BEARING CAPACITY OF FOOTINGS CLOSE TO SLOPES OF COHESIONLESS SOIL

by

JEAN-HUGUES DESCHENES

Submitted in partial fulfillment of the
requirements for the degree of
Doctor of Philosophy

Department of Civil Engineering
School of Graduate Studies
University of Ottawa
Ottawa, Canada

March, 1978

PREFACE

The bearing capacity of a shallow foundation at the top of a natural or man-made slope is a topic of soil mechanics which is important in civil engineering design. At the present time the geotechnical engineer is not in a very good position to evaluate the safety of a particular design configuration and, therefore, is uncertain as to whether or not his design is the most economical. No experimental proof exists that the present methods of design for footings near slopes -- based mainly on the theory of perfect plasticity -- are satisfactory both from the point of view of safety and economy.

The scope of the present study is limited to the determination of ultimate bearing pressures of a thirty centimeter wide footing at the top of a slope with an inclination of two horizontal to one vertical slope of both dense and compact sand.

The program consisted of twenty-three tests, twelve with the sand in a compact state and eleven with the sand in a dense state. Five tests were performed to determine whether or not the experiments are reproducible.

An extensive literature survey was carried out to find the existing theoretical and experimental accounts of the problem. Certain improvements have been contributed to these existing accounts. A theoretical approach, involving

the finite element method is also presented to find a lower bound value to the problem.

The findings from this first large scale test program reveal that the theories do not predict adequately the failure loads. Furthermore the relationship between the experimental bearing capacity factors $N_{\gamma q}$ and the angle of internal friction Φ is not as clear as that which theory would predict. From this study, it is concluded that the safe design approach might be to use a lower bound solution in conjunction with a shear box Φ angle for the particular sand.

ACKNOWLEDGEMENTS

The writer is indebted to his advisor Dr. D.H. Shields, Professor of Geotechnical Engineering, for his guidance, valuable advice, and suggestions throughout this investigation. He also has to be complimented for his interest and dedication to the project.

Thanks are due to Dr. J.D. Scott, and Dr. G.E.A. Bauer, who enormously helped to get the project started and completed efficiently, and to Dr. Selvadurai, Professor of Civil Engineering at Carleton University, for his interest. Dr. J.M. Duncan, Professor of Geotechnical Engineering at the University of California at Berkeley must be thanked for making the computing facilities available to the writer.

Thanks and appreciation are due to all members of the technical staff who made the project possible especially MM. O.H. Siret and R. Moore. The machine shop staff under Mr. C. Lavigne rendered very valuable assistance.

Thanks are also extended to P. Lai, J.-L. Briaud, H. Abu-Sitta, G. Haile, and G. McEniry, fellow graduate students for their encouragement and constructive criticism.

A special word of thanks is due to my wife, Madeleine, for providing for me the ideal atmosphere for study and for her invaluable assistance and patience in typing the manuscript. Thanks are also due to Mrs. Carol Shields, M.A., for reviewing the manuscript.

TABLE OF CONTENTS

LIST OF TABLES AND ILLUSTRATIONS

NOTATIONS

$[A]$ = Position displacement matrix.

A_o = Original area (Bowles 1977).

A_1 = Transformed area (Bowles 1977).

A_2 = Bearing capacity factor due to weight (Kovalev).

b = Horizontal distance from the slope crest to the leading edge of the footing.

B = Footing width.

B_2 = Bearing capacity factor due to surcharge (Kovalev).

c = Cohesion.

$[C]$ = Material property matrix.

D = Depth of footing embedment.

D_{BC} = Dissipated energy along BC.

D_{BCD} = Dissipated energy in BCD.

f_o = Pressure on BC (Mizuno).

$\{F_e\}$ = Force vector matrix at the nodes of the element.

F_m = Force acting on the m^{th} wedge (Mizuno).

F_n = Normal force.

F_o = Force on BC (Mizuno)

F_t = Tangential force.

G = $\gamma B/2c$ = Dimensionless soil weight parameter (Chen).

G_{Rm} = Weight resultant (Mizuno).

H = Height of slip surface.

K = Constant relating forces and displacements.

K = Empirical constant (pressuremeter).

K_A = Active earth pressure coefficient.

$[K_A]$ = Overall stiffness matrix.

$[K_e]$ = Stiffness matrix of the element.

K_o = Coefficient of earth pressure at rest.

K_p = Passive earth pressure coefficient.

L_m = Wedge reaction (Mizuno).

m = Fraction of shear strength mobilized along a slip surface.

M_1 = Function of the angle of internal friction (Bowles 1975).

N_c = Bearing capacity factor due to cohesion (Terzaghi and Meyerhof).

$N_{c\alpha}$ = Bearing capacity factor due to cohesion and effect of a slope (Giroud).

N_q = Bearing capacity factor due to surcharge (Terzaghi and Meyerhof).

$N_{q\alpha}$ = Bearing capacity factor due to surcharge and effect of slope (Giroud).

N_γ = Bearing capacity factor due to weight (Terzaghi and Meyerhof).

$N_{\gamma\alpha}$ = Bearing capacity factor due to weight and effect of slope (Giroud).

$N_{\gamma q}$ = Bearing capacity factor combining effect of weight and surcharge (Meyerhof).

p = Normal stress on equivalent free surface (or simply γD = surcharge).

P_o = At rest horizontal in-situ total stress at the level of the pressuremeter test.

P_L = Limit pressure (pressuremeter).

P_p = Passive earth pressure.

q = Bearing pressure.

q_L = Vertical limit pressure (pressuremeter).

q_o = In-situ total vertical stress at the foundation depth after construction.

q_p = Applied pressure.

r_o = Length of plane BC.

r_m = Length of plane BD (Mizuno).

s = Tangential stress on the equivalent free surface.

S_m = Reaction stress (Mizuno).

S_t = Shearing force along slip surface.

u = Displacement in the horizontal direction.

$[u_e]$ = Displacement vector matrix at the nodes of the element.

v = Displacement in the vertical direction.

V = Velocity.

W = Weight of a slice.

W_{ABC} = Rate of work done along ABC.

α = Slope angle.

$[\alpha]$ = Coefficient matrix.

β = Angle of the equivalent free surface to the horizontal.

β_1 = Angle of rigid wedge at footing edge (Giroud).

γ = Unit weight of the soil (Density).

T^1 = $\sin^{-1}(\frac{\sin\alpha}{\sin\Phi})$ (Giroud).

δ = Angle of friction between soil and footing.

$[\delta]$ = Transformed displacement matrix.

δ^1 = Angle on the Mohr-Coulomb circle that defines the fraction of cohesion in a particular soil (Giroud).

$[\delta_{(x,y)}]$ = Nodal displacements.

ε = Strain.

$[\varepsilon]$ = Strain matrix.

ζ = Bearing capacity reduction factor (Brinch Hansen).

ζ_{qg} = Bearing capacity reduction factor due to surcharge for ground inclination (Brinch Hansen and Vésic).

$\zeta_{\gamma g}$ = Bearing capacity reduction factor due to weight for ground inclination (Brinch Hansen and Vésic).

η = Angle between the equivalent free surface and a slip- line (Meyerhof and Chen).

θ = Sweep angle of a log spiral.

θ_{η} = Angle $\hat{ABD}$ (Mizuno).

θ_{o} = Angle $\hat{ABC}$ (Mizuno).

λ = Slope angle of OB with the vertical (Absi).

μ = Angle between two slip-lines.

ν = Poisson's ratio.

ξ = Angle of rigid wedge at footing edge

ρ = Base angle of a slice.

σ = Standard deviation.

σ = Mean stress.

$\sigma_{(D)}$ = Stress at point D.

$\sigma_{(o)}$ = Stress at point O.

σ_{n} = Normal stress.

σ_{x} = Stress in the horizontal direction.

σ_{z} = Stress in the vertical direction.

$\sigma_{z(o)}$ = Vertical stress at O.

$\sigma_{z(D)}$ = Vertical stress at D.

$[\sigma_{(x,y)}]$ = Nodal stresses.

τ = Shear stress

τ_{xz} = Shear stress acting on the xz plane

Φ = Angle of internal friction

Ψ = Angle of rigid wedge at footing edge.

ω = Inclination of load q.

Ω = Construction angle (Kovalev).

CHAPTER I

INTRODUCTION

1.1 General

The bearing capacity of a shallow foundation at the top of a natural or man-made slope is a topic of soil mechanics which is important in civil engineering design. Figure 1.1 depicts situations where a slope is a major feature in the evaluation of bearing capacity. In these situations the geotechnical engineer is faced with two, often conflicting concerns -- safety and cost. He must ensure that the structure (building, bridge, machinery, or vehicle) will not be endangered by the presence of the slope; he must also ensure that his analysis does not err so far on the side of safety that financial resources are wasted.

At the present time the geotechnical engineer is not in a very good position to evaluate the safety of a particular design configuration and, therefore, is uncertain as to whether or not his design is the most economical. The engineer's understanding of the problem is hampered by its broad scope and the many variables which affect the bearing capacity of shallow footings.

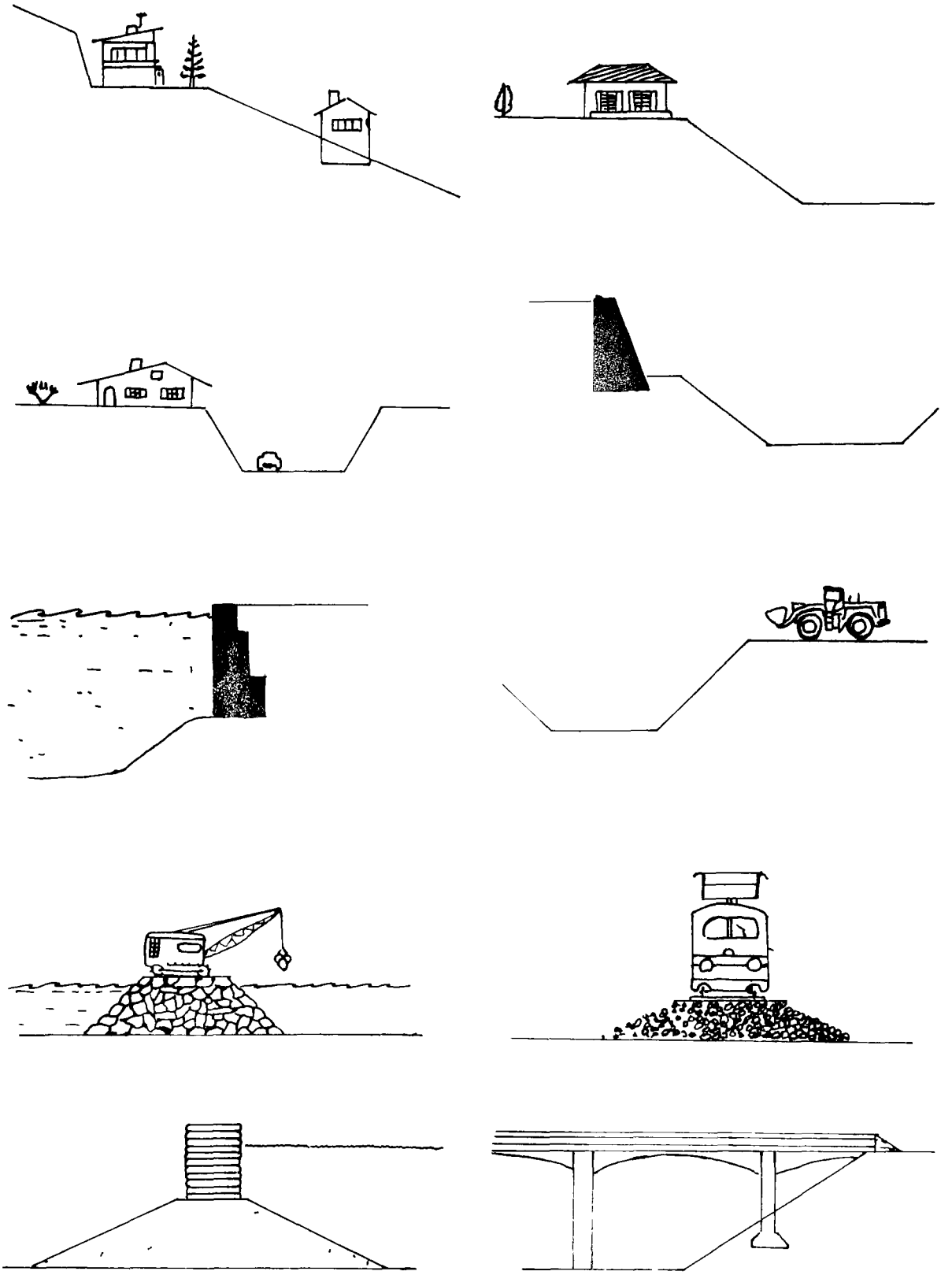

Foundations on Top of Slopes (According to Giroud)

Figure 1.1

1.1.1 Statement of the Problem

No experimental proof exists that the present methods of design for footings near slopes -- based mainly on the theory of perfect plasticity -- are satisfactory both from the point of view of safety and economy. It is appreciated that this problem has been studied experimentally by several investigators; however, the small scale of the models they used makes their findings suspect.

It is presently possible to carry out tests of reasonable scale at the University of Ottawa. A large sandbox, holding fifty tons of sand, has been constructed. The box is equipped with a spreading device so that a wide range of relative densities (and therefore shearing resistances) can be achieved for the sand. It is the purpose of this project to measure the ultimate capacity of a thirty centimeter wide strip footing at the crest of a slope of both compact and dense sand. The results provide the experimental test that is lacking to determine whether or not existing design theories are valid.

1.1.2 Objectives and Scope of the Study

The scope of the present study includes six major topics. These topics are, (in order of consideration in the thesis), 1) a literature survey of previous theoretical and experi-

mental work on bearing capacity of sands and, in particular, of footings at the top of slopes; 2)extensions of existing theories were required to meet the needs of this particular research project; 3)a testing program which is described in greater detail in the following paragraphs; 4) a comparison of the test results with theory; 5)a search for a lower bound theoretical solution to the problem; and 6)the drawing of conclusions and the making of suggestions for additional research.

The scope of the testing program is limited to the determination of ultimate bearing pressures of a thirty centimeter wide footing at the top of a slope with an inclination of $\tan^{-1}(\frac{1}{2})$ (two horizontal to one vertical) of both dense and compact sand. The reasons for this particular choice of variables are given in Sections 1.2 and 1.3. In order to assess the influence of the proximity of the slope on the bearing capacity the footing is located at various distances from the crest of the slope and at various depths in the sand mass.

The work intends to simulate the case of a strip footing which assumes to deform under conditions of plane strain. Two-dimensional loading conditions are imposed by the footing stretched across the rigid box, so that the strip footing case is simulated even though the footing is of finite length (180 cm.).

The program consists of twenty-four tests, twelve with the sand in a compact state and twelve with the sand in a

dense state. The footing locations are shown in Figure 1.2. Extra tests are carried out to determine whether or not the experiments are reproducible.

1.1.3 Outline of the Thesis

In Chapter I, a general introduction to the problem is given. Chapters II and III respectively present the findings of a literature survey of the main theoretical and experimental studies treating the problem of bearing capacity of footings located at the top of slopes.

Two chapters deal with the present experiments; Chapter IV describes the experimental model, while Chapter V discusses the test procedure.

The experimental results are given in Chapter VI, and they are discussed and compared with theory and other experiments in Chapter VII. A special look at the problem, using finite elements, forms Chapter VIII.

A summary and conclusions are given in Chapter IX. The appendices contain a list of references and the mathematical formulations for some of the theories which are discussed in Chapter II.

1.2 The Variables that Make up the Problem

Figure 1.3 attempts to categorize the main variables

Location of Tests

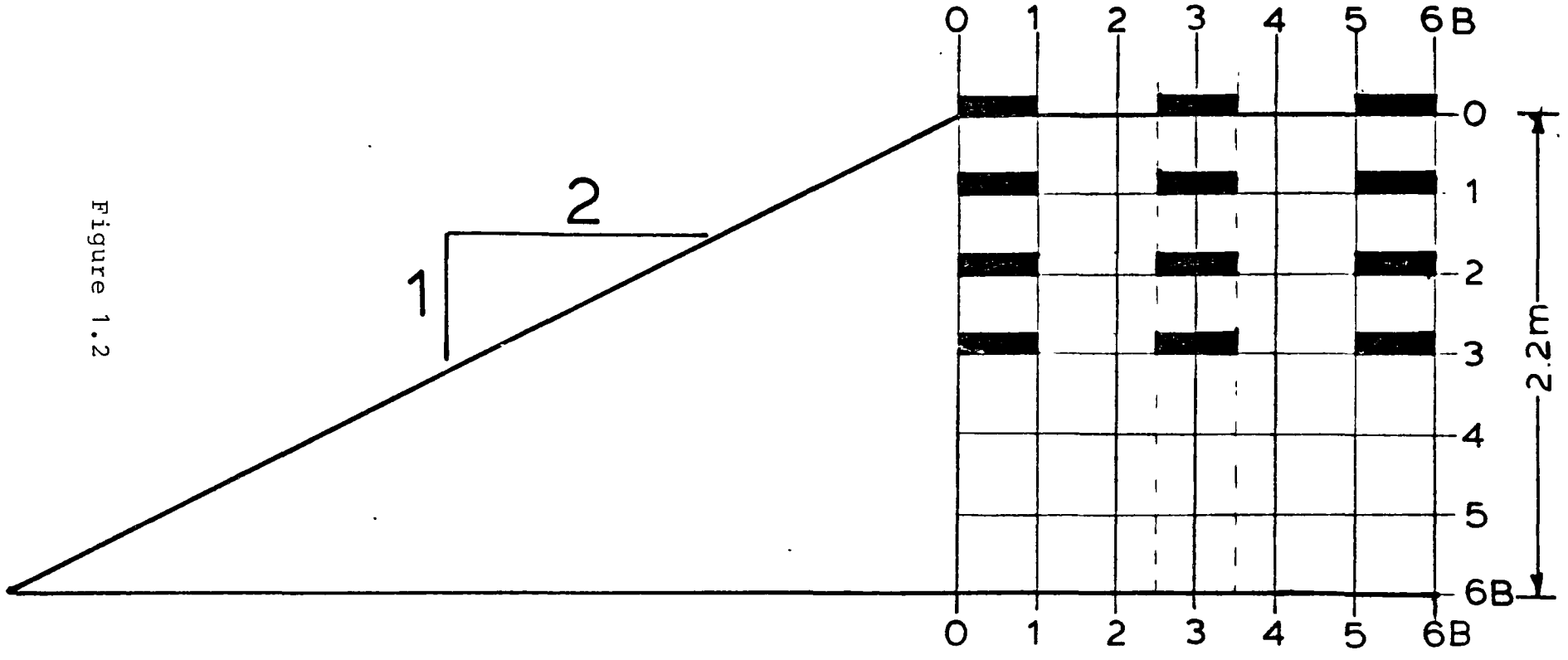

Figure 1.2

that influence bearing capacity according to 1)the properties of the footing itself, 2)the soil, 3)external considerations, and 4)other factors. These categories (except for 'other factors') are subdivided into subcategories, with the provision that each variable is present only once in the list.

A typical example of a set of variables making up a particular problem could be "a square footing, at the crest of a slope of soft compressible clay, subjected to an eccentric load, and with seepage in the slope". In the same way, the extent of the present study lies within the variables given in Figure 1.3; the choice of these variables is explained in the following paragraphs.

1.3 Ministry of Transportation and Communications of Ontario Requirements

Undertaking the present study necessitated important financial support. Funds were available from the Ministry of Transportation and Communications of Ontario (MTC), provided that certain conditions were met:

1- the slope should be two horizontal to one vertical to represent MTC design practice.

2- crushed sand be used to simulate "Granular A" frictional properties.

3- the footings be tested to their ultimate capacity under vertical, central load.

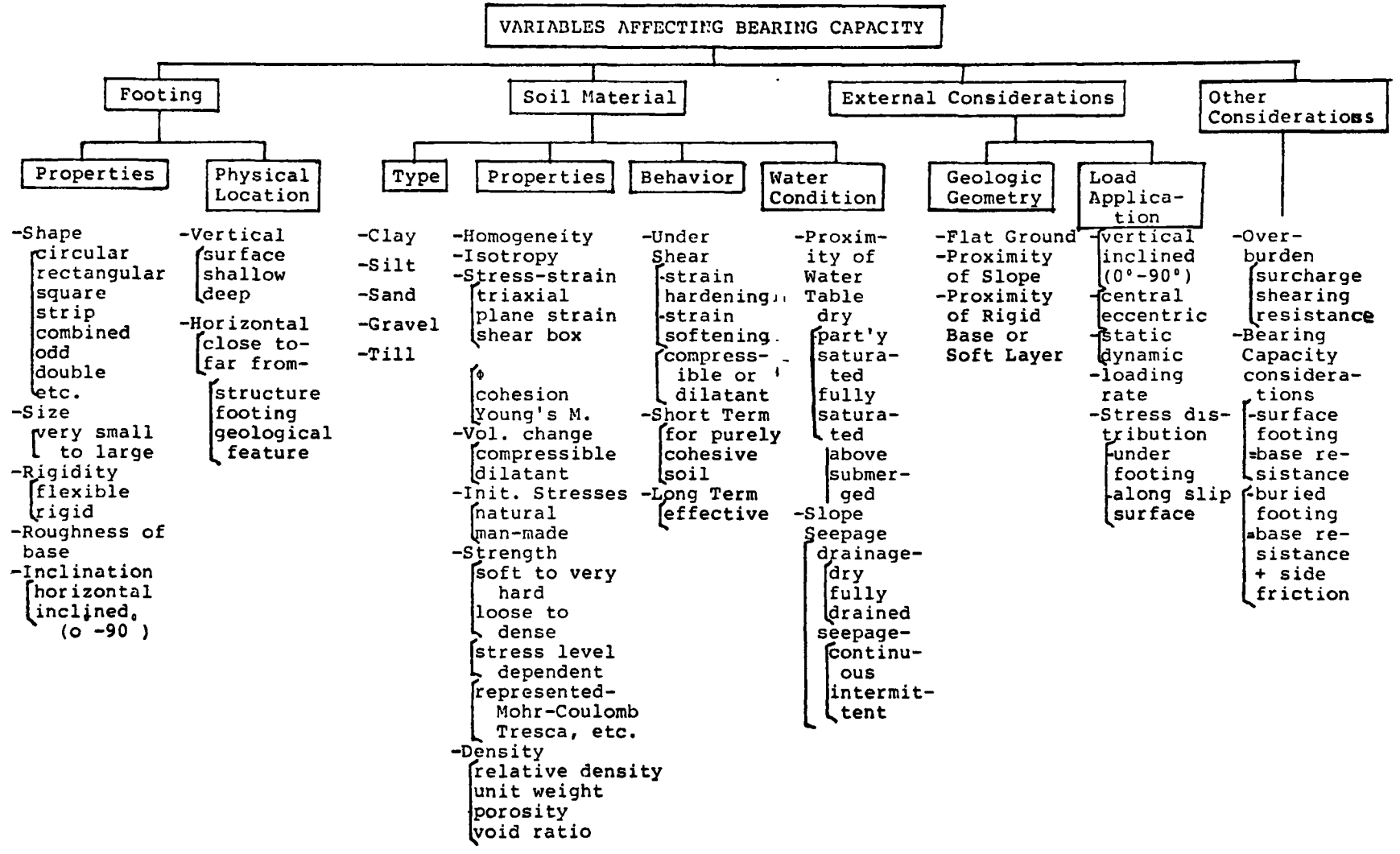
VARIABLES AFFECTING BEARING CAPACITY
Footing
Soil Material
External Considerations
Other Considerations
Properties
Physical Location
Type
Properties
Behavior
Water Condition
Geologic Geometry
Load Application
-Shape
circular
rectangular
square
strip
combined
odd
double
etc.
-Size
very small to large
-Rigidity
flexible
rigid
-Roughness of base
-Inclination
horizontal
inclined, (o -90)
-Vertical
surface
shallow
deep
-Horizontal
close to-far from-
structure
footing
geological feature
-Clay
-Silt
-Sand
-Gravel
-Till
-Homogeneity
-Isotropy
-Stress-strain
triaxial
plane strain
shear box
φ
cohesion
Young's M.
-Vol. change
compressible
dilatant
-Init. Stresses
natural
man-made
-Strength
soft to very hard
loose to dense
stress level dependent
represented-
Mohr-Coulomb
Tresca, etc.
-Density
relative density
unit weight
porosity
void ratio
-Under Shear
-strain hardening
-strain softening
compress-ible or dilatant
-Short Term
for purely cohesive soil
-Long Term
effective
-Proximity of Water Table
dry
part'y saturated
fully saturated
above submerged
-Slope Seepage
drainage-
dry
fully drained
seepage-
continuous
intermittent
-Flat Ground
-Proximity of Slope
-Proximity of Rigid Base or Soft Layer
-vertical
inclined (0°-90°)
-central
eccentric
-static
dynamic
-loading rate
-Stress distribution
-under footing
-along slip surface
-Over-burden
surcharge
shearing resistance
-Bearing Capacity considera-tions
-surface footing
-base re-sistance
-buried footing
-base re-sistance + side friction

Figure 1.3

4- the tests be carried out at two different sand densities to simulate two different degrees of compaction of embankment material.

5- the test results be compared with certain theoretical evaluations so that the present MTC method of design can be assessed.

6- at least twenty-four tests be carried out, in addition to a certain number of repeat tests.

All these requirements are specified in a formal contract with the MTC.

Many of the remaining variables, such as the size of the footings and the properties of the sand are dictated by the size of the sandbox and the materials handling equipment. Other factors, such as the surface roughness of the footing, are chosen to conform with current practice.

CHAPTER II

BEARING CAPACITY

2.1 Introduction

Usually, problems of soil mechanics are divided into two distinct groups -- deformation problems and stability problems. Deformation problems deal with the distribution of stress and deformation of the soil when no collapse of the soil is involved. Stability problems, on the other hand, deal with the conditions of ultimate failure of a soil mass; the most important feature of such problems is the determination of the loads which will cause general failure of the soil mass. In between deformation and stability lie the problems of progressive failure.

This thesis discusses only the stability aspect of the problem of foundation analysis. Chapter II is divided into three parts: the first part gives a general discussion of the methods which are used in determining ultimate bearing capacity; the second part presents and discusses existing theories of bearing capacity of footings on top of a slope; and, finally, the third part is an original contribution to the topic, demonstrating the ways in which previously conceived ideas can be extended and presented.

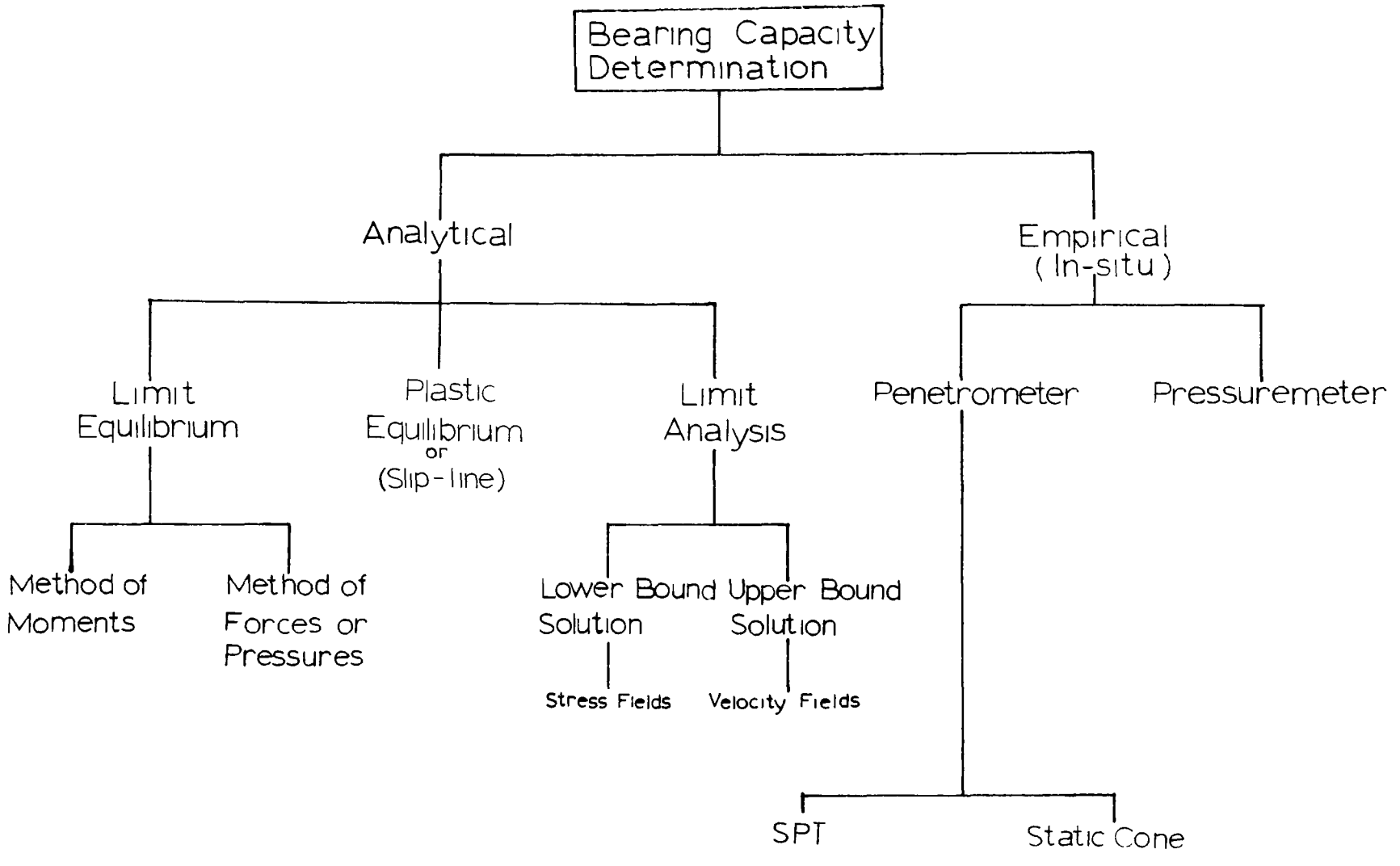
Bearing Capacity Determination
Analytical
Empirical (In-situ)
Limit Equilibrium
Plastic Equilibrium or (Slip-line)
Limit Analysis
Penetrometer
Pressuremeter
Method of Moments
Method of Forces or Pressures
Lower Bound Solution
Upper Bound Solution
Stress Fields
Velocity Fields
SPT
Static Cone

Figure 2.1

2.2 Determination of Bearing Capacity

2.2.1 General

Figure 2.1 shows a chart of the principal methods used at the present time for the determination of bearing capacity. These methods are divided into the two major categories: analytical and empirical. The analytical methods are the mathematical processes which link theoretical assumptions of soil and foundation behavior to seemingly realistic values of ultimate bearing capacity. The empirical methods, on the other hand, attempt to relate a form of measurement, usually an in-situ field test, to ultimate bearing capacity. Both these methods are discussed in the following paragraphs.

2.2.2 Analytical Methods

2.2.2.1 General

Soil mechanics uses a variety of mathematical techniques that assume perfect soil plasticity to determine failure loads. These techniques can be divided into three groups: limit equilibrium, the plastic equilibrium method, and the limit analysis concept. In following sections, each of these techniques is described as they apply to bearing capacity. However, before describing the techniques, a general overview of the bearing capacity problem is given, based on the solution proposed by Terzaghi in 1943.

At that time and even today, the mathematical investigations concerning the state of equilibrium beneath continuous footings under loading are not fully satisfactory. No general bearing capacity equation has been found that rigorously satisfies the Mohr-Coulomb equation

$$\tau = c + \sigma_n \tan\Phi \qquad (2.2.2.1)$$

and at the same time takes into account the weight of soil, the influence of the depth of surcharge D, and the real distribution of vertical and horizontal forces on the base of the footing.

Terzaghi proposed that the ultimate normal load that could be applied to the soil surface could be approximately estimated by superposing the limit loads obtained for each of the following cases, considered separately: 1)weightless soil possessing cohesion, 2)for a weightless soil whose ability to sustain a surface stress depends only on the presence of a counterbalancing surcharge, and 3)for a soil having weight and carrying footing stresses in the absence of a surcharge. These contributions are added together and are represented by the expression:

$$q = cN_c + pN_q + \tfrac{\gamma}{2}BN_\gamma \qquad (2.2.2.2)$$

where q is the ultimate bearing pressure; the bearing capa-

city factors N_c, N_q, and N_γ represent the effects due to soil cohesion, surcharge $p = \gamma D$ and soil unit weight γ respectively. B is the footing width. The factors N are all functions of the angle of internal friction Φ of the soil.

The solution consists of a two stage approach. The first stage is based on the analytical work of Prandtl and Reissner [Terzaghi (1943)]; this assumes the material to be weightless in order to find the N_c and N_q factors of the general bearing capacity equation. Prandtl's failure mechanism is shown on Figure 2.2. In this case, the N_c value is given by:

$$N_c = \cot\Phi\,[e^{\pi \tan\Phi} \tan^2(\tfrac{\pi}{4} + \tfrac{\Phi}{2}) - 1] \qquad (2.2.2.3)$$

According to Reissner, the effect of the surcharge is found to be:

$$N_q = e^{\pi \tan\Phi} \tan^2(\tfrac{\pi}{4} + \tfrac{\Phi}{2}) \qquad (2.2.2.4)$$

It can be seen from the general equation that if the surcharge stress is zero, the weightless frictional mass cannot sustain any load. N_c and N_q are interrelated by the following expression:

$$N_c = (N_q - 1)\cot\Phi \qquad (2.2.2.5)$$

Prandtl's Mechanism

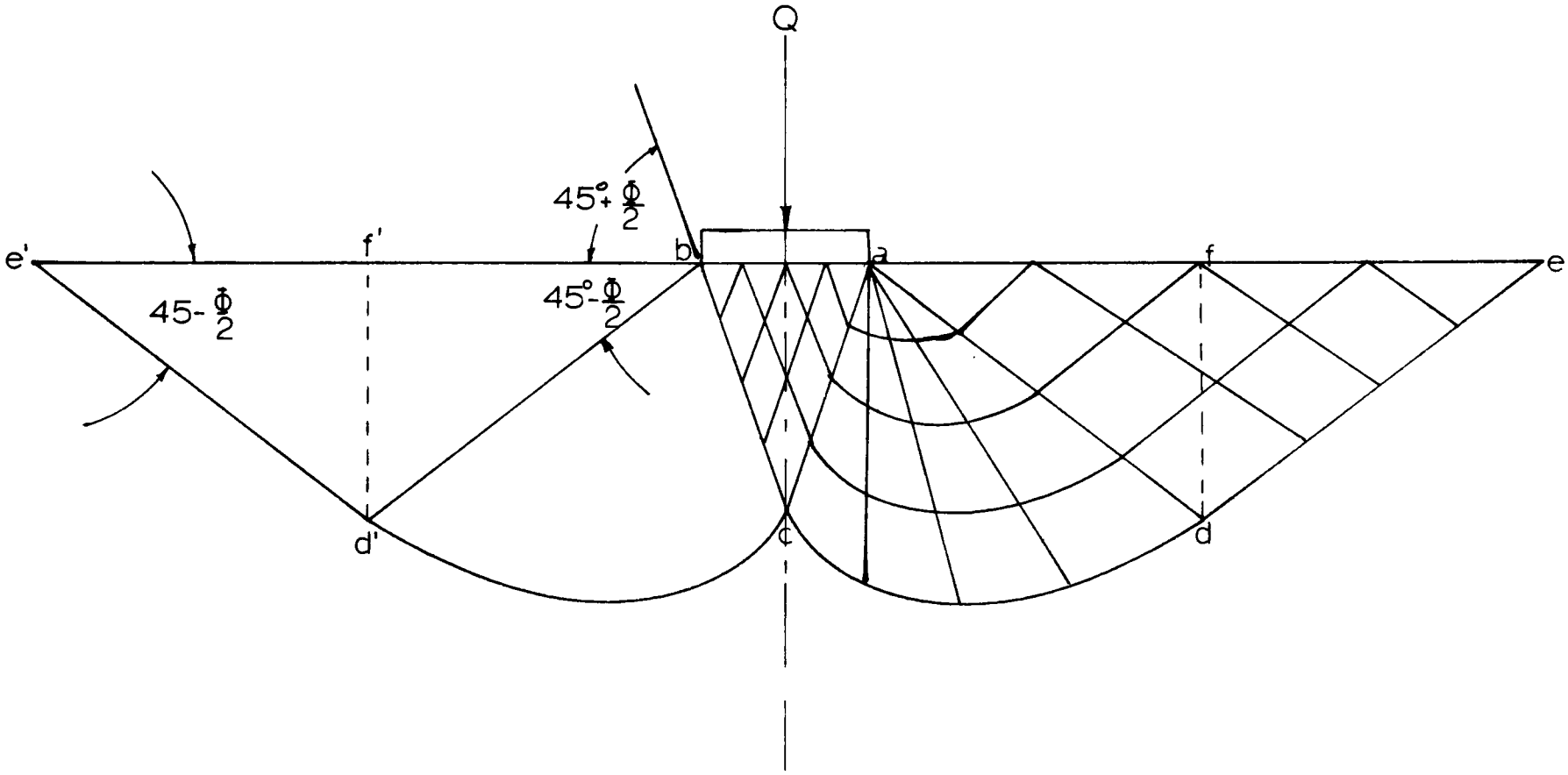

Figure 2.2

The second stage is a semigraphical treatment, based on an extension of the work of Ohde [Terzaghi (1943)] or the numerical integration scheme of Sokolovskii (1965); this stage takes the weight of the soil material into account, and gives values for N_γ. While there is a variety of other, more involved solutions available, all investigators agree that there is no completely correct theoretical solution for the weight factor N_γ for the shallow footing problem. For example, Meyerhof (1961), Brinch Hansen (1961), and A. Vésic (1973) suggested the following relationships with N_q for the computation of N_γ on flat ground:

Meyerhof: $$N_\gamma = (N_q - 1)\tan(1.4\Phi) \qquad (2.2.2.6)$$

Brinch Hansen: $$N_\gamma = 1.8(N_q - 1)\tan\Phi \qquad (2.2.2.7)$$

A. Vésic: $$N_\gamma = 2(N_q - 1)\tan\Phi \qquad (2.2.2.8)$$

The validity of the superposition process can be questioned because soil behavior is nonlinear in the plastic range. Although superposition does not lead to a correct solution, in many instances it enables one to find an approximate but realistic answer.

2.2.2.2 Limit Equilibrium

The limit equilibrium method is an approximate approach

to the construction of a slip line and generally entails an assumed failure surface of simple shape -- plane, circular, or log spiral. An indication of the stress distribution on the failure surface is required. Once the failure surface and the stress distribution are assumed, the analysis requires only that conditions of equilibrium are satisfied. The object is to find the most dangerous slip surface with respect to static loads, pressures, or moments. This method assumes the soil to be rigid-plastic.

Terzaghi (1943) was the first to apply the limit equilibrium method as proposed by Odhe to the analysis of bearing capacity and retaining wall problems. Terzaghi proposes, for the case of a soil with weight, a failure pattern which is similar to the one analysed by Prandtl for weightless soil. In this case, the slip surface is divided into the three zones shown in Figure 2.3. Zone I is an active wedge which can be considered to be part of the footing as it is pushed into the soil. Zone II is a zone of radial shear and is called the transition zone between the active zone, I, and the passive zone, III. These zones are defined by the Mohr circle of stress. The transition (or radial shear zone) in the Prandtl case is a sector of a logarithmic spiral.

Terzaghi determined his N_γ values from the equilibrium of moments about the center of the log spiral at the footing edge (point B). Meyerhof (1951) started with the same zone I as Terzaghi assumed, but found that the most critical

The Three Zones of Bearing Capacity

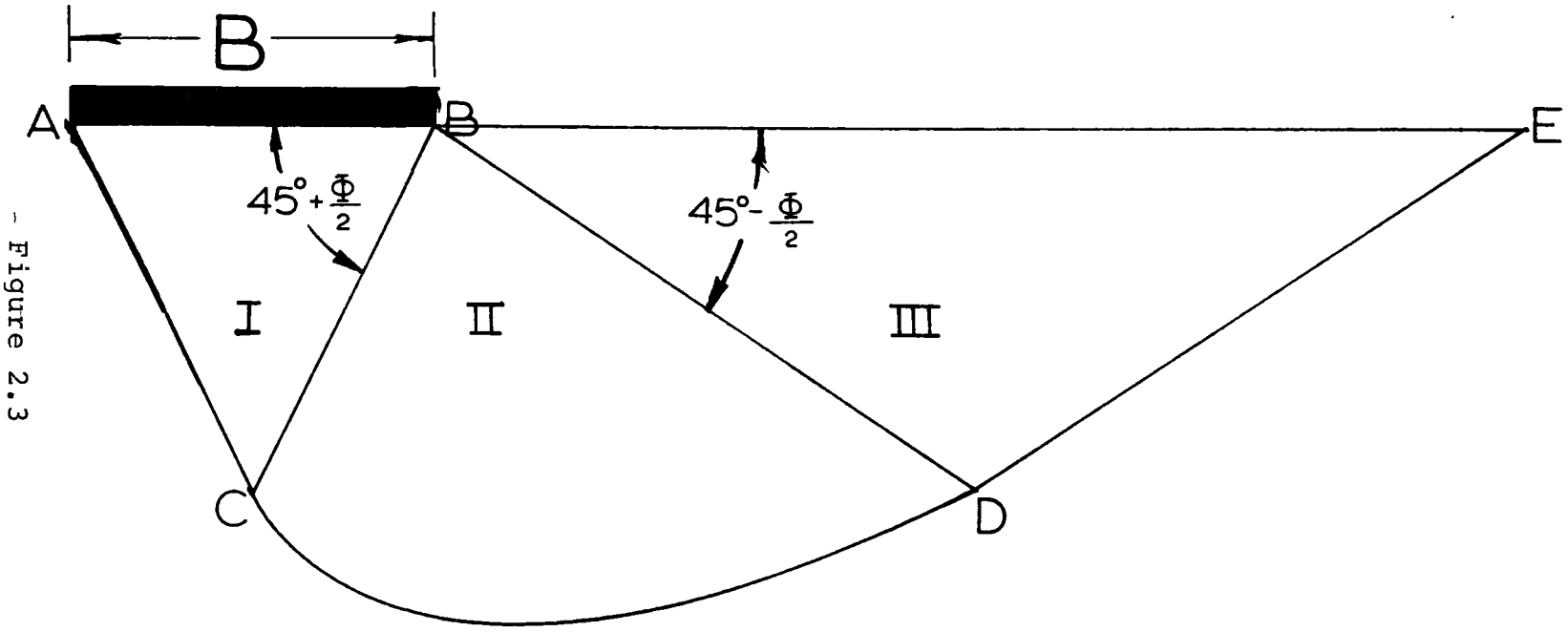

- Figure 2.3

location of the logspiral center is not at the footing edge but somewhere inside zone BCDE, close to point B on either side of line BD. Later, Meyerhof (1955) changed zone I but returned the center of the log spiral to the footing edge. Meyerhof varied the active wedge angle ABC until minimum N_γ values were found.

Other investigators used the same basic method as Terzaghi and Meyerhof but with different assumed failure surfaces. Brinch Hansen (1966) reviewed some of the methods which consider the equilibrium of forces within the slip surface. Mizuno (1948) used a Prandtl type slip surface. All these failure analyses consider the static equilibrium of the forces which are involved and the distribution of the stresses which act on radial planes taken from the edge of the footing to the slip surface.

In a series of articles, DeBeer (1967) attempted to correlate experimental data with the existing theories. Most of the theories used in this comparison are based on limit equilibrium. As a result of this work, DeBeer proposed improvements to the theories. Vésic (1973), also went through a similar process, and the result was a table of bearing capacity values that have proven useful for the practicing engineers.

As previously mentioned, the limit equilibrium method is an approximate solution to the problem of bearing capacity. It is found to yield results of practical importance in Geo-

technical Engineering design. A principal drawback is that the method must make assumptions regarding the stress distribution along the failure surface. Chen (1974) contributes these comments about this aspect of the limit equilibrium method:

> "Since the stress distribution is not precisely defined everywhere inside and outside of the assumed failure surface, one cannot say definitely that a stress distribution, compatible with the assumed failure surface and satisfying equilibrium, stress boundary conditions, and the yield function, exists."

2.2.2.3 Plastic Equilibrium Method(or Stress Characteristics Method or Slip-line Method)

A combination of the Mohr-Coulomb criterion, expressed as:

$$\sqrt{\frac{(\sigma_z - \sigma_x)^2}{4} + \tau_{xz}^2} - \frac{\sigma_z + \sigma_x}{2} \sin\Phi = c \cos\Phi \qquad (2.2.2.9)$$

and the two-dimensional equations of equilibrium,

$$\frac{\partial \sigma_x}{\partial x} + \frac{\partial \tau_{xz}}{\partial z} = 0 \qquad (2.2.2.10a)$$

$$\frac{\partial \tau_{xz}}{\partial x} + \frac{\partial \tau_z}{\partial z} = \gamma \qquad (2.2.2.10b)$$

yields a set of differential equations of plastic equilibrium where σ_x is the normal stress at a point acting in the x direction, σ_z is the normal stress at the same point acting in the z direction and τ_{xz} is the shearing stress at the point. Together with the boundary stress conditions, this set of differential equations can be used to investigate the stresses in the soil beneath the footing at the instant of impending plastic flow. This leads to the formation of slip directions which yield a network of slip-lines. An illustration of the network is given in Figure 2.4.

Sokolovski (1965) adopts a numerical procedure based on a finite difference approximation of the slip line equations. He obtains a number of interesting solutions for the bearing capacity problem. Harr (1966), Scott (1963), Graham (1968), and I.K. Lee (1968) also adopt this method to find bearing capacity factors and earth pressures coefficients.

One of the major drawbacks of the plastic equilibrium method is that it neglects the stress-strain properties of the soil. The method assumes the soil to be rigid-plastic. A realistic flow rule for the soil must be considered to obtain a solution which takes into account the displacement along the slip lines.

2.2.2.4 Limit Analysis

The usefulness of the classical theory of plasticity was greatly improved by the development of limit analysis tech-

Slip Line Network

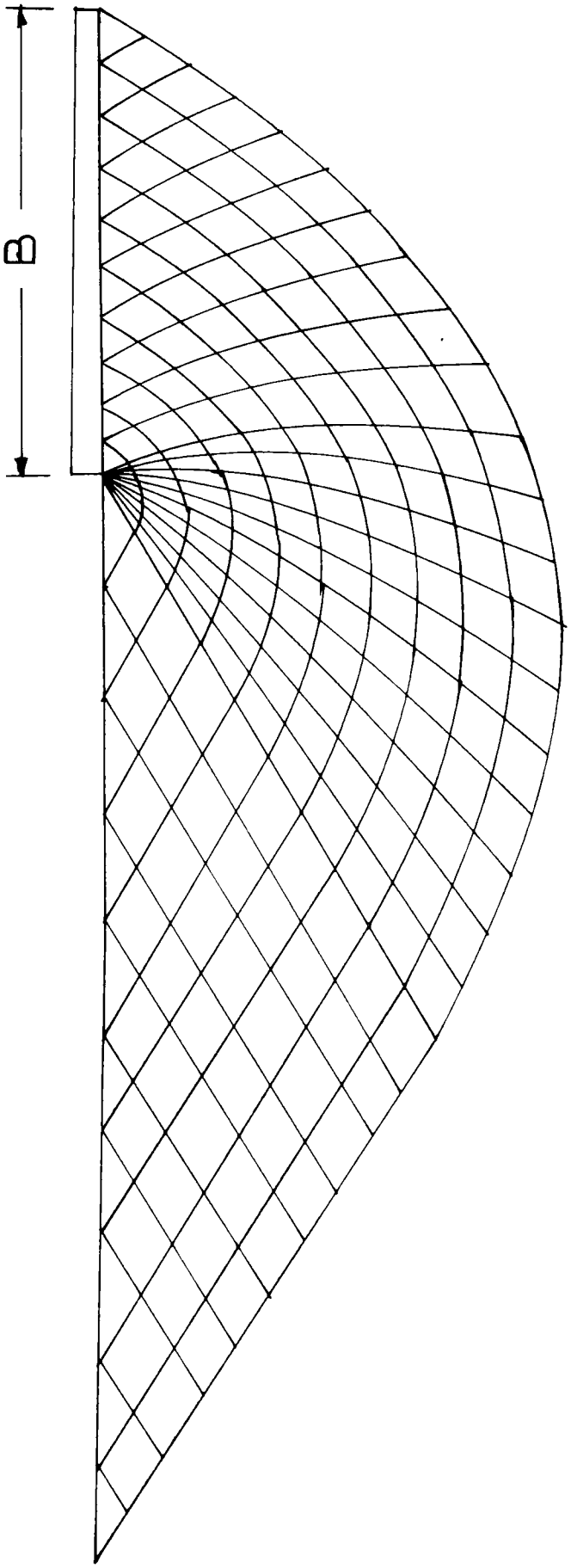

Figure 2.4

niques and the associated bound theories by Drucker, Greenberg, and Prager [Chen (1974)]. These methods enable bounds to be placed on the load at which general plastic collapse occurs, even when the problem is quite complex and the determination of the true collapse load is virtually impossible. Frequently, the bounds are close enough to define the true collapse load with sufficient accuracy for engineering purposes.

As applied to soil mechanics, the basic assumptions made by the theory of limit analysis are the following:

a) the material exhibits an elasto-plastic or rigid-plastic behavior
b) the Mohr-Coulomb or other failure criteria are valid
c) the kinematics of the problem are given by the concept of the flow rule.
d) there are small changes in geometry at failure
e) the equation of virtual work applies.

The two main limit theorems will be examined in the following paragraphs. Their corresponding mathematical techniques will also be introduced.

2.2.2.4.1 Lower Bound Theorem

The lower bound theorem states that if a distribution of stress (over the domain in question) can be found which satisfies the equations of equilibrium, the stress boundary conditions and the yield criterion, the load associated with

this stress distribution is less than or at best equal to the true collapse load or limit load.

The technique used to obtain lower bound values is called a statically admissible stress field. This stress field is usually obtained through engineering intuition and trial and error. Chen (1974) discusses the technique at great length. An illustration of a typical stress field is given in Figure 2.5.

The requirements for the validity of this technique are the following:

a) a complete stress distribution or stress field must be found, everywhere satisfying the differential equations of equilibrium.
b) the stress field at the boundary must satisfy the boundary stress condition.
c) the stress field must nowhere violate the yield condition.

The formulation of stress fields can be found, for example, in Lee (1968) and Chen (1974). Another acceptable lower bound analysis is the one proposed by Lysmer (1970), but this analysis is mainly computer oriented and closely resembles the finite element method.

2.2.2.4.2 Upper Bound Theorem

The upper bound theorem states that if the rate at which work is being done by the external load is greater than or equal to the rate of internal energy dissipation associated

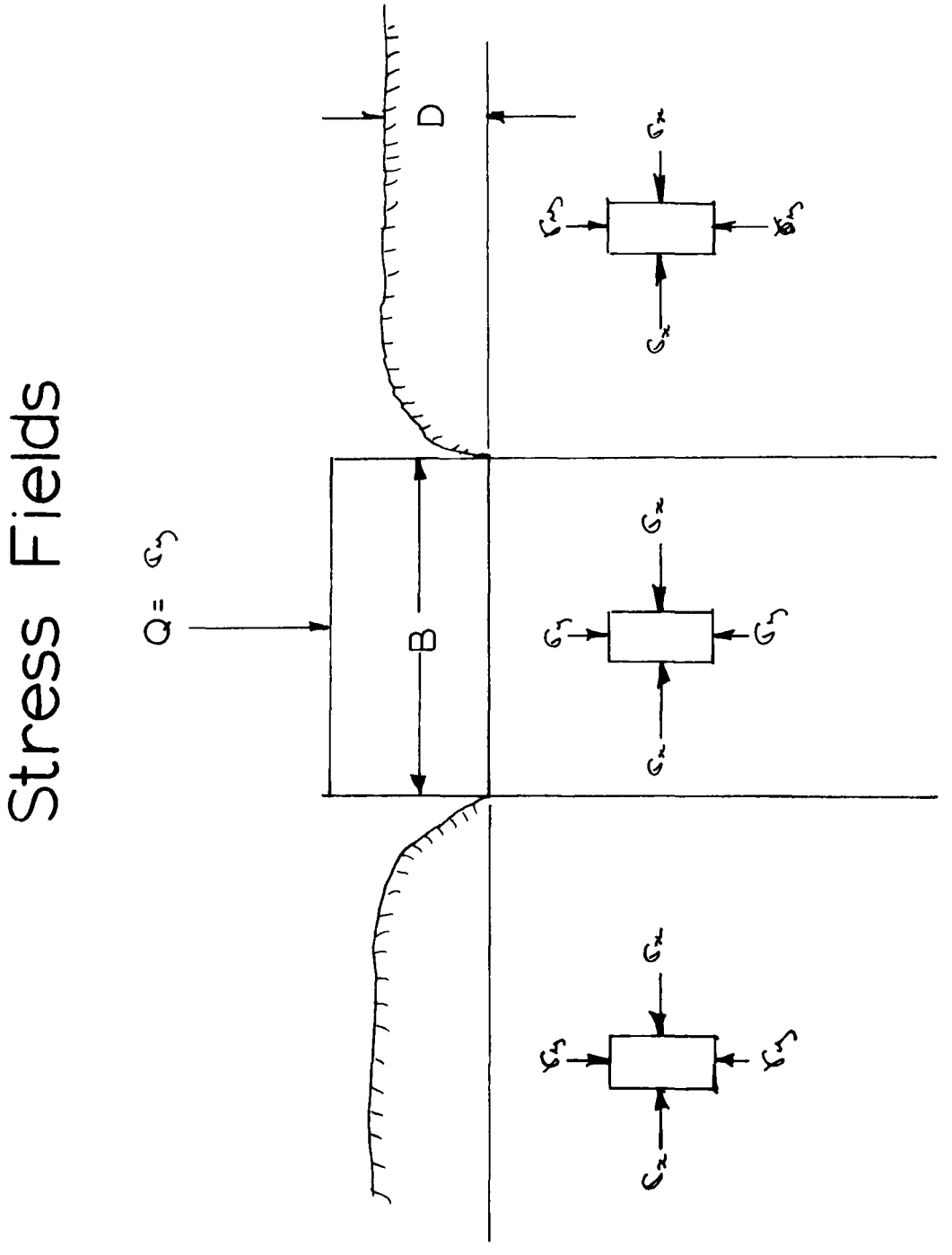

Figure 2.5

with a kinematically admissible velocity field, the load must be greater than, or at best equal to, the true ultimate or limit load. A corollary to the limit analysis method states that if the upper and the lower bounds coincide, the limit load is the true collapse load.

The technique used to obtain upper bound values requires the generation of velocity fields using well defined mathematical rules. The method is described in books by Wu (1968), Lee (1968) and Chen (1974). An illustration of a typical velocity field is given in Figure 2.6.

The requirements for the validity of this technique are the following:

a) a valid mechanism of collapse must be assumed which satisfies the mechanical boundary conditions.
b) the expenditure of energy by the external load (including soil weight) as it is displaced according to the assumed mechanism must be calculated.
c) the internal dissipation of energy by the plastically deforming regions associated with the mechanism must be calculated.
d) the most critical upper-bound solution is generally obtained via the work equation.

Velocity Fields

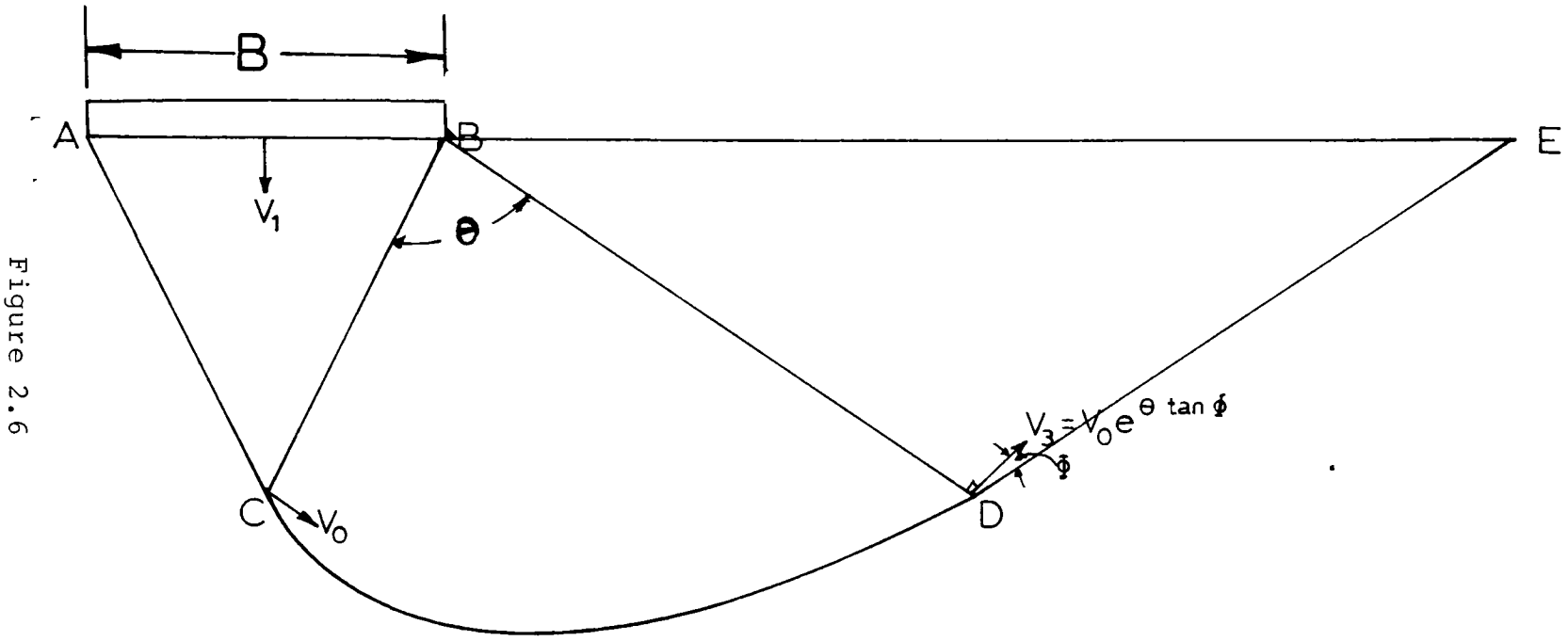

Figure 2.6

2.2.2.5 Conclusions Regarding Analytical Determination of Bearing Capacity

2.2.2.5.1 General

In the foregoing paragraphs, mathematical processes used to determine ultimate bearing capacity are presented. These mathematical techniques are: the limit equilibrium method, the plastic equilibrium method and limit analysis techniques.

As previoulsy seen limit equilibrium takes into account the yield criterion and the conditions of equilibrium but the stress on the failure surface must be sssumed and the resulting velocity field may be inadmissible. On the other hand, the plastic equilibrium method takes into account the equations of equilibrium, the yield criterion and the stress boundary conditions but nothing is known of the velocities. The limit analysis method was developed originally for solid mechanics, but has been applied successfully to soil mechanics. Limit analysis has proven to be quite powerful in assessing the values of ultimate loads.

Because limit analysis can yield solutions for bearing capacity which take into account a variety of soil properties, it seems to be more exact and more adequate for solving the bearing capacity problem than the other two techniques which are more limited. It must be pointed out that in the case of both the limit equilibrium method and the slip-line method, the stress state is specified only along the slip line or in a local plastic zone around the load, and not everywhere in

the soil mass; therefore a limit equilibrium solution or a slip-line solution does not give a complete equilibrium solution.

Chen and Davidson (1973) computed bearing capacity results for a soil which has weight and which exhibits cohesion and friction. They used the upper-bound technique of limit analysis. The study was carried out for different footing embedment depths and for an assumed failure mechanism which was similar to Prandtl's. These results have been compared with limit equilibrium and slip-line solutions. The limit analysis solutions for smooth, surface footings have been shown to compare favorably with slip-line solutions. Meyerhof's solutions and the limit analysis solutions for rough subsurface footings were shown to agree. Thus it appears that the Meyerhof values, obtained by the limit equilibrium method, are close to the upper bound results.

Because of its recent introduction to soil mechanics, limit analysis methods have not been favored by many investigators. Instead, the limit equilibrium method has been the technique most widely used in determining bearing capacity. Some of the practical advantages of limit analysis methods are:

a) the stress-strain relationship can be either rigid-plastic or elasto-plastic
b) the true collapse loads can be assumed to lie between a lower and an upper bound.

c) the superposition technique is not required.

d) the kinematics of the problem are satisfied.

A limitation is that the material cannot strain harden or soften in the plastic region.

The basic procedure for using limit analysis to determine bearing capacity values would involve an iterative process where different stress fields would be analysed to yield a maximum lower bound value and different failure mechanisms would be studied by velocity field techniques to yield a minimum upper bound.

2.2.2.5.2 Bearing Capacity

Brinch Hansen (1970) and Vésic (1973) (1975) embodied previously published theoretical and experimental results in a new bearing capacity equation:

$$q = \tfrac{1}{2}\gamma B\, N_\gamma\, \zeta_{\gamma_1} \circ \zeta_{\gamma_2} \circ \zeta_{\gamma_3} \circ \text{----} \zeta_{\gamma n} \quad \text{[weight]}$$

$$+pN_q\, \zeta_{q_1} \circ \zeta_{q_2} \circ \zeta_{q_3} \circ \text{----} \zeta_{qn} \quad \text{[surcharge]}$$

$$+cN_c\, \zeta_{c_1} \circ \zeta_{c_2} \circ \zeta_{c_3} \circ \text{----} \zeta_{cn} \quad \text{[cohesion]} \qquad (2.2.2.11)$$

where ζ represent reduction factors (greater than or less than 1.0) which correspond to variables affecting bearing capacity (as in Figure 1.3). There will be as many factors as there are variables; Brinch Hansen and Vésic introduced

factors which take into account each of the following variables:

a) foundation shape
b) inclination and eccentricity of the load
c) base tilt and ground surface slope
d) shearing resistance of the surcharge
e) soil compressibility and scale effect
f) roughness of the foundation base
g) vicinity of adjacent footings
h) ground water location
i) non-homogeneity of the soil
j) loading rate

The equation, even though of considerable interest to the practicing engineer, is based on limit equilibrium and maintains the concept of superposition. The equation therefore has all the limitations of the limit equilibrium method and the uncertainties included in the concept of superposition.

Aside from the principle of superposition, Equation (2.2.2.11) often makes the following questionable assumptions:

a) the shear strength properties of the soil are defined by a single straight-line Mohr envelope, that is by a strength intercept (cohesion) c and an angle of shearing resistance Φ, both of which are constants for a particular problem. This is incorrect for many soils because the shear strength at any point is dependent on the stress level.

(This criticism also applies to classical plasticity theory and limit analysis).

b) the shear strength at any point is independent of strain. It has been shown that most bearing capacity failures occur by progressive failure. This assumes that the shearing resistance mobilized along a potential slip surface during shearing is not the same at every point along the slip surface.

c) The elastic deformations are negligible compared to plastic deformation; the material is assumed to possess a rigid-plastic stress-strain relationship. This assumes that the elastic modulus is infinite or completely rigid. This is not the case in a real soil.

d) The volume change in soil due to shear or compression is negligible. Based on the work by Rowe (1962) volume compression and dilatancy are major factors affecting the shearing resistance of a particular soil.

Another point which is worth mentioning is the interpretation of the surcharge "p". For practical purposes, the surcharge "p" is equated to the vertical pressure at the footing level. In fact, it shoud be the effective vertical in-situ stress at the footing level before the principal stresses are being rotated.

2.2.3 Empirical Methods

The empirical method of foundation design usually

revolves around a method of field testing and a correlation between the test and bearing capacity. The test may be more or less sophisticated and may apply in only a limited range of soils. For the most part empirical methods can be divided into two groups based on the field test which is used: penetrometer-based methods and pressuremeter-based methods.

Penetrometer investigations fall into two categories; those based on static penetrometers and those based on dynamic penetrometers. Usually a cone is used in the static tests, while the standard penetration test (which can be referred to as SPT) is the preferred dynamic test. The static cone is used mainly in Europe, and the test consists of registering the point resistance of the cone and the shaft resistance of a special mantle located at the cone as they continuously penetrate the soil. Correlations have been made between cone resistance and bearing capacity.

The SPT is used mainly in North and South America. Extensive correlations between blow count and bearing capacity values have been established. Both Sanglerat (1972) and Meyerhof (1956) have published in this field; their work is probably the best documented and the most practical from an engineering standpoint. The dynamic penetrometer method, though quite useful and widespread, remains very crude.

The pressuremeter method consists of expanding a cylindrical probe in a borehole. Self-boring pressuremeters which do not require a pre-drilled borehole are now used in research.

The pressuremeter method is widely used in France. It offers to the user deformation observations in addition to resistance measurements. Through extensive field work, a bearing capacity equation has been developed which can take into account the following:

a) the resistance of the soil through the determination of the limit pressure
b) the soil type
c) the foundation shape
d) the foundation depth.

The empirical bearing capacity formula is:

$$q_L - q_o = K(P_L - p_o) \qquad (2.2.3.1)$$

where q_o is the in-situ total vertical stress at the foundation depth after construction

p_o is the at rest horizontal in-situ total stress at the level of the pressuremeter test at the time of the test

P_L is the limit pressure found by the pressuremeter

q_L corresponds to the limiting vertical pressure which can be applied by the foundation

K is an empirical constant based on experimental data and depends on the footing depth, footing shape and the type of material. It usually varies between 8 and 9 for sand.

One of the advantages of the pressuremeter method is that the test deforms the soil in much the same way as the foundation. Since the test is carried out in-situ, most of the variables shown in Figure 1.3 which are pertinent to the soil properties, are thought to be taken into account. Other variables pertaining to foundation properties and geometry are contained in the factor K. Variables concerning load applications are estimated through sound engineering judgment.

For some reason the pressuremeter has had little recognition in North America eventhough it has been a viable alternative to the Standard Penetration Test for some 20 years. While the SPT is a much cruder test than the pressuremeter test it represents, nevertheless, a method that has been proven to work to the satisfaction of many American engineers, particularly those working with sand.

2.2.4 Conclusion Regarding Analytical and Empirical Design Methods

In the foregoing paragraphs, analytical and empirical methods for determining bearing capacity have been presented. It seems that limit analysis is the analytical method which offers the greatest possibilities. Of the empirical methods, the pressuremeter seems to be the better tool for predicting the true collapse load.

2.3 Theoretical Investigations of Bearing Capacity for Foundations on Top of Slopes of Cohesionless Soil

2.3.1 Introduction

For the purpose of simplicity this thesis will make use of the bearing capacity factor $N_{\gamma q}$ which was introduced by Meyerhof (1951). This factor combines the effect of surcharge and weight. The bearing capacity equation then becomes (for cohesionless soil):

$$q = \tfrac{1}{2} \gamma B N_{\gamma q} \qquad (2.3.1.1)$$

which can be related to the Terzaghi equation by the following expression:

$$N_{\gamma q} = N_{\gamma} + \frac{2D}{B} N_{q} \qquad (2.3.1.2)$$

The factor $N_{\gamma q}$ is used to compare the results of different theories with the present experimental work.

A disadvantage of the Meyerhof factor $N_{\gamma q}$ arises if the sand is not completely dry or completely submerged. Where the ground water table is located within the depth of influence of the footing, the bearing capacity factor $N_{\gamma q}$ should be modified to account for the varying effective unit weight of the sand. The usual approach in this case is to revert back to the Terzaghi equation using N_{γ} and N_{q} or $N_{\gamma q}$ with the use of the effective weight modification by Meyerhof (1955).

The major difference between the theoretical bearing capacity of a footing located on flat ground and one located on the top of a slope, is that in the case with a slope, the failure zones are modified to conform to the geometry of the slope as shown in Figure 2.7. It follows that the bearing capacity factors N_γ, N_q or $N_{\gamma q}$ for this sloping ground will be smaller than the flat ground values.

An extensive literature survey was undertaken in order to gather together theoretical treatment of the topic. A total of nine theoretical and one empirical investigations has been assembled. All theoretical treatments make the assumption of plane strain. Chronologically these theories have been presented by Meyerhof (1957), Mizuno (1960), Kovalev (1964), Brinch Hansen (1970), Giroud et al (1972), Absi (1972), Chen (1974), Bowles (1975), Bowles (1977), and the empirical account by Ménard (1964). Of all the theories mentioned above only those of Meyerhof, Giroud, Bowles, and Chen offer the possibility of deriving a bearing capacity value for all vertical and horizontal footing locations with respect to the slope crest, while others yield values for footings located exclusively at the crest of the slope.

These accounts of bearing capacity of footings close to slopes can be divided into two groups: complete and incomplete solutions. The complete solution group would embody all the theories that yield bearing capacity values based on assumed material properties and found by mathematical

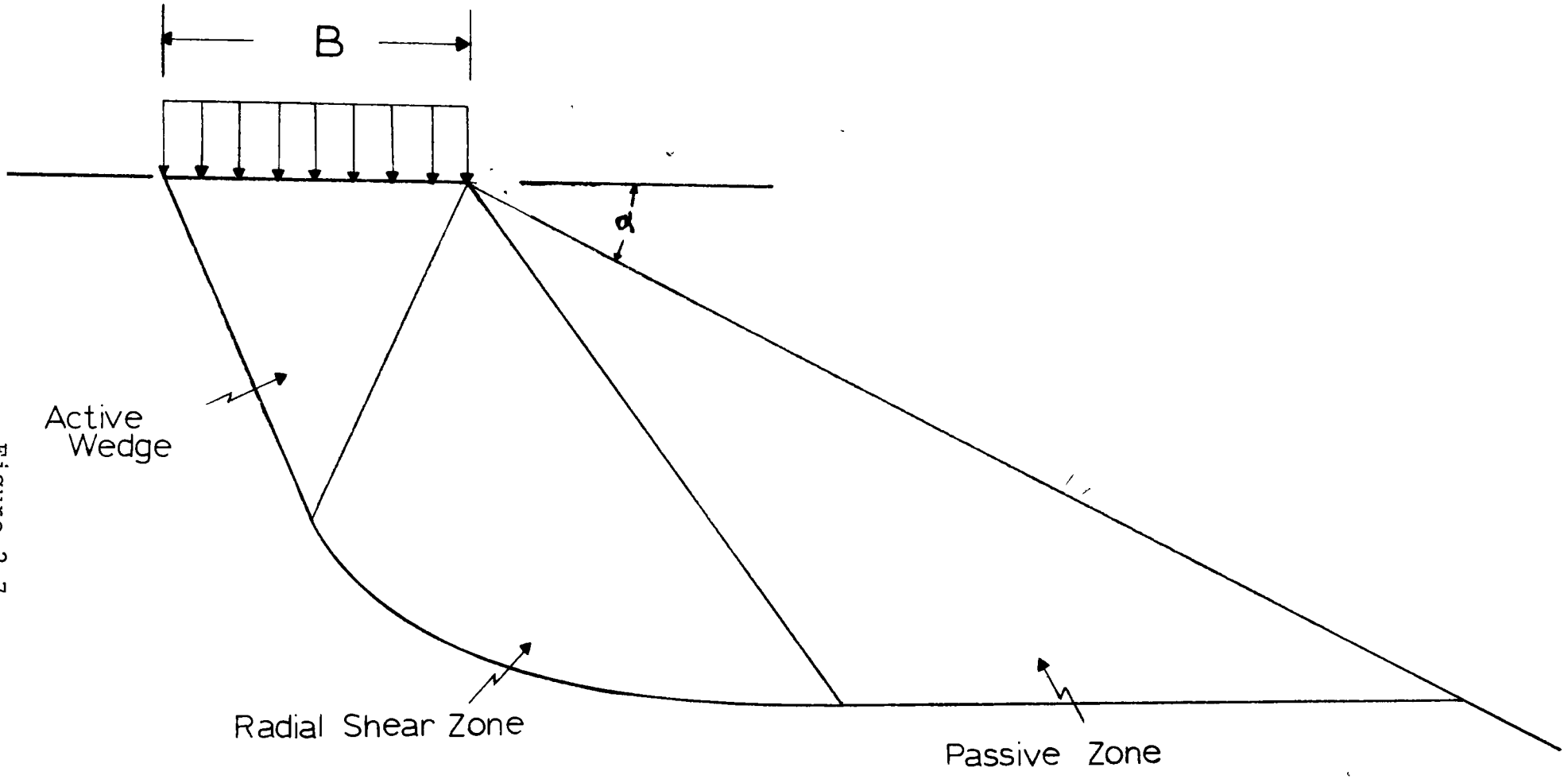

Figure 2.7

The 3 Zones of Bearing Capacity on Slope

techniques. The Giroud, Meyerhof, Mizuno, Absi, Chen, Bowles, and Kovalev theories are considered to fall into this category. The incomplete solution implies that bearing capacity values for the case of a footing located on top of a slope are found by applying correction factors to the flat ground case. The theoretical solution of Brinch Hansen and the empirical treatment of Ménard are considered to be in this category.

With the exception of Chen's, all theories assume the material to be rigid-plastic. Meyerhof, Giroud, Bowles and Mizuno obtain their solutions using limit equilibrium. Kovalev's and Absi's methods are a type of plastic equilibrium solution. Brinch Hansen makes a simple postulation to obtain his factors. Chen employs the concept of limit analysis and velocity fields; he assumes the bearing material possesses an elasto-plastic stress-strain relationship. Finally, Ménard (1964) presents empirical slope influence factors based on experiment. All nine theories and the one empirical treatment are thoroughly investigated in the following paragraphs.

2.3.2 Meyerhof (1957)

Meyerhof (1957) proposed bearing capacity factors $N_{\gamma q}$ for foundations on top of slopes of cohesionless soil. The values are presented in the form of graphs for soils having two different angles of shearing resistance, $\phi = 30°$ and

φ = 40°; these graphs are reproduced as Figures 2.8 and 2.9.

All of these values are based on Meyerhof's 1951 theory for flat ground in which he develops an expression that takes into account the shearing strength of the overburden. To take this shearing strength into consideration, Meyerhof modified Terzaghi's slip surface as shown on Figure 2.10. The analysis involves two steps: first Meyerhof considers the effect of the surcharge N_q and the cohesion N_c, secondly he finds the most critical value of the weight-friction term N_γ by a series of trial slip surfaces.

In evaluating the surcharge term N_q (ignoring the cohesion term N_c for the purpose of the present study), Meyerhof considers zone ABC to be an active wedge that remains part of the foundation, as shown in Figure 2.6. To simplify the analysis, the weight of soil in wedge BEF is replaced by the equivalent normal "p" and tangential "s" stresses on the plane BE. This plane may then be considered as an "equivalent free surface" subjected to these stresses. The radial zone is BCD, which is that area within the log spiral having its center at B with an angle of

$$\theta = 135^\circ + \beta - \eta - \Phi/2 \qquad (2.3.2.1)$$

where θ = the sweep angle of the log spiral

β = angle of the equivalent free surface BE to the horizontal

η = the angle between the two slip-lines BD and BE. The value of η depends on the percentage of mobilized shear along BD. This value is found from the Mohr circle of stress.

Φ = angle of internal friction

Area BDEB represents a passive zone. Meyerhof also takes into account the friction along the foundation shaft BF (this force will be ignored in the present analysis).

Along BD and DE, Meyerhof assumes that the shearing strength of the soil is fully mobilized. The actual shear stress which is mobilized along BE at failure is assumed to be a fraction "m" of the full shear strength mobilized along BD. Therefore the position of BD with respect to BE is a function of the angle η determined by the Mohr circle (Figure 2.12). From the Mohr circle it can be seen that if no shearing resistance occurs along BE, i.e. "m" equals zero, angle η is then $45 - \frac{\Phi}{2}$. In this case, a passive zone BDEB forms. In the case where the resistance is fully mobilized along the equivalent free surface BE, angle η becomes 0 which means that BD is identical to BE, thus "m" = 1.

Meyerhof is led to the following expression for the surcharge factor N_q:

$$N_q = \frac{(1 + \sin\Phi)\, e^{2\theta\tan\Phi}}{1 - \sin\Phi \sin(2\eta + \Phi)} \qquad (2.3.2.2)$$

These values are shown on Figure 2.12 a). It is inter-

Strip foundation on top of slope of cohesionless material

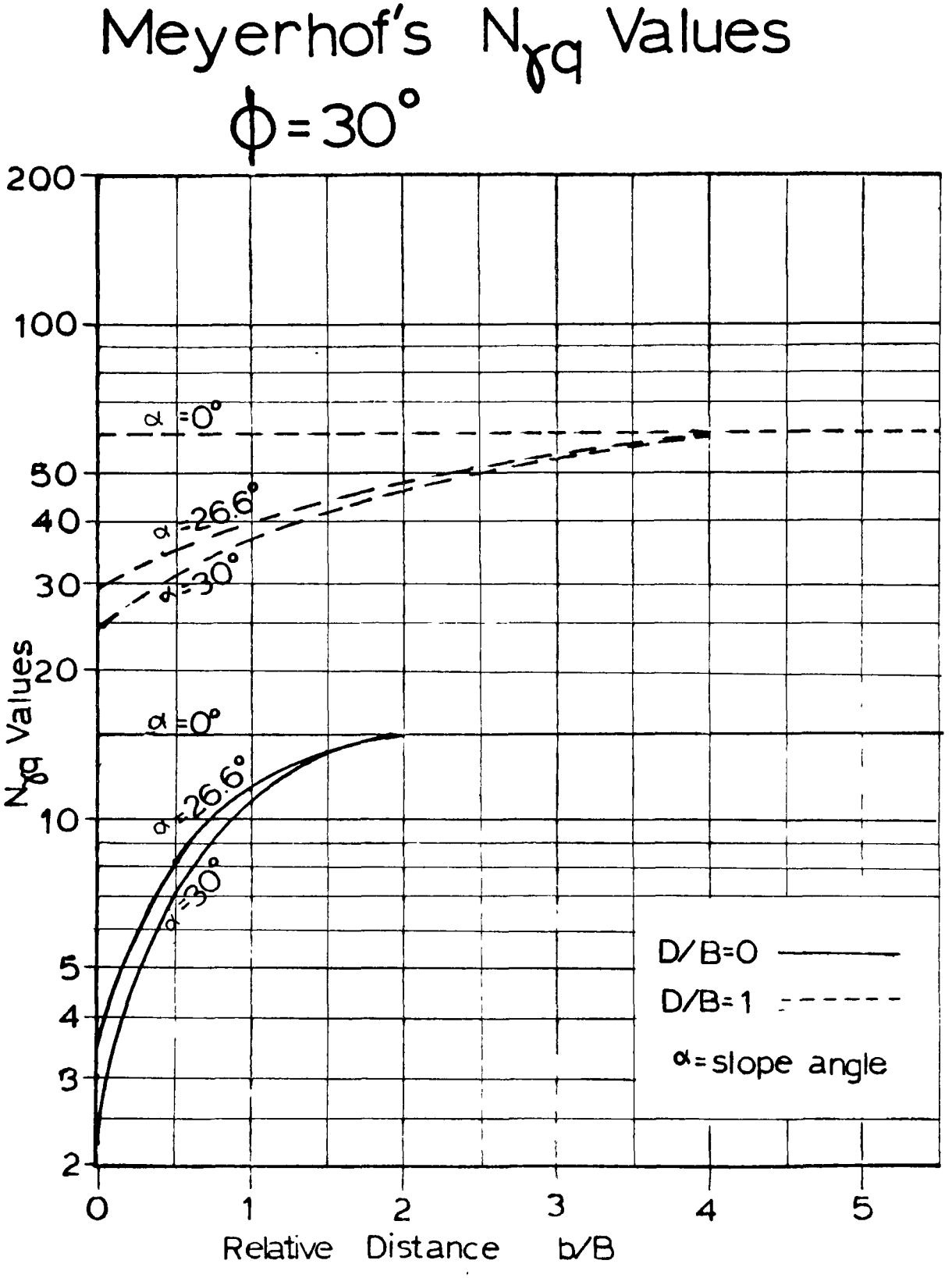

Figure 2.8

Strip foundation on top of slope of cohesionless material

Meyerhof's $N_{\gamma q}$ Values

$\phi = 40°$

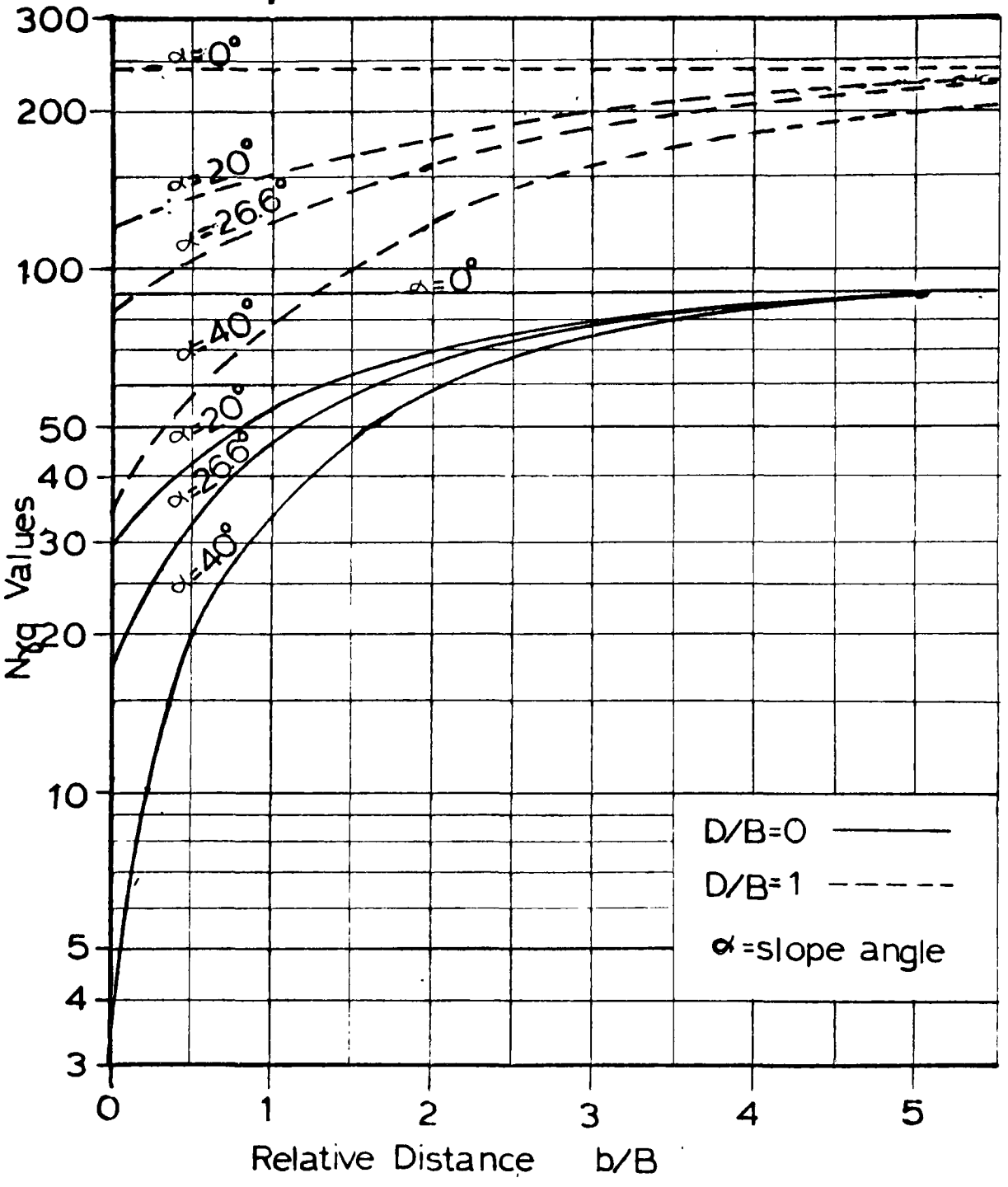

Figure 2.9

Meyerhof's Failure Mechanism

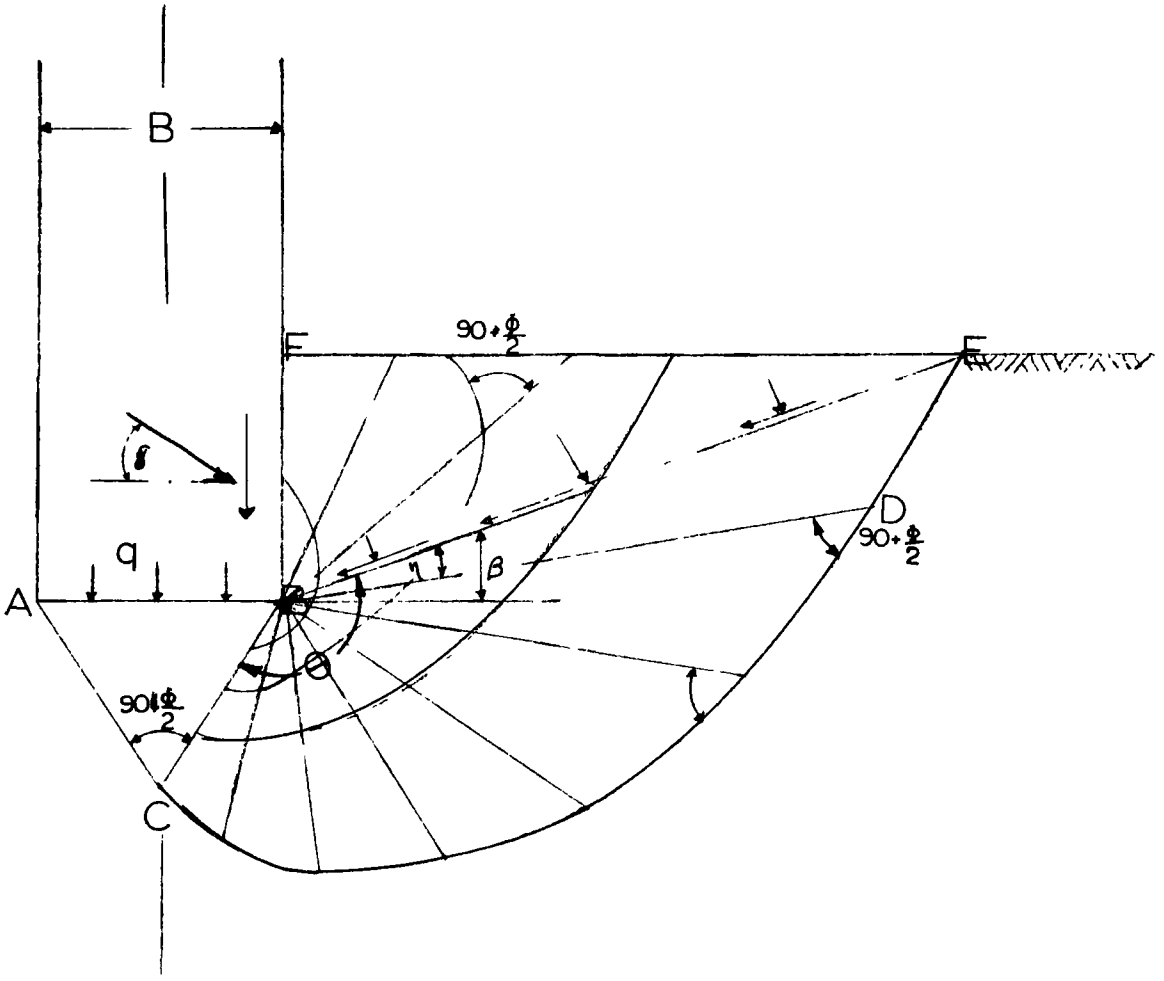

Figure 2.10

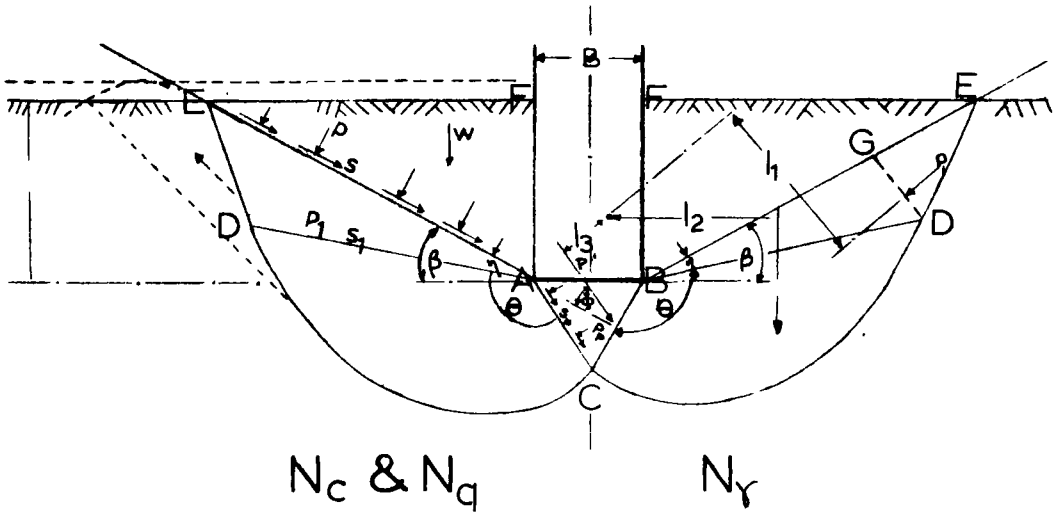

Figure 2.11

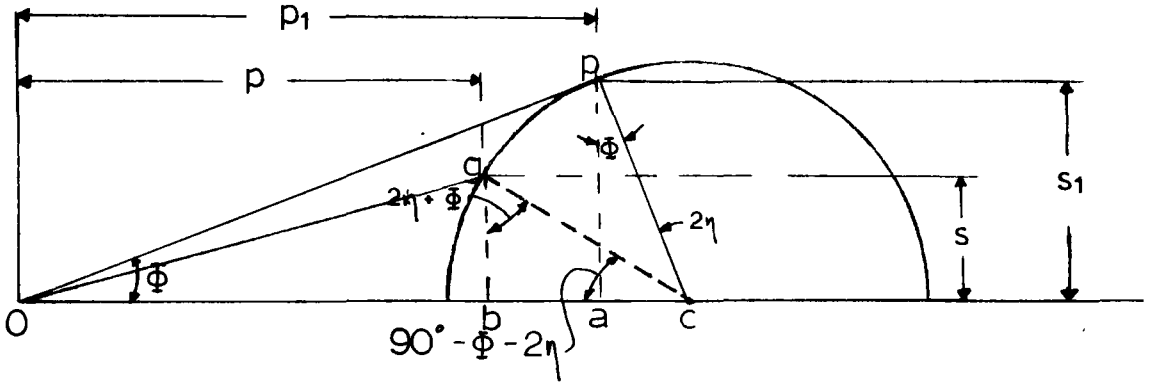

Mohr Circle of Stress

Figure 2.12

esting to note that N_q is not very sensitive to a change of "m". The difference in N_q between m=0 and m=1 is within 15% of the value N_q.

The term N_γ (Figure 2.11) is found through a similar procedure except that by a trial and error solution the center of the log-spiral is positioned at different locations to yield the minimum value of N_γ.

$$N_\gamma = \frac{4P_p'' \sin(45^\circ + \Phi/2)}{\gamma B^2} - \tfrac{1}{2}\tan(45^\circ + \Phi/2) \qquad (2.3.2.3)$$

Here also, the N_γ term is found to be almost independent of "m". The values are given in Figure 2.14b).

Finally, Meyerhof gives values of $N_{\gamma q}$ which combine the effect of surcharge and weight.

$$N_{\gamma q} = N_\gamma + \frac{2p}{\gamma B} N_q \qquad (2.3.2.4)$$

When Meyerhof adapted this method to the case of sloping ground, the result was a simple method of finding bearing capacity factors for footings at any depth and at any distance from the slope. These factors take into account the shearing resistance of the surcharge by means of the equivalent stresses acting on the equivalent free surface. This analysis does not, however, take into account the fact that zone BDE will take the shape of a simple, passive Rankin wedge. The failure surface in this zone will not be curved but will be a

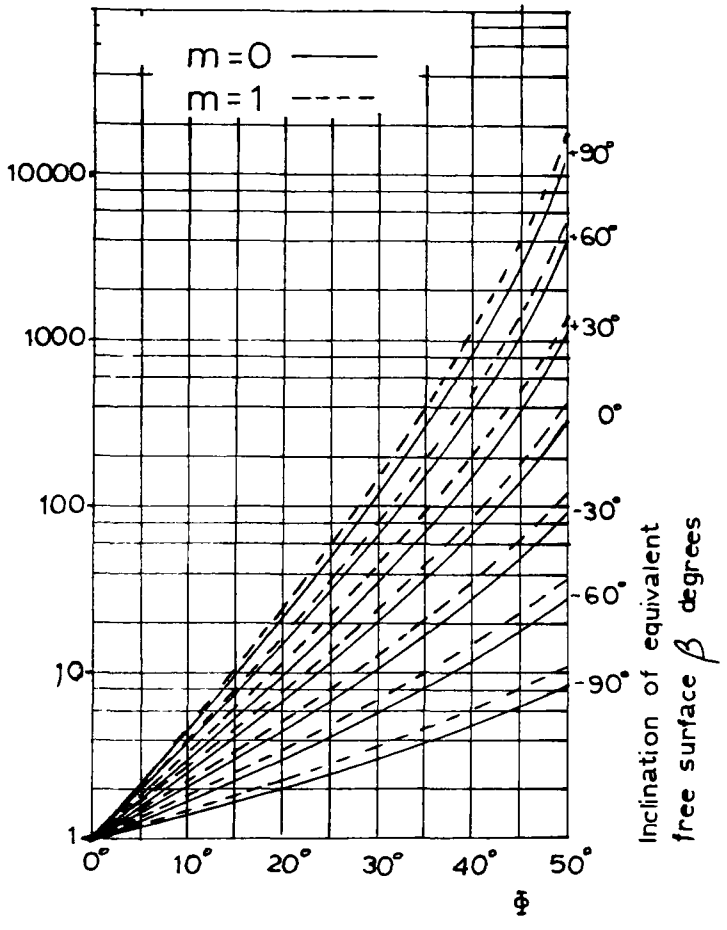

N_q Values

(a)

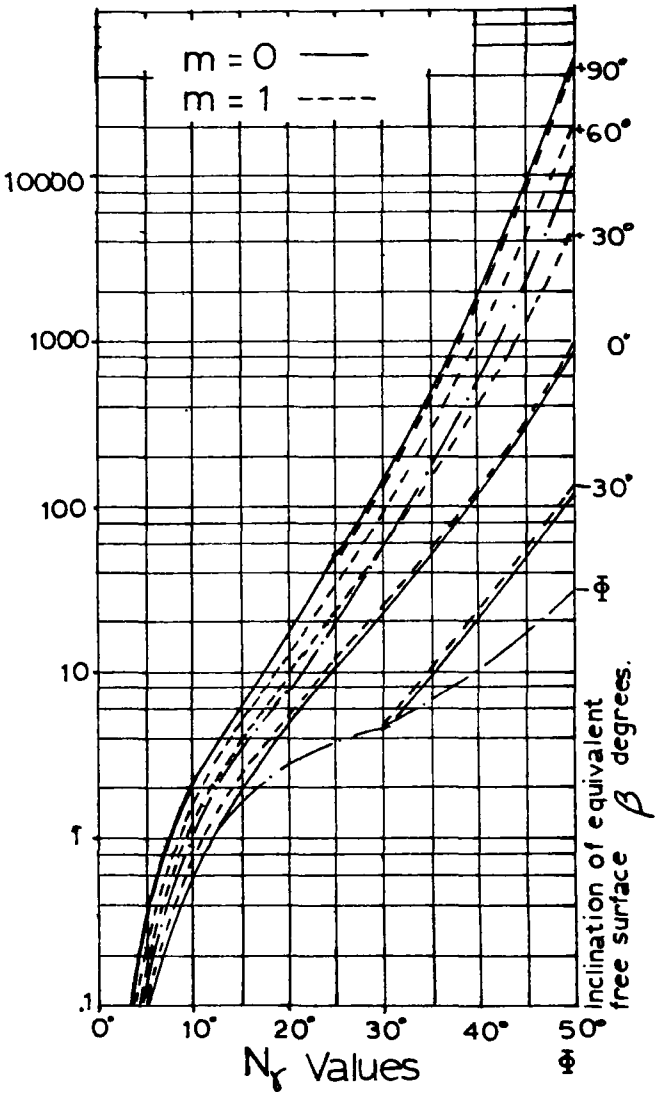

N_γ Values

(b)

Figure 2.13

straight line which slopes at an angle which depends on the orientation of principal stresses. In other words, the analysis ignores the existing stresses in the slope. In actual fact, the $N_{\gamma q}$ values that Meyerhof presented in 1957 for sloping ground (as shown in Figures 2.8 and 2.9) incorporate the improvement in his 1951 theory which he made in 1955. This improvement consists of finding a minimum value of N_γ by varying the angle $\hat{ABC}$ of the elastic wedge. Meyerhof finds that the angle $\hat{ABC}$ should be approximately equal to 1.2Φ to yield a minimum value of N_γ.

2.3.3 Mizuno (1960)

Mizuno first presented a method for estimating the bearing capacity of flat ground in 1948. In 1960, the original method was adapted to sloping ground.

Mizuno's theoretical model has the same three zones as described previously in Figure 2.7 and as shown on Figure 2.14. Zone I is called the active pressure wedge ABC. This zone is found by a procedure which is similar to the one used by Meyerhof, with the angle $\hat{ABC} = \theta_o = 45^o + \Phi/2$. The stress acting at $90 - \varphi$ along BC is found to be

$$f_o = 2r_o q \cot\theta_o + \frac{B}{2}\gamma \qquad (2.3.3.1)$$

where f_o = pressure on plane BC

r_o = length of plane BC

q = vertical pressure on the footing or bearing capacity

θ_o = angle $\hat{ABC}$

Zone III is then found by the Mohr circle (Figure 2.15). Line BD in Figure 2.14 is parallel to the line TQ on the Mohr circle (Figure 2.15) taken from the pole Q to the failure point T. The stress acting on this plane is denoted by f_n which is equal to:

$$f_n = \frac{\gamma r_n \sin(\theta_n + \alpha) \sec\alpha \cos\Phi}{1 - \sqrt{1 - \cos^2\Phi \sec^2\alpha}} \qquad (2.3.3.2)$$

where α = slope angle

θ_n = angle $\hat{ABD}$

r_n = length of BD (which is unknown)

and makes an angle of Φ to the normal of BD. Line DE has the same direction as f_n, the stress acting on plane BD. Zone II is called a transition zone whose slip line is a semi-circular arc from C to D.

Mizuno then considers the triangular distribution of stress along planes BC and BD and finds the resultant on both of these planes. The stress factors f_o on plane BC have a resultant which acts in a direction parallel to AC. The value r_o is equal to BC, which is found from the footing width and angle θ_o; r_n remains an unknown but has the same direction and orientation as BD. Mizuno describes the resultant force along BC as

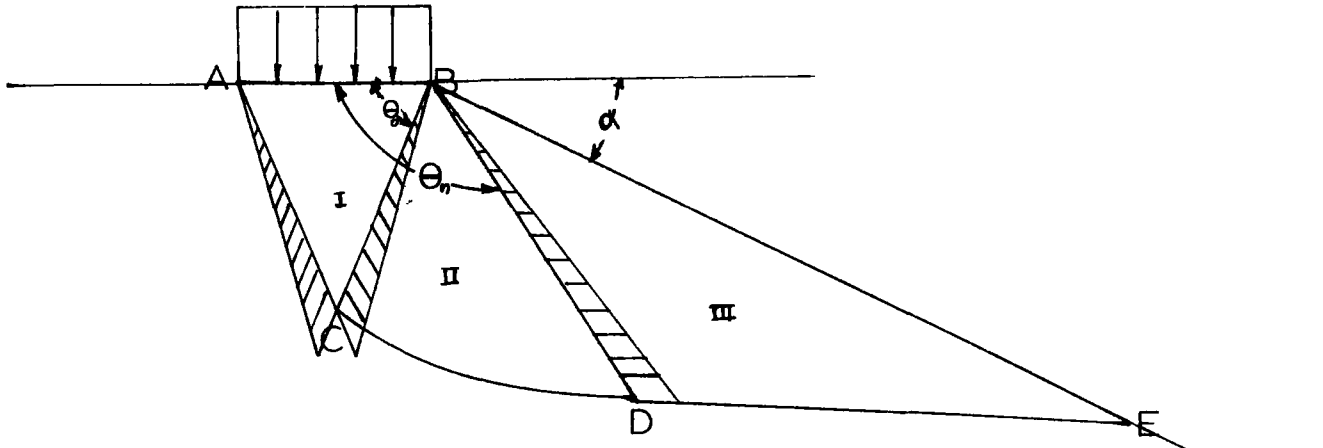

Mizuno's Failure Mechanism

Figure 2.14

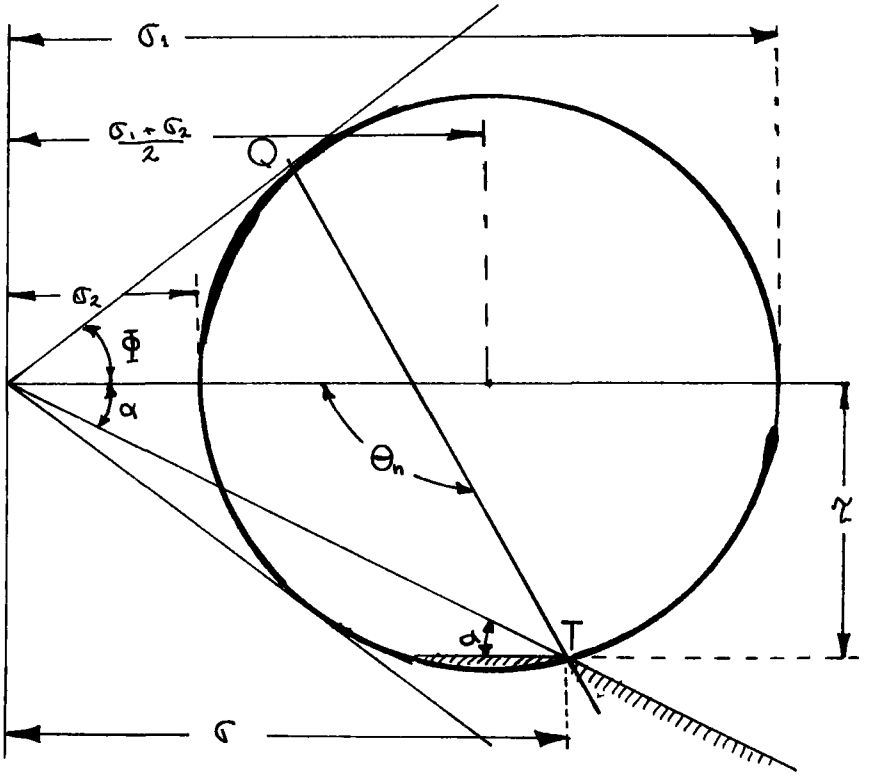

Mohr Circle of Stress

Figure 2.15

$$F_o = \tfrac{1}{2} [f_o] \frac{B}{2} \sec \qquad (2.3.3.3)$$

while on BD

$$F_n = \tfrac{1}{2} r_n [f_n] \qquad (2.3.3.4)$$

is the resultant along BD. Now that the magnitude and the direction of the forces acting on these planes are known, Mizuno considers the transition zone.

The transition zone BCD is divided into a number of small wedges, and then the equilibrium of one small wedge BRT is studied. This is done by dividing the wedge into two halves (BRS and BST) as shown in Figure 2.16. The forces acting upon the left half BRS are $F_{m-\frac{1}{2}}$ and F_m, which are resultants of the triangularly distributed stresses on the surfaces BR and BS respectively, the reaction L_m along the sliding surface RS, and the weight of wedge G_{Lm}. Similarly, the right half BST is acted upon by the forces F_m and $F_{m+\frac{1}{2}}$, the reaction R_m and the weight of wedge G_{Rm}.

The reaction stress S_m which is assumed to be constant over the base of wedge BRT can be found by the Mohr circle shown on Figure 2.13. The values of L_m and R_m are given by:

$$L_m = S_m \times \overline{RS} \qquad (2.3.3.5)$$

$$R_m = S_m \times \overline{ST}$$

Also: $G_{Lm} = \gamma \Delta BRS$

$$G_{Rm} = \gamma \Delta BST \qquad (2.3.3.6)$$

Mizuno designates the stresses at R, S and T along BR, BS and BT by $[f_{m-\frac{1}{2}}]$, $[f_m]$ and $[f_{m+\frac{1}{2}}]$ where the resulting forces are given by

$$F_{m-\frac{1}{2}} = \tfrac{1}{2}[f_{m-\frac{1}{2}}]\ \overline{BR}$$

$$F_m = \tfrac{1}{2}[f_m]\ \overline{BS} \qquad (2.3.3.7)$$

$$F_{m+\frac{1}{2}} = \tfrac{1}{2}[f_{m+\frac{1}{2}}]\ \overline{BT}$$

From the Mohr circle it is possible to find α_m which is the angle between radial line BS and the sliding surface. Angle α_m also represents the angle between F_m and the radial along BS. If the length $r_{m-\frac{1}{2}}$ along BR is known, the angle α_m, the length r_m of BS, and the weight of wedge G_{Lm} are obtained by assuming the value of δ_m. The value of F_m can be expressed as:

$$F_m = \tfrac{1}{2}[f_m]\ r_m \qquad (2.3.3.8)$$

By successive trials with various values of δ_m until the direction of the resultant $F_{m-\frac{1}{2}}$ and G_{Lm} coincides with the

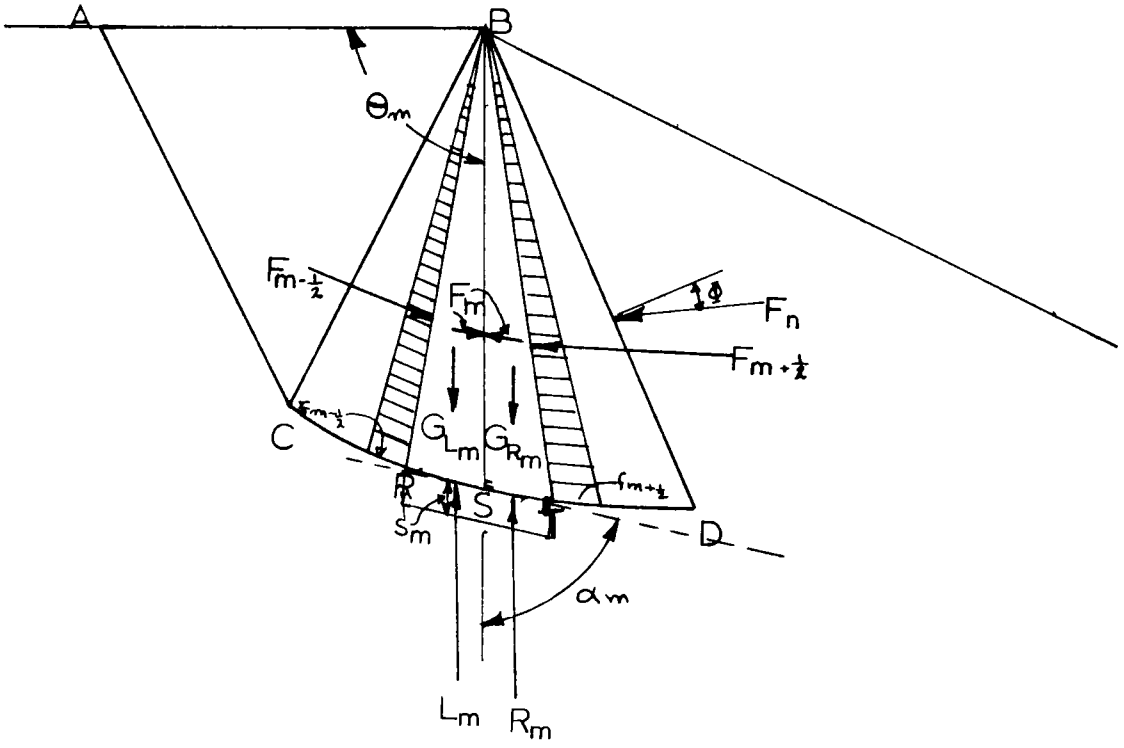

Transition Zone Divided into Wedges
Figure 2.16

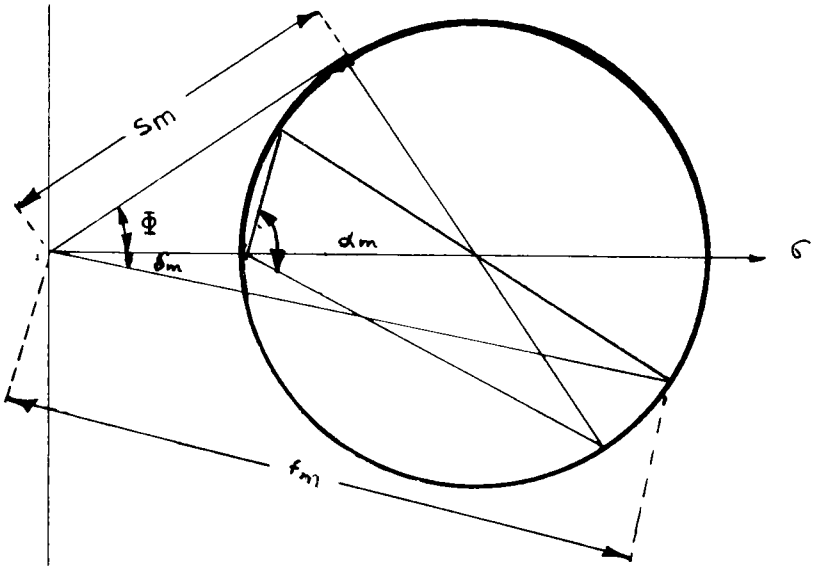

Mohr Circle of Stress
Figure 2.17

direction of the resultant of F_m and L_m, the value of F_m is found and subsequently $[f_m]$. Then point T is determined, and the value of $F_{m+\frac{1}{2}}$ is obtained by means of the equilibrium conditions for $\triangle$BST.

This procedure is repeated for every wedge until finally plane BT coincides with plane BD and subsequently point T coincides with D. The distance r_n along BD becomes known and the exact force F_n on BD is found by the use of equation (2.3.3.3). Working back into the transition zone, $F_{m+\frac{1}{2}}$, F_m and $F_{m-\frac{1}{2}}$ are found for every wedge until $F_{m-\frac{1}{2}}$ has the same value as F_o. From this value of F_o, the value of f_o is obtained from equation (2.3.3.1) and in turn, q can be found.

Mizuno presents the results of this analysis in graphical form (Figure 2.18). Unlike Meyerhof's method, Mizuno takes into account the stresses in the slope; Mizuno also makes the slip surface have the same direction as the forces acting on the radial planes. On the other hand, Mizuno only gives solutions for a footing at the crest of the slope and makes no suggestions for the effect of depth and distance from the slope for footings at other locations.

Another point worth mentioning is that the Mizuno bearing capacity $N_{\gamma q}$ factors tend towards a common value where the angle of the slope is equal to Φ. This is the only theory which makes this finding.

Mizuno's $N_{\gamma q}$ Values

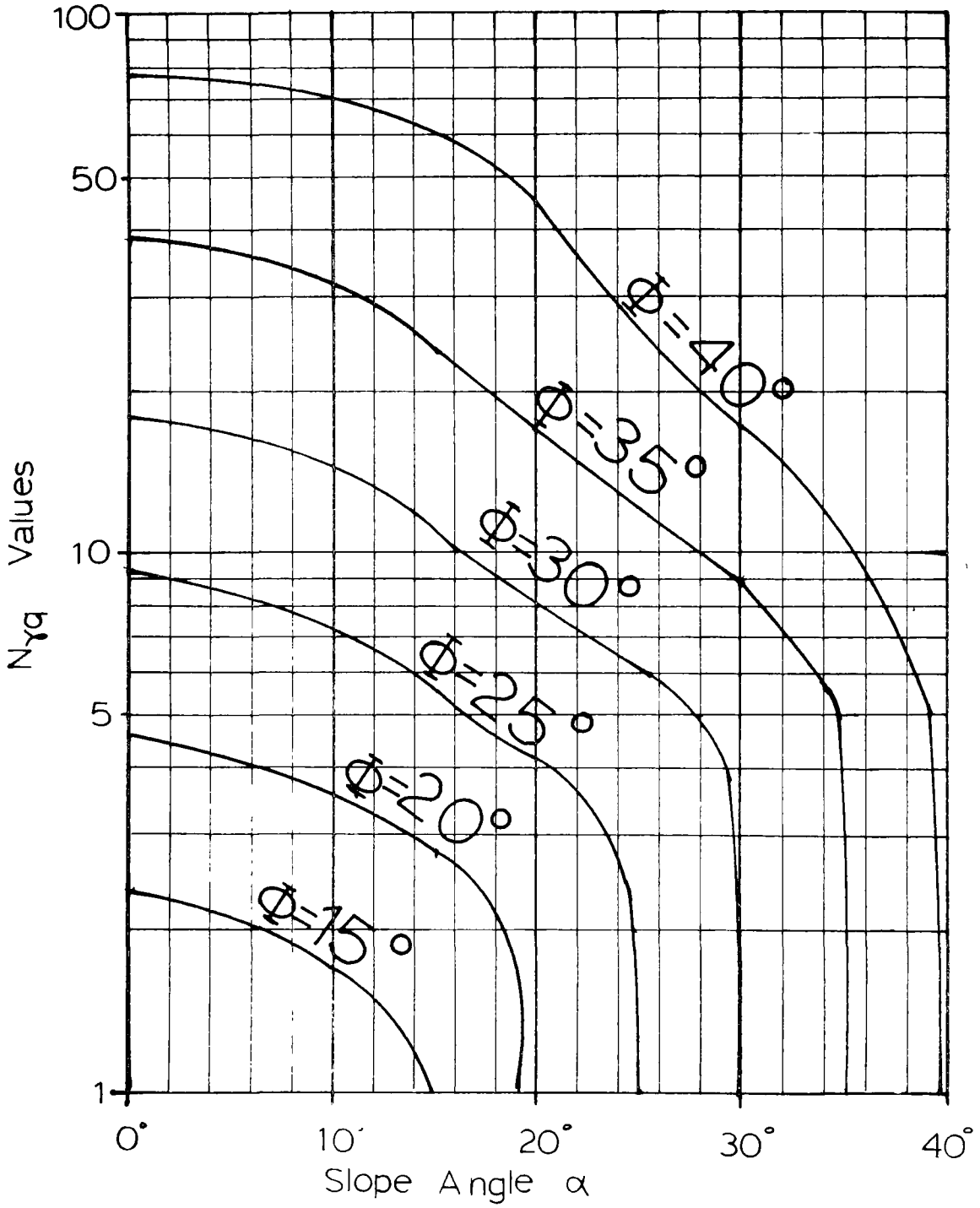

Figure 2.18

2.3.4 Kovalev (1964)[1]

In 1960 Sokolovski proposed a method for solving bearing capacity problems by the method of characteristics. This method is a plastic-equilibrium solution by which the stresses in the failure mass can be determined form the solution of the governing differential equations which are subjected to appropriate traction boundary conditions. The result is a family of curves similar to the one shown on Figure 2.19. However the method is long and involved. Kovalev (1964) recognized this fact and proposes an approximate solution.

Based on the position of the slip-line obtained by Sokolovski's method, the approximate solution consists of defining the outermost slip-line of the slip-line field by straight lines and arcs. Once the failure slip surface has been approximated in this way, the method integrates the equation of equilibrium along this simplified surface.

To achieve this solution some of the basic principles of the stress characteristic technique must be described. At failure, the Mohr-Coulomb yield condition can be expressed in terms of the componants of the state of stress (σ_x, σ_z, τ_{xz}) in the following form:

---

1. Kovalev published in Russian. This interpretation of his work is based on a French translation by the translation department of Laboratoire des Ponts et Chaussees, Paris, Fr.

$$\sqrt{\frac{(\sigma_z - \sigma_x)^2}{4} + \tau_{xz}^2} - \frac{\sigma_z + \sigma_x}{2} \sin\varphi = c \cos\varphi \qquad (2.3.4.1)$$

However, it is more convenient to write this equation in the following form:

$$\sqrt{\frac{(\sigma_z - \sigma_x)^2}{4} + \tau_{xz}^2} = \frac{\sin\varphi}{2} (\sigma_x + \sigma_z + 2\, c \cot\varphi) \qquad (2.3.4.2)$$

In Figure 2.20a), the circle represents the stresses on planes through the element shown in Figure 2.20b). The major principal stress σ_1 on the element is directed at an angle of θ to the z axis. By construction, the pole P of the Mohr diagram is located in Figure 2.20a). From the position of the pole, the directions of two slip-lines can be found parallel to the straight lines passing through the pole and C and C^1, the points of tangency of the circle of stress with the failure envelope. These slip-lines, PC and PC^1, make equal angles $\pm\mu$ with the direction PB of the major principal stress plane BP on Figure 2.20a), where

$$\mu = \frac{\pi}{4} - \frac{\varphi}{2} \qquad (2.3.4.3)$$

The slip-lines of Figure 2.20b) are drawn through the element parallel to the lines PC and PC^1, of Figure 2.20a). It is seen that the slip-lines at the element of Figure

2.20b) make angles of $\theta \pm \mu$ with the z-axis.

From all the stresses shown on Figure 2.20a), a new yield stress can be defined as

$$\sigma = \tfrac{1}{2}(\sigma_x + \sigma_z + 2c \cot\varphi) \qquad (2.3.4.4)$$

or $$\sigma = \tfrac{1}{2}(\sigma_1 + \sigma_3 + 2c \cot\varphi) \qquad (2.3.4.5)$$

In Figure 2.20a), σ is represented by the distance O^1D. It is possible now to express σ_x, σ_z and τ_{xz} at yield in terms of the two variables σ and θ, the angle that the major principal stress makes with the x-axis, as follows:

$$\sigma_x = \sigma(1 + \sin\varphi \cos 2\theta) - c \cot\varphi \qquad (2.3.4.6)$$

$$\sigma_z = \sigma(1 - \sin\varphi \cos 2\theta) - c \cot\varphi \qquad (2.3.4.7)$$

$$\tau_{xz} = \sigma \sin\varphi \sin 2\theta \qquad (2.3.4.8)$$

The stresses σ_x, σ_z, and τ_{xz} are represented on the Mohr diagram by points E and F, obtained by drawing lines through the pole P parallel to the x and z axes respectively. It can be seen that a given problem of plastic yielding is solved if σ and θ are known throughout the region, since, by equations (2.3.4.5), (2.3.4.6), (2.3.4.7), and (2.3.4.8), the other stresses may be determined in terms of σ and θ. Therefore σ

and θ may be considered the unknown variables.

Since the material being studied is yielding in static equilibrium, the stresses at yield must also satisfy the two-dimensional equations of equilibrium,

$$\frac{\partial \sigma_x}{\partial x} + \frac{\partial \tau_{xz}}{\partial z} = 0 \qquad (2.3.4.9)$$

$$\frac{\partial \tau_{xz}}{\partial x} + \frac{\partial \sigma_z}{\partial z} = \gamma \qquad (2.3.4.10)$$

where these equations assume that the z-axis is oriented vertically, with the positive direction downward, as shown in Figure 2.20b). Here the unit weight of the soil is taken to be only a body force, i.e. these body forces arise through the action of gravity.

By substituting equations (2.3.4.6), (2.3.4.7) and (2.3.4.8) into equations (2.3.4.9) and (2.3.4.10) Sokolovski (1965) obtains a family of two differential equations describing the slip-lines. Kovalev used only one differential equation which was integrated along the approximate slip-line that he had assumed. This differential equation is:

$$\frac{d\sigma}{ds} - 2\sigma \tan\varphi \frac{d(\theta+\alpha)}{ds} = -\gamma \frac{\cos(\theta+\alpha)}{\cos\varphi} \qquad (2.3.4.11)$$

From the boundary conditions and the stress character-

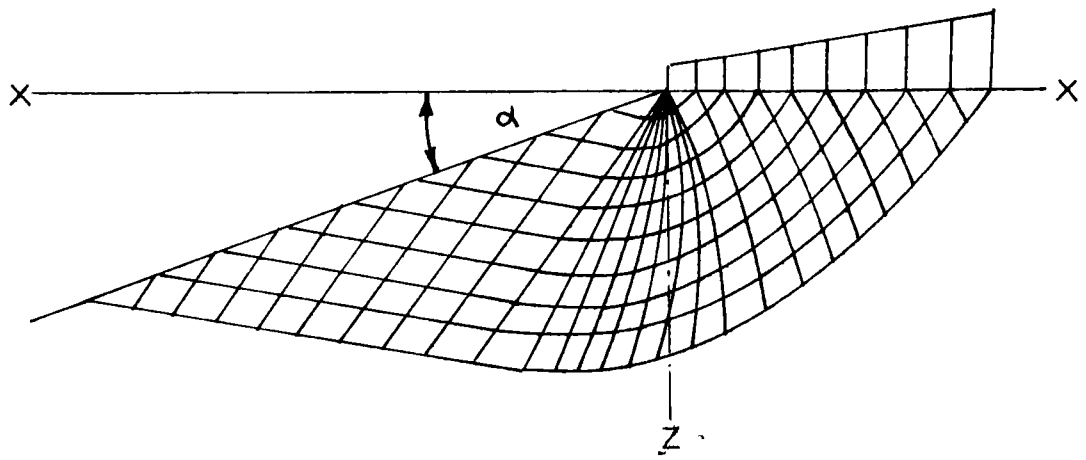

Slip-line Field

Figure 2.19

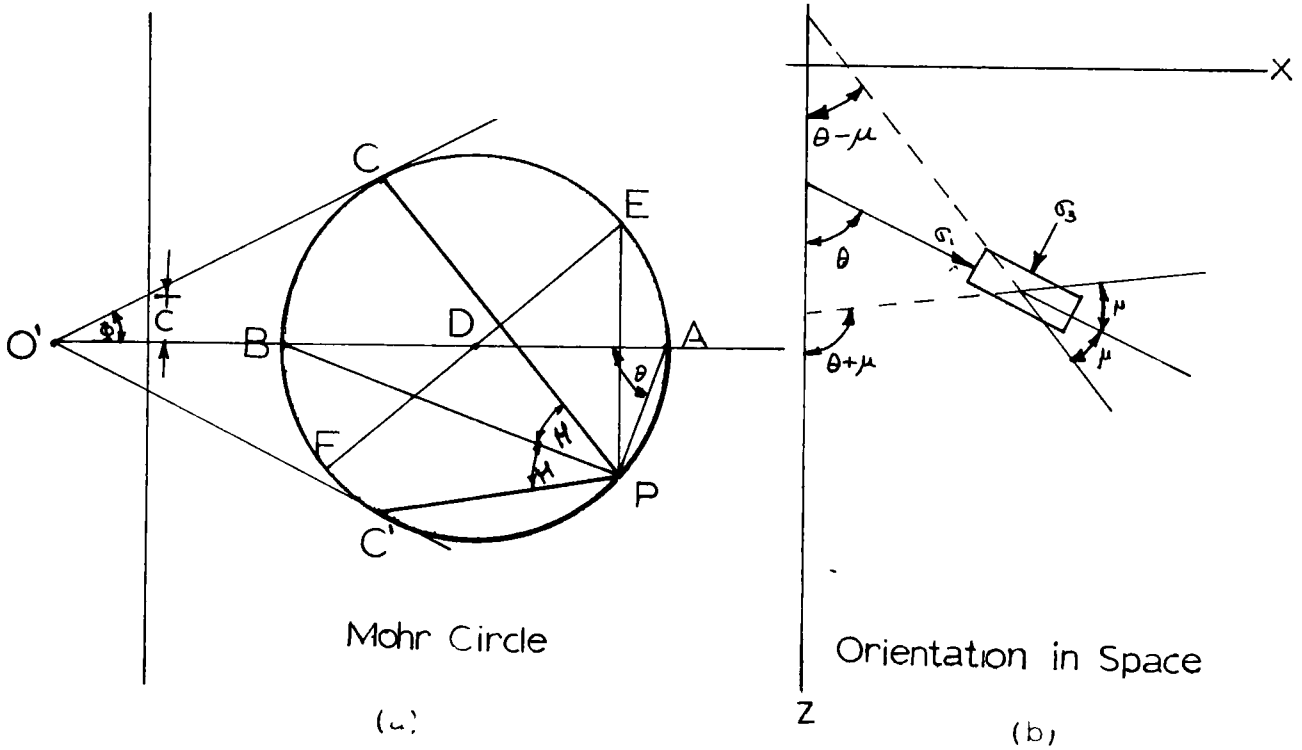

Figure 2.20

Kovalev's Approximate Mechanism

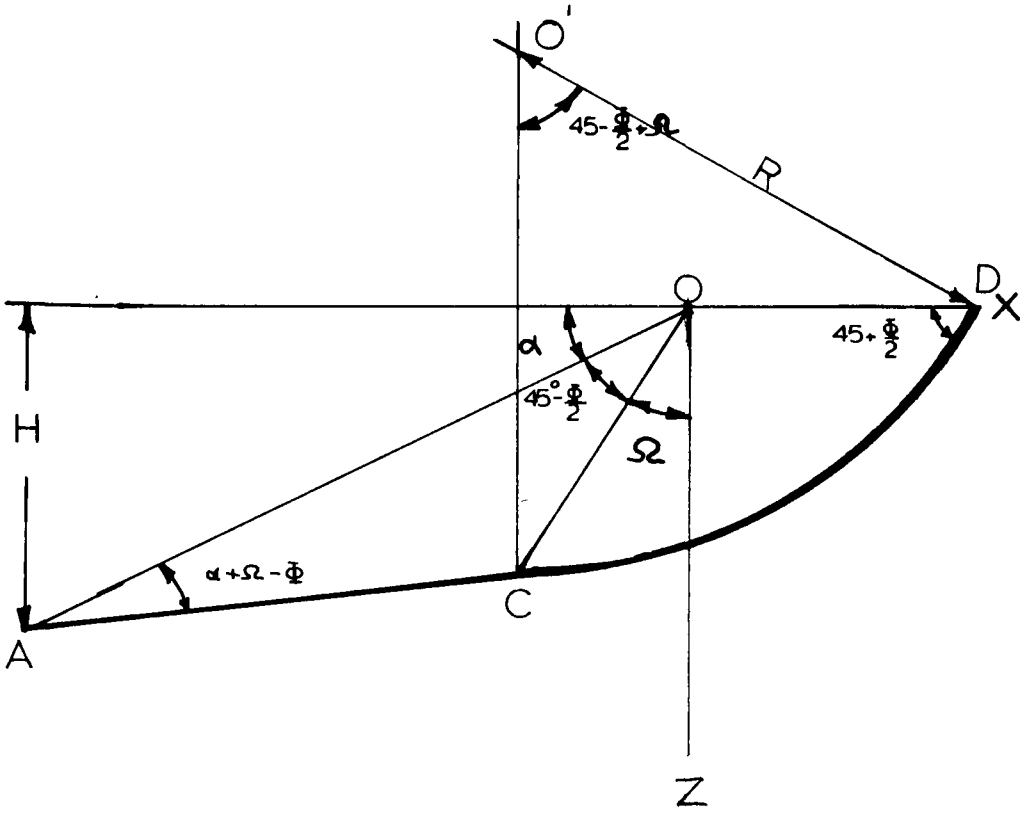

Figure 2.21

istic solution, Kovalev proposes a failure geometry for foundations on top of slopes of cohesionless material as shown on Figure 2.21. Furthermore this figure shows the slip surface, divided into two segments: a straight line AC and an arc CD. Point C is determined by construction using angle Ω. This angle is found to be equal to

$$\Omega = \tfrac{1}{2}\left[90^0 - \sin^{-1}\left(\frac{\sin\alpha}{\sin\Phi}\right) - \alpha + \Phi\right] \qquad (2.3.4.12)$$

Point C is determined as the point of intersection of OC and AC; the value of angle $\hat{AOC}$ is $\frac{\pi}{4} - \frac{\Phi}{2}$, while from point C a vertical is drawn to O'. This length is R, which is defined as:

$$R = \frac{H}{\sin\beta}\,\frac{\sin(\Omega + \alpha - \Phi)\,\cos(\frac{\pi}{4} + \frac{\Phi}{2} - \alpha)\,\sin(\frac{3}{8}\pi - \frac{\Omega}{2} + \frac{\Phi}{4})}{\cos(\frac{\pi}{4} - \Omega - \alpha + \frac{3}{2}\Phi)\,\sin(\frac{\pi}{8} - \frac{\Omega}{2} + \frac{3}{4}\Phi)\,\sin(\frac{\pi}{4} + \Omega - \frac{\Phi}{2})} \qquad (2.3.4.13)$$

and H is a function of footing width B

$$\frac{B}{H} = \frac{\sin(\Omega + \alpha - \Phi)\,\sin(\frac{\pi}{8} + \frac{\Omega}{2} + \alpha - \frac{5}{4}\Phi)}{\sin\alpha\,\cos(\frac{\pi}{4} - \Omega - \alpha + \frac{3}{2}\Phi)\,\sin(\frac{\pi}{8} - \frac{\Omega}{2} + \frac{3}{4}\Phi)} \qquad (2.3.4.14)$$

Once O' is found and R is determined, the circular arc CD can be drawn.

In solving equation (2.3.4.11), the normal stress at point D of Figure 2.21 is given by

$$\sigma_{(D)} = \left[\frac{p \cos\alpha}{1-\sin\Phi \cos(\sin^{-1} \frac{\sin\alpha}{\sin\Phi} - \alpha)} + \gamma \frac{\sin\Omega \, H\sin(\frac{\pi}{4} - \frac{\Phi}{2})}{\cos\Phi \sin\alpha \cos(\frac{\pi}{4} - \alpha - \Omega + \frac{3}{2}\Phi)} \right.$$

$$\left. - \frac{\gamma R(\cos\Omega - 2\tan\Phi \sin\Omega)}{\cos\Phi(4\tan^2\Phi + 1)} \right] e^{\tan\Phi(\frac{\pi}{2} - \Phi + 2\Omega)}$$

$$+ \frac{\gamma[R \cos(\frac{\pi}{4} - \frac{\Phi}{2}) + 2\tan\Phi \sin(\frac{\pi}{4} - \frac{\Phi}{2})]}{\cos\Phi(4\tan^2\Phi + 1)} \qquad (2.3.4.15)$$

at point O

$$\sigma_{(o)} = \frac{p \cos\alpha}{1 - \sin\Phi \cos 2(\theta - \alpha)} e^{2(\frac{\pi}{2} - \theta)\tan\Phi} \qquad (2.3.4.16($$

Now the vertical stresses are equal to

$$\sigma_{z(O)} = \sigma_{(O)} (1 + \sin\Phi) \qquad (2.3.4.18)$$

$$\sigma_{z(D)} = \sigma_{(D)} (1 + \sin\Phi) \qquad (2.3.4.18)$$

Equation (2.3.4.18) can be expressed in the form of the following bearing capacity equation:

$$q = A_2 \gamma B + B_2 p \qquad (2.3.4.19)$$

which is equivalent to the Meyerhof equation of

$$q = \frac{N_\gamma}{2} \gamma B + N_q \gamma D \qquad (2.3.4.20)$$

where $\frac{N_\gamma}{2} = A_2$ (2.3.4.21)

and $N_q = B_2$ (2.3.4.22)

Thus $N_{\gamma q} = 2A_2 + 2\frac{D}{B} B_2$ (2.3.4.23)

The resulting values of A_2 and B_2 are given in Figure 2.22. The ratios of B/H and R/H are found in Figures 2.23 and 2.24 respectively.

2.3.5 Brinch Hansen (1970)

Brinch Hansen (1970) presents a revised and extended formula for bearing capacity which embodies as many variables as possible. (This topic was taken up later by Vésic in 1975.) In actual fact Brinch Hansen's bearing capacity equation is similar to the one discussed previously (2.2.2.1); the novelty of Brinch Hansen's equation is the introduction of reduction factors to take into account such things as inclination of load, eccentricity, and so on. The reduction factor which takes into account the presence of a slope is given by the following expression:

$$\zeta qg = \zeta \gamma g = [1 - 0.5\tan\alpha]^5 \quad (2.3.5.1)$$

By means of this simple formula, Brinch Hansen (1970) finds values for ζqg and $\zeta \gamma g$. These slope reduction factors

Values of A_2

α \ Φ	26°	28°	30°	32°	34°	36°	38°	40°	42°
20	4.03	5.48	7.26	9.73	13.04	18.16	25.45	36.10	53.00
25	2.61	3.82	5.28	7.15	9.80	13.38	18.41	25.71	36.89
30	-	-	-	4.61	6.61	9.20	12.91	17.76	25.01
35	-	-	-	-	-	5.11	7.82	11.27	16.11

Values of B_2

α \ Φ	26°	28°	30°	32°	34°	36°	38°	40°	42°
20	5.44	6.78	8.46	10.56	12.90	16.64	21.14	27.01	34.71
25	3.60	4.83	6.26	7.44	10.02	12.70	16.15	20.62	26.48
30	-	-	-	5.25	6.99	9.12	11.78	15.13	19.55
35	-	-	-	-	-	5.42	7.64	10.35	13.55

Figure 2.22

Values of B/H

α \ Φ	26°	28°	30°	32°	34°	36°	38°	40°	42°
20	1.85	1.89	1.89	1.87	1.83	1.78	1.73	1.67	1.61
25	0.93	1.32	1.38	1.43	1.44	1.44	1.42	1.39	1.36
30	-	-	-	0.94	1.09	1.16	1.19	1.19	1.18
35	-	-	-	-	-	0.63	0.91	1.00	1.03

Figure 2.23

Values of R/H

α \ Φ	26°	28°	30°	32°	34°	36°	38°	40°	42°
20	0.78	0.80	0.79	0.76	0.72	0.66	0.59	0.52	0.44
25	0.25	0.40	0.46	0.49	0.48	0.47	0.44	0.40	0.36
30	-	-	-	0.23	0.29	0.32	0.32	0.31	0.29
35	-	-	-	-	-	0.13	0.19	0.22	0.22

Figure 2.24

are considered by Brinch Hansen to be only approximate since they are based on a theory which he devised to take into account the effect of inclination of load on a footing on flat ground. In the case of flat ground the reduction factor is a function of the ratio of the horizontal to the vertical components of the inclined load. Applying the reasoning that a vertical load on a footing in or near a slope is similar to the case of an inclined load on a footing on flat ground, Brinch Hansen concluded that the reduction factor which should be applied when the ground surface is not horizontal is only a function of the angle of the slope.

Therefore, according to Brinch Hansen (1970), the bearing capacity of a footing located at the crest of a slope is not influenced by the properties of the soil. For example, in the case of a slope of 2:1, the reduction factor is unique, independent of Φ and has a value of 0.24. But N_γ and N_q is dependent on Φ.

2.3.6 Giroud and Tran-Vo-Nhiem (1972)

In 1972, Giroud presented a general theory for foundations in or at the crest of a slope; this theory is adapted to handle the case of a footing on top of a slope, that is to say with the footing being located at a certain distance back from the edge of the slope. The theory gives solutions for three types of soil:

a) frictionless soil ($\Phi = 0$)

b) soil exhibiting cohesion and friction ($\tau = c + \sigma_n \tan\Phi$)

c) cohesionless soil (c = 0)

Giroud used the principle of superposition previously discussed, and his bearing capacity equation for the present situation is

$$q = cN_{c\alpha} + \gamma D\cos\alpha\ N_{q\alpha} + \tfrac{1}{2}N_{\gamma\alpha}\gamma B \qquad (2.3.6.1)$$

To suit the present study, certain portions of Giroud's work are not considered; only that part of his theory dealing with cohesionless material is reviewed. Thus $N_{c\alpha}$ and c are not included in this study and this means that the angle δ' (Figure 2.27b)) is equal to the slope angle α.

To obtain $N_{q\alpha}$ Giroud, like Meyerhof, starts by considering the surcharge acting on a weightless material. The elastic wedge immediately under the footing is denoted by $0'S_1 0$ on Figure 2.26. Angle β' is referred to as the angle $S_1\hat{0}'0$ and is found by differentiation to be a minimum when it is equal to $\frac{\pi}{4} + \frac{\Phi}{2}$.

From the Mohr circle (Figure 2.27) the zone within S_1OS_2 is divided into two parts by a line OL_2 which is parallel to P_2T_2 in the circle of stress. This procedure is the same as the one described in the Mizuno case.

Therefore, full mobilization of shearing strength is encountered on plane OL_2. The angle $L_2\hat{O}S_2$ is defined as E. The curved line that joins points S_1 to L_2 is a sector of a logarithmic spiral that has its center at O and sweeps

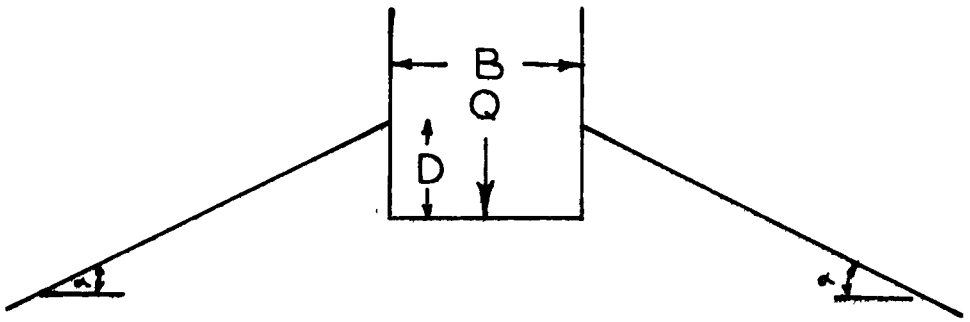

Giroud's Assumptions

Figure 2.25

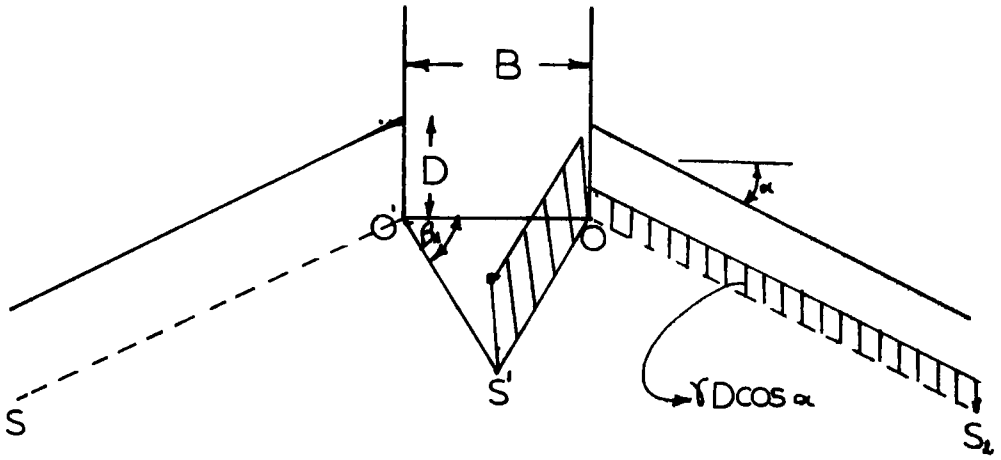

Giroud's Assumptions

Figure 2.26

through an angle of

$$\Theta = \tfrac{3}{4}\pi + \tfrac{\Phi}{2} - \tfrac{\Gamma}{2} - \tfrac{\alpha}{2} - \beta_1 \qquad (2.3.6.2)$$

where $\Gamma = \sin^{-1} \frac{\sin\alpha}{\sin\Phi}$ (2.3.6.3)

Considering the forces acting on these zones and the shearing strength along the slip surface, Giroud arrives at the following expression for the surcharge term

$$N_{q\alpha} = \frac{\cos\alpha\ (1 + \sin\Phi)}{1 - \sin\Phi\ \cos(\Gamma - \alpha)}\ e^{(\pi - \Gamma - \alpha)\tan\Phi} \qquad (2.3.6.4)$$

The vertical surcharge acting on the plane OS_2 is taken to be $\gamma D\cos\alpha$ as shown on Figure 2.18.

To find the weight term $N_{\gamma\alpha}$, Giroud considers segment OS_1 as a retaining wall pushing on wedge S_1OS_2, as seen in Figure 2.20.

The weight term is expressed as

$$N_{\gamma\alpha} = \tfrac{1}{2}\left[\frac{\cos(\beta_1 - \Phi)\ K_p - \tan\beta_1}{\cos^2\beta_1}\right] \qquad (2.3.6.5)$$

which is similar to the Terzaghi and Meyerhof expressions.

The method consists of finding a minimum value of equation (2.3.6.5) by changing the value of β_1 for different values of K_p. Using this procedure Giroud noticed that for

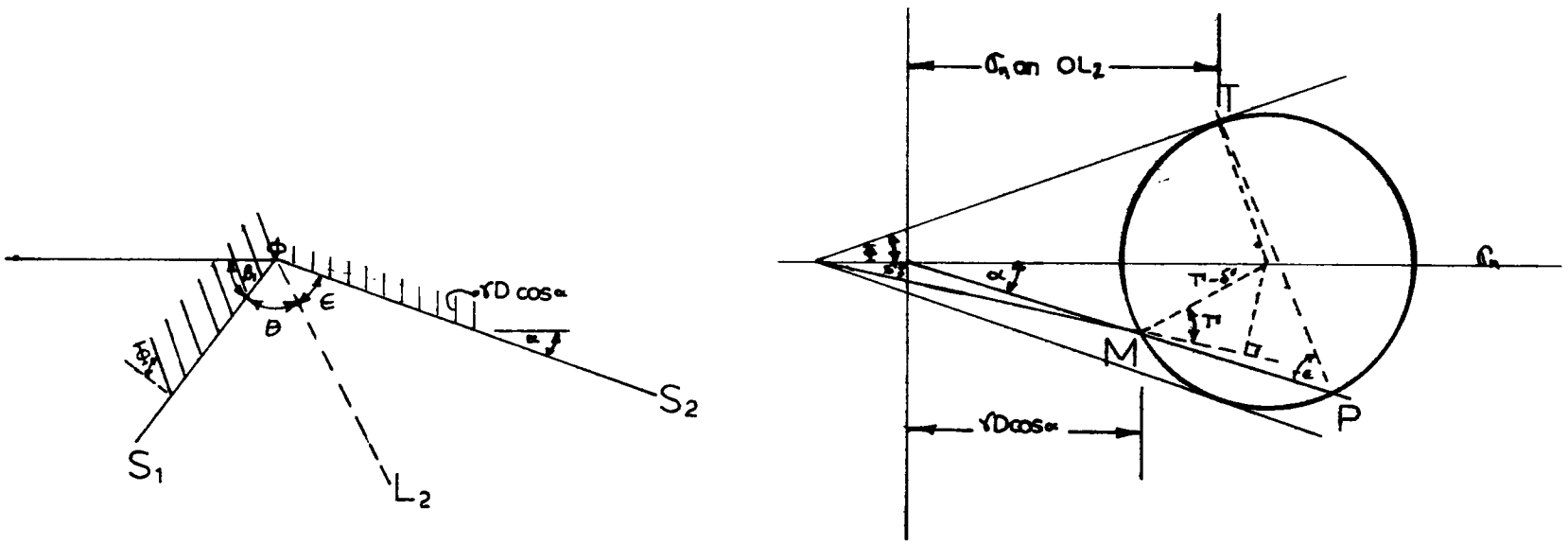

Figure 2.27

Initial Stresses in the Slope

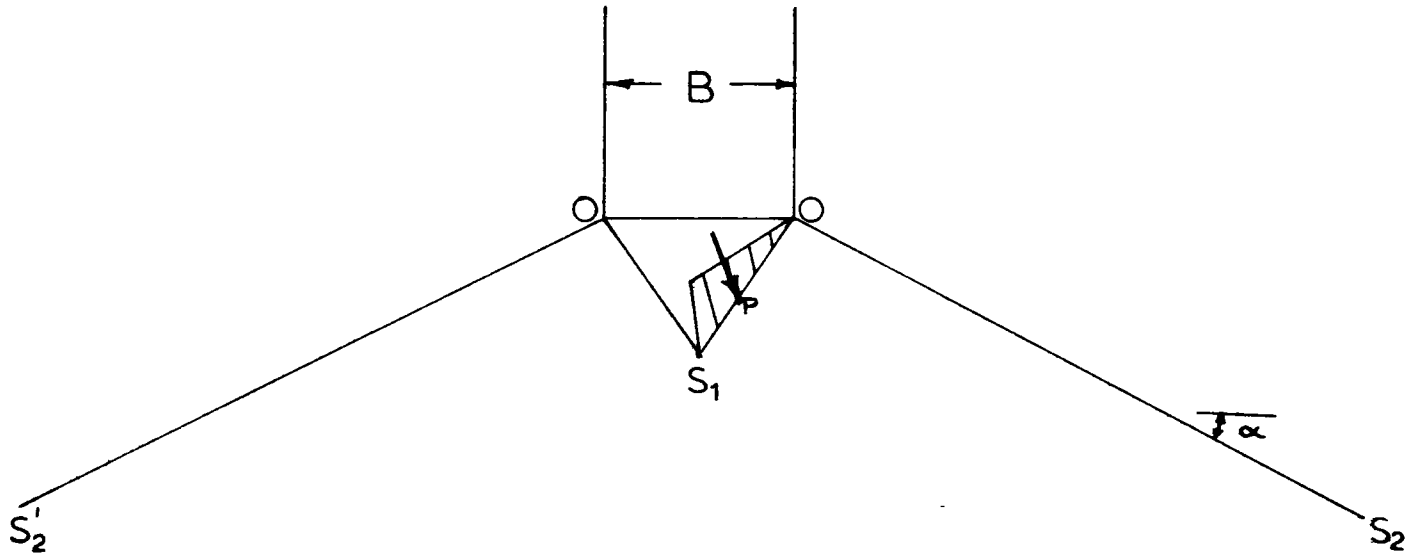

Forces Acting on the Active Wedge

Figure 2.28

a minimum value of the weight term $N_{\gamma\alpha}$, the angle β_1 was not equal to $45 - \frac{\Phi}{2}$, but closer to 1.2Φ, which is almost identical to that which Meyerhof (1955) found.

The method which Giroud devised to consider the bearing capacity of footings at a certain distance from the crest of the slope is called the equivalent slope method. Special charts enable the failure geometry for a particular case to be determined; knowing the failure geometry, the bearing capacity factor can be found. The procedure consists of drawing the slope, the footing and the location of the footing, to the scale of the footing width. The Giroud chart is then superimposed on this drawing; a graphical construction is used to place the footing at the crest of the equivalent slope of angle α'.

Giroud does not actually give bearing capacity factors for footings on top of a slope; he limits himself to presenting the charts. Since bearing capacity factors are required for the present study, the Giroud method is further elaborated in Section 2.4 of the present chapter where the required factors are computed. Since Giroud's method leads to values of $N_{\gamma\alpha}$ and $N_{q\alpha}$, the following expression is used to find $N_{\gamma q}$:

$$N_{\gamma q} = N_{\gamma\alpha} + 2\frac{D}{B} \cos\alpha \, N_{q\alpha} \qquad (2.3.6.6)$$

Giroud's $N_{q\alpha}$ and $N_{\gamma\alpha}$ values are given in Figures 2.29 and 2.30.

$N_{q\alpha}$ Values (according to Giroud)

α \ Φ	50°	45°	40°	35°	30°	25°	20°	15°	10°	5°
0°	319	135	64	33	18	11	6	4	2	2
5°	250	109	53	28	16	9	6	3	2	1
10°	193	86	43	23	13	8	5	3	2	-
15°	148	68	34	19	11	6	4	2	-	-
20°	112	52	27	15	9	5	2	-	-	-
25°	83	40	21	11	6	3	-	-	-	-
30°	60	29	15	8	3	-	-	-	-	-
35°	42	21	10	4	-	-	-	-	-	-
40°	28	13	4	-	-	-	-	-	-	-
45°	17	5	-	-	-	-	-	-	-	-
50°	6	-	-	-	-	-	-	-	-	-

Figure 2.29

$N_{\gamma\alpha}$ Values (according to Giroud)

α \ Φ	50°	45°	40°	35°	30°	25°	20°
0°	720	254	100	41	18	8	4
5°	550	193	75	33	14	6	3
10°	400	142	58	26	11	5	2
15°	281	107	43	20	9	4	2
20°	200	76	32	15	7	4	2
25°	139	55	24	11	5	3	1
30°	95	38	16	7	2	2	–
35°	61	25	10	4	–	–	–
40°	37	15	5	–	–	–	–
45°	21	7	–	–	–	–	–
50°	10	–	–	–	–	–	–

Figure 2.30

2.3.7 Absi (1972)

Using the Caquot (1934) equations for equilibrium along a potential slip-line,

$$\frac{d\sigma'}{d\theta} = 3\tau - \gamma \sin\theta \qquad (2.3.7.1)$$

$$\frac{d\tau}{d\theta} = 2\sigma - \sigma' - \gamma \cos\theta$$

Caquot and Kérisel (1948) were able to compile tables of K_p and K_a for different values of:

a) angle of shearing resistance

b) backfill angle

c) wall inclination

d) load obliquity on wall

The failure analysis used by Caquot and Kérisel, and subsequently adapted for sloping ground by Absi, is shown on Figure 2.31 where

ω = inclination of the contact stress under footing of width B

α = inclination of slope OA

Φ = angle of internal friction

In this problem, Absi defines two zones as shown on Figure 2.31. Zone I is a Rankine passive zone, while in zone II the stress distribution is known from the boundary conditions along OT and along OB. From these boundary

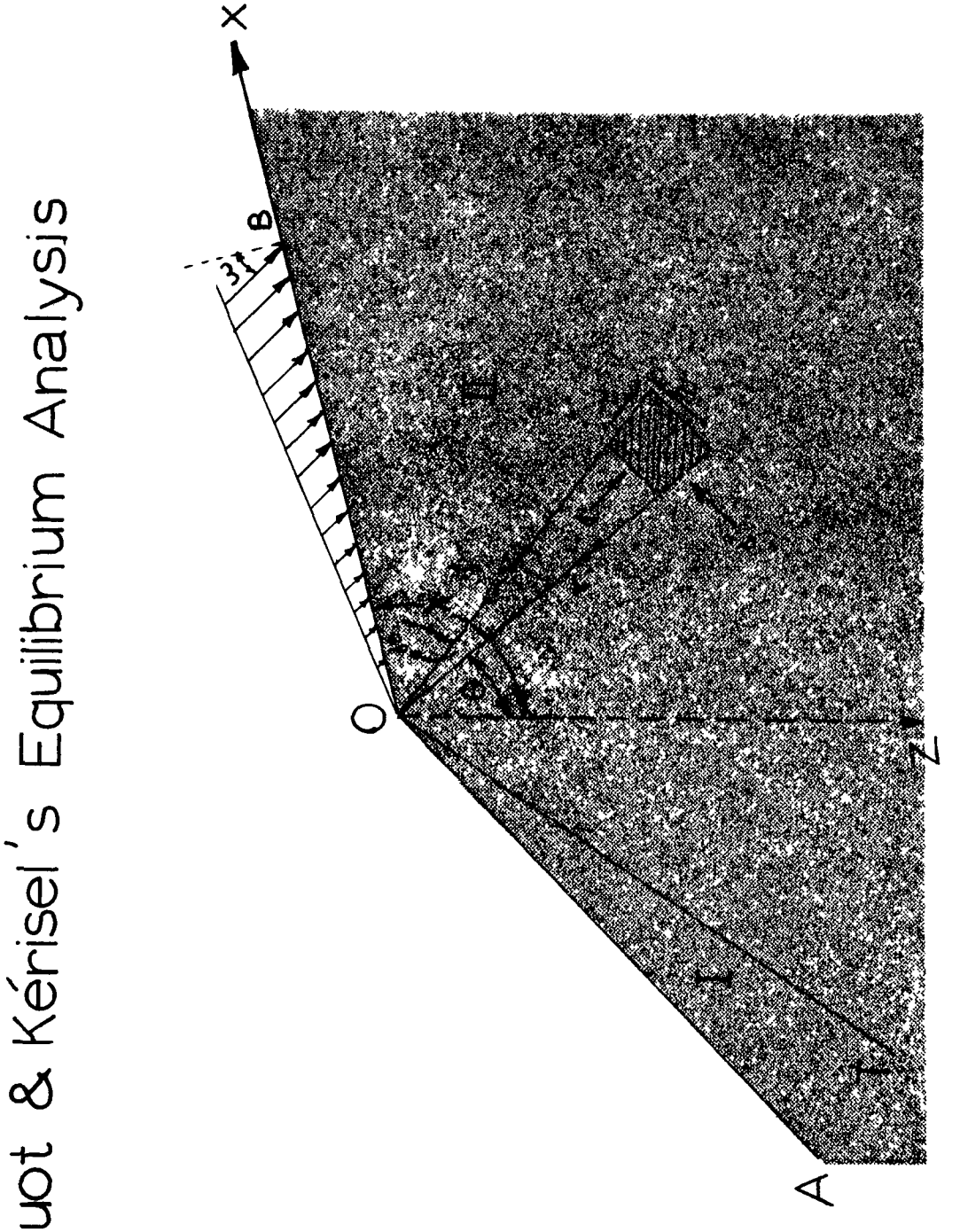

Figure 2.31

conditions equation (2.3.7.1) can be solved. A numerical integration solution for this equation is given in Caquot (1934).

From this solution, Absi is led to the following integration across the width of the footing to determine the bearing capacity:

$$q = \int_0^{\frac{B}{2}} \frac{B}{2}\gamma x \quad K_p dx = \gamma K_p \frac{B^2}{4} \qquad (2.3.7.2)$$

where K_p is a coefficient of passive earth pressure and

$$N_\gamma = N_{\gamma q} = \frac{K_p}{2} \qquad (2.3.7.3)$$

This expression is valid only for cohesionless material which possesses weight and for the case where the footing is located at the crest of the slope. For practical purposes the values of K_p are represented graphically for different load inclination angles . These results are shown in Figure 2.32.

2.3.8 Chen (1974)

Chen (1974), using the technique of velocity fields, found an upper bound solution to the problem of bearing capacity close to a slope. He assumed a Prandtl mechanism divided into three zones as shown on Figure 2.33. In accordance with the upper bound theorem of limit analysis,

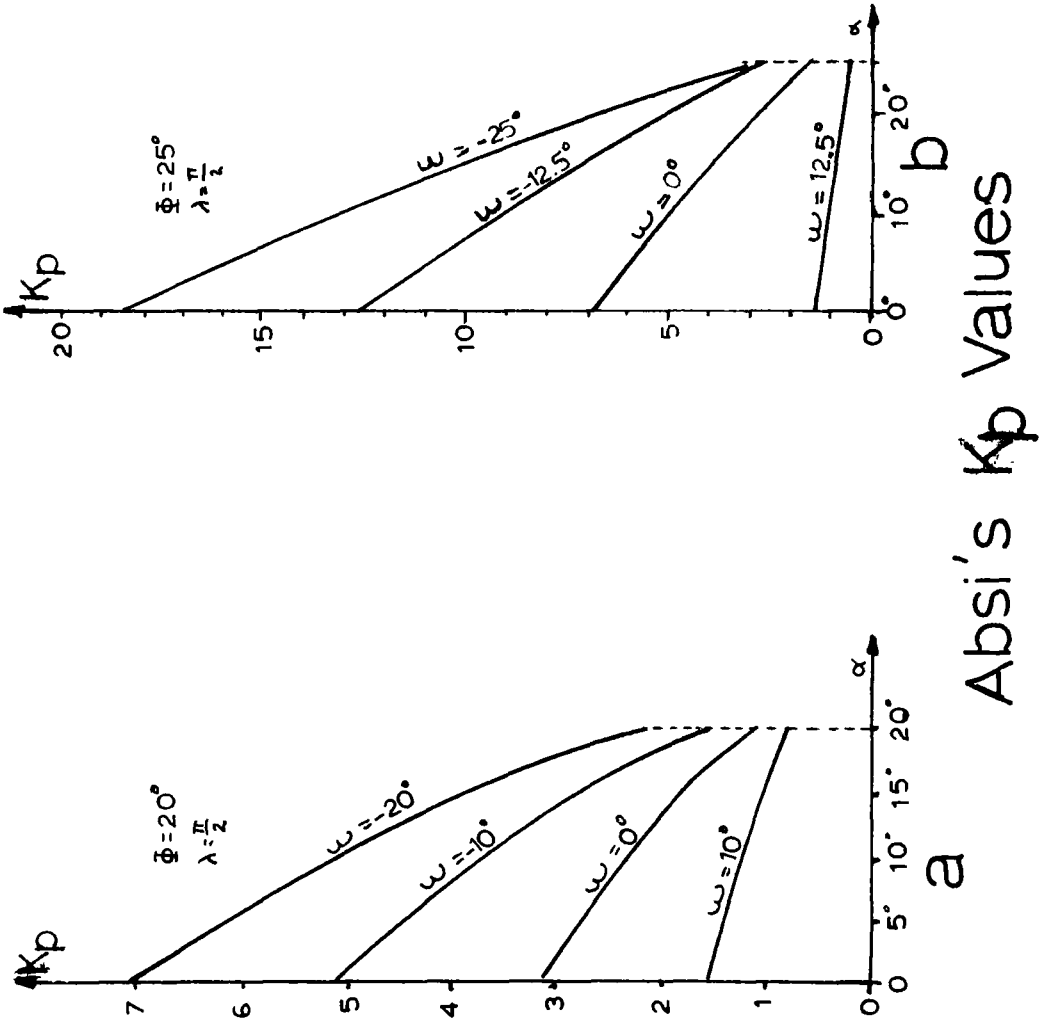
Kp
Φ=20°
λ=π/2
ω=-20°
ω=-10°
ω=0°
ω=10°
α
0 5° 10° 15° 20°
a
Absi's Kp Values
Kp
Φ=25°
λ=π/2
ω=-25°
ω=-12.5°
ω=0°
ω=12.5°
α
0 5° 10° 20°
b

Figure 2.32

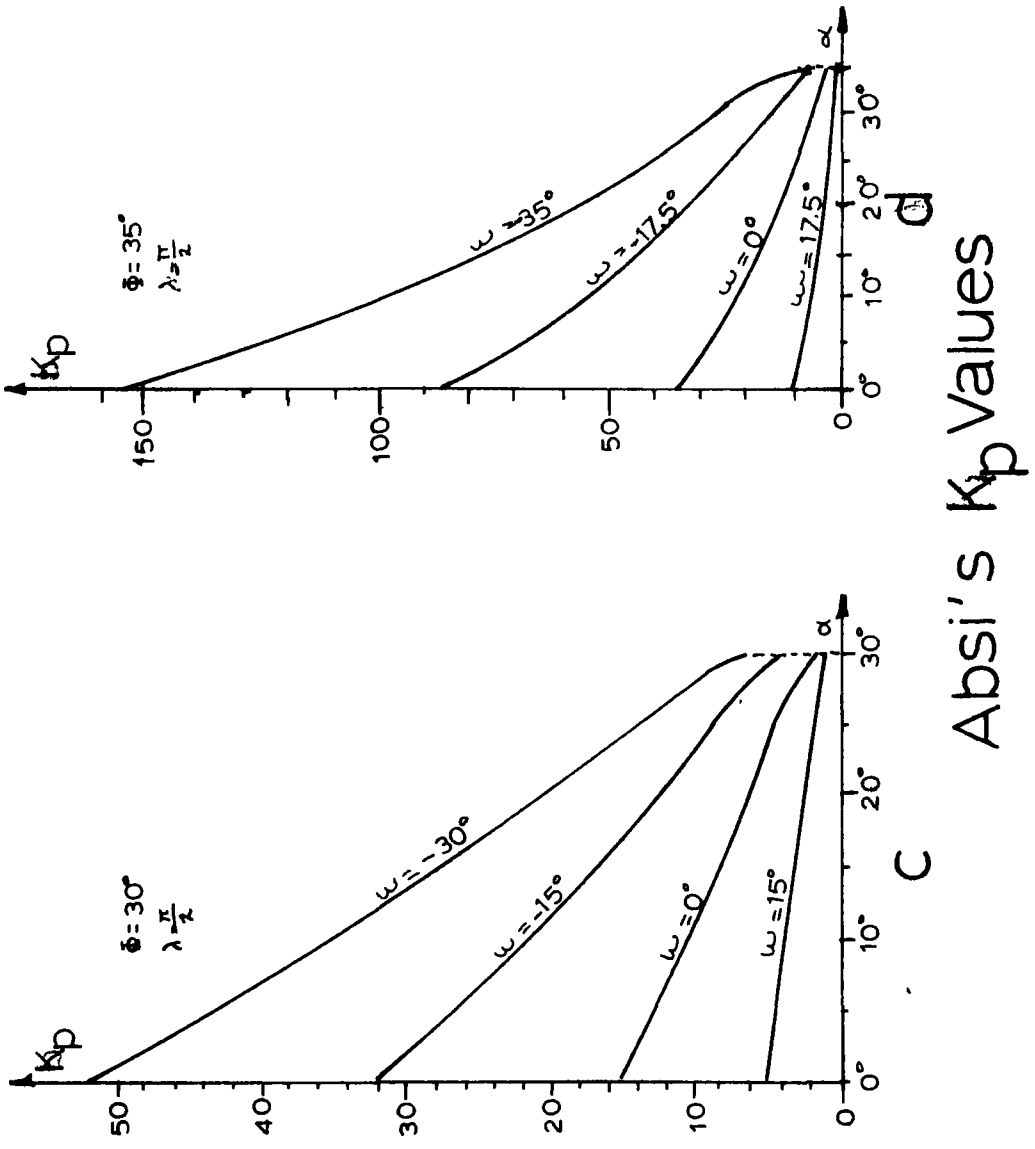
Absi's K_p Values
C
d
K_p
α
$\Phi = 30°$
$\lambda = \frac{\pi}{2}$
$\omega = -30°$
$\omega = -15°$
$\omega = 0°$
$\omega = 15°$
$\Phi = 35°$
$\lambda = \frac{\pi}{2}$
$\omega = -35°$
$\omega = -17.5°$
$\omega = 0°$
$\omega = 17.5°$
0°
10°
20°
30°
0
10
20
30
40
50
50
100
150

Figure 2.32

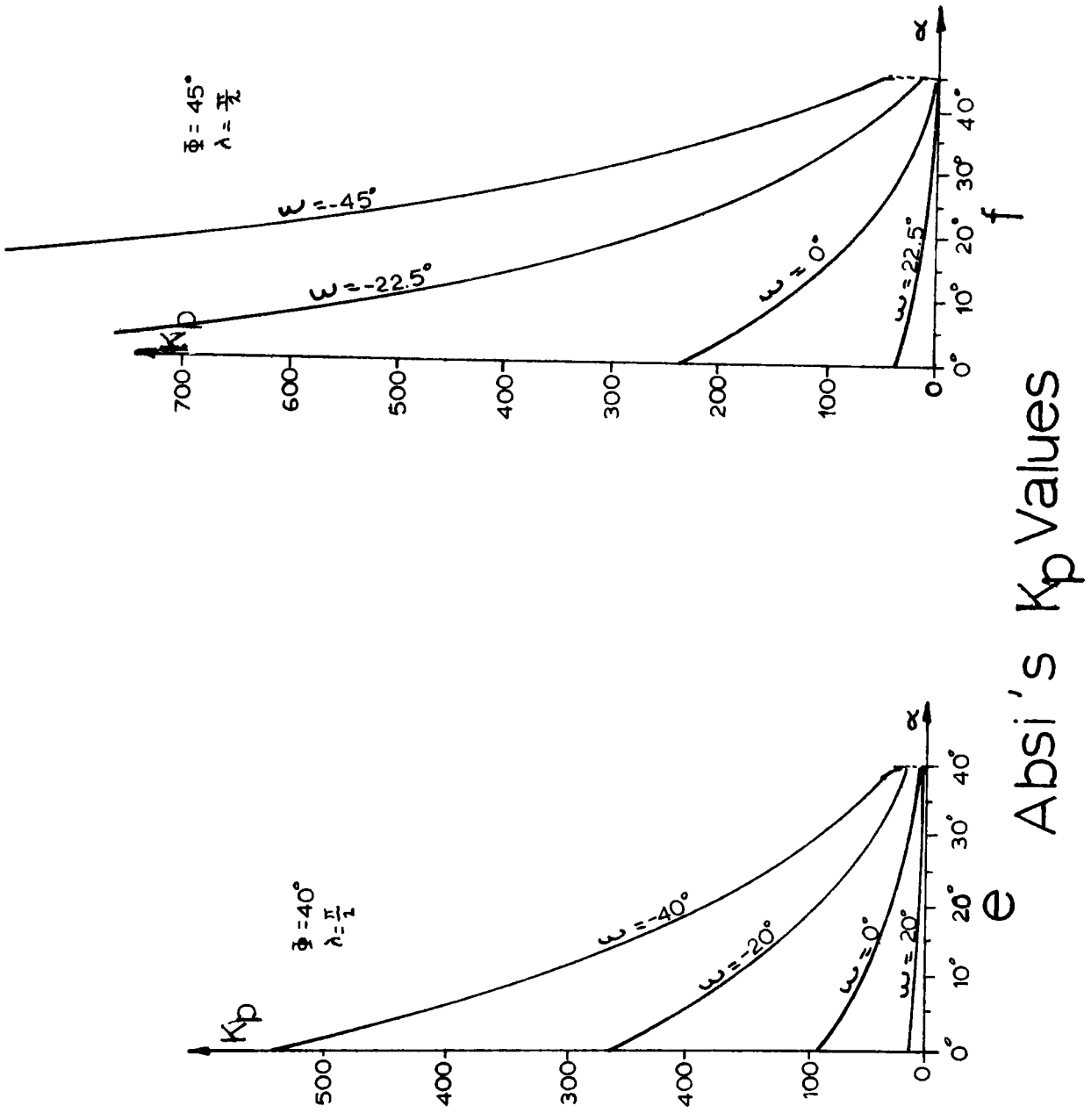
Φ = 45°
λ = π/2
ω = -45°
ω = -22.5°
ω = 0°
ω = 22.5°
Kp
α
0° 10° 20° 30° 40°
0 100 200 300 400 500 600 700
f
Φ = 40°
λ = π/2
ω = -40°
ω = -20°
ω = 0°
ω = 20°
Kp
α
0° 10° 20° 30° 40°
0 100 400 300 400 500
e
Absi's Kp Values

Figure 2.32

for a kinematically admissible velocity field the rate at which work is done by the external loads is identical to the rate of internal energy dissipation. To be kinematically admissible, the velocity field must satisfy velocity boundary conditions.

Figure 2.33a) shows the general mechanism which is used to determine the bearing capacity of a buried footing. The mechanism is similar to the one used by Meyerhof (1951). Angle β is the direction of the equivalent free surface. Figure 2.33b) illustrates the Prandtl mechanism modified to conform to the problem of a footing on top of a slope.

In his solution for footings on top of a slope, Chen starts by defining the rate of internal energy dissipation along the slip surface. Energy is dissipated at the discontinuity between material at rest and material in motion and in the radial shear zone BCD. The rate of energy dissipation is found by multiplying together the length of each discontinuity line (such as BC), the velocity difference across the line, and c $\cos\Phi$. The resulting products for all such lines are summed.

From the velocity diagram along a discontinuity line such as BC, shown in Figure 2.34, it is possible to find the following relationships between velocities:

$$V_r = \frac{V_o \sin\xi}{\cos(\xi - \Phi)} \qquad (2.3.8.1)$$

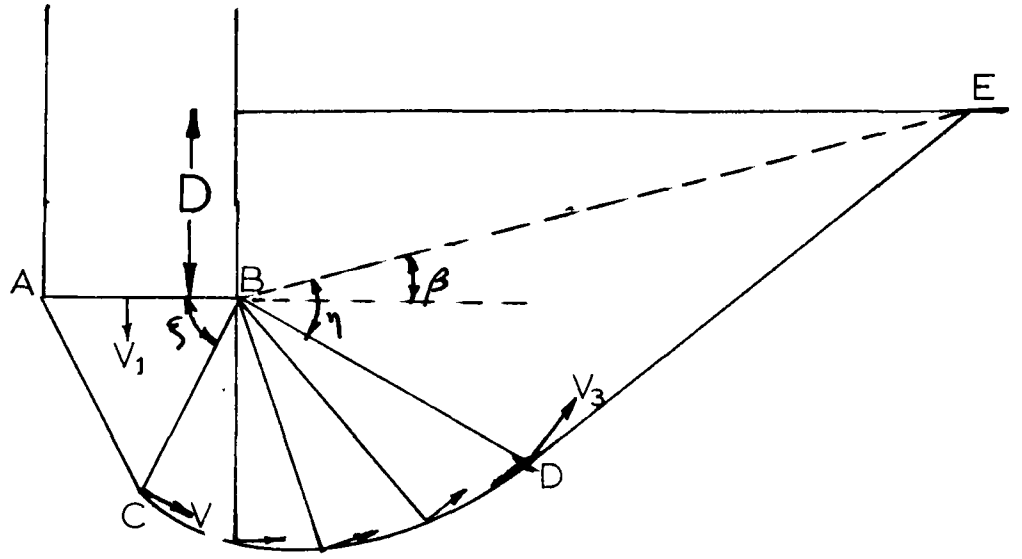

a

Velocity Fields

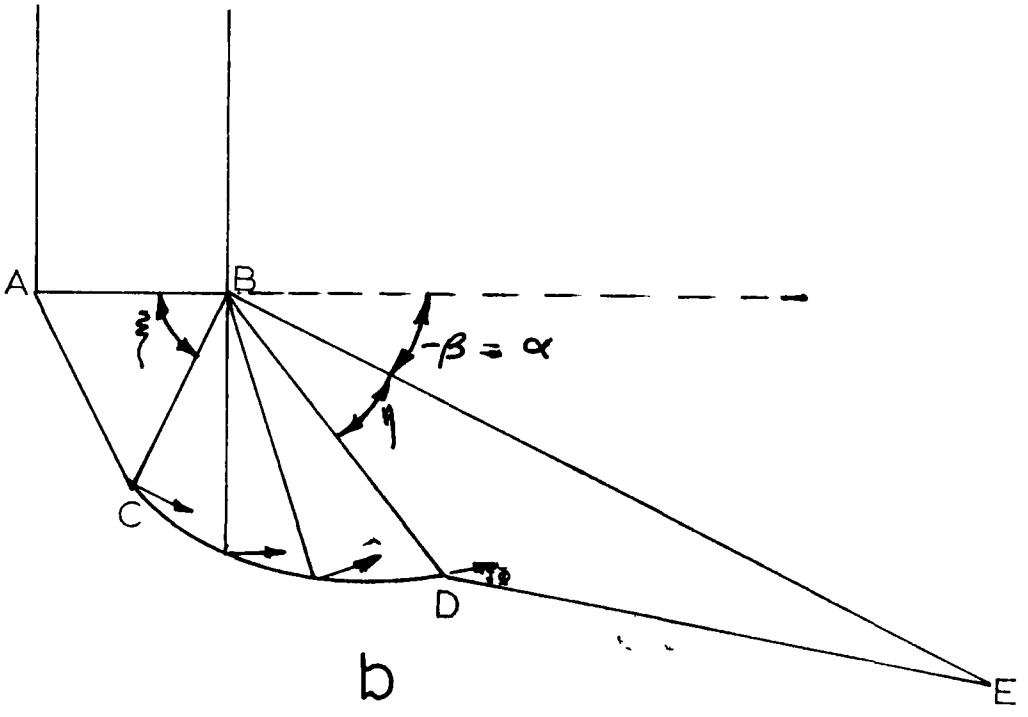

b

Figure 2.33

$$V_1 = \frac{V_o \cos\Phi}{\cos(\xi - \Phi)} \qquad (2.3.8.2)$$

Hence the rate at which energy is dissipated along line BC is:

$$D_{BC} = c\, V_o r_o \, \frac{\sin\xi \cos\Phi}{\cos(\xi - \Phi)} \qquad (2.3.8.3)$$

The energy dissipated in the radial shear zone BCD is obtained by dividing the logarithmic spiral sector into an infinite number of small rigid triangles. The total rate of energy dissipation within the shear zone is:

$$D_{BCD} = \tfrac{1}{2}\, cV_o r_o \, \frac{e^{2(\pi + \beta - \xi - \eta)\tan\Phi} - 1}{\tan\Phi} \qquad (2.3.8.4)$$

It can also be shown that the energy dissipation along the spiral CD is defined by equation (2.3.8.4) as well.

Since the velocity field is continuous across line BD, no energy is dissipated there. The dissipation rate along line DE can be computed easily once the length DE is known and is:

$$D_{DE} = c\, V_o r_o \, \frac{\sin\eta \cos\Phi \; e^{2(\pi + \beta - \xi - \eta)\tan\Phi}}{\cos(\eta + \Phi)} \qquad (2.3.8.5)$$

The rate at which work is done by the soil weight is found by multiplying the area of each rigid body by γ, times the vertical component of the velocity of the rigid body; the individual products are summed over all the areas in motion.

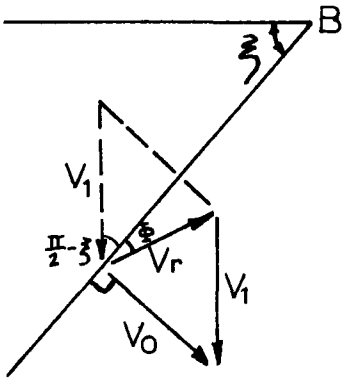

Velocity Diagram along BC

Figure 2.34

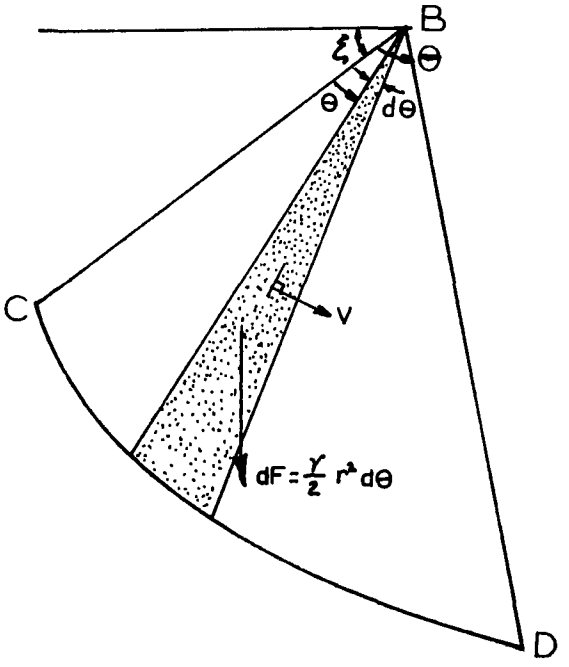

Gravity Force Acting on an Element

Figure 2.35

In the triangular region ABC

$$W_{ABC} = -\gamma V_o r_o^2 - \frac{\sin\xi \cos\xi \cos\Phi}{\cos(\xi - \Phi)} = -\gamma V_o r_o^2 h_1(\xi) \qquad (2.3.8.6)$$

where $h_1(\xi)$ has the value given with the brackets of Equation (2.3.8.5)

The external rate of work done by the soil weight in the log spiral region BCD can be computed by summing over the region the products of each elemental triangle's component of vertical velocity and its weight. Referring to Figure 2.35, the gravity force acting on a triangular element is $dF = \frac{1}{2}\gamma r^2 d\theta$ and the rate of external work is:

$$W_{BCD} = [V \cos(\theta + \xi)]\ [\tfrac{1}{2}\gamma r^2 d\theta] \qquad (2.3.8.7)$$

Using the following velocity relations:

$$V = V_o\, e^{\theta \tan\Phi} \qquad (2.3.8.8a)$$

$$r = r_o e^{\theta \tan\Phi} \qquad (2.3.8.8b)$$

the total rate of external work done by the soil becomes

$$W_{BCD} = \tfrac{1}{2}\gamma \int^{\theta} r^2 V \cos(\theta + \xi) d\theta = -\frac{\gamma V_o r_o^2}{2} h_2(\xi, \eta) \qquad (2.3.8.9)$$

where:

$$h_2(\xi,\eta) = \frac{(3\tan\Phi\cos\xi+\sin\xi)+[3\tan\Phi\cos(\beta-\eta)+\sin(\beta-\eta)]e^{3(\pi+\beta-\xi-\eta)\tan\Phi}}{(1+9\tan^2\Phi)} \qquad (2.3.8.10)$$

In region BDEF the rate of external work is

$$W_{BDEF} = \frac{\gamma V_o r_o^2}{2} h_3(\xi,\eta) \qquad (2.3.8.11)$$

where

$$h_3(\xi,\eta) = \frac{\sin\eta\cos\Phi}{\cos(\eta+\Phi)} + \frac{\sin\beta\cos\beta\cos^2\Phi}{\cos^2(\eta+\Phi)}\cos(\beta-\eta)e^{3(\pi+\beta-\xi-\eta)\tan\Phi} \qquad (2.3.8.12)$$

in which the first and the second terms in the square bracket represent the contribution from zone BDE and zone BEF respectively. The rate of work done by the footing load W_f is given by the following expression:

$$W_f = q\, V_o r_o \frac{2\cos\Phi\cos\xi}{\cos(\xi-\Phi)} \qquad (2.3.8.13)$$

Equating the total rate at which work is done by the force on the foundation and the soil weight in motion to the total rate of energy dissipation along the lines of velocity discontinuity, it is found, after some simplifications, that the upper bound bearing capacity of the soil is:

$$\frac{q(\xi,\eta)}{c} = Nc(\xi,\eta) + GN_\gamma(\xi,\eta) \qquad (2.3.8.14)$$

in which $G(=\gamma\frac{B}{2c})$ is a dimensionless soil weight parameter and the bearing capacity factors $N_c(\xi,\eta)$ and $N_\gamma(\xi,\eta)$ can be expressed in terms of the two angles (ξ,η) under the condition $\eta>\beta$

$$N_{c(\xi,\eta)} = \cot\Phi \quad \frac{\cos\eta\cos(\xi-\Phi)\ e^{2(\pi+\beta-\xi-\eta)\tan\Phi}}{\cos\xi\ \cos(\eta+\Phi)} \qquad (2.3.8.15)$$

$$N\gamma(\xi,\eta) = \frac{\cos(\xi-\Phi)}{2c\cos\Phi\ \cos^2\xi}\ [h_1(\xi) + h_2(\xi,\eta) + h_3(\xi,\eta)] \qquad (2.3.8.16)$$

The best upper bound is found by minimizing the function $q_o(\xi_1\eta)/c$ with respect to variables ξ and η for the given values Φ, G and $\frac{D}{B}$.

The bearing capacity of a footing on a slope can be obtained directly from a simple modification of the above solution. If area BEF in Figure 2.33 is set to zero, the case $-\frac{1}{2}\pi<\beta<0$ represents the bearing capacity of a footing on a slope. The equation for computing the bearing capacity factor N_γ for this case is as follows:

$$N_\gamma(\xi_1\eta) = \frac{\cos(\xi-\Phi)}{2\cos\Phi\ \cos^2\xi}\ [h_1(\xi) + h_2(\xi,\eta)] \qquad (2.3.8.17)$$

$$+ \frac{\cos(\xi-\Phi)\ \sin\eta}{2\cos(\eta+\Phi)\ \cos^2\xi}\ \cos(\beta-\eta)\ e^{3(\pi+\beta-\xi-\eta)\tan\Phi}$$

Minimum values of the factor N_γ computed from the Prandtl mechanism for the case of a rough footing on a slope have been calculated by Chen (1974) for the slope angle $\alpha = \beta$ varying

$N_{\gamma q}$ Values at Slope Crest

Upper Bound Solution

(Chen 1974)

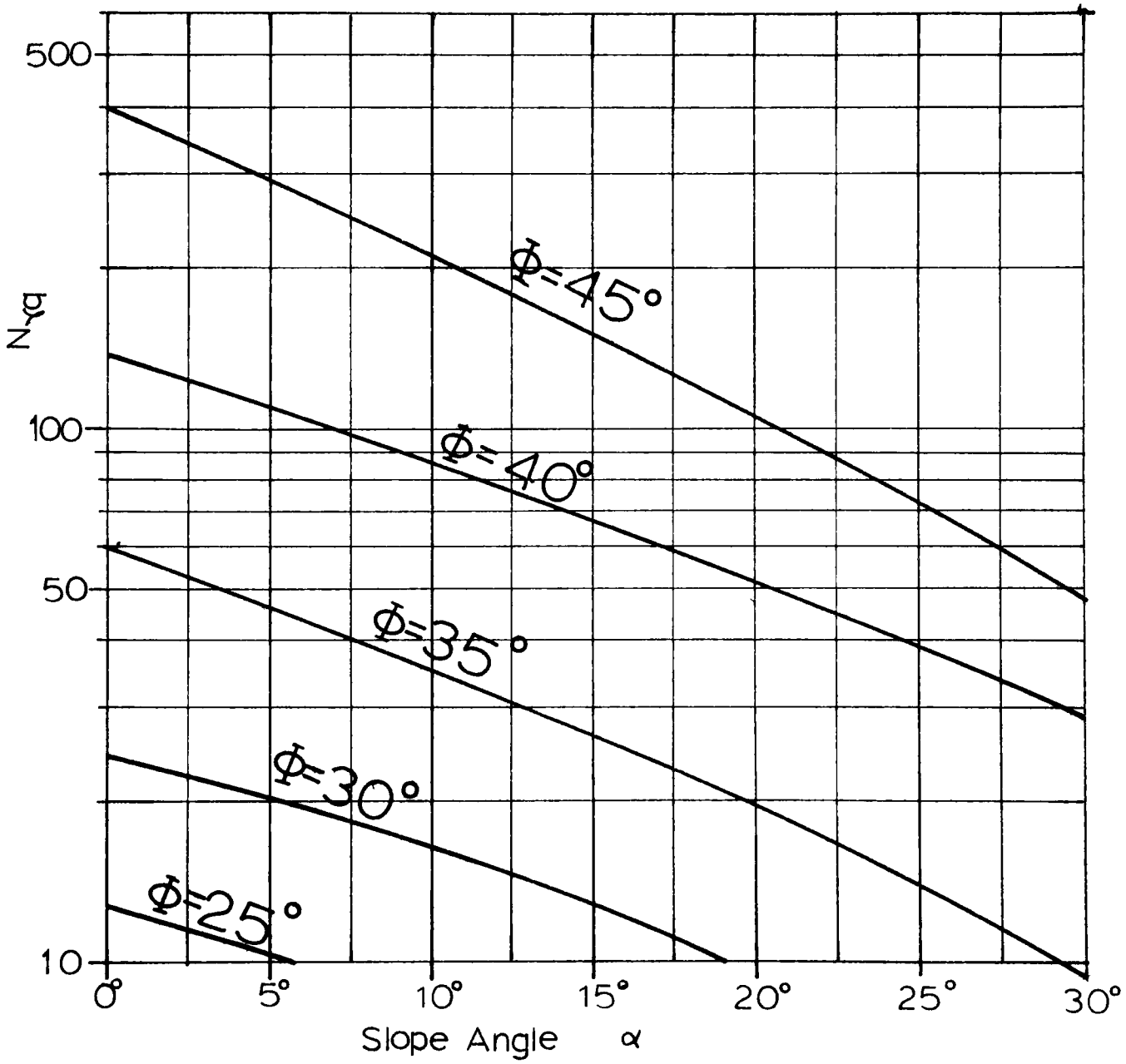

Figure 2.36

from 0 to -30° and friction Φ angles ranging from 10° to 45°. The results are plotted in Figure 2.36.

2.3.9 Bowles (1975)

Bowles (1975) proposes a graphical method based on Brinch Hansen's [(1953), (1957), (1966)] equilibrium method to establish a safe soil pressure on the top of sloping ground. The method is illustrated in Figure 2.37

The graphical procedure consists of drawing a possible slip surface under a footing, close to a slope. This slip surface is divided into three portions. The first portion is line DC, which is part of the elastic wedge ADC immediately under the footing. Angle $\hat{ADC}$ is always equal to $45° + \frac{\Phi}{2}$. Length AC equals R_o.

To obtain line BC, line Ga must be constructed at an angle of $45° - \frac{\Phi}{2}$ to the horizontal, BC is determined as an arc whose radius is equal to $m_1 R_o$ where the center of this arc is located on line GA. The value of "m_1"[1] is a function of the angle of internal friction and is given by Bowles (1975) to be equal to the following:

Φ	m_1
0°	1.00
10°	1.18

1 The method to obtain "m_1" is not explained.

Bowles' Construction Solution

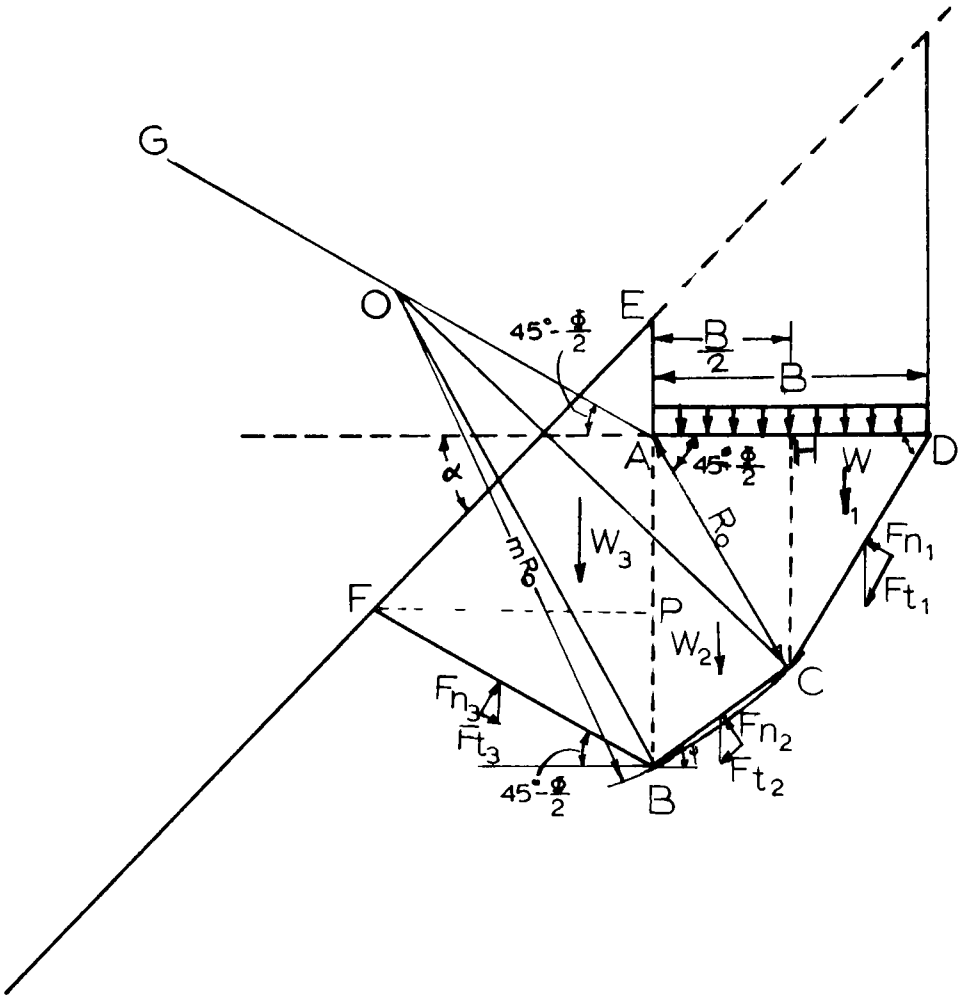

Figure 2.37

Φ	m_1
20°	1.48
30°	2.00
40°	3.09

Point B is defined as the intersection of the arc BC and a vertical line drawn from the leading edge of the footing at point A.

The segment of the slip surface given by the line FB is constructed from B at an angle of $45° - \frac{\Phi}{2}$ to the horizontal. This portion of the slip surface reaches the slope at point F. Now, the complete slip surface is determined.

The weights of soil W_1, W_2 and W_3 can be computed. W_1 corresponds to the volume of soil within HDC, while W_2 corresponds to the volume inside AHCB, and finally W_3 corresponds to the volume of soil FBAE.

The frictional resistance along all three portions of the slip surface can be computed from the respective weights and the footing pressure q. Then, through a process which is similar to the Swedish method for slope stability analysis, the sum of the shear forces which are mobilized along the slip surface is equated to the shearing resistance along the slip surface. At equilibrium a value for q is found.

Bowles gives only the steps to achieve the method; no bearing capacity values may be found in the literature. An example is worked out in Section 2.4.5. This section contains contributions to the theories for bearing capacity of footings

on top of slopes.

2.3.10 Bowles (1977)

Bowles develops another bearing capacity expression which takes into account the proximity of a slope. The failure mechanism used by Bowles (1977) is illustrated in Figure 2.38.

This method consists of constructing the failure mechanism in three sections. First the mechanism has an active wedge- fac - which is directly below the footing. Then a log spiral arc - ad - links this elastic wedge with the third zone Edf. The slip-line at E strikes the slope surfaced at an angle of $45^{\circ} - \frac{\phi}{2}$. Bowles assumes this angle because he states that the slope line is a principal plane.

Once the failure mechanism is found for situations similar to those shown on Figure 2.38, the method consists of computing a reduced N_q based on the ratio of area DfE = A_o (the surcharge) for the case of flat ground and the area Efg of Figure 2.3.10.1a) or the alternative Figure 2.3.10.1b) where Efgh = A_1 to obtain

$$N'_q = N_q \frac{A_1}{A_o} \qquad (2.3.10.1)$$

The bearing capacity is computed using Equation (2.2.1) and the reduced bearing capacity factor N'_q.

Bowles stated that since N_γ depends only on the soil wedge cfa of Figure 2.3.10.1, this requires no modification

Bowles' (1977) Solution

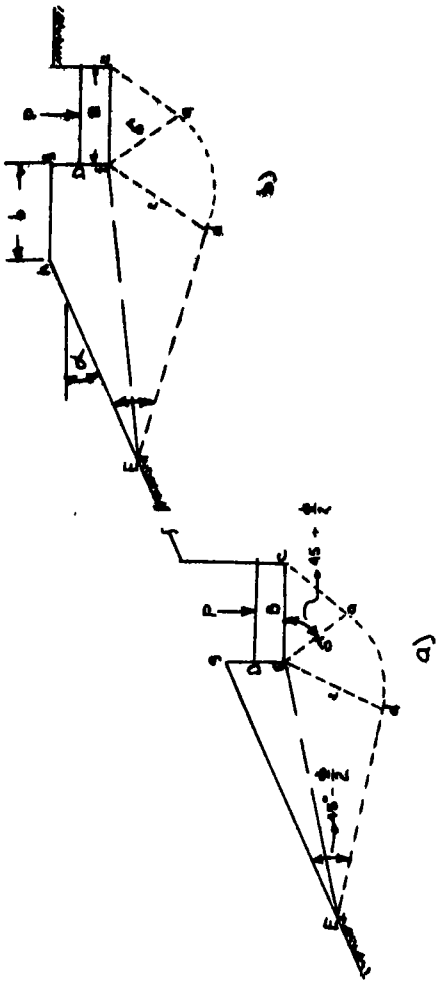

Figure 2.38

for slope effects. This statement is in direct contradiction to the preceeding theories where it is shown that the slope has an influence on the bearing capacity factor N_γ. The statement that N_γ depends on the soil wedge cfa alone is false because N_γ is also dependent on the passive wedge Egfd (Figure 2.3.10.1a) and the log spiral sector.

Bowles' assumption leads to erroneous bearing capacity results for a footing located on top of a slope; the Bowles results for a surface footing are the same whether the footing is located at the slope crest or at a certain horizontal distance from the slope crest.

Bowles only gives the steps to achieve the method; no bearing capacity values could be found. An example is worked out in Section 2.4.5.

2.3.11 Ménard (1964)

Ménard (1964) presents the experimental results of tests on footings close to the slope of an excavation. These experiments are discussed in more detail in Chapter three.

The contribution to the present discussion is that Ménard proposes empirical slope influence factors based on these full scale test results. These factors are meant to be applied to the bearing capacity obtained from the pressuremeter equation for flat ground:

$$q_L - q_o = k(p_L - p_o) \qquad (2.2.3.1)$$

The Ménard slope influence factors are similar to those of Brinch Hansen in that they take into account only the slope angle and not other features such as the soil strength and its deformation properties. Ménard's factors are given in the form of a graph, as shown in Figure 2.39. Ménard appears to assume that the properties of the soil material are taken care of by the constant K of Equation(2.2.3.1).

2.3.12 Conclusions on the Theoretical Investigations

In the foregoing sections, nine theoretical and one empirical investigations have been surveyed. This survey shows that only certain theories consider the possibility that the footing may be located at any horizontal and vertical distance from the slope crest. Among these are the theories of Meyerhof (1955), Giroud (1972) and Bowles (1975) and (1977). The remaining theories deal only with the footing located at the slope crest. This section compares the various theories on the basis of the bearing capacity values obtained for footings located at the slope crest. The values obtained for other footing locations are discussed in Section 2.4.

Given a certain slope angle and Φ value, the theories yield values of bearing capacity which differ from one another as shown in Figure 2.40. Some results are relatively close together, while others are widely different. Since Ménard's account is empirical, it is not included in this graph.

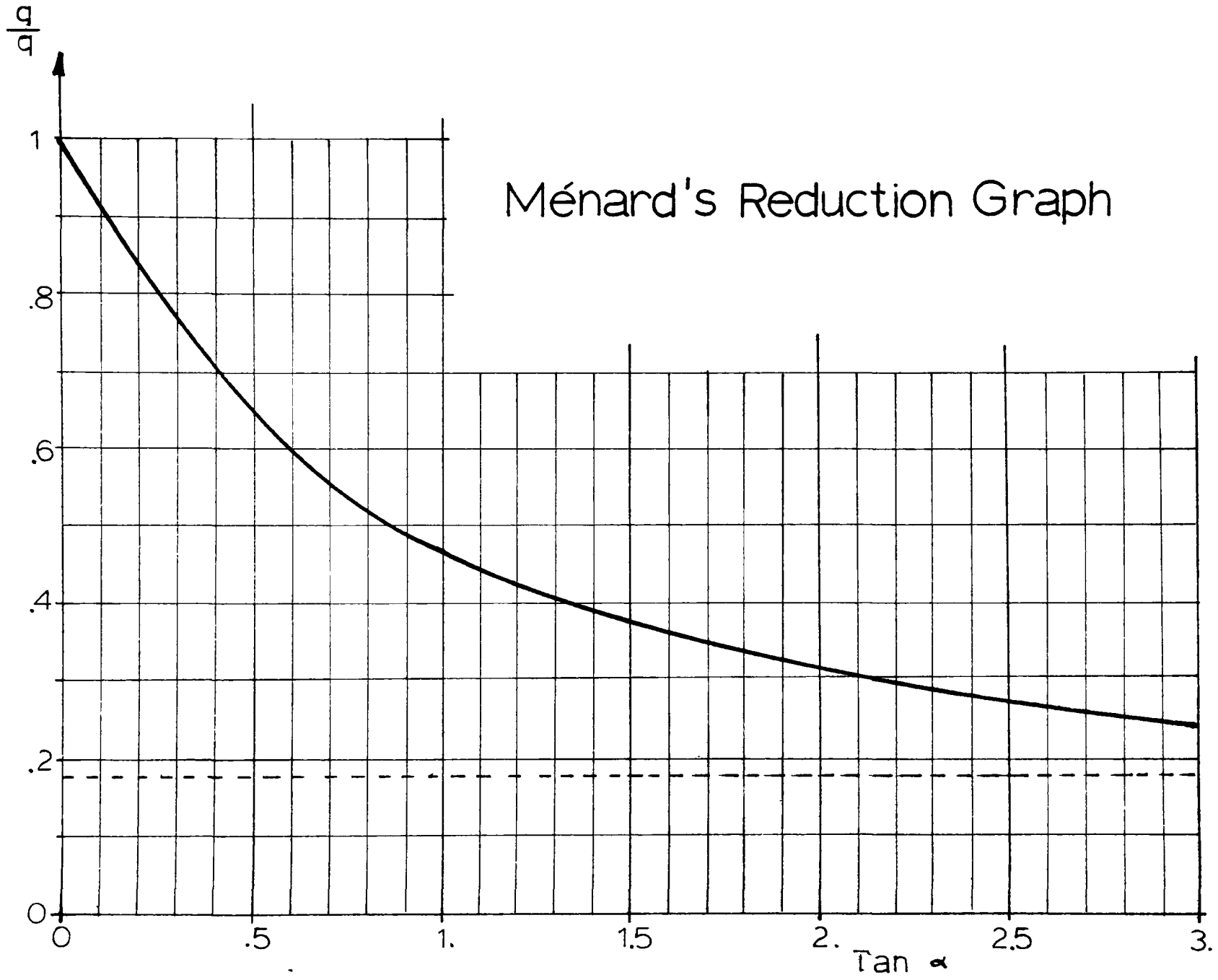

Figure 2.39

Figure 2.41 gives in tabular form a summary of all the basic assumptions that are made in the various theories. This list of assumptions is compatible with the list of variables presented in Figure 1.3. From this table it is possible to see that most theories are based on identical assumptions.

The Meyerhof theory neglects the stresses in the slope, but considers the shearing strength of the surcharge above the footing level. Giroud neglects the shearing strength of the surcharge, but considers the effect of the stresses induced by the slope. The Mizuno model, which considers surface footings only, takes into account the stresses in the slope and, in addition, assumes that the direction of the slip surface has the same direction as the resultant forces acting on the radial planes in the transition zone. The stress distribution along these radial planes is assumed to be triangular. Kovalev computed values of the bearing capacity of footings near slopes using the slip surface he obtained from a stress characteristics mathematical solution. Brinch Hansen's approach is unique because it simply reduces the bearing capacity on flat ground by a factor which is a function of only the angle of the slope. The Absi method is entirely based on the theory proposed by Caquot and Kérisel which considers the initial state of stress in the ground due to self weight. Chen is the only investigator to present results obtained from velocity fields, while Bowles introduces graphical methods where the problem must be constructed to scale.

Ménard, after a number of field experiments, offers reduction factors to take into account the angle of the slope (this is the same as Brinch Hansen's approach).

From Figure 2.40, it can be seen that the Absi theory gives the lowest values of $N_{\gamma q}$, while the Kovalev values are the highest, even higher than the upper bound values of Chen. The other five theories seem to vary only slightly from one another; the exception is the Mizuno case in which $N_{\gamma q}$ goes to zero as the slope angle approaches the value of the angle of internal friction Φ.

The comparison established here is valid only when the footing is located at the top of the slope, that is to say, at its crest.

2.4 Contributions to the Theories of Bearing Capacity on Top of Slopes of Cohesionless Material

2.4.1 General

As previously mentioned in Sections 1.1.3 and 1.3, the experimental program calls for tests to be carried out at certain vertical and horizontal distances from the slope crest. If comparisons are to be made between theory and experiment, theoretical bearing capacity values must be available in the soil mass at the experimental footing locations.

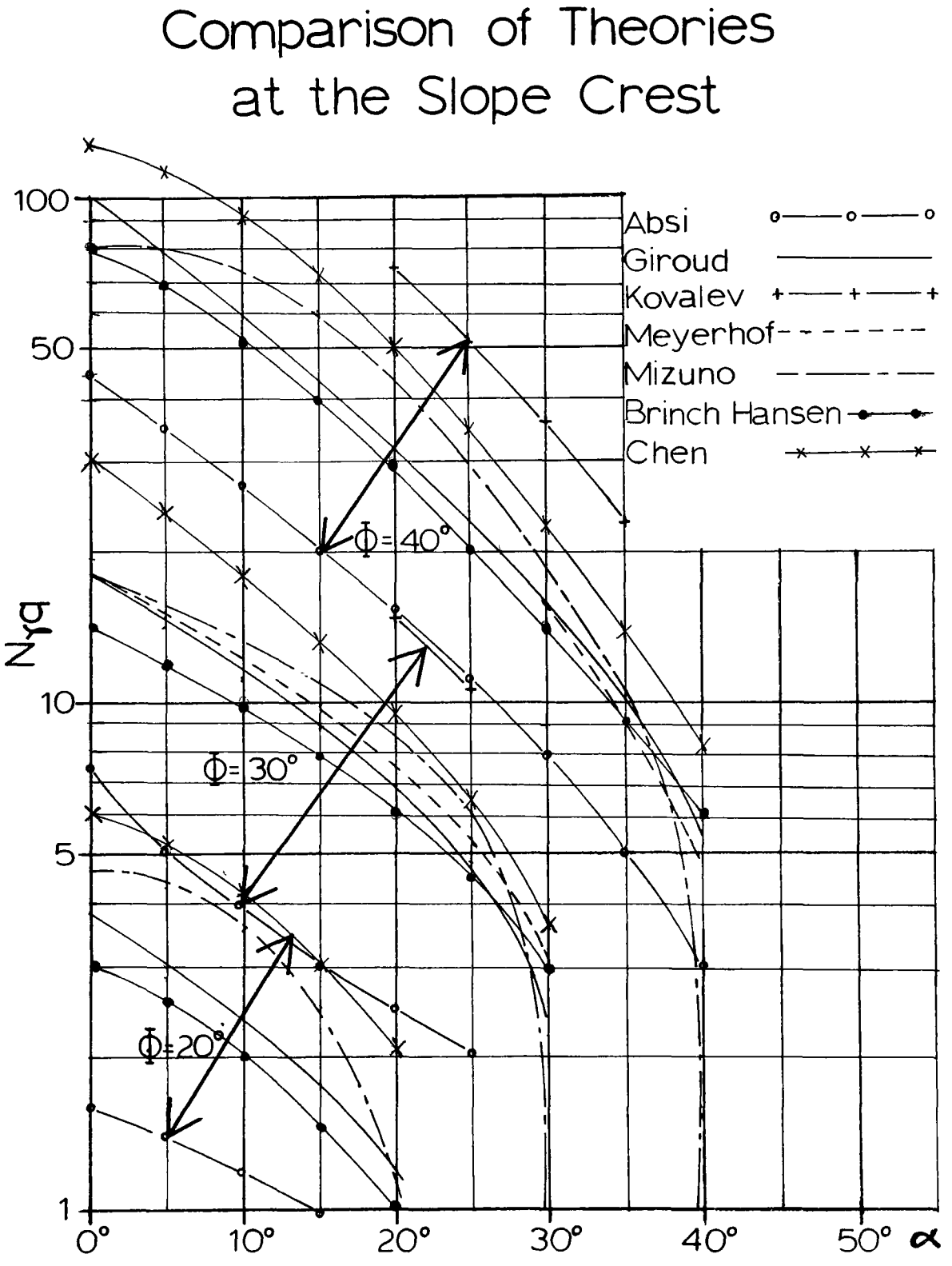
Comparison of Theories
at the Slope Crest
Absi
Giroud
Kovalev
Meyerhof
Mizuno
Brinch Hansen
Chen
Φ= 40°
Φ= 30°
Φ=20°
Nγq
100
50
10
5
1
0°
10°
20°
30°
40°
50°
α

Figure 2.40

Figure 2.41

Basic Assumptions for Each Theory

Assumptions Category \ Theories	Meyerhof (1957)	Mizuno (1960)	Kovalev (1964)	Brinch Hansen (1970)	Giroud (1972)	Absi (1972)	Chen (1974)	Bowles (1975) Bowles (1977)	Ménard (1964)
1-0 Footing									
1-1 Footing properties									
a) shape rectangular	x	x	x	x	x	x	x	x	square
b) size (plane strain)	x	x	x	x	x	x	x	x	--
c) rigidity	x	x	x	x	x	x	x	x	x
d) roughness of base (rough)	x	x	x	x	x	x	x	x	x
e) inalination: horizontal	x	x	x	x	x	x	x	x	x
1-2 Physical location									
a) vertically (surface)	x	x	x	x	x	x	x	x	x
(shallow)	x	-	x	x	x	-	-	x	-
b) horizontally: on top of a slope									
-at slope crest only	x	x	x	x	x	x	x	x	x
-any distance from the slope crest	x	-	-	-	x	-	-	x	-
2-0 Soil Material									
2-1 Type considered									
-cohesionless only	x	x	x	x	x	x	x	x	x

Figure 2.41 (cont'd)

Assumptions Category \ Theories	Meyerhof (1957)	Mizuno (1960)	Kovalev (1964)	Brinch Hansen (1970)	Giroud (1972)	Absi (1972)	Chen (1974)	Bowles (1975) Bowles (1977)	Ménard (1964)
2-2 Properties									
a) homogeneity of footing	x	x	x	x	x	x	x	x	x
b) stress-strain: rigid plastic	x	x	x	x	x	x	-	x	pressure-meter
c) volume change incompressible	x	x	x	x	x	x	x	x	-
d) strength: Mohr-Coulomb representation: straight line	x	x	x	x	x	x	x	x	-
2-3 Water condition: dry and no seepage	x	x	x	x	x	x	x	x	-
3-0 External consideration									
3-1 Geologic geometry									
a) proximity of slope	x	x	x	x	x	x	x	x	x
b) proximity of rigid base or soft layer	-	-	-	-	-	-	-	-	-

Figure 2.41 (cont'd)

Theories / Assumptions Category	Meyerhof (1957)	Mizuno (1960)	Kovalev (1964)	Brinch Hansen (1970)	Giroud (1972)	Absi (1972)	Chen (1974)	Bowles (1975) Bowles (1977)	Ménard (1964)
3-2 Load Application									
a) vertical	x	x	x	x	x	x	x	x	x
b) centric	x	x	x	x	x	x	x	x	x
c) static	x	x	x	x	x	x	x	x	x
4-0 Other Considerations									
a) overburden pressure has shearing resistance	x	-	-	-	-	-	-	-	-
or surcharge only	-	-	x	x	x	-	-	x	-
b) base resistance only	x	x	x	x	x	x	x	x	-
c) mathematical process used									
-limit equilibrium	x	x	-	x	x	x	-	x	-
-stress characteristics	-	-	x	-	-		-	-	-
-velocity fields	-	-	-	-	-	-	x	-	-
-empirical approach	-	-	-	-	-	-	-	-	x

Certain theories, like Meyerhof's (1957), Giroud's (1972) and Bowles' (1975) can be extended or made to yield values of bearing capacity for any footing location in the soil mass. This work has been undertaken and is considered to be a contribution to the topic; the methods used are described in the following paragraphs. To show the theoretical values of bearing capacity at any point in the soil mass, a new presentation of the bearing capacity factors is used and this is described first.

2.4.2 New Presentation of the Results

The Meyerhof (1957) $N_{\gamma q}$ values , which consider the proximity of a slope, are shown in Figures 2.8 and 2.9. A new presentation of these values is found in Figure 2.43; here the theoretical bearing capacity factors are shown as contour lines for a slope of 2 to 1. Presenting the results in this way is intended to give a better idea of the influence of the slope on bearing capacity. The distribution of bearing capacity is applicable to any granular soil. The scale of the diagram is the footing width B.

As an example of how the figure can be used to compare bearing capacities, if a footing is located at a horizontal distance equal to 2B, away from the slope, and at a depth of D = ½B, the bearing capacity is predicted to be twice that of a footing of the same width but located at the same depth at the crest of the slope (32 vs 16 in terms of $N_{\gamma q}$ for Φ =

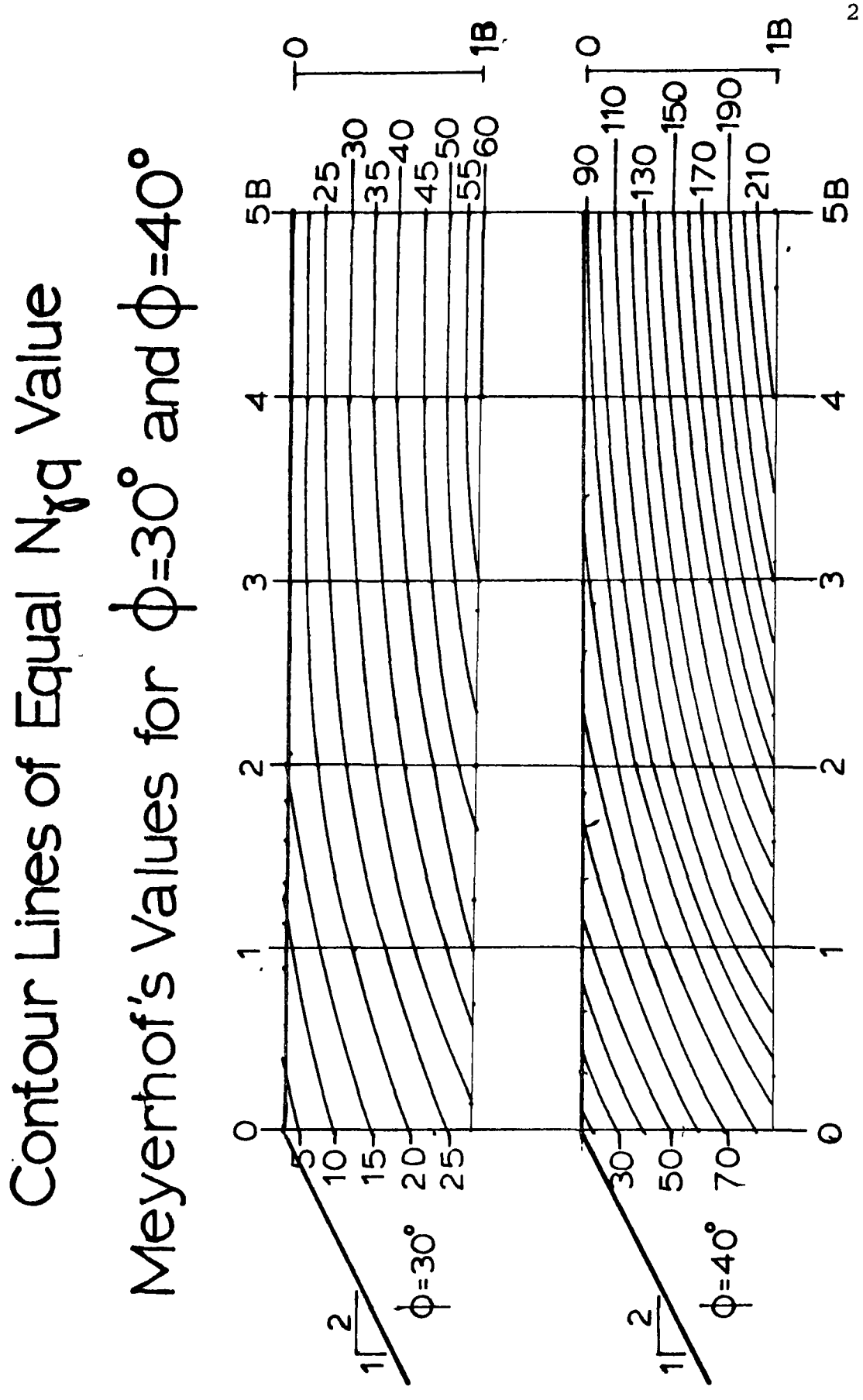
Contour Lines of Equal $N_{\gamma q}$ Value
Meyerhof's Values for $\phi=30°$ and $\phi=40°$
0
1B
5B
25
30
35
40
45
50
55
60
90
110
130
150
170
190
210
4
3
2
1
0
5
10
15
20
25
30
50
70
$\phi=30°$
$\phi=40°$
2
1

Figure 2.42

30° and 110 vs 55 for Φ = 40°).

2.4.3 Extension of the Meyerhof (1957) Values

Meyerhof (1957) presented values of $N_{\gamma q}$ for footings located on top of a slope for only two Φ angles, 30° and 40°, and for two depths, $\frac{D}{B}$ = 0, and $\frac{D}{B}$ = 1. Using the theories of Meyerhof (1951) Meyerhof (1955) and the discussion of Vogel and Baracos (1973), it was possible to set up a computer program to find $N_{\gamma q}$ values for the following conditions:

Φ = 30°, 35°, 40° and 45°.

$\frac{D}{B}$ = 0, 1, 2 and 3

The program pinpoints the center of the log spiral at different locations above and beneath the leading edge of the footing. The corner angle of the elastic wedge underneath the footing was also varied as recommended by Meyerhof (1955) and Vogel and Baracos (1973). The method is presented, described and discussed at length in appendix B.

The results from this computerized method are found in Figures 2.43, 2.44, 2.45, and 2.46. It is noted that the values are identical to those of Meyerhof (1957) for Φ = 30° and Φ = 40° and for $\frac{D}{B}$ = 0 and 1. The slope angle α was kept constant at 2:1 throughout the analysis.

Meyerhof's Extended $N_{\gamma q}$ Values

for $\Phi = 30^\circ$ and $\alpha = 26.6^\circ$

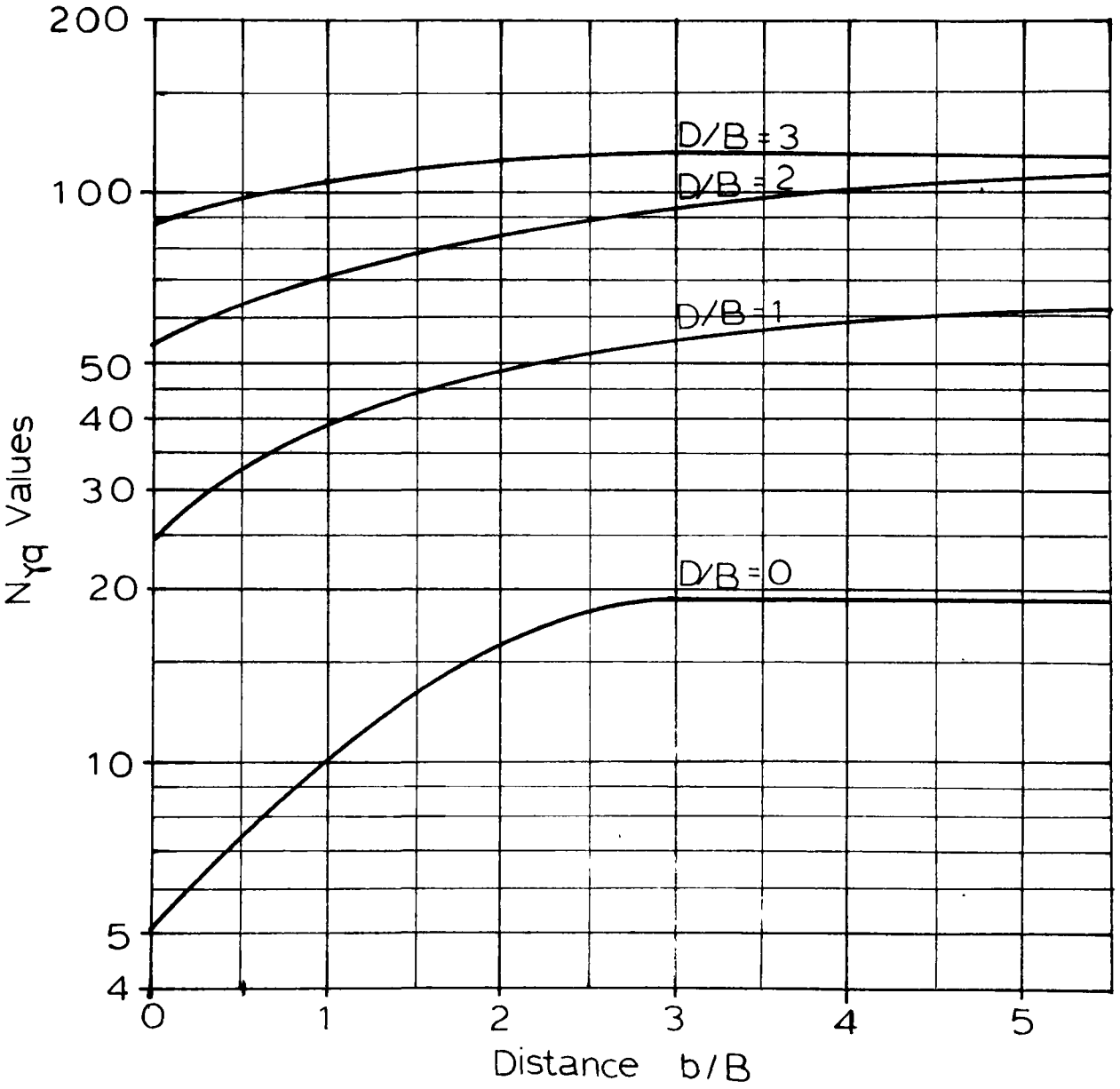

Figure 2.43

Meyerhof's Extended $N_{\gamma q}$ Values

for $\Phi = 35°$ and $\alpha = 26.6°$

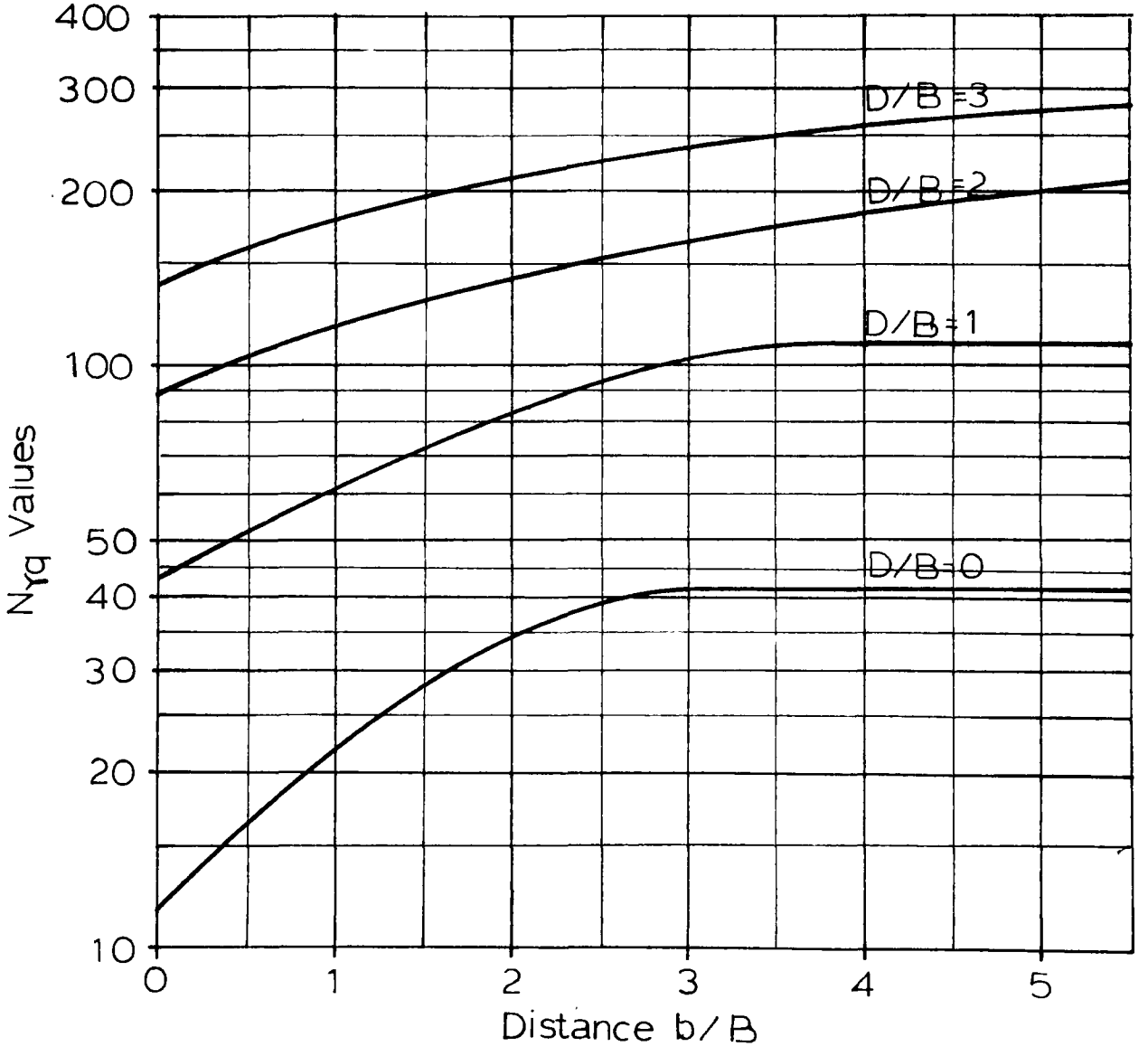

Figure 2.44

Meyerhof's Extended $N_{\gamma q}$ Values

for $\Phi = 40°$ and $\alpha = 26.6°$

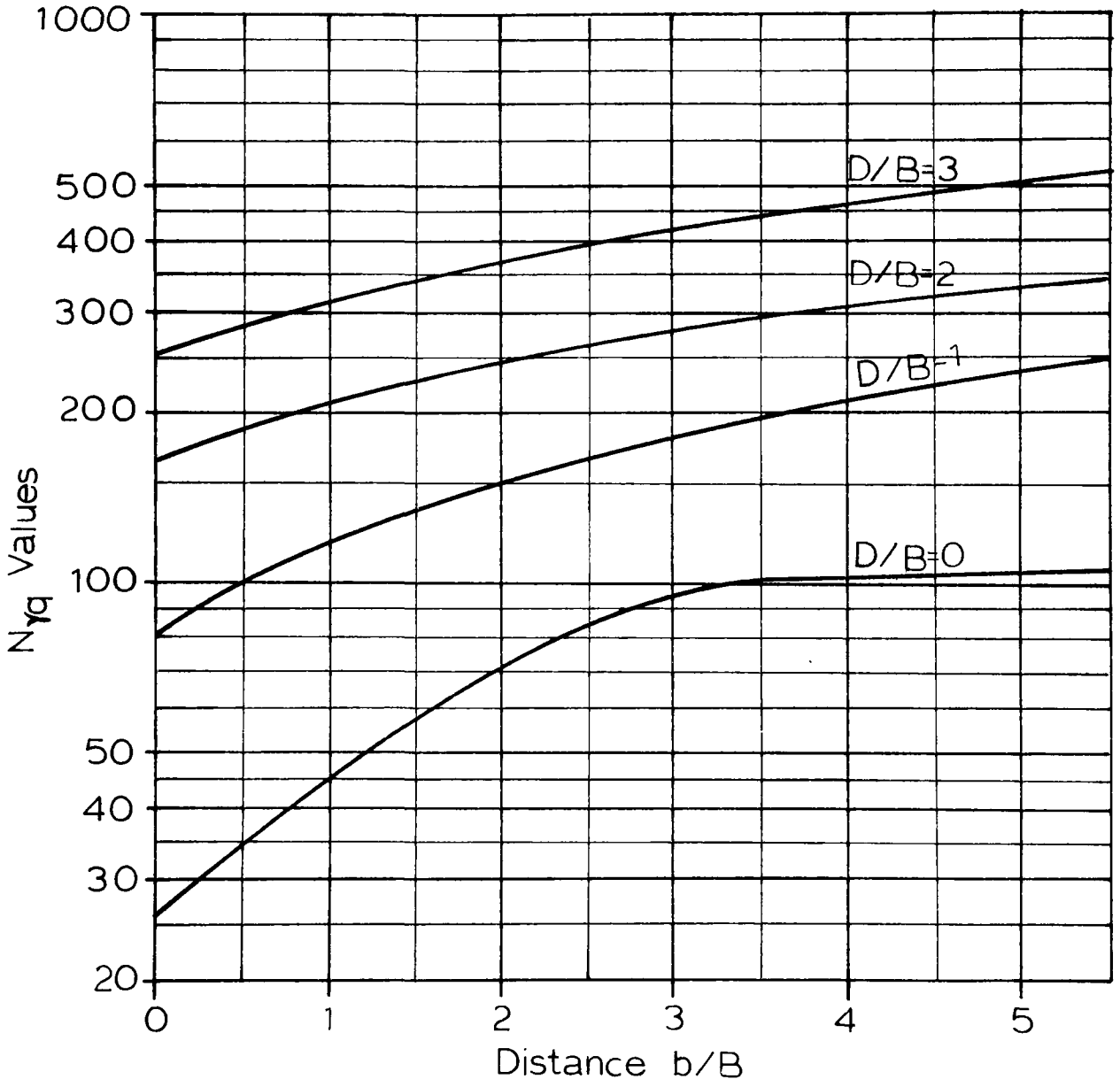

Figure 2.45

Meyerhof's Extended $N_{\gamma q}$ Values

for $\Phi = 45°$ and $\alpha = 26.6°$

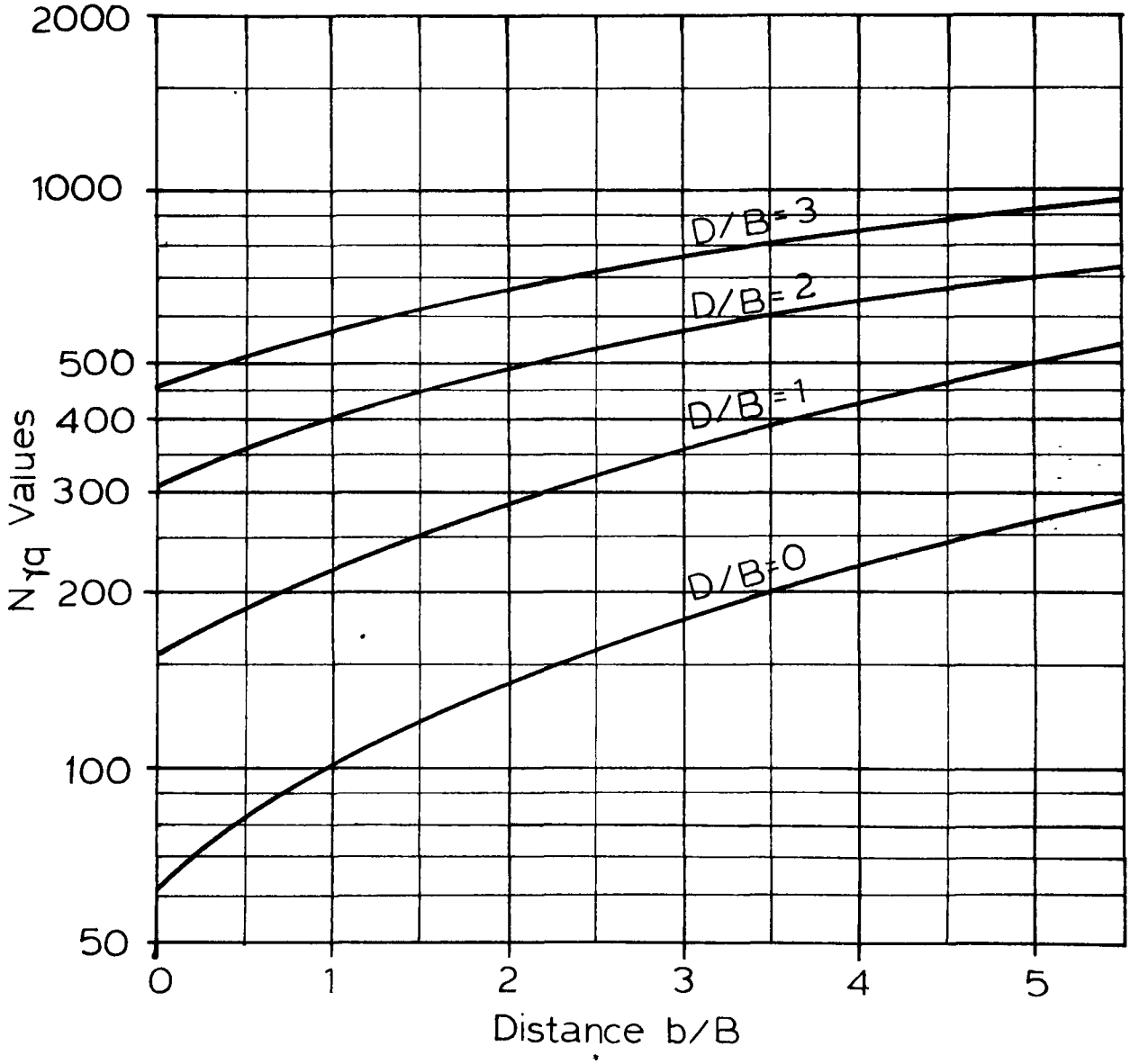

Figure 2.46

2.4.4 Extension of Giroud Values

Giroud and Tran-Vo-Nhiem (1972) presented a means of finding bearing capacity factors for a footing located at the slope crest. They also introduced a method by which the value of $N_{\gamma q}$ can be found for footings located at any horizontal distance from the slope crest. This method involves assuming that a fictitious slope exists from the footing edge to the sloping ground surface as shown in Figure 2.47. The fictitious slope is called the equivalent slope α' and its location and angle are determined by means of charts which are constructed from the equation of the slip surface. These charts are given for different Φ angles in Figures 2.48 through 2.56.

In order to use the charts, the geometric configuration of the problem is drawn to the scale of the charts in terms of the footing width B. Then the particular chart for the Φ value of the soil is superimposed on the geometric configuration. As shown in Figure 2.47, the point of intersection of the curved line on the chart and the sloping ground surface is noted. From this point of intersection a straight line is drawn to the leading edge of the footing; the slope of this straight line is the equivalent slope α'. Now the footing is located at the crest of a slope - albeit a fictitious one - and Giroud gives values of $N_{\gamma\alpha}$ and $N_{q\alpha}$ for footings at the crest of a slope. The two expressions, $N_{\gamma\alpha}$ and $N_{q\alpha}$ combine to give $N_{\gamma q}$.

Giroud's Equivalent Slope

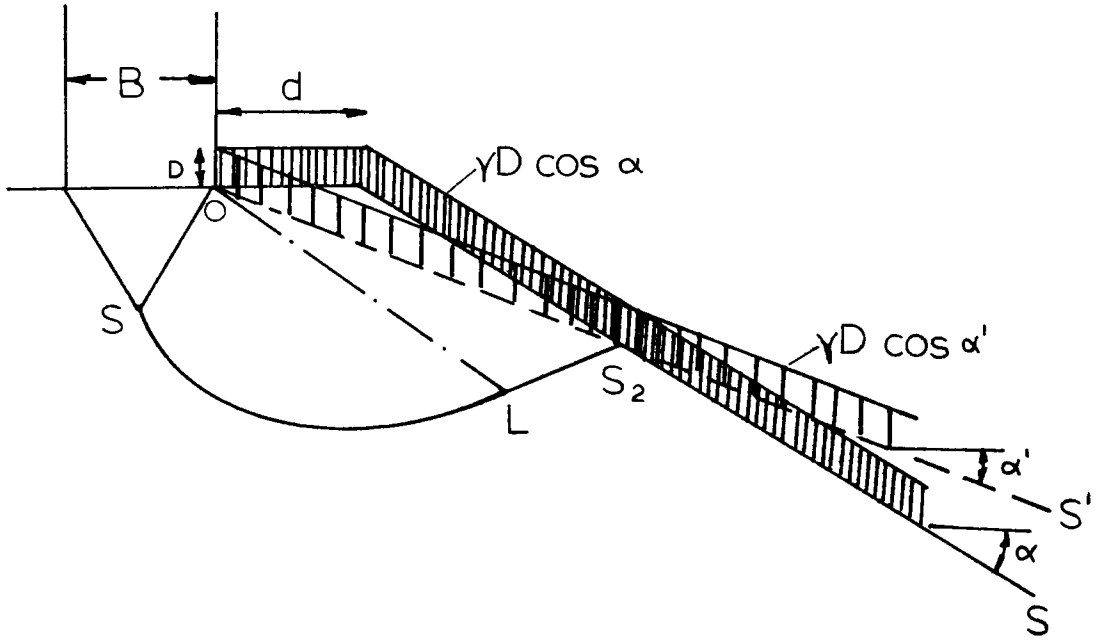

Figure 2.47

Giroud's Equivalent α' Slope Chart

For $\phi = 30°$

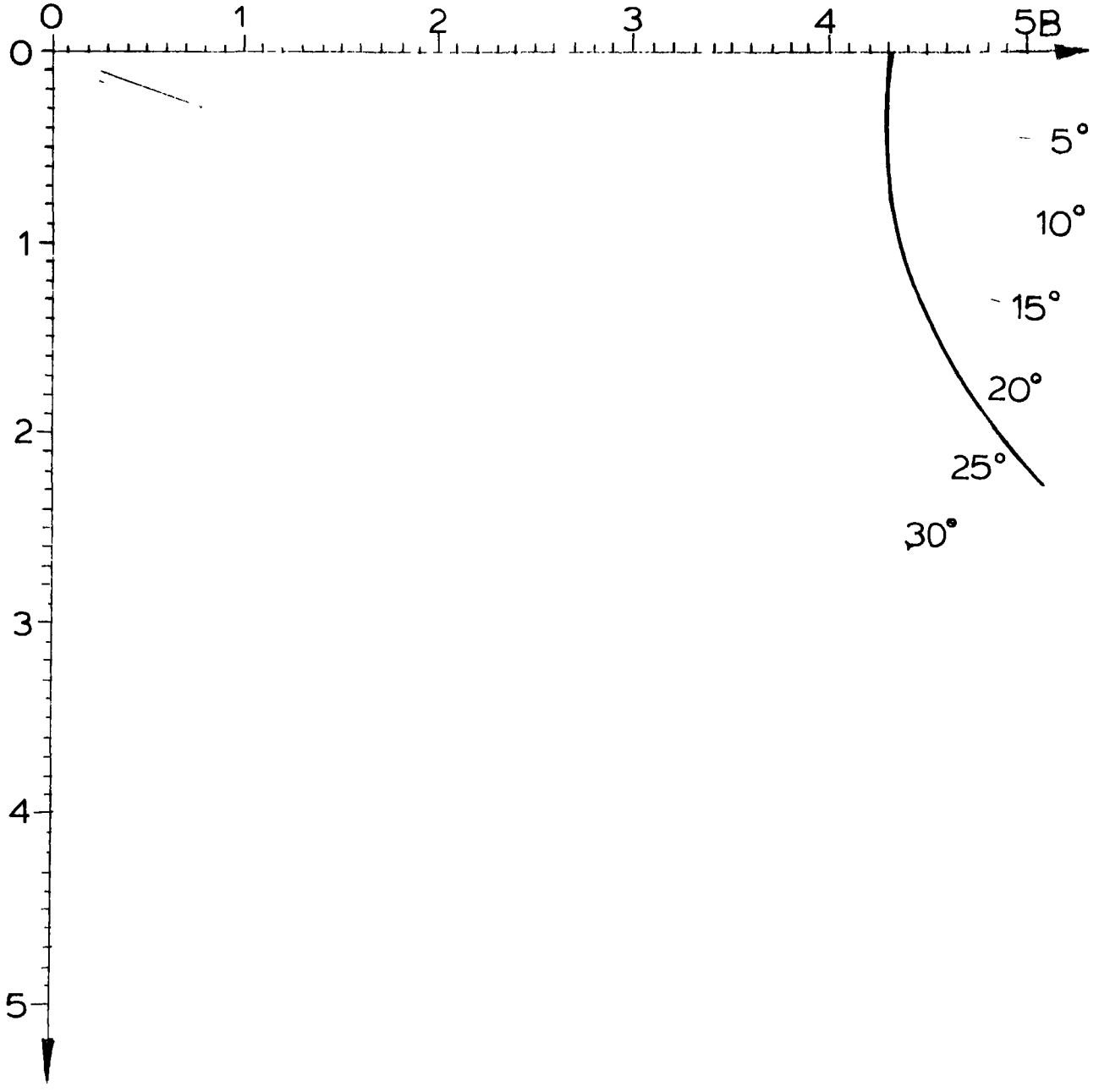

Figure 2.48

Giroud's Equivalent α' Slope Chart

For $\phi = 35°$

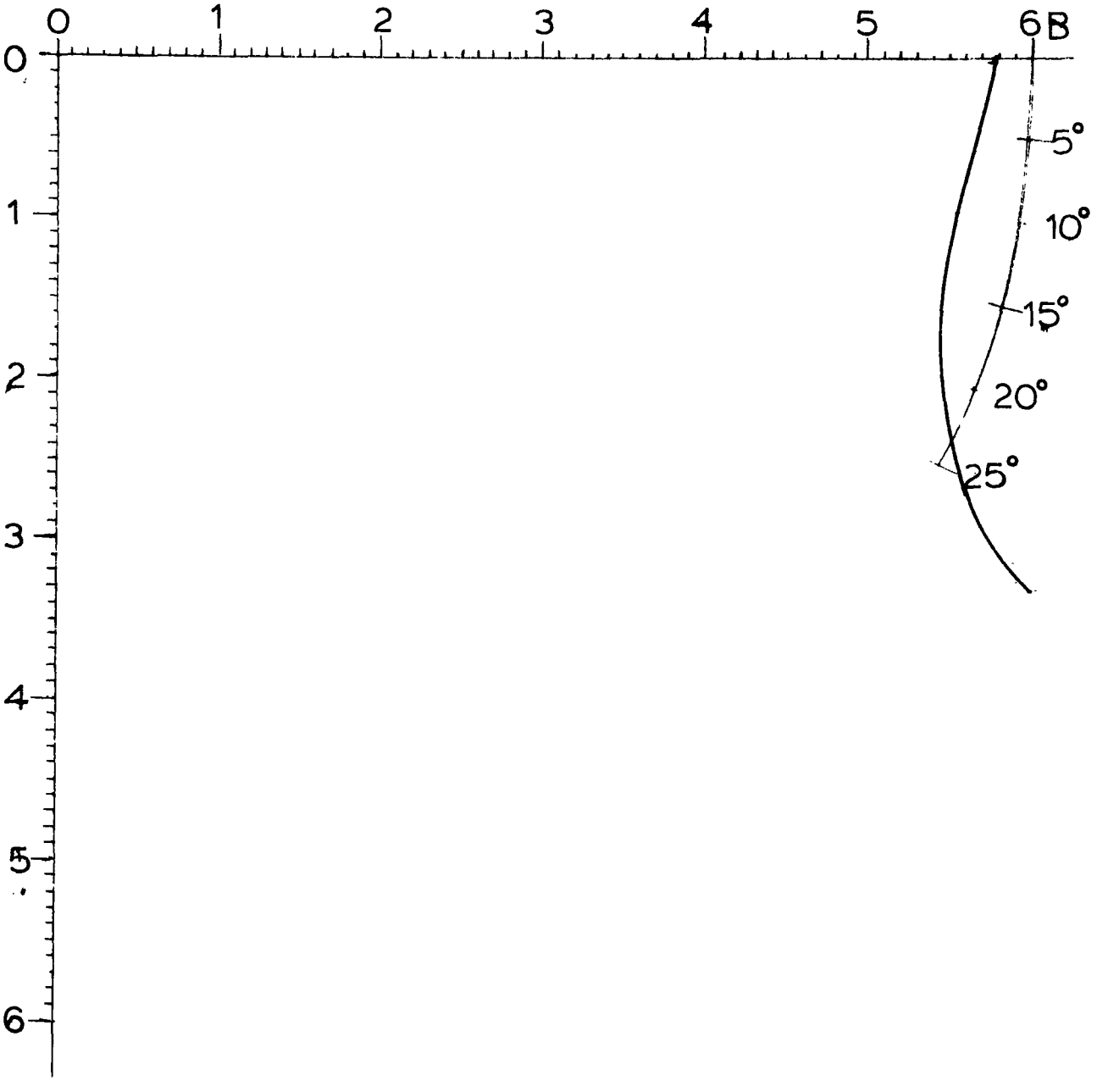

Figure 2.49

Giroud's Equivalent α' Slope Chart

For $\Phi = 37°$

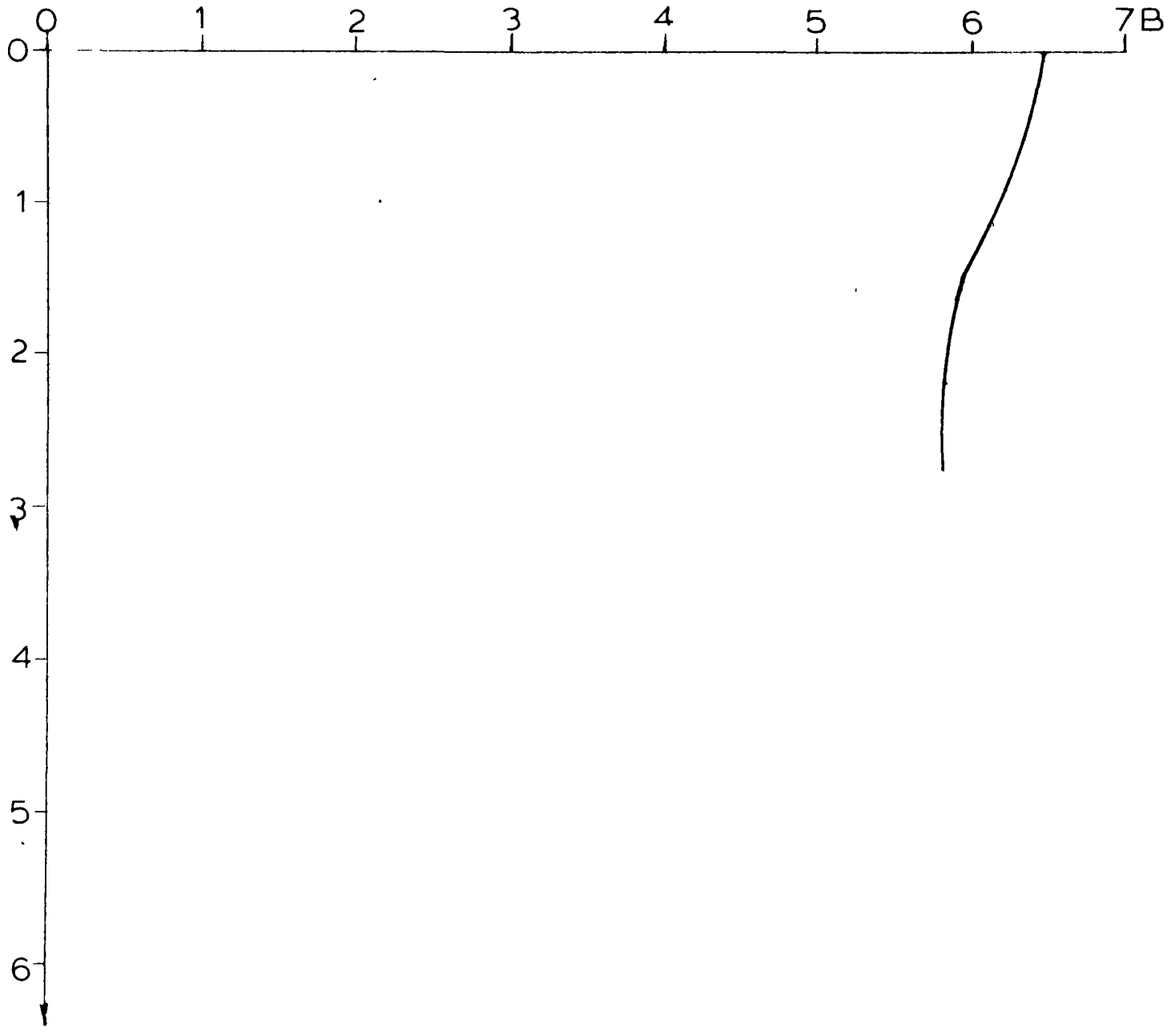

Figure 2.50

Giroud's Equivalent α' Slope Chart

For $\phi = 40°$

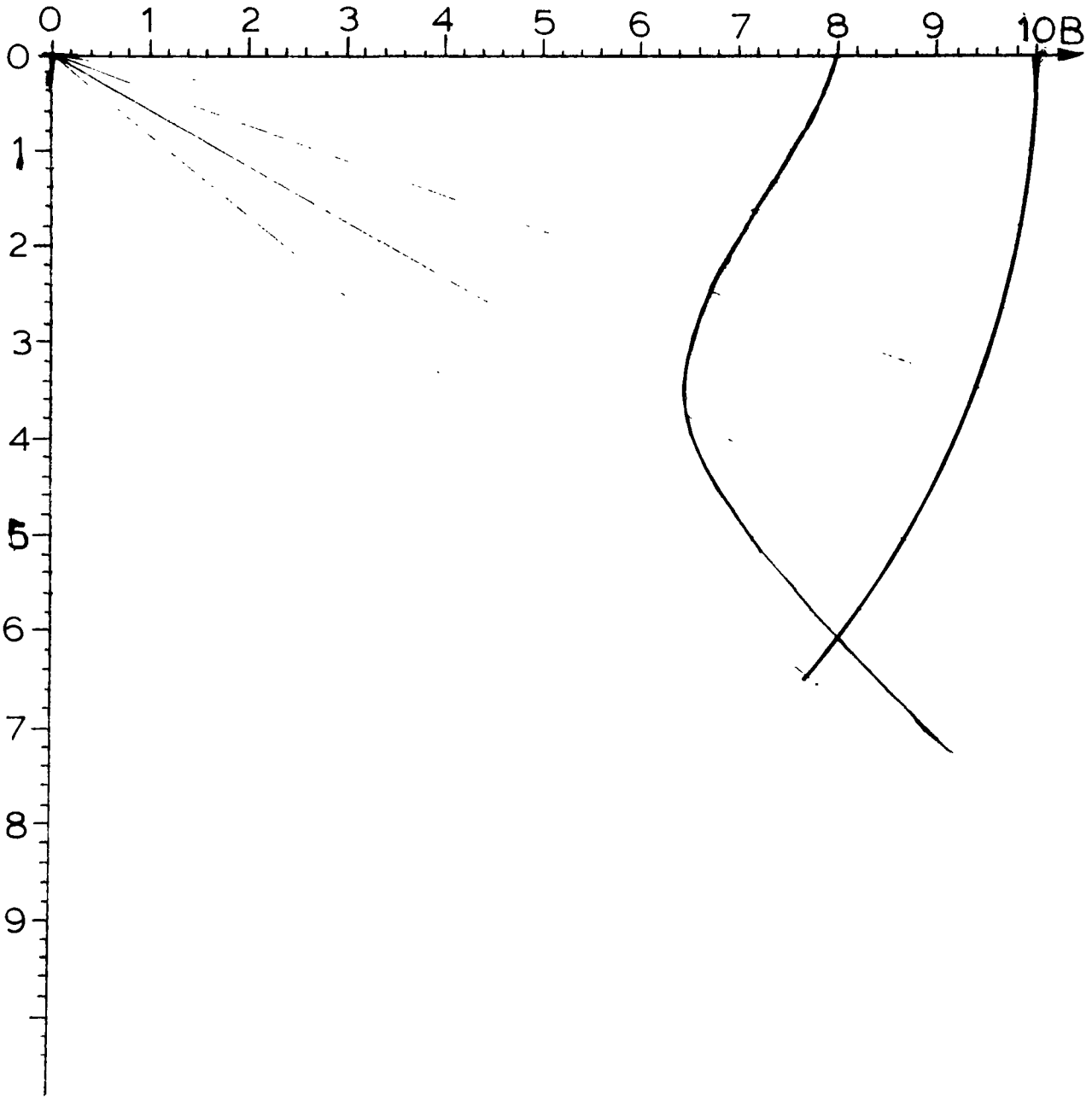

Figure 2.51

Giroud's Equivalent α' Slope Chart

For $\Phi = 41°$

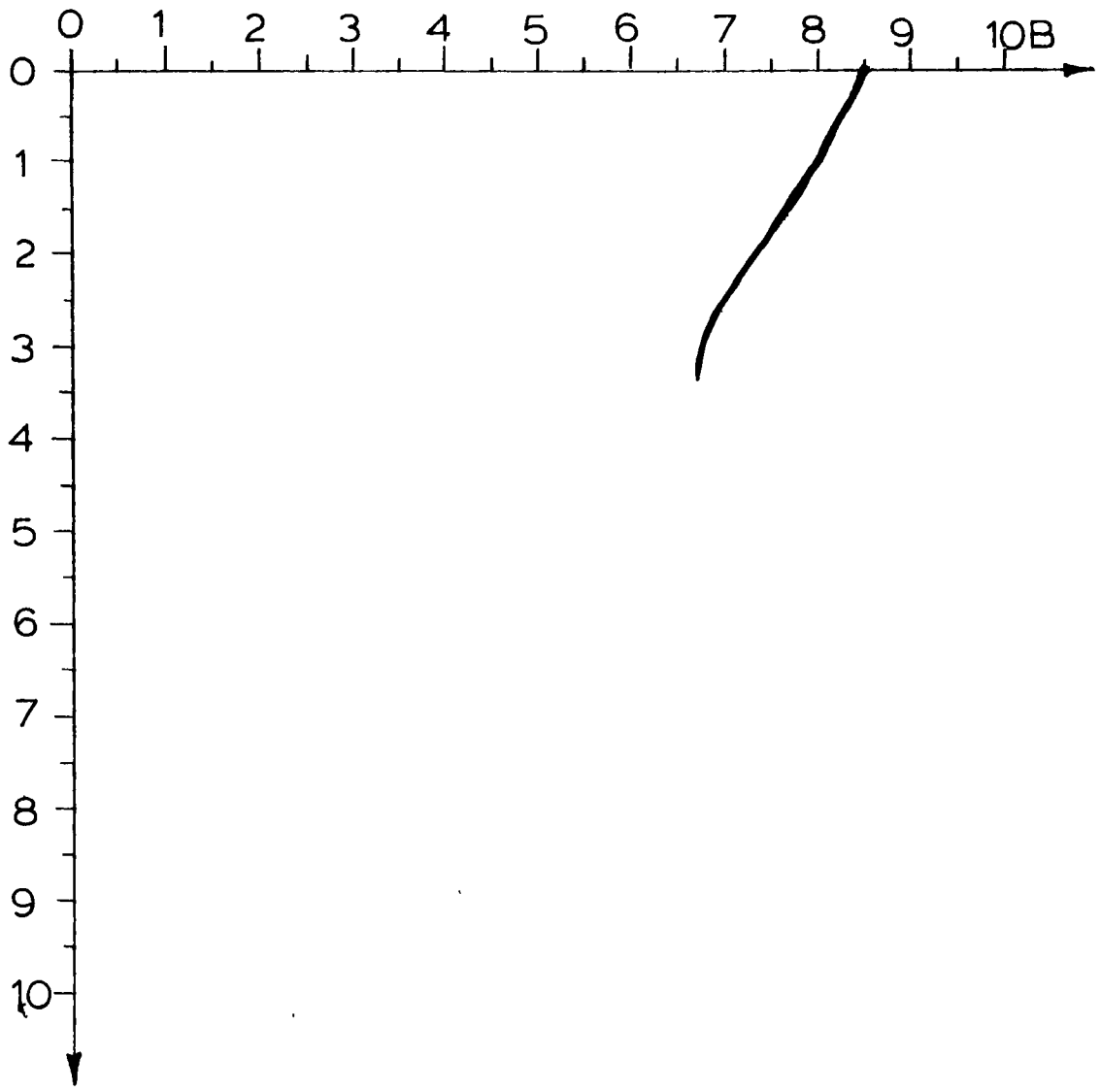

Figure 2.52

Giroud's Equivalent α' Slope Chart

For $\phi = 45°$

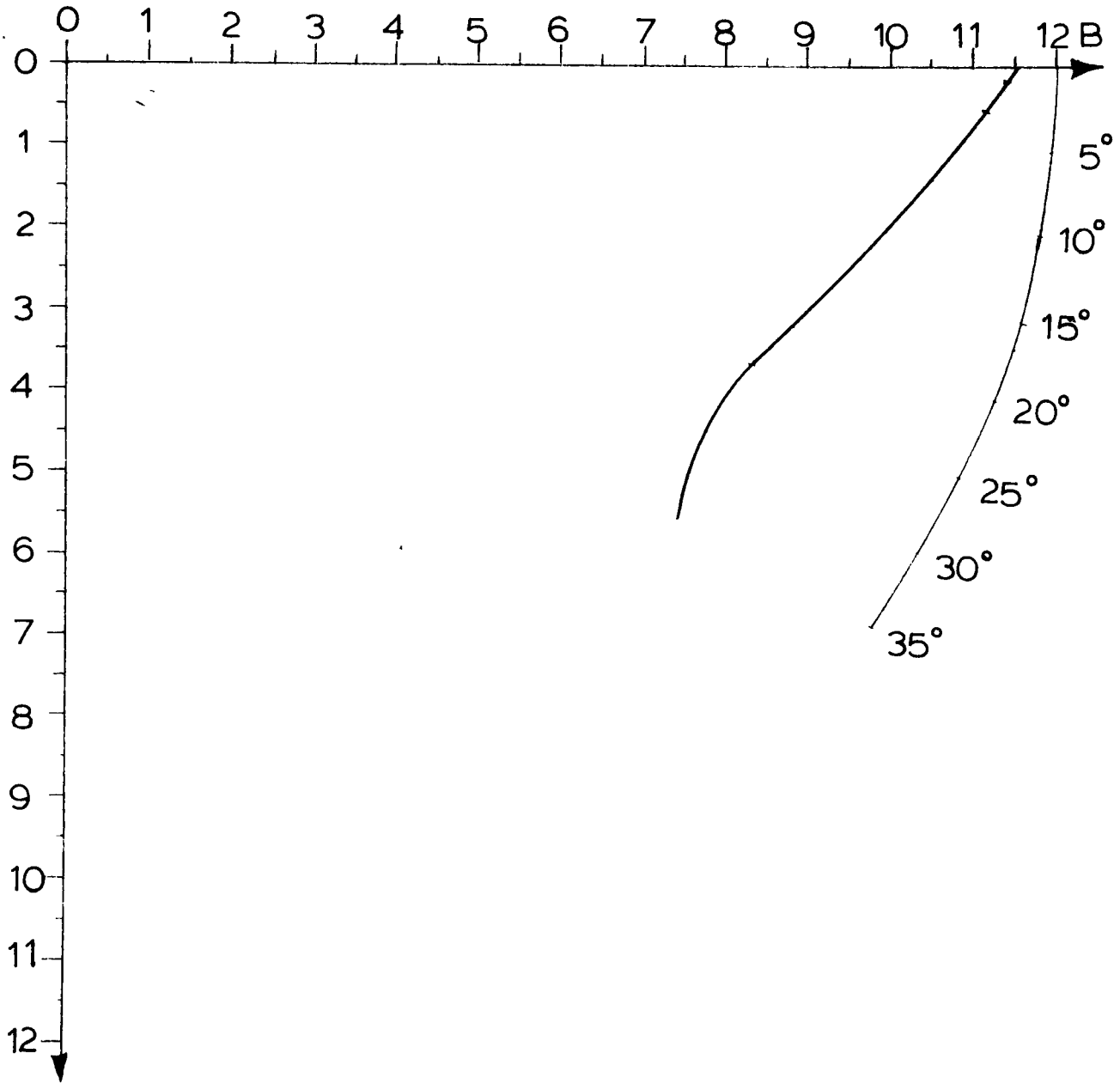

Figure 2.53

Giroud's Equivalent α' Slope Chart

For $\Phi = 48°$

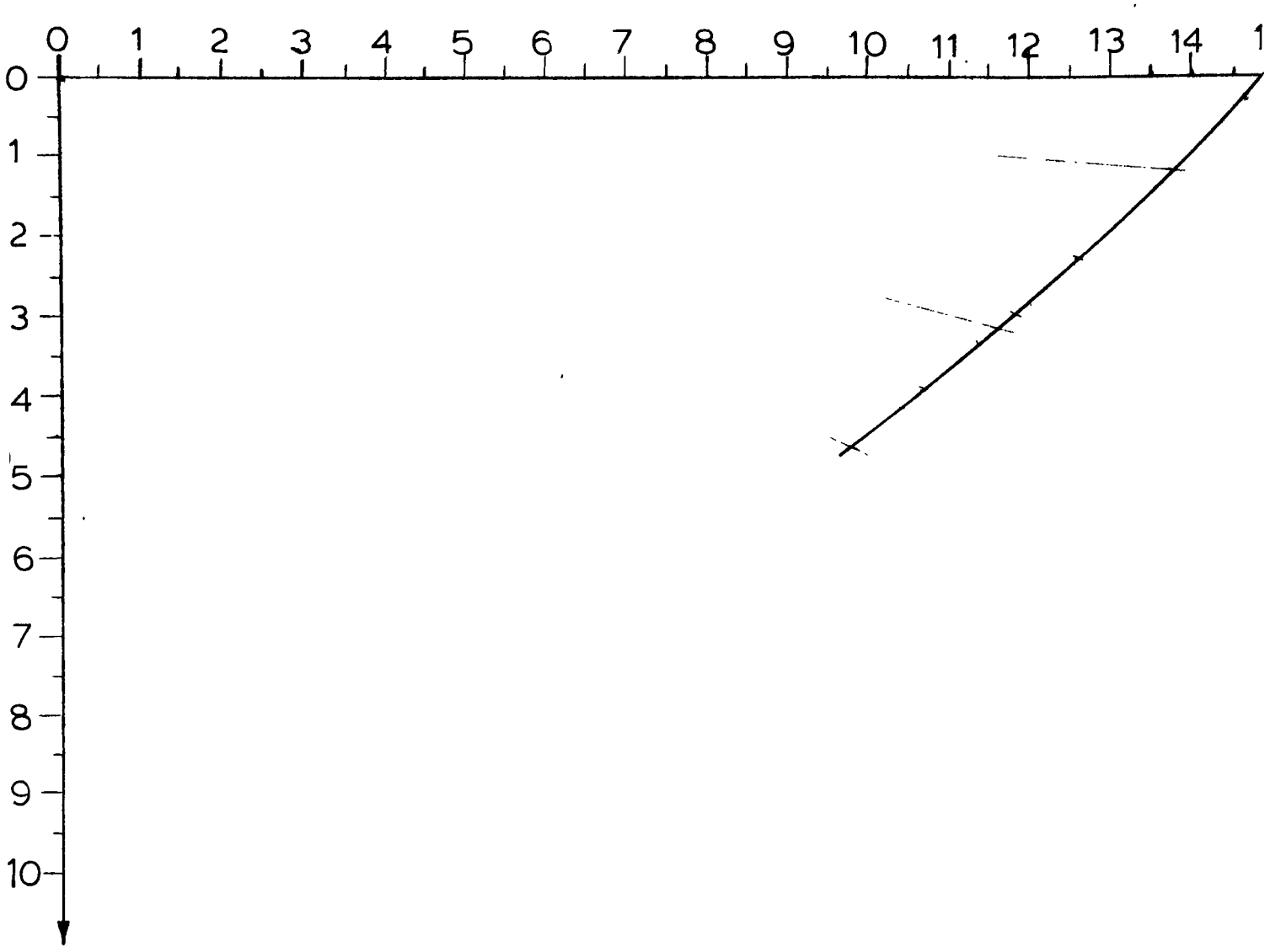

Figure 2.54

Giroud's Equivalent α' Slope Chart

For $\phi = 50°$

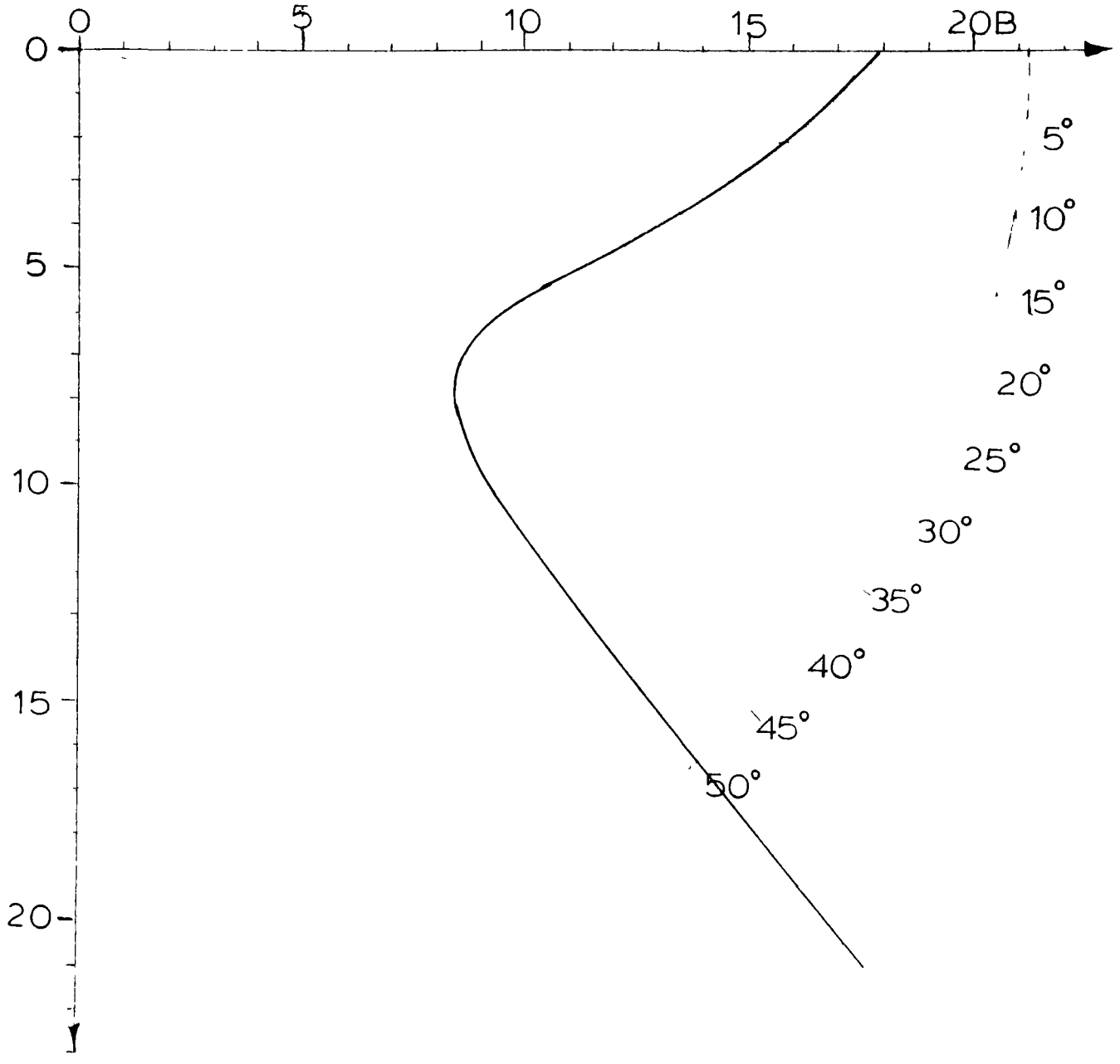

Figure 2.55

Use of Giroud's Equivalent α' Slope Charts

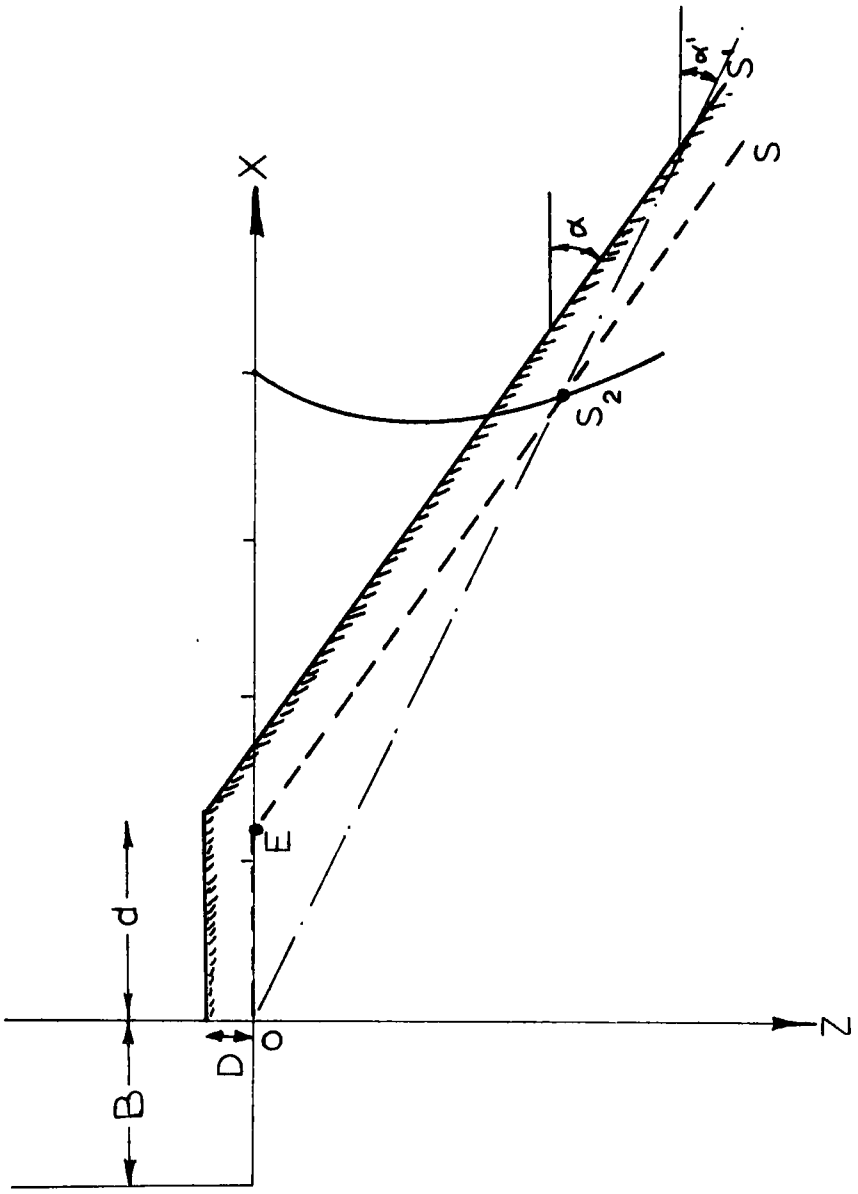

Figure 2.56

$$N_{\gamma q} = N_{\gamma \alpha} + 2\frac{D}{B} \cos\alpha \, N_{q\alpha} \qquad (2.4.4.1)$$

Values for $N_{\gamma q}$ were found using the method of the equivalent slope for a 2:1 real slope; for Φ angles of 30°, 35°, 40°, 45° and 50°; for depths of $\frac{D}{B}$ = 0, 1, 2, 3; and for horizontal distances from the slope crest of $\frac{b}{B}$ = 0, 1, 2, 3, 4 and 5. These $N_{\gamma q}$ values are presented in graphical form in Figures 2.57 to 2.61. These values are also presented in Figures 2.62 to 2.66 as contour lines of bearing capacity.

2.4.5 Example of Bowles' (1975) Solution

Bowles (1975) suggested a method for determining the safe bearing capacity of a footing on top of a slope of cohesionless material. The method is described in Section 2.3.9. Since no examples of the method were worked out in the original reference, an example is given here of the way in which the method can be used for the case of a footing located at the crest of a slope of soil having Φ = 30°. Using the construction given in Section 2.3.9, the geometry at failure is as shown in Figure 2.67.

The equilibrium conditions are checked by a method similar to the Swedish method of slices used in slope stability analyses. The tangential forces acting along the slip surfaces are equated to the shearing resistance along the same slip surfaces.

For each slice the following equation can be established:

Giroud's $N_{\gamma q}$ Values

for $\phi = 30°$ and $\alpha = 26.6°$

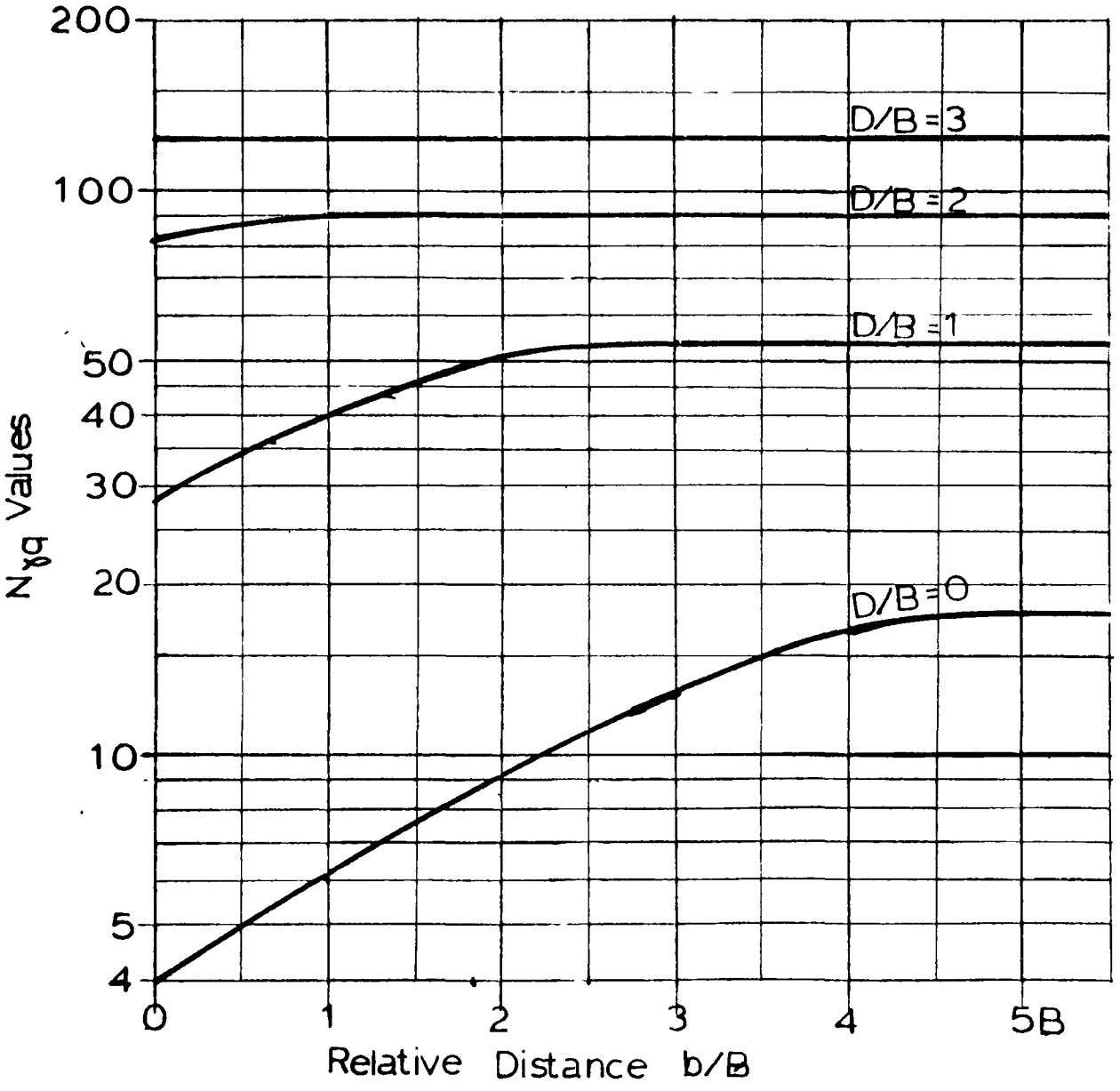

Figure 2.57

Giroud's $N_{\gamma q}$ Values

for $\phi = 35°$ and $\alpha = 26.6°$

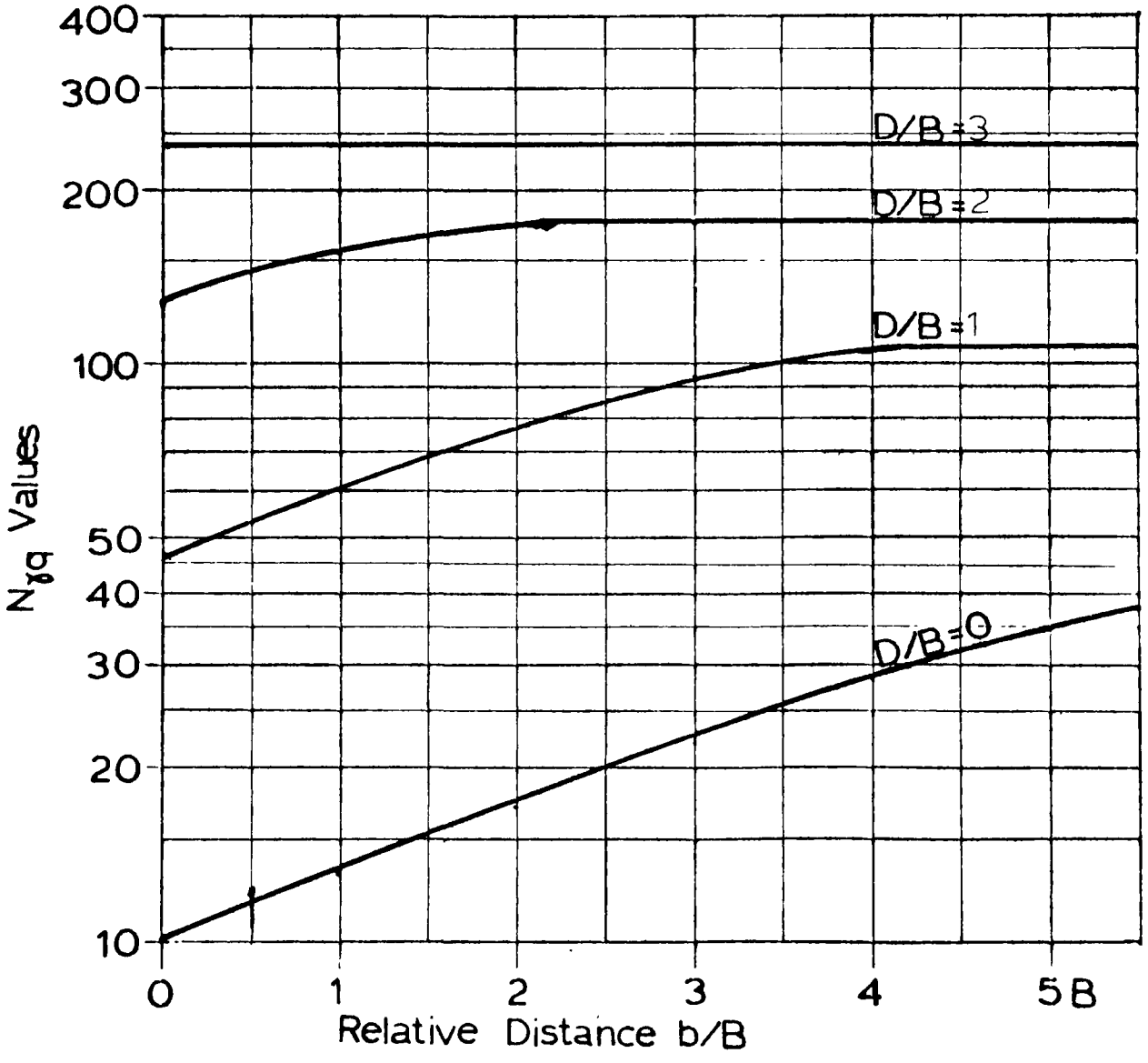

Figure 2.58

Giroud's $N_{\gamma q}$ Values

for $\phi = 40°$ and $\alpha = 26.6°$

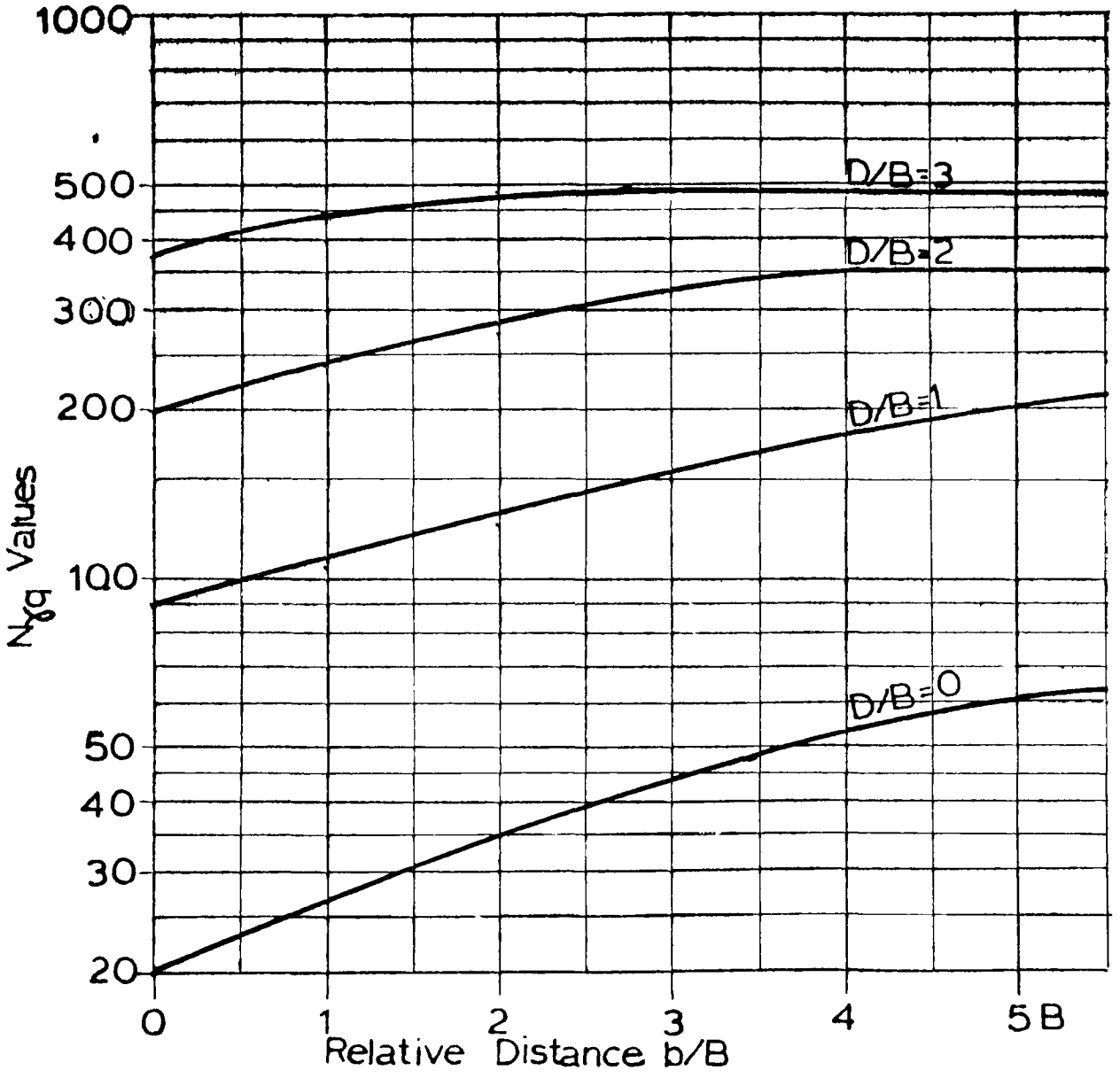

Figure 2.59

Giroud's $N_{\gamma q}$ Values

for $\phi = 45°$ and $\alpha = 26.6°$

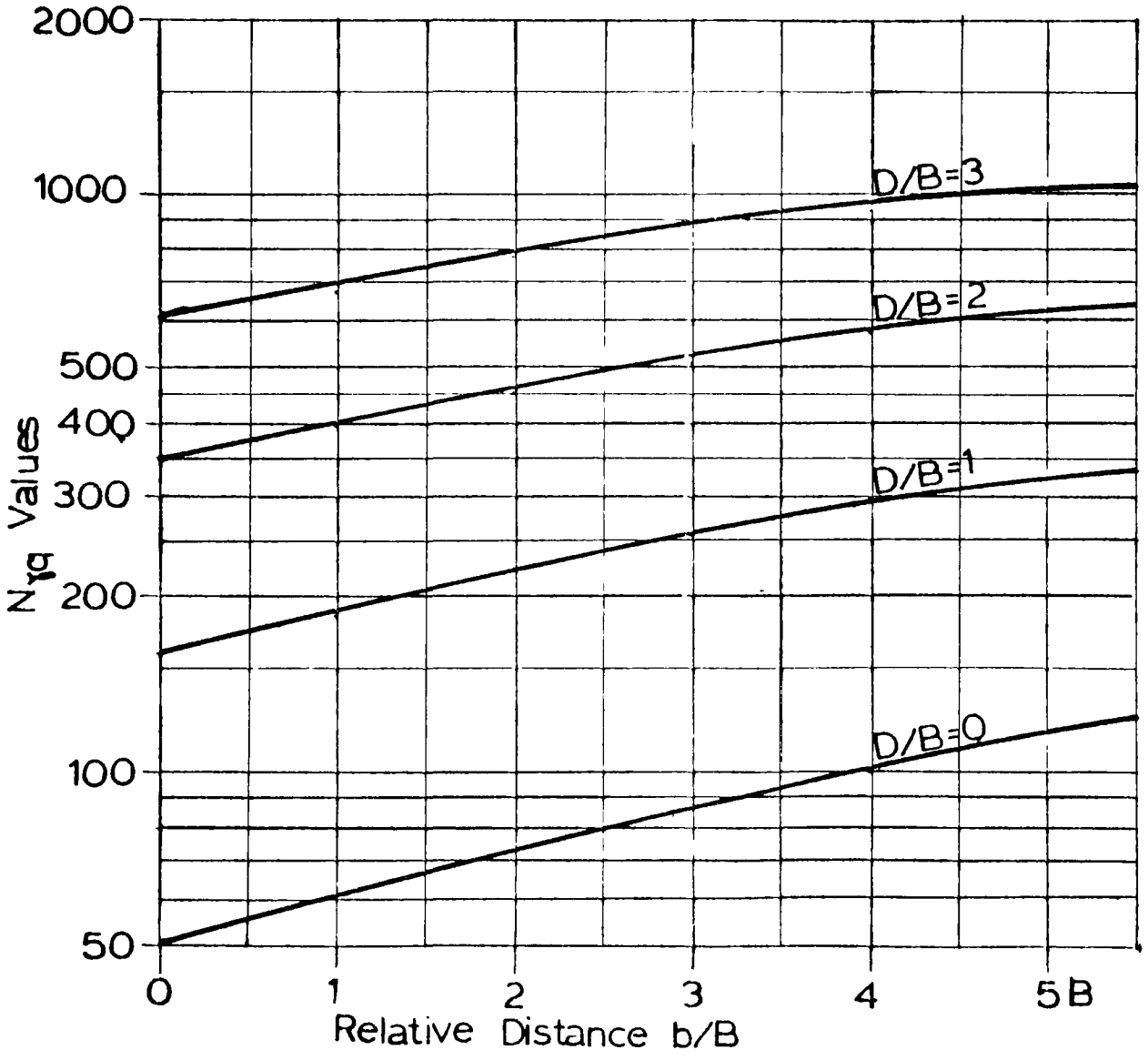

Figure 2.60

Giroud's $N_{\gamma q}$ Values

for $\phi = 50°$ and $\alpha = 26.6°$

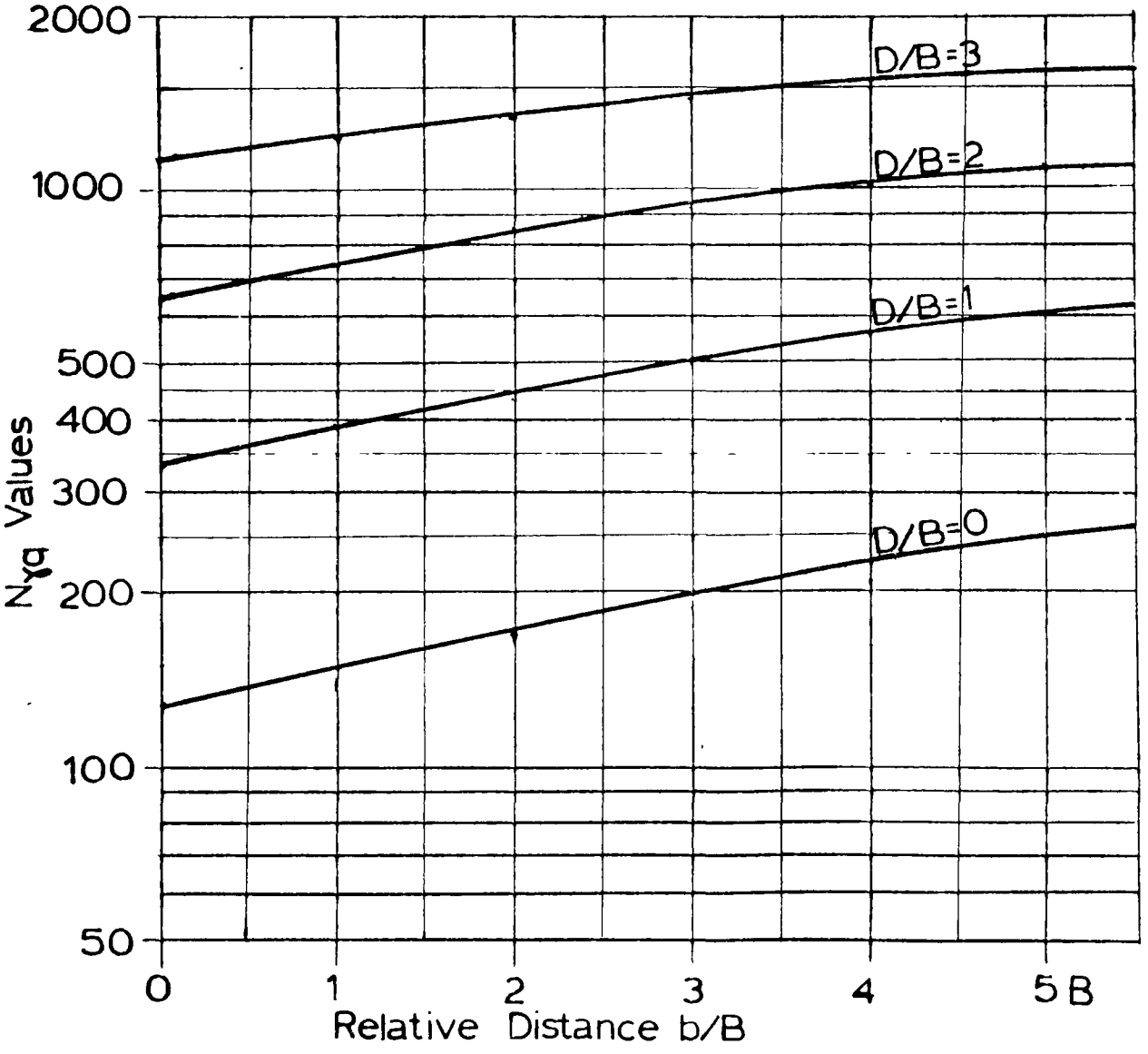

Figure 2.61

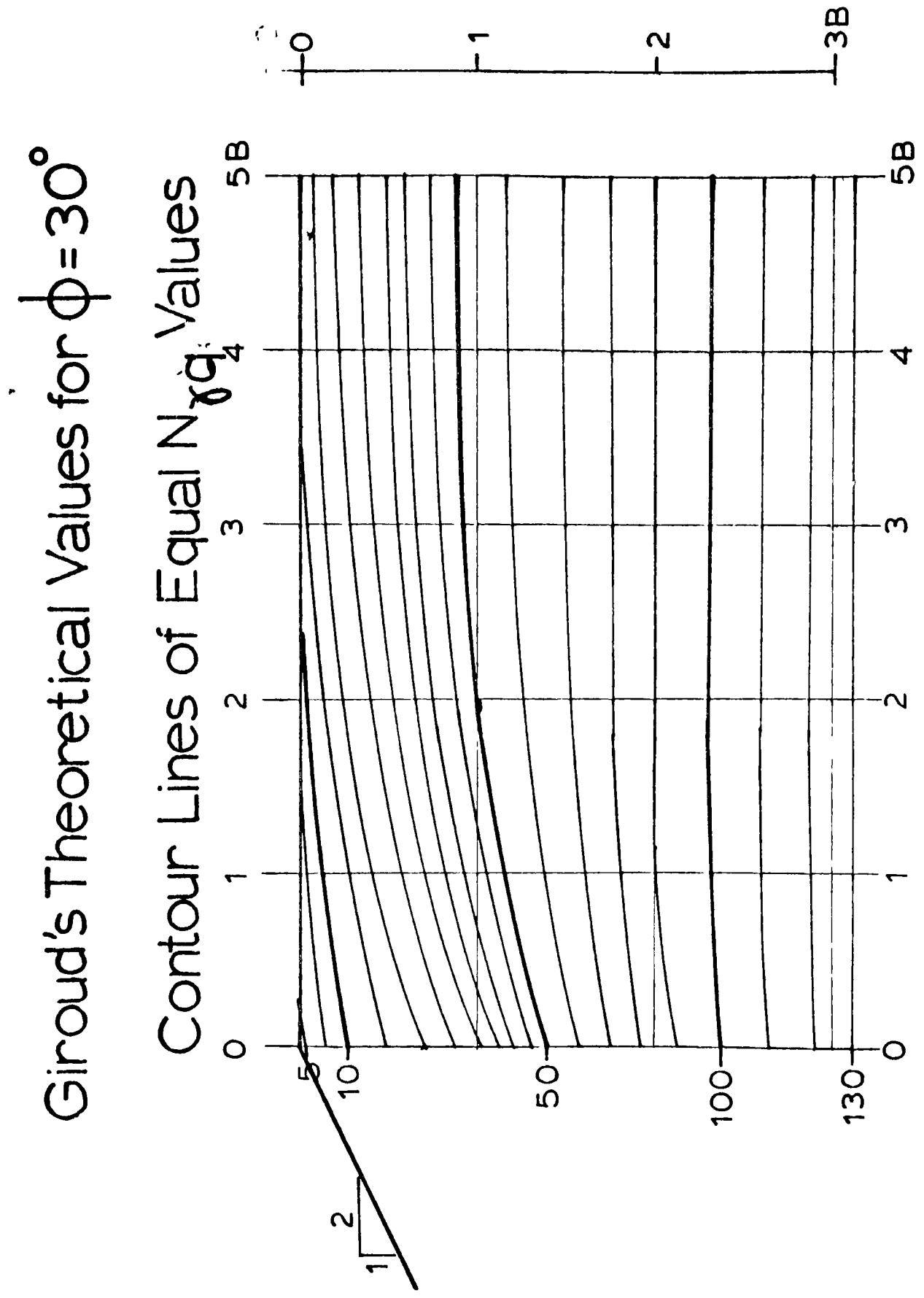
Giroud's Theoretical Values for $\phi = 30^\circ$
Contour Lines of Equal $N_{\gamma q_4}$ Values
0
1
2
3B
5B
0
1
2
3
4
5B
5
10
50
100
130
2
1

Figure 2.62

Contour Lines of Equal $N_{\gamma q}$ Value

Giroud's Theoretical Values for $\phi = 35°$

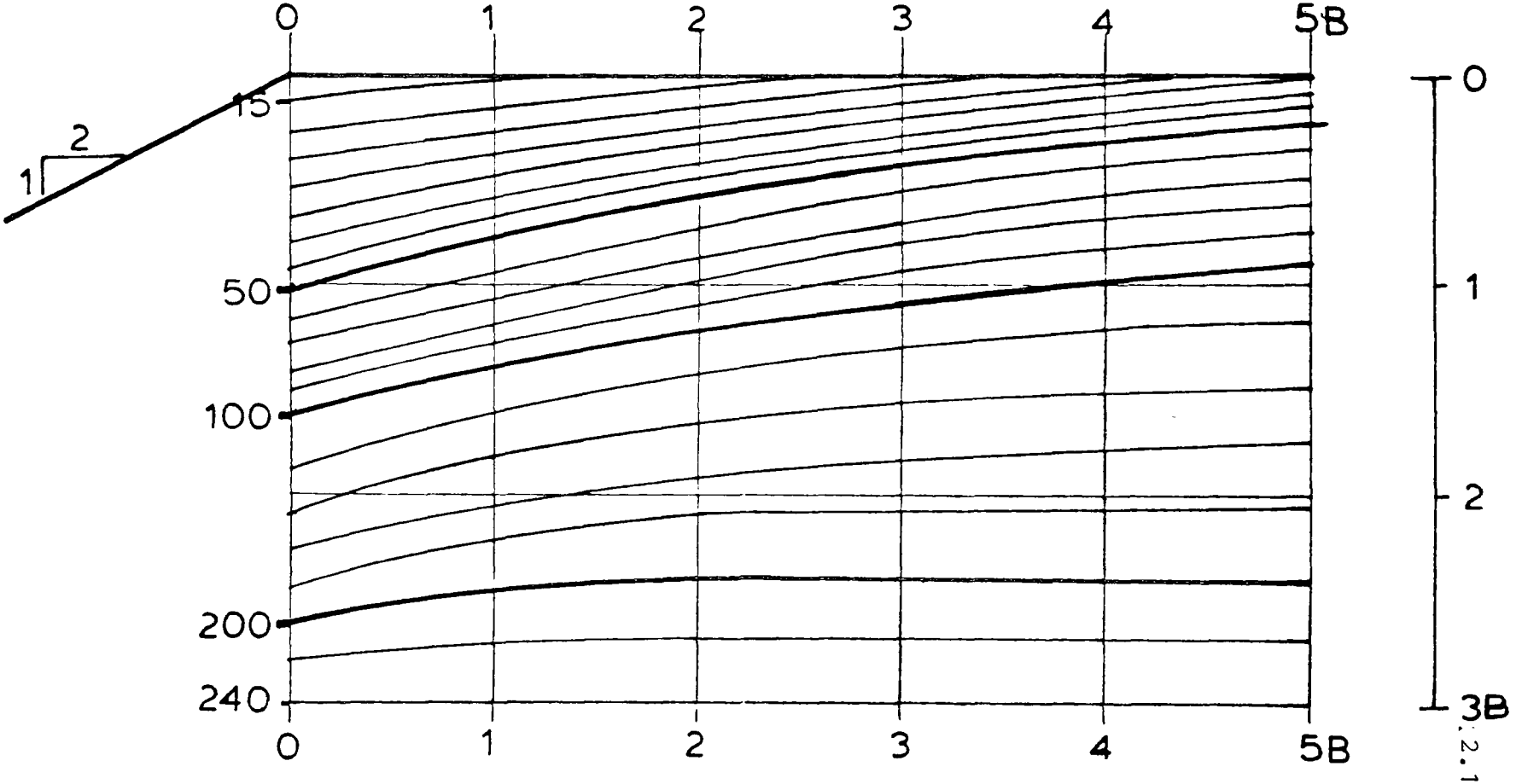

Figure 2.63

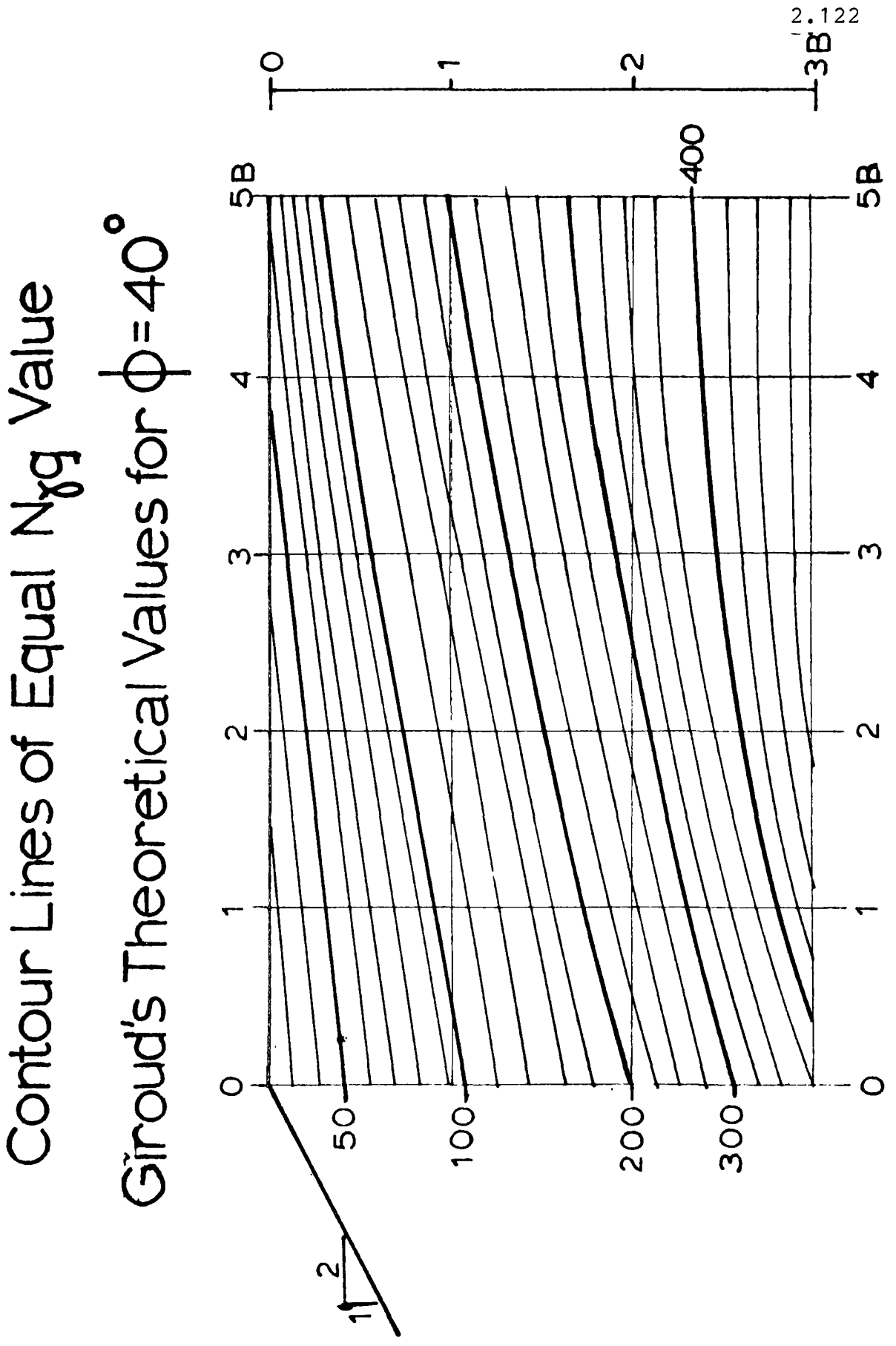
Contour Lines of Equal $N_{\gamma q}$ Value
Giroud's Theoretical Values for $\phi = 40°$
0
1
2
3B'
5B
400
5B
4
3
2
1
0
50
100
200
300
2
1

Figure 2.64

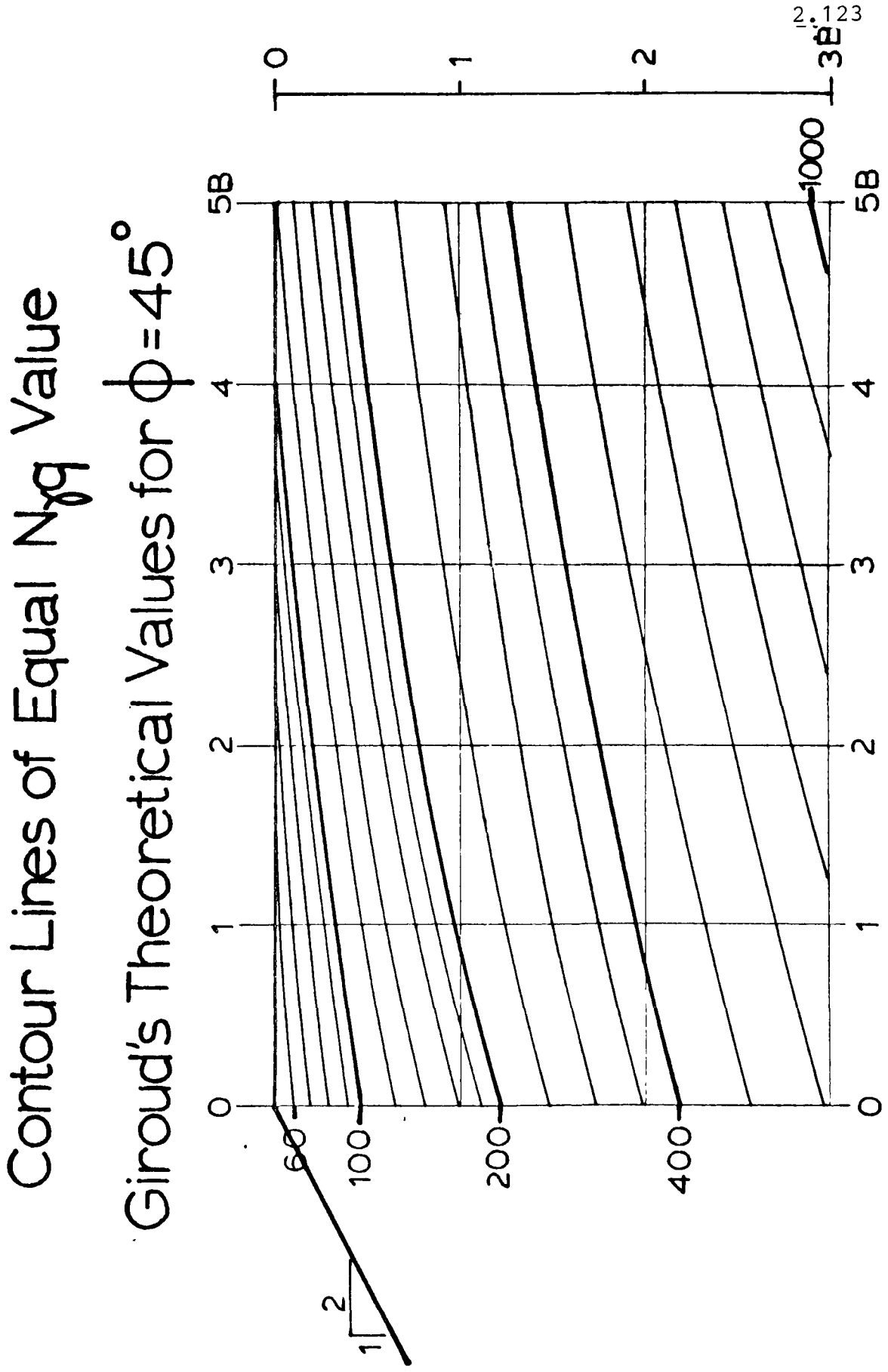
Contour Lines of Equal $N_{\phi q}$ Value
Giroud's Theoretical Values for $\phi = 45°$
0
1
2
3B
1000
5B
5B
0
1
2
3
4
60
100
200
400
2
1

Figure 2.65

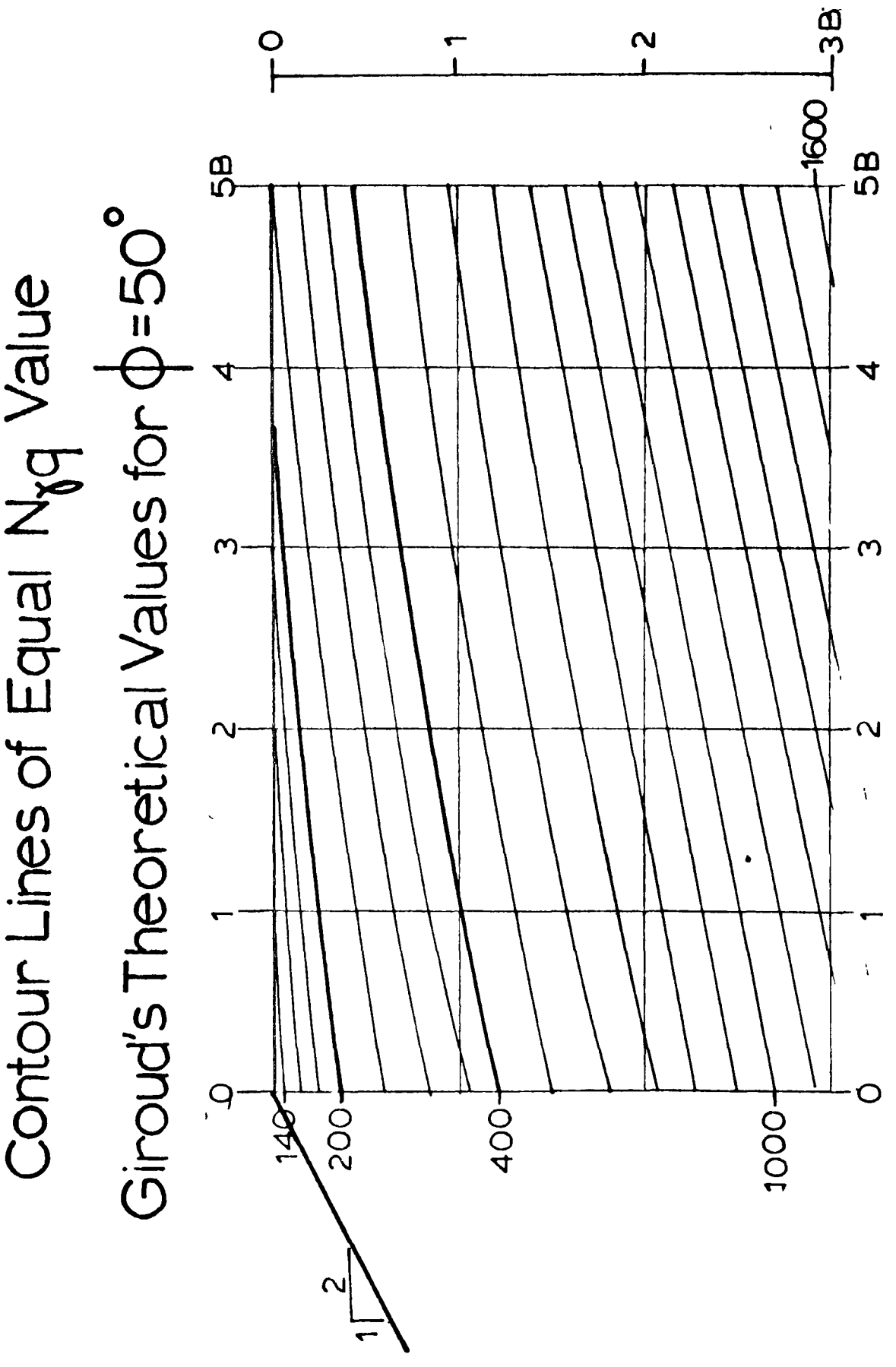
Contour Lines of Equal $N_{\gamma q}$ Value
Giroud's Theoretical Values for $\phi = 50°$
0
1
2
3B
1600
5B
5B
4
4
3
3
2
2
1
1
0
0
140
200
400
1000
2
1

Figure 2.66

Bowles' Solution for $\Phi = 30°$

(1975)

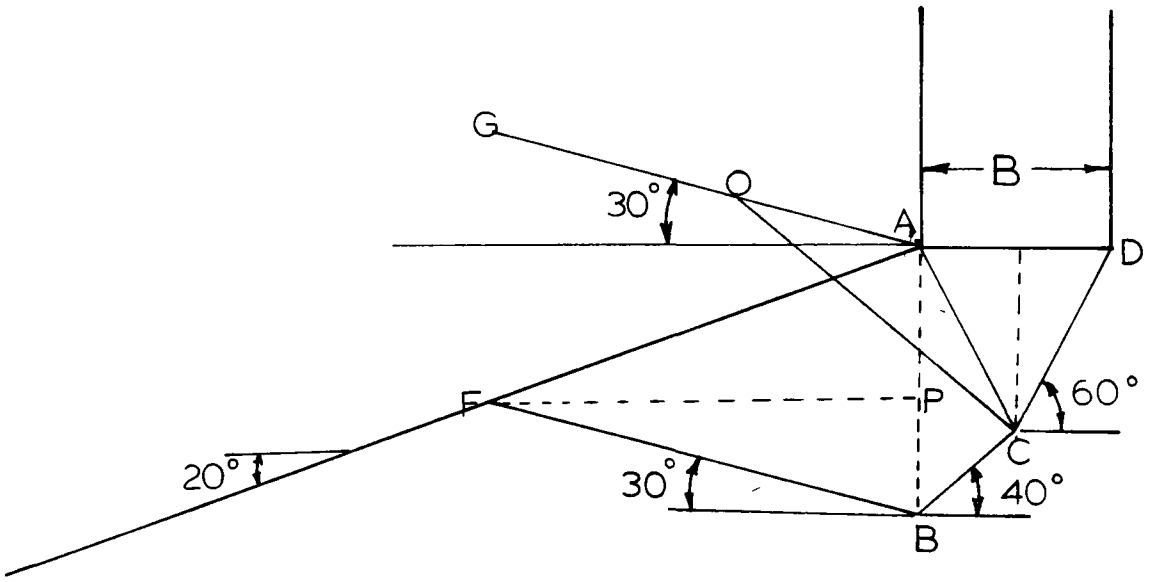

Figure 2.67

$$F_n = (W + q\frac{B}{2}) \cos\rho \qquad (2.4.5.1)$$

$$F_t = (W + q\frac{B}{2}) \sin\rho \qquad (2.4.5.2)$$

$$S_t = F_n \tan\Phi \qquad (2.4.5.3)$$

where F_n = normal force along slip surface

F_t = tangential force along slip surface

S_t = shearing resistance along slip surface

W = weight of the slice

B = footing width

q = bearing pressure

ρ = base angle of the slice

In the present example,

$$W_1 = \gamma[\frac{B^2}{8} \tan(45^\circ + \frac{\Phi}{2})] \qquad (2.4.5.4)$$

$$W_2 = \gamma\frac{B}{4} [\overline{AB} + \frac{B}{2} \tan(45^\circ + \frac{\Phi}{2})] \qquad (2.4.5.5)$$

$$W_3 = \gamma [\frac{\overline{AB} \times \overline{FP}}{2}] \qquad 2.4.5.6)$$

Then $F_{t1} = (W_1 + q\frac{B}{2}) \sin (45^\circ + \frac{\Phi}{2})$ (2.4.5.7)

$$F_{t2} = (W_2 + q\frac{B}{2}) \sin\rho \qquad (2.4.5.8)$$

$$F_{t3} = W_3 \sin [-(45^\circ - \frac{\Phi}{2})] \qquad (2.4.5.9)$$

$$S_{t1} = (W_1 + q\frac{B}{2}) \cos(45^\circ + \frac{\Phi}{2}) \tan\Phi \qquad (2.4.5.10)$$

$$S_{t2} = (W_2 + q\frac{B}{2}) \cos\rho \tan\Phi \qquad (2.4.5.11)$$

$$S_{t3} = (W_3) \cos [-(45^\circ - \frac{\Phi}{2})] \tan\Phi \qquad (2.4.5.12)$$

Now equating $\Sigma F_t = \Sigma S_t$ (2.4.5.13)

Substituting the values of the present example

$$\Sigma F_t = .04 B^2\gamma + .75qB \qquad (2.4.5.14)$$

$$\Sigma S_t = .84 B^2\gamma + .37qB \qquad (2.4.5.15)$$

From (2.4.5.13) an expression for solving q is obtained:

$$q = 2B_\gamma = \tfrac{1}{2}N_{\gamma q}B\gamma \qquad (2.4.5.16)$$

Where $N_{\gamma q} = 4$.

The value of $N_{\gamma q} = 4$ (for $\Phi = 30^\circ$ for the case of a slope of 20°) compares with other theories. Results have been worked out for a 2 to 1 slope. These are given in Figures 2.68 to 2.75.

Approach (1) and (2) applies to deep tests only. In approach (1), the overburden was taken to act as a surcharge only, while approach (2) takes into account the shearing resistance of the overburden.

Contour Lines of Equal $N_{\gamma q}$ Value
Bowles' (1975) Theoretical Values for $\Phi = 30°$

Approach (1)

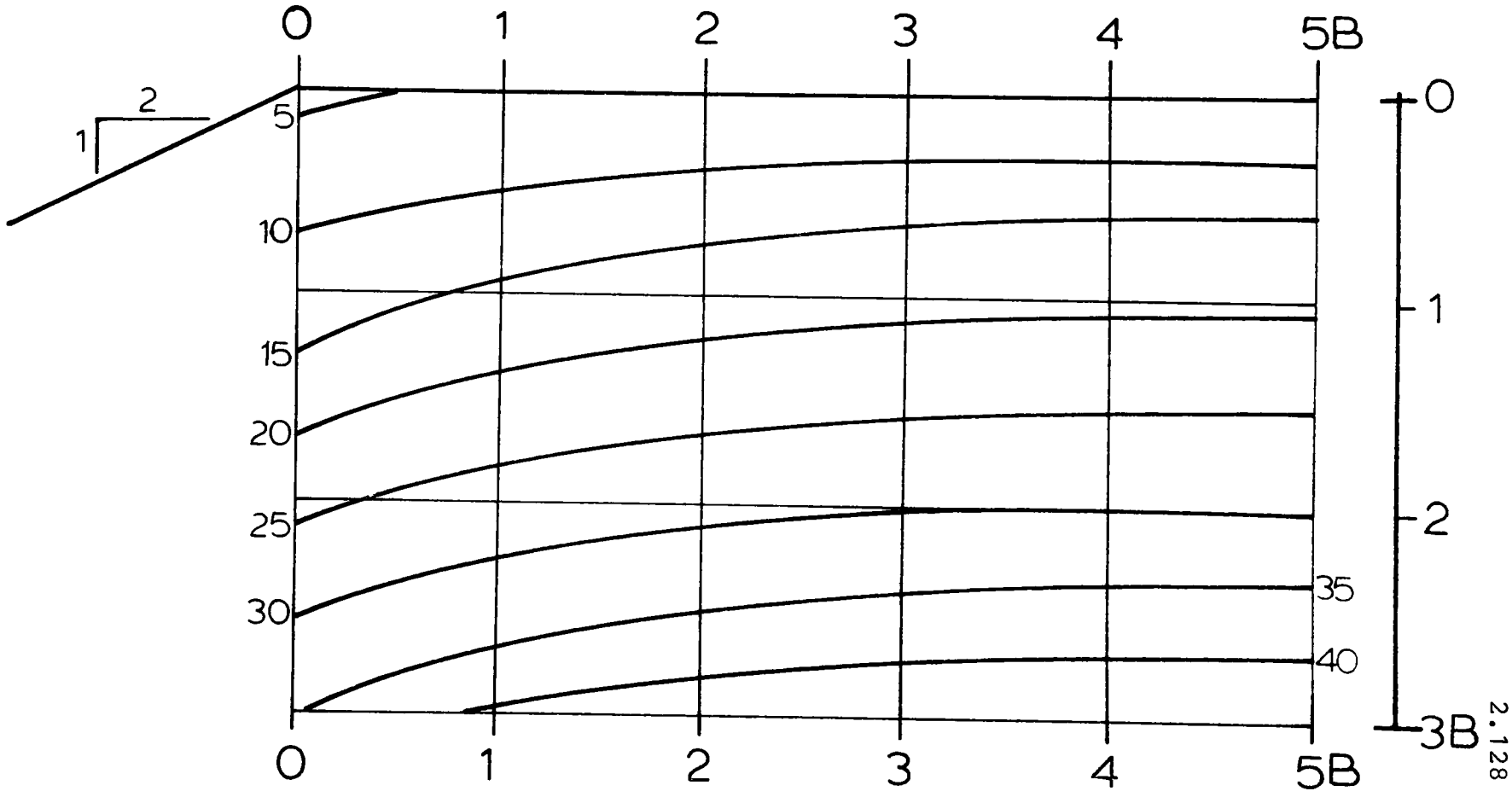

Figure 2.68

Contour Lines of Equal $N_{\gamma q}$ Value
Bowles'(1975) Theoretical Values for $\Phi = 30^{\circ}$

Approach (2)

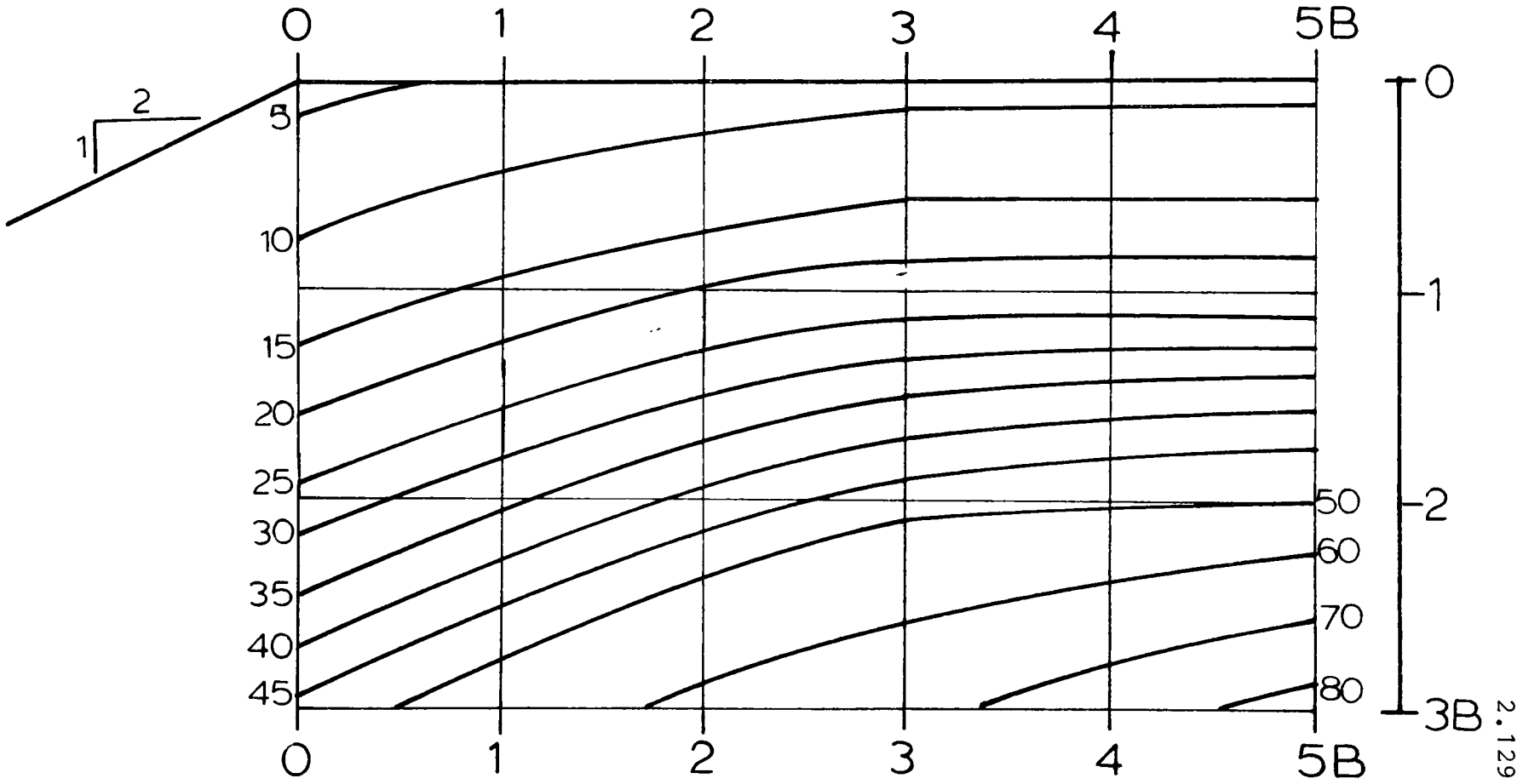

Figure 2.69

Contour Lines of Equal $N_{\gamma q}$ Value
Bowles'(1975) Theoretical Values for $\Phi = 35°$

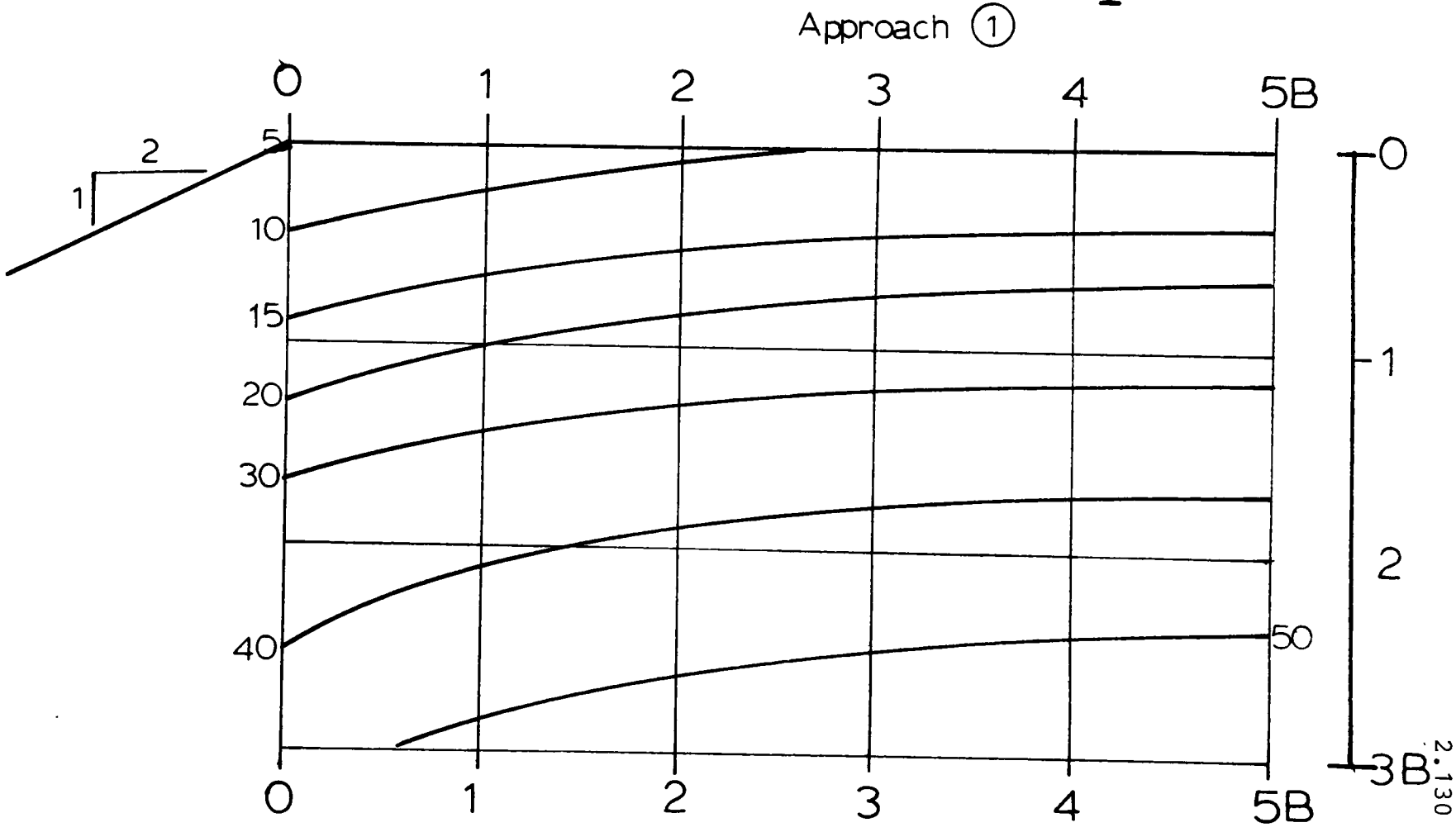

Figure 2.70

Contour Lines of Equal $N_{\gamma q}$ Value
Bowle's (1975) Theoretical Values for $\Phi = 35°$

Approach ②

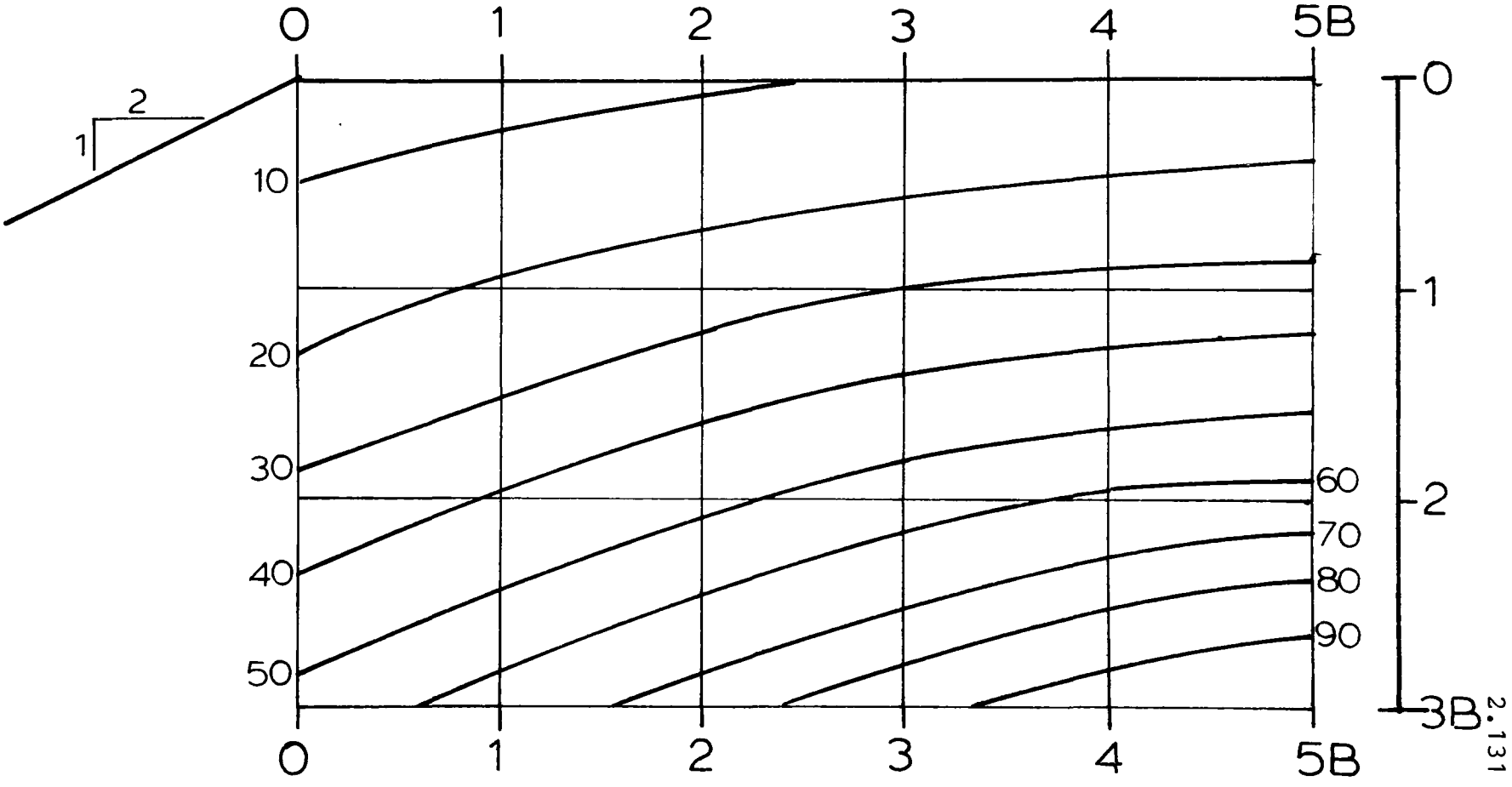

Figure 2.71

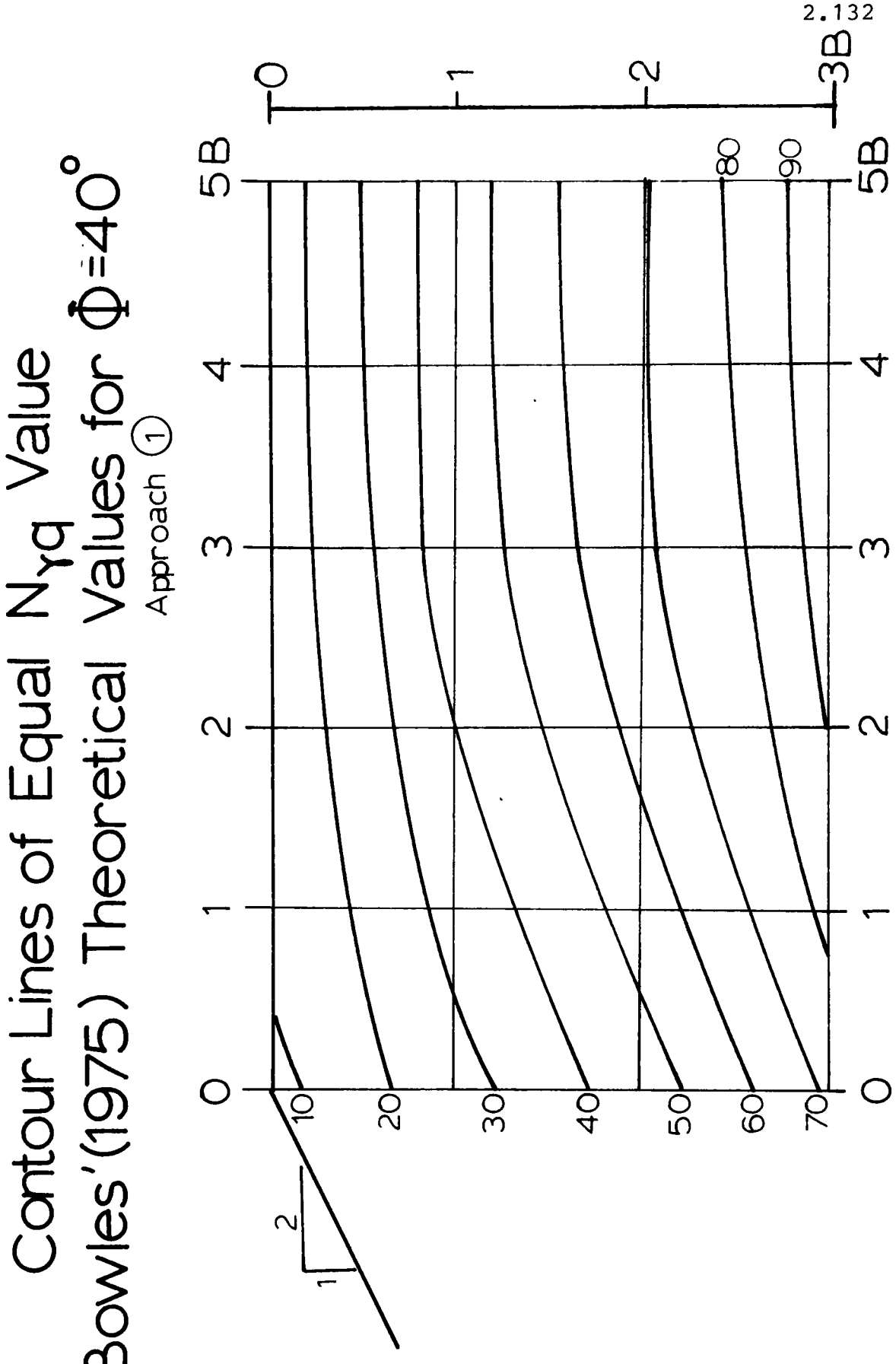
Contour Lines of Equal $N_{\gamma q}$ Value
Bowles' (1975) Theoretical Values for Φ=40°
Approach ①
0
1
2
3B
5B
0
1
2
3
4
5B
10
20
30
40
50
60
70
80
90
2
1

Figure 2.72

Contour Lines of Equal $N_{\gamma q}$ Value
Bowle's (1975) Theoretical Values for $\Phi = 40°$

Approach ②

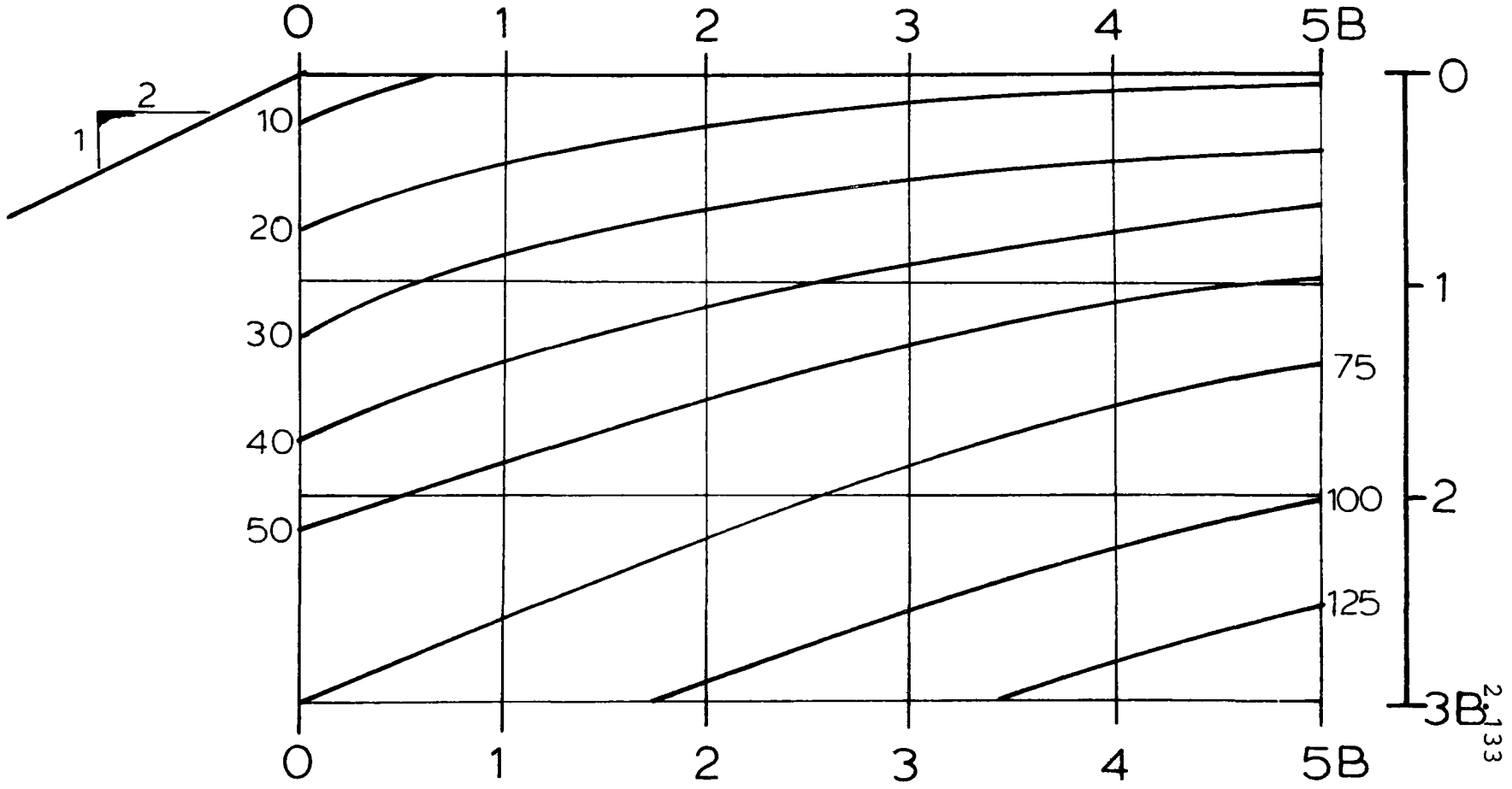

Figure 2.73

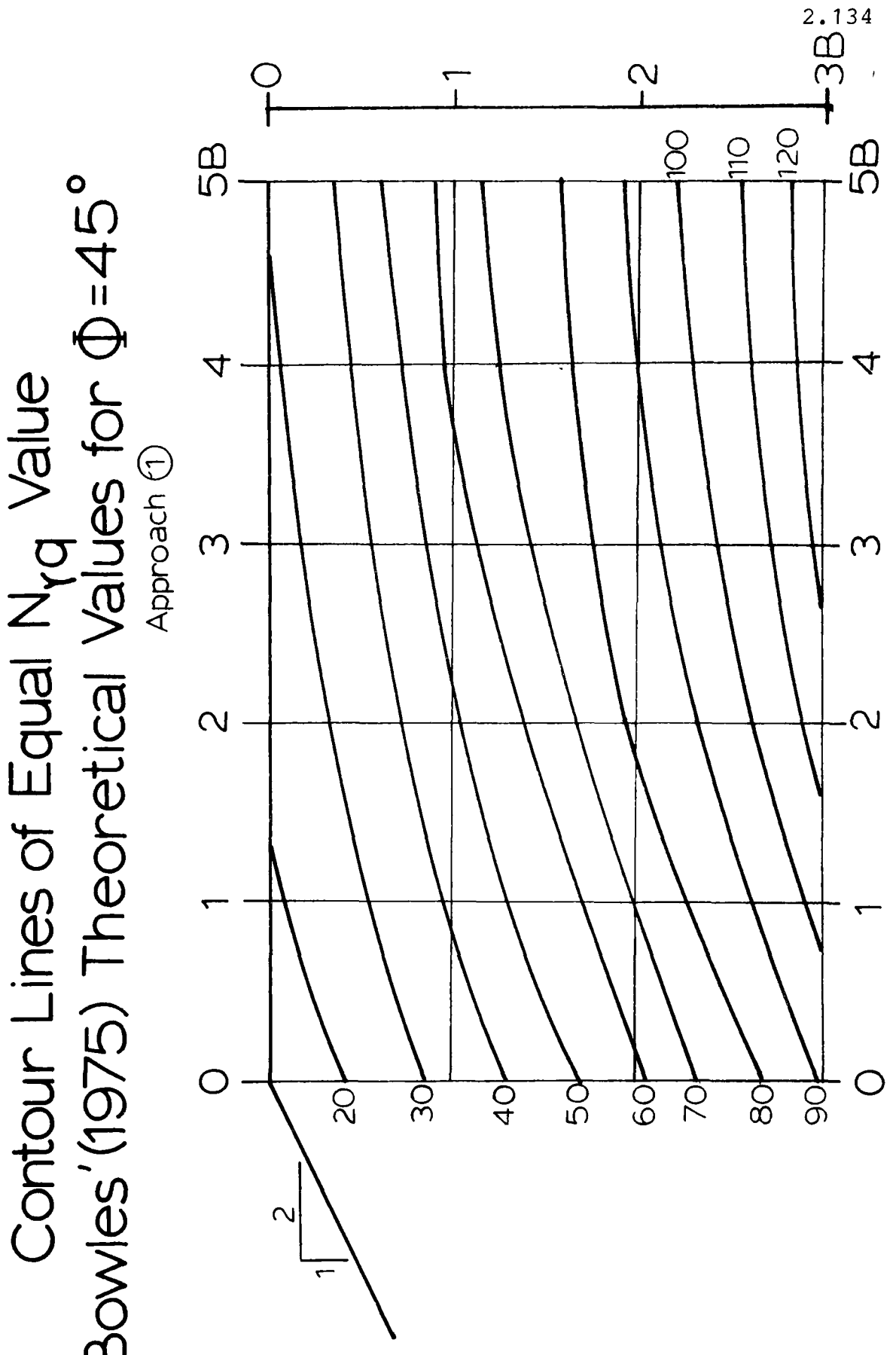
Contour Lines of Equal $N_{\gamma q}$ Value
Bowles' (1975) Theoretical Values for Φ=45°
Approach ①
0
1
2
3B
5B
0
1
2
3
4
5B
20
30
40
50
60
70
80
90
100
110
120
2
1

Figure 2.74

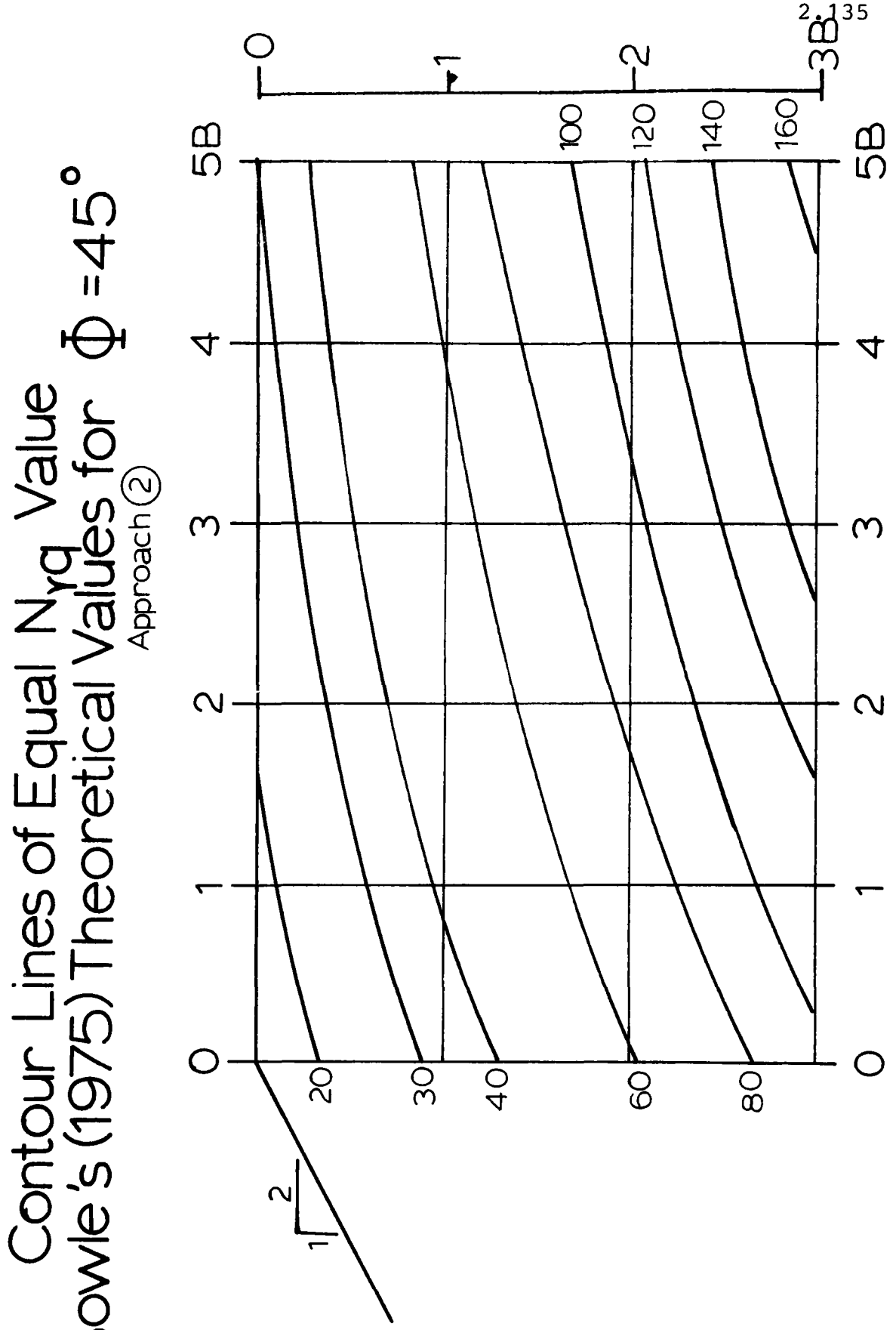
Contour Lines of Equal $N_{\gamma q}$ Value
Bowle's (1975) Theoretical Values for $\Phi = 45°$
Approach ②
0
1
2
3B
5B
100
120
140
160
20
30
40
60
80
2
1

Figure 2.75

2.4.6 Example of Bowles' (1977) Solution

Bowles (1977) suggested a method for determining the safe bearing capacity of a footing on top of a slope of cohesionless material. The method is described in Section 2.3.10. Since no examples of the method were worked out in the original reference, an example is giben here of the way in which the method can be used for the case of a footing located at the crest of a 2:1 slope having $\Phi = 30^0$. Using the construction given in Section 2.3.10, the geometry at failure is as shown in Figure 2.68.

The construction consists in establishing the failure geometry as in Figure 2.76. To obtain this the following steps

a) The active wedge under the footing is obtained thus:

$$\text{Angle } \hat{cfa} = f\hat{c}a = 45^0 + \frac{\Phi}{2} = 45 + \frac{30^0}{2} = 60^0$$

b) Length $fa = r_o = \dfrac{fc}{2\cos(45 + \frac{\Phi}{2})}$

$$= \frac{1}{2\cos(60^0)} = 1.05B$$

c) Length of $d = r_o e^{\theta \tan\Phi}$

where $\theta = 90^0 - \alpha = 90^0 - 26.6^0 = 63.4^0$

$$fd = 1.05 \times e^{\frac{63.4^0 \pi \tan 30^0}{180^0}} = 1.97B$$

d) Position of E is found because angle $qEd = 45^0 - \frac{\Phi}{2}$

$$= 45^0 - \frac{30^0}{2} = 30^0$$

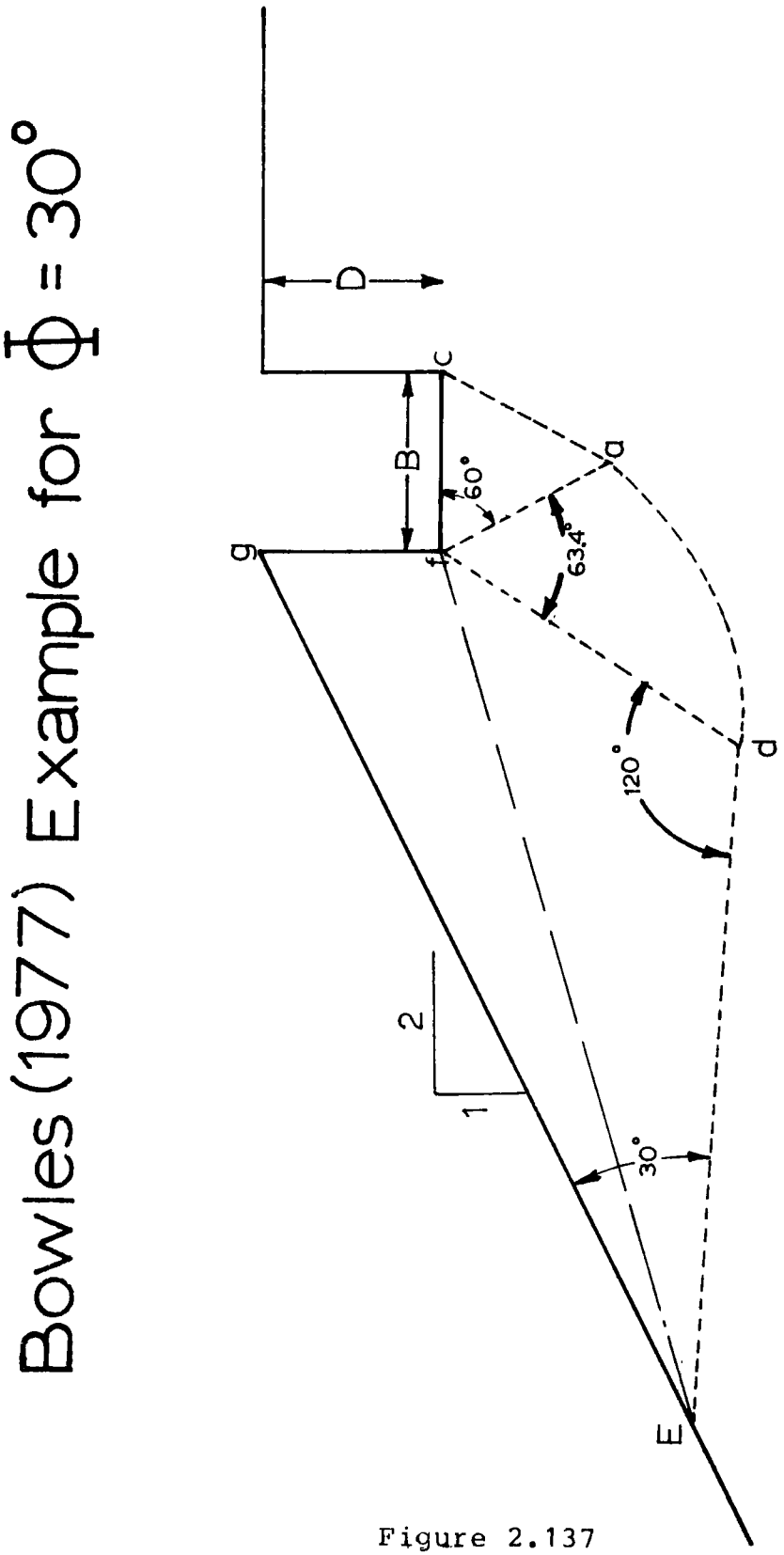

Figure 2.137

e) Area of surcharge if the footing was on flat ground =

$B \times 4B = 4B^2$

f) Area of surcharge gEf =

$\frac{\text{length gf}}{2}$ x the perpendicular from E to the extension of gf=

$= \frac{B \times 4.8B}{2} = 2.4B^2$

g) Revised $N_q' = N_q \frac{2.4}{4}$

$N_q = 25 \times \frac{2.4}{4} = 15$

Finally the complete bearing capacity is:

$$N_q = N + 2\frac{D}{B} N_q'$$
$$= 20 + 2 \times 1 \times 15$$
$$= 50$$

The Bowles (1977) values have been found and are given in Figures 2.77 to 2.80

2.5 Conclusion

This chapter begins by reviewing the methods used in determining bearing capacity. The different theoretical treatments of the problem of the bearing capacity of foundations on top of slopes of cohesionless material are reported. Some contributions to the existing theories have been presented.

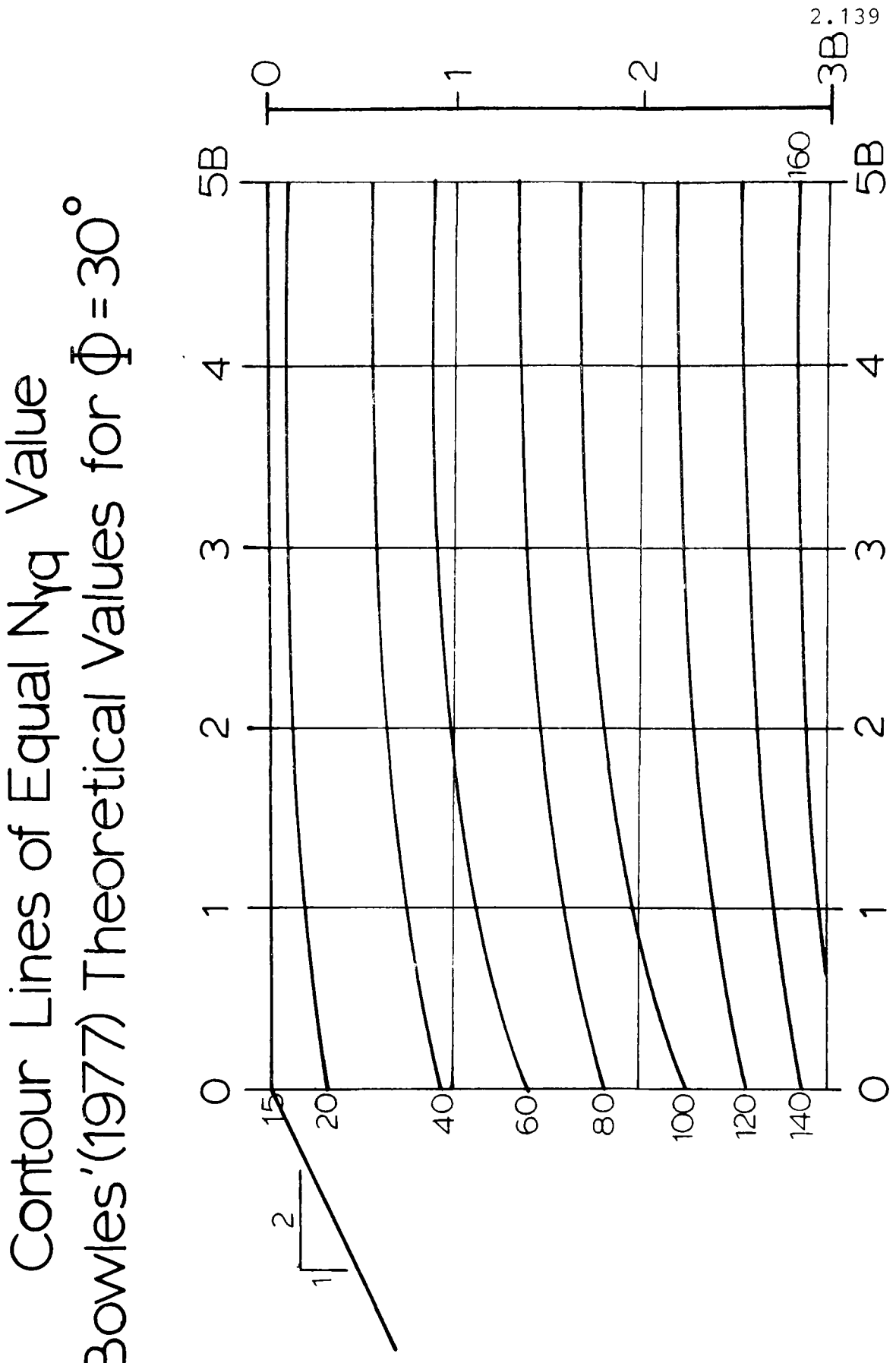
Contour Lines of Equal $N_{\gamma q}$ Value
Bowles'(1977) Theoretical Values for $\Phi = 30°$
0
1
2
3B
5B
0
1
2
3
4
5B
160
15
20
40
60
80
100
120
140
2
1

Figure 2.77

Contour Lines of Equal $N_{\gamma q}$ Value
Bowles'(1977) Theoretical Values for $\Phi = 35°$

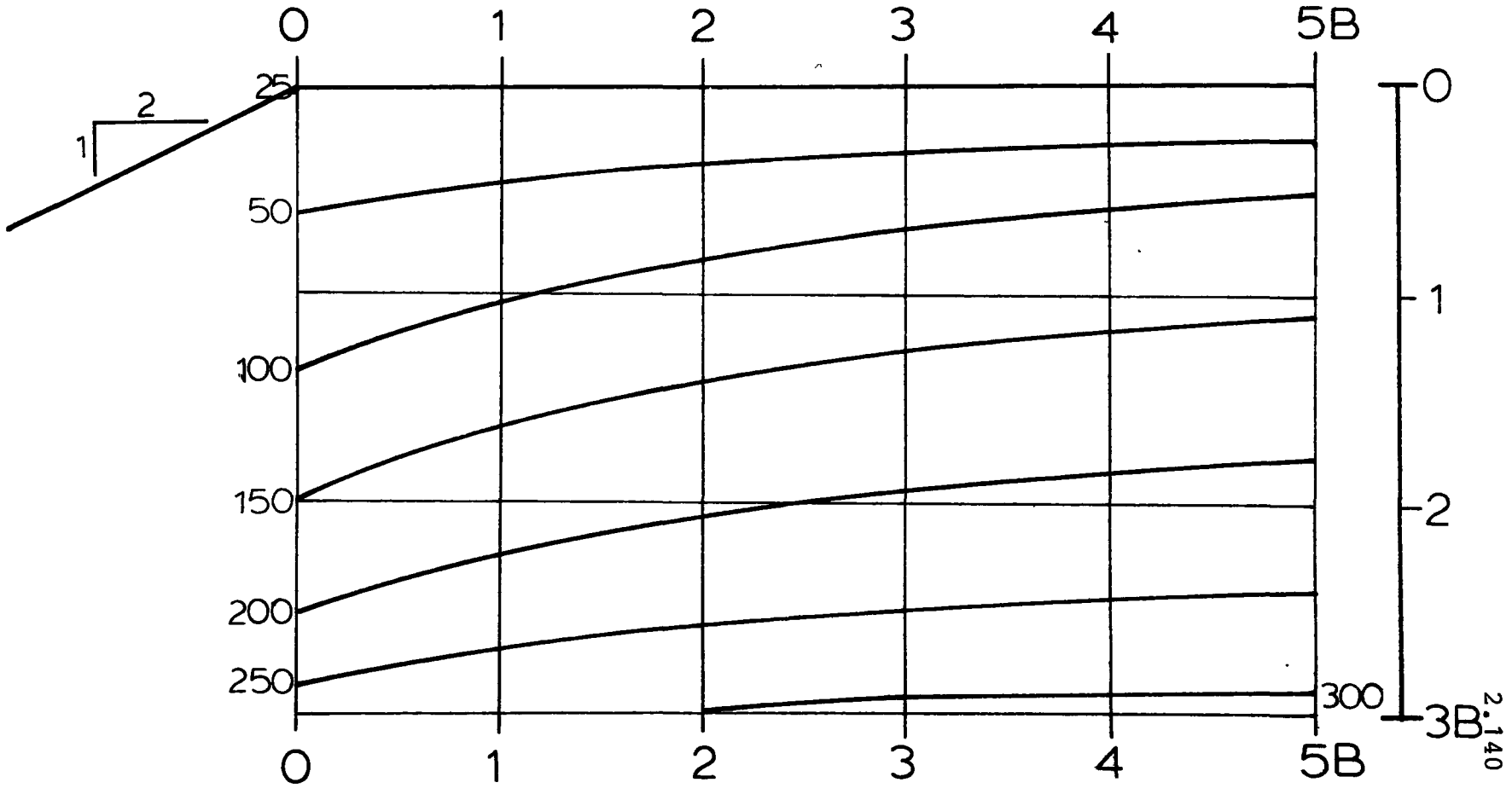

Figure 2.78

Contour Lines of Equal $N_{\gamma q}$ Value
Bowles' (1977) Theoretical Values for $\Phi = 40^{\circ}$

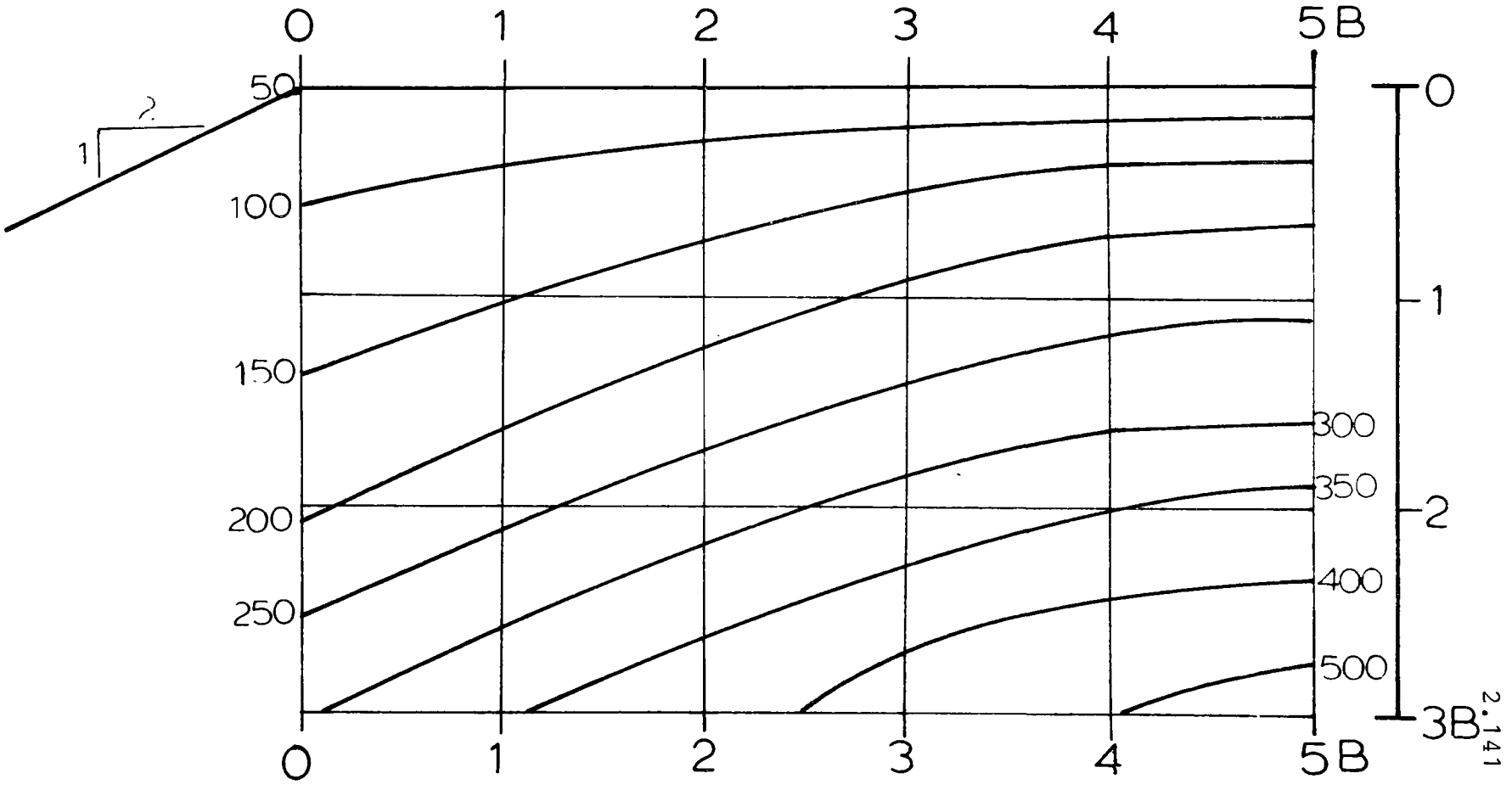

Figure 2.79

Contour Lines of Equal $N_{\gamma q}$ Value
Bowles'(1977) Theoretical Values for $\Phi = 45°$

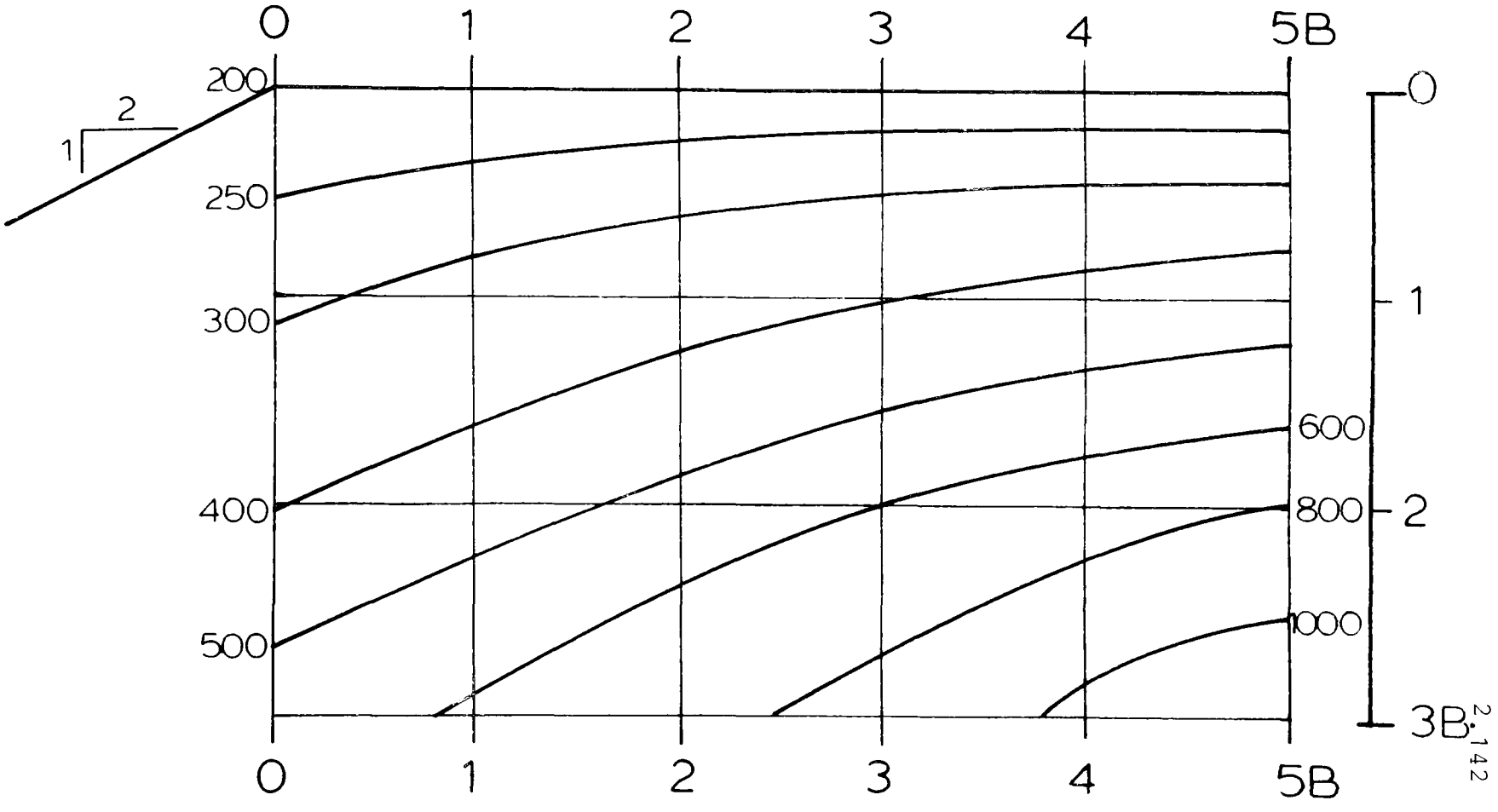

Figure 2.80

Because they are general in the sense that they consider a footing located anywhere with respect to the crest of a slope, the bearing capacity values of Meyerhof and Giroud are used in this study for comparison with the experimental results (Chapter 3). Since Meyerhof takes into account the shear strength of the overburden, his values are always larger than the Giroud values, as substantiated by Figures 2.81 and 2.82 (where the Meyerhof results are compared to Giroud's for $\Phi = 30^{\circ}$ and $\Phi = 40^{\circ}$ respectively). It can be observed on Figure 2.81 ($\Phi = 30^{\circ}$) that the values are almost identical, while Figure 2.82 ($\Phi = 40^{\circ}$) shows an important discrepency between the results.

Furthermore, since the Meyerhof values compare closely with those of Chen (1974) values which were obtained by the velocity fields technique, it would be fair to assume that the Meyerhof values constitute a realistic upper bound to the solution of bearing capacity of foundations located on top of slopes of cohesionless material, eventhough Meyerhof's solution does not meet all the requirements of the upper bound theorem.

Contours of Theoretical $N_{\gamma q}$ Values for $\phi = 30^\circ$

Giroud:—— Meyerhof:- - - -

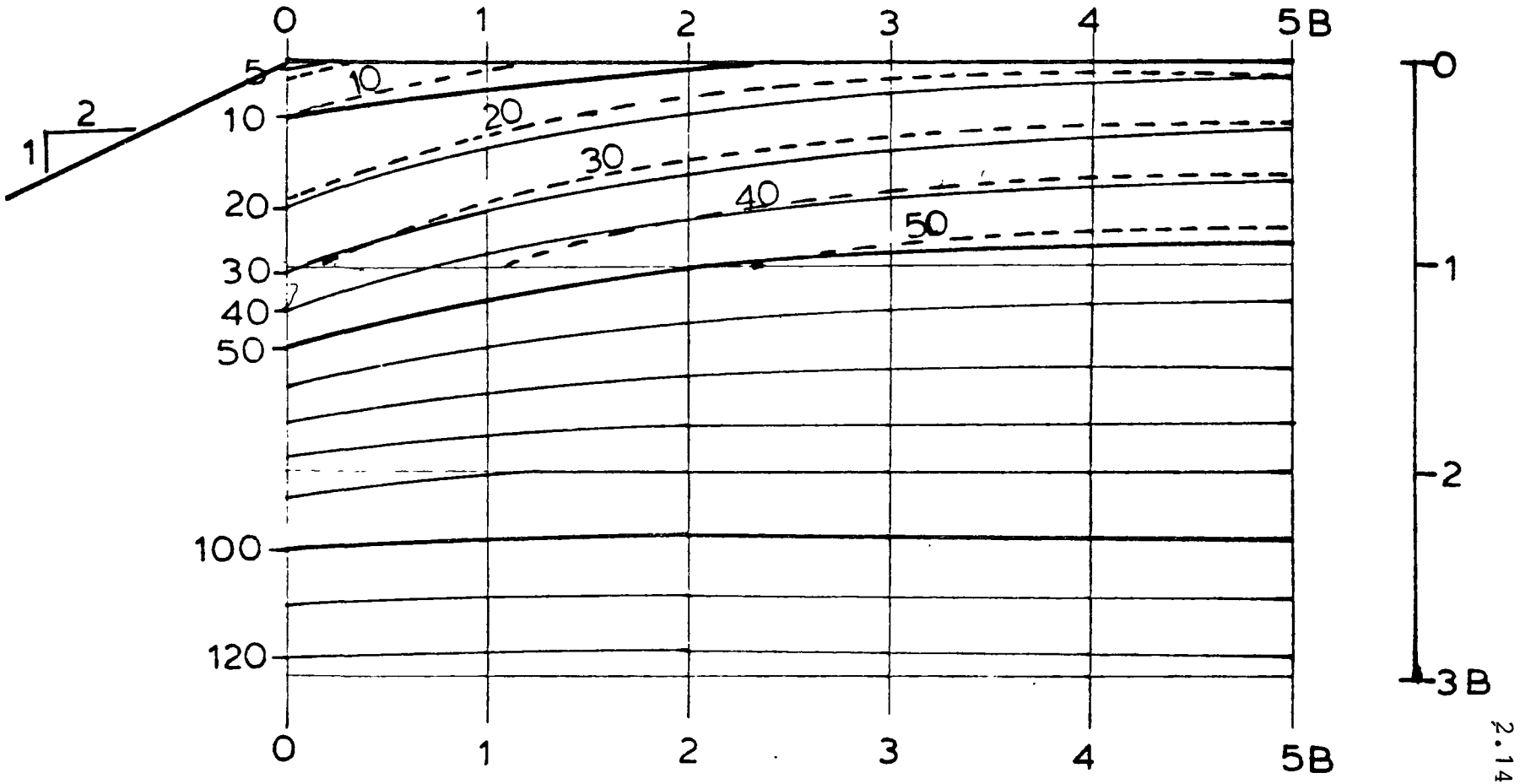

Figure 2.82

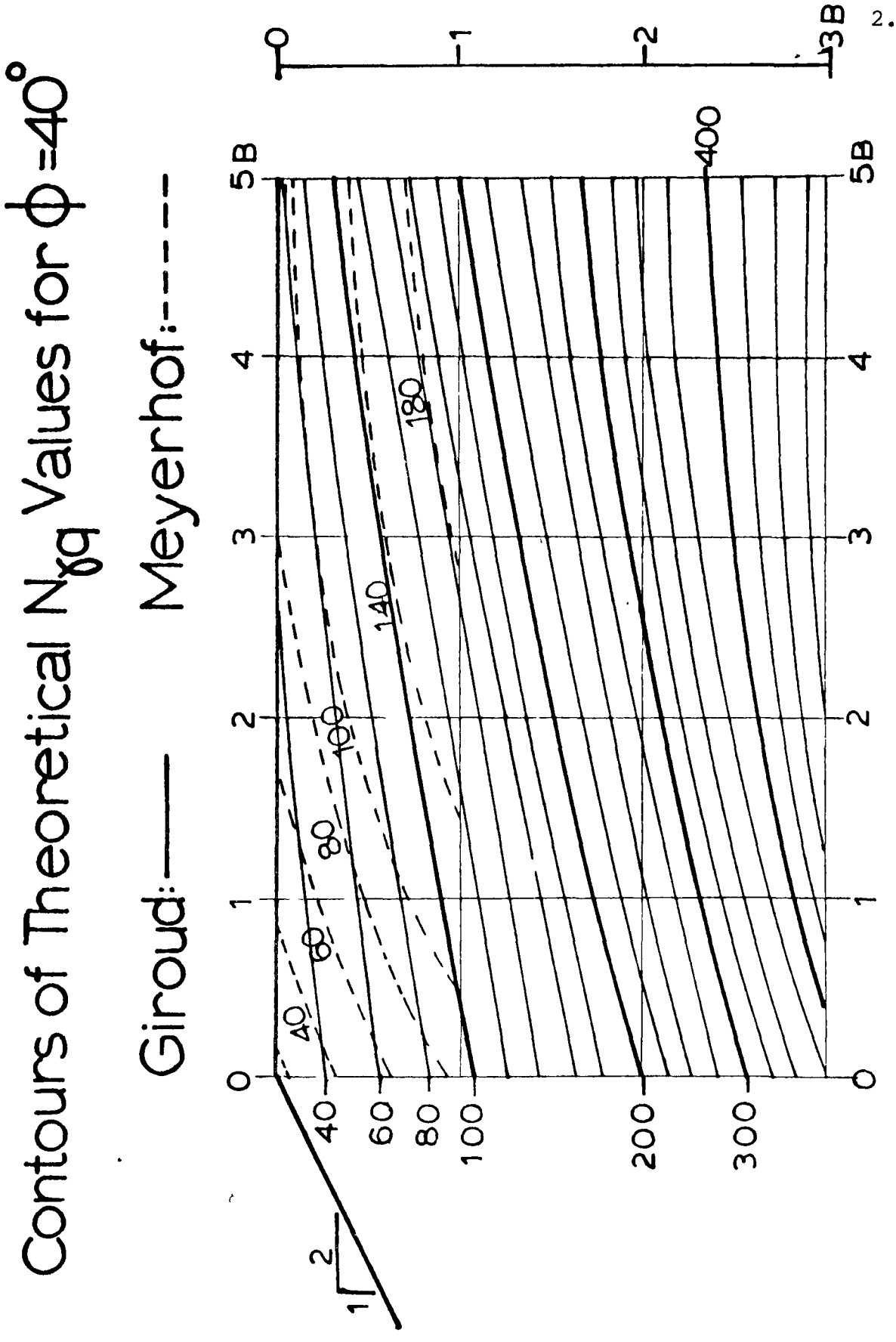
Contours of Theoretical $N_{\gamma q}$ Values for $\phi = 40°$
Giroud: ——— Meyerhof: - - - -
0
1
2
3B
5B
400
180
140
100
80
60
40
0
1
2
3
4
5B
40
60
80
100
200
300
2
1

Figure 2.82

CHAPTER III

EXPERIMENTAL INVESTIGATIONS

3.1 General

Despite the importance of the present topic, very few experimental tests have been undertaken to check the theoretical models proposed above. Peynircioglu (1948) carried out small scale tests using fine sand to find the failure geometry of footings on an embankment. This was done without monitoring the failure loads. Other investigations have been carried out on small stick models: Mizuno (1960), Giroud (1972) and University of Ottawa (1975). Tests using a larger model were attempted by Lebègue (1973). Only one report of a large scale field testing investigation was found in the literature; this investigation was carried out by Ménard (1964).

3.2 Small Scale Models (Stick Models)

Small scale models make use of long, thin cylinders (sticks). The sticks are made of various materials having unit weights and angle of shearing resistance. Various investigators have used the following materials having the properties which are indicated:

Investigator	Material	Dimensions (mm.)	Angle of Internal Friction
Mizuno (1960)	bamboo	5	30°
Giroud (1972)	duralumin	3 - 5	26° - 27°
University of Ottawa (1975)	wood	------	25°

Mizuno (1960) states that tests were carried but he does not mention the results. All his tests were at crest of the slope. He simply gave sketches of the failure surfaces for different angles of internal friction. These surfaces were somewhat different in form from the usual Prandtl type of failure surface.

The University of Ottawa tests were carried out in order to study the mechanics of failure, and bearing capacity values are only incidental to this. The results are shown in graphical form in Figure 3.1. On the same figure, Meyerhof's $N_{\gamma q}$ values are plotted, and very poor agreement is noted between the two curves.

Giroud has examined a number of different situations including a footing on top of a non-symmetric fill, foundation with eccentric loading, footing in a slope and so on. He measured the position of the slip surface in addition to the failure load. His results which are of value to the present study are shown in Figure 3.2. It is seen that in some cases

the experimental values are lower than the ones predicted by Giroud's theory.

From these experiments it is obvious that the weight of the sticks is too low to influence the results. By this it is meant that small scale models do not allow the significance of the weight term in the theories to be evaluated. This is seen in Giroud's results where the use of duralumin, the heaviest of the three materials, did not lead to results which were appreciably different from the University of Ottawa and Mizuno results. In the latter two cases the models of wood could be considered to be weightless. A further complication of these particular small scale tests is that the angles of internal friction of the material is unusually low in comparison with most sands. As a result, according to theory at low friction angles, the N_γ and N_q terms are of approximately equal significance and both are small numbers.

While these small scale experimental models are very interesting as a classroom aid to explain the kinematic formation of the failure geometry, they are not very relevent for practical purposes because of the very low unit weight, confining pressures and friction angles.

3.3 Large Scale Models

Very few large scale footing tests appear to have been undertaken in the laboratory to check the effects of sloping ground. In the case of sand supporting footings carrying a

University of Ottawa Small Scale Experimental Results

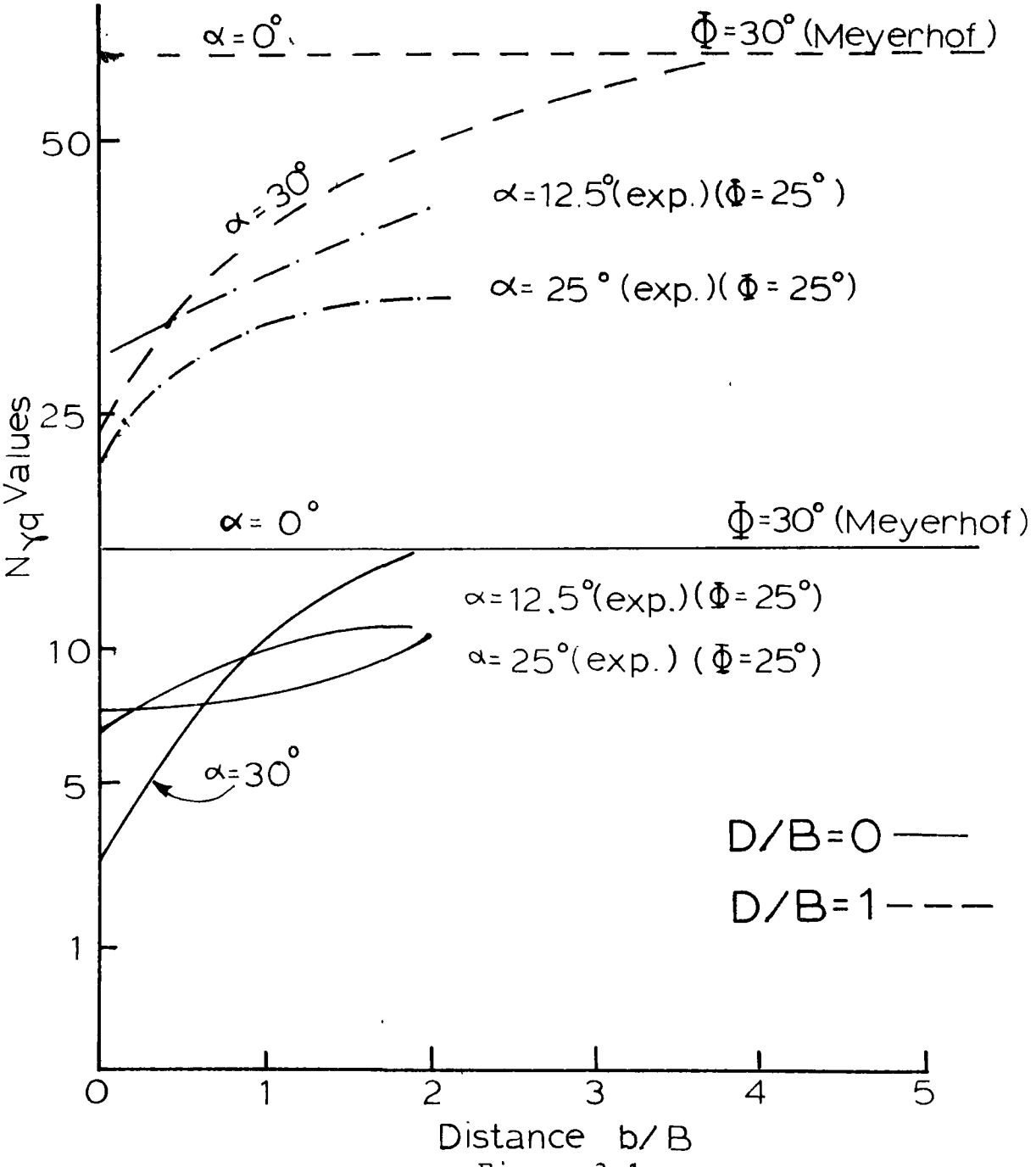

Figure 3.1

Giroud's Small Scale Experimental Test Results

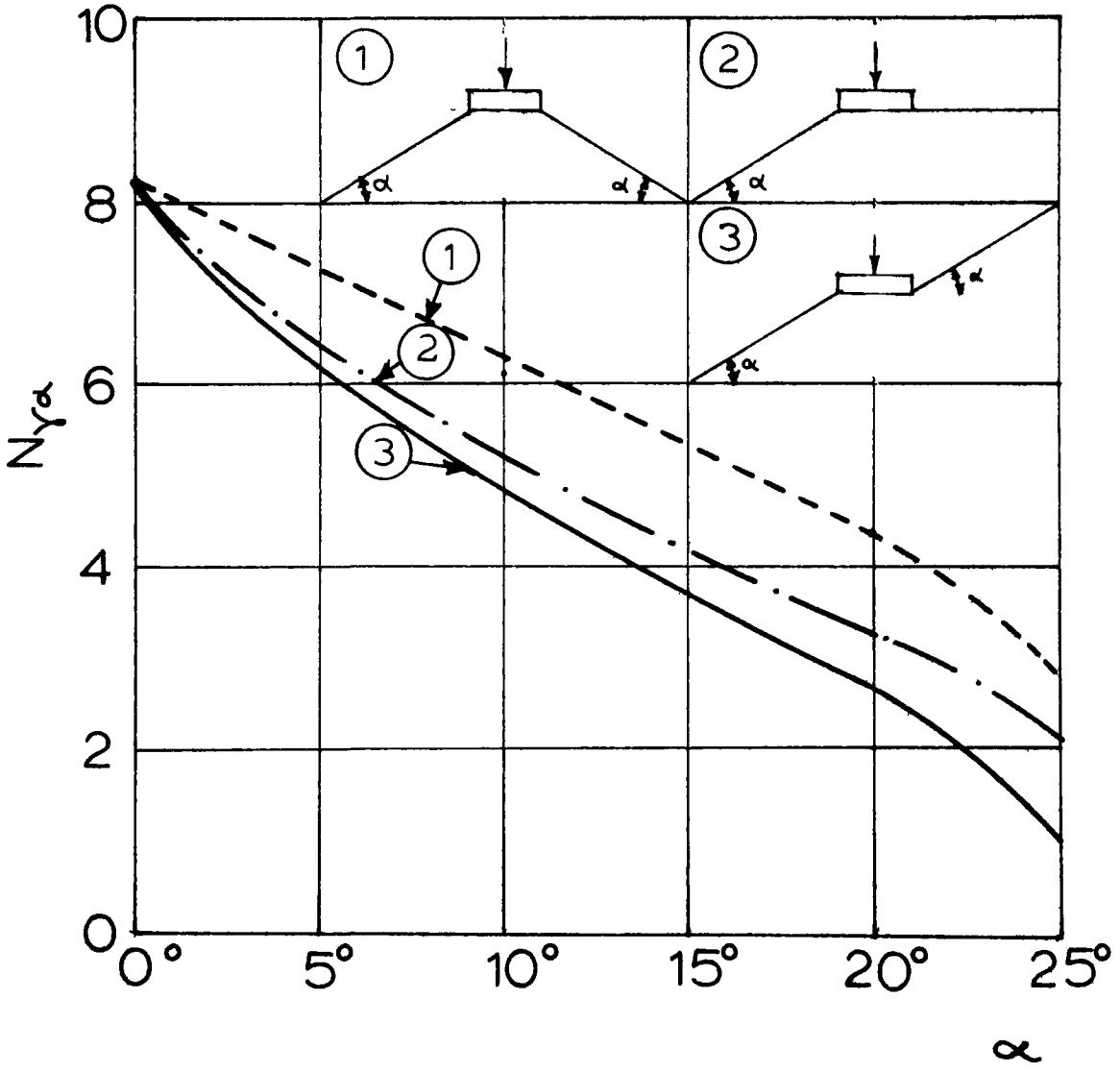

Figure 3.2

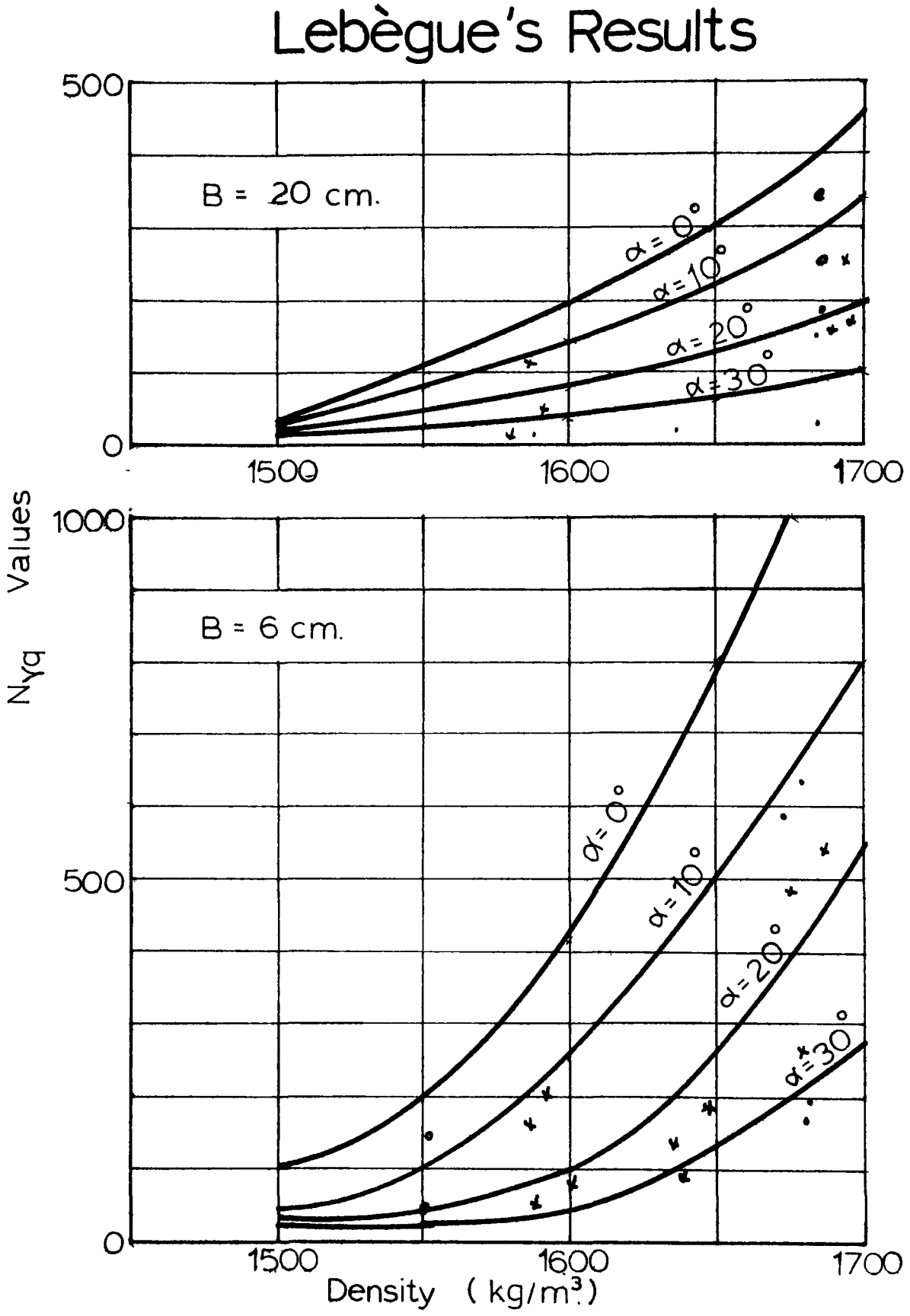
Lebègue's Results
500
B = 20 cm.
α = 0°
α = 10°
α = 20°
α = 30°
0
1500
1600
1700
1000
B = 6 cm.
Nγq Values
500
0
1500
1600
1700
Density (kg/m³)

Figure 3.3

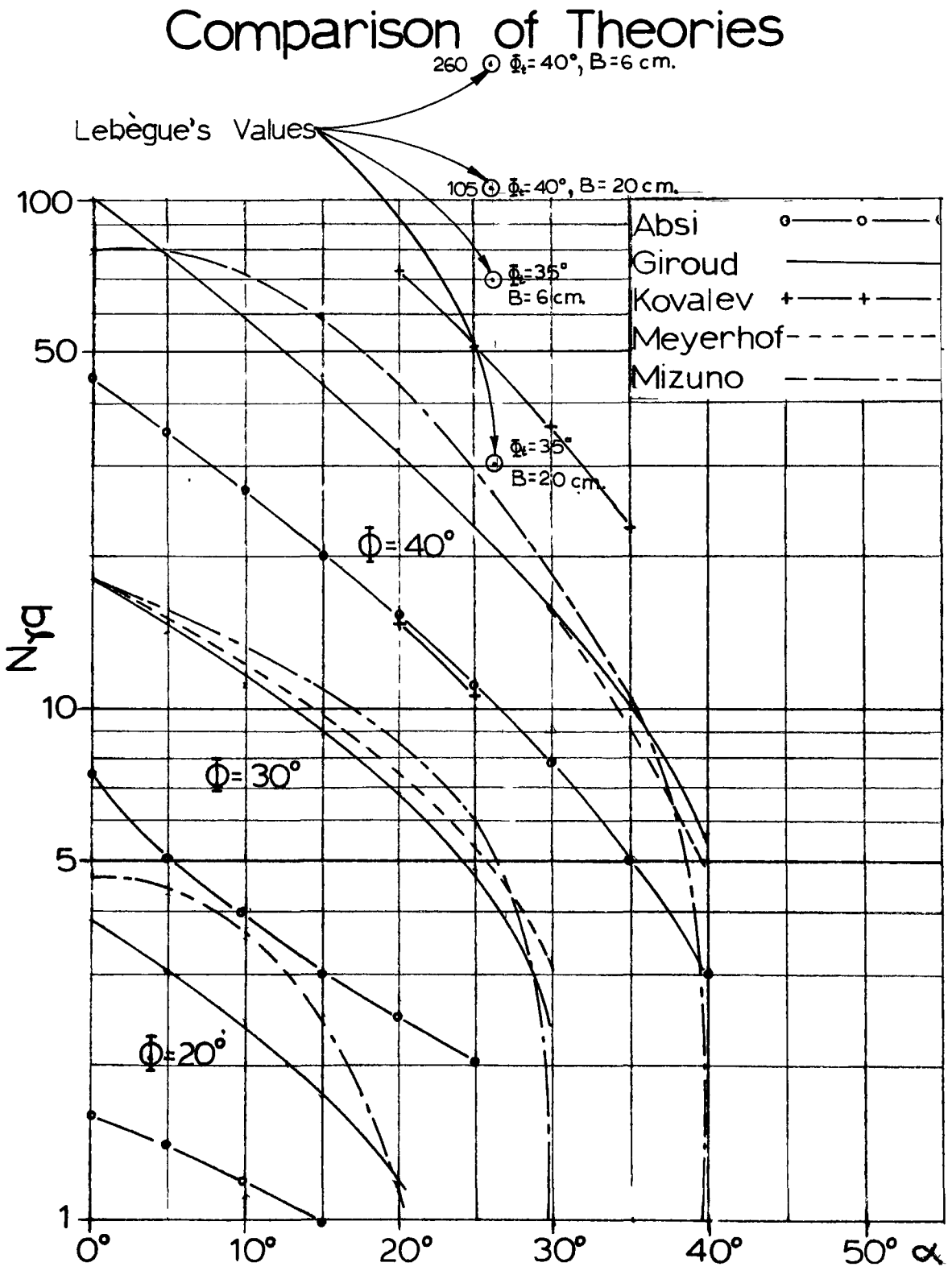
Comparison of Theories
260 ⊙ Φt=40°, B=6 cm.
Lebègue's Values
105 ⊙ Φt=40°, B=20 cm.
Φt=35°
B=6 cm.
Φt=35°
B=20 cm.
Absi
Giroud
Kovalev
Meyerhof
Mizuno
Φ=40°
Φ=30°
Φ=20°
N1q
100
50
10
5
1
0°
10°
20°
30°
40°
50°
α

Figure 3.4

vertical central load, only two series of tests are known. One series consisted of twenty-four tests as reported by Kovalev (1965); while no results and no details of the experimental procedure are given in the reference, the investigators estimated that the results were within 22.7% of the theoretical values.

Y. Lebègue tested 6cm. and 20 cm. wide footings located on top of a slope of cohesionless soil. These experiments were part of a general testing program that started in the mid 1960's at le Centre expérimental de recherches et d'études du bâtiment et des travaux publics, Paris, France. The experimental apparatus and procedure are described by Lebègue (1974).

Lebègue was able to study the effects of scale by comparing the bearing capacity values from the 6 cm. wide and 20cm. wide test.

The results are plotted on Figure 3.3 as a function of density and slope angle, with the angle of internal friction for the sand being obtained by using triaxial apparatus. His tests were performed for two densities; namely 1570 kg/m^3 which corresponded to a Φ triaxial of 35° and 1690 kg/m^3 which corresponded to a Φ triaxial of 40°. A comparison of these results with the theories presented in Chapter II are shown in Figure 3.4. It is seen from this graph that most of the theoretical values are smaller than Lebègue's experimental results.

3.4 Field Testing

As previously mentionned in Section 2.3.10, Ménard (1964) reported on tests which were carried out in the field. These were done to correlate the bearing capacity on flat ground with the bearing capacity close to an excavation. The work was done in conjunction with the study Ménard carried out to establish empirical rules relating bearing capacity to pressuremeter test results.

The tests were performed on a silty sand. The footing was square, having dimensions of 0.9m x 0.9m, and was founded at a depth of 0.5m below the ground surface. The groundwater level was at a depth of 10m below the surface.

The tests consisted of first loading 3 footings on flat ground. After a few months the soil on one side of the footings was excavated, and then the footing was loaded to failure. This was done for 3 different excavation slopes.

For these different excavation slopes, the footings were loaded to failure to determine the ultimate bearing capacity. The values of bearing capacity were then related to those which were measured with the footing on flat ground. These results are presented in Figure 3.5. They are of interest since they can be used to compare the bearing capacity on flat ground to the bearing capacity of a footing located close to a slope. Since no mention was made of the material properties of the soil in terms of Φ and γ, these tests cannot be used in our present study for comparison purposes.

Ménard's Results

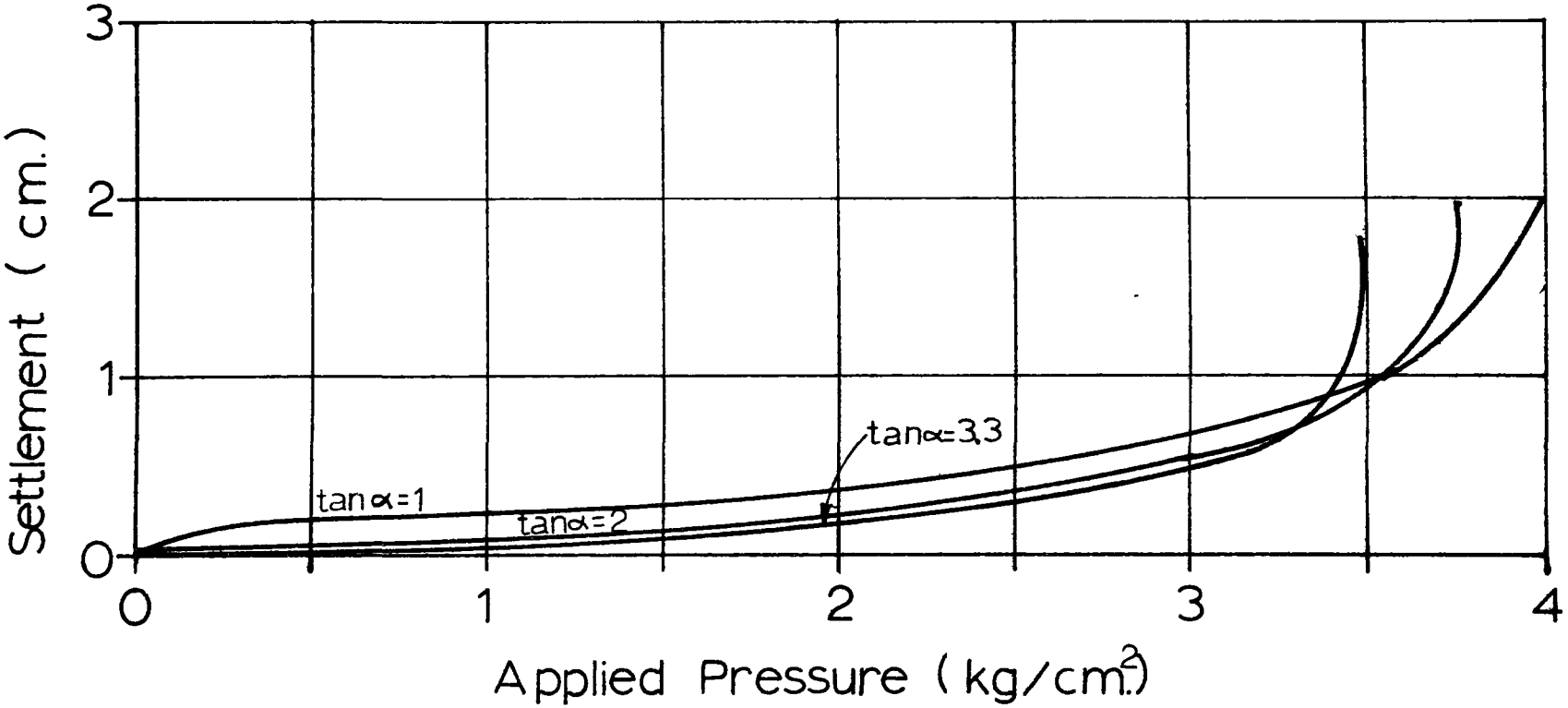

Figure 3.5

3.5 Conclusion and Comparison with Theories

Experimental investigations of the topic are surveyed in the preceeding sections. Only the Lebègue (1973) experiments seem to offer worthwhile information; there is a similarity of 1)scale, 2)material properties and 3)the types of tests with the present study.

Lebègue's experimental results are compared with the pertinent theoretical values in Figure 3.4. The Giroud values fall almost in the middle of the band formed by all bearing capacity theories. This theory is compared with the Lebègue test results in Figure 3.6. This figure indicates that the test results are higher than the theoretical predictions. DeBeer (1965) tries to explain why such discrepencies exist. He discusses such factors as: the improper choice of the angle of internal friction, the scale effects, the assumptions of plane strain, and so on. Most of these factors are discussed in the analysis of the experimental data in Chapter VII.

Comparison of Lebègue's Results with Giroud's Theory

	ϕ = 35°			ϕ = 40°		
Slope angle α	Lebègue's values ϕ_t = 35°		Giroud's Theoretical Values	Lebègue's values ϕ_t = 40°		Giroud's Theoretical values
	B= 6cm	B= 20cm		B= 6cm	B= 20cm	
0°	330	150	41	1000	400	100
10°	200	100	26	600	300	58
20°	100	50	15	400	150	32
26.6°	70	30	10	260	105	20
30°	50	20	7	180	75	16

Notes: 1. All tests conducted with footing on surface at slope crest.

2. ϕ_t = were determined from triaxial testd.

Figure 3.6

CHAPTER IV

EXPERIMENTAL MODEL

4.1 Introduction

Because so few experiments in soil have been carried out on a reasonnable scale, the problem of the bearing capacity of footings in or near slopes remains unresolved for practical purposes. It is safe to say that useful experiments could be undertaken on any and all aspects of the bearing capacity of spread footings in or near slopes. It seems worthwhile, then, to list and discuss briefly the variables that exist when attempting to define the problem as introduced in Chapter I.

The main variable involved in the problem is the dimension of the slope. The height of the slope can vary between a few centimeters for a stepped footing in an excavation and a thousand meters or more in mountainous terrain. The slope angle can vary from 0 to 90 degrees to the horizontal.

The slope can be made up of one or any combination of the following materials: clay, silt, sand, gravel and rock. The material could have been deposited by a natural or by mechanical process. The soil strength can vary from soft to very hard (cohesive material) or it can range from weak to strong (very loose to very dense frictional material).

Water conditions can influence the stability of the slope. The soil can be dry, partially saturated, or fully

saturated; the drainage conditions can be fully drained or dry, submerged, or there can be seepage either continuously or intermittently (during rainfalls or sudden drawdown, for example).

The footings can be placed close to, far from, or in the slope. At any of these positions, surface, shallow or deep foundations can be constructed.

Depending upon the type of construction, the footings can be horizontal, as in the usual case, or inclined, as for a raker shore near an elevator pit. In some cases the loads may be vertical and concentric with the footing; in other cases they may be eccentric and inclined.

Time also can be a major factor influencing the properties and the behavior of the soil. This is particularly noticeable in the case of clay slopes. The clay in a freshly cut slope will behave as a purely cohesive material immediately after the cut; this is known as its "short term behavior." A certain period after the cut is made, the clay properties will change. This is refered to as "long term behavior"; then the clay 'loses' most of its cohesive characteristics and becomes more frictional. Presumably the bearing capacity of a footing at the crest of a clay slope also changes from the short term to the long term condition.

Given all of these variables and the wide scope of the problem, it is fortunate that there is a rational grouping of variables that can be considered to be the starting point for

a research project. This grouping would be based on the following considerations:

- It seems practical to start by considering the top of the slope to be horizontal.
- Sand and gravel slopes usually have an inclination within a fairly narrow range of angles as do long term slopes in silt or clay.
- A purely frictional material simulates many of the soils which are encountered; this material represents directly sand, gravel, broken rock, and sandy silt. Based on their long term behavior, normally consolidated clays can be considered to be a purely frictional material as can over-consolidated clays when their cohesion drops to zero with time.
- The complication brought about by the flow of ground water should be avoided in any preliminary study of the bearing capacity problem.
- The loading condition can be limited to vertical central loads on horizontal footings because this condition represents many of the cases which are encountered in practice and is the fundamental case.

The foregoing rationalization of the problem considerably reduces the breadth of the variables. There are also physical, cost, and time constraints which will limit the scope of any research. These constraints are real and are probably the reason why so little experimental work of value

has been carried out to date; these constraints which are interdependent are discussed in the following paragraphs.

A physical constraint arises from the testing facilities. Testing should be performed in a laboratory to ensure ideal, reproducible conditions. The slope must have finite dimensions, but must be of reasonable size. Since the slope will have to be rebuilt after each test, some convenient way of handling and depositing the material must be provided. The handling of this material could create an enormous quantity of dust; thus, the testing facilities should have a separate enclosure to limit the migrating effect of the dust. This is particularly true of the deposition process where segregation could prove to be an additional problem.

Financial restrictions also have to be considered. Only limited funds are available for the testing facilities and for the technical staff. The present facilities available at the University of Ottawa are provided by a number of grants and donations and are worth approximately $140,000.00. Operating funds are available from the Ministry of Transportation and Communications of Ontario, provided that the conditions mentioned in Chapter I are met.

Considering that the first stage of the research will be carried out as part of a Ph. D. program, the proposed experimental research must be achieved in a reasonable time frame. Calibration and preliminary tests indicated that about thirty tests would probably be completed within one and one half years.

4.2 Facilities

4.2.1 General

The testing program makes use of the facilities which are available at the University of Ottawa. These facilities can be divided into three categories: the testing box, the sand handling equipment, and the loading frame. Each of these is described in the following paragraphs.

4.2.2 Sand Box

4.2.2.1 Dimensions

The sand box, shown in Figures 4.1 and 4.2, has a length of 14.6m, a width of 1.8m and a depth of 2.2m; it has been divided into two equal compartments (A and B) by two bulkheads. While one compartment was used as a testing box, the other served as a storage bin for the sand not used in a particular test and for the entire amount of sand between tests. The sand box is made of 1.27cm thick steel plates held rigidly in place by 10 WF sections 2.2m long, with a web thickness of 6.4mm, spaced at 900mm centers. These WF columns and steel plates are held in place by horizontal I-beams (254mm x 203mm) spaced at 900mm centers. These horizontal I-beams are connected to a 900mm thick concrete reaction floor, by 12mm diameter steel anchors spaced at 900mm centers. With the sand box thus constructed, it was anticipated that no appreciable deflections would take place off the walls and floor of the sand box.

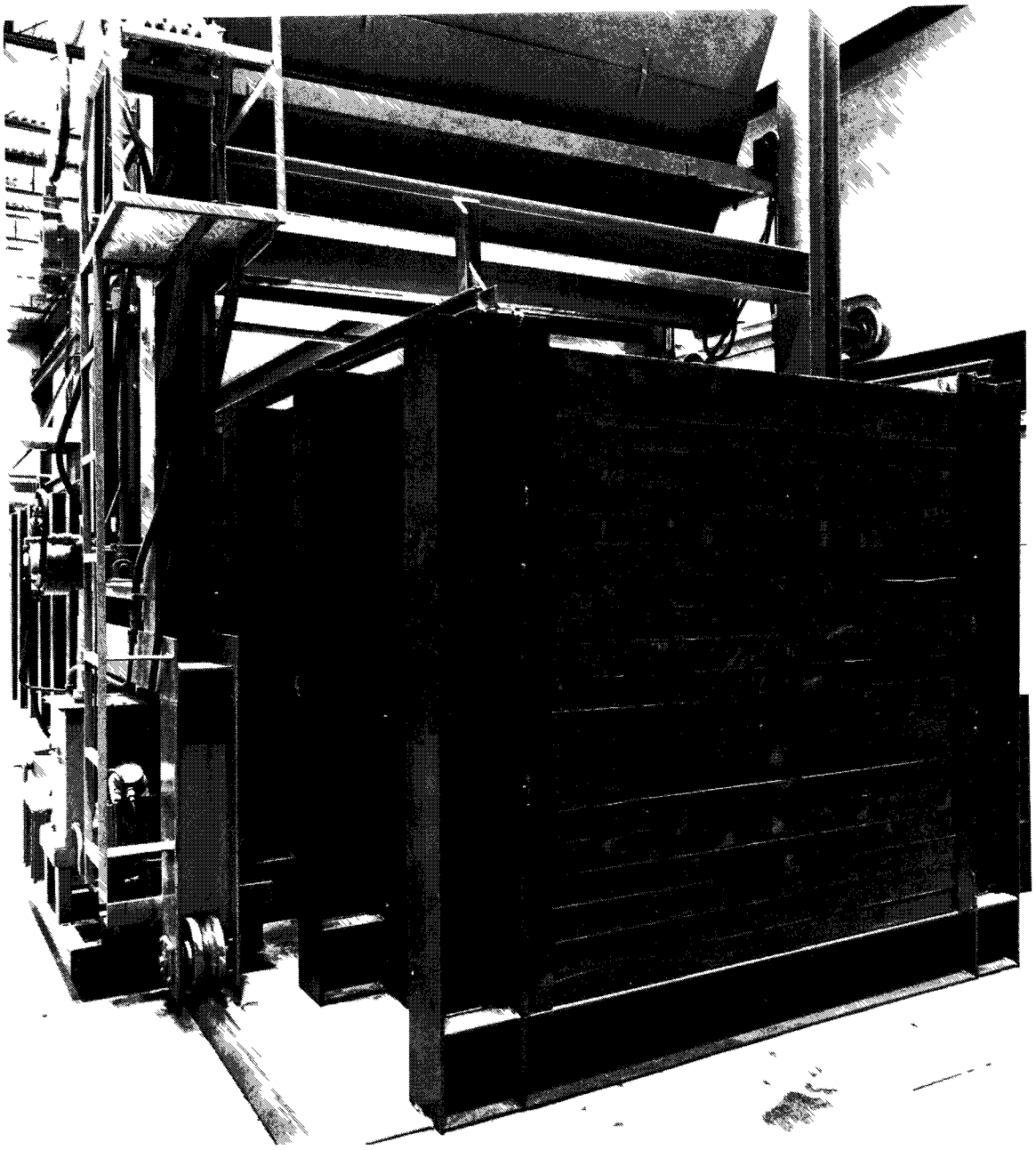

Sample box

Figure 4.1

Sand box

Figure 4.2

In order to maintain plane strain condition during the tests, it is important that the width of the box not change.

4.2.2.2 Effective Use of the Box

As previously mentioned, only one compartment of the box is used for testing and the other for storage. One compartment has an effective length of 6.7m. The maximum effective height of the slope is 1.8m and with a 2:1 slope, the length taken by the slope is 3.6m. This leaves a horizontal distance from the slope crest to the end of the sand box of 3.1m.

4.2.3 Sand Handling Equipment

4.2.3.1 General

For the purpose of the present study, a method of forming artificial beds of sand which are homogeneous and reproducible over a wide range of densities is required.

Walker and Whitaker (1967) report that Kolbuszenski (1948) has shown experimentally that a wide range of densities in dry sand could be produced by allowing the sand to be rained into place while building up the required sand beds. This can be achieved by the use of a raining device. The one used at the University of Ottawa is shown in Figure 4.3.

By controlling a certain set of variables, various densities can be achieved. These variables can be summarized as follows:

a) height of fall

b) drum rotating speed

c) horizontal travelling speed

The raining process has a problem which is inherent to it; when advancing, the curtain of falling sand displaces air in the container (sand box). Displacement of air becomes of particular concern as the curtain approaches the end wall of the box. The air current then bounces back into the sand curtain and reduces the intensity of fall in the central part, creating an uneven sand surface. This process can also affect the sand density close to the end wall of the box.

4.2.3.2 Physical Description

The sand spreader consists of three major parts: the frame, the hopper and the controls.

a) The Frame

The frame is a large assembly of I beams on which the hopper is mounted. The frame spans across the box and is equipped with wheels which travel on rails placed on both sides of the box. The frame also supports various motors and an oil reservoir.

Steel ladders were welded on to the frame in order to provide easy access to the control deck and the hopper.

b) The Hopper

The hopper is of triangular cross-section. It is an upside-down triangle with the point at the bottom. The

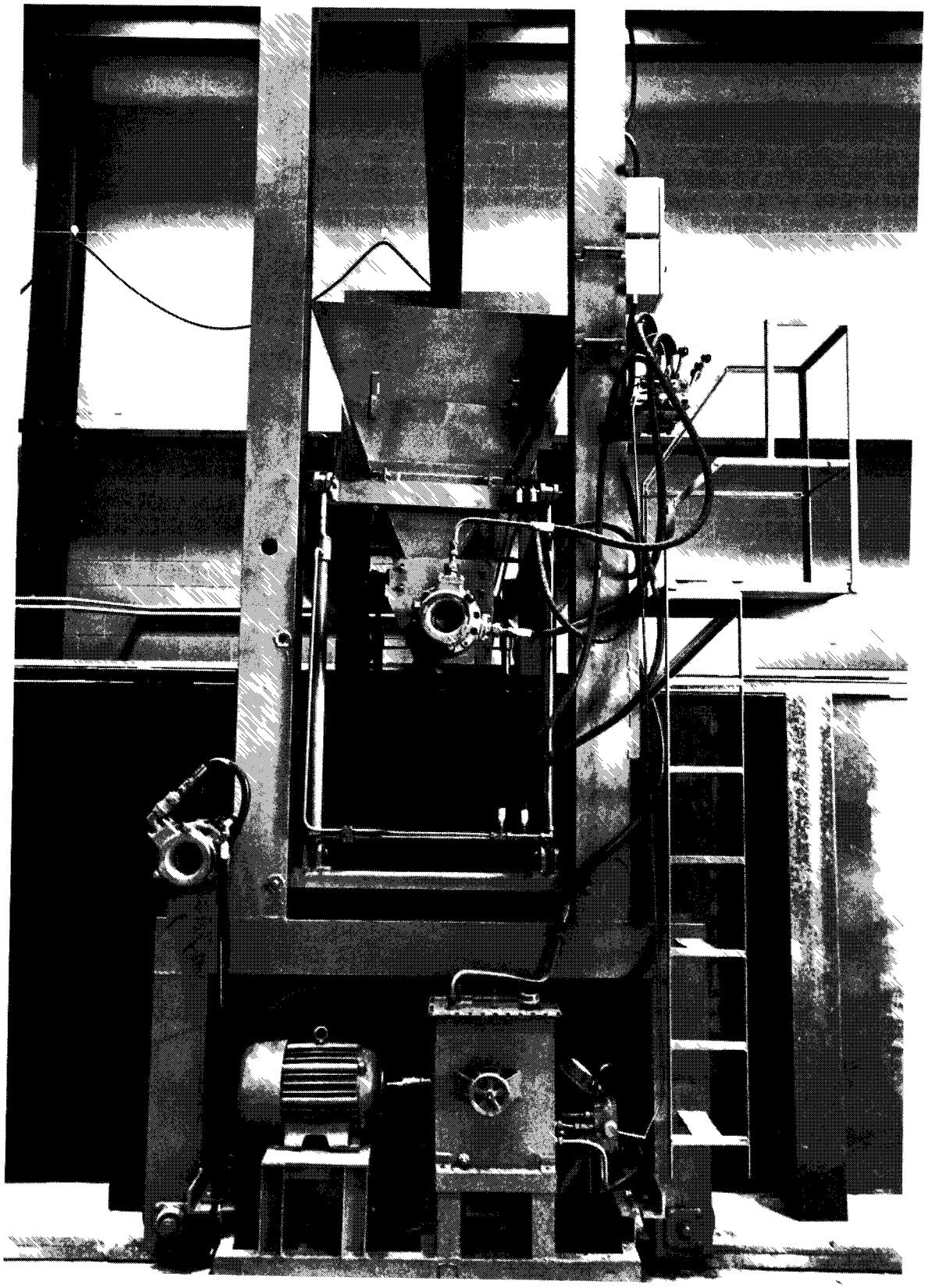

Spreading device

dimensions are 1.2m high, 1.2m wide at the top, and 1.9, long.

The whole hopper is mounted on the frame 1.8m from the ground and a few centimeters from the top of the box. It can be raised to a maximum of 0.6m above that level by activating hydraulic jacks mounted on each side of the frame.

At the bottom of the hopper, there is a rotating drum. The sand in the hopper falls onto the drum and is rotated into free fall. The drum speed can be controlled to achieve different intensities of fall.

There is also a deflector plate at the sand exit which can be adjusted to give different angles of deflection.

c) The Controls

There is a valve on the side of the oil reservoir which restricts the flow of oil to the rotating drum at the bottom of the hopper. This valve controls the rotating speed of the drum.

Four handles control the flow of oil to the various parts of the apparatus:

- two valves are needed to raise or lower the hopper
- one valve is needed to let the drum rotate
- one valve controls the horizontal speed of the whole frame. This horizontal control is designed so that the frame can go back and forth along the length of the box.

d) Sand Elevator

To feed the spreader an apparatus called a sand elevator was designed. It has a series of small buckets assembled on

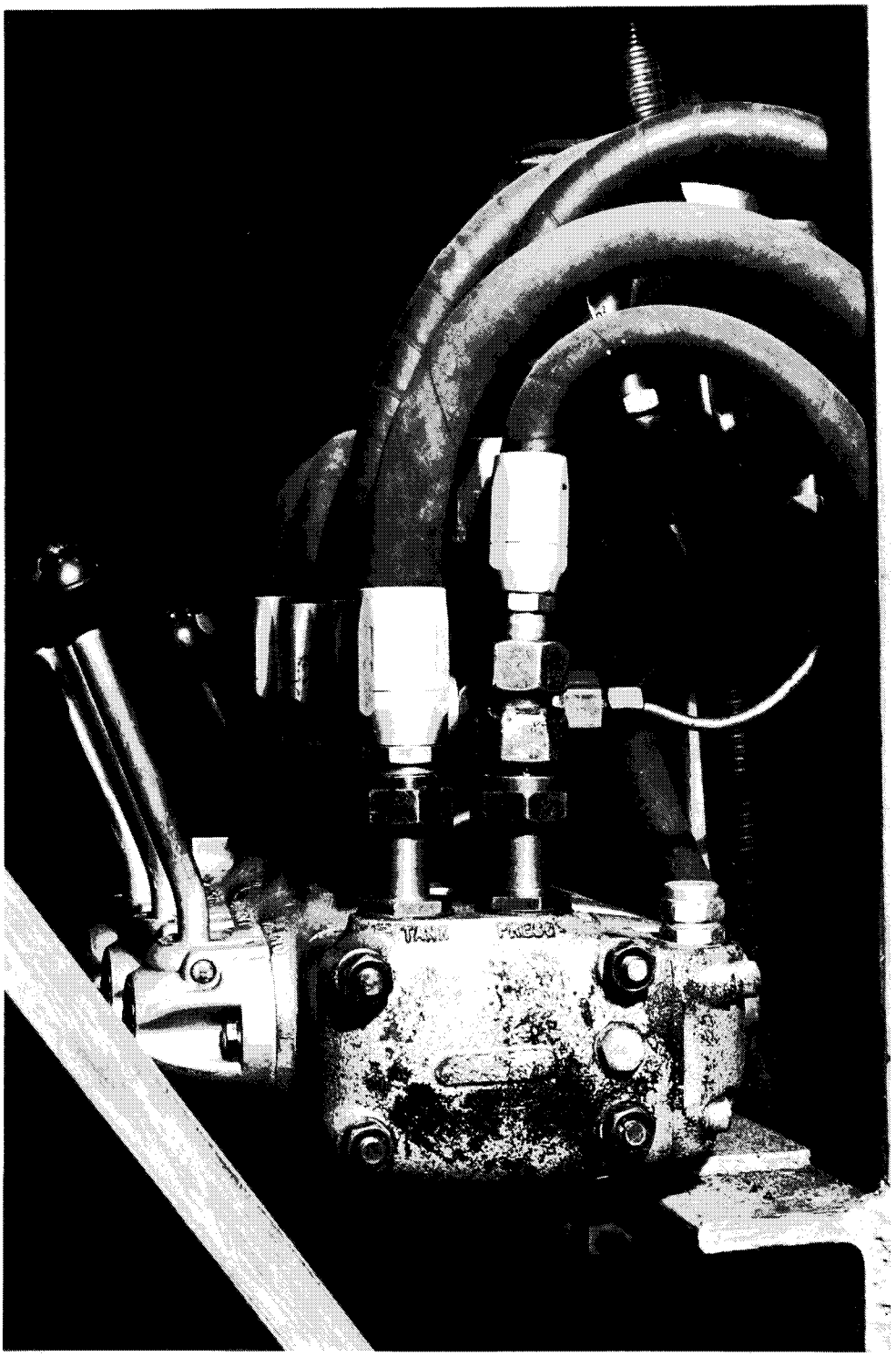

Control handles

Figure 4.4

a chain; these buckets pick up the sand. The sand dug up by the buckets is discharged into a funnel by centrifugal action, and is then directed into the hopper by a chute attached to the funnel. The bucket-elevator is held in place by a rigid rectangular frame structure which travels on rails built on the sand box. During a testing operation, the elevator usually stays in the compartment of the sand box which is being used for storage. The elevator is shown in Figures 4.5 and 4.6.

4.2.3.3 Speed Calibration of the Raining Device (Spreader)

The spreader was calibrated to ensure that it could carry out the raining process satisfactorily. Firstly the quantity of sand in the hopper (load of sand) was varied in order to see whether this might influence the horizontal speed of the spreader and the speed of rotation of the drum. Secondly, the influence of the speed of rotation of the drum and height of fall of the sand on the sand density was studied.

4.2.3.3.1 Influence of the Hopper Load on the Horizontal Speed of the Spreader

In order to get an idea of the change in horizontal speed of the spreader with a variation in the quantity of sand in the hopper, the following procedure was carried out: a) the quantities of sand in the hopper were divided into

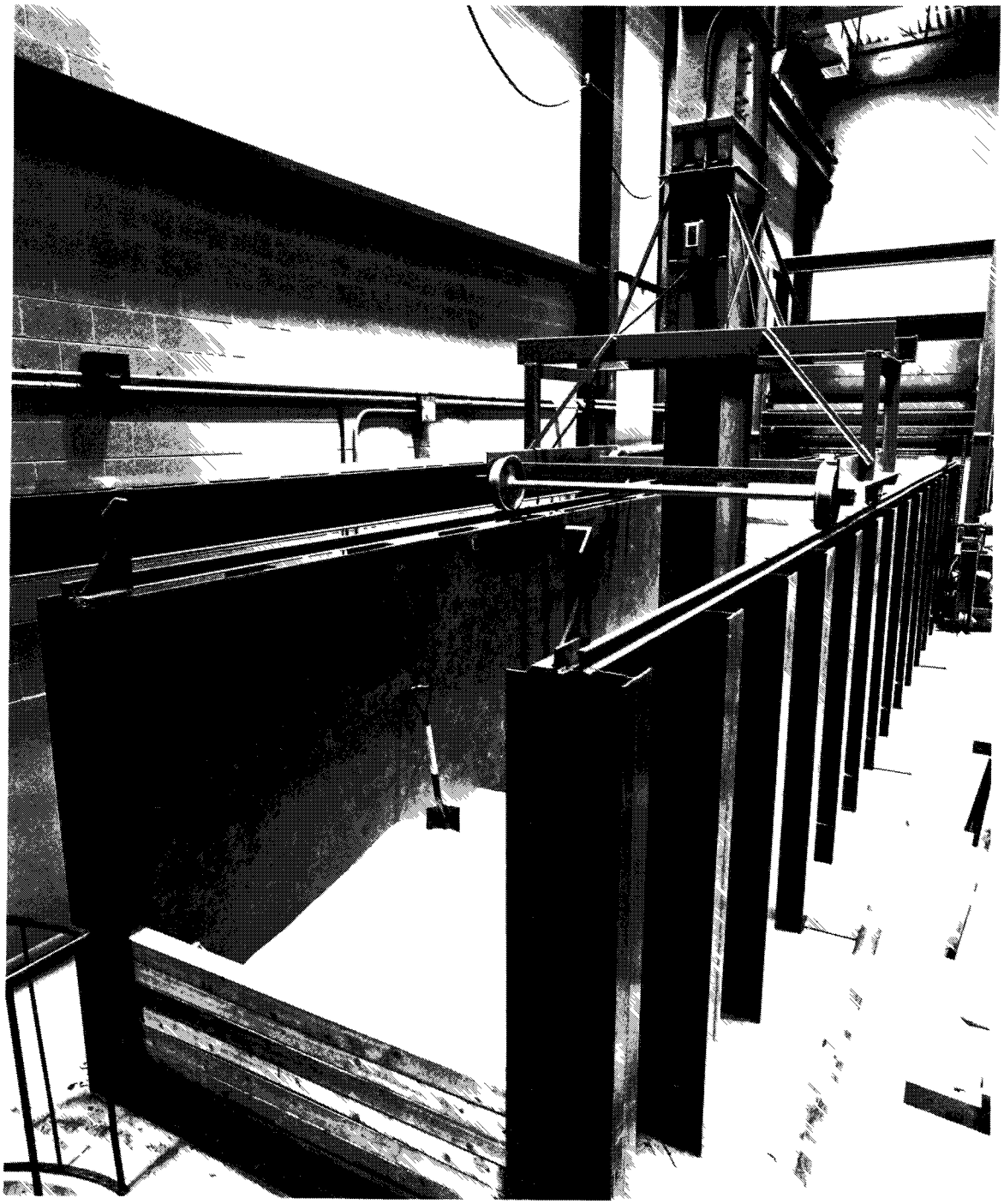

Sand Elevator

Figure 4.5

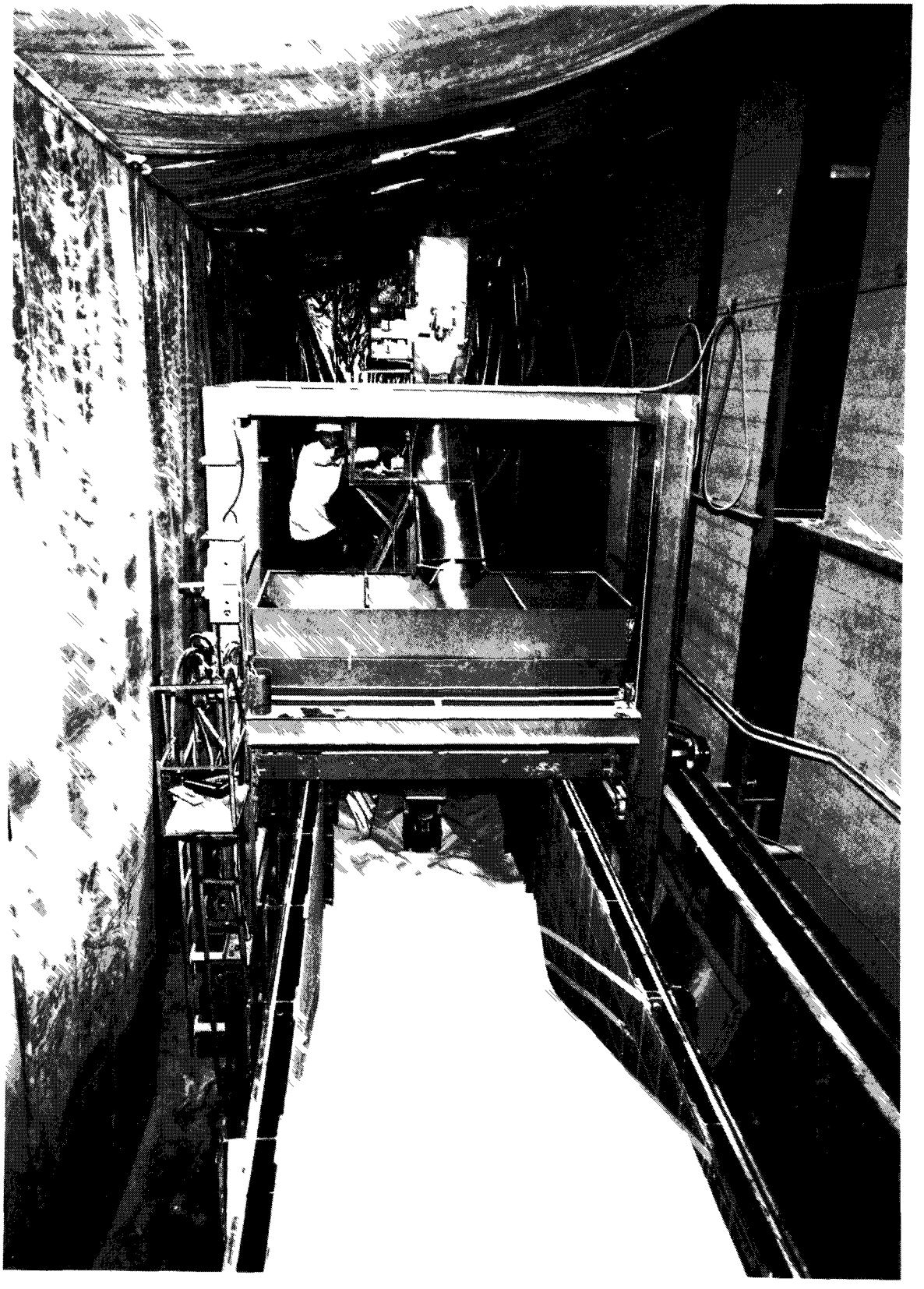

Sand elevator

Figure 4.9

five load conditions:

i) full hopper load

ii) 3/4 hopper load

iii) 1/2 hopper load

iv) 1/4 hopper load

v) empty

b) for each load condition described above the spreader was made to travel 6m along its rails while the time required to cover this distance was monitored using a stop watch. This process was repeated six times for each load condition in both directions. The results are presented in the table of Figure 4.7. It must be pointed out that the last two columns are for statistical purposes, one giving the average of the six values and the other the standard deviation.

The results presented in Figure 4.7 are also shown as a graph on Figure 4.8. From these figures one may say that the loading condition has a slight influence on the horizontal speed. In order to minimize even this slight influence of the hopper load, the spreading operation is only carried out when the hopper is more than half full; in this condition almost no variation in horizontal speed is noticed.

4.2.3.3.2 Influence of the Hopper Load on the Speed of Rotation of the Drum

The influence of the hopper load on the speed of rotation

of the drum was checked. A rotating speed of 3.5 r.p.m. was set for the no load condition (empty hopper) and then the speed was measured for different hopper loads. The results are shown in the table of Figure 4.9.

As can be seen the hopper load has very little influence on the rate of rotation of the drum. Therefore it is concluded that no adjustment has to be made to ensure that the speed of rotation of the drum does not change with hopper load.

4.2.4 Loading Frame

4.2.4.1 Description

The loading frame is shown in Figure 4.12. It consists of a 514mm x 159mm I-beam with a web and flange thickness of 13mm and a length of 2.52cm; two sets of channels 2.41m long are welded to each end of the I-beam to form the vertical sides of the frame. The I-beam is stiffeend by 13mm thick plates at points where the hydraulic jacks are installed.

Six holes were drilled on either side of the center line of the I-beam which support the sides of the box at the positions where the loading frame is placed. The first hole is at a distance of 229mm from the top of the sand box. The holes were drilled at 76mm centers. Compatible holes were also drilled in the channels of the loading frame, leaving the loading frame standing at a height of 1.72m above the sand box.

Horizontal Speed (m./sec.)

Loading cot.	Direction	1	2	3	4	5	6	ave.	σ std devi.
empty	east	.23	.23	.23	.23	.23	.23	.23	0
	west	.22	.23	.23	.23	.22	.22	.23	0
¼ load	east	.23	.23	.23	.23	.23	.23	.23	0
	west	.22	.22	.23	.23	.22	.22	.22	.01
½ load	east	.22	.22	.22	.22	.22	.22	.22	0
	west	.21	.21	.21	.21	.21	.21	.21	0
3/4 load	east	.21	.21	.21	.21	.21	.21	.21	0
	west	.20	.21	.20	.20	.20	.20	.20	.01
full	east	.20	.21	.21	.20	.20	.20	.20	.01
	west	.20	.20	.20	.20	.20	.20	.20	0

Figure 4.7

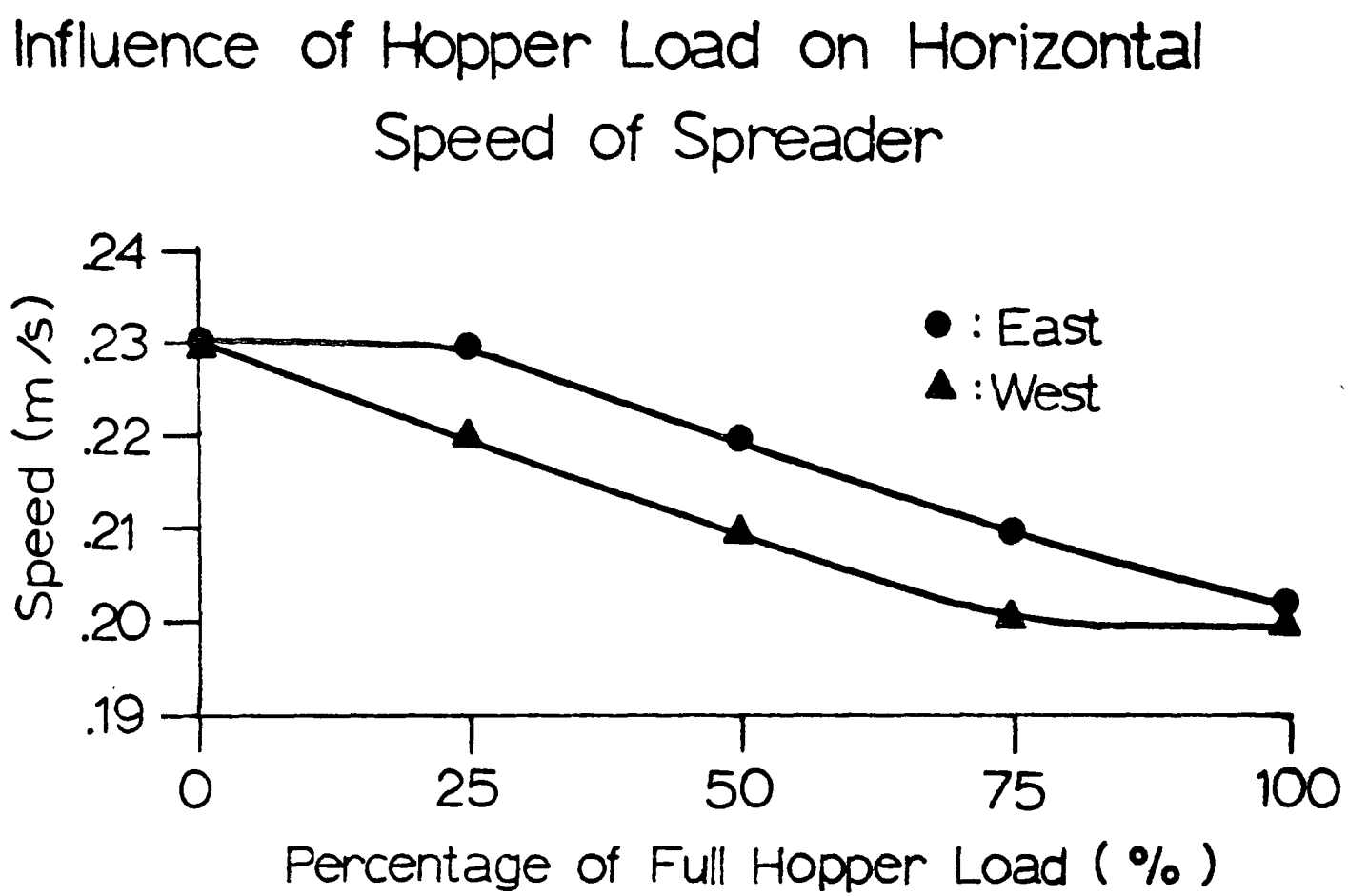
Influence of Hopper Load on Horizontal Speed of Spreader
Speed (m/s)
.24
.23
.22
.21
.20
.19
● : East
▲ : West
0
25
50
75
100
Percentage of Full Hopper Load (%)

Figure 4.8

Drum Speed (r.p.m.)

Load cot.	Drum speed fixed at	1	2	3	4	5	6	ave	σ std dia.
empty	3.5	3.5	3.5	3.5	3.5	3.5	3.5	3.5	0
¼ load	3.5	3.6	3.6	3.6	3.6	3.6	3.6	3.6	0
½ load	3.5	3.6	3.6	3.6	3.6	3.6	3.6	3.6	0
3/4 load	3.5	3.5	3.6	3.6	3.5	3.5	3.5	3.5	.1
full	3.5	3.5	3.5	3.4	3.5	3.4	3.4	3.4	.1

Figure 4.9

Test footing

Figure 4.10

An additional I-beam had to be installed at lower levels in the frame during the deep bearing capacity tests since the travel of the jacks was insufficient to reach all the way from the permanent I-beam to the founding level. The frame was moved out of the way of the sand handling operation on wheels which ran on the rails built along the top of the sides of the sand box.

This type of apparatus was designed so that the mechanism for applying loads to the model foundations could be set up over the sand, without touching or interfering with it in any way, thus avoiding any risk of altering the initial state of compaction of the sand.

Three hydraulic jacks were welded to 152mm x 152mm x 16mm plates. These plates were subsequently bolted to the reaction beam at a distance of 60cm from the end channels and at 61cm centers. The cylinders of the jacks had an internal diameter of 12.5cm. The pressures exerted by these jacks were monitored by hydraulic gauges and in the case of the central jack only by an electronic load transducer mounted between the jack and the reaction beam.

4.2.4.2 Loading Frame Calibration

During a test, the vertical movement of the footing was referenced to the loading frame. In order to plot the true settlement of the footing it was necessary to subtract the deformation of the loading frame from the measurements of

movement.

The deformation of the frame was calibrated over the full range of capacity of the jacks - see Figure 4.11 and 4.12. Measurements were made of the horizontal displacement of the central jack during calibration in order to ensure that the load remained vertical.

As it can be seen, in this table, the horizontal displacements of the central jack are negligeable and are considered to have no effect on the test results. The vertical movement of the loading frame is sufficiently significant that a correction is made to the measured movements of the footing.

4.3 Sand Used in the Experiments

4.3.1 Description

The sand used in these experiments is a crushed white silica sand. The strength properties of the sand were determined by M.M. Hasnain (1974) who performed a variety of triaxial and direct shear box tests on the sand. Furthermore, a special plane strain triaxial testing program was carried out on the sand in the geotechnical laboratory of the Department of Civil Engineering at Queen's University in Kingston, Ontario. All test samples were prepared in the same manner.

The manufacturer designates the sand as Silica - 24. It is sharp and angular. With a uniformity coefficient of about 2.1, it can be classified as a uniform sand. From the grain size distribution curves (Figure 4.16) it is seen to be a fine

Applied pressure kPa	Horizontal displacement of central jack cm.	Vertical movement of frame cm.
0	0	0
5	.01	.01
25	.24	.03
50	.46	.17
75	.46	.18
100	.47	.20
125	.47	.21
150	.47	.23
175	.46	.23
200	.46	.23
225	.46	.25
250	.46	.25
275	.47	.26
300	.46	.26
325	.46	.26
350	.46	.26
375	.45	.26
400	.45	.28
425	.44	.30
450	.44	.30
475	.44	.31

Figure 4.11

Applied pressure kPa	Horizontal displacement of central jack cm.	Vertical movement of frame cm.
500	.43	.31
525	.43	.32
550	,43	.32
575	.43	.32
600	.45	.34
625	.45	.37
650	.44	.37
675	.44	.37
700	.44	.38
725	.46	.38
750	.44	.40
775	.43	.40
800	.43	.42
825	.46	.44
850	.45	.45
875	.44	.45

Figure 4.11 (cont'd)

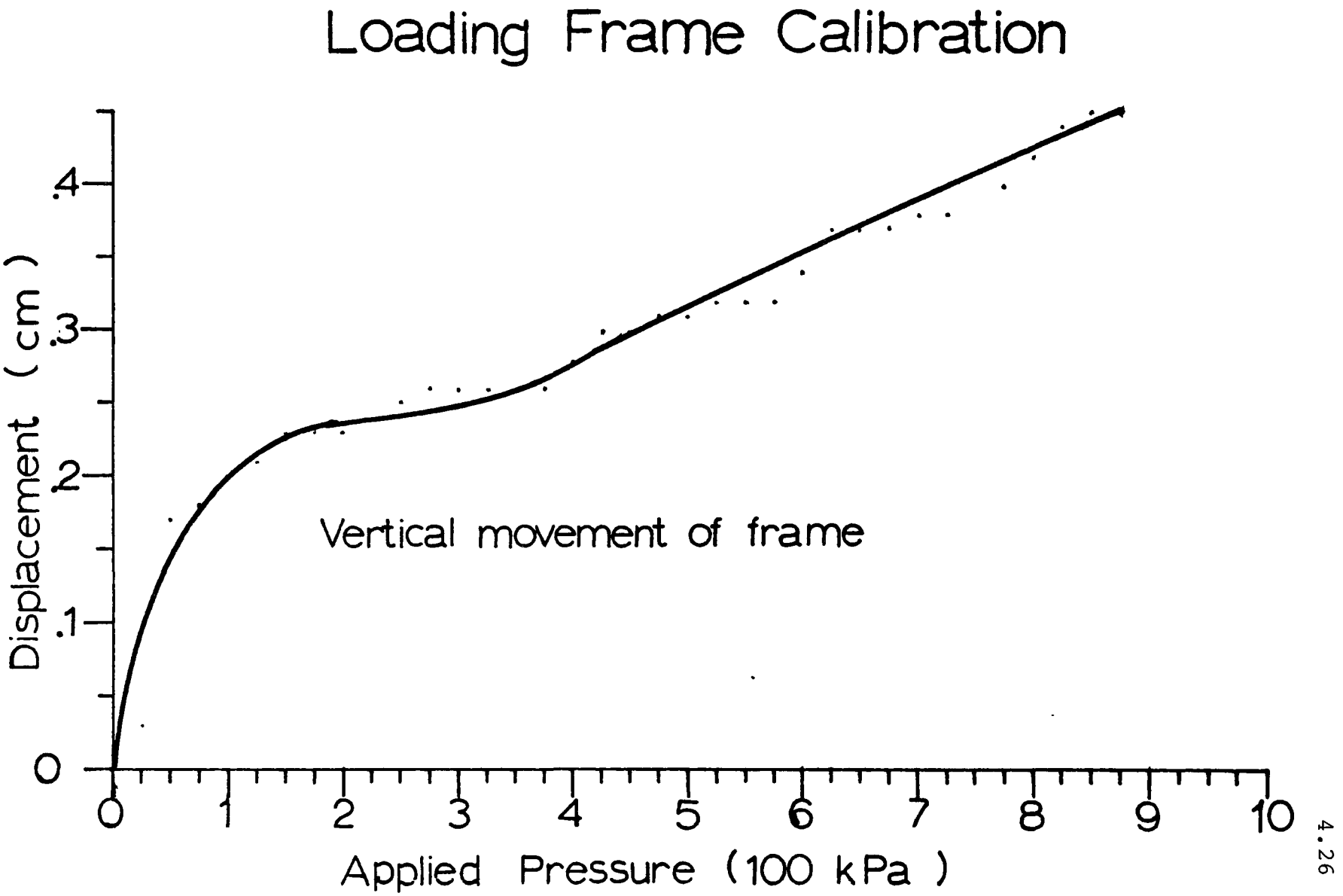
Loading Frame Calibration
Displacement (cm)
0
.1
.2
.3
.4
Vertical movement of frame
0
1
2
3
4
5
6
7
8
9
10
Applied Pressure (100 kPa)

Figure 4.12

to medium sand. Four tests were conducted for grain size distribution before the testing program started.

Since there was some concern that the sand might break down during handling as the tests were carried out, the grain size distribution of the sand was checked at various times during the test program, and these check tests were compared with the 4 initial grain size curves. No significant change was noticed during testing.

The maximum and minimum densities of the sand using A.S.T.M. procedures, were 1660 kg/m^3 and 1250 kg/m^3 respectively. The conversion of densities into relative densities is shown on Figure 4.14 . The specific gravity of the particles was found to 2.66. The minimum and maximum void ratios were 0.61 and 1.13, and the corresponding porosities were 0.38 and 0.53 respectively.

As previously stated, the determination of the shearing properties of the sand was by means of triaxial, shear box, and plane strain tests. In addition constant diameter K_o tests were performed. The results of these tests are given in Figures 4.15 to 4.25.

All results are summarized on Figure 4.2 entitled "Influence of Normal Stress on Shearing Resistance." As shown in table 4.2 the strain at failure for this sand is very high. This behavior of uniform angular sand is to be expected. As reported by Holubec and D'Appolinia (1973); angular uniform sand fails at much larger strains than uni-

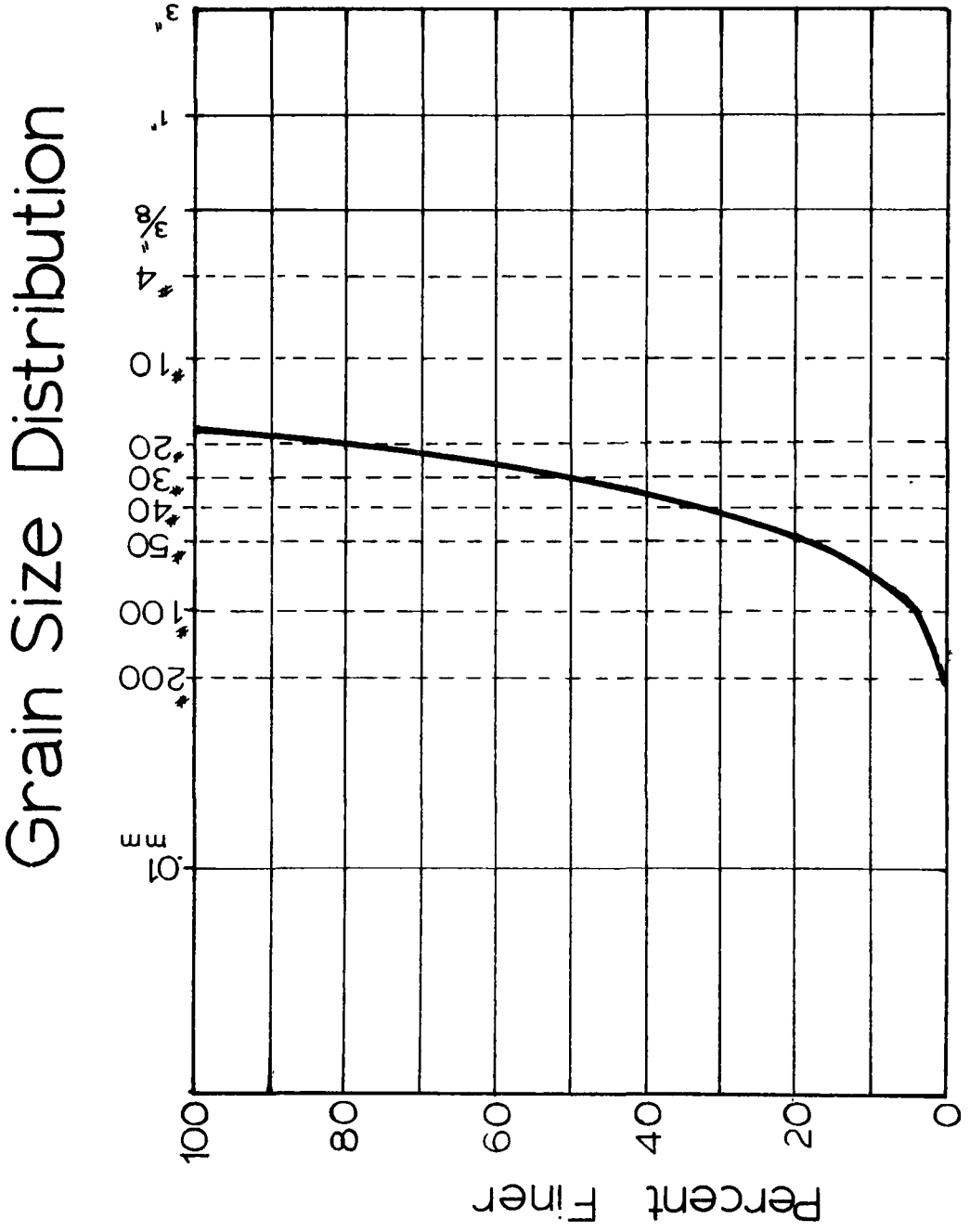
Grain Size Distribution
Percent Finer
100
80
60
40
20
0
3"
1"
3/8"
#4
#10
#20
#30
#40
#50
#100
#200
.01 mm

Figure 4.13

Relative Density Relationship

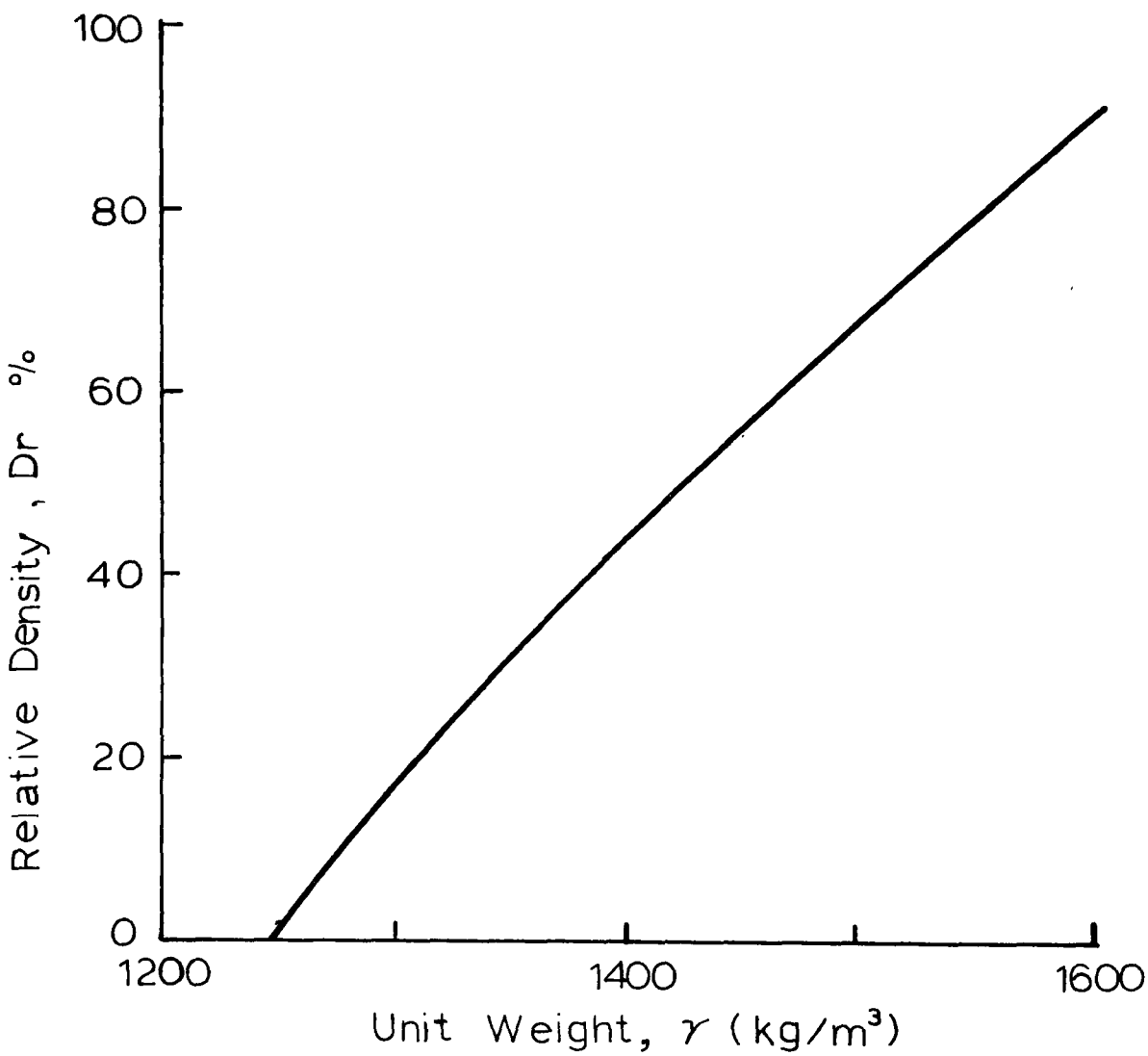

Figure 4.14

Triaxial Test Results - Very Dense Sand

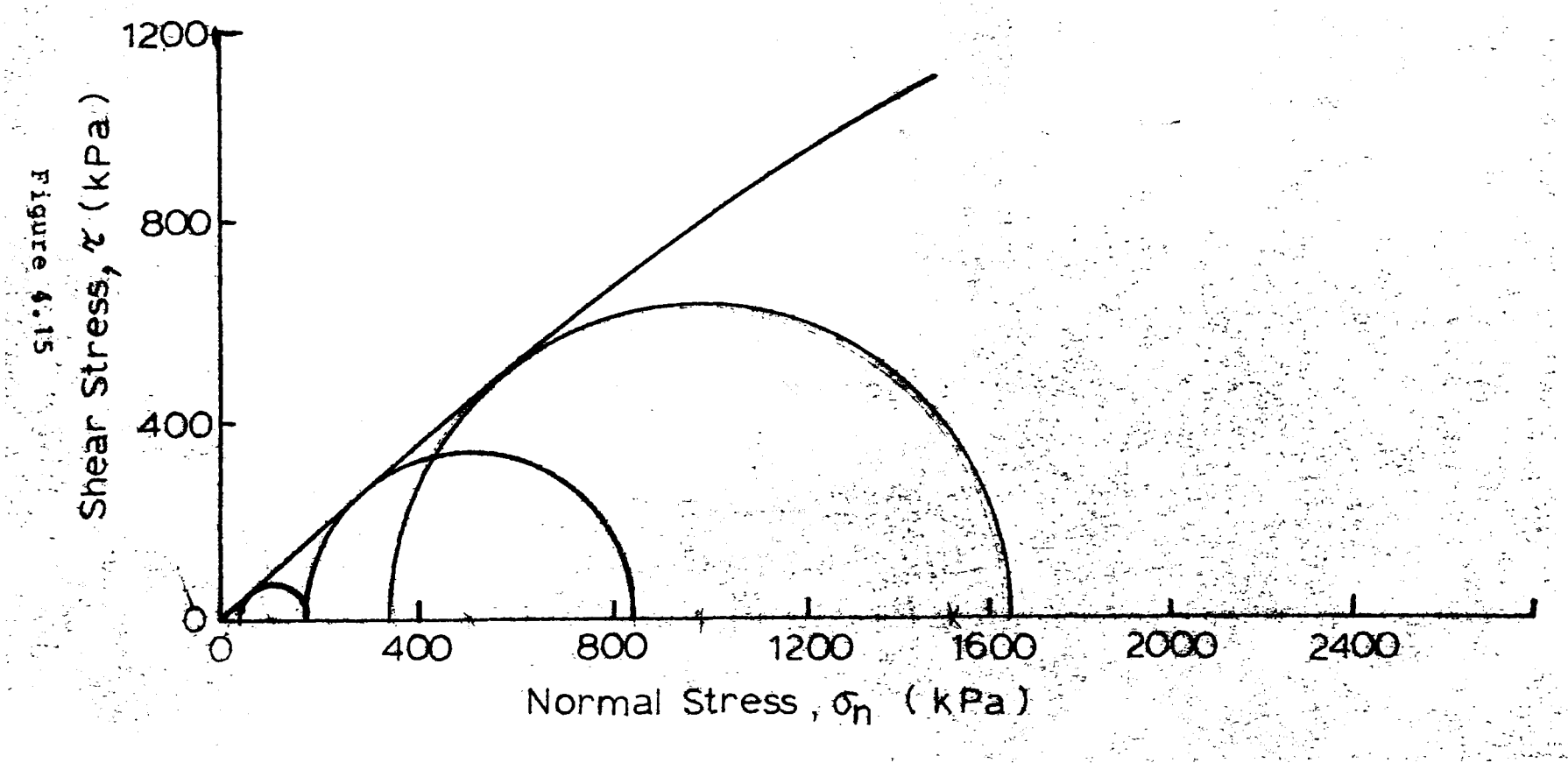

Figure 4.15

4.30

Triaxial Test Results - Dense Sand

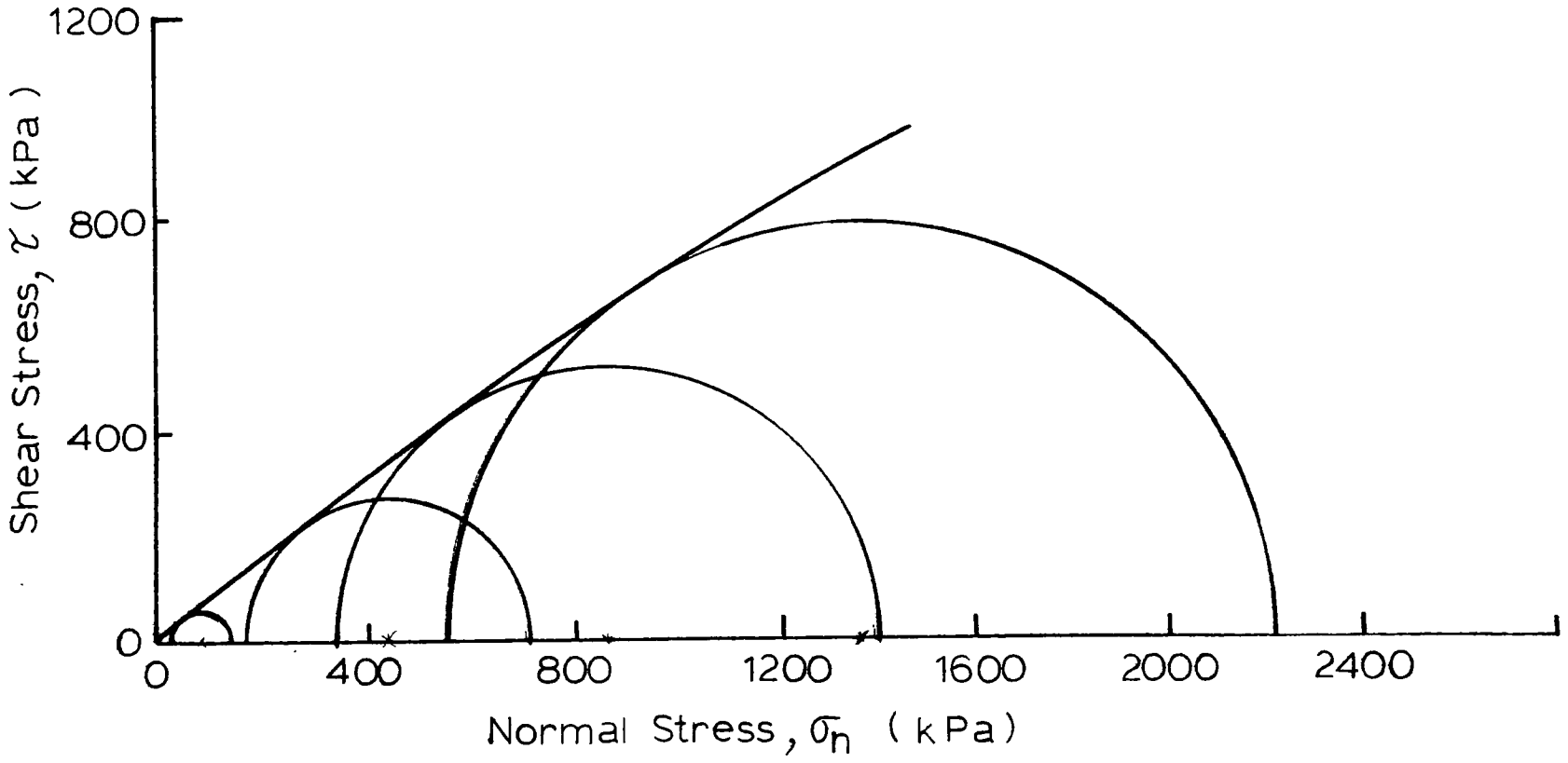

Figure 4.16

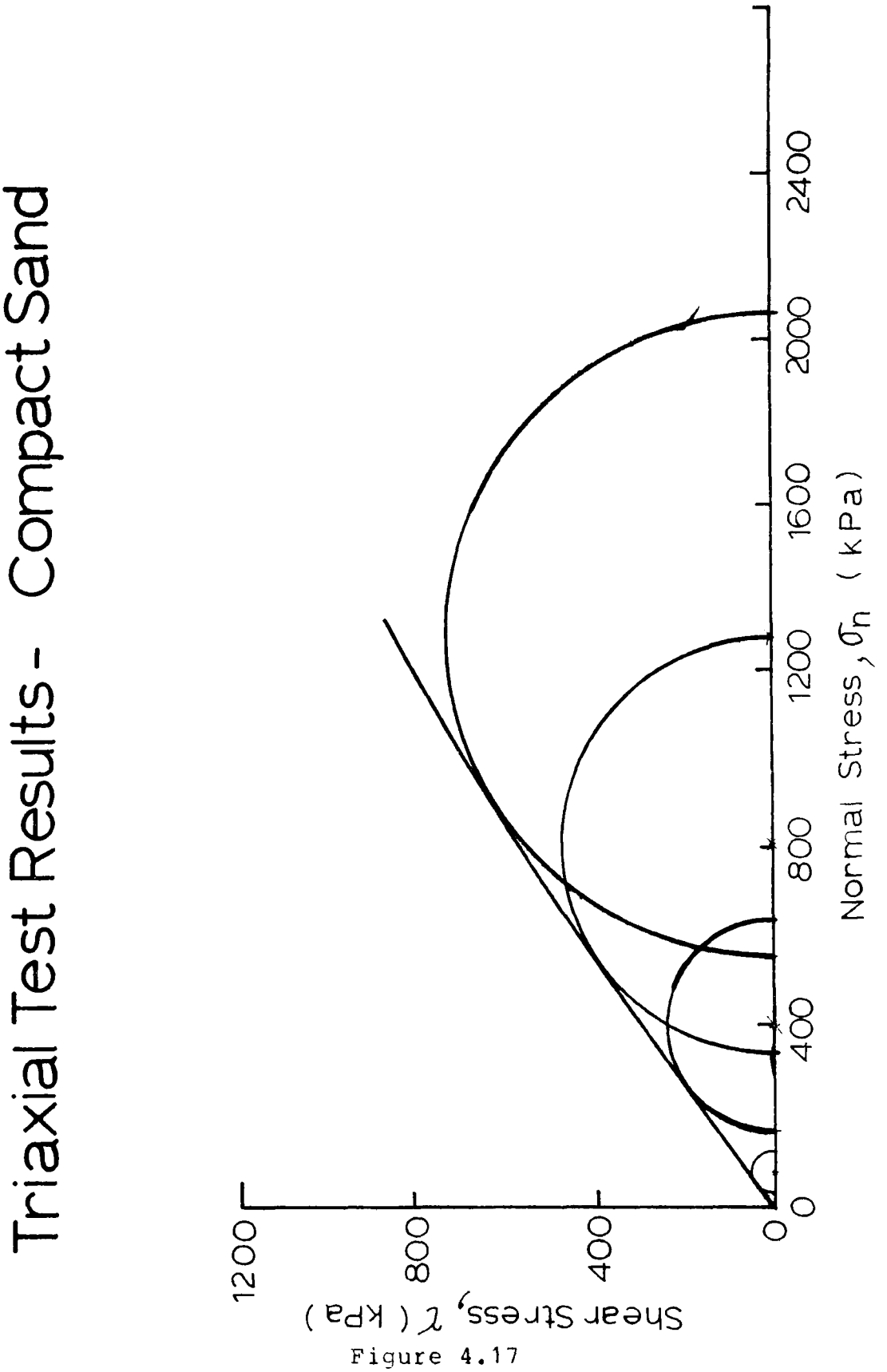
Triaxial Test Results - Compact Sand
Shear Stress, τ (kPa)
0
400
800
1200
Normal Stress, σn (kPa)
0
400
800
1200
1600
2000
2400

Figure 4.17

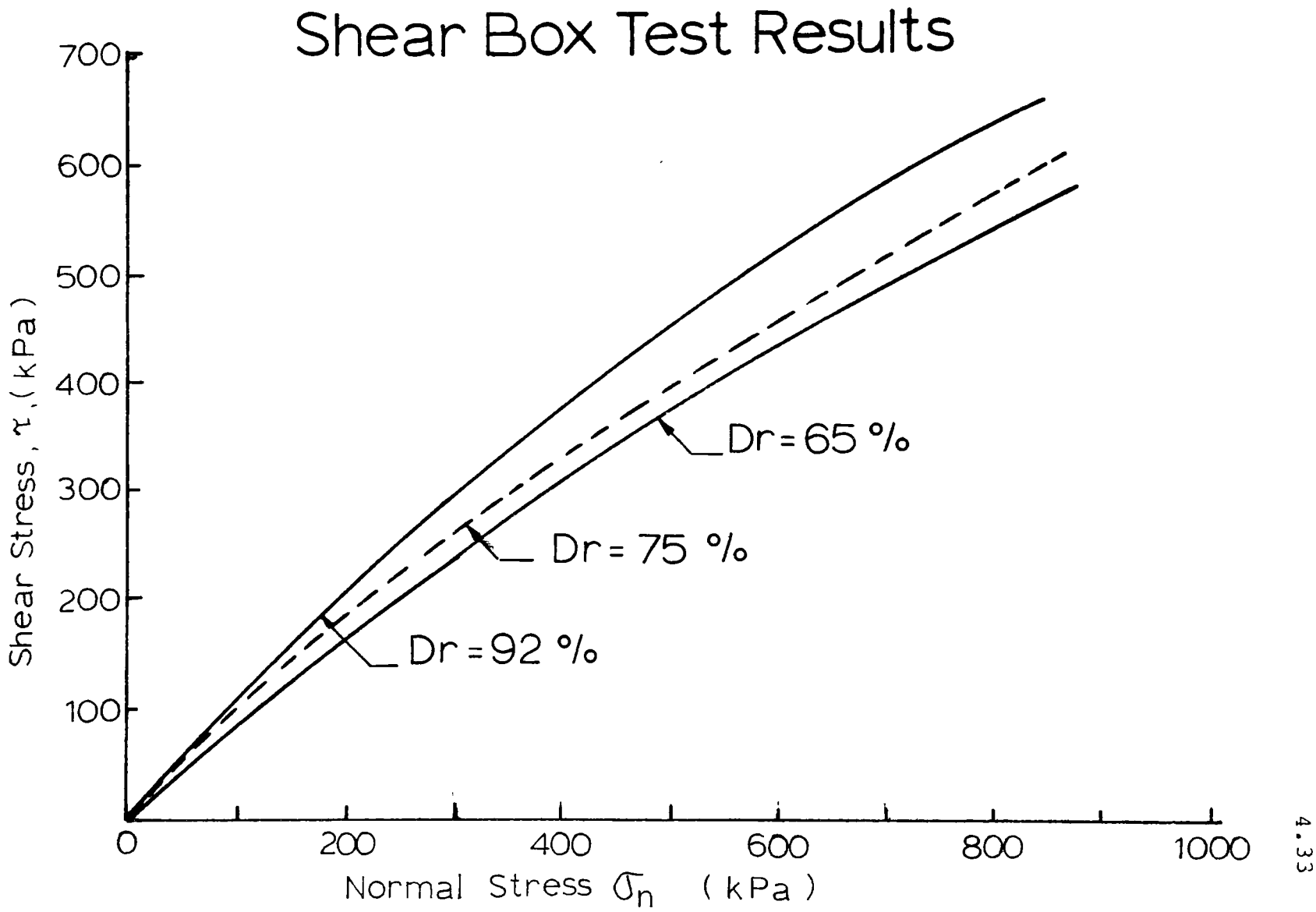
Shear Box Test Results
700
600
500
400
300
200
100
Shear Stress, τ, (kPa)
Dr = 65 %
Dr = 75 %
Dr = 92 %
0
200
400
600
800
1000
Normal Stress σn (kPa)

Figure 4.18

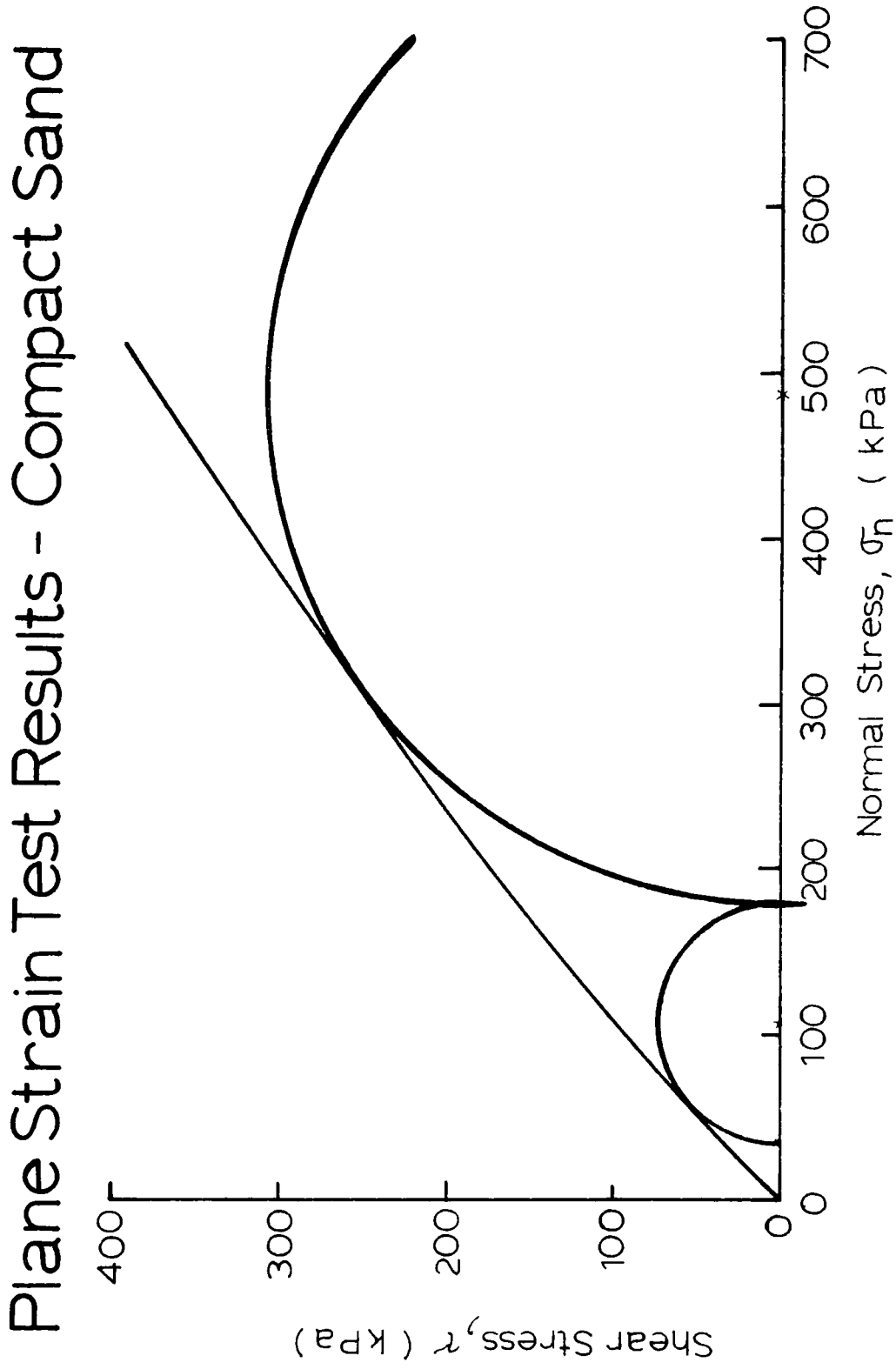
Plane Strain Test Results - Compact Sand
Shear Stress, τ (kPa)
Normal Stress, σn (kPa)
0
100
200
300
400
500
600
700

Figure 4.19

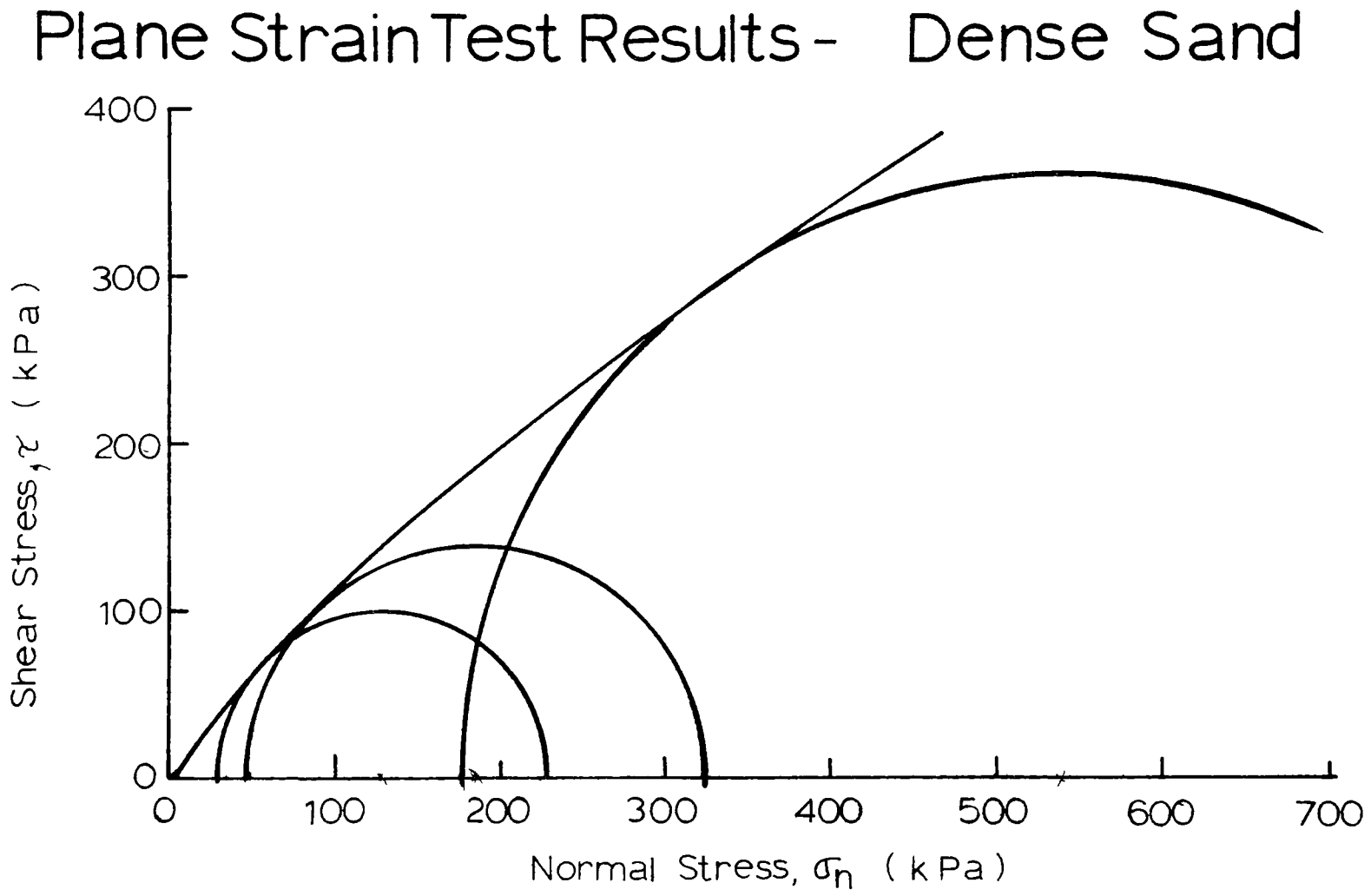
Plane Strain Test Results - Dense Sand
400
300
200
100
0
Shear Stress, τ (kPa)
0
100
200
300
400
500
600
700
Normal Stress, σn (kPa)

Figure 4.20

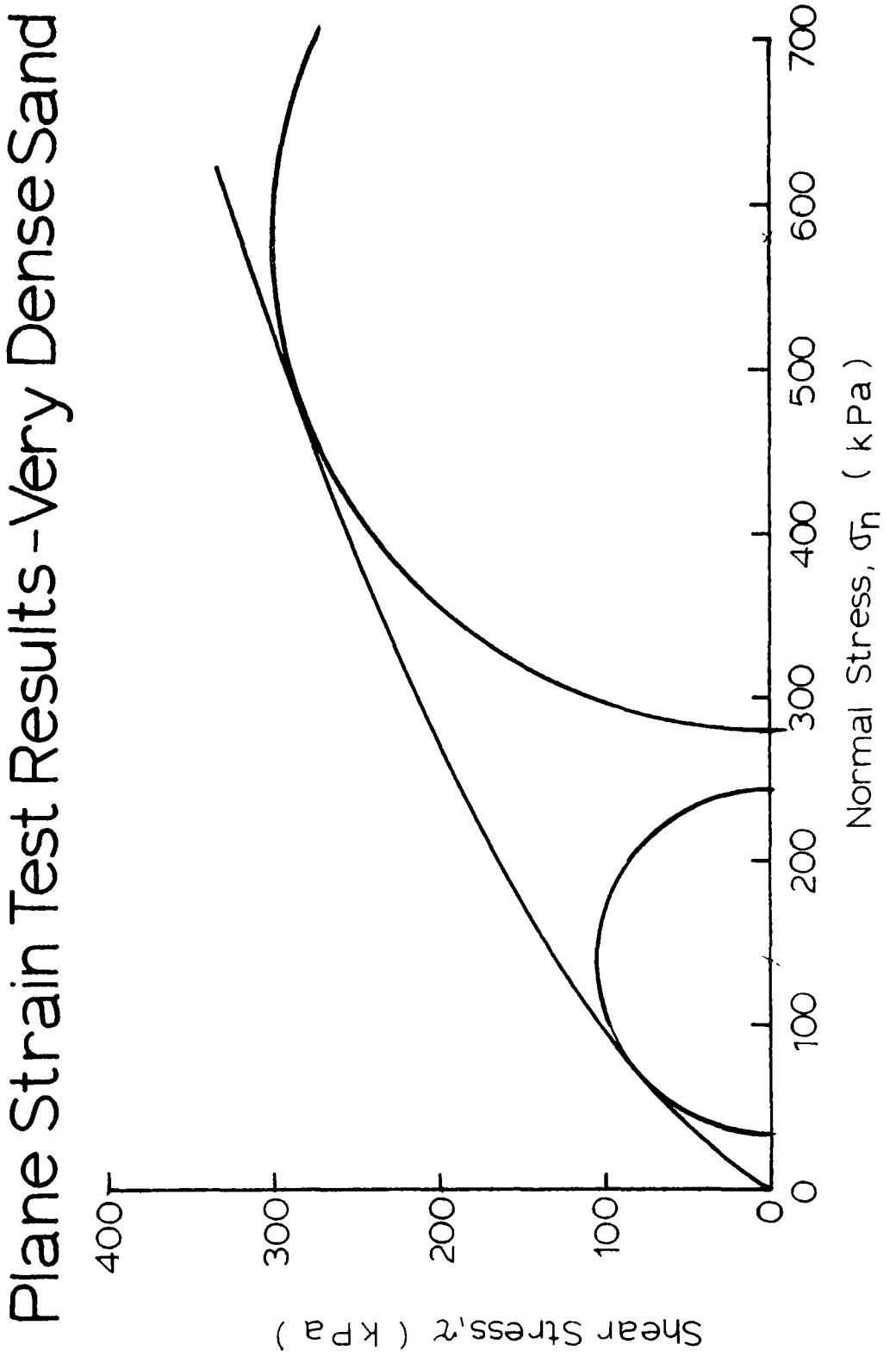
Plane Strain Test Results - Very Dense Sand
Shear Stress, τ (kPa)
0
100
200
300
400
Normal Stress, σn (kPa)
0
100
200
300
400
500
600
700

Figure 4.21

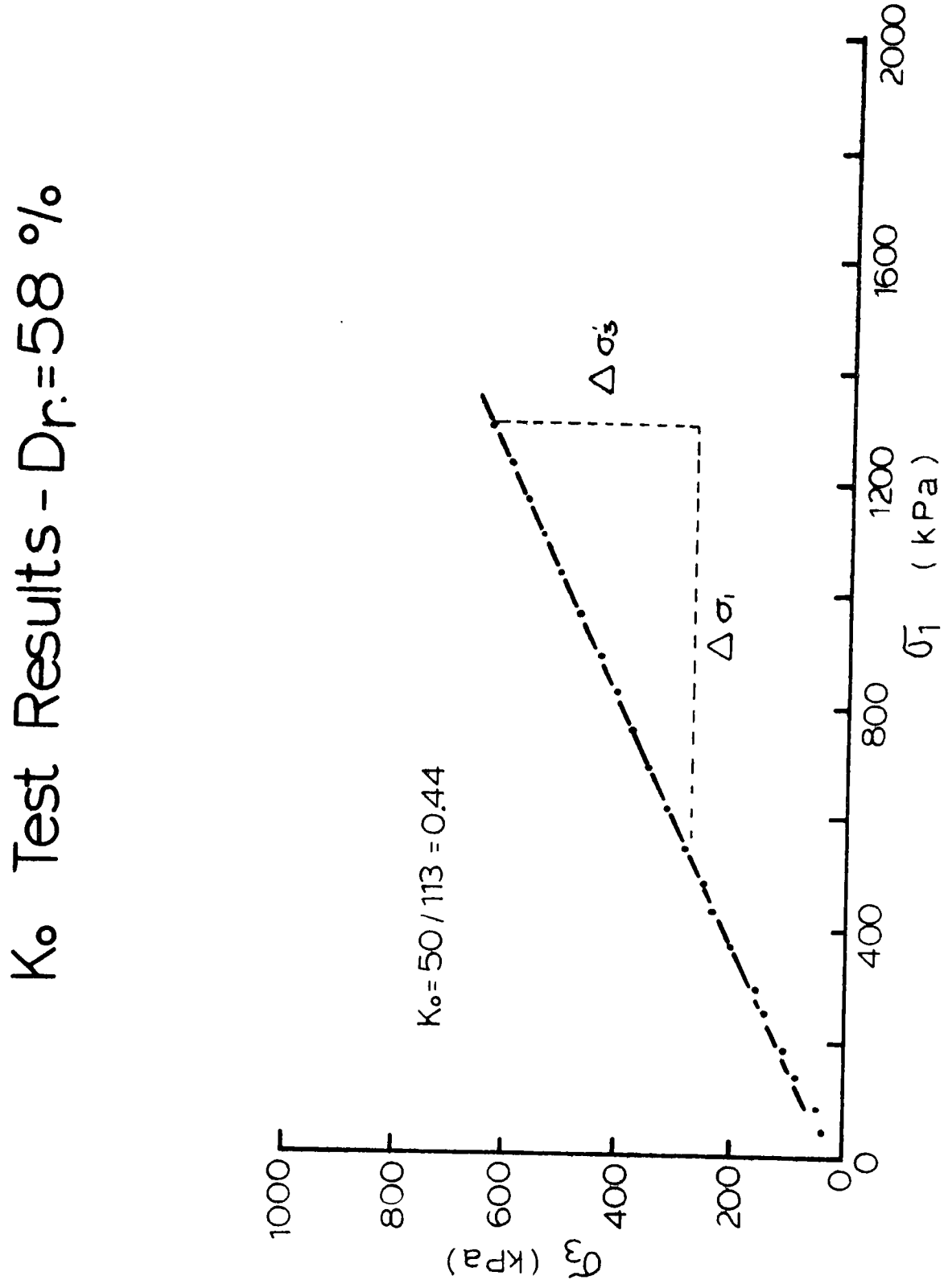
Ko Test Results - Dr.=58 %
Ko= 50 / 113 = 0.44
Δσ3
Δσ1
σ3 (kPa)
σ1 (kPa)
0
200
400
600
800
1000
400
800
1200
1600
2000

Figure 4.22

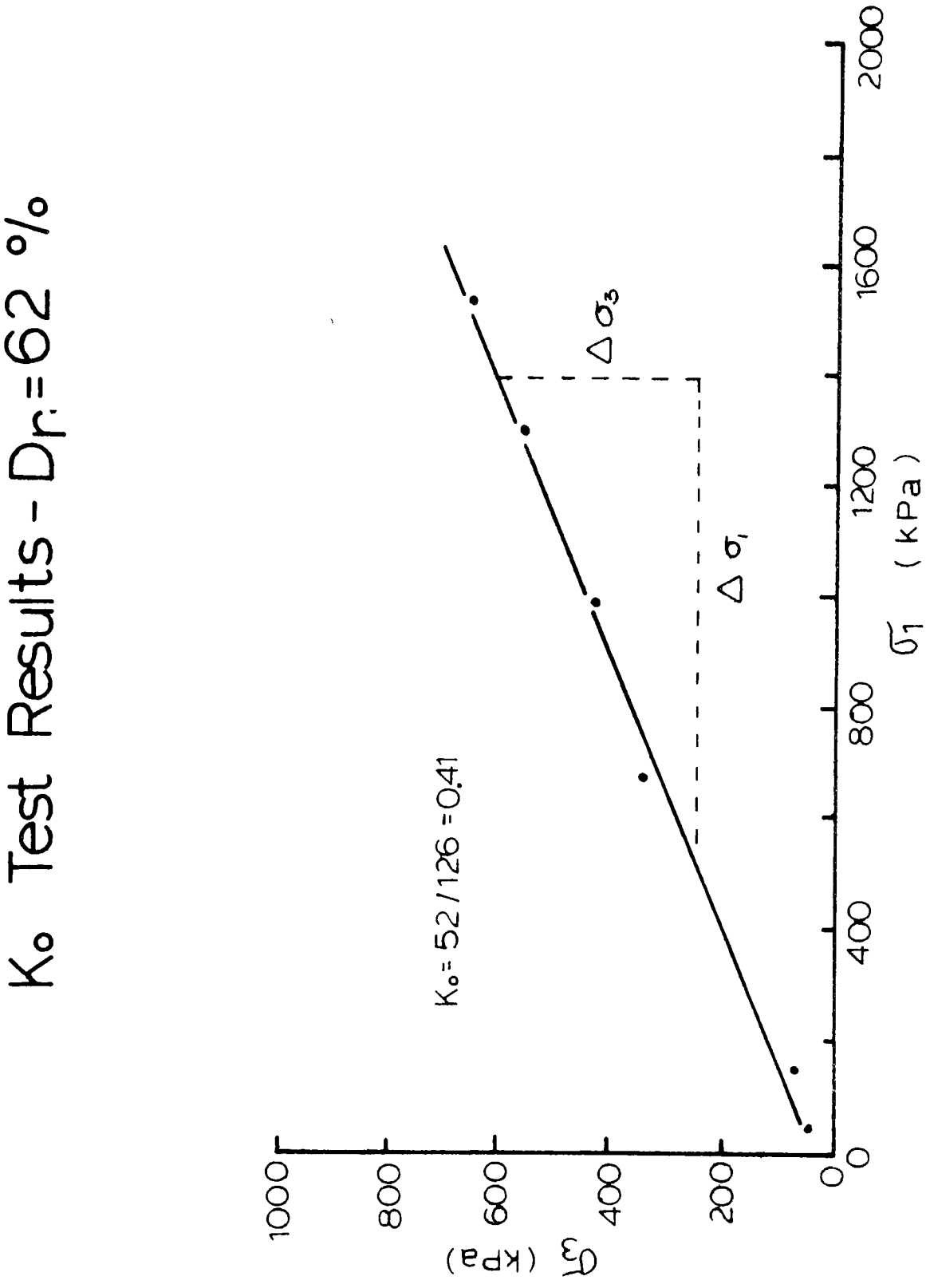
Ko Test Results - Dr=62 %
Ko= 52/126 =0.41
Δσ3
Δσ1
σ3 (kPa)
σ1 (kPa)
0
200
400
600
800
1000
400
800
1200
1600
2000

Figure 4.23

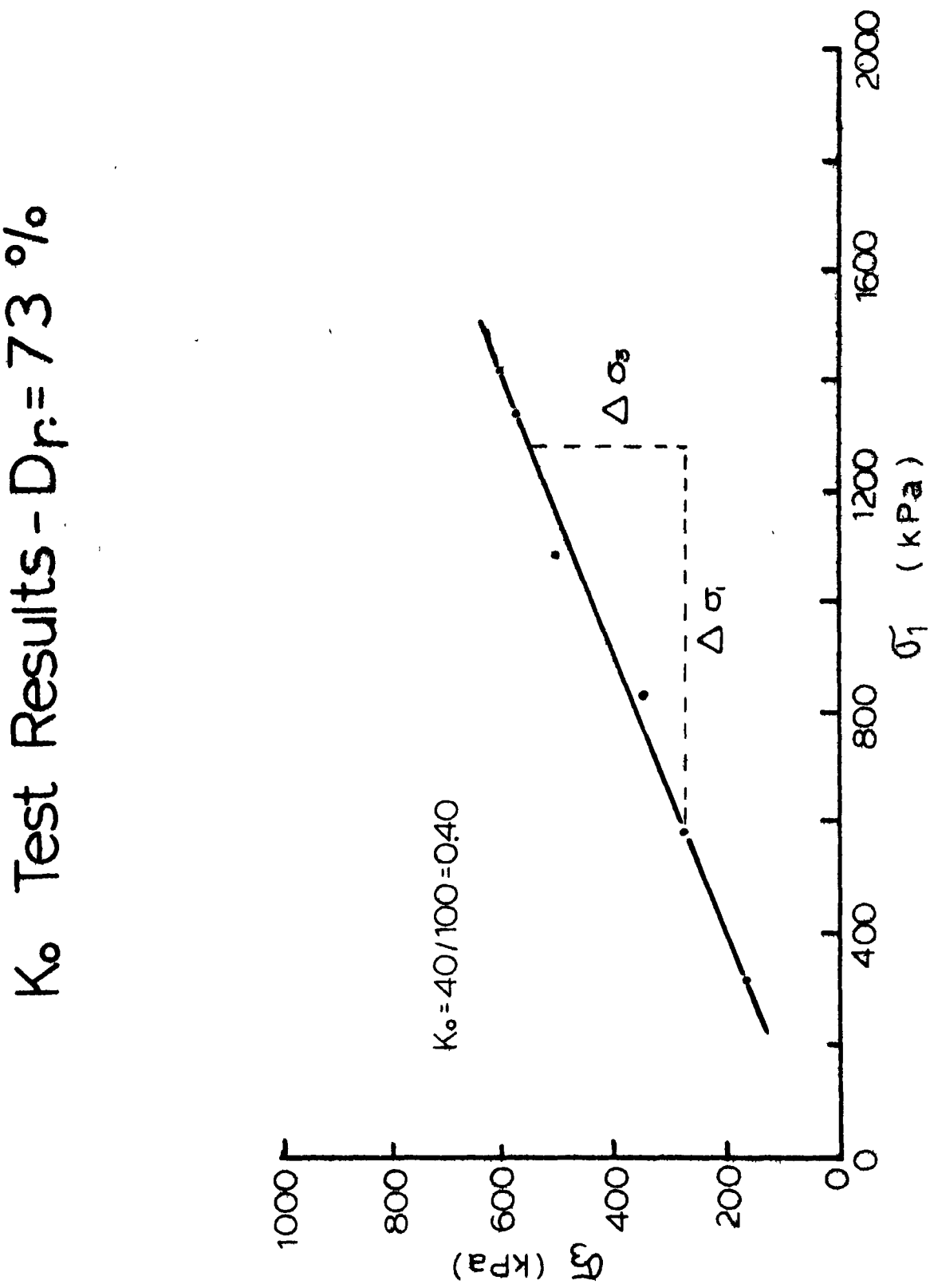
K_o Test Results - D_r = 73 %
K_o = 40/100 = 0.40
$\Delta\sigma_3$
$\Delta\sigma_1$
σ_3 (kPa)
σ_1 (kPa)
0
200
400
600
800
1000
400
800
1200
1600
2000

Figure 4.24

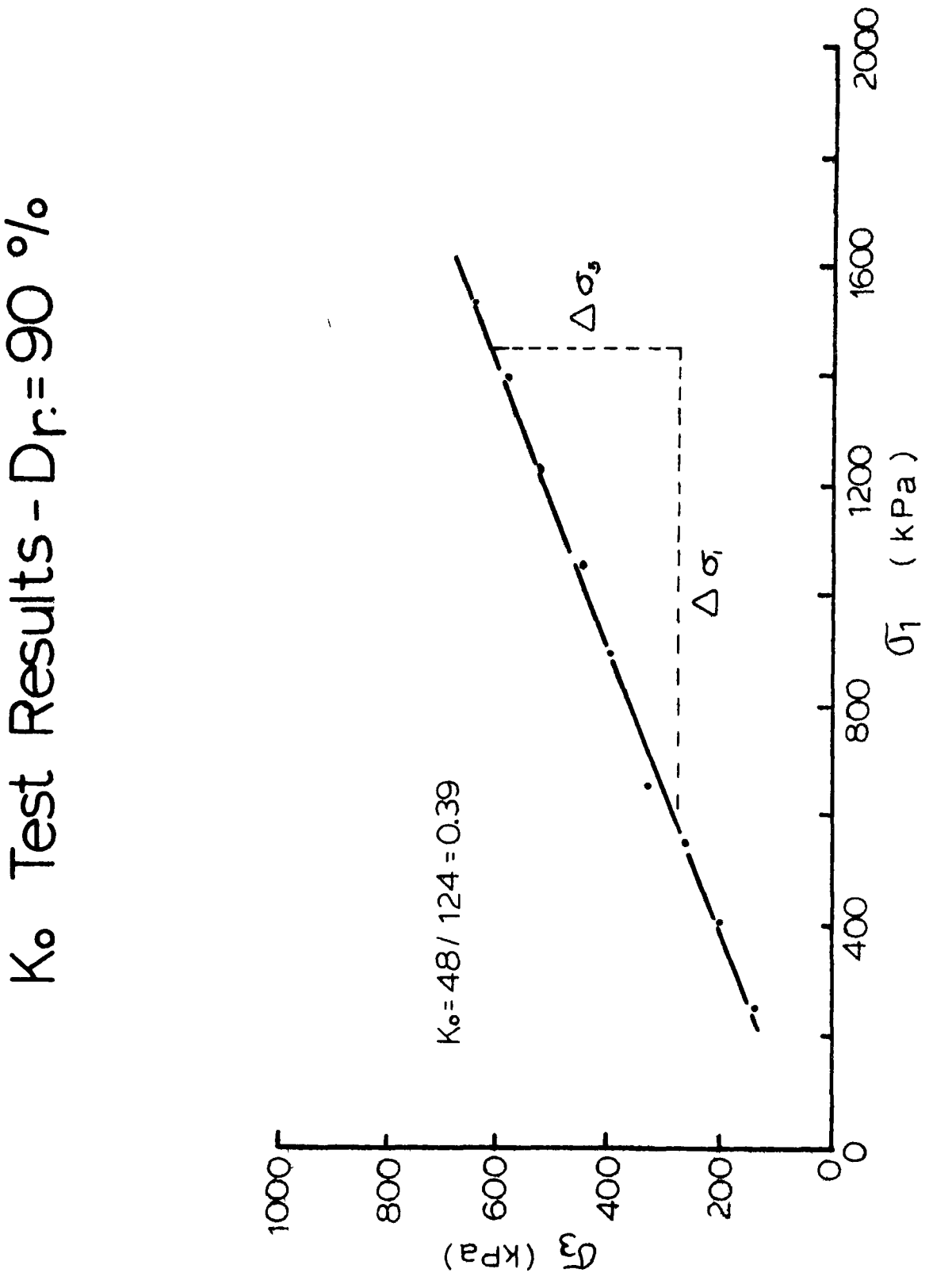
Ko Test Results - Dr.= 90 %
Ko= 48/ 124 = 0.39
Δσ3
Δσ1
σ3 (kPa)
σ1 (kPa)
0
200
400
600
800
1000
400
800
1200
1600
2000

Figure 4.25

Influence of Normal Stress on Shearing Resistance

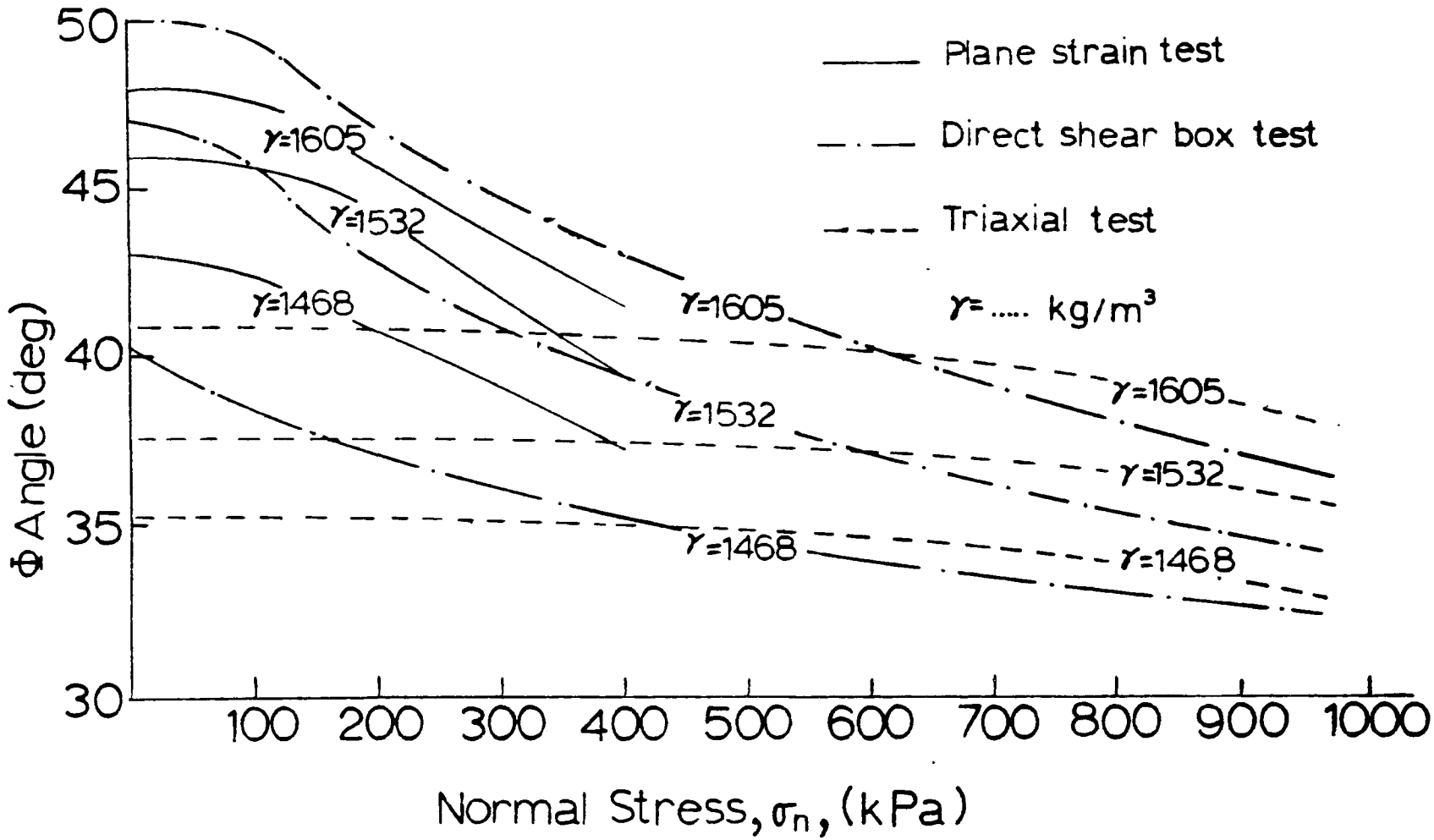

Figure 4.26

Typical Triaxial Test Results on Sand

Unit Weight kg/m³	σ_3 kPa	σ_1/σ_3	ϵ_f %	Φ^0	$(\frac{\Delta V}{V})_f$	Remarks
1610	34.5	4.9	5.50	41.5	0.042	
1620	172.5	4.8	7.00	41.0	0.035	Dense
1620	345.0	4.6	9.00	40.0	0.021	Sand
1630	552.0	4.4	9.60	39.0	0.014	
1510	34.5	4.1	7.60	37.3	0.032	
1510	172.5	4.1	7.61	37.2	0.011	Compact
1520	345.0	4.0	10.80	36.8	0.007	Sand
1530	552.0	3.9	14.70	36.2	0.006	
1490	34.5	3.8	11.10	35.4	0.028	
1450	172.5	3.7	13.20	35.2	0.004	Loose
1470	345.0	3.7	16.30	35.0	0.011	Sand
1480	552.0	3.6	19.20	34.5	0.022	

Figure 4.27

form rounded sand and well graded sand. This fact is of importance in the evaluation of settlement of the test footings.

The production of dust during spreading of the sand is a major concern. For this reason, the whole testing facility was enclosed in an airtight polyethylene tent. The enclosure was outfitted with a dust collecting system which is essentially a large vacuum cleaner. When the sand was being rained the workers inside the polyethylene tent were required to wear special dust masks.

4.3.2 Sand Density Calibration

One of the most important features of the raining device is that it can deposit sand at various densities and porosities by changing certain variables:

a) the height of fall of the sand
b) the rotation speed of the drum
c) the horizontal travel speed of the raining device

The third variable, horizontal travel speed, is not used in this study. Instead, the travel speed is kept constant for all tests. Therefore, only the first two variables, height of fall and the speed rotation of the drum, are of interest.

The density of the sand which is deposited by the raining device is measured by means of special perspex glass pots. As the sand is rained into place, some of it drops into the

pots. When full, the pots are recovered and weighed. With the volume and the weight of the pots known, the density of the sand is calculated.

To calibrate densities against drum speed and height of fall, platforms were built at various heights in the box. A number of density pots was placed on each platform and the spreader made to travel over the platforms from east to west and west to east. The speed of rotation was held constant until the pots were filled and the densities measured. The rotation speed was then changed and the procedure repeated.

Six pots were placed on each level so that a statistical analysis of the density results could be worked out. The procedure is illustrated schematically in Figure 4.28.

The procedure was repeated for six drum speeds: 3, 8, 12, 23, 30 and 33 r.p.m. The results of these tests are listed in the table of Figure 4.29 shown graphically in Figure 4.30.

4.4 Footing

4.4.1 Choice of Footing Size

The problem of the effect of scale on bearing capacity has been studied by several investigators (namely DeBeer (1965), Tcheng and Iseux (1966), and Graham (1972))but only for flat ground. The conclusions reached by these investigators are illustrated in Figures 4.30 to 4.32. All curves give the bearing capacity factor versus footing width or a

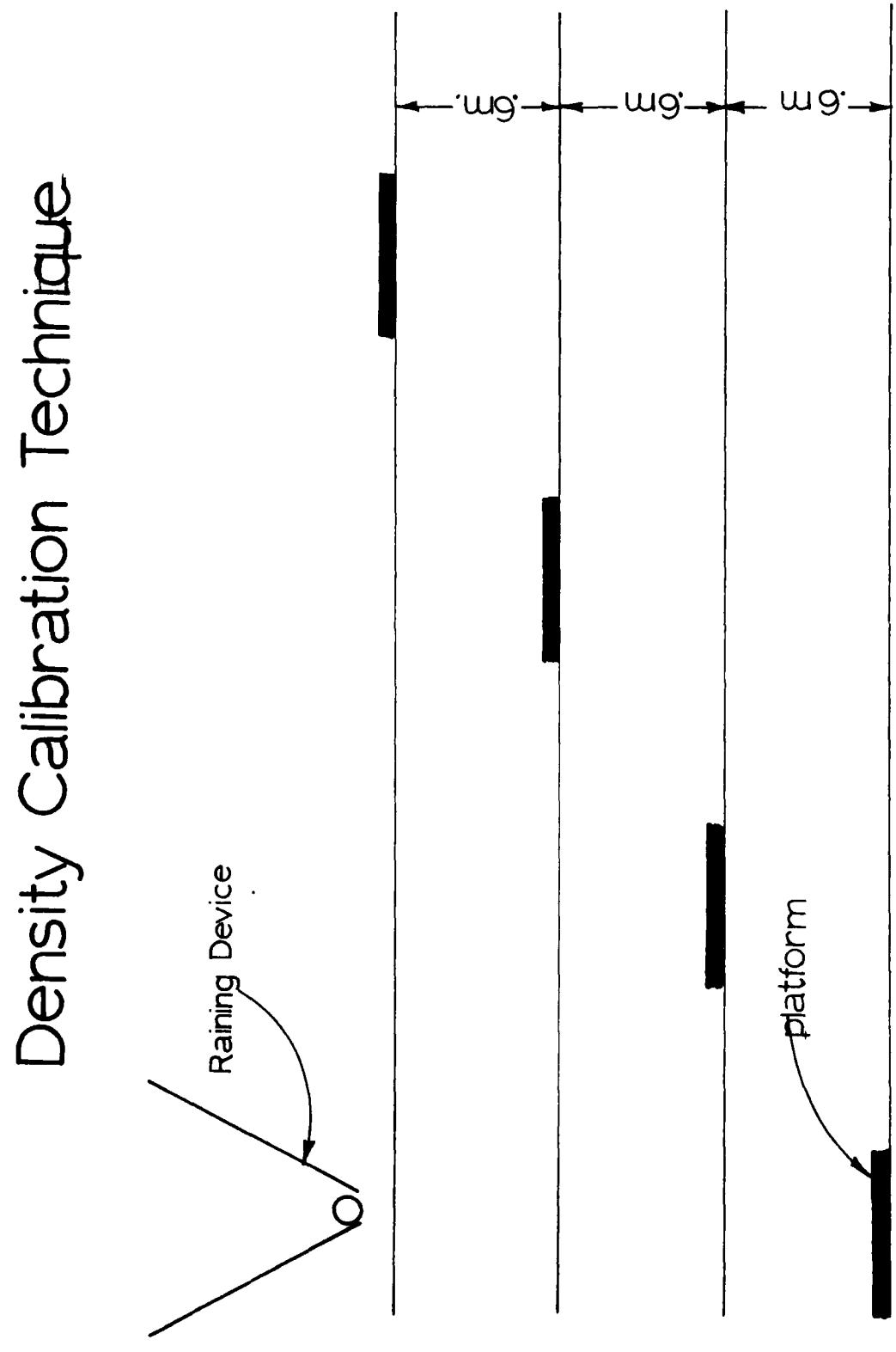
Density Calibration Technique
.6m
.6m
.6m
Raining Device
platform

Figure 4.28

Density(kg/m^3) Vs. Height of Fall Vs. Drum Speed

Height of fall (m.)	Drum Speed (r.p.m.) 3	8	12	23	30	33
	1560	1470	1400	1380	1410	1380
	1580	1510	1410	1380	1370	1370
	1570	1480	1420	1380	1420	1390
.15	1570	1480	1400	1380	1380	1370
	1580	1480	1400	1380	1420	1380
	1570	1490	1400	1380	1380	1380
	1570	1480	1410	1380	1390	1380
average	1570	1480	1410	1380	1390	1380
σ	9	14	6	2	22	7
	1600	1550	1500	1450	1420	1410
	1590	1540	1490	1440	1420	1410
	1620	1560	1480	1440	1410	1410
0.6	1610	1560	1500	1440	1420	1420
	1610	1550	1500	1430	1410	1430
	1610	1550	1480	1440	1420	1410
average	1610	1550	1490	1440	1420	1410
σ	9	7	6	5	5	7
	1600	1580	1520	1460	1450	1450
	1600	1560	1520	1470	1450	1440
	1610	1560	1520	1480	1460	1430
.12	1610	1570	1530	1480	1440	1450
	1610	1560	1520	1490	1440	1420
	1610	1560	1520	1460	1450	1420
average	1610	1560	1520	1470	1450	1440
σ	5	8	6	10	8	14
	1580	1540	1500	1500	1480	1490
	1590	1540	1510	1510	1500	1470
	1600	1560	1490	1500	1450	1450
.18	1610	1540	1510	1510	1480	1470
	1600	1540	1510	1500	1490	1480
	1600	1560	1510	1510	1450	1460
average	1600	1540	1510	1510	1480	1470
σ	10	10	9	6	19	13

Figure 4.29

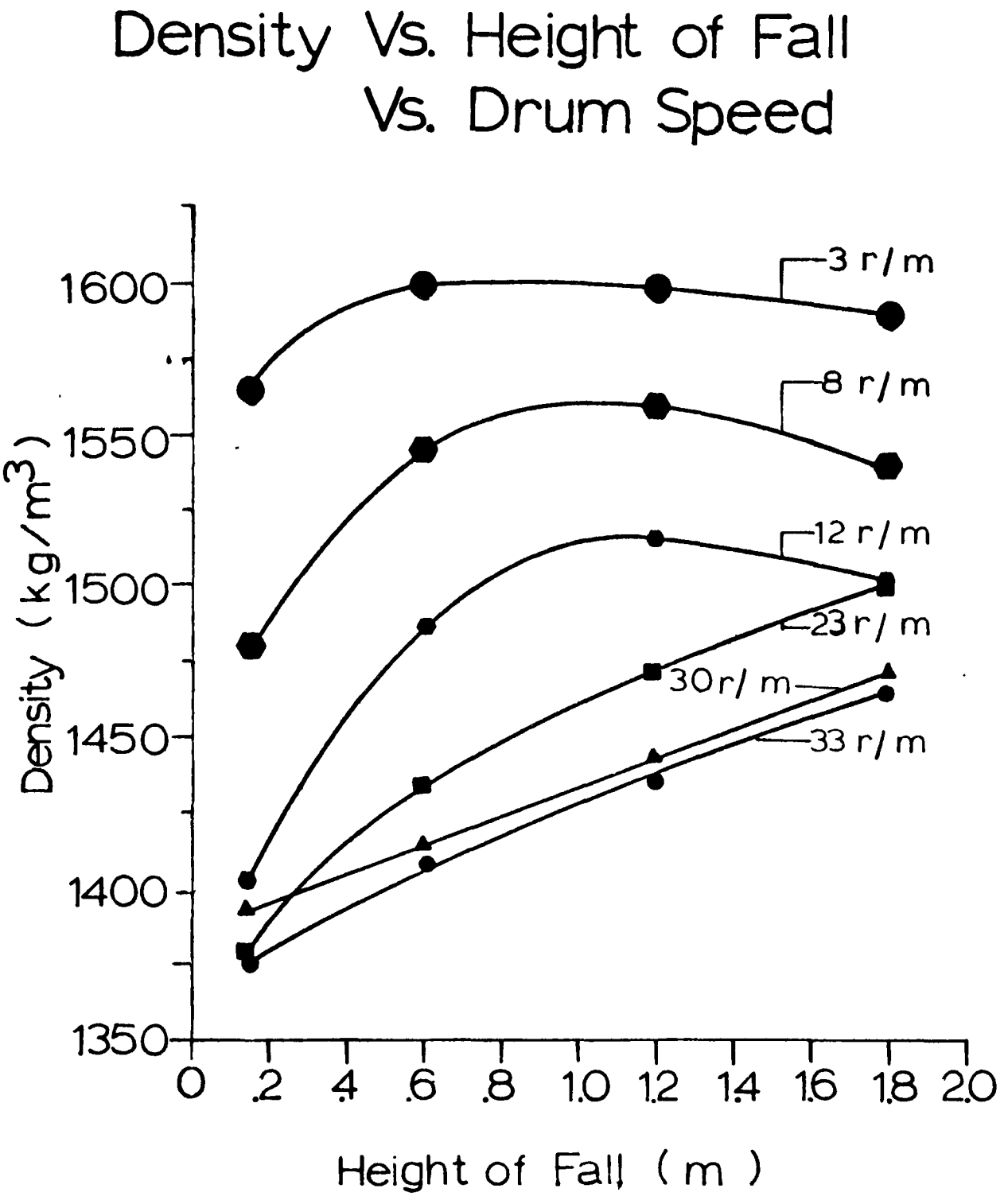
Density Vs. Height of Fall
Vs. Drum Speed
3 r/m
8 r/m
12 r/m
23 r/m
30 r/m
33 r/m
1600
1550
1500
1450
1400
1350
Density (kg/m3)
0
.2
.4
.6
.8
1.0
1.2
1.4
1.6
1.8
2.0
Height of Fall (m)

Figure 4.30

function of the footing width.

These curves show the same trend. For very small footings (where the footing width is less than 10 cm), the corresponding bearing capacity factors are extremely high. Between footing widths of 10 to 20cm, the bearing capacity factors decrease rapidly. For footings more than 30cm wide, the bearing capacity values seem to decrease very slowly.

It is reasonable to conclude from these findings that footings as large as possible should be used for meaningful experimental work. A reasonable lower limit would be a 30cm wide footing.

However, from an experimental point of view, the footing size must be small enough to avoid the possible influence of the rigid bottom of the bin. The problem of a rough rigid base has been studied theoretically by Mandel and Salençon (1972) and experimentally by Tournier (1972). The conclusions reached by these researchers are summarized in Figures 4.33 and 4.34. From these two figures, it is obvious that the bearing capacity increases because of the presence of a rigid base only if the thickness H of the soil below the base of the footing is smaller than 2B. Both theory and experimentation confirm that if the thickness of the soil layer between the footing and the rigid base is thicker than 2B, the footing will behave exactly as if there were no rigid base.

Taking B = 30cm means that with a 2.2m depth of sand, there would be 1.3m of sand below the footing, when it is

Scale Effect

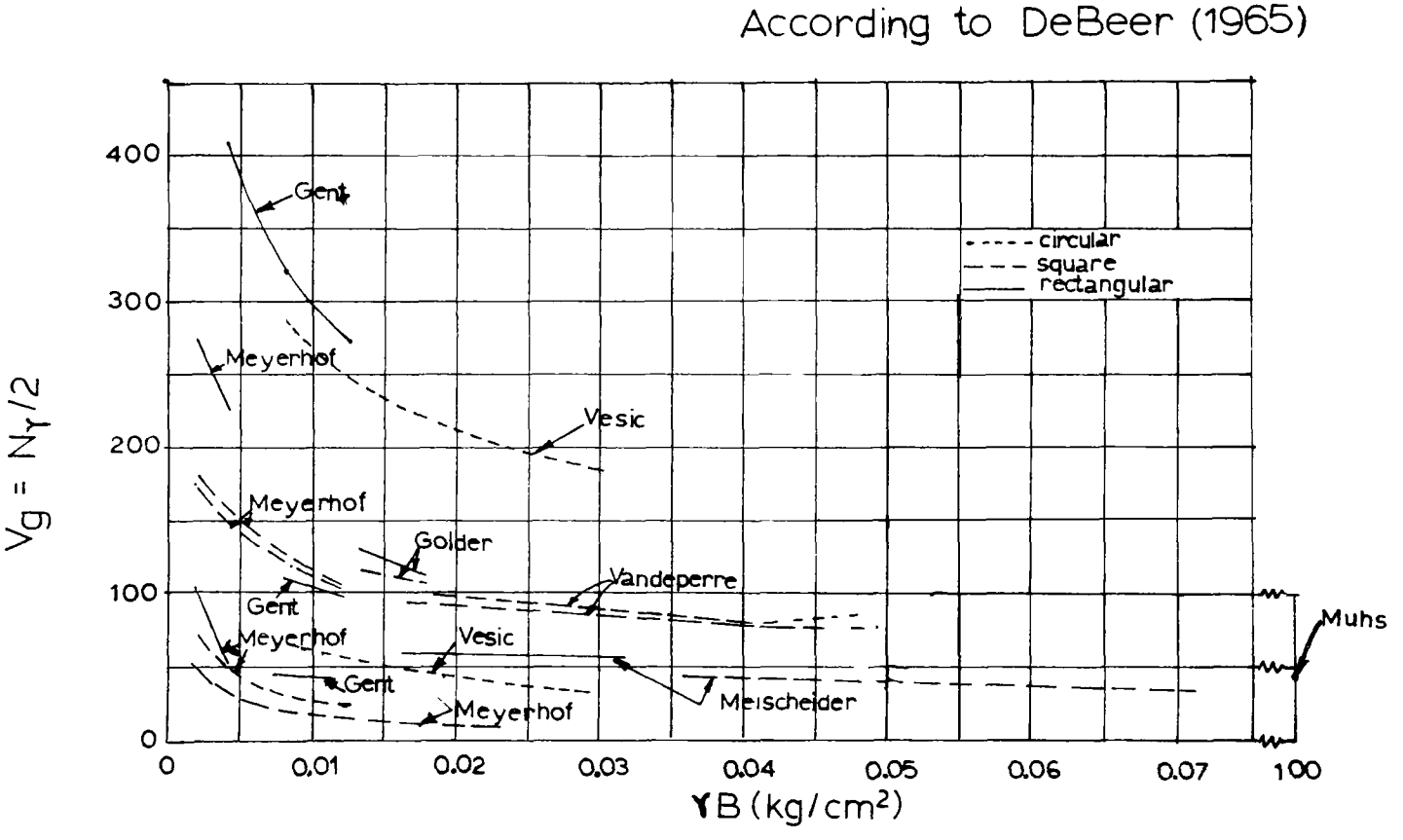

Figure 4.31

Scale Effect

According to Tcheng & Iseux (1965)

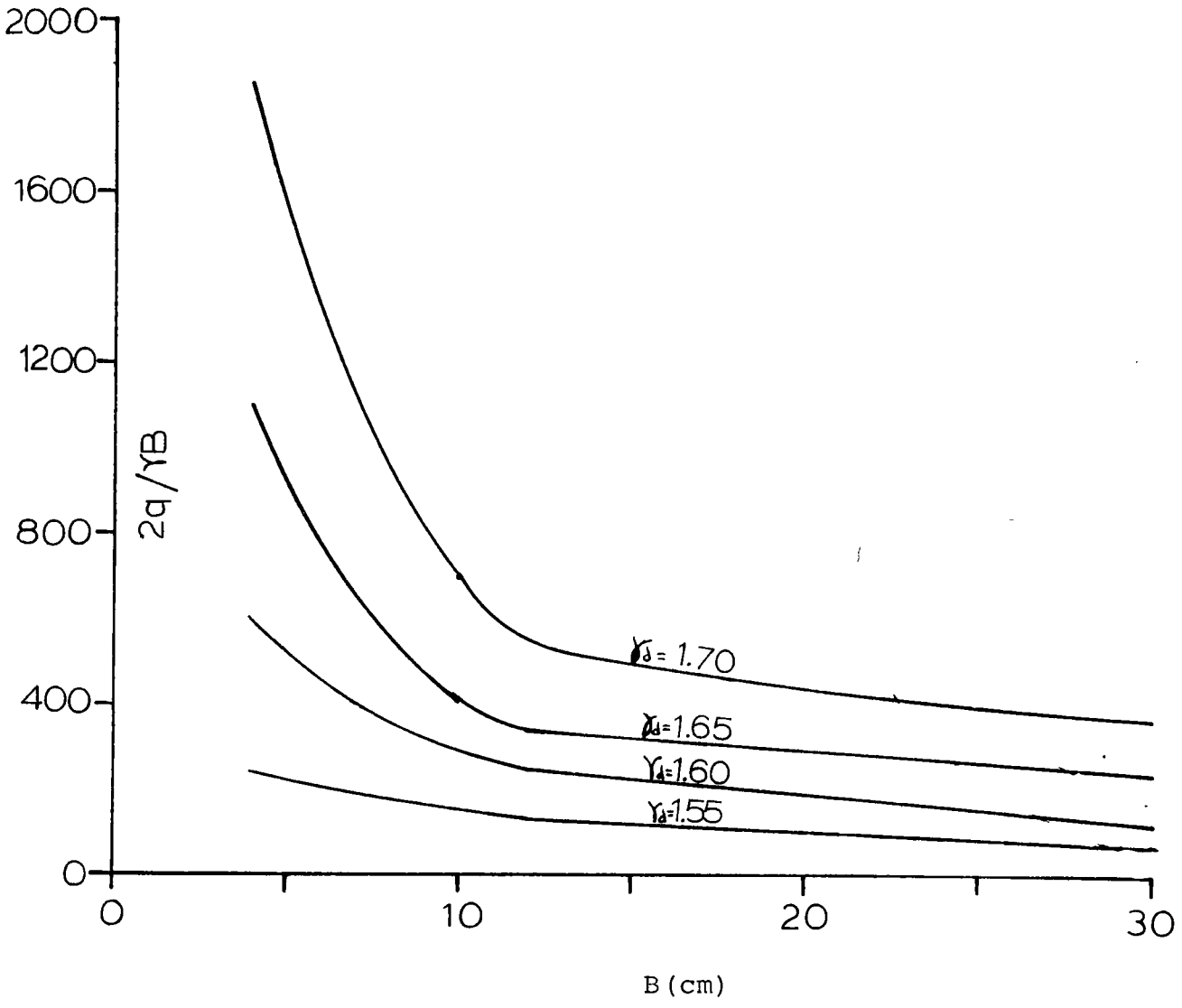

Figure 4.32

Scale Effect

According to Graham (1974)

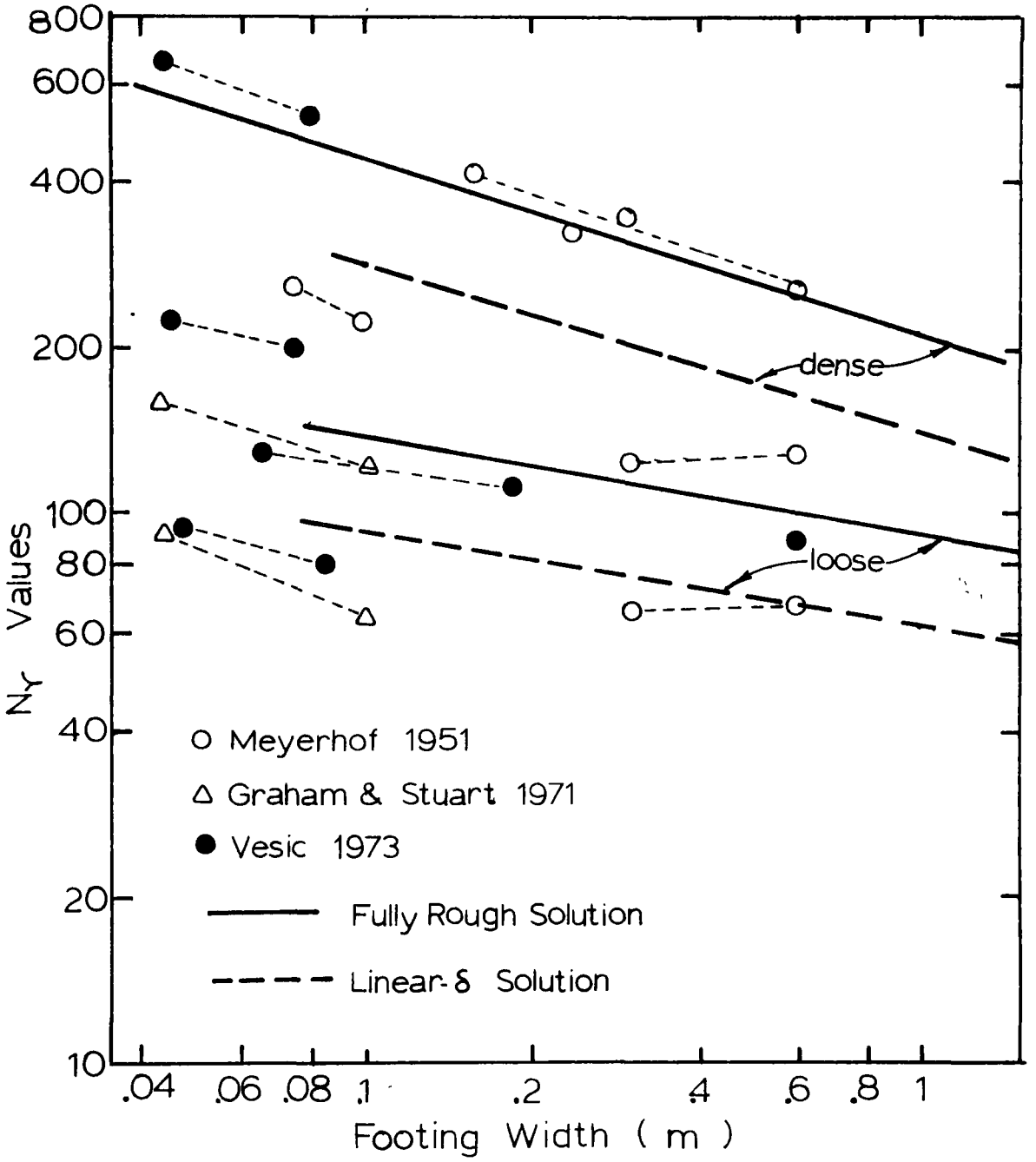

Figure 4.33

at a depth of 3B. This minimum depth of sand would appear to be ample since it is equivalent to 4B.

4.4.2 Description of the Footing

As shown in Figure 4.12, a three-sectional footing was used in the tests. Two of the sections were dummy footings used to nullify wall friction effects at the center footing [Peaker (1964)]. These three segments taken together simulate the action of a footing 1.8m long, by 0.3m wide failing in plane strain.

The surfaces of the footing were made rough by gluing sand onto them. The footings were kept from rotating [as recommended by Ko and Davidson (1973)], by fixing them rigidly to the jacks.

4.5 Slope

Throughout the testing program, the slope angle is kept fixed at 2:1 (horizontal to vertical) to meet M.T.C. requirements, as stated previously in Section 1.3.

Influence of Rigid Base on Bearing Capacity

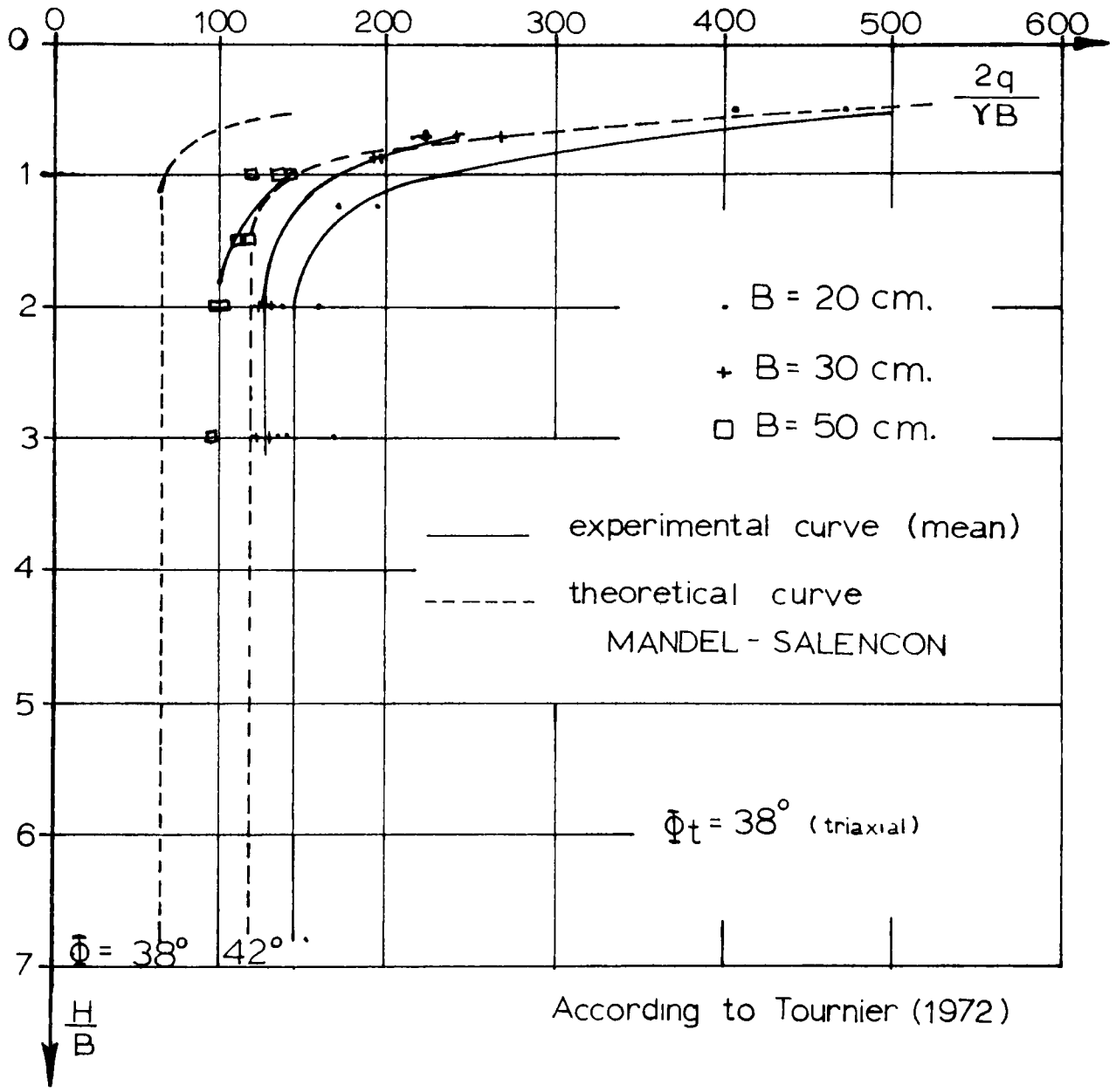

Figure 4.34

Influence of Rigid Base on Bearing Capacity

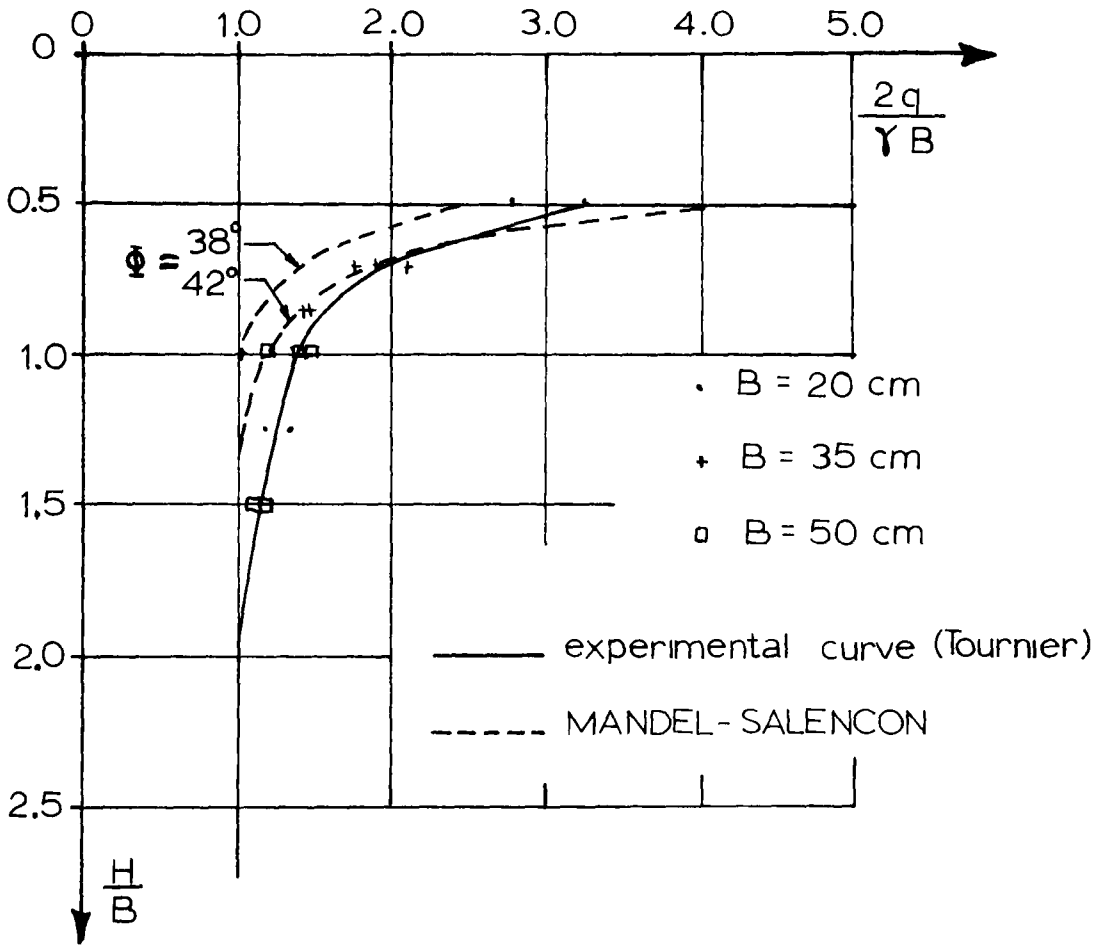

According to Tournier (1972)

Figure 4.35

CHAPTER V

EXPERIMENTAL PROCESS

5.1 Introduction

The M.T.C. requirements, described in Chapter I, call for two different sand densities to simulate two different degrees of compaction of embankment material. The two densities represent a compact and a dense sand and correspond approximately to 1520 kg/m^3 and 1610 kg/m^3 respectively for the sand used in the testing program.

The present Chapter discusses the elements that make up the testing program and describes the test procedure.

5.2 Testing Program

5.2.1 Aims

The aim of the present research project is to study the influence of a 2:1 slope on footings located at different horizontal distances from the slope crest and at different depths below the ground surface.

5.2.2 Measurement and Instrumentation

For every test, the density of the sand in the test bin has to be known. Density measurements are taken at two depths below the footing level, namely at 1B and 2B. A minimum of

four tests at each level are made using the procedure described in article 4.3.2.

The bearing pressure for the first two footing tests was measured by means of pressure gauges mounted in the pressure line of the central jack. However, it was observed that the pressure gauges were not as accurate as had been anticipated; thus a load cell was installed between the central hydraulic jack and the reaction beam.

The settlement of the footing is obtained directly from measuring tapes which are rigidly attached to the jacks. The distances through which the pistons of the jacks move can be read to an accuracy of 0.8mm.

For the first five tests, settlement of the footing was obtained from two dial gauges, one with a travel of 20cm. and the other, 15cm. The dial gauges were attached to a rigid reference channel which was fixed to the sand box. The gauges were placed on either end of the footing. With this arrangement, it was possible to observe if there was any tilting of the footing in a longitudinal direction during a test. After the first five tests, it was noted that tilting of the footing was minimal, and no further measurements of this nature were made.

The deformation of the soil surface which took place during the failure of the footings was recorded initially using linear transducers. The transducers were connected to an electronic readout unit which allowed the deformation to

be read automatically. After a few trials, the transducers proved to be totally unreliable. Thereafter, small wooden rulers were simply embedded in the slope at various locations and were used as reference points to register the vertical and tangential movement of the soil along the surface during load application.

5.2.3 Test Locations

All footing tests were carried out in the flat ground adjacent to the slope, rather than beneath the slope itself. This simulates present M.T.C. practice for the design of spill through bridge abutments. Footings were positioned horizontally at 0, 2.5 and 5 footing widths from the slope crest (with respect to the leading edge of the footing) and vertically at 0, 1, 2 and 3 footing widths from the ground surface. This gave a grid of twelve positions. The program calls for the completion of twenty-four tests, twelve with the sand in a compact state and twelve with the sand in a dense state. Locations of the tests are given in Figure 5.1. Furthermore, a bearing capacity test was performed on a dense sand bed with a horizontal surface and no slope.

5.2.4 Reproducibility

A certain number of tests were repeated in order to check whether the results were reproducible. The program calls for three particular tests to be repeated once, while

Location of Tests

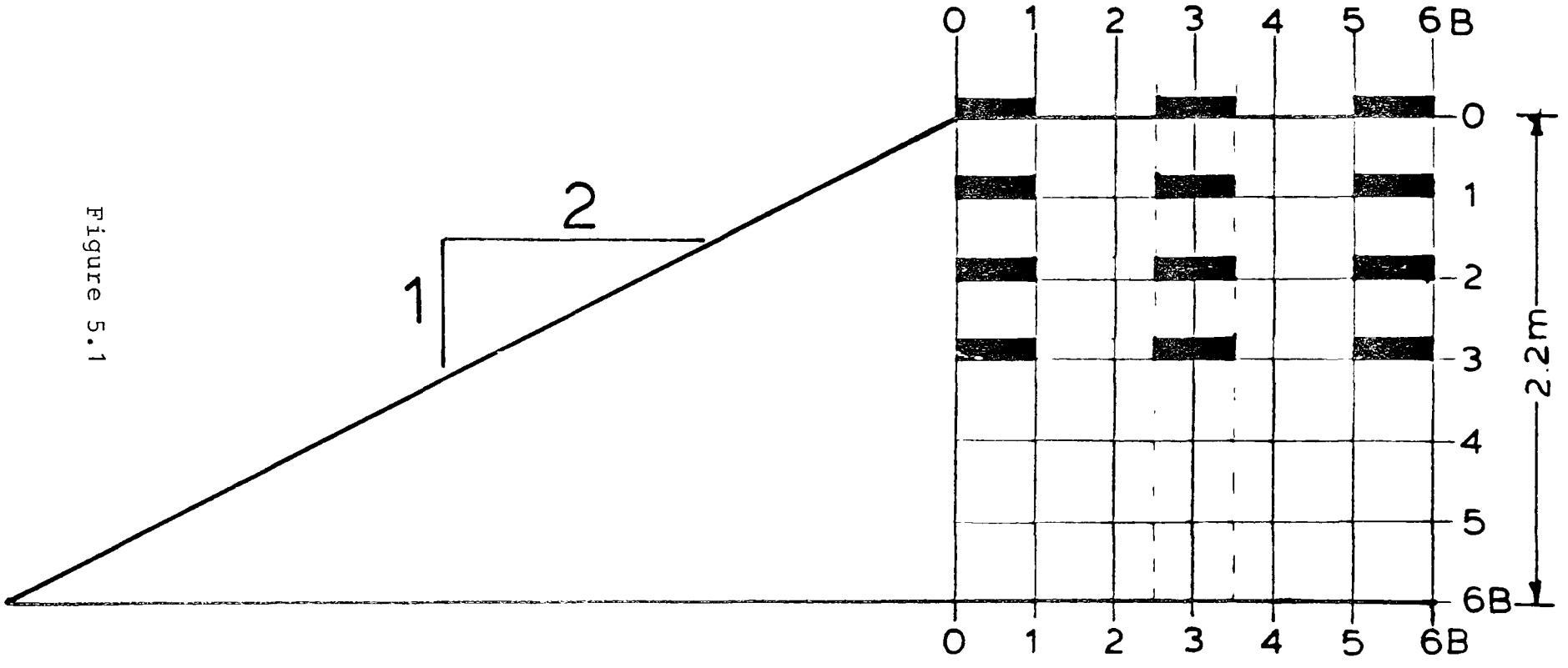

Figure 5.1

another test is repeated twice.

5.3 Test Procedure

5.3.1 Spreading of the Sand

This operation consists of transfering the sand from one end of the test bin to the other. The sand is picked up by the elevator, and dropped into the hopper. Once the desired drum speed is selected, the sand is then deposited in the test compartment of the bin.

To place the sand in the dense state, the slowest drum speed is selected; this causes the sand to fall in a curtain at low intensity. Only a small amount of sand is deposited by each pass of the spreader. To obtain a density of approximately 1600 kg/m^3, the sand layers are less than 3mm thick. To obtain compact sand the rotating drum of the spreader is set at a very high speed which causes a high intensity of sand and thick layers.

The sand is deposited uniformly throughout the length of the bin except close to the end bulkheads (see Section 4.2.3.1); these end effects are inherent to the process and cannot be avoided. The surface of the sand was levelled from time to time as required to ensure that the final bed of sand had a smooth, uniform surface. The spreading operation is shown in Figure 5.2.

Spreading operation

Figure 5.2

5.3.2 Making the Slope

Making the slope requires no special technique. First the outline of the slope is drawn on both sides of the box and this outline serves as a guide during the deposition of the sand. It is only necessary to reverse the spreader when it reaches the proper point in its travel. Any unevenness in the slope was removed by raking. Care was taken to alter the state of the sand as little as possible during the raking operation.

5.3.3 Uniformity of Density

Since the slope is not cut to shape out of a homgeneous bed of sand but formed during the deposition process, it is conceivable that the density of the sand at the slope may differ from the bulk or average density. This is because the spreader stops and starts at the slope surface.

As all of the density measurements are taken away from the slope crest, namely beyond 5B out of the way of the test zone, no factual information is normally available to confirm the state of density at the slope crest. A special density measurement program was set up to study the uniformity of density throughout the test bin.

The study was carried out using three types of measuring apparatus. The first type is the cylindrical pots which are used to determine the density during the bearing capacity tests. Six of these pots were placed at a horizontal distance

of at least 5B from the slope crest. The density values were avaraged for the six results. The resulting mean value was compared to other density values which were obtained by the other two density measuring devices. A nuclear densimeter (Troxler type) was used to measure directly the density of the sand at the slope and in the mass at three different elevations. The nucelar density values were supported by the results from a third type of measuring apparatus, namely a square box having no bottom which was pushed into the soil. Once the box was in place, the soil inside the box was removed carefully with a special shovel. The soil was weighed and the density was thus known.

This particular program was carried out for two densities (compact and dense sands), and the results appear in Figures 5.3 and 5.4 and have been consolidated in Figure 5.5. From these figures it can be seen that the state of density throughout the soil mass is uniform.

5.3.4 Tests Done Below the Surface

The testing program calls for experiments to be carried out at depths of 1B, 2B and 3B (B = footing width). These tests require the construction of a pit into the sand so that the footings can be embedded the proper depth.

Rigid wooden walls were used to keep the sand from falling into the footing pit. The load registered on the experimental footing gives only the base resistance of the founda-

Uniformity of Density
(kg/m^3)

(Compact State)

Level	Distance from crest	Pots	Nuclear Densimeter	Box
2B	0	----	1450	1450
	2B	----	1450	1450
	6B	1450	1450	1450
1B	0	----	1450	1450
	4B	----	1450	14.28
	6B	1450	1450	1440
0B	0	----	1450	1450
	2B	----	1470	1470
	4B	1470	1470	1470

Figure 5.3

Uniformity of Density
(kg/m^3)

(Dense State)

Level	Distance from crest	Pots	Nuclear Densimeter	Box
2B	0	----	1600	1590
	6B	----	1610	1610
	10B	1600	1610	1600
1B	0	----	1600	1610
	4B	----	1610	1610
	8B	1600	1610	1610
0B	0	----	1600	1600
	2B	----	1610	1600
	6B	1610	1610	1610

Figure 5.4

Uniformity of Density

Measurements: ○ Pots (ave of 6)
□ Nuclear Densimeter
△ Square Box
γ: kg/m³

Compact State

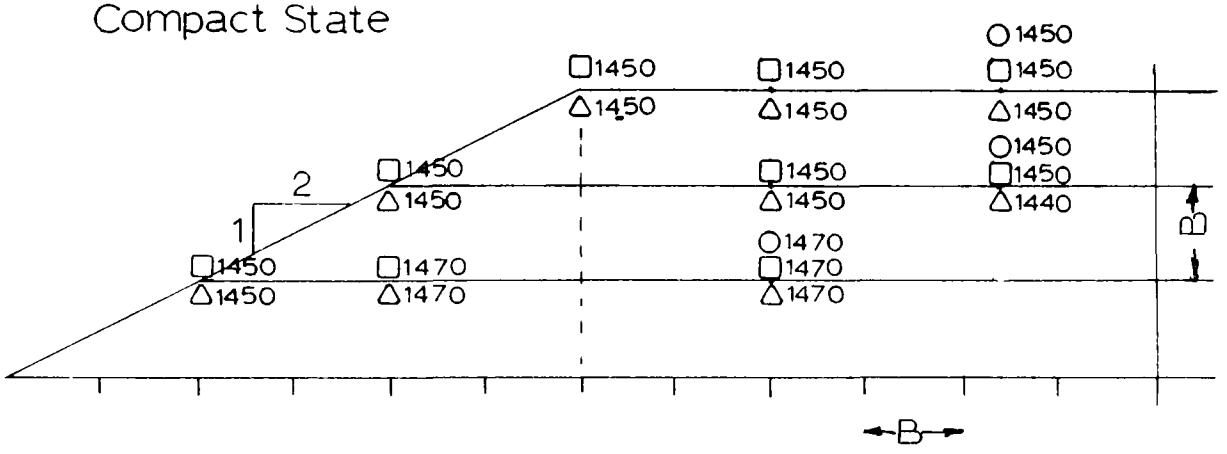

Dense State

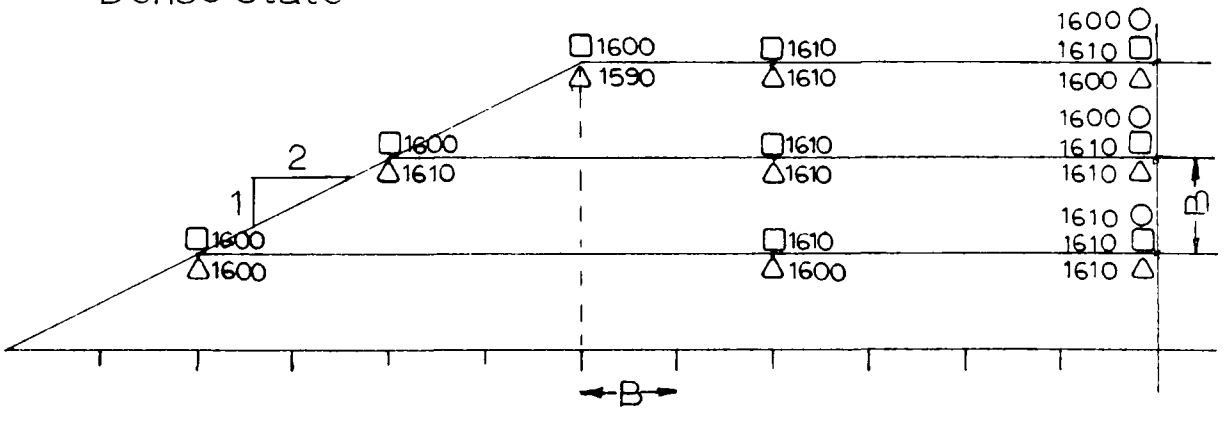

Figure 5.5

tion and does not take into account skin friction that would be encountered along the walls retaining the sand.

5.3.5 Application of Loads

Once the sand box is filled to the required height the loading frame is positioned and bolted to the box.

Loading is by increments of approximately 25 kPa. For each increment, load and settlement of the footing are recorded at five minute intervals until settlement stops, usually within 15 minutes. At every increment, surface movements are also recorded.

5.3.6 Determination of the Failure Load

The determination of the failure load follows the method suggested by Vésic (1973). Three modes of bearing capacity failure are defined: general shear, local shear, and punching shear. Figure 5.6 illustrates the different types of failure mode.

Failure of a footing is clearly defined only in the case of general shear. In this case, the peak or ultimate load is approached gradually until sudden failure occurs. General shear failure is characteristic of dense sands.

In compact sand, failure occurs by local shear, and the failure load is not easy to determine. In this case,the sand is compressed under the footing load, and the failure load can

The Three Modes of Failure

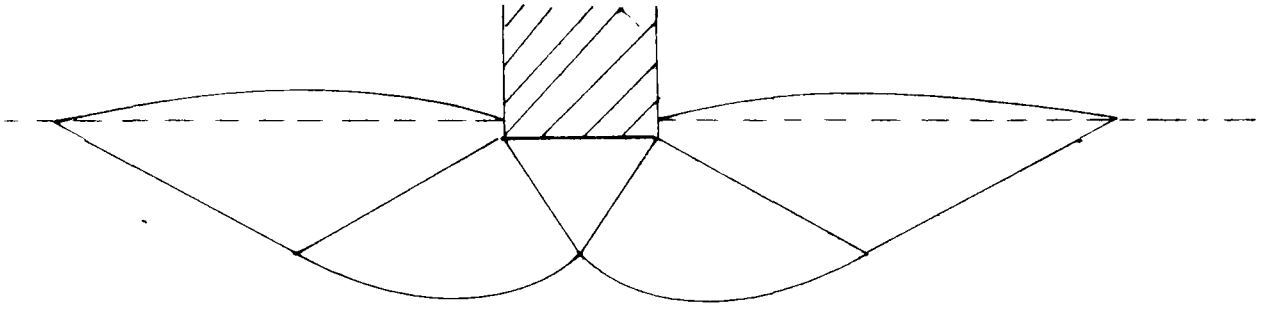

A) General Shear

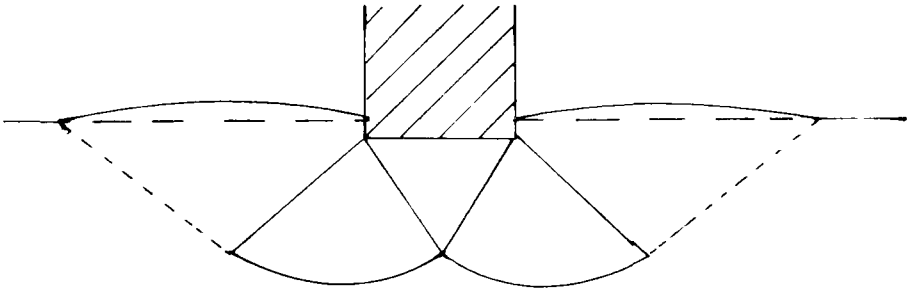

B) Local Shear

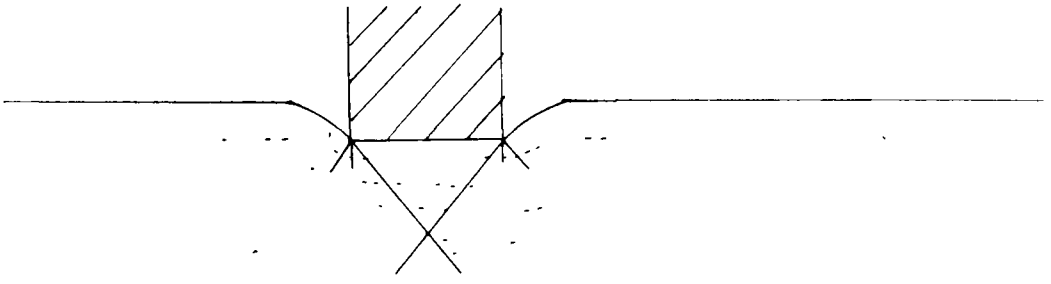

C) Punching Shear

Figure 5.6

be defined only from an examination of the load-settlement curve.

In all cases Vésic recommends that the ultimate load be taken at the point at which the slope (load/settlement) of the load-settlement curve first reaches zero or a steady, minimum value.

J.-H. DESCHENES

BEARING CAPACITY OF FOOTINGS CLOSE TO SLOPES OF COHESIONLESS SOIL

CHAPTERS

VI-IX

CHAPTER VI

RESULTS

6.1 Introduction

This chapter presents the results which were obtained during the experimental program and consists mainly of the applied pressure-settlement curves, density measurements and surface movement curves.

6.2 Numbering System

Each test is labelled according to the test location with respect to the slope crest and to the density of the sand. The labels are described by three or four characters separated by a dash.

The first character is a number which refers to the horizontal position of the leading edge of the footing with respect to slope crest as shown in Figure 5.1. This number may be 0, 2.5, or 5, corresponding to the number of footing widths from the slope edge. The second character is also a number, representing the depth of the bearing surface of the footing with respect to horizontal surface of the sand at the top of the slope. This number may be 0, 1, 2 or 3, and is the number of footing widths at which the tests were carried out. The third character is a letter refering to the state of

density in the sand during the test. This letter may be a C (compact state), or D(dense state).

The fourth and final character is used only in special cases and can be one of two letters; the letter R would correspond to a repeat test, and, if the test is repeated more than once, the letter R is then followed by the number 1 or 2.

This can be better illustrated by the example:

2.5 - 1 - C - R

2.5 is the horizontal location of the leading edge of the footing. The footing is located 2.5 times the footing width from the crest of the slope.

1 is the vertical distance (depth) from the horizontal surface. Therefore, the footing is located at one footing width down from the surface.

C the test was performed in compact sand.

R the test was a repeat test.

The test carried out on flat ground in dense sand is refered to as: ∞ - 1 - D - S.

6.3 Units Used

English units were used for the actual measurements; the results were converted and are presented in S.I. units.

In this thesis, stress and pressure are expressed in

terms of kilo pascals where 100 kPa is approximately equal to 1 ton per square foot. The S.I. unit for density is kilograms per meter cubed.

6.4 Figures and Tables

In the following pages the results are tabulated and plotted for each of 29 tests. The following factual information is found for each test:

a) table of pressure-settlement values

b) curve of pressure-settlement

c) summary of density measurements

d) table of surface movements

e) plot of surface movements.

The table of pressure-settlement gives the increment of pressure and the corresponding settlement. Two other columns are added to express applied load and settlement as dimensionless values. The dimensionless pressure is expressed as $\frac{2q}{\gamma B}$ which yields the $N_{\gamma q}$ term at failure. The settlement is expressed as a percentage of the footing width.

The figures containing the pressure-settlement curves are designed to give the pertinent information on each test:

i) graph of footing location

ii) density state

iii) failure $N_{\gamma q}$

iv) settlement curve

The densities are tabulated for each test, giving the

measurements at different levels throughout the sand mass. A statistical analysis of the results is made. The average density found in those tables is the one given on the pressure settlement curve. Tests # 5 - 0 - C, 5 - 0 - D, 5 - 0 - D - R, ∞ - 1 - D - S have no density measurements. The density in these cases was assessed from the density versus drum speed curve discussed in Section 4.3.2.

The tabulation of surface movements is represented on the curve of the same name and gives an appreciation of the migration of sand grains during a test. Surface movements are not available for the following six tests because no measurements were made: 2.5 - 1 - C - R, 5 - 0 - C, 0 - 0 - D, 2.5 - 0 - D, 5 - 0 - D, ∞ - 1 - D - S.

Test: 0 - 0 - C

PRESSURE - SETTLEMENT

TEST: 0 - 0 - C

$\gamma = 1490\ kg/m^3$

B = .3 m.

Pressure q kPa	Settlement cm.	$\frac{2q}{\gamma B}$	Relative settlement $(\frac{W}{B} \times 100)$
0	0	0	0
25	0.3	10	1.0
38	0.5	16	1.7
50	1.4	22	4.7
56	1.9	24	5.7
63	3.4	28	11.3
75	7.1	32	23.7
88	10.1	38	33.7
100	12.3	44	41

Figure 6.1

b/B : 0 D/B : 0

Density : Compact

$N_{\gamma q}$: 24

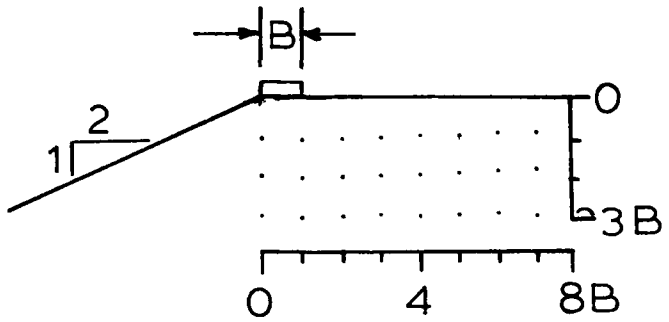

Figure 6.2

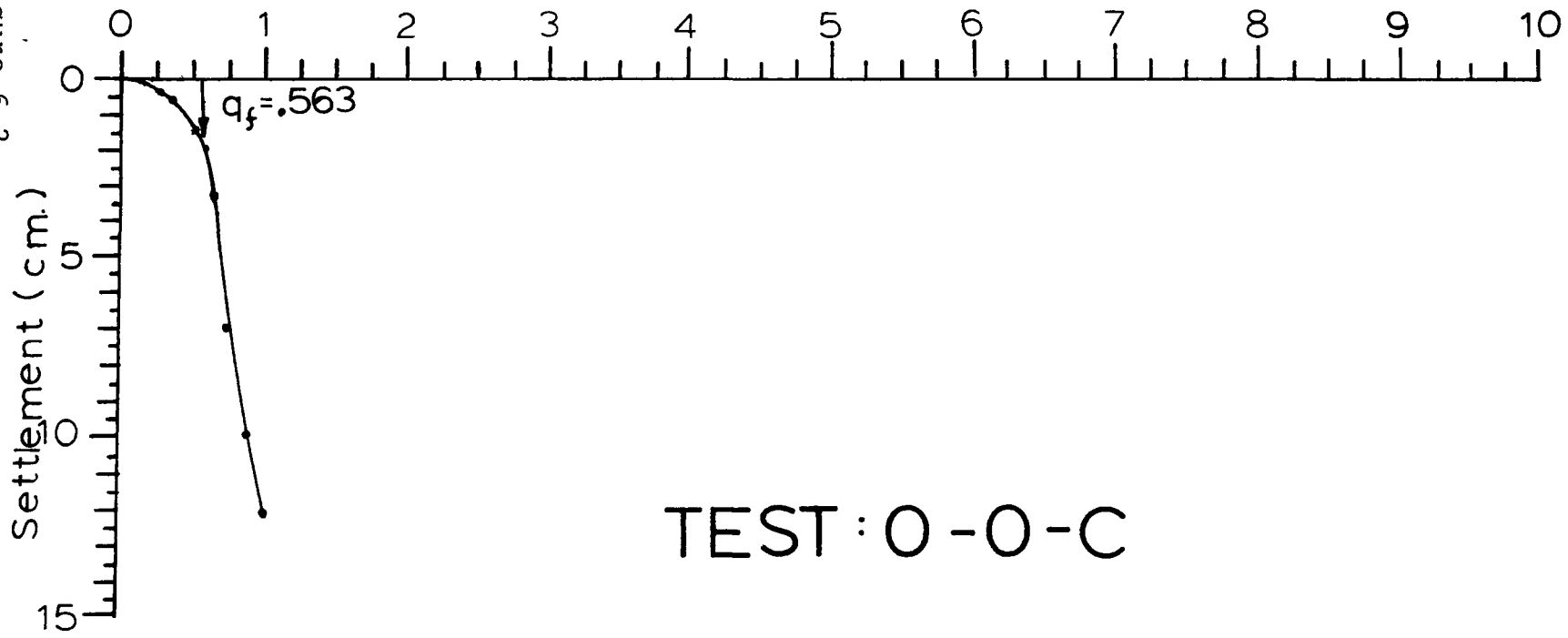

TEST : 0-0-C

DENSITY MEASUREMENTS (kg/m^3)

TEST: 0 - 0 - C

Location of measurement under footing	Measurements	Average	Standard deviation
1B*	1490		
	1470		
	1480		
	1490		
	1490		
	1470		
2B*	1490		
	1500		
	1500		
	1520		
	1510		
	1490		
		1490	1515

* B = footing width

Figure 6.3

Surface Movements
Test:O-O-C

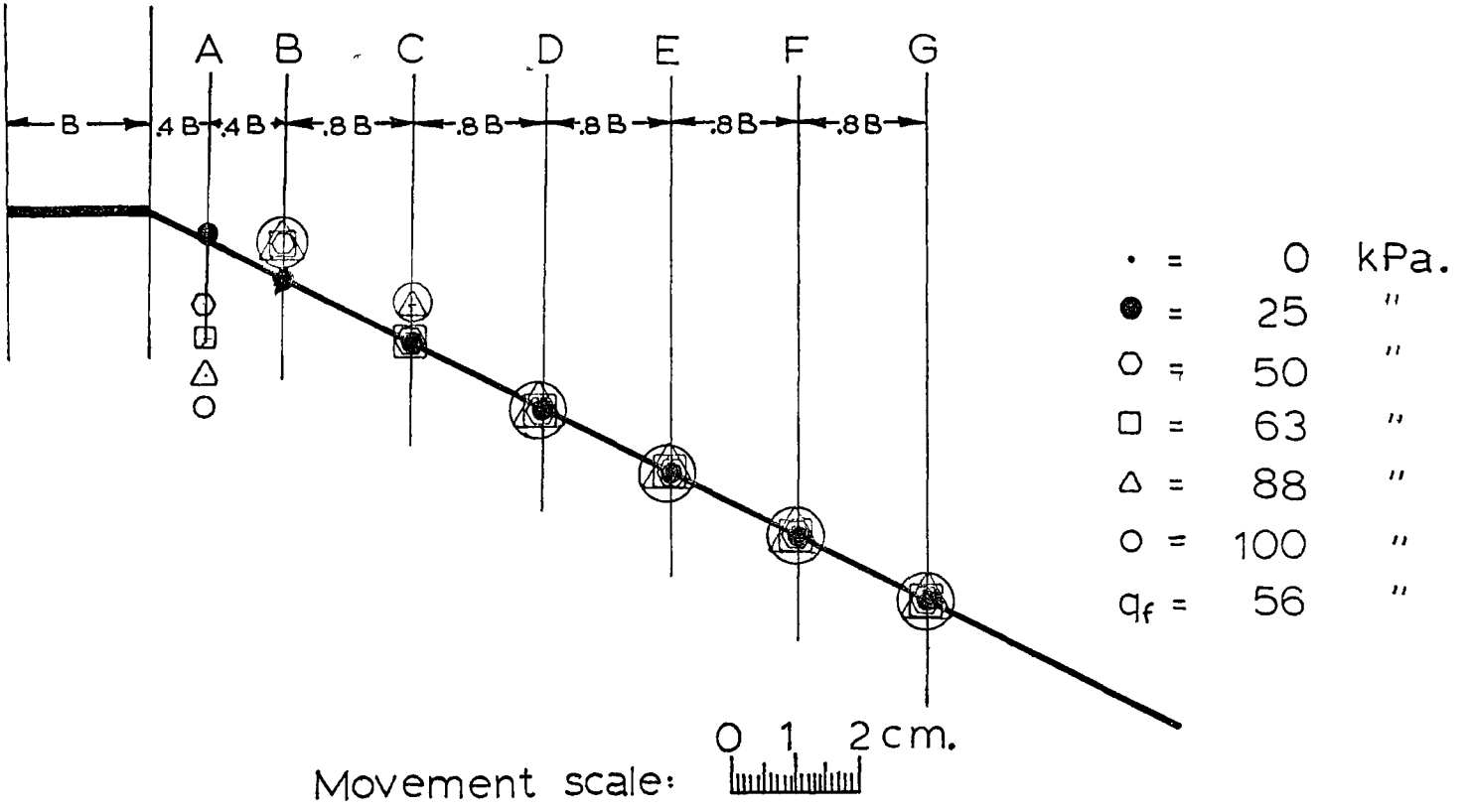

Figure 6.4

SURFACE MOVEMENTS (cm)

TEST: 0 - 0 - C

Positions		A	B	C	D	E	F	G
Horizontal distance from footing (B = footing width)		.4B	.8B	1.6B	2.4B	3.2B	4B	4.8B
Pressure (kPa)								
0	V	0	0	0	0	0	0	0
25	V	0.1	0	0	0	0	0	0
38	V	-1.9	0.5	0	0	0	0	0
50	V	-0.9	0.5	0	0	0	0	0
56	V	-1.5	0.5	0	0	0	0	0
63	V	-1.5	0.5	0	0	0	0	0
75	V	-1.5	0.5	0.5	0	0	0	0
88	V	-2.0	0.5	0.5	0	0	0	0
100	V	-2.5	0.5	0.5	0	0	0	0

Figure 6.5

Test: 0 - 1 - C

PRESSURE - SETTLEMENT

TEST: 0 - 1 - C

γ = 1500 kg/m^3

B = .3 m.

Pressure q kPa	Settlement cm.	$\frac{2q}{\gamma B}$	Relative settlement $\frac{W}{B}$ x 100)
0	0	0	0
25	0.3	10	1.0
38	0.5	16	1.7
50	0.8	22	2.7
63	1.0	28	3.3
75	1.2	32	4.0
88	1.4	38	4.7
100	1.6	43	5.3
113	1.8	49	6.0
125	2.0	54	6.7
138	2.2	60	7.3
150	2.5	65	8.3
163	2.7	70	9.0
175	4.6	76	15.3
200	8.0	86	26.7
225	11.5	97	38.3
250	14.7	108	49.0

Figure 6.6

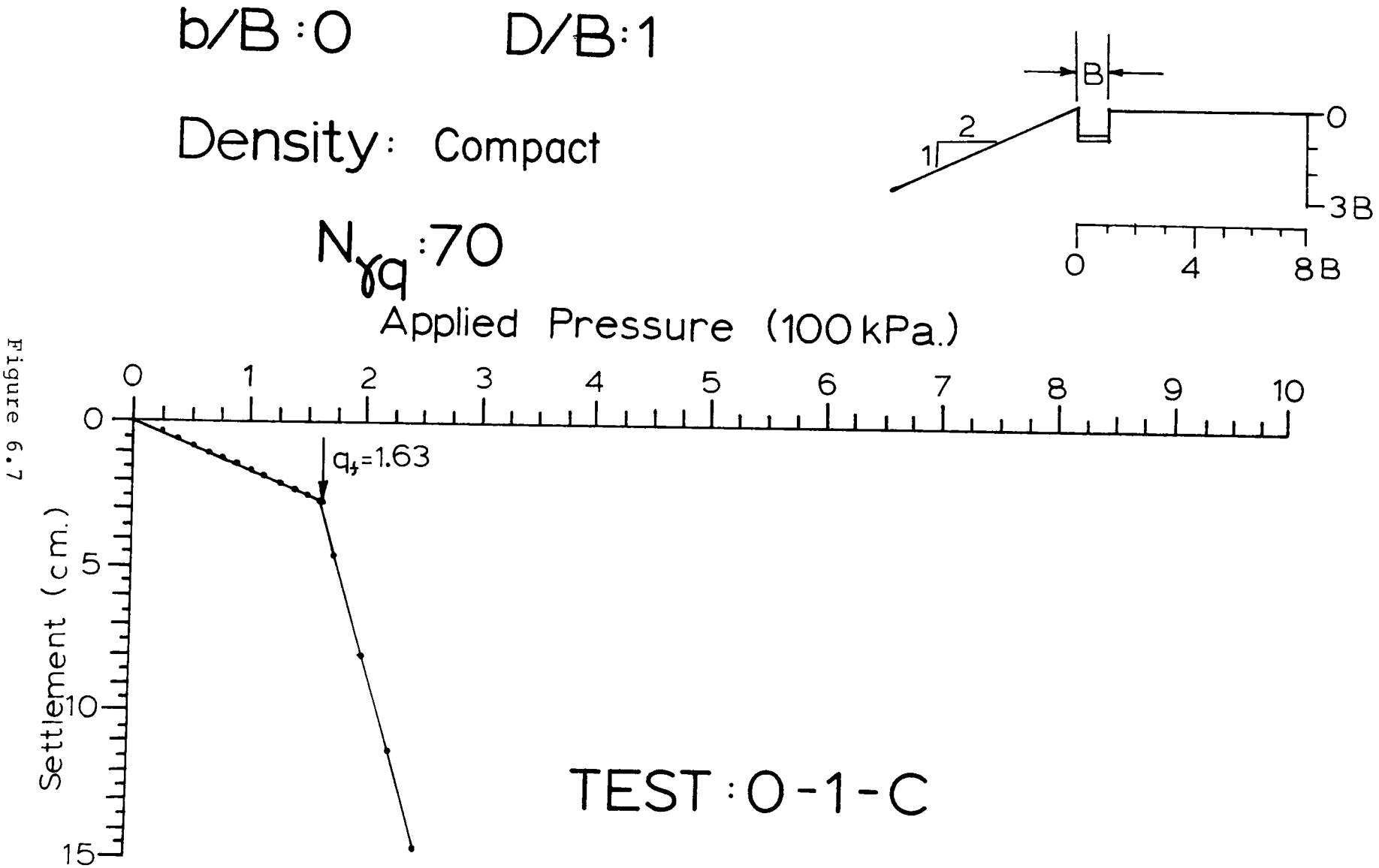
b/B : 0
D/B : 1
Density : Compact
$N_{\gamma q}$: 70
B
2
1
0
3B
0
4
8B
Applied Pressure (100 kPa.)
0
1
2
3
4
5
6
7
8
9
10
q_f = 1.63
Settlement (cm.)
0
5
10
15
TEST : 0-1-C

Figure 6.7

DENSITY MEASUREMENTS (kg/m^3)

TEST: 0 - 1 - C

Location of measurement under footing	Measurements	Average	Standard deviation
1B*	1490		
	1500		
	1490		
	1510		
	1500		
	1510		
2B*	1490		
	1500		
	1490		
	1490		
	1490		
	1500		
		1500	7

* B = footing width

Figure 6.8

Surface Movements
Test: 0 - 1 - C

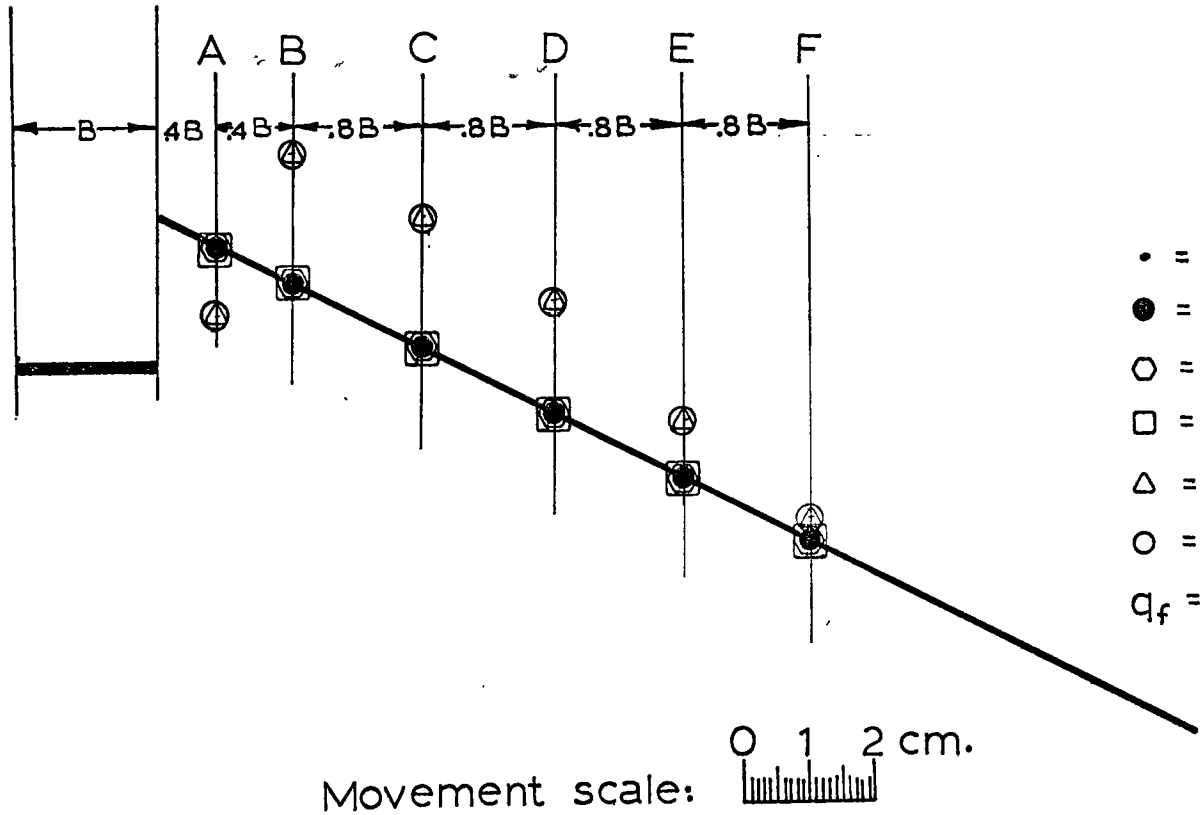

• = 0 kPa.
● = 50 "
○ = 100 "
□ = 150 "
△ = 175 "
o = 225 "
q_f = 163 "

Movement scale: 0 1 2 cm.

Figure 6.9

SURFACE MOVEMENTS (cm)

TEST: 0 - 1 - C

Positions		A	B	C	D	E	F
Horizontal distance from footing (B = footing width)		B	2B	3B	4B	5B	6B
Pressure (kPa)							
0	V	0	0	0	0	0	0
50	V	0	0	0	0	0	0
75	V	0	0	0	0	0	0
100	V	0	0	0	00	0	0
125	V	0	0	0	0	0	0
150	V	0	0	0	0	0	0
175	V	-1	2	2	1.7	0.8	0.3
225	V	-1	2	2	1.7	0.8	0.3

Figure 6.10

Test: 0 - 2 - C

PRESSURE - SETTLEMENT

TEST: 0 - 2 - C

$\gamma = 1530 \text{ kg/m}^3$

B = .3 m.

Pressure q $\overline{kPa}$	Settlement cm.	$\frac{2q}{\gamma B}$	Relative settlement $(\frac{W}{B} \times 100)$
0	0	0	0
63	0.2	27	0.7
125	0.5	53	1.7
188	0.7	80	2.3
250	1.0	105	3.3
275	1.1	116	3.7
300	1.2	127	4.0
325	1.3	138	4.3
350	1.4	148	4.7
363	1.5	152	5.0

Figure 6.11

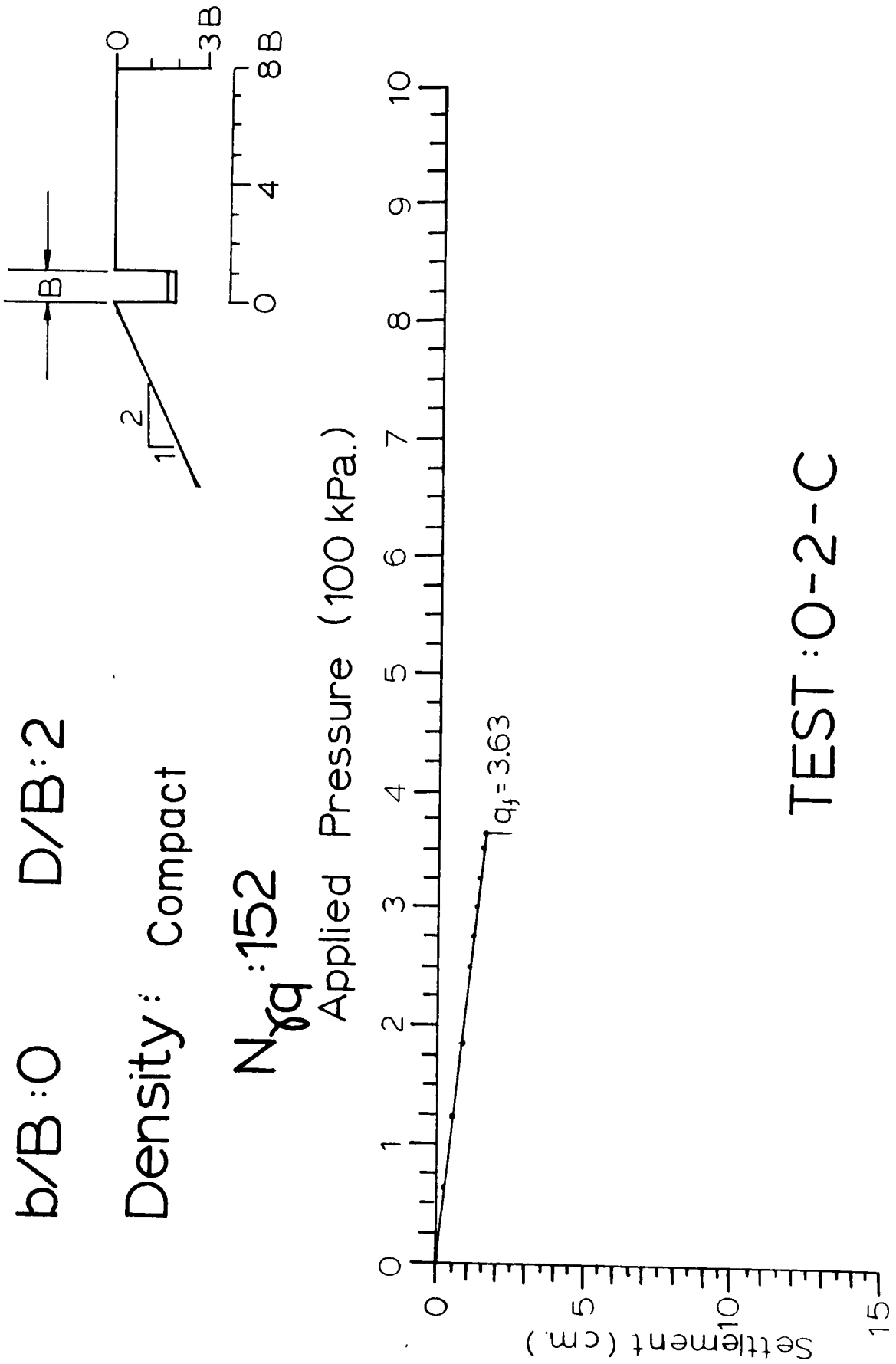
TEST:O-2-C
b/B:O
D/B:2
Density: Compact
$N_{\gamma q}$:152
Applied Pressure (100 kPa.)
Settlement (cm.)
q_f=3.63
B
2
1
O
3B
8B
4

Figure 6.12

DENSITY MEASUREMENTS (kg/m^3)

TEST: 0 - 2 - C

Location of measurement under footing	Measurements	Average	Standard deviation
-B*	1530		
	1500		
	1530		
	1520		
0	1520		
	1510		
	1520		
	1520		
B*	1540		
	1520		
	1550		
	1550		
2B*	1540		
	1550		
	1560		
	1560		
	1540		
		1530	15

* B = footing width

Figure 6.13

Surface Movements
Test:0-2-C

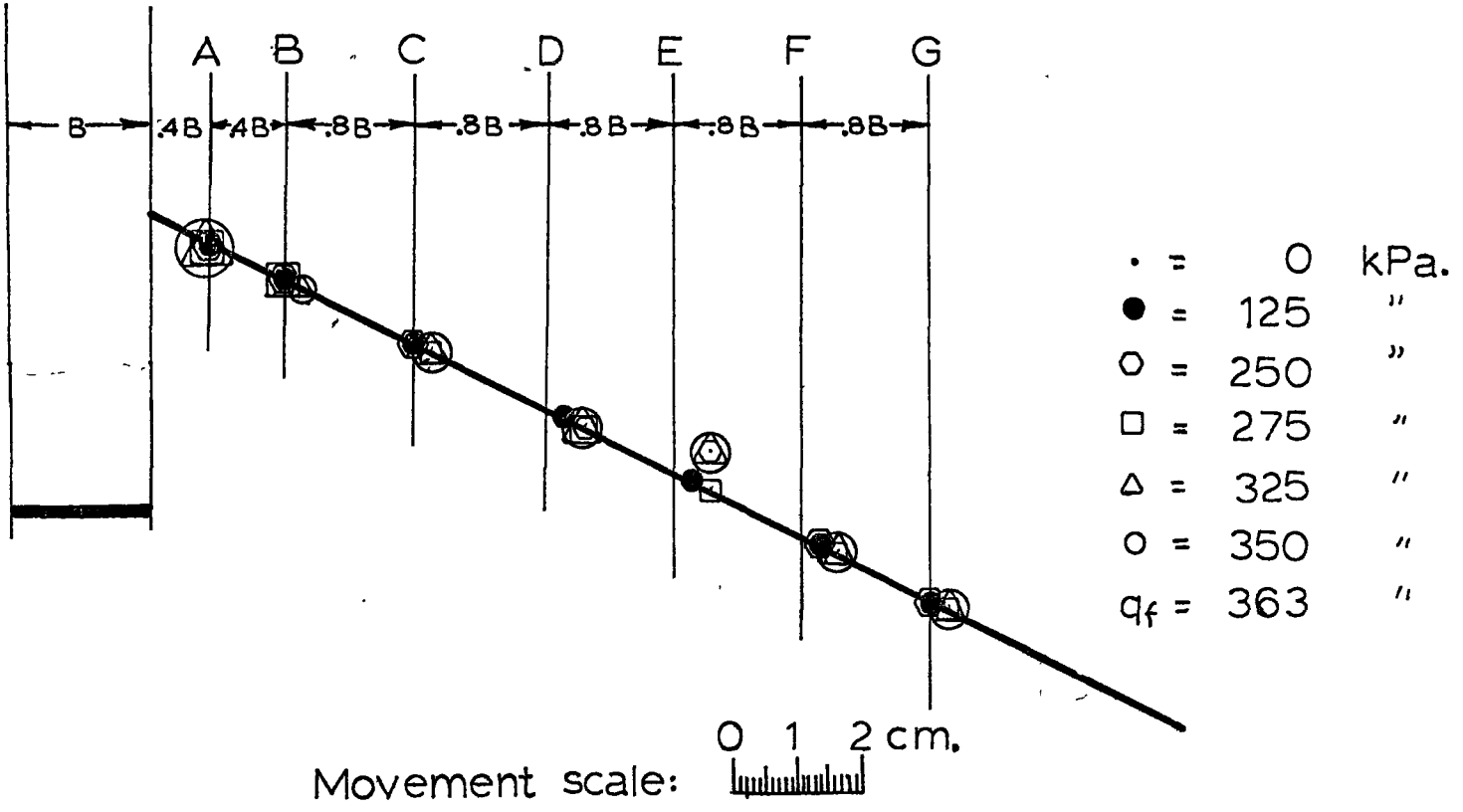

Figure 6.14

SURFACE MOVEMENTS (cm)

TEST: 0 - 2 - C

Positions		A	B	C	D	E	F	G
Horizontal distance from footing (B = footing width)		.4B	.8B	1.6B	2.4B	3.2B	4B	4.8B
Pressure (kPa)								
0	H	0	0	0	0	0	0	0
	V	0	0	0	0	0	0	0
63	H	0	0	0	0	0	0	0
	V	0	0	0	0	0	0	0
125	H	0	0	0	0.3	0.3	0.3	0
	V	0	0	0	0	0	0	0
188	H	0	0	0	0.6	0.3	0.3	0
	V	0	0	0	0	0.6	0	0
250	H	0	0	0	0.6	0.6	0.3	0
	V	0	0	0	0	0.6	0	0
275	H	0	0	0.3	0.6	0.6	0.6	0.3
	V	0	0	0	0	0	0	0
300	H	0	0	0.3	0.6	0.6	0.6	0.3
	V	0	0	0	0	0.6	0	0
325	H	0	0.3	0.3	0.6	0.6	0.6	0.3
	V	0	0	0	0	0.6	0	0
350	H	0	0.3	0.3	0.6	0.6	0.6	0.3
	V	0	0	0	0	0.6	0	0
Past failure	H	1.3	1	1.9	1.6	1.6	1.6	1.3
	V	-0.5	1	1	1	1	1	0.8

Figure 6.15

Test: 0 - 3 - C

PRESSURE - SETTLEMENT

TEST: 0 - 3 - C

γ = 1530 kg/m^3

B = .3 m.

Pressure q kPa	Settlement cm.	$\frac{2q}{\gamma B}$	Relative settlement $(\frac{W}{B} \times 100)$
0	0	0	0
63	0.2	27	0.7
125	0.4	51	1.3
188	0.7	79	2.3
250	1.0	105	3.3
313	1.3	132	4.3
375	1.6	158	5.3
433	2.0	182	6.7
500	2.6	211	8.7
525	2.8	221	9.3
550	3.1	230	10.3

Figure 6.16

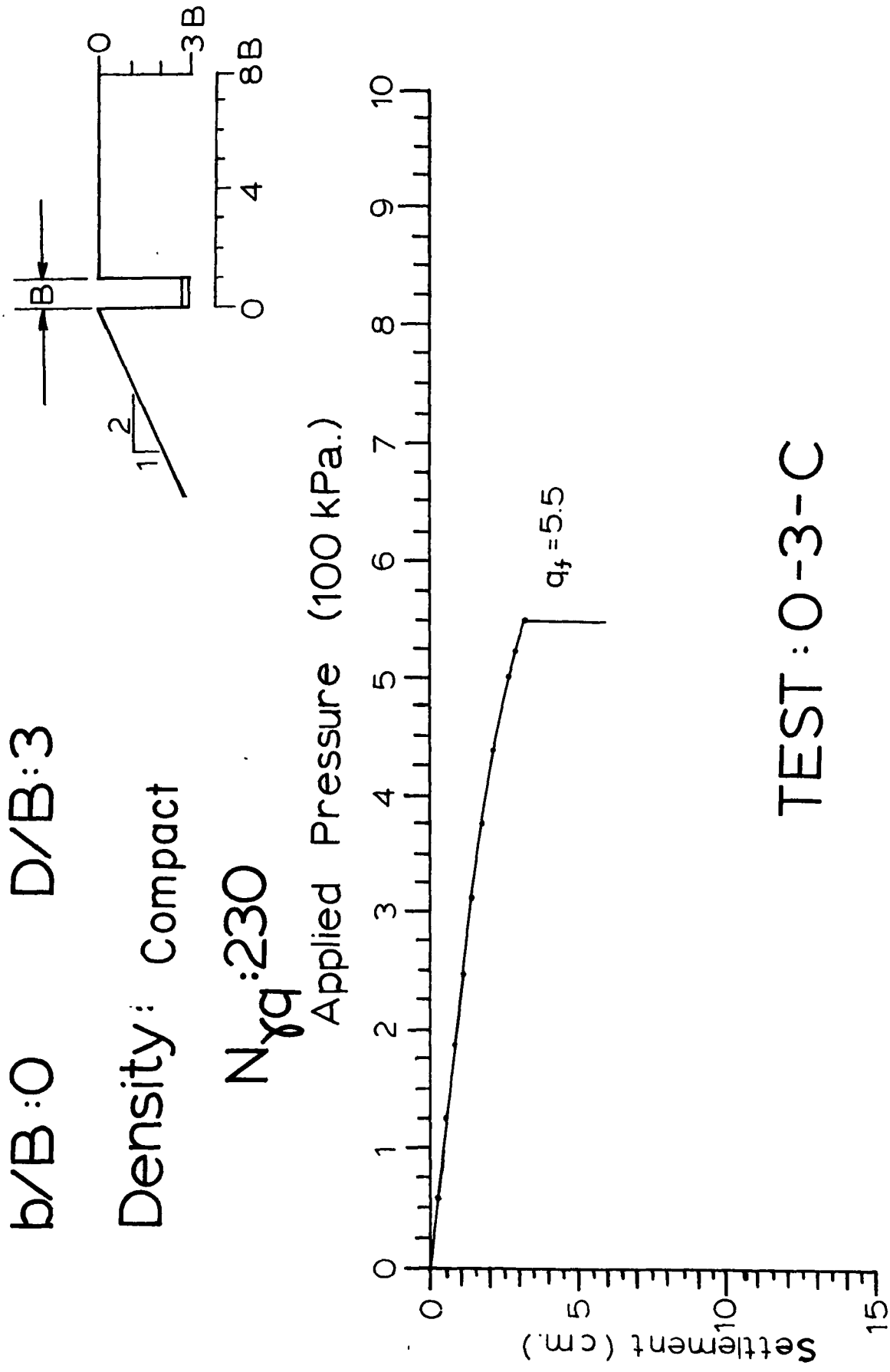
b/B :0
D/B :3
Density : Compact
$N_{\gamma q}$:230
Applied Pressure (100 kPa.)
Settlement (cm.)
TEST : O-3-C
q_f =5.5
B
2
1
0
4
8B
3B

Figure 6.17

DENSITY MEASUREMENTS (kg/m^3)

TEST: 0 - 3 - C

Location of measurement under footing	Measurements	Average	Standard deviation
B*	1540		
	1530		
	1530		
	1530		
2B*	1530		
	1530		
	1540		
	1540		
		1530	3

*B = footing width

Figure 6.18

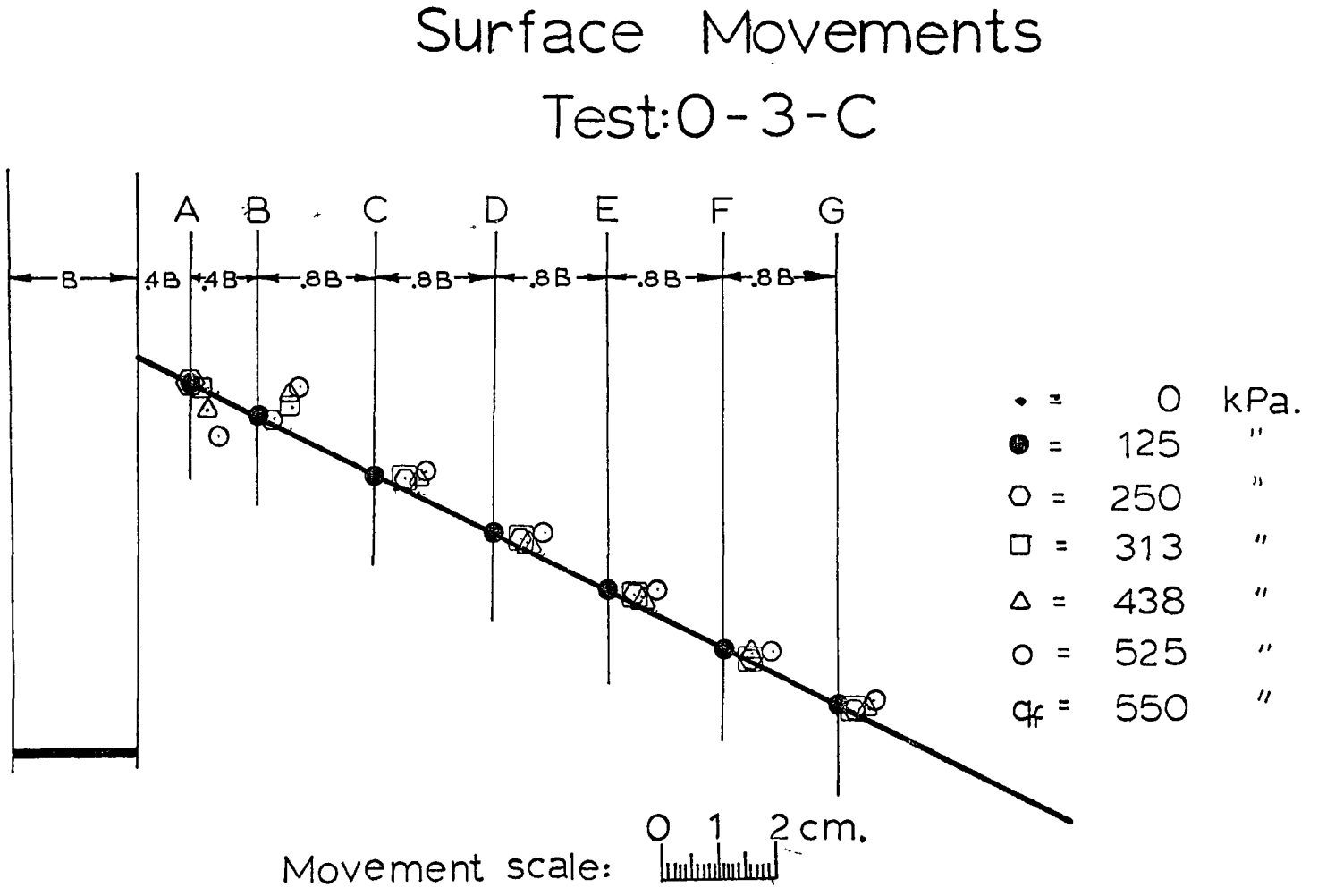
Surface Movements
Test:0-3-C
A
B
C
D
E
F
G
B
.4B
.4B
.8B
.8B
.8B
.8B
.8B
• = 0 kPa.
● = 125 "
○ = 250 "
□ = 313 "
△ = 438 "
○ = 525 "
qf = 550 "
0 1 2 cm.
Movement scale:

Figure 6.19

SURFACE MOVEMENTS (cm)

TEST: 0 - 3 - C

Positions		A	B	C	D	E	F	G
Horizontal distance from footing (B = footing width)		.4B	.8B	1.6B	2.4B	3.2B	4B	4.8B
Pressure (kPa)								
0		0	0	0	0	0	0	0
125	H	0	0	0	0	0	0	0
	V	0	0	0	0	0	0	0
188	H	0	0	0	0	0	0	0
	V	0	0	0	0	0	0	0
250	H	0	0.3	0.6	0.5	0.5	0.5	0.3
	V	0	0.1	0.2	0.1	0.1	0	0
313	H	0.2	0.6	0.6	0.5	0.5	0.5	0.3
	V	0	0.4	0.2	0.1	0.1	0	0
375	H	0.3	0.6	0.6	0.6	0.6	0.5	0.5
	V	-0.2	0.5	0.2	0.1	0.1	0.1	0.1
438	H	0.3	0.6	0.8	0.6	0.6	0.5	0.5
	V	-0.3	0.6	0.2	0.1	0.1	0.1	0.1
500	H	0.5	0.8	0.9	0.9	0.9	0.9	0.6
	V	-0.6	0.9	0.3	0.3	0.3	0.2	0.2
525	H	0.5	0.8	0.9	0.9	0.9	0.9	0.6
	V	-0.6	0.8	0.4	0.4	0.4	0.3	0.3

Figure 6.20

Test: 2.5 - 0 - C

PRESSURE - SETTLEMENT

TEST: 2.5 - 0 - C

$\gamma = 1520\ kg/m^3$

B = .3 m.

Pressure q kPa	Settlement cm.	$\frac{2q}{\gamma B}$	Relative settlement $\frac{W}{B} \times 100$
0	0	0	0
25	0.2	10	0.7
33	0.3	14	1.0
50	0.5	21	1.7
63	0.8	27	2.7
75	1.0	31	3.3
88	1.4	37	4.7
100	2.0	43	6.7
113	2.6	48	8.7
125	3.6	53	12.0
150	5.8	64	19.3
163	7.1	69	23.7
175	8.3	74	27.7

Figure 6.21

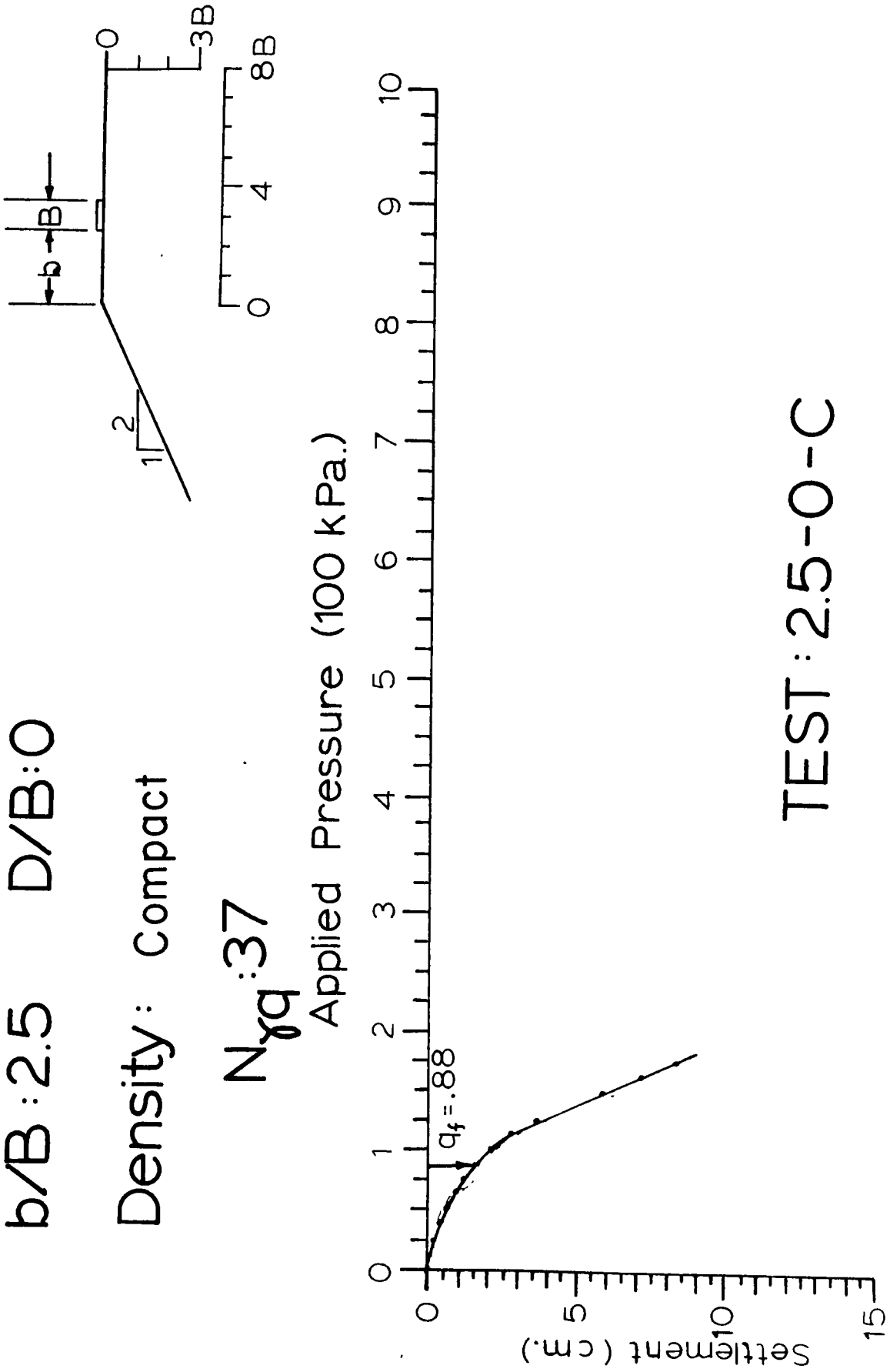
b/B :2.5 D/B:0
Density: Compact
$N_{\gamma q}$:37
TEST : 2.5-O-C
Applied Pressure (100 kPa.)
Settlement (cm.)
q_f=.88
0
1
2
3
4
5
6
7
8
9
10
0
5
10
15
b
B
2
1
0
3B
8B
0
4

Figure 6.22

DENSITY MEASUREMENTS (kg/m^3)

TEST: 2.5 - 0 - C

Location of measurement under footing	Measurements	Average	Standard deviation
B*	1510		
	1520		
	1510		
	1530		
2B*	1530		
	1530		
	1540		
	1530		
		1520	11

* B = footing width

Figure 6.23

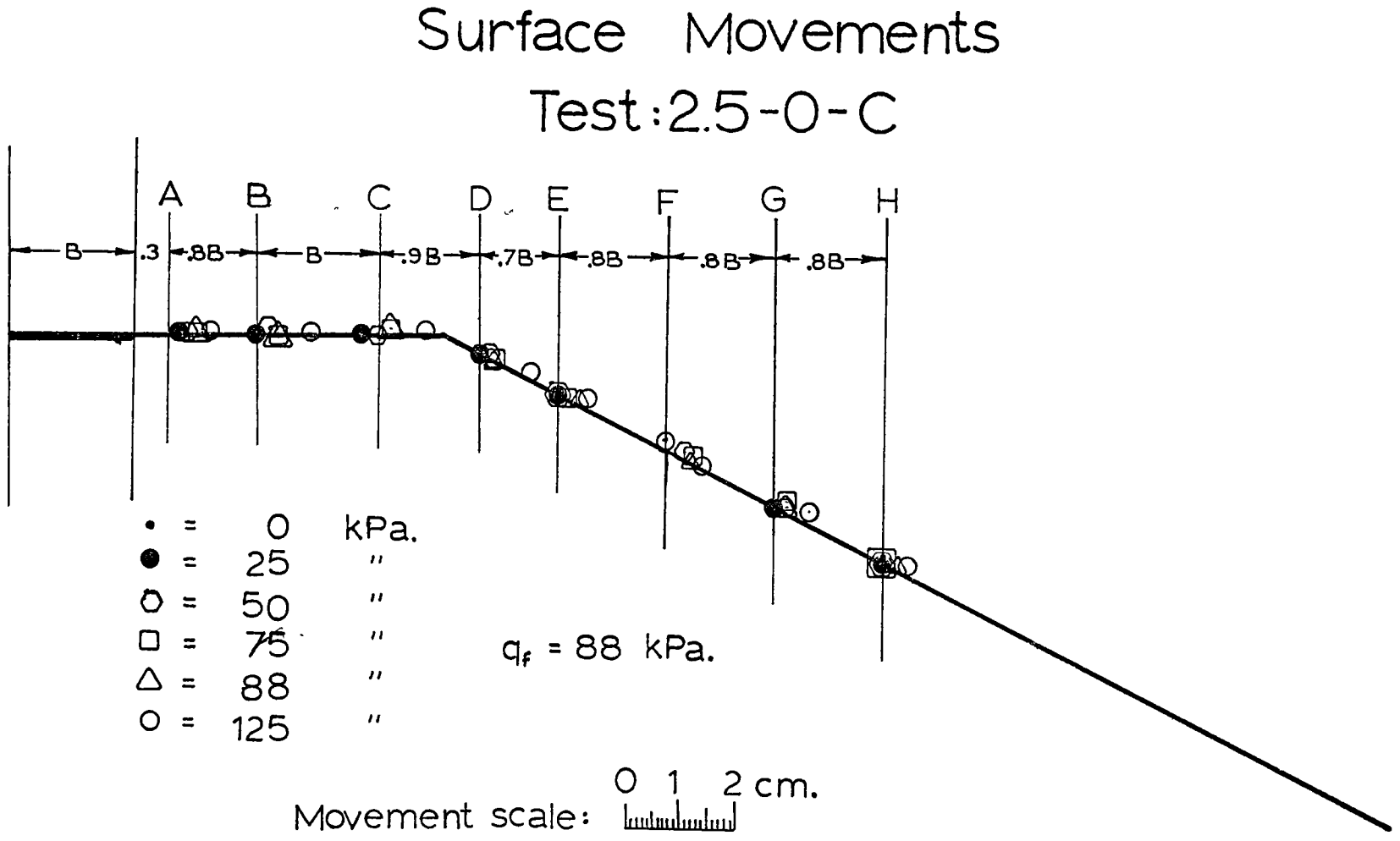
Surface Movements
Test: 2.5-0-C
A
B
C
D
E
F
G
H
B
.3
.8B
B
.9B
.7B
.8B
.8B
.8B
• = 0 kPa.
● = 25 "
⬡ = 50 "
□ = 75 "
△ = 88 "
○ = 125 "
q_f = 88 kPa.
0 1 2 cm.
Movement scale:

Figure 6.24

SURFACE MOVEMENTS (cm)

TEST: 2.5 - 0 - C

Positions		A	B	C	D	E	F	G	H
Horizontal distance from footing (B = footing width)		.3B	B	2B	2.9B	3.6B	4.4B	5.2B	6B
Pressure (kPa)									
13	H	0	0	0	0	0	0	0	0
	V	0	0	0	0	0	0	0	0
25	H	0.2	0	-0.2	0	0	0	0	0
	V	0	0	0	0	0	0.1	0	0
38	H	0.3	0.2	-0.2	0	0	0	0.2	0
	V	0	0	0	0	0	0.1	0	0
50	H	0.3	0.2	0	0.2	0	0.3	0.2	0
	V	0	0.1	0	0.1	0	0.1	0.1	0
63	H	0.5	0.3	0.2	0.2	0	0.2	0.2	0
	V	0	0	0.1	0.1	0	0.1	0	0
75	H	0.5	0.3	0.2	0.3	0.2	0.3	0.3	0.2
	V	0	0	0.1	0.1	0	0.2	0	0
88	H	0.5	0.3	0.2	0.3	0.3	0.3	0.3	0.2
	V	0	0	0.1	0	0.1	0.1	0	0.1
100	H	0.6	0.6	0.5	0.6	0.5	0.6	0.5	0.3
	V	0	0.1	0	0	0	0	0.1	0.1
113	H	0.6	0.6	0.5	0.6	0.6	0.6	0.5	0.3
	V	-0.1	0.2	0	0	0.1	0.1	0.1	0.1
125	H	0.8	1.0	0.8	1.0	0.6	0.6	0.6	0.3
	V	-0.1	0.2	0.1	0.1	0.2	0	0.2	0.2
138	H	0.8	1.1	1.0	1.1	0.8	0.8	0.6	0.3
	V	-0.1	0.2	0.1	0.2	0.3	0	0.3	0.2
150	H	1.3	1.6	1.3	1.3	1.1	1.0	1.0	0.6
	V	-0.5	0.2	0.1	0.4	0.4	0.1	0.3	0.4

Figure 6.25

Test: 2.5 - 0 - C - R

PRESSURE - SETTLEMENT

TEST: 2.5 - 0 - C - R

γ = 1470 kg/m^3

B = .3 m.

Pressure q kPa	Settlement cm.	$\frac{2q}{\gamma B}$	Relative settlement $(\frac{W}{B} \times 100)$
0	0	0	0
25	0.7	11	2.3
50	1.5	22	5.0
63	2.8	28	9.3
75	5.7	33	19.0
88	9.0	39	30.0
100	11.5	44	38.3
113	14.1	49	47.0

Figure 6.26

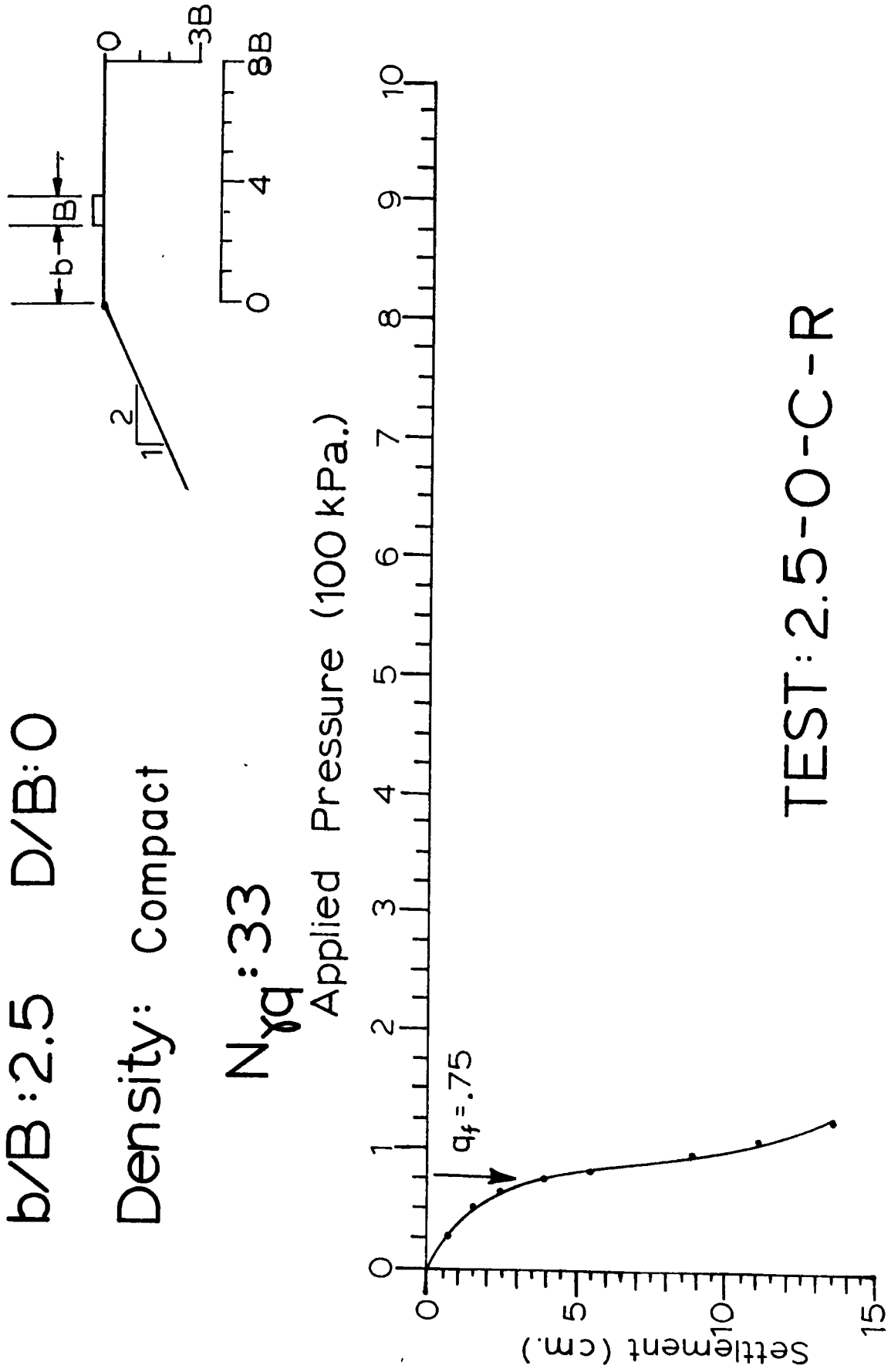
b/B:2.5 D/B:0
Density: Compact
$N_{\gamma q}$:33
TEST: 2.5-O-C-R
Applied Pressure (100 kPa.)
Settlement (cm.)
q_f=.75
b
B
2
1
0
3B
8B
4

Figure 6.27

DENSITY MEASUREMENTS (kg/m^3)

TEST: 2.5 - 0 - C - R

Location of measurement under footing	Measurements	Average	Standard deviation
B*	1470		
	1460		
	1450		
	1460		
	1470		
	1470		
2B*	1470		
	1450		
	1480		
	1460		
	1470		
		1470	8

* B = footing width

Figure 6.28

Surface Movements
Test: 2.5-0-C-R

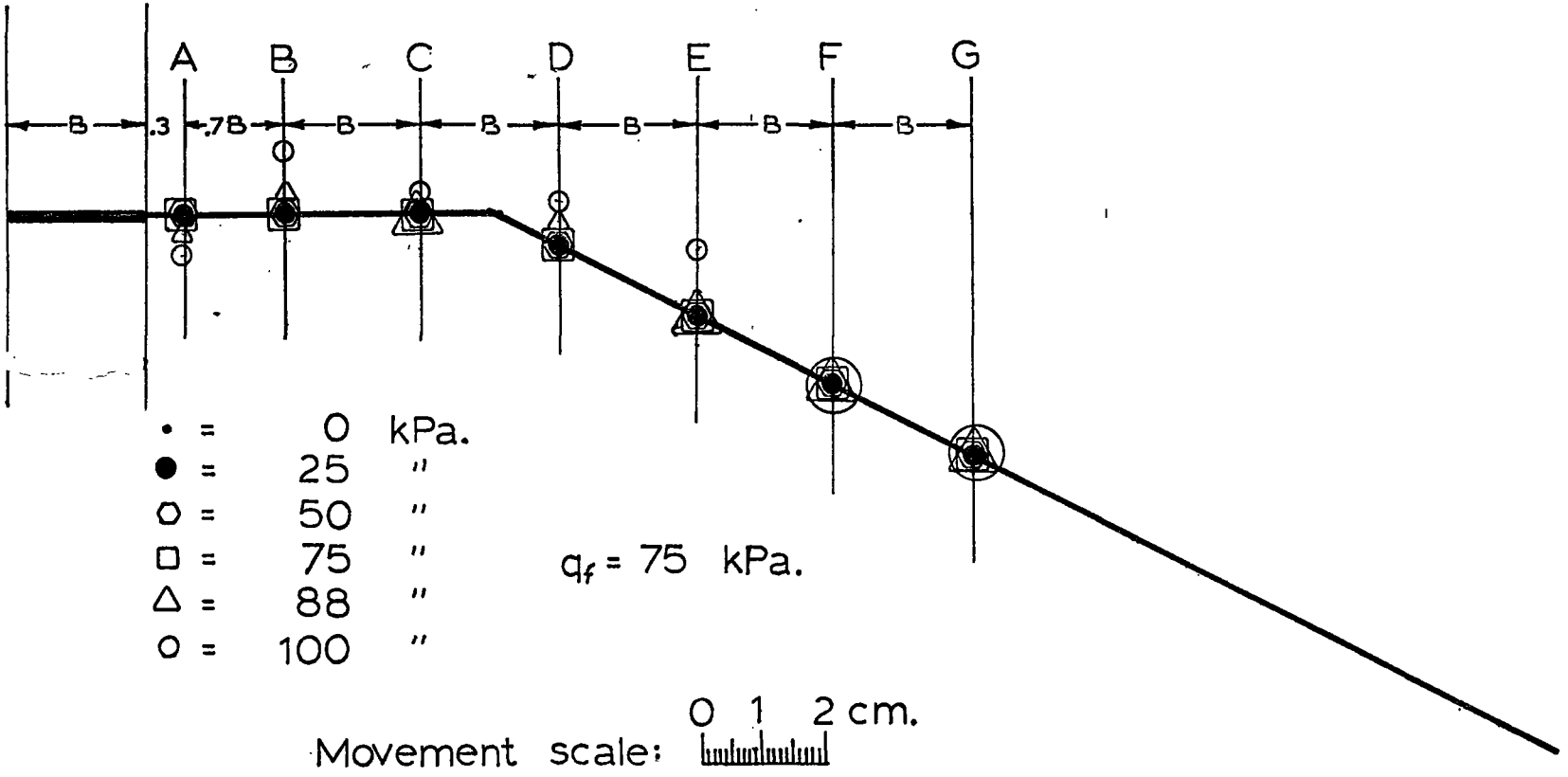

Figure 6.29

SURFACE MOVEMENTS (cm)

TEST: 2.5 - 0 - C - R

Positions		A	B	C	D	E	F	G
Horizontal distance from footing (B = footing width)		.3B	B	2B	3B	4B	5B	6B
Pressure (kPa)								
0	V	0	0	0	0	0	0	0
25	V	0	0	0	0	0	0	0
50	V	0	0	0	0	0	0	0
75	V	0	0	0	0	0	0	0
88	V	-0.3	0.3	0	0.3	0	0	0
100	V	-0.6	1.0	0.3	0.6	1.0	0	0
113	V	-1.2	1.0	0.6	0.6	1.2	0	0

Figure 6.30

Test: 2.5 - 1 - C

PRESSURE - SETTLEMENT

TEST: 2.5 - 1 - C

γ = 1510 kg/m^3

B = .3 m.

Pressure q kPa	Settlement cm.	$\frac{2q}{\gamma B}$	Relative settlement $(\frac{W}{B} \times 100)$
0	0	0	0
13	0.1	6.0	0.3
25	0.3	10	1.0
50	0.7	22	2.3
75	1.1	32	3.7
100	1.5	43	5.0
125	2.0	53	6.7
150	2.4	65	8.0
163	2.6	69	8.7
175	2.9	75	9.7
188	3.1	80	10.3
200	3.6	86	12.0
225	5.1	96	17.0
250	6.5	107	22.0
263	7.6	112	25.3

Figure 6.31

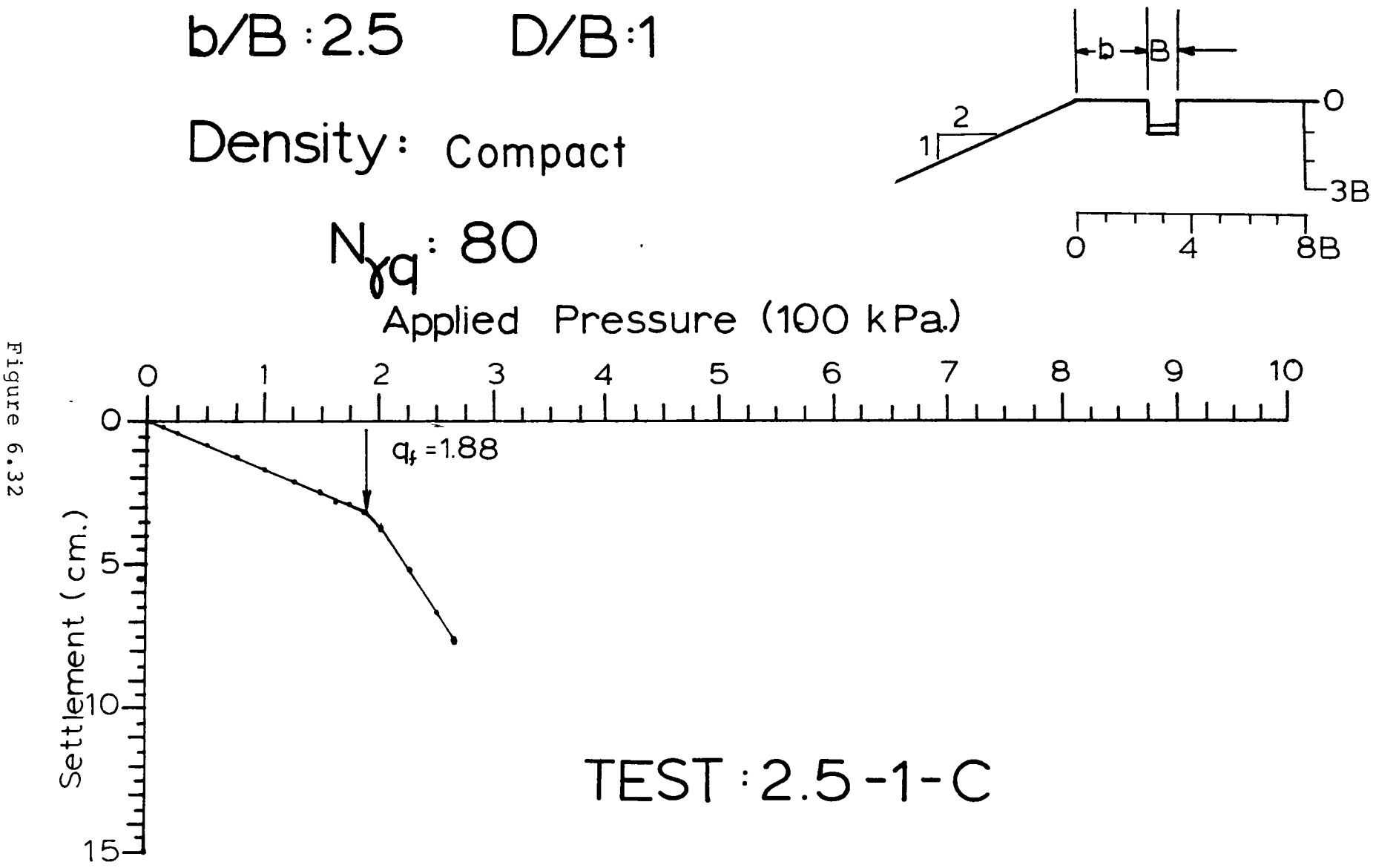
b/B : 2.5 D/B : 1
Density : Compact
$N_{\gamma q}$: 80
b
B
2
1
0
3B
0
4
8B
Applied Pressure (100 kPa.)
0 1 2 3 4 5 6 7 8 9 10
q_f = 1.88
Settlement (cm.)
0
5
10
15
TEST : 2.5 - 1 - C

Figure 6.32

DENSITY MEASUREMENTS (kg/m^3)

TEST: 2.5 - 1 - C

Location of measurement under footing	Measurements	Average	Standard deviation
B*	1500		
	1520		
	1510		
	1500		
2B*	1510		
	1520		
	1510		
	1530		
		1510	12

* B = footing width

Figure 6.33

Surface Movements
Test: 2.5-1-C

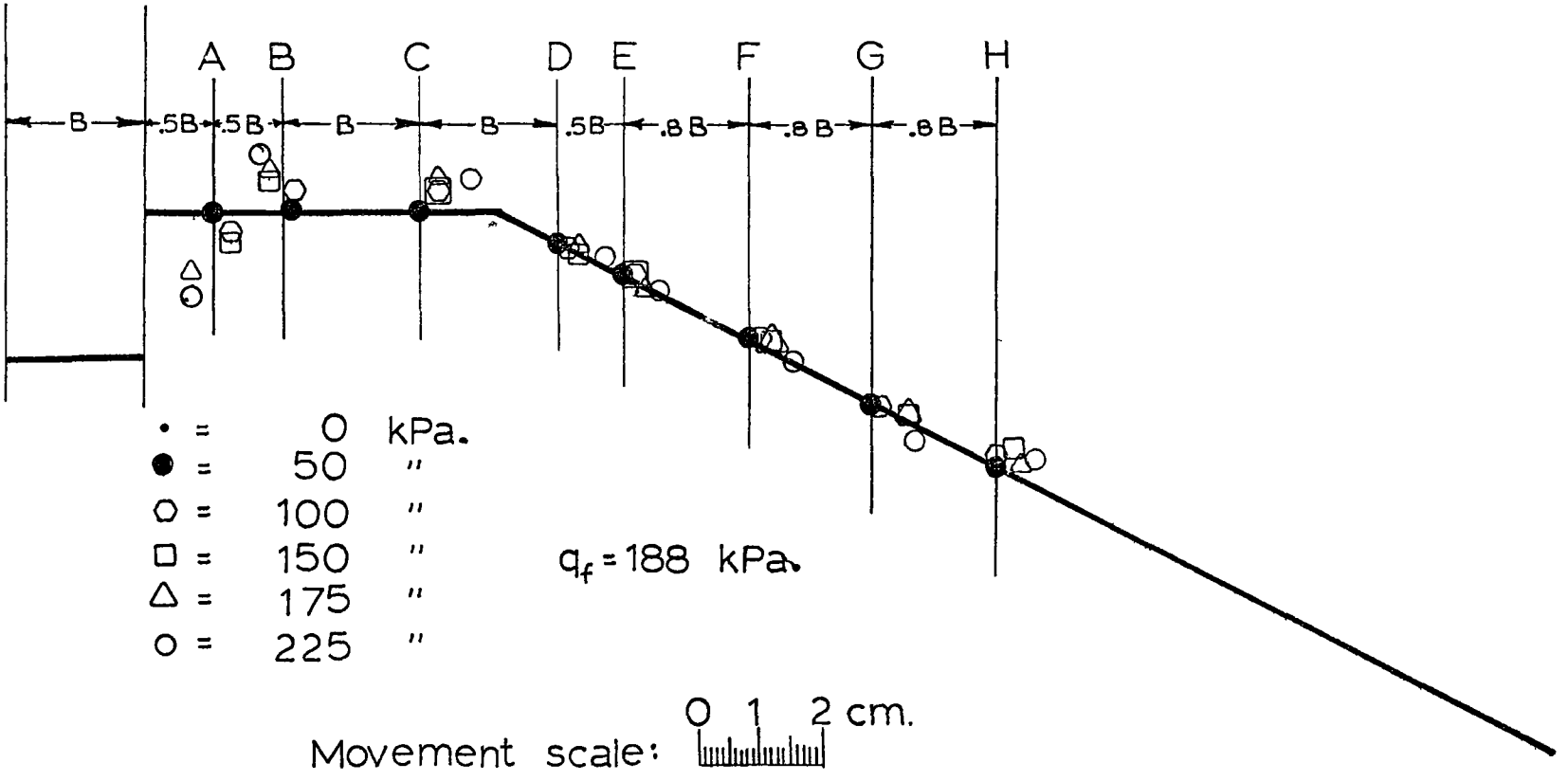

Figure 6.34

SURFACE MOVEMENTS (cm)

TEST: 2.5 - 1 - C

Positions		A	B	C	D	E	F	G	H
Horizontal distance from footing (B = footing width)		.5B	B	2B	3B	3.5B	4.3B	5.1B	5.9B
Pressure (kPa)									
0	H	0	0	0	0	0	0	0	0
	V	0	0	0	0	0	0	0	0
25	H	0	0.2	0	0	0	0	0	0
	V	0	0	0	0	0	0	0	0
50	H	0	0.2	0	0	0	0	0	0
	V	0	0.1	0.1	0	0.1	0.1	0	0
75	H	0	0.2	0.2	0.2	0.2	0.2	0	0
	V	-0.1	0.1	0.2	0	0.1	0.1	0	0.1
100	H	0.3	0.2	0.3	0.2	0.2	0.2	0.2	0
	V	-0.2	0.3	0.3	0	0.1	0.1	0	0.2
150	H	-0.2	-0.2	0.3	0.3	0.2	0.3	0.6	0.2
	V	-0.4	0.5	0.3	0	0.1	0.1	0.1	0.3
175	H	-0.3	-0.2	0.3	0.3	0.3	0.3	0.6	0.3
	V	-0.9	0.6	0.4	0.1	0	0.1	0	0.2
200	H	-0.3	-0.2	0.5	0.5	0.5	0.5	0.6	0.3
	V	-1.0	0.8	0.5	0	0	0.1	-0.1	0.3
225	H	-0.3	-0.3	0.8	0.8	0.6	0.6	0.8	0.6
	V	-1.3	0.9	0.5	0.1	0	0	-0.2	0.4
250	H	-0.5	-0.2	1.0	1.0	1.0	0.8	1.3	0.8
	V	-1.5	1.0	0.5	-0.2	-0.2	-0.1	-0.3	0.3
263	H	-0.6	0	1.2	1.9	1.3	1.6	1.6	1.3
	V	-1.5	0.8	0.4	-0.6	-0.4	-0.4	-0.5	0.5

Figure 6.35

Test: 2.5 - 1 - C - R

PRESSURE - SETTLEMENT

TEST: 2.5 - 1 - C - R

γ = 1480 kg/m^3

B = .3 m.

Pressure q kPa	Settlement cm.	$\frac{2q}{\gamma B}$	Relative settlement $(\frac{W}{B} \times 100)$
0	0	0	0
25	0.2	10	0.7
38	0.4	16	1.3
50	0.6	22	2.0
63	0.8	28	2.7
75	1.1	32	3.7
88	1.3	38	4.3
100	1.6	44	5.3
113	1.8	49	6.0
125	2.0	54	6.7
138	2.3	60	7.7
150	2.6	66	8.7
163	2.8	71	9.3
175	3.1	76	10.3
188	4.0	82	13.3
200	4.9	87	16.3
225	6.9	98	23.0
250	8.5	109	28.3
275	10.5	120	35.0
300	12.7	131	42.3

Figure 6.36

b/B : 2.5 D/B : 1

Density : Compact

$N_{\gamma q}$: 76

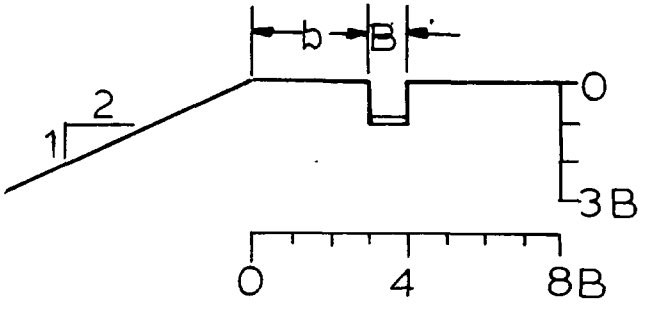

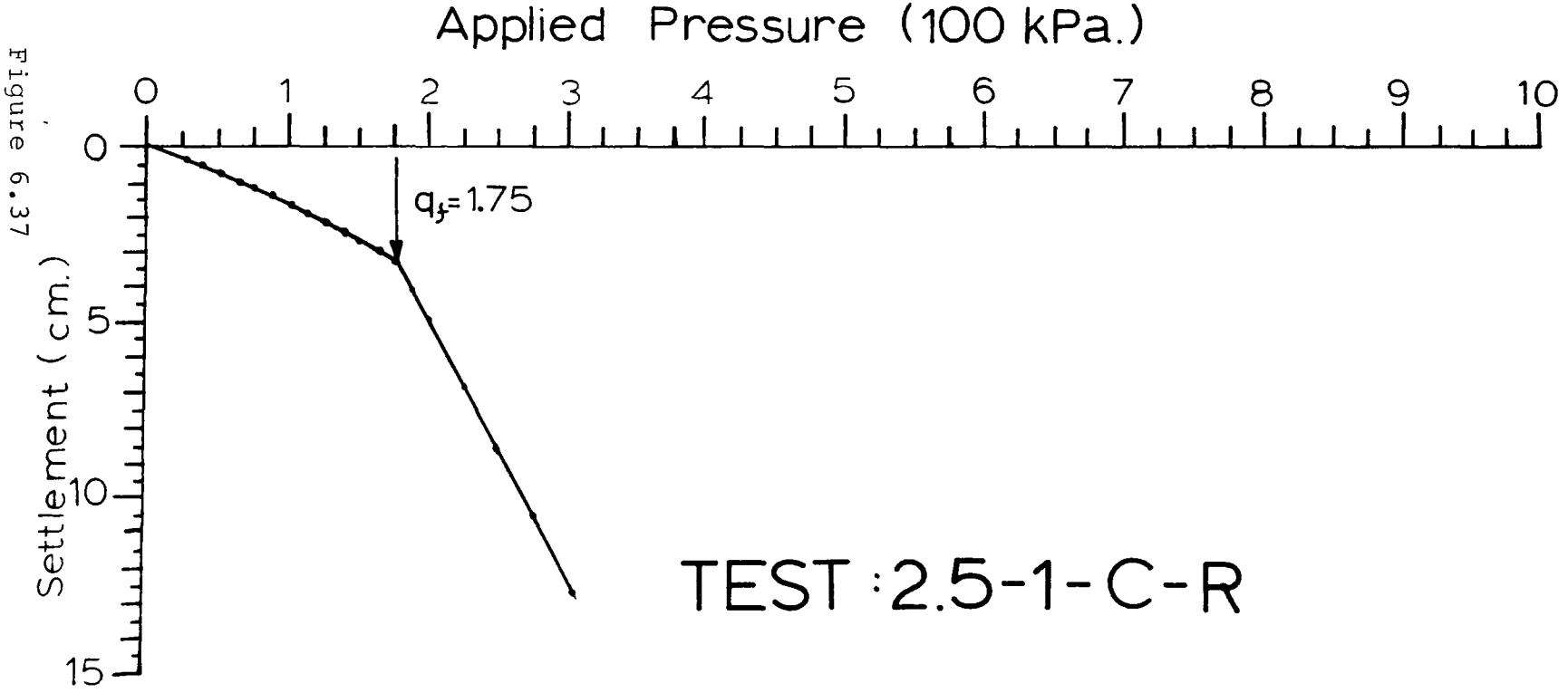

TEST : 2.5-1-C-R

Figure 6.37

DENSITY MEASUREMENTS (kg/m^3)

TEST: 2.5 - 1 - C - R

Location of measurement under footing	Measurements	Average	Standard deviation
-B*	1480		
	1470		
	1500		
	1490		
	1490		
2B*	1470		
	1460		
	1460		
	1450		
	1450		
3B*	1480		
	1490		
	1480		
	1490		
	1490		
4B*	1510		
	1480		
	1500		
	1500		
		1480	17

* B = footing width

Figure 6.38

Test: 2.5 - 2 - C

PRESSURE - SETTLEMENT

TEST: 2.5 - 2 - C

γ = 1520 kg/m^3

B = .3 m.

Pressure q kPa	Settlement cm.	$\frac{2q}{\gamma B}$	Relative settlement $(\frac{W}{B} \times 100)$
0	0	0	0
63	.2	27	.7
125	.3	53	1.0
188	.5	80	1.7
250	.8	106	2.7
313	1.2	133	4
350	1.3	149	4.3
375	1.5	160	5
400	1.6	170	5.3
425	1.8	181	6.0
450	2.1	190	7
475	2.3	202	7.7
500	2.8	213	9.3
525	3.4	223	11.3
550	4.0	234	13.3
575	4.7	244	15.7
600	5.6	255	18.7
625	6.6	266	22

Figure 6.39

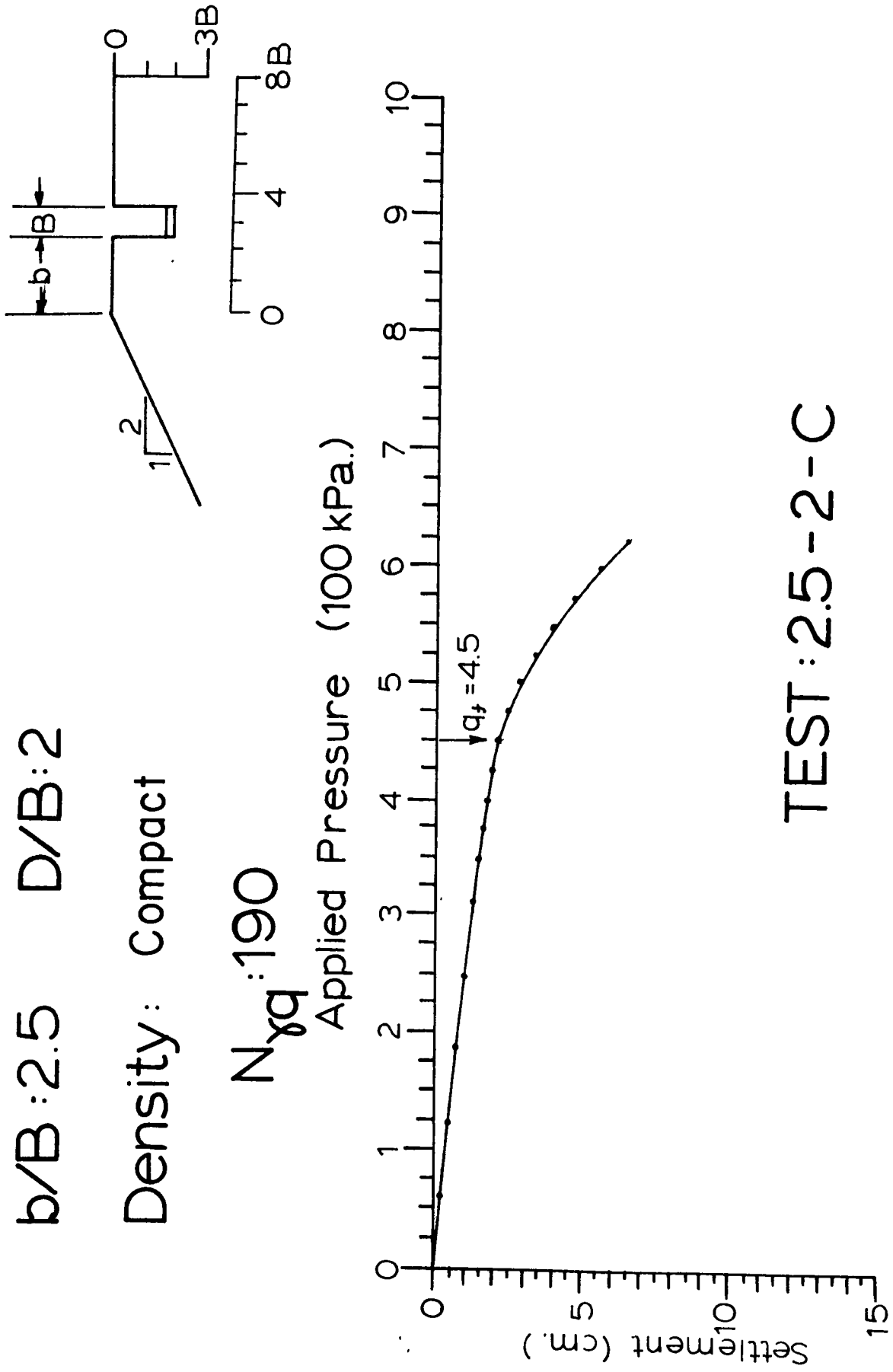
b/B :2.5 D/B:2
Density: Compact
$N_{\gamma q}$:190
TEST :2.5-2-C
Applied Pressure (100 kPa.)
Settlement (cm.)
q_f =4.5
b
B
2
1
0
3B
8B
0
4
0
1
2
3
4
5
6
7
8
9
10
0
5
10
15

Figure 6.40

DENSITY MEASUREMENTS (kg/m^3)

TEST: 2.5 - 2 - C

Location of measurement under footing	Measurements	Average	Standard deviation
0	1530		
	1510		
	1530		
	1530		
B*	1510		
	1500		
	1520		
	1500		
2B*	1530		
	1500		
	1530		
	1520		
3B*	1530		
	1510		
	1540		
	1530		
		1520	14

* B = footing width

Figure 6.41

Surface Movements
Test: 2.5-2-C

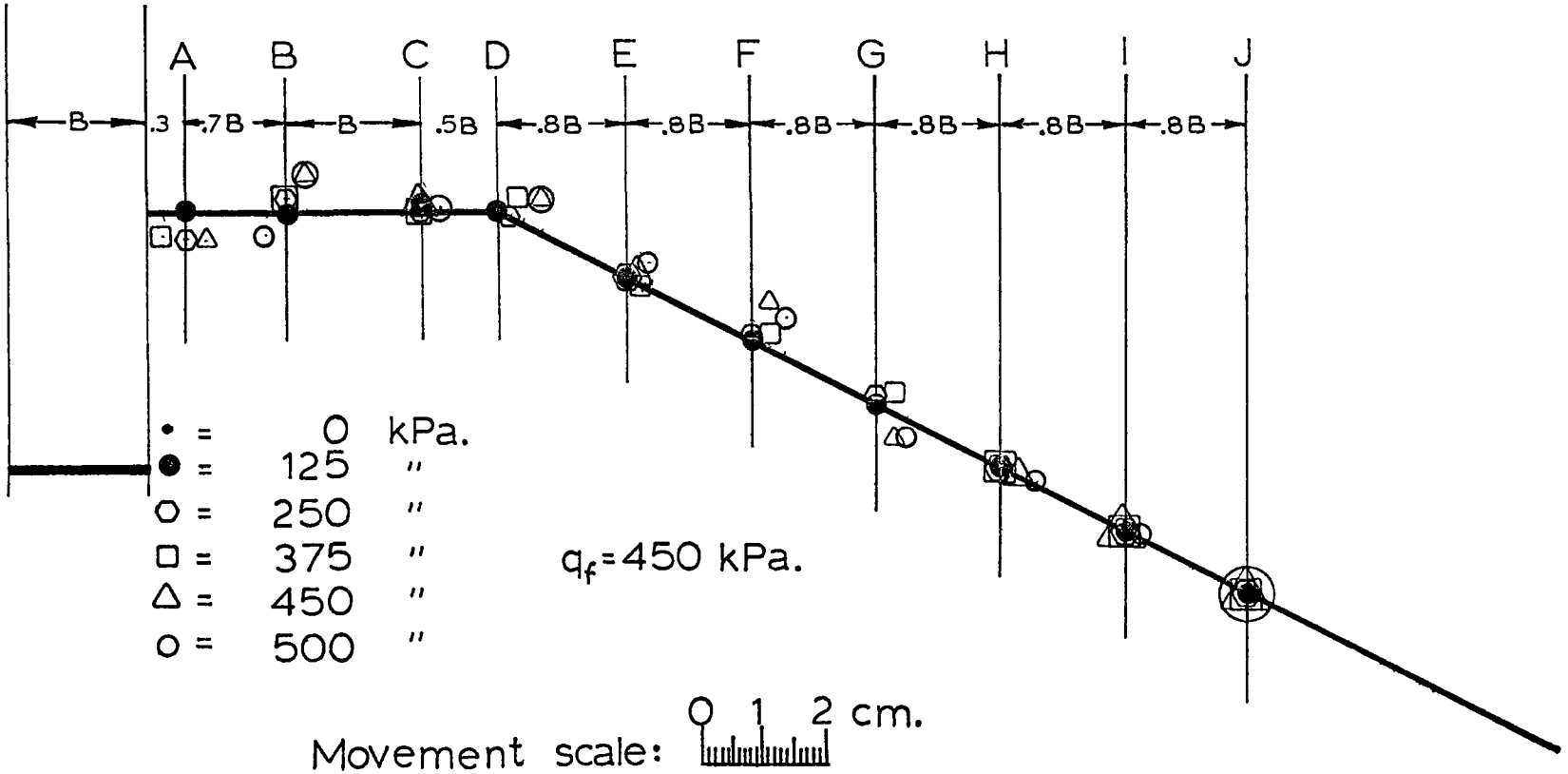

Figure 6.42

SURFACE MOVEMENTS (cm)

TEST: 2.5 - 2 - C

Positions		A	B	C	D	E	F	G	H	I	J
Horizontal distance from footing (B = footing width)		.3B	B	2B	2.5B	3.3B	4.1B	4.9B	5.7B	6.5B	7.3B
Pressure (kPa)											
0	H	0	0	0	0	0	0	0	0	0	0
	V	0	0	0	0	0	0	0	0	0	0
125	H	0	0	0	0	0	0	0	0	0	0
	V	0	0	0.1	0	0	0	0	0	0	0
250	H	0	0	0	0.2	0	0	0	0	0	0
	V	-0.4	0.2	0	0	0	0.1	0.1	0	0	0
313	H	0.3	0	0	0.3	0	0	0	0	0	0
	V	-0.4	0.2	0	0.1	0	0.3	0.2	0	0	0
350	H	0.3	0	0	0.3	0	0.2	0	0	0	0
	V	-0.4	0.4	0.1	0.2	0	0.2	0.2	0	0	0
375	H	0.3	0	0	0.3	0	0.3	0.3	0	0	0
	V	-0.3	0.2	0	0.4	0.3	0.2	0.3	0	0	0
400	H	0.3	0.3	0	0.6	0.2	0.3	0.3	0.2	0	0
	V	-0.3	0.4	0.3	0.6	0.2	0.4	0.3	0	0	0
425	H	0.3	0.3	0	0.8	0.2	0.3	0.3	0.2	0	0
	V	-0.3	0.6	0.3	0.4	0	0.4	0	0	0	0
450	H	0.3	0.3	0	0.8	0.2	0.3	0.3	0.2	0	0
	V	-0.4	0.6	0.1	0.5	0.2	0.8	-0.4	0	0	0
475	H	0.3	0.3	0	0.8	0.2	0.3	0.3	0.2	0	0
	V	-0.3	0.6	0.3	0.5	0.2	0.6	-0.4	0	0	0
500	H	1.3	0.3	0	1.0	0.4	0.6	0.6	0.2	0	0
	V	-0.3	0.6	0.3	0.5	0.4	0.6	-0.4	0	0	0
525	H	1.3	0.3	0	0.8	0.4	0.5	0.5	0.6	0.2	0.2
	V	-0.3	0.6	0.3	0.5	0.4	0.6	-0.4	0	0	0
550	H	1.3	0.6	0	0.8	0.4	0.5	0.5	0.6	0.2	0.2
	V	-0.3	0.7	0.3	0.5	0.4	0.6	-0.4	-0.2	0	0
575	H	1.3	0.6	0.2	1.0	0.8	0.6	0.6	0.6	0.5	0.2
	V	-0.3	0.7	0.3	0.5	0.4	-0.4	-0.2	-0.2	0	0
600	H	1.3	0.6	0.2	1.0	0.8	0.6	0.6	0.6	0.5	0.2
	V	-0.3	0.7	0.3	0.5	0.4	-0.4	-0.2	-0.3	0	0

Figure 6.43

Test: 2.5 - 3 - C

PRESSURE - SETTLEMENT

TEST: 2.5 - 3 - C

γ = 1530 kg/m^3

B = .3 m.

Pressure q kPa	Settlement cm.	$\frac{2q}{\gamma B}$	Relative settlement $(\frac{W}{B} \times 100)$
0	0	0	0
63	0.2	27	0.7
125	0.4	52	1.3
188	0.7	79	2.3
250	0.9	105	3.0
313	1.3	132	4.3
375	1.6	158	5.3
433	2.0	182	6.7
500	2.4	211	8.0
525	2.6	221	8.7
550	2.8	232	9.3
575	2.9	242	9.7
600	3.0	250	10.0

Figure 6.44

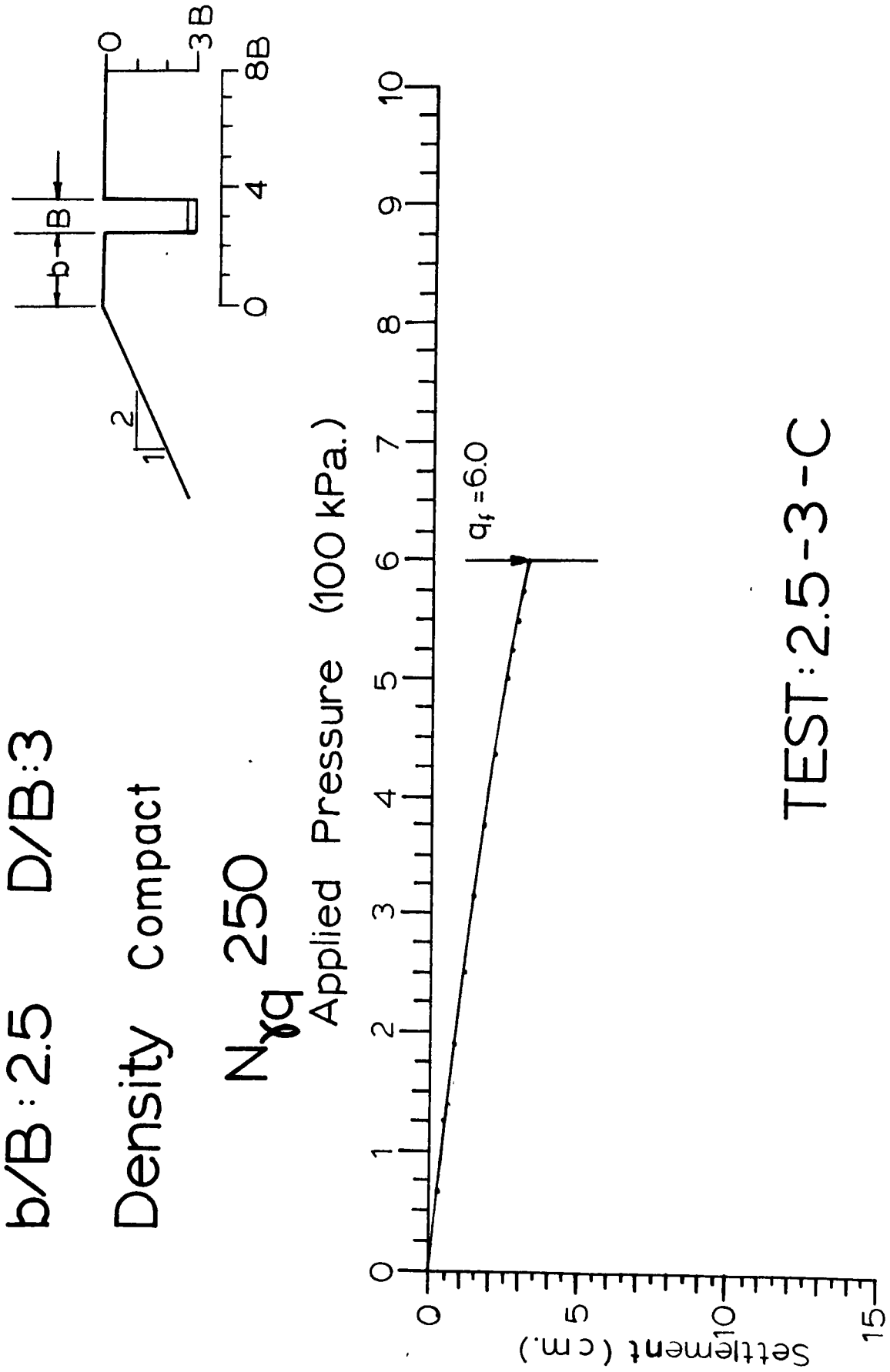
b/B : 2.5
D/B : 3
Density Compact
$N_{\gamma q}$ 250
Applied Pressure (100 kPa.)
Settlement (cm.)
q_f = 6.0
TEST : 2.5-3-C
b
B
2
1
0
3B
8B
4

Figure 6.45

DENSITY MEASUREMENTS (kg/m^3)

TEST: 2.5 - 3 - C

Location of measurement under footing	Measurements	Average	Standard deviation
B*	1540		
	1540		
	1540		
	1530		
2B*	1540		
	1520		
	1530		
	1530		
		1530	8

* B = footing width

Figure 6.46

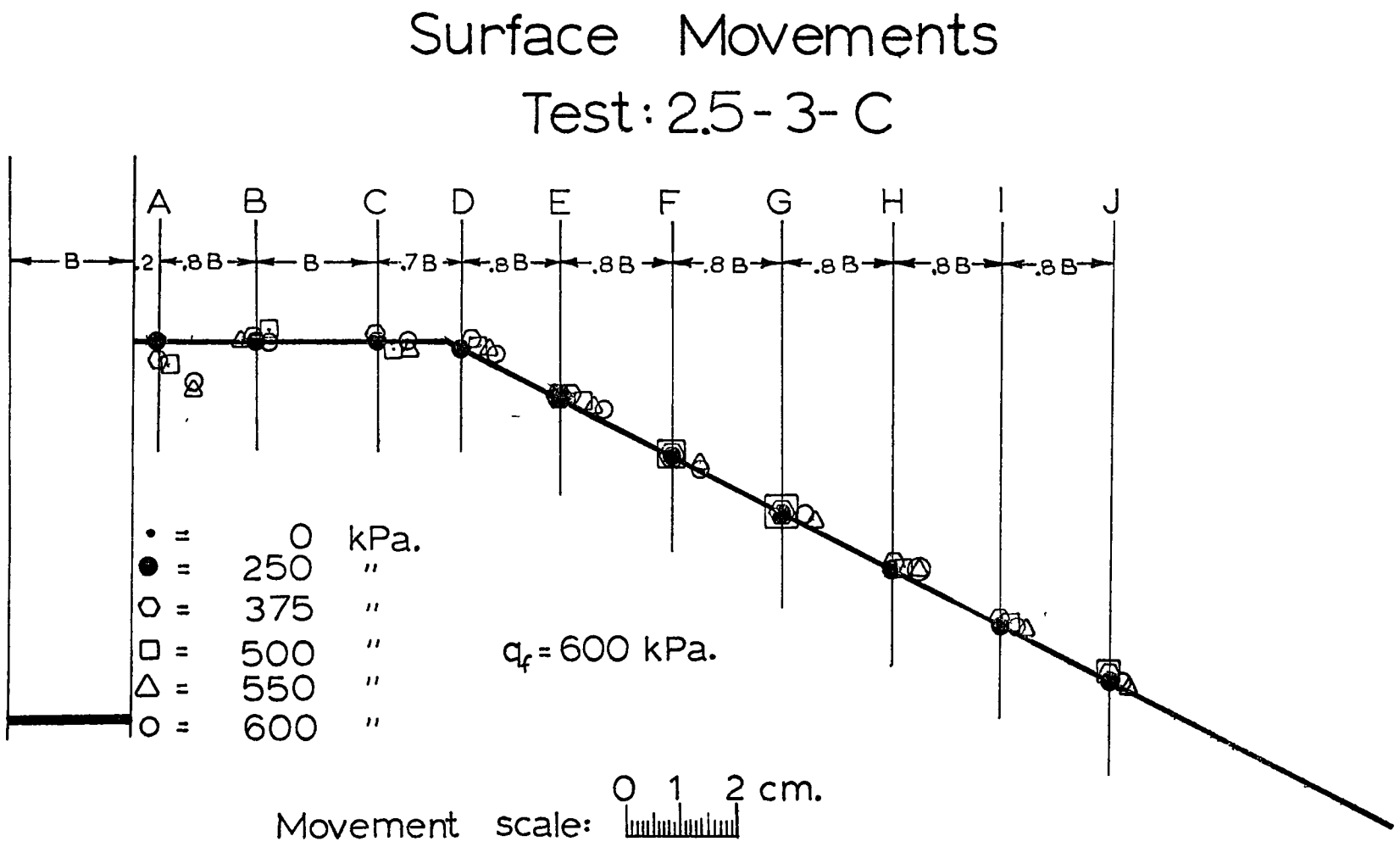
Surface Movements
Test: 2.5 - 3 - C
A
B
C
D
E
F
G
H
I
J
B
.2
.8B
B
.7B
.8B
.8B
.8B
.8B
.8B
.8B
• = 0 kPa.
● = 250 "
○ = 375 "
□ = 500 "
△ = 550 "
○ = 600 "
q_f = 600 kPa.
0 1 2 cm.
Movement scale:

Figure 6.47

SURFACE MOVEMENTS (cm)

TEST: 2.5 - 3 - C

Positions		A	B	C	D	E	F	G	H	I	J
Horizontal distance from footing (B = footing width)		.2B	B	2B	2.7B	3.5B	4.3B	5.1B	5.9B	6.7B	7.5B
Pressure (kPa)											
0	H	0	0	0	0	0	0	0	0	0	0
	V	0	0	0	0	0	0	0	0	0	0
125	H	0	0	0	0	0	0	0	0	0	0
	V	0	0	0	0	0	0	0	0	0	0
250	H	0	0	0	0	0	0	0	0	0	0
	V	0	0	0	0	0	0	0	0	0	0
375	H	0	0	0	0.2	0.2	0	0	0	0	0
	V	-0.3	0.1	0.1	0.2	0.2	0	0	0.1	0.1	0.1
500	H	0.2	0.3	0.3	0.3	0.3	0	0	0.2	0.2	0
	V	-0.4	0.2	-0.1	0.2	0.1	0	0	0.1	0.1	0.1
550	H	0.6	-0.2	0.5	0.5	0.6	0.5	0.5	0.5	0.5	0.3
	V	-0.8	0	-0.1	0.2	0.2	0.1	0.1	0.2	0.1	0
575	H	0.6	-0.3	0.6	0.6	0.6	0.5	0.5	0.5	0.5	0.3
	V	-0.7	0.2	-0.1	0.2	0.1	0	0.1	0.2	0.1	0.1
600	H	0.6	0	0.5	0.6	0.8	0.5	0.3	0.5	0.3	0.2
	V	-0.7	0.2	0	0.2	0.2	0	0.1	0.2	0.1	0

Figure 6.48

Test: 5 - 0 - C

PRESSURE - SETTLEMENT

TEST: 5 - 0 - C

γ = 1490 kg/m^3

B = .3 m.

Pressure q kPa	Settlement cm.	$\frac{2q}{\gamma B}$	Relative settlement $(\frac{W}{B} \times 100)$
0	0	0	0
25	0.2	10	0.7
50	0.4	22	1.3
75	0.8	32	2.7
100	1.4	44	4.1
125	2.2	54	7.3
138	5.1	60	17.0
150	6.1	65	20.3
163	7.2	70	24.0
175	8.2	76	27.3
188	10.0	82	33.3
200	10.8	86	36.0
225	12.5	98	41.6
238	14.3	104	47.6
250	15.3	108	50.9

Figure 6.49

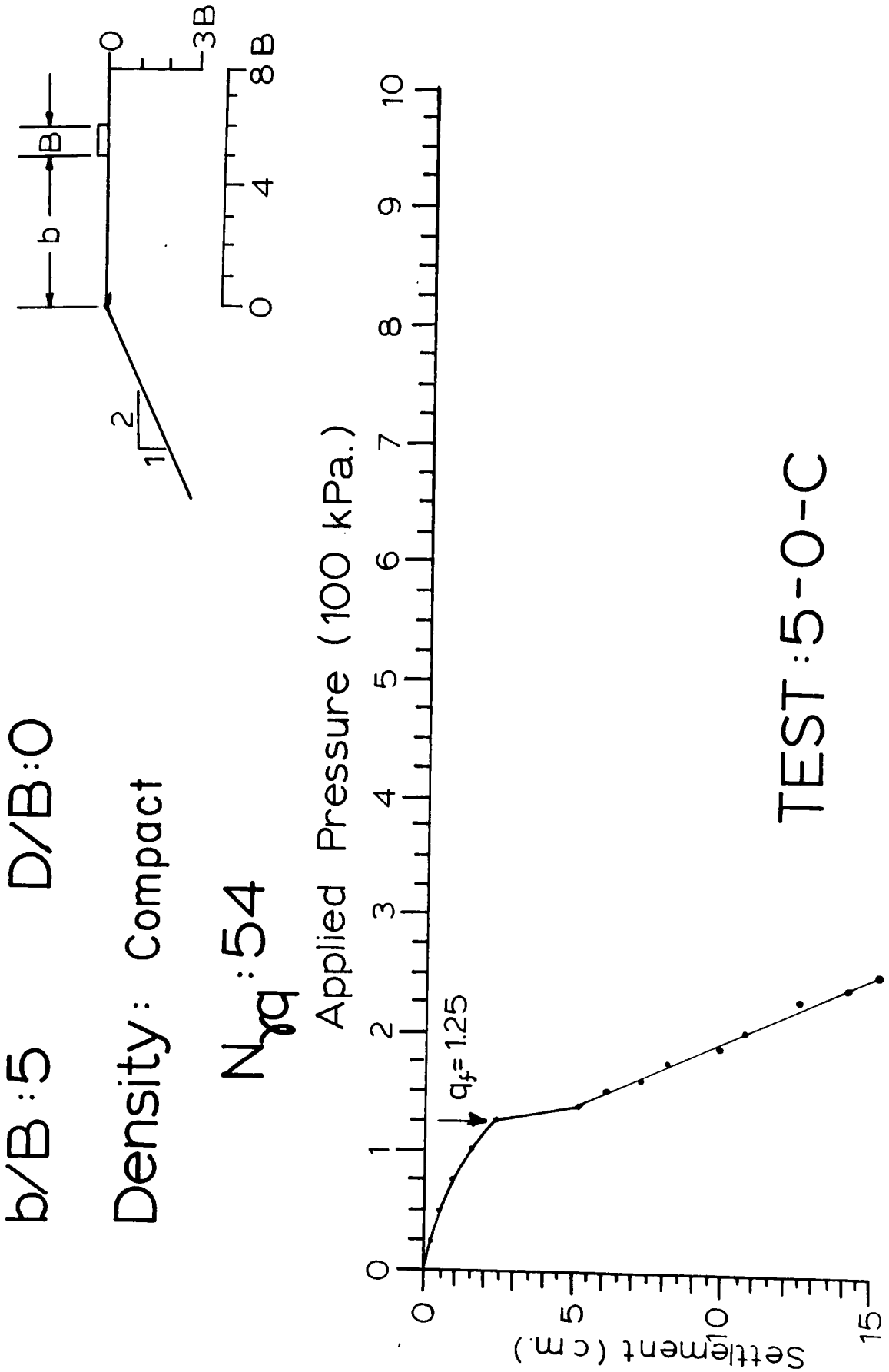
b/B :5
D/B:0
Density: Compact
$N_{\gamma q}$:54
TEST:5-O-C
Applied Pressure (100 kPa.)
Settlement (cm.)
q_f= 1.25
b
B
O
3B
8B
0
4
2
1
0
1
2
3
4
5
6
7
8
9
10
0
5
10
15

Figure 6.50

Test: 5 - 1 - C

PRESSURE - SETTLEMENT

TEST: 5 - 1 - C

$\gamma = 1510\ kg/m^3$

B = .3 m.

Pressure q $\overline{kPa}$	Settlement cm.	$\frac{2q}{\gamma B}$	Relative settlement $(\frac{W}{B} \times 100)$
0	0	0	0
13	0.1	6	0.3
25	0.2	10	0.7
50	0.5	22	1.7
75	0.9	32	3.0
100	1.3	43	4.3
125	2.0	53	6.7
150	2.5	65	8.3
175	3.3	76	11.0
200	4.2	86	14.0
225	5.3	95	17.7
250	7.5	107	25.0
275	9.7	118	32.3
300	13.0	128	43.3

Figure 6.51

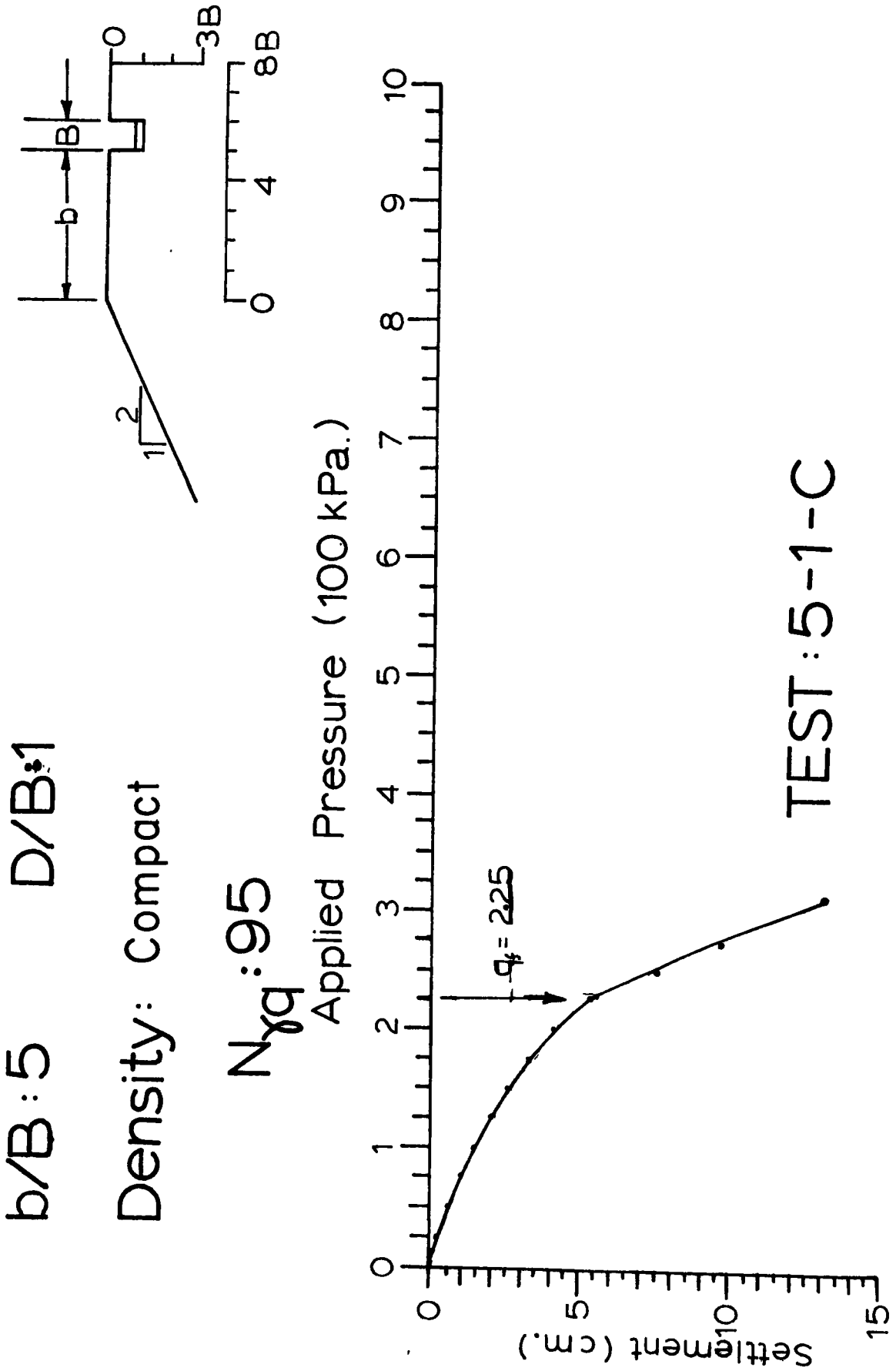
b/B : 5
D/B : 1
Density : Compact
$N_{\gamma q}$: 95
TEST : 5-1-C
Applied Pressure (100 kPa.)
Settlement (cm.)
q_f = 225
B
b
2
1
0
3B
8B
4

Figure 6.52

DENSITY MEASUREMENTS (kg/m^3)

TEST: 5 - 1 - C

Location of measurement under footing	Measurements	Average	Standard deviation
B*	1510		
	1510		
	1520		
	1520		
2B*	1510		
	1490		
	1500		
	1500		
		1510	10

* B = footing width

Figure 6.53

Surface Movements
Test:5-1-C

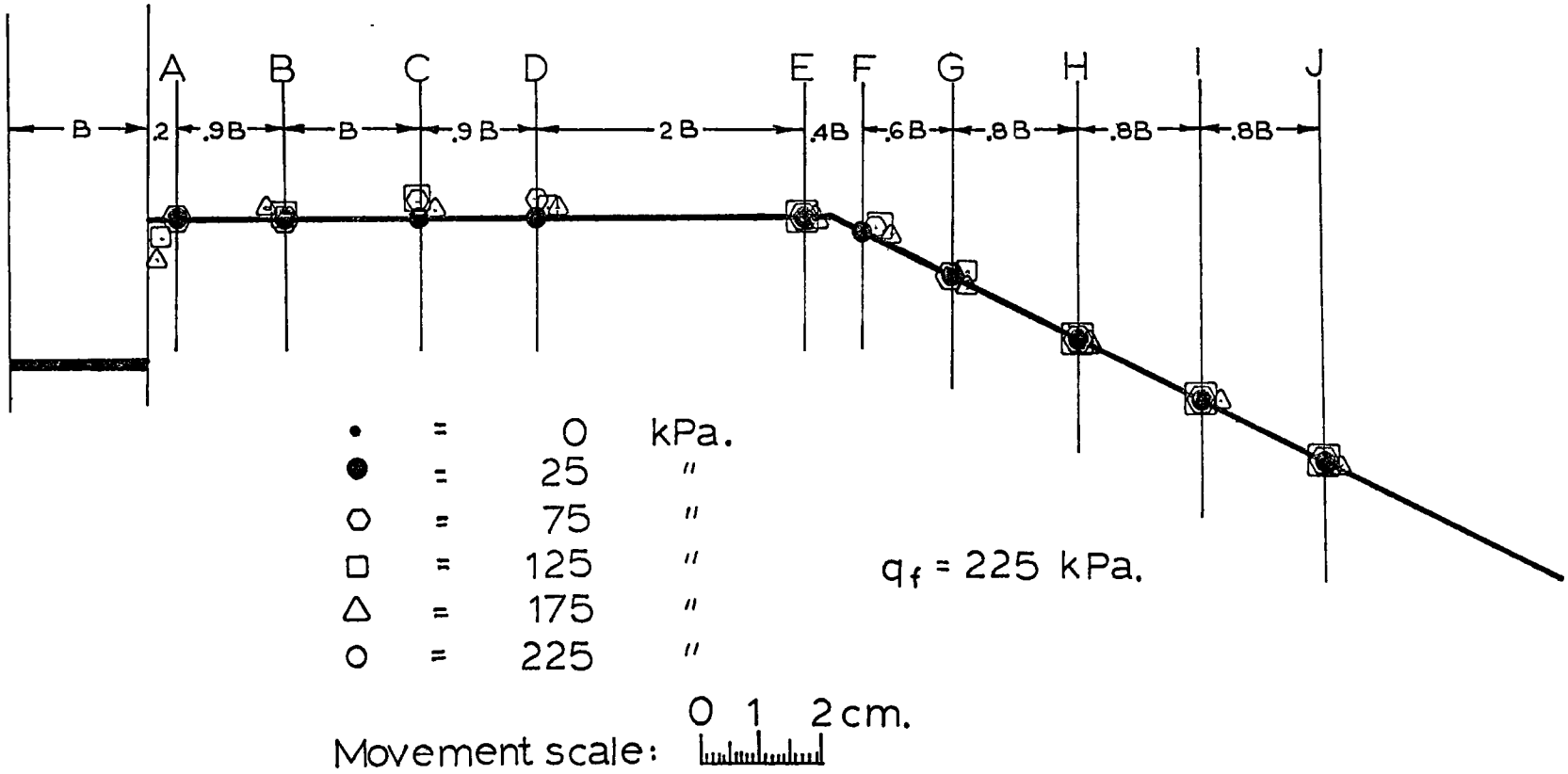

Figure 6.54

SURFACE MOVEMENTS (cm)

TEST: 5 - 1 - C

Positions		A	B	C	D	E	F	G	H	I	J
Horizontal distance from footing (B = footing width)		.2B	1.1B	2.1B	3B	5B	5.4B	6B	6.8B	7.6B	8.4B
Pressure (kPa)											
0	H	0	0	0	0	0	0	0	0	0	0
	V	0	0	0	0	0	0	0	0	0	0
25	H	0	0	0	0	0	0	0	0	0	0
	V	0	0	0	0	0	0	0	0	0	0
50	H	0	0	0	0	0	0	0	0	0	0
	V	0	0	0.1	0	0	0.1	0	0	0	0
75	H	0	0	0	0	0	0.2	0	0	0	0
	V	0	0	0.2	0.2	0	0.1	0	0	0	0
100	H	-0.2	0	0	0	0	0.2	0.2	0	0	0
	V	-0.1	0	0.2	0.3	0.1	0.1	0	0	0	0
125	H	-0.2	0	0	0.1	0	0.2	0.2	0	0	0
	V	-0.2	0.1	0.1	0.1	0	0.1	0.1	0	0	0
150	H	-0.3	-0.2	0.1	0.2	0.2	0.3	0.2	0.2	0.2	0
	V	-0.4	0.1	0.2	0.2	0	0.1	0	0.1	0	0
175	H	-0.3	-0.2	0.2	0.3	0.2	0.5	0.3	0.2	0.3	0.2
	V	-0.6	0.1	0.1	0.1	0	0.1	0	0	0.1	0
200	H	-0.3	0	0.3	0.3	0.3	0.5	0.3	0.3	0.3	0.2
	V	-0.6	0.1	0.2	0.3	0.1	0.1	0	0.1	0.1	0
225	H	-0.3	0	0.6	0.5	0.3	0.6	0.6	0.3	0.3	0.2
	V	1.0	0	0.6	0.4	0.1	0	0	0	0.1	0

Figure 6.55

Test: 5 - 2 - C

PRESSURE - SETTLEMENT

TEST: 5 - 2 - C

γ = 1520 kg/m^3

B = .3 m.

Pressure q kPa	Settlement cm.	$\frac{2q}{\gamma B}$	Relative settlement $(\frac{W}{B} \times 100)$
0	0	0	0
63	0.1	27	0.3
125	0.3	53	1.0
188	0.5	80	1.7
250	0.8	106	2.7
313	1.2	133	4.0
375	2.0	160	6.7
438	2.8	186	9.3
500	4.4	212	14.7
525	6.7	223	22.3
550	7.2	234	24.0
575	8.8	244	29.3
600	9.3	256	31.0
650	11.3	276	37.7
675	13.3	287	44.3
700	14.8	297	49.3
725	16.0	309	53.3

Figure 6.56

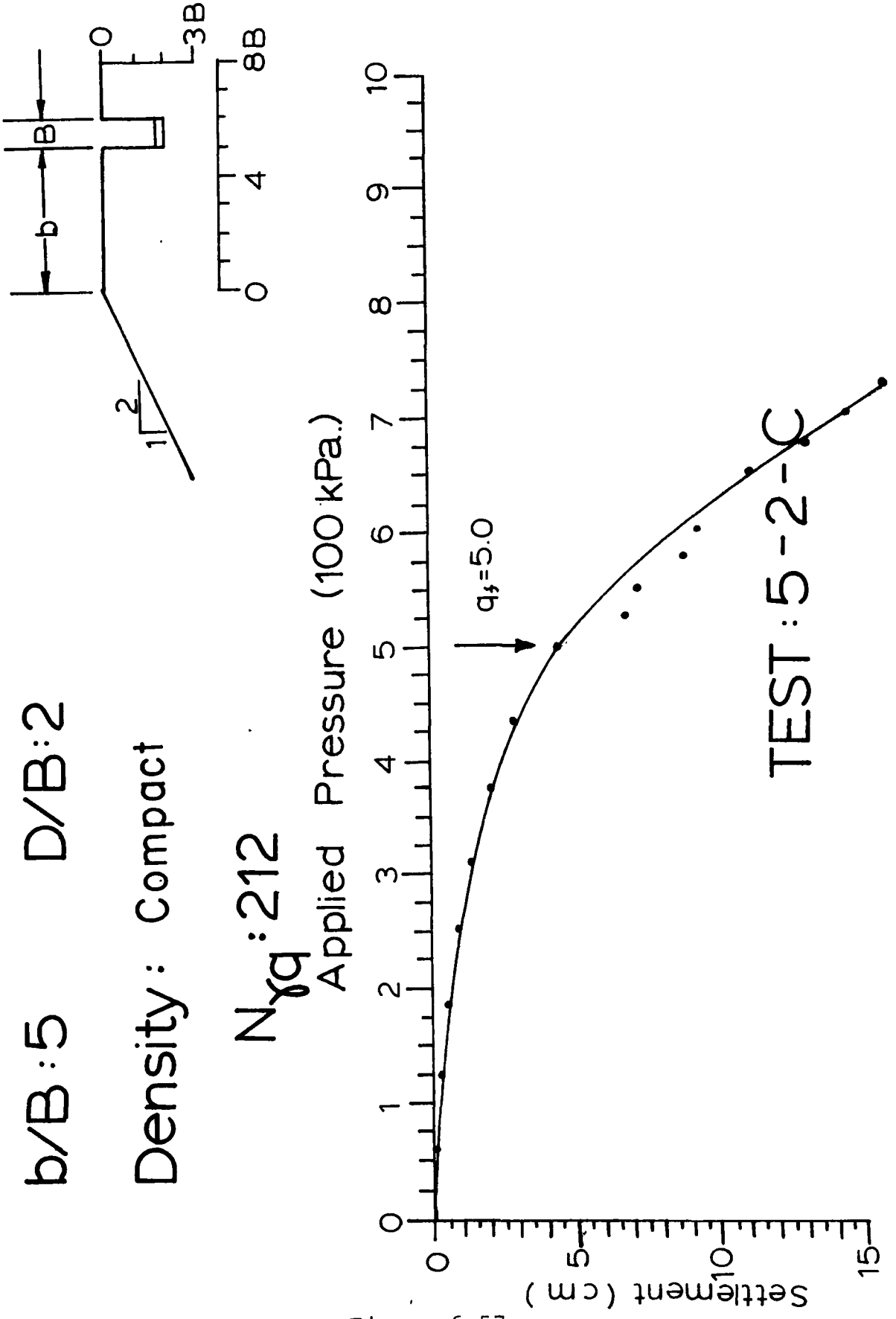
b/B:5
D/B:2
Density: Compact
$N_{\gamma q}$:212
Applied Pressure (100 kPa.)
Settlement (cm)
TEST: 5-2-C
q_f=5.0
B
b
2
1
0
3B
8B
0
4

Figure 6.57

DENSITY MEASUREMENTS (kg/m^3)

TEST: 5 - 2 - C

Location of measurement under footing	Measurements	Average	Standard deviation
B*	1520		
	1500		
	1520		
	1520		
2B*	1520		
	1500		
	1520		
	1520		
3B*	1530		
	1520		
	1540		
	1540		
		1520	12

*B = footing width

Figure 6.58

Surface Movements

Test: 5-2-C

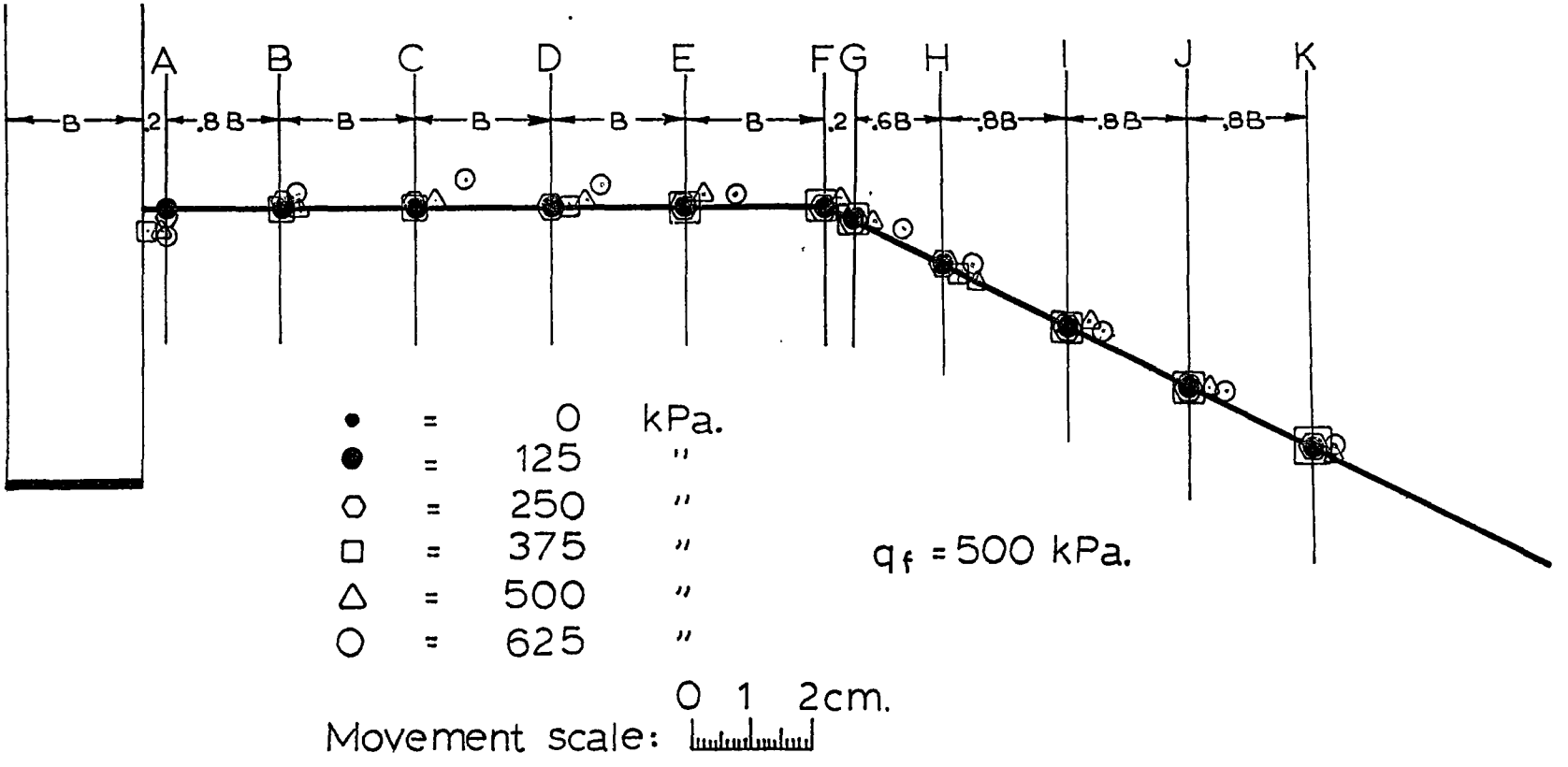

Figure 6.59

SURFACE MOVEMENTS (cm)

TEST: 5 - 2 - C

Positions		A	B	C	D	E	F	G	H	I	J	K
Horizontal distance from footing (B = footing width)		.2B	B	2B	3B	4B	5B	5.2B	5.8B	6.6B	7.4B	8.2B
Pressure (kPa)												
0	H	0	0	0	0	0	0	0	0	0	0	0
	V	0	0	0	0	0	0	0	0	0	0	0
125	H	0	0	0	0	0	0	0	0	0	0	0
	V	0	0	0	0	0	0	0	0	0	0	0
250	H	0	0	0	0	0	0	0	0	0	0	0
	V	-0.1	0.1	0.1	0	0	0	0	0	0	0	0
375	H	-0.3	0	0	0.3	0	0	0	0.3	0	0	0
	V	-0.2	0	0	0	0	0	0	0	0	0	0
500	H	-0.2	0.3	0.3	0.6	0.3	0.3	0.3	0.6	0.3	0.3	0.3
	V	-0.1	0	0.1	0.1	0.1	0.1	0.1	0	0.2	0.1	0
525	H	-0.2	0.3	0.6	0.6	0.6	0.8	0.6	0.2	0.6	0.6	0.3
	V	-0.2	0.1	0.3	0.1	0.1	0	0.2	0.2	0.2	0.1	0
550	H	-0.2	0.3	0.6	0.6	0.6	0.8	0.6	0.2	0.6	0.6	0.3
	V	-0.2	0.1	0.3	0.2	0.1	0	0.2	0.2	0.2	0.1	0
575	H	0	0.3	0.8	0.8	0.8	0.8	0.8	0.2	0.6	0.6	0.3
	V	-0.1	0.2	0.4	0.3	0.2	0	0.2	0.1	0.3	0.2	0
600	H	0	0.3	0.8	0.8	0.8	0.8	0.8	0.4	0.6	0.6	0.3
	V	-0.2	0.2	0.4	0.3	0.2	0	0.2	0.1	0.2	0.2	0.1
625	H	0	0.3	0.8	0.8	0.8	0.8	0.8	0.4	0.6	0.6	0.3
	V	-0.3	0.2	0.4	0.4	0.2	0.1	0.2	0.1	0.2	0.2	0.1
650	H	0	0.3	0.8	0.8	0.8	0.8	0.8	0.4	0.6	0.6	0.3
	V	-0.3	0.2	0.4	0.7	0.2	0.1	0.2	0.1	0.2	0.2	0.1
675	H	0.3	0.3	0.8	0.8	1.0	1.0	1.0	0.6	1.0	1.0	0.5
	V	-0.4	0.2	0.4	0.7	0.4	0.2	0.4	0.3	0.4	0.3	0.2

Figure 6.60

Test: 5 - 3 - C

PRESSURE - SETTLEMENT

TEST: 5 - 3 - C

γ = 1530 kg/m^3

B = .3 m.

Pressure q kPa	Settlement cm.	$\frac{2q}{\gamma B}$	Relative settlement $(\frac{W}{B} \times 100)$
0	0	0	0
63	0.3	27	1.0
125	0.6	53	2.0
188	1.1	80	3.7
250	1.6	105	5.3
313	2.1	132	7.0
375	2.5	159	8.3
400	2.6	169	8.7
425	2.9	180	9.7
450	3.1	190	10.3
475	3.3	200	11.0
500	3.7	212	12.3
525	4.1	222	13.7
550	4.5	233	15.0
575	5.1	243	17.0
600	5.6	254	18.7
625	7.0	264	23.3
650	7.1	275	23.7
675	7.2	285	24.0
700	7.3	296	24.3

Figure 6.61

PRESSURE - SETTLEMENT

TEST: 5 - 3 - C

γ = 1530 kg/m^3

B = .3 m.

Pressure q kPa	Settlement cm.	$\frac{2q}{\gamma B}$	Relative settlement $(\frac{W}{B} \times 100)$
725	7.4	307	24.7
750	7.6	317	25.0
775	7.6	328	25.3
800	7.7	338	25.7
825	7.8	349	26.0
850	7.9	359	26.3
875	8.0	370	26.7
900	8.3	381	27.7
925	8.5	391	28.3
950	8.8	402	29.3
975	9.0	412	30.0
1000	9.5	423	31.7

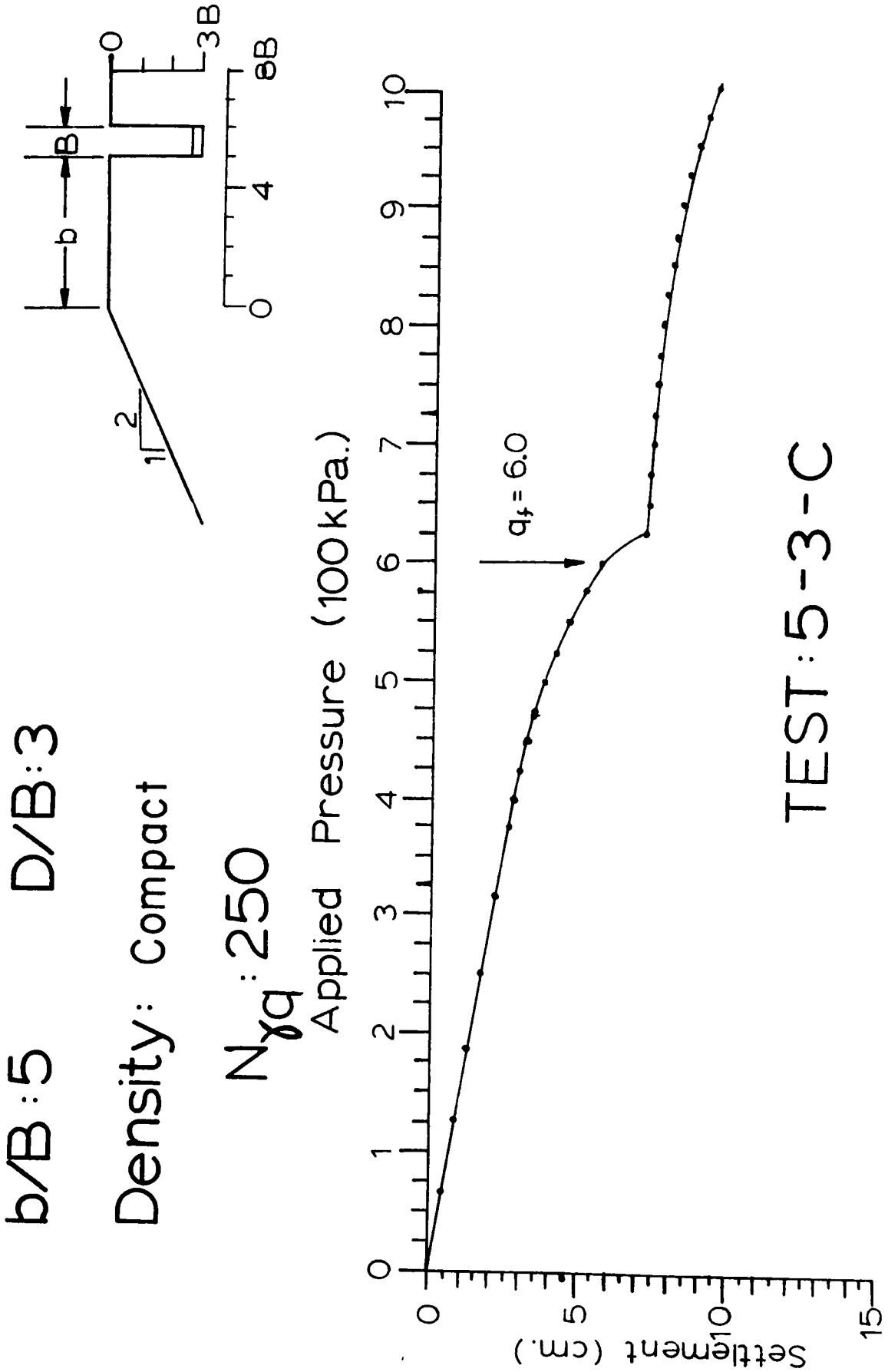
b/B:5
D/B:3
Density: Compact
$N_{\gamma q}$:250
Applied Pressure (100 kPa.)
Settlement (cm.)
q_f= 6.0
TEST:5-3-C
b
B
2
1
0
3B
8B
4

Figure 6.62

DENSITY MEASUREMENTS (kg/m^3)

TEST: 5 - 3 - C

Location of measurement under footing	Measurements	Average	Standard deviation
B*	1510		
	1510		
	1500		
	1510		
2B*	1540		
	1550		
	1550		
	1550		
		1530	20

* B = footing width

Figure 6.63

Surface Movements
Test: 5-3-C

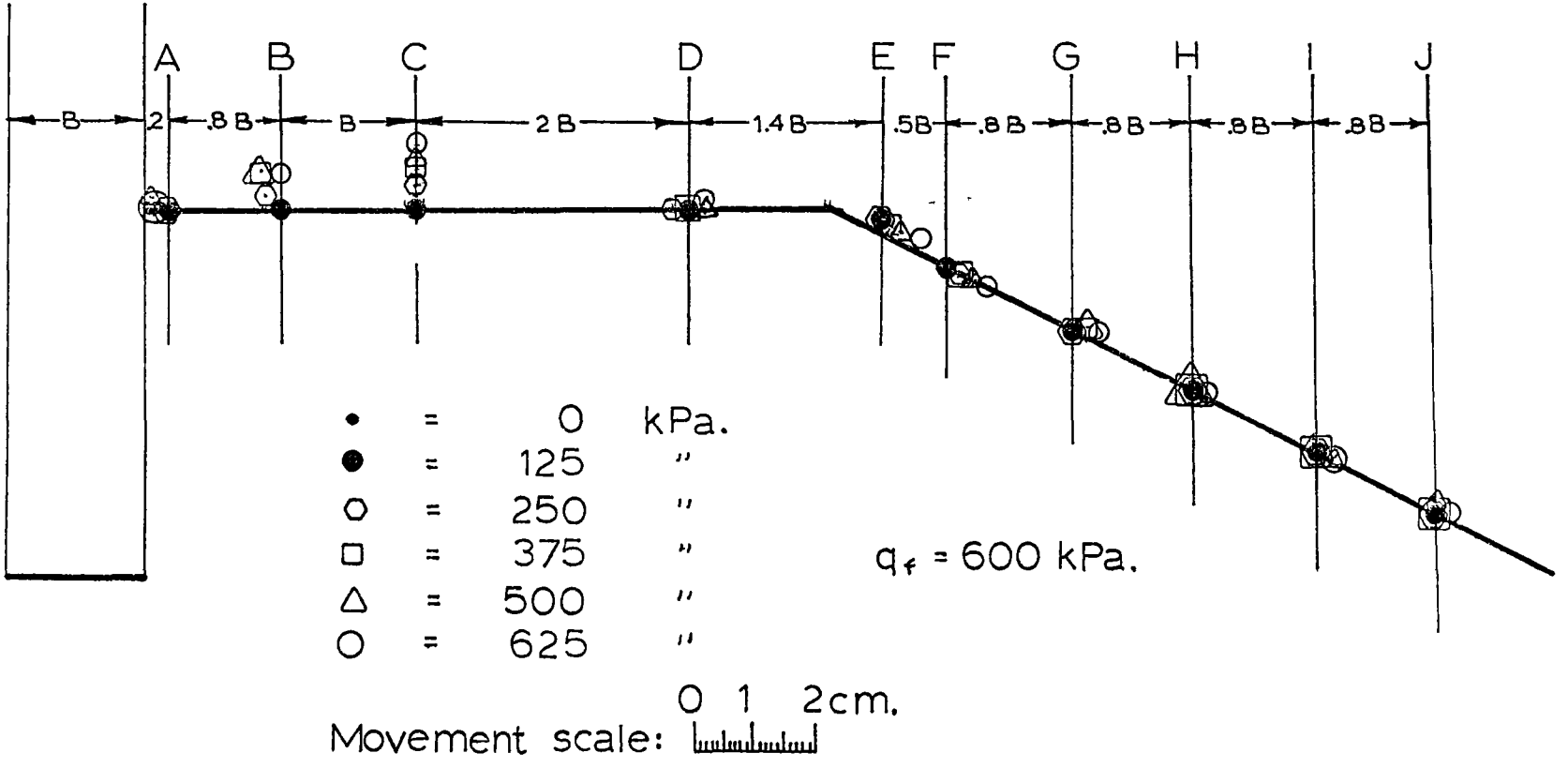

Figure 6.64

SURFACE MOVEMENTS (cm)

TEST: 5 - 3 - C

Positions		A	B	C	D	E	F	G	H	I	J
Horizontal distance from footing (B = footing width)		.2B	B	2B	4B	5.4B	5.9B	6.7B	7.5B	8.3B	9.1B
Pressure (kPa)											
0	H	0	0	0	0	0	0	0	0	0	0
	V	0	0	0	0	0	0	0	0	0	0
125	H	0	0	0	0	0	0	0	0	0	0
	V	0	0	0	0	0.2	0	0	0	0	0
250	H	0	-0.2	0	-0.2	0	0.2	0	0	0	0
	V	0	0.2	0.4	0	0.2	0	0	0	0	0
375	H	-0.2	-0.3	0	0.2	0.3	0.3	0.2	0	0.2	0
	V	0.1	0.6	0.8	0	0.1	0	0.1	0	0	0.1
500	H	-0.2	-0.3	0	0.2	0.3	0.3	0.2	0	0.2	0
	V	0.1	0.6	0.8	0	0.1	0	0.1	0	0	0.1
625	H	-0.2	0	0	0.2	0.5	0.5	0.3	0.2	0.2	0.2
	V	0	0.6	1.1	0.1	0.1	0	0.1	0.1	0	0.1
750	H	0	0	0.2	0.3	0.6	0.6	0.5	0.3	0.2	0.2
	V	-0.1	0.6	1.0	0	0.1	0.1	0.1	0	0	0.2
875	H	0	0	0.3	0.5	0.6	0.6	0.5	0.3	0.3	0.2
	V	-0.1	0.7	1.1	0	0	0	0.1	0.1	0	0
1000	H	0	0	0.3	0.3	0.6	0.6	0.5	0.3	0.3	0.2
	V	-0.1	0.8	1.2	0	0	0.1	0.1	0.1	0	0

Figure 6.65

Test: 0 - 0 - D

PRESSURE - SETTLEMENT

TEST: 0 - 0 - D

$\gamma = 1620 \text{ kg/m}^3$

B = .3 m.

Pressure q kPa	Settlement cm.	$\frac{2q}{\gamma B}$	Relative settlement $(\frac{W}{B} \times 100)$
0	0	0	0
25	0.1	10	0.33
50	0.2	20	0.7
75	0.3	30	1.0
100	0.5	40	1.7
125	0.7	49	2.3
150	1.0	60	3.3
175	1.2	70	4.0
200	1.5	80	5.0
225	1.8	89	6.0
250	2.2	99	7.3

Figure 6.66

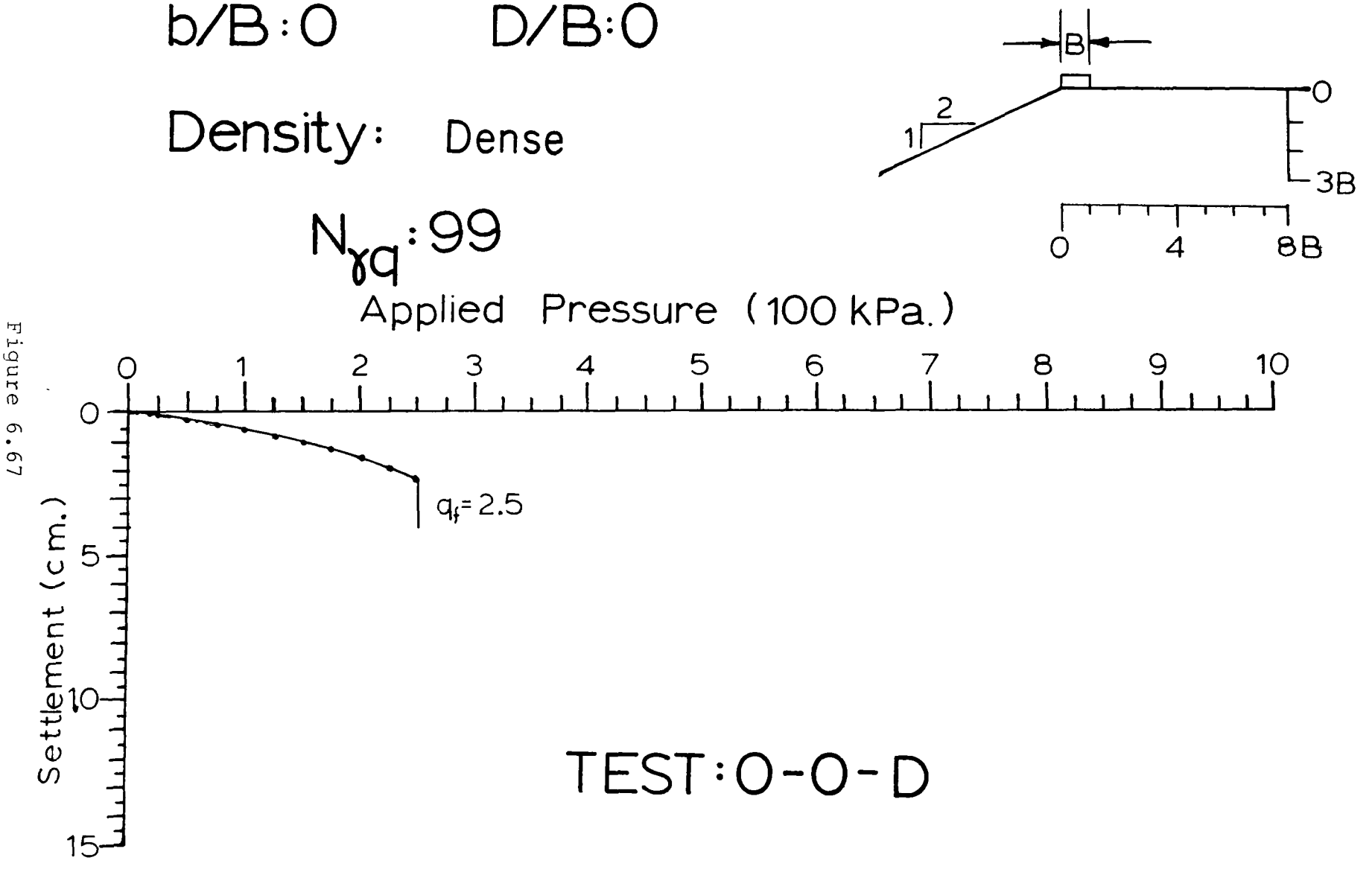
b/B:0
D/B:0
Density: Dense
$N_{\gamma q}$:99
B
2
1
0
3B
0
4
8B
Applied Pressure (100 kPa.)
0
1
2
3
4
5
6
7
8
9
10
Settlement (cm.)
0
5
10
15
q_f= 2.5
TEST:O-O-D

Figure 6.67

DENSITY MEASUREMENTS (kg/m^3)

TEST: 0 - 0 - D

Location of measurement under footing	Measurements	Average	Standard deviation
B*	1620		
	1620		
	1610		
	1610		
2B*	1620		
	1620		
	1620		
	1630		
3B*	1640		
	1610		
	1630		
	1630		
		1620	10

* B = footing width

Figure 6.68

Test: 0 - 1 - D

PRESSURE - SETTLEMENT

TEST: 0 - 1 - D

$\gamma = 1590 \text{ kg/m}^3$

B = .3 m.

Pressure q kPa	Settlement cm.	$\frac{2q}{\gamma B}$	Relative settlement $(\frac{W}{B} \times 100)$
0	0	0	0
63	0.3	26	1.0
125	0.6	50	2.0
188	1.0	76	3.3
250	1.1	102	3.7
300	1.7	122	5.7
325	1.9	132	6.3
350	2.1	143	7.0
363	2.2	146	7.3
363	4.2	146	14.0

Figure 6.69

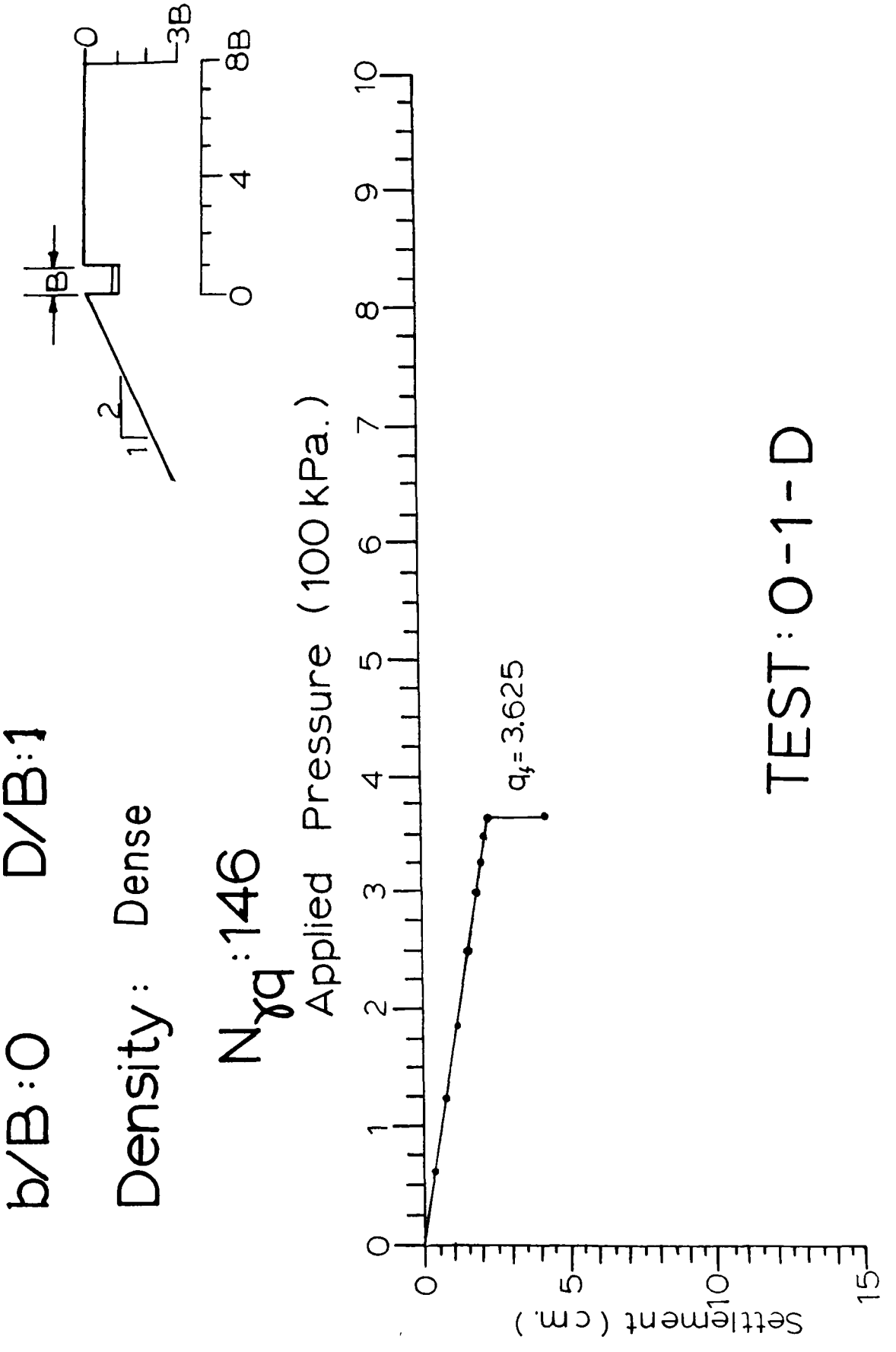
b/B:0
D/B:1
Density: Dense
$N_{\gamma q}$:146
TEST:O-1-D
Applied Pressure (100 kPa.)
Settlement (cm.)
q_f= 3.625
0
3B
8B
B
2
1

Figure 6.70

DENSITY MEASUREMENTS (kg/m^3)

TEST: 0 - 1 - D

Location of measurement under footing	Measurements	Average	Standard deviation
0B*	1570		
	1600		
	1600		
	1600		
	1600		
B*	1570		
	1590		
	1570		
	1580		
	1590		
2B*	1590		
	1590		
	1590		
	1590		
3B*	1590		
	1600		

Figure 6.71

DENSITY MEASUREMENTS (kg/m^3)

TEST: 0 - 1 - D(cont'd)

Location of measurement under footing	Measurements	Average	Standard deviation
3B*	1590		
	1590		
4B*	1570		
	1590		
	1610		
	1590		
	1610		
	1610		
		1590	12

* B = footing width

Surface Movements
Test:O-1-D

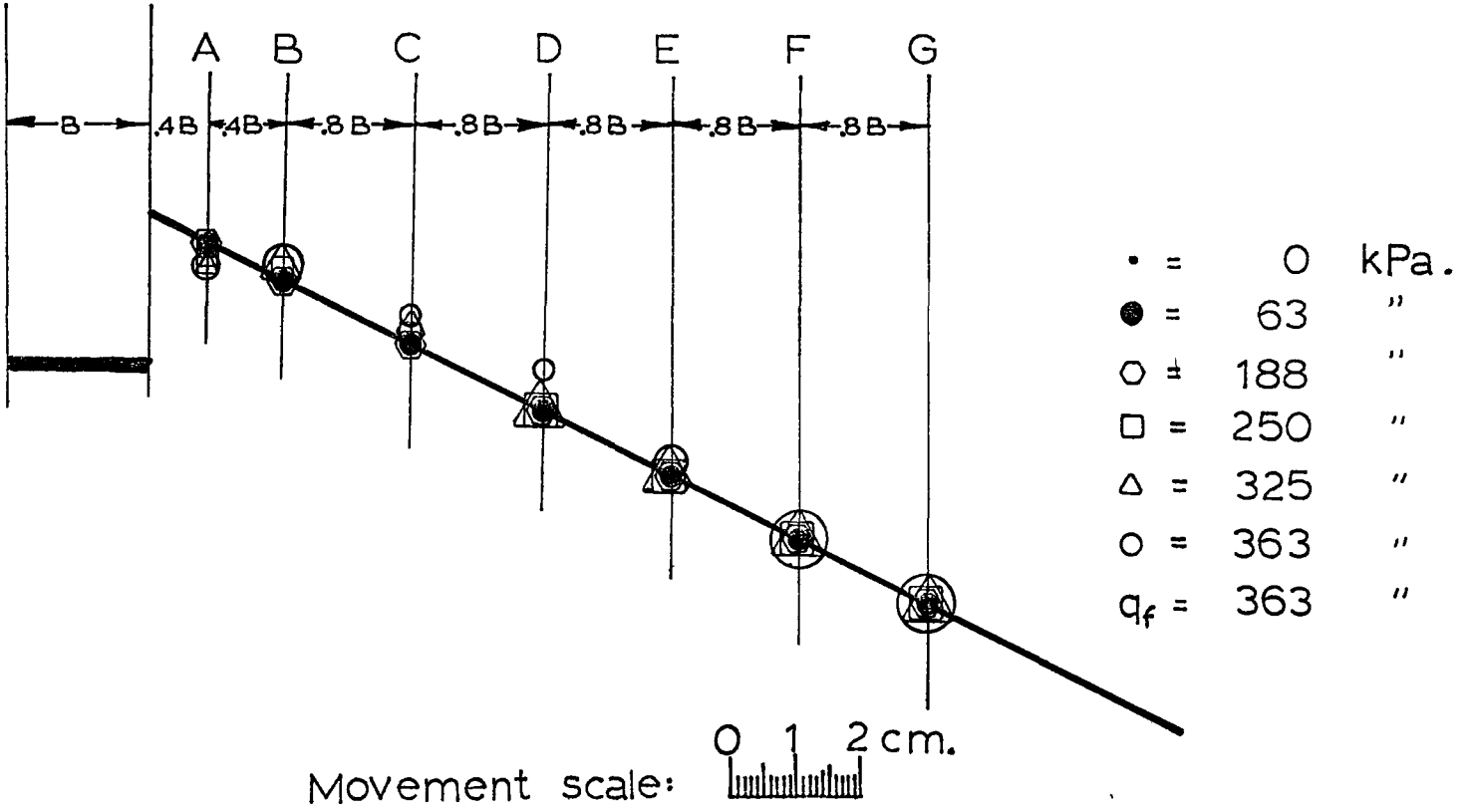

Figure 6.72

SURFACE MOVEMENTS (cm)

TEST: 0 - 1 - D

Positions		A	B	C	D	E	F	G
Horizontal distance from footing (B = footing width)		.4B	.8B	1.6B	2.4B	3.2B	4B	4.8B
Pressure (kPa)								
0	V	0	0	0	0	0	0	0
63	V	0	0	0	0	0	0	0
188	V	0	0	0	0	0	0	0
250	V	-0.2	0.1	0.1	0	0	0	0
300	V	-0.2	0.1	0.1	0	0	0	0
325	V	-0.4	0.1	0.2	0.4	0	0	0
350	V	-0.4	0.1	0.2	0.4	0	0	0
363	V	-0.4	0.1	0.5	1.0	0.2	0	0

Figure 6.73

Test: 0 - 2 - D

PRESSURE - SETTLEMENT

TEST: 0 - 2 - D

γ = 1620 kg/m^3

B = .3 m.

Pressure q kPa	Settlement cm.	$\frac{2q}{\gamma B}$	Relative settlement $(\frac{W}{B} \times 100)$
0	0	0	0
63	0.2	25	0.7
125	0.4	49	1.3
188	0.7	75	2.3
250	1.0	100	3.3
313	1.4	124	4.7
375	1.8	149	6.0
438	2.2	175	7.3
500	2.5	200	8.3
525	2.8	208	9.3

Figure 6.74

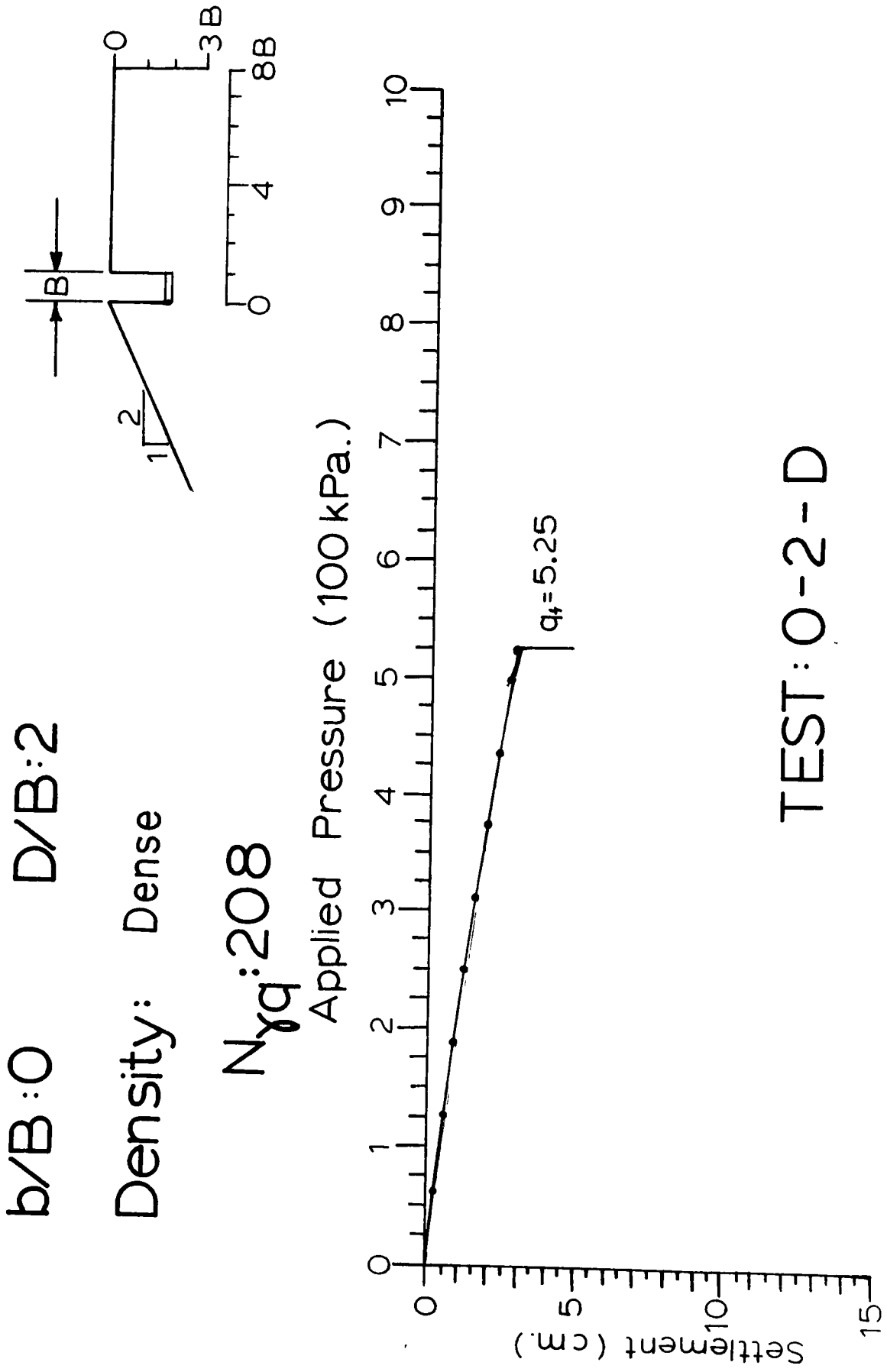
b/B:0
D/B:2
Density: Dense
$N_{\gamma q}$:208
TEST: O-2-D
Applied Pressure (100 kPa.)
Settlement (cm.)
q_f=5.25
B
2
1
0
3B
8B
4

Figure 6.75

DENSITY MEASUREMENTS (kg/m^3)

TEST: 0 - 2 - D

Location of measurement under footing	Measurements	Average	Standard deviation
0B*	1610		
	1590		
	1610		
	1620		
1B*	1640		
	1620		
	1640		
	1640		
2B*	1620		
	1610		
	1630		
	1630		
3B*	1630		
	1610		
	1630		
	1630		
		1620	14

* B = footing width

Figure 6.76

Surface Movements
Test: O-2-D

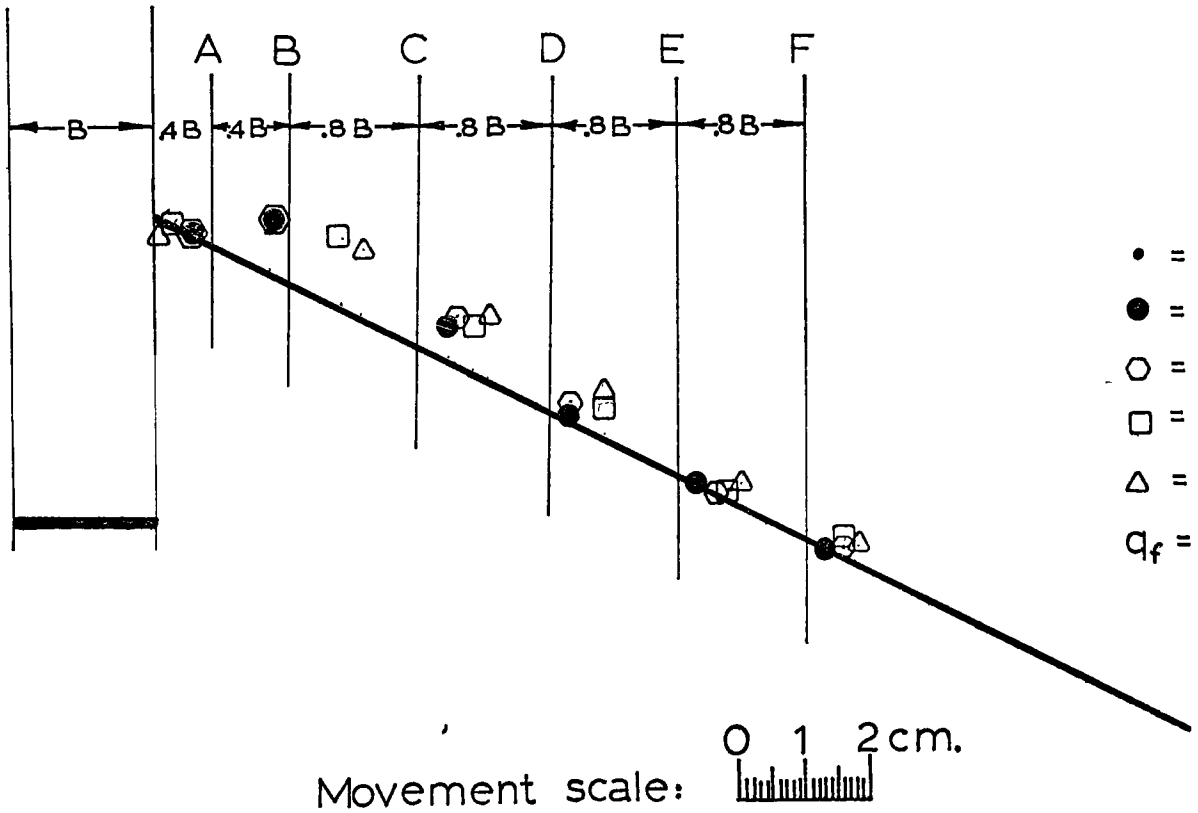

• = 0 kPa.
● = 338 "
○ = 375 "
□ = 500 "
△ = 525 "
q_f = 525 "

Movement scale: 0 1 2 cm.

Figure 6.77

SURFACE MOVEMENTS (cm)

TEST: 0 - 2 - D

Positions		A	B	C	D	E	F
Horizontal distance from footing (B = footing width)		.4B	.8B	1.6B	2.4B	3.2B	4B
Pressure (kPa)							
0	H	0	0	0	0	0	0
	V	0	0	0	0	0	0
338	H	-0.3	-0.3	0.5	0.3	0.3	0.3
	V	0	0.8	0.5	0.1	0	0
375	H	-0.3	-0.3	0.6	0.3	0.6	0.6
	V	0	0.8	0.7	0.3	0	0.1
500	H	-0.6	0.9	0.9	0.9	0.8	0.6
	V	0	1.0	0.7	0.5	0.1	0.2
525	H	-0.9	1.2	1.2	0.9	1.0	0.8
	V	-0.2	1.0	1.0	0.7	0.3	0.2

Figure 6.78

Test: 0 - 3 - D

PRESSURE - SETTLEMENT

TEST: 0 - 3 - D

$\gamma = 1620\ kg/m^3$

B = .3 m.

Pressure q $\overline{kPa}$	Settlement cm.	$\frac{2q}{\gamma B}$	Relative settlement $(\frac{W}{B} \times 100)$
0	0	0	0
63	0.1	25	0.3
125	0.2	50	0.7
188	0.4	75	1.3
250	0.5	100	1.7
313	0.7	125	2.3
375	0.8	150	2.7
400	0.9	160	3.0
425	1.0	170	3.3
450	1.1	180	3.7
475	1.1	190	3.7
500	1.2	200	4.0
525	1.2	210	4.0
550	1.3	219	4.3
575	1.3	230	4.3
600	1.4	239	4.7
625	1.4	250	4.7
650	1.5	259	5.0
675	1.6	270	5.3
700	1.7	279	5.7
725	1.8	288	6.0

Figure 6.79

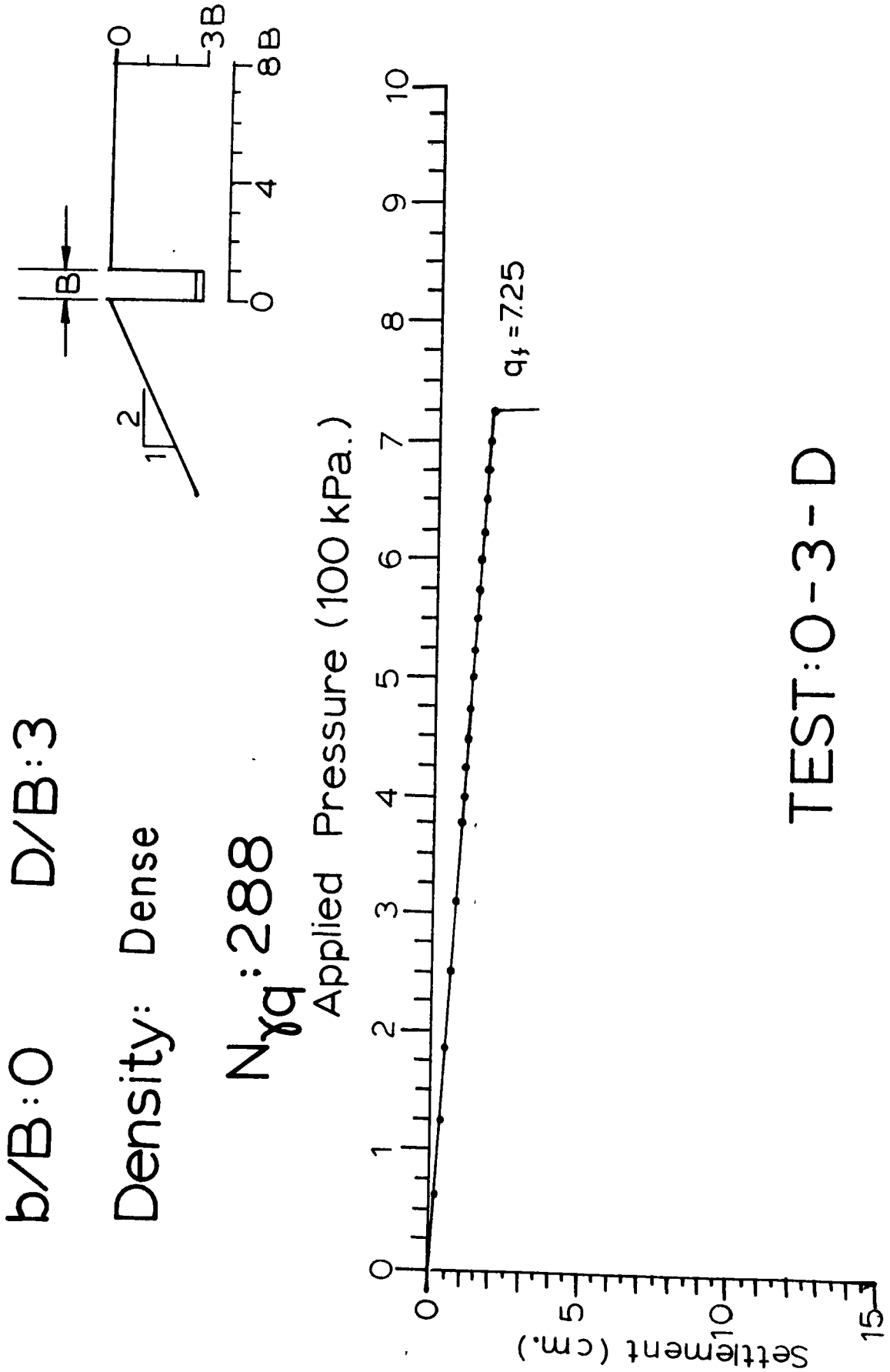
b/B:0
D/B:3
Density: Dense
$N_{\gamma q}$:288
TEST:O-3-D
Applied Pressure (100 kPa.)
Settlement (cm.)
q_f=7.25
B
2
1
0
3B
8B
0
4
0
1
2
3
4
5
6
7
8
9
10
0
5
10
15

Figure 6.80

DENSITY MEASUREMENTS (kg/m^3)

TEST: 0 - 3 - D

Location of measurement under footing	Measurements	Average	Standard deviation
-2B*	1630		
	1610		
	1620		
	1620		
-1B*	1620		
	1600		
	1620		
	1620		
0B*	1600		
	1580		
	1600		
	1610		
1B*	1620		
	1610		
	1630		
	1630		
2B*	1630		
	1610		
	1620		
	1630		
		1620	13

* B = footing width

Figure 6.81

Surface Movements
Test: O-3-D

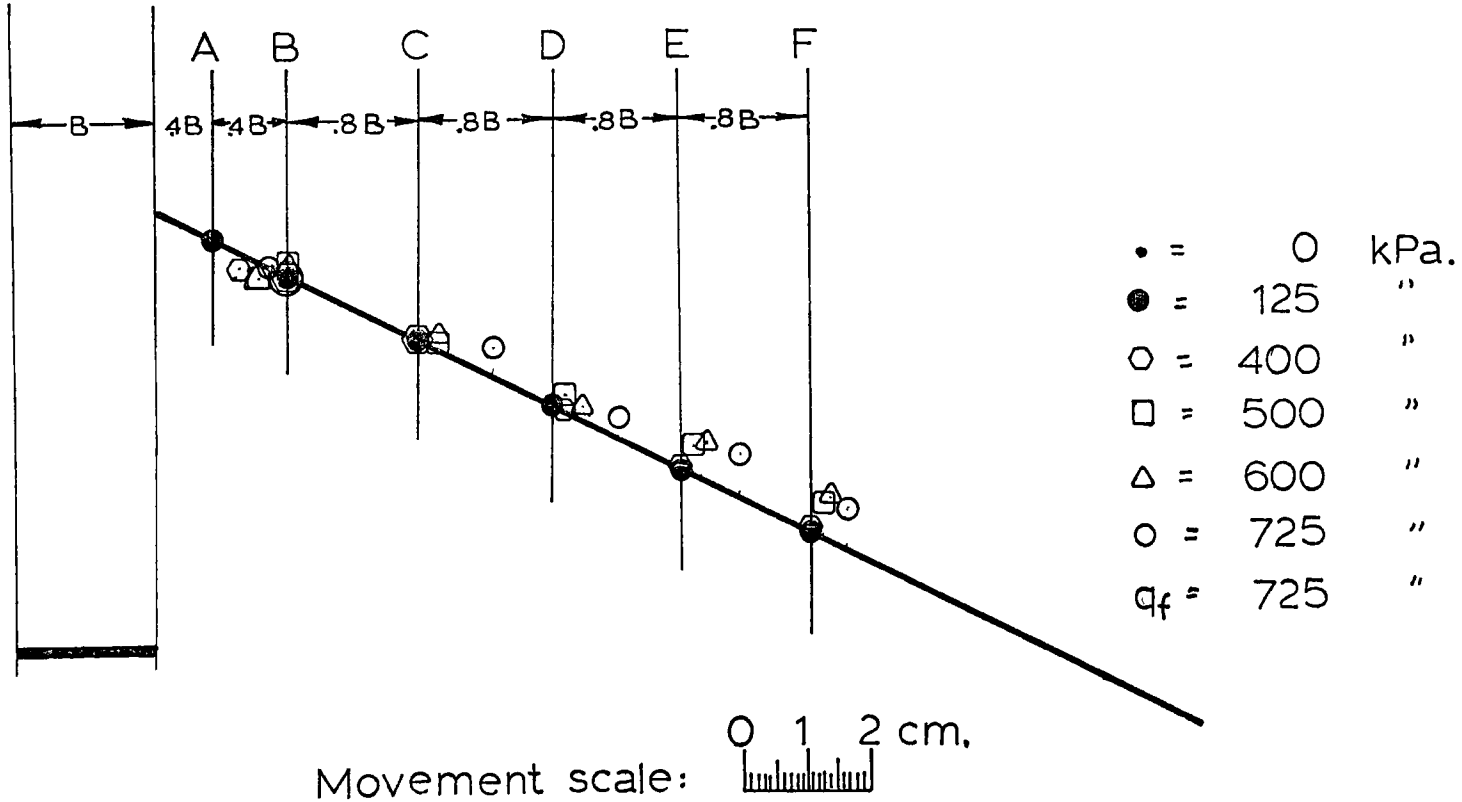

Figure 6.82

SURFACE MOVEMENTS (cm)

TEST: 0 - 3 - D

Positions		A	B	C	D	E	F
Horizontal distance from footing (B = footing width)		.4B	.8B	1.6B	2.4B	3.2B	4B
Pressure (kPa)							
0	H	0	0	0	0	0	0
	V	0	0	0	0	0	0
125	H	0	0	0	0	0	0
	V	0	0	0	0	0	0
250	H	0.2	-0.2	0	0	0	0
	V	-0.2	0	0	0	0	0
375	H	0.2	-0.3	0	0	0	0
	V	-0.2	0.1	0	0	0	0.1
400	H	0.5	0	0	0.2	0	0
	V	-0.2	0	0	0	0.1	0.1
425	H	0.4	-0.3	0	0.2	0	0
	V	-0.2	0	0	0.1	0.1	0.1
450	H	0.8	-0.3	0.3	0.2	0	0
	V	-0.2	0.1	0.1	0	0.2	0.4
475	H	0.8	0	0.3	0.2	0	0.2
	V	-0.2	0.1	0.2	0.1	0.4	0.5
500	H	0.8	0	0.3	0.2	0.3	0.3
	V	-0.2	0.2	0.1	0.2	0.4	0.5
525	H	0.8	0	0.3	0.2	0.3	0.3
	V	-0.2	0.1	0.2	0.2	0.4	0.5
550	H	0.8	0	0.3	0.3	0.3	0.3
	V	-0.2	0.1	0.3	0.2	0.5	0.6
575	H	0.8	0	0.3	0.2	0.3	0.3
	V	-0.3	0.1	0.2	0.2	0.5	0.6
600	H	0.8	0	0.3	0.5	0.3	0.3
	V	-0.2	0.1	0.2	0.2	0.5	0.6

Figure 6.83

SURFACE MOVEMENTS (cm)

TEST: 0 - 3 - D(cont'd)

Positions		A	B	C	D	E	F
Horizontal distance from footing (B = footing width)		.4B	.8B	1.6B	2.4B	3.2B	4B
Pressure (kPa)							
625	H	0.8	0	0.3	0.5	0.3	0.3
	V	-0.2	0.1	0.2	0.2	0.5	0.6
700	H	0.8	0.3	0.6	1.1	0.5	0.3
	V	-0.1	0.1	0.2	0.3	0.6	0.7
725	H	1.0	0	1.2	1.1	1.0	0.6
	V	0	0	0.4	0.3	0.6	0.6

Test: 2.5 - 0 - D

PRESSURE - SETTLEMENT

TEST: 2.5 - 0 - D

γ = 1610 kg/m^3

B = .3 m.

Pressure q kPa	Settlement cm.	$\frac{2q}{\gamma B}$	Relative settlement $\frac{W}{B}$ x 100)
0	0	0	0
25	0.1	11	0.3
50	0.1	20	0.3
75	0.2	30	0.7
100	0.3	40	1.0
125	0.4	50	1.3
150	0.5	60	1.7
188	0.6	75	2.0
250	1.0	100	3.3
300	1.2	121	4.0
325	1.3	130	4.3
350	1.4	141	4.7
375	1.6	150	5.3
400	1.8	159	6.0

Figure 6.84

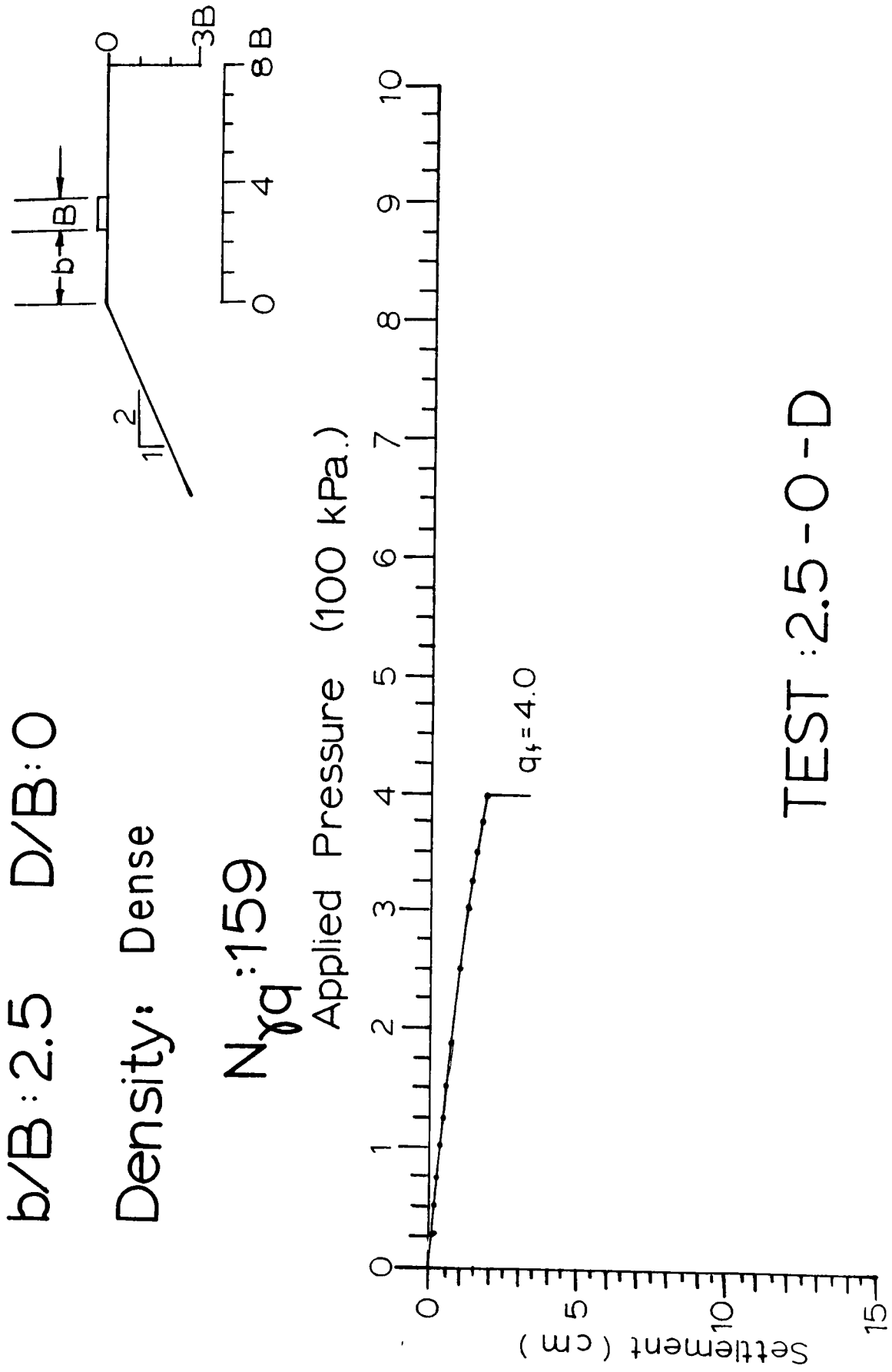
b/B : 2.5 D/B : 0
Density: Dense
$N_{\gamma q}$:159
TEST :2.5-0-D
q_f = 4.0
Applied Pressure (100 kPa.)
Settlement (cm)
0
1
2
3
4
5
6
7
8
9
10
0
5
10
15
b
B
2
1
0
3B
8B
0
4

Figure 6.85

DENSITY MEASUREMENTS (kg/m^3)

TEST: 2.5 - 0 - D

Location of measurement under footing	Measurements	Average	Standard deviation
1B*	1600		
	1590		
	1610		
	1620		
	1600		
2B*	1630		
	1630		
	1620		
	1620		
	1620		
3B*	1610		
	1600		
	1600		
	1600		
	1610		
4B*	1620		

Figure 6.86

DENSITY MEASUREMENTS (kg/m^3)

TEST: 2.5 - 0 - D(cont'd)

Location of measurement under footing	Measurements	Average	Standard deviation
4B*	1600		
	1620		
	1620		
	1630		
5B*	1610		
	1610		
	1620		
	1620		
	1610		
	1620		
	1600		
	1610		
	1620		
	1610		
	1610		
	1610		
	1610		
	1620		
	1610		
		1610	11

* B = footing width

Test: 2.5 - 0 - D - R1

PRESSURE - SETTLEMENT

TEST: 2.5 - 0 - D - R.1

γ = 1610 kg/m^3

B = .3 m.

Pressure q $\overline{kPa}$	Settlement cm.	$\frac{2q}{\gamma B}$	Relative settlement $(\frac{W}{B} \times 100)$
0	0	0	0
63	0.3	26	1.0
125	0.6	50	2.0
188	1.1	76	3.7
250	1.4	101	4.7
275	1.6	110	5.3
300	1.7	121	5.7
325	1.9	130	6.3
350	2.0	141	6.7
375	2.1	150	7.0

Figure 6.87

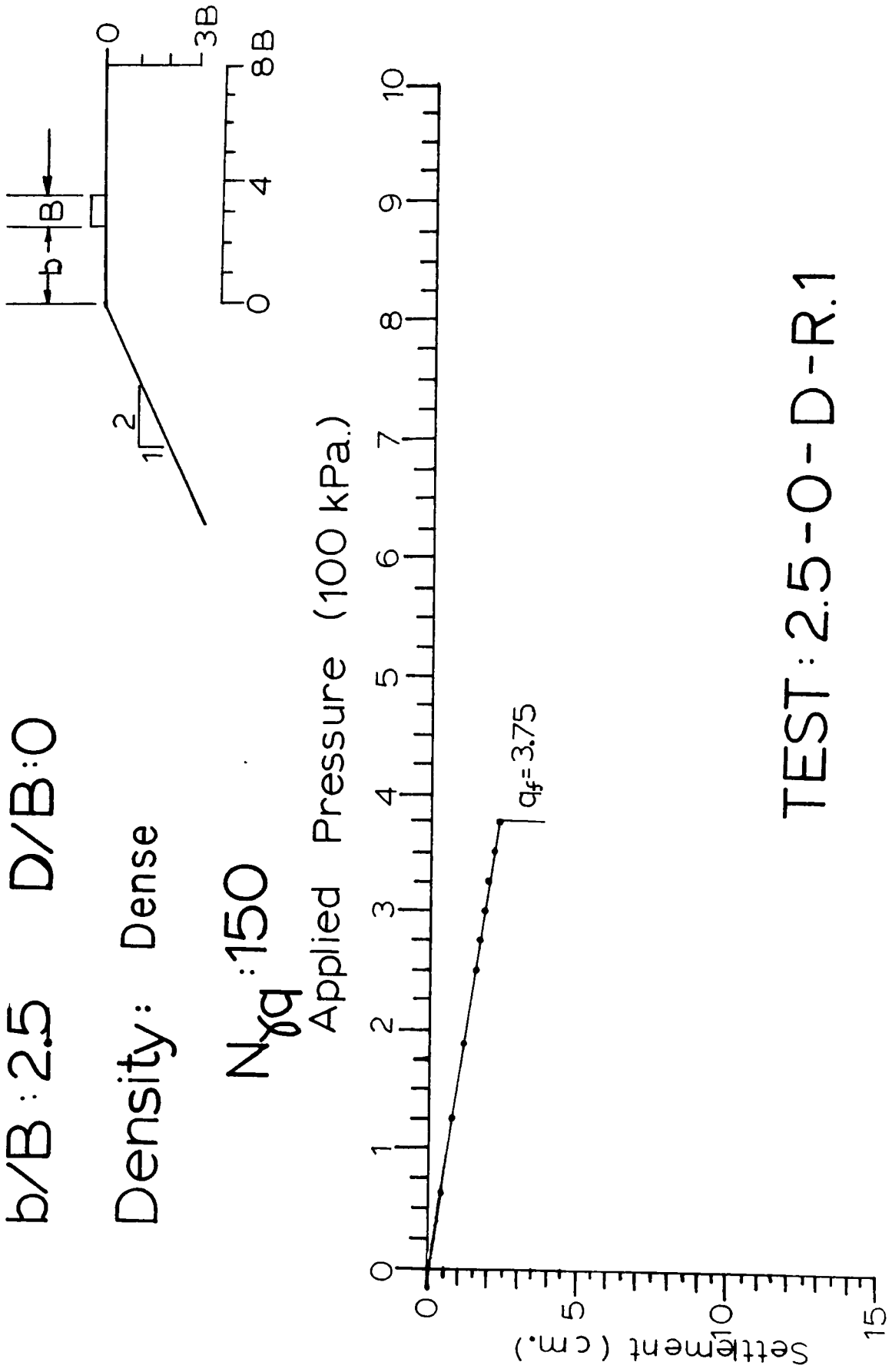
b/B : 2.5 D/B:0
Density: Dense
$N_{\gamma q}$:150
TEST : 2.5-0-D-R.1
Applied Pressure (100 kPa.)
Settlement (cm.)
q_f= 3.75
b
B
0
3B
8B
4
2
1
0
1
2
3
4
5
6
7
8
9
10
0
5
10
15

Figure 6.88

DENSITY MEASUREMENTS (kg/m^3)

TEST: 2.5 - 0 - D - R.1

Location of measurement under footing	Measurements	Average	Standard deviation
0B*	1610		
	1600		
	1610		
	1610		
1B*	1600		
	1590		
	1600		
	1610		
2B*	1610		
	1600		
	1620		
	1610		
3B*	1620		
	1600		
	1620		
	1630		
		1610	11

* B = footing width

Figure 6.89

Surface Movements

Test: 2.5-0-D-R.1

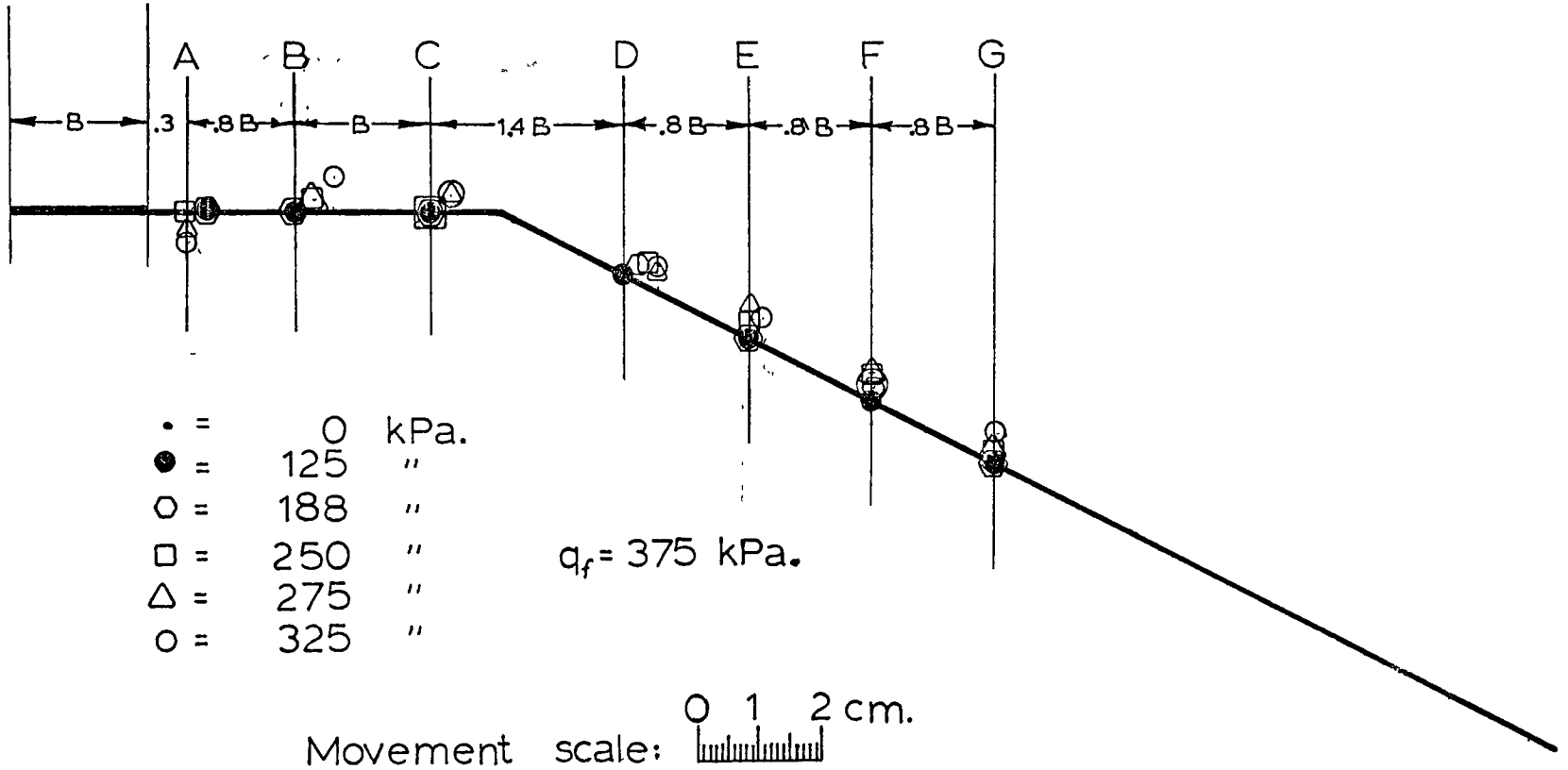

Figure 6.90

SURFACE MOVEMENTS (cm)

TEST: 2.5 - 0 - D - R.1

Positions		A	B	C	D	E	F	G
Horizontal distance from footing (B = footing width)		.3B	B	2B	3.4B	4.2B	5B	5.8B
Pressure (kPa)								
0	H	0	0	0	0	0	0	0
	V	0	0	0	0	0	0	0
125	H	0.3	0	0	0	0	0	0
	V	0	0	0	0	0	0	0
188	H	0.3	0	0	0.2	0	0	0
	V	0	0	0	0.2	0	0.2	0
250	H	0	0.3	0	0.3	0	0	0
	V	0	0.2	0	0.3	0.3	0.4	0.2
275	H	0	0.3	0.3	0.6	0	0	0
	V	-0.1	0.2	0.2	0.3	0.5	0.4	0.2
300	H	0	0.3	0.3	0.6	0.2	0	0
	V	-0.1	0.4	0.3	0.3	0.5	0.3	0.4
325	H	0	0.6	0.3	0.6	0.2	0	0
	V	-0.4	0.5	0.2	0.4	0.5	0.2	0.4

Figure 6.91

Test: 2.5 - 0 - D - R2

PRESSURE - SETTLEMENT

TEST: 2.5 - 0 - D - R.2

γ = 1620 kg/m^3

B = .3 m.

Pressure q kPa	Settlement cm.	$\frac{2q}{\gamma B}$	Relative settlement $(\frac{W}{B} \times 100)$
0	0	0	0
63	0.3	25	1.0
125	0.6	50	2.0
188	0.9	75	3.0
250	1.4	100	4.7
275	1.5	110	5.0
300	1.7	120	5.7
325	1.8	130	6.0
350	1.9	140	6.3
375	2.1	150	7.0
400	2.2	159	7.3

Figure 6.92

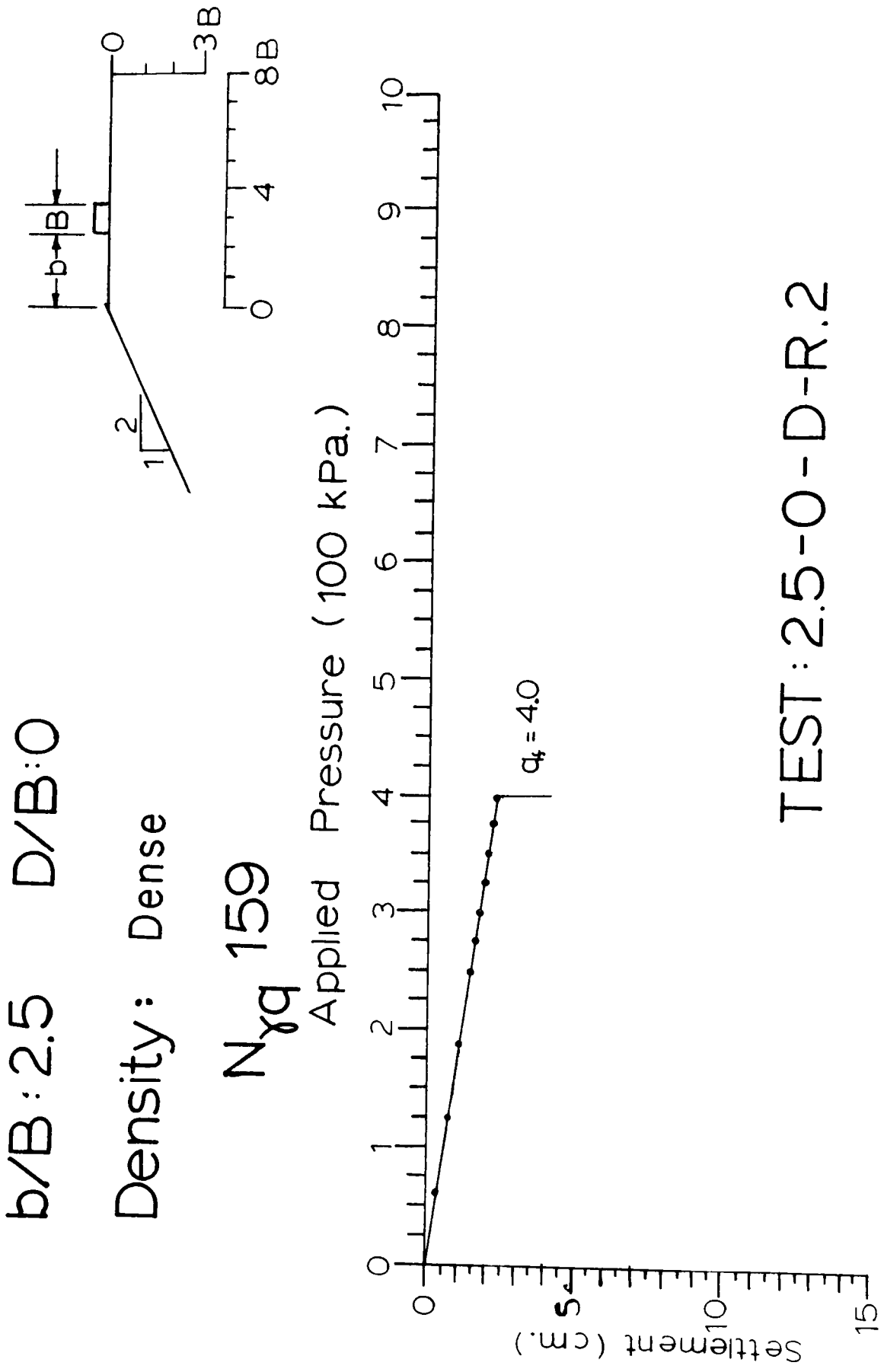
b/B : 2.5 D/B:0
Density: Dense
$N_{\gamma q}$ 159
TEST : 2.5-0-D-R.2
Applied Pressure (100 kPa.)
Settlement (cm.)
$q_f = 4.0$
s
b
B
0
3B
8B
0
4
1
2
0
1
2
3
4
5
6
7
8
9
10
0
5
10
15

Figure 6.93

DENSITY MEASUREMENTS (kg/m^3)

TEST: 2.5 - 0 - D - R.2

Location of measurement under footing	Measurements	Average	Standard deviation
0B*	1620		
	1610		
	1620		
	1620		
1B*	1620		
	1610		
	1620		
	1620		
2B*	1620		
	1600		
	1630		
	1630		
3B*	1630		
	1610		
	1630		
	1620		
		1620	10

* B = footing width

Figure 6.94

Surface Movements
Test: 2.5-0-D-R.2

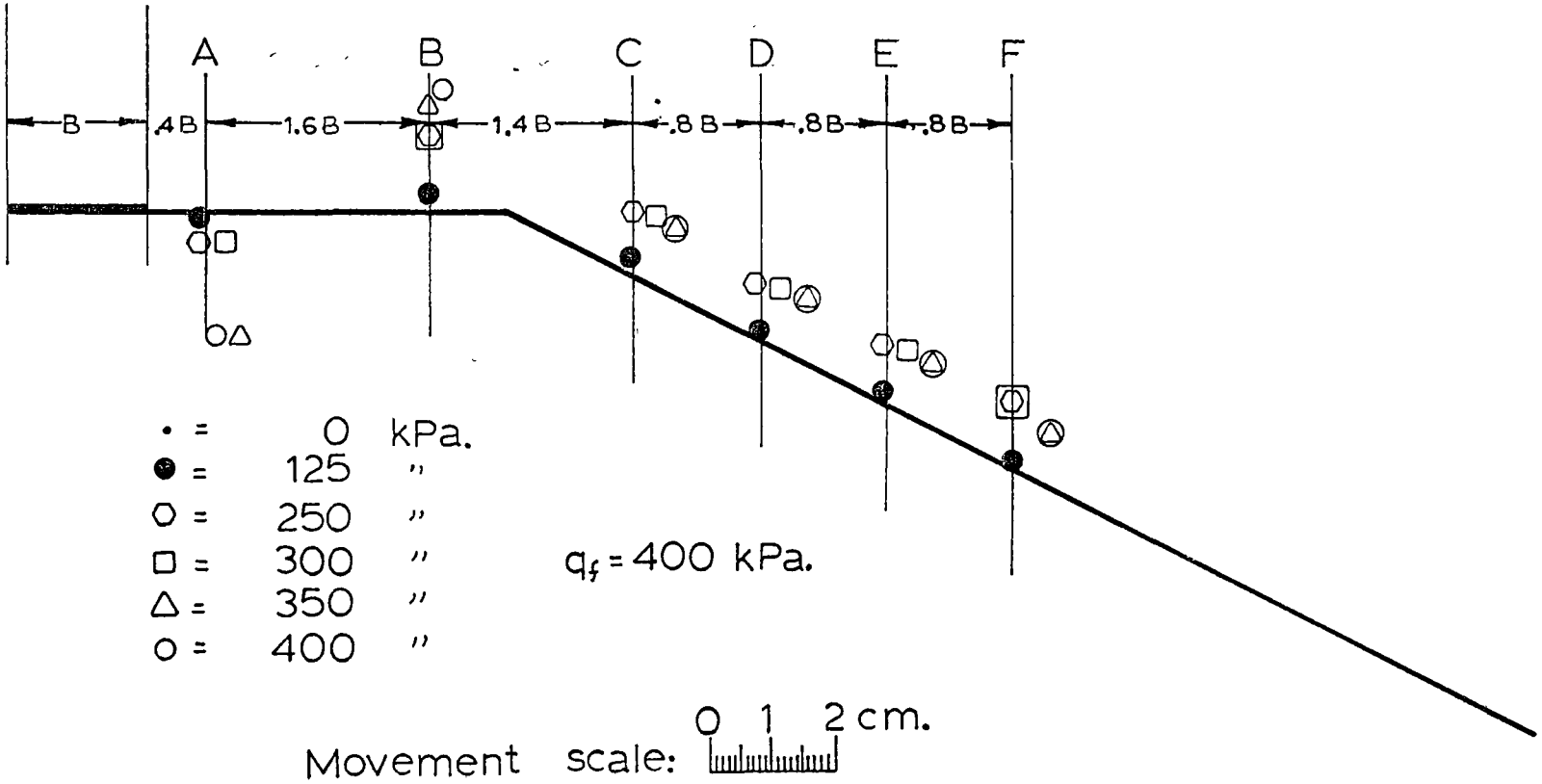

Figure 6.95

SURFACE MOVEMENTS (cm)

TEST: 2.5 - 0 - D - R.2

Positions		A	B	C	D	E	F
Horizontal distance from footing (B = footing width)		.4B	2B	3.4B	4.2B	5B	5.8B
Pressure (kPa)							
0	H	0	0	0	0	0	0
	V	0	0	0	0	0	0
63	H	0	0	0	0	0	0
	V	0	0.2	0	0.1	0	0
125	H	0	0	0	0	0	0
	V	-0.1	0.3	0	0.2	0.2	0
188	H	0	0	0	0	0	0
	V	-0.1	1.4	0.5	1.2	0.8	0.5
250	H	0	0	0	0	0	0
	V	-0.5	1.7	1.5	1.5	1.3	1.0
275	H	0	0	0.3	0	0.3	0
	V	-0.5	1.7	1.5	1.5	1.4	1.0
300	H	0.3	0	0.3	0.3	0.3	0
	V	-0.5	1.7	1.6	1.5	1.4	1.0
325	H	0.3	0	0.3	0.3	0.3	0
	V	-1.8	1.6	1.6	1.5	1.4	0.8
350	H	0.6	0	0.6	0.6	0.6	0.6
	V	-2.0	1.8	1.6	1.5	1.4	0.8
375	H	0.6	0	0.6	0.6	0.6	0.6
	V	-2.0	2.0	1.6	1.5	1.4	0.8
400	H	0.3	0.3	0.6	0.6	0.6	0.6
	V	-2.0	2.0	1.6	1.5	1.4	0.7

Figure 6.96

Test: 2.5 - 1 - D

PRESSURE - SETTLEMENT

TEST: 2.5 - 1 - D

γ = 1590 kg/m^3

B = .3 m.

Pressure q kPa	Settlement cm.	$\frac{2q}{\gamma B}$	Relative settlement $(\frac{W}{B} \times 100)$
0	0	0	0
63	0.3	26	1.0
125	0.6	50	2.0
188	1.0	76	3.3
250	1.4	102	4.7
313	1.8	127	6.0
375	2.2	152	7.3
438	2.6	178	8.7
500	2.9	202	9.7
513	3.0	206	10.0

Figure 6.97

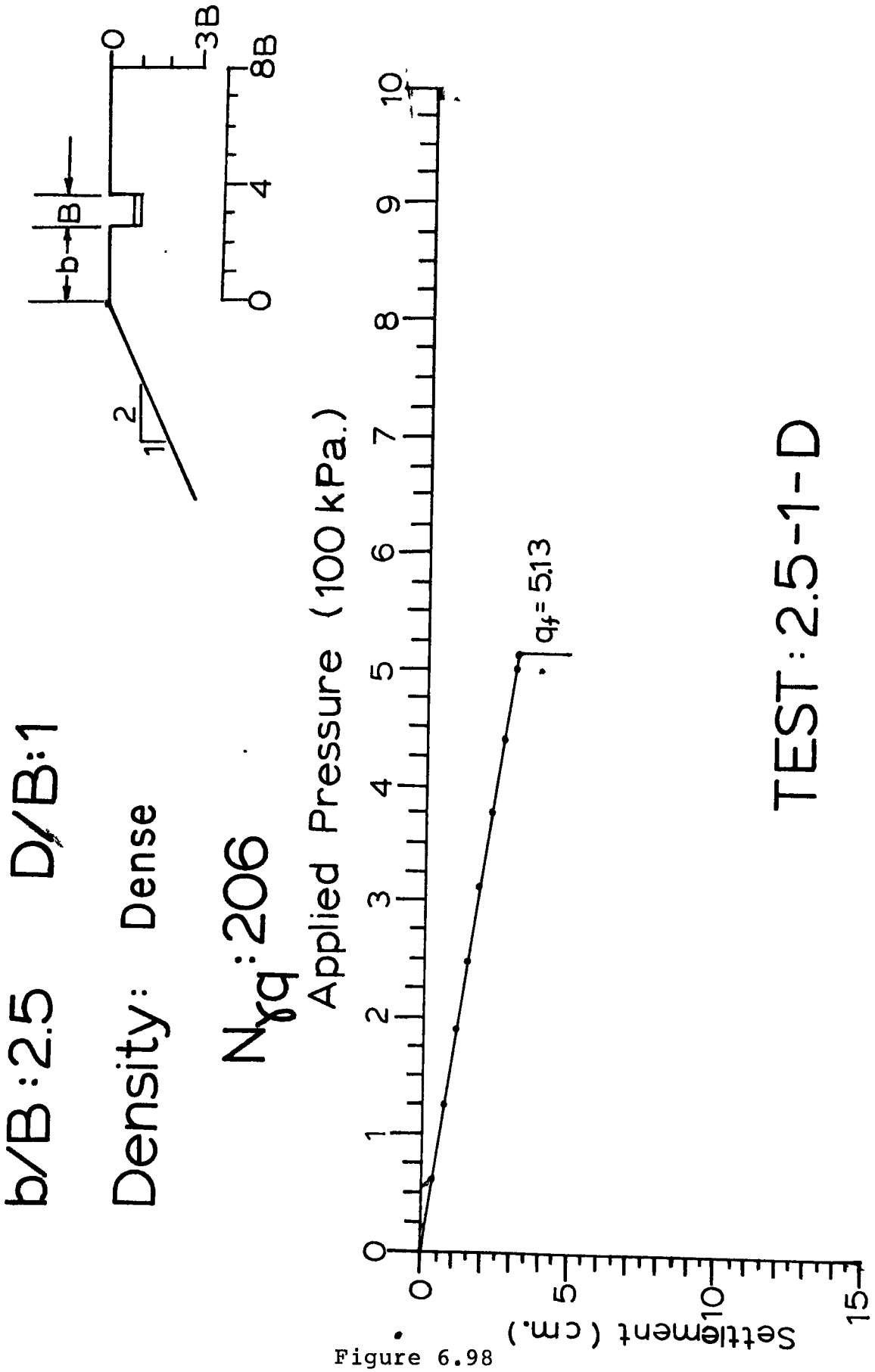
b/B:2.5
D/B:1
Density: Dense
$N_{\gamma q}$:206
TEST:2.5-1-D
Applied Pressure (100 kPa.)
Settlement (cm.)
q_f= 5.13
0
3B
8B
b
B
2
1
0
1
2
3
4
5
6
7
8
9
10
0
5
10
15

Figure 6.98

DENSITY MEASUREMENTS (kg/m^3)

TEST: 2.5 - 1 - D

Location of measurement under footing	Measurements	Average	Standard deviation
0B*	1620		
	1600		
	1620		
	1630		
	1570		
1B*	1610		
	1630		
	1610		
	1610		
	1590		
2B*	1570		
	1570		
	1580		
	1590		
3B*	1590		
	1590		
	1590		
	1580		
	1580		
4B*	1580		
	1570		
	1590		
	1580		
		1590	20

* B = footing width

Figure 6.99

Surface Movements
Test: 2.5-1-D

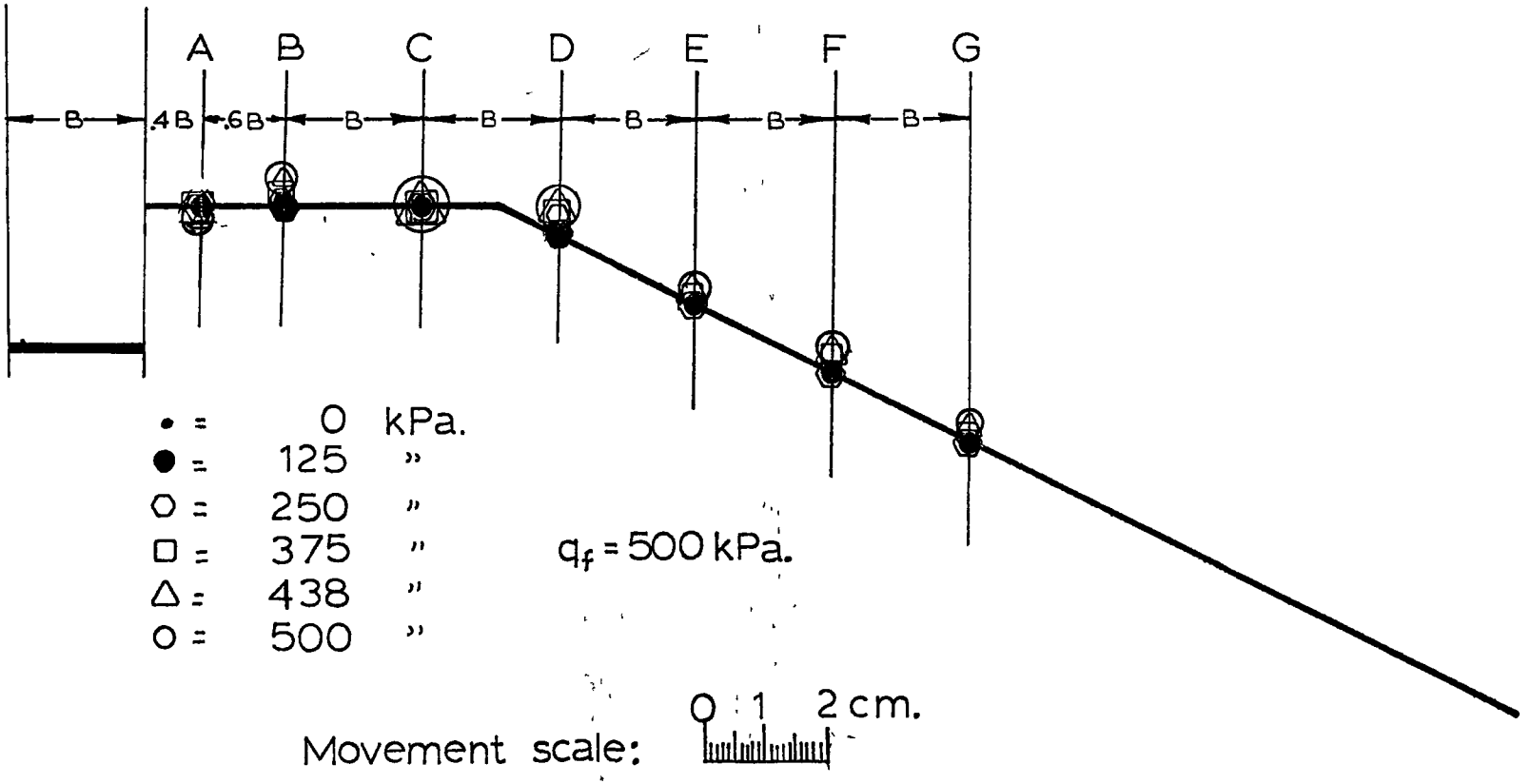

Figure 6.100

SURFACE MOVEMENTS (cm)

TEST: 2.5 - 1 - D

Positions		A	B	C	D	E	F	G
Horizontal distance from footing (B = footing width)		.4B	B	2B	3B	4B	5B	6B
Pressure (kPa)								
0	V	0	0	0	0	0	0	0
125	V	0	0	0	0	0	0	0
250	V	0	0.1	0	0.4	0	0.2	0.1
375	V	0	0.1	0	0.4	0.2	0.3	0.1
438	V	-0.3	0.3	0	0.4	0.2	0.3	0.2
500	V	-0.3	0.3	0	0.4	0.2	0.3	0.2

Figure 6.101

Test: 2.5 - 2 - D

PRESSURE - SETTLEMENT

TEST: 2.5 - 2 - D

γ = 1620 kg/m^3

B = .3 m.

Pressure q kPa	Settlement cm.	$\frac{2q}{\gamma B}$	Relative settlement $(\frac{W}{B} \times 100)$
0	0	0	0
63	0.2	26	0.7
125	0.6	50	2.0
188	0.8	75	2.7
250	1.2	100	4.0
313	1.5	125	5.0
375	1.8	150	6.0
438	2.1	175	7.0
500	2.4	200	8.0
525	2.6	210	8.7
550	2.7	219	9.0
575	2.8	230	9.3
600	2.9	240	9.7
625	3.1	250	10.3
650	3.2	260	10.7
675	3.4	270	11.3
700	3.5	280	11.7
725	3.6	290	12.0
750	3.7	300	12.3
775	3.8	310	12.7
800	4.0	320	13.3
825	4.2	328	14.0

Figure 6.102

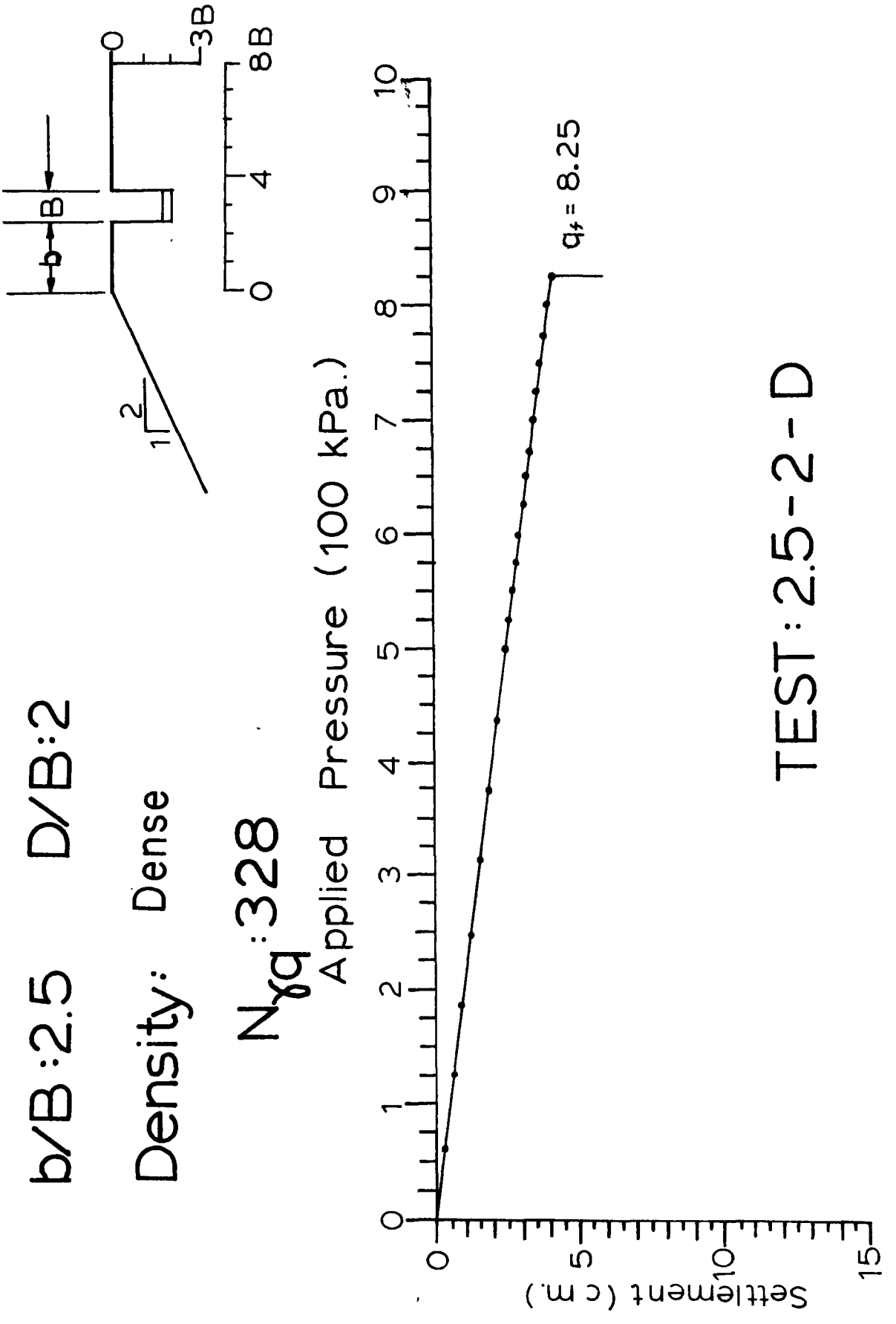
b/B:2.5
D/B:2
Density: Dense
$N_{\gamma q}$:328
TEST: 2.5-2-D
Applied Pressure (100 kPa.)
Settlement (c m.)
q_f = 8.25
B
b
2
1
0
4
8B
3B
0
1
2
3
4
5
6
7
8
9
10
0
5
10
15

Figure 6.103

DENSITY MEASUREMENTS (kg/m^3)

TEST: 2.5 - 2 - D

Location of measurement under footing	Measurements	Average	Standard deviation
0B*	1620		
	1610		
	1620		
	1610		
1B*	1610		
	1600		
	1620		
	1620		
2B*	1620		
	1600		
	1610		
	1620		
3B*	1630		
	1610		
	1630		
	1630		
		1620	10

* B = footing width

Figure 6.104

Surface Movements
Test: 2.5-2-D

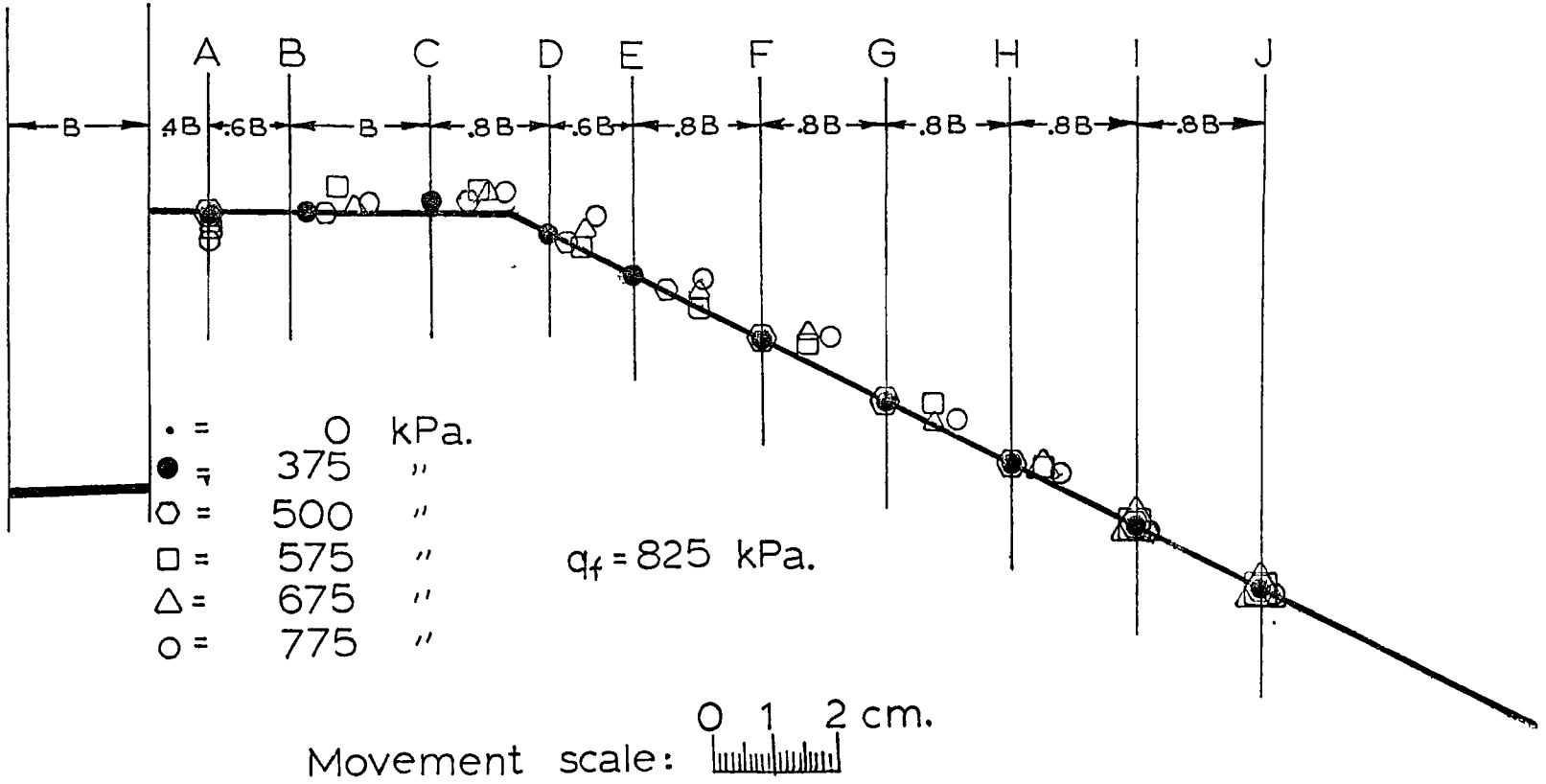

Figure 6.105

SURFACE MOVEMENTS (cm)

TEST: 2.5 - 2 - D

Positions		A	B	C	D	E	F	G	H	I	J
Horizontal distance from footing (B = footing width)		.4B	B	2B	2.8B	3.4B	4.2B	5B	5.8B	6.6B	7.4B
Pressures (kPa)											
0	H	0	0	0	0	0	0	0	0	0	0
	V	0	0	0	0	0	0	0	0	0	0
250	H	0	0	0	0	0	0	0	0	0	0
	V	0	0	0	0	0	0	0	0	0	0
375	H	0	0.3	0	0	0	0	0	0	0	0
	V	0	0	0.2	0	0	0	0	0	0	0
500	H	0	0.6	0.6	0.3	0.6	0	0	0	0	0
	V	0	0	0.2	0	0	0	0	0	0	0
525	H	0	0.6	0.6	0.6	0.8	0.2	0.5	0.3	0	0
	V	-1.0	0	0.2	0	0.2	0.5	0.5	0	0	0
550	H	0	0.8	0.6	0.6	0.8	0.6	0.8	0.6	0	0
	V	-0.2	0	0.2	0.2	0.2	0.5	0.5	0.2	0	0
575	H	0	0.8	0.8	0.6	1.2	0.8	0.8	0.6	0	0
	V	-0.2	0.4	0.3	0	0	0.5	0.3	0.2	0	0
600	H	0	0.9	1.0	0.6	1.2	0.8	0.8	0.6	0	0
	V	-0.1	0.2	0.3	0.2	0	0.5	0	0.2	0	0
625	H	0	1.0	1.0	0.6	1.2	0.8	0.8	0.6	0	0
	V	-0.1	0.1	0.3	0.3	0.2	0.4	0	0.2	0	0
650	H	0	1.0	1.0	0.6	1.2	0.8	0.8	0.6	0	0
	V	-0.1	0.1	0.3	0.3	0.2	0.4	0	0.2	0	0
675	H	0	1.0	1.0	0.6	1.2	0.8	0.8	0.6	0	0
	V	-0.1	0.1	0.3	0.3	0.2	0.4	0	0.2	0	0
700	H	0	1.3	1.1	0.8	1.2	1.2	1.2	0.6	0.2	0
	V	-0.1	0.2	0.3	0.4	0.1	0.5	0	0.2	0	0
725	H	0	1.3	1.3	0.8	1.2	1.2	1.2	0.6	0.2	0
	V	-0.1	0.3	0.3	0.4	0.2	0.5	0	0.2	0	0
750	H	0	1.3	1.2	0.8	1.2	1.2	1.2	0.8	0.2	0.2
	V	-0.3	0.4	0.3	0.6	0.3	0.4	0.2	0.2	0	0
775	H	0	1.3	1.2	0.8	1.2	1.2	1.2	0.8	0.2	0.2
	V	-0.3	0.2	0.3	0.6	0.4	0.5	0.2	0.2	0	0

Figure 6.106

Test: 2.5 - 3 - D

PRESSURE - SETTLEMENT

TEST: 2.5 - 3 - D

γ = 1620 kg/m^3

B = .3 m.

Pressure q kPa	Settlement cm.	$\frac{2q}{\gamma B}$	Relative settlement $(\frac{W}{B} \times 100)$
0	0	0	0
63	0.2	26	0.7
125	0.3	50	1.0
188	0.4	75	1.3
250	0.5	100	1.7
313	0.6	125	2.0
375	0.7	150	2.3
438	0.8	175	2.7
500	0.9	200	3.0
563	1.1	225	3.7
625	1.2	250	4.0
688	1.3	276	4.3
750	1.4	300	4.7
800	1.5	320	5.0
825	1.6	330	5.3
850	1.6	340	5.3
875	1.7	350	5.7
900	1.7	360	5.7
925	1.8	370	6.0
950	1.8	380	6.0
975	1.9	390	6.3
1000	1.9	397	6.3

Figure 6.107

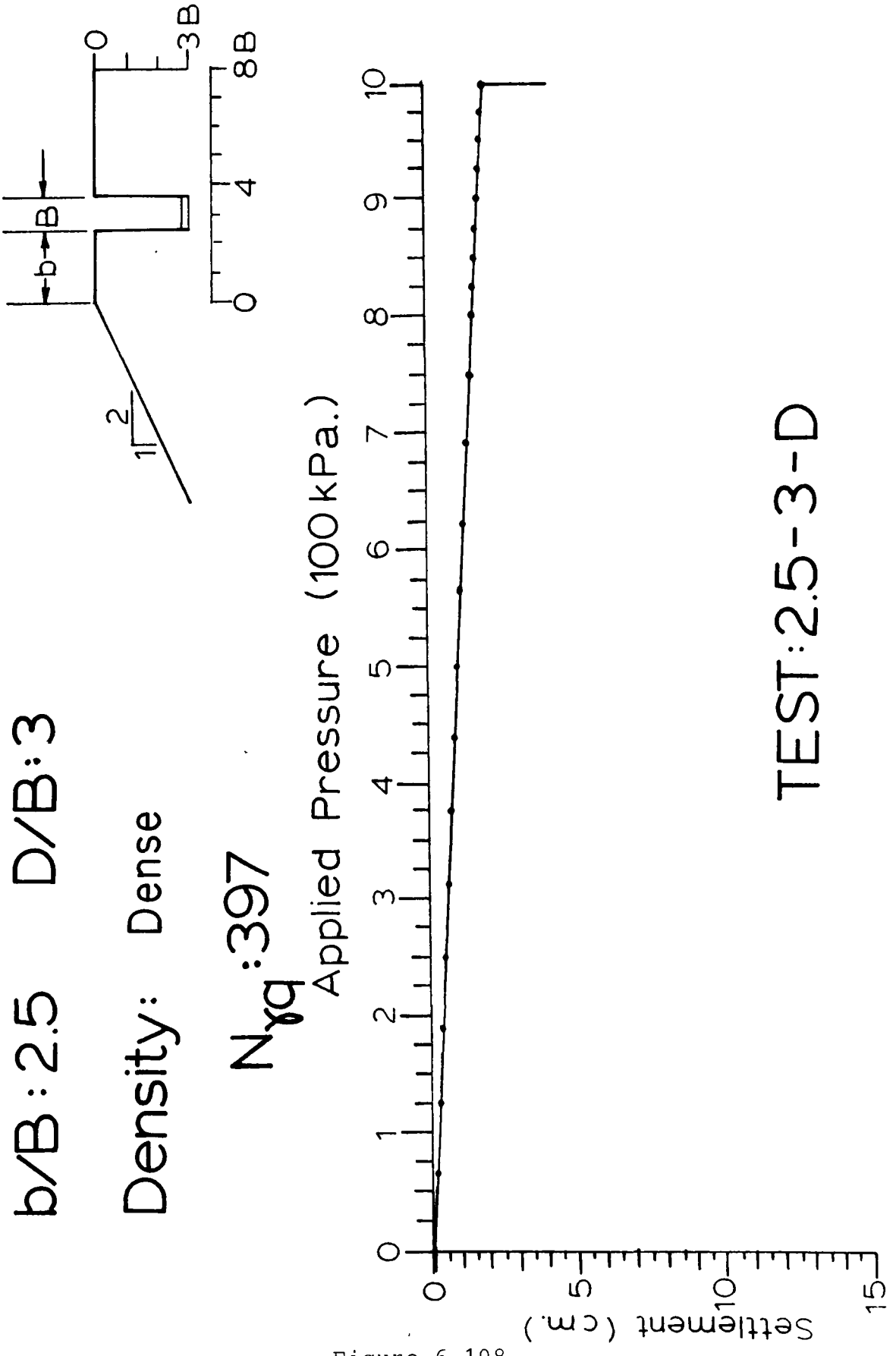
b/B:2.5
D/B:3
Density: Dense
$N_{\gamma q}$:397
TEST:2.5-3-D
Applied Pressure (100 kPa.)
Settlement (cm.)
0
1
2
3
4
5
6
7
8
9
10
0
5
10
15
b
B
0
3B
8B
0
4
1
2

Figure 6.108

DENSITY MEASUREMENTS (kg/m^3)

TEST: 2.5 - 3 - D

Location of measurement under footing	Measurements	Average	Standard deviation
1B*	1610		
	1620		
	1610		
	1610		
2B*	1630		
	1620		
	1610		
	1630		
		1620	9

* B = footing width

Figure 6.109

Surface Movements
Test 25-3-D

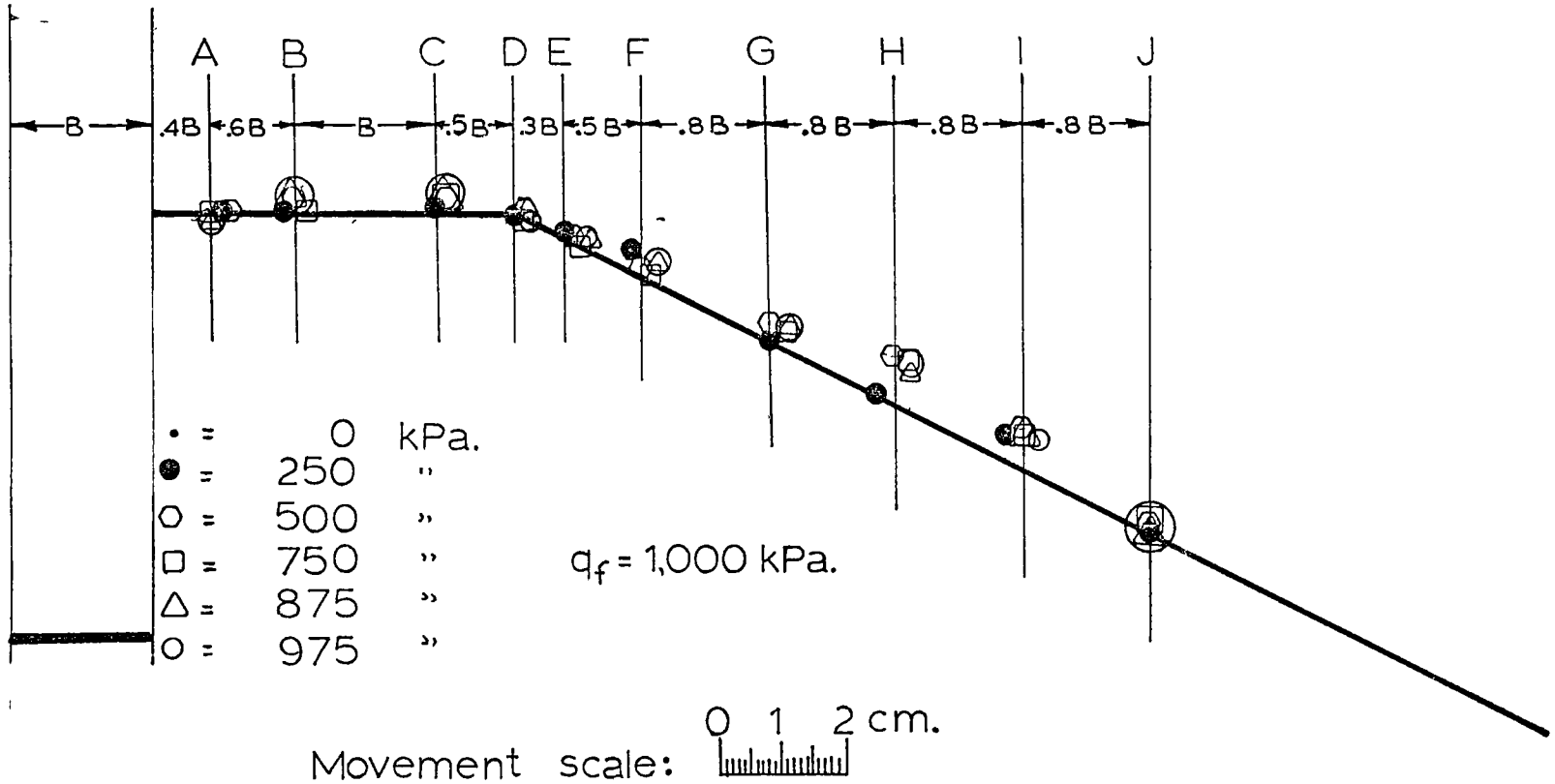

Figure 6.110

SURFACE MOVEMENTS (cm)

TEST: 2.5 - 3 - D

Positions		A	B	C	D	E	F	G	H	I	J
Horizontal distance from footing (B = footing width)		.4B	B	2B	2.5B	2.8B	3.3B	4.1B	4.9B	5.7B	6.5B
Pressure (kPa)											
0	H	0	0	0	0	0	0	0	0	0	0
	V	0	0	0	0	0	0	0	0	0	0
125	H	0	0	0	0	0	0	0	0	0	0
	V	0	0	0	0	0	0	0	0	0	0
250	H	0.2	-0.2	0	0	0	-0.2	0	-0.3	-0.3	0
	V	0	0	0.1	0	0.1	0.3	0	0	0.4	0
375	H	0.3	-0.3	0	0	0	-0.2	0	-0.3	-0.3	-0.2
	V	0	0.3	0.1	0.1	0.1	0.1	0.3	0.6	0.6	0.1
500	H	0.3	0	0.2	0	0.2	0	0	0	0	0
	V	0	0.2	0.2	0.1	0.1	0.1	0.1	0.7	0.6	0.1
625	H	0.2	0	0.2	0.2	0.2	0	0	0	0	0
	V	-0.1	0.3	0.1	0.1	0.1	0.1	0.3	0.8	0.5	0.1
750	H	0	0	0.3	0.2	0.3	0.3	0.2	0.2	0	0
	V	0	0.2	0.2	0	0	0.1	0.3	0.8	0.5	0.1
775	H	0	0	0.2	0.2	0.3	0.2	0.2	0.2	0	0
	V	-0.1	0.1	0.3	0	0	0.1	0.3	0.4	0.6	0.1
800	H	0	-0.2	0.2	0.2	0.3	0.2	0.2	0.2	0	0
	V	-0.1	0.1	0.2	0	0.1	0.1	0.2	0.8	0.6	0.1
825	H	0	-0.2	0.2	0.2	0.3	0.2	0.2	0.2	0	0
	V	-0.1	0.2	0.1	0	0.1	0.3	0.2	0.7	0.5	0
875	H	0	0	0.2	0.2	0.3	0.2	0.2	0.2	0	0
	V	-0.1	0.1	0.2	0.1	0.1	0.2	0.1	0.5	0.5	0
900	H	0	0	0.2	0.2	0.3	0.2	0.2	0.2	0	0
	V	-0.1	0.1	0.2	0.1	0	0.2	0.3	0.8	0.5	0
925	H	0	0	0.2	0.3	0.3	0.2	0.2	0.2	0.2	0
	V	-0.1	0.1	0.3	0	0.1	0.2	0.2	0.7	0.5	0
950	H	0	0	0.2	0.3	0.3	0.2	0.2	0.2	0.2	0
	V	-0.1	0.1	0.2	0	0.1	0.2	0.2	0.7	0.5	0
975	H	0	0	0.2	0.3	0.3	0.2	0.2	0.2	0.2	0
	V	-0.1	0.1	0.2	0	0.1	0.2	0.2	0.7	0.5	0

Figure 6.111

Test: 5 - 0 - D

PRESSURE - SETTLEMENT

TEST: 5 - 0 - D

γ = 1610 kg/m^3

B = .3 m.

Pressure q kPa	Settlement cm.	$\frac{2q}{\gamma B}$	Relative settlement $(\frac{W}{B} \times 100)$
0	0	0	0
25	0.1	10	0.3
50	0.2	20	0.7
125	0.6	50	2.0
275	1.4	111	4.7
300	1.5	121	5.0
375	1.8	151	6.0
425	2.2	171	7.3
450	2.3	180	7.7

Figure 6.112

b/B : 5 D/B : 0

Density : Dense

$N_{\gamma q}$: 180

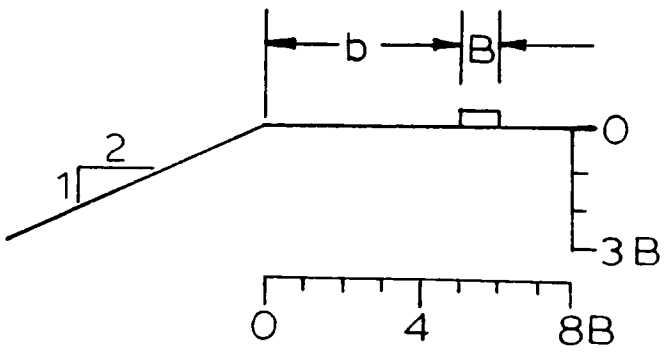

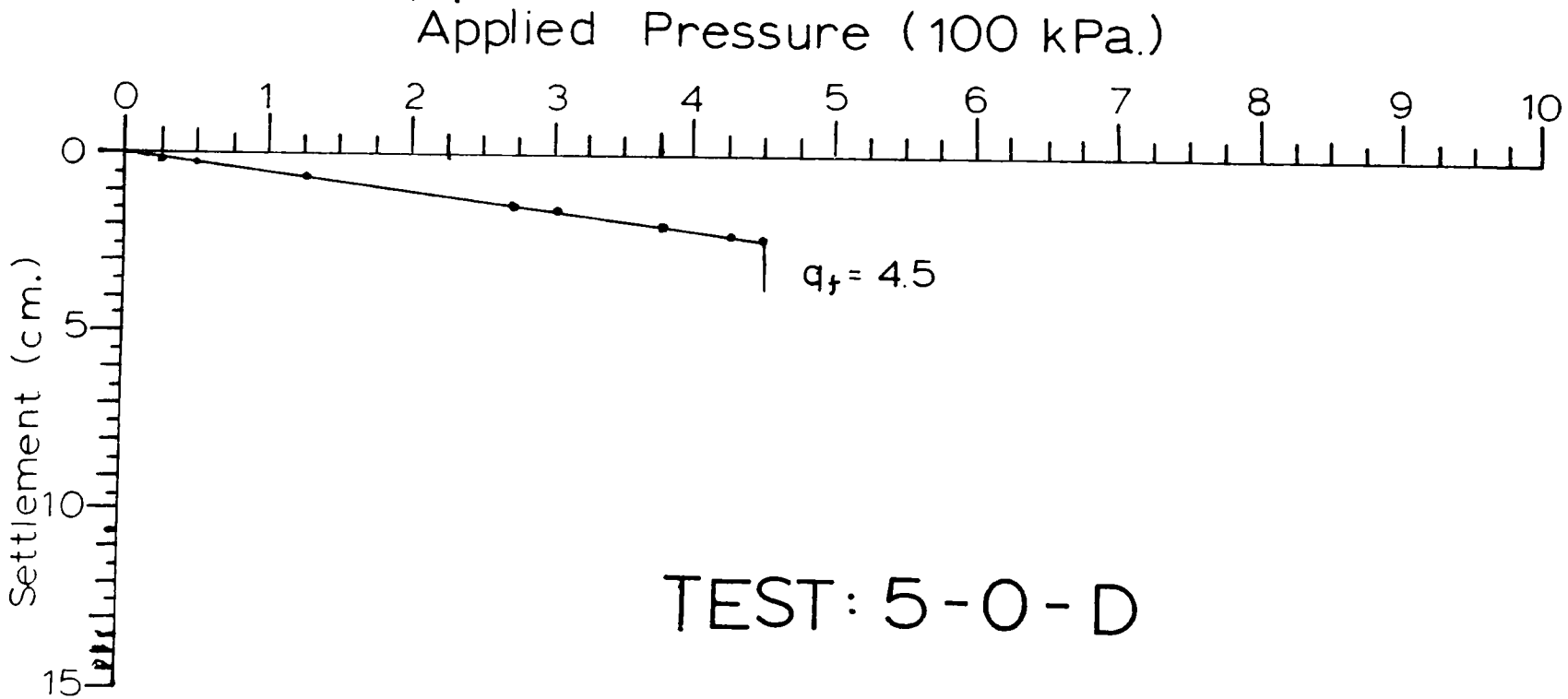

TEST : 5 - 0 - D

Figure 6.113

Test: 5 - 0 - D - R

PRESSURE - SETTLEMENT

TEST: 5 - 0 - D - R

γ = 1610 kg/m^3

B = .3 m.

Pressure q kPa	Settlement cm.	$\frac{2q}{\gamma B}$	Relative settlement $(\frac{W}{B} \times 100)$
0	0	0	0
25	0.1	10	0.3
50	0.2	20	0.7
75	0.3	30	1.0
100	0.5	40	1.7
125	0.6	50	2.0
150	0.7	60	2.3
175	0.8	70	2.7
200	0.9	81	3.0
225	1.0	91	3.3
300	1.5	121	5.0
350	1.7	141	5.7
400	1.9	161	6.3
425	2.0	171	6.7
450	2.3	180	7.7

Figure 6.114

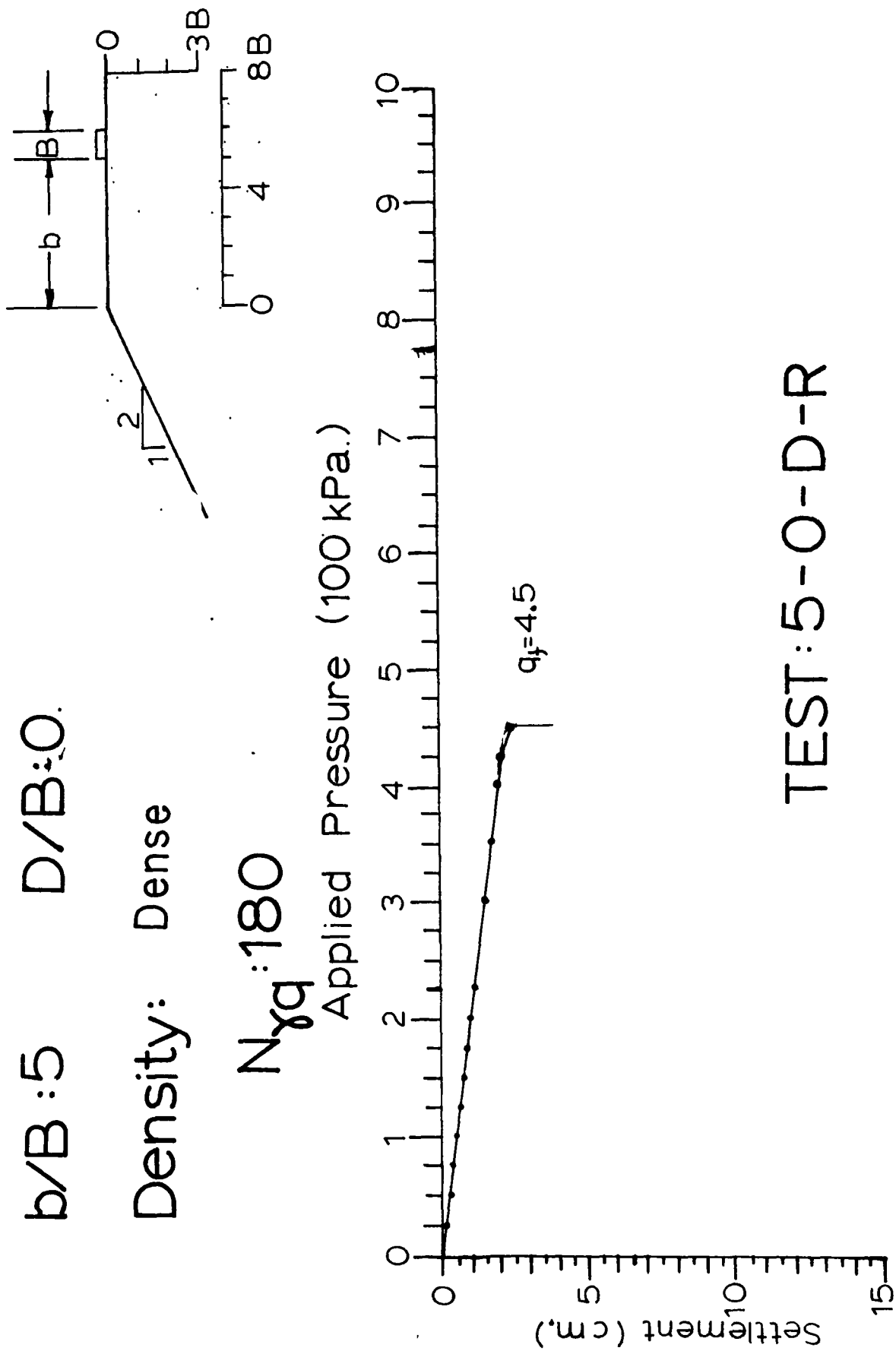
b/B :5
D/B:0
Density: Dense
$N_{\gamma q}$:180
TEST:5-O-D-R
Applied Pressure (100 kPa.)
Settlement (cm.)
q_f=4.5
b
B
0
3B
8B
2
1
0
1
2
3
4
5
6
7
8
9
10
0
5
10
15

Figure 6.115

Test: 5 - 1 - D

PRESSURE - SETTLEMENT

TEST: 5 - 1 - D

γ = 1600 kg/m^3

B = .3 m.

Pressure q $\overline{kPa}$	Settlement cm.	$\frac{2q}{\gamma B}$	Relative settlement $(\frac{W}{B} \times 100)$
0	0	0	0
63	0.2	26	0.7
125	0.6	50	2.0
188	0.9	76	3.0
225	1.1	91	3.7
300	1.5	122	5.0
375	1.9	152	6.3
438	2.3	177	7.7
500	2.6	202	8.7
550	2.9	221	9.7

Figure 6.116

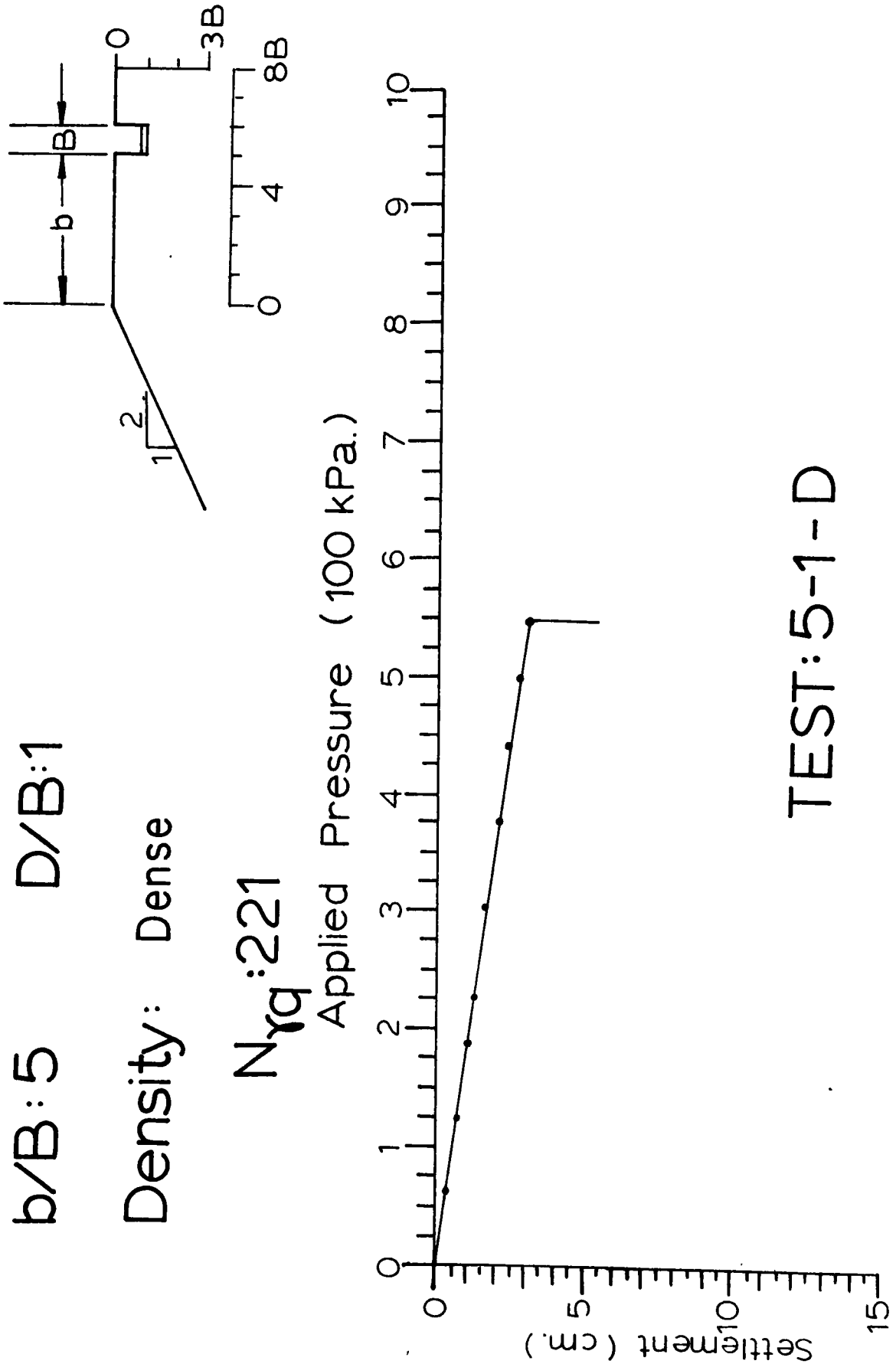
b/B:5
D/B:1
Density: Dense
$N_{\gamma q}$:221
TEST:5-1-D
Applied Pressure (100 kPa.)
Settlement (cm.)
0
1
2
3
4
5
6
7
8
9
10
0
5
10
15
b
B
2
1
0
3B
0
4
8B

Figure 6.117

DENSITY MEASUREMENTS (kg/m^3)

TEST: 5 - 1 - D

Location of measurement under footing	Measurements	Average	Standard deviation
1B*	1590		
	1590		
	1600		
	1590		
2B*	1610		
	1590		
	1610		
	1600		
		1600	9

* B = footing width

Figure 6.118

Surface Movements
Test:5-1-D

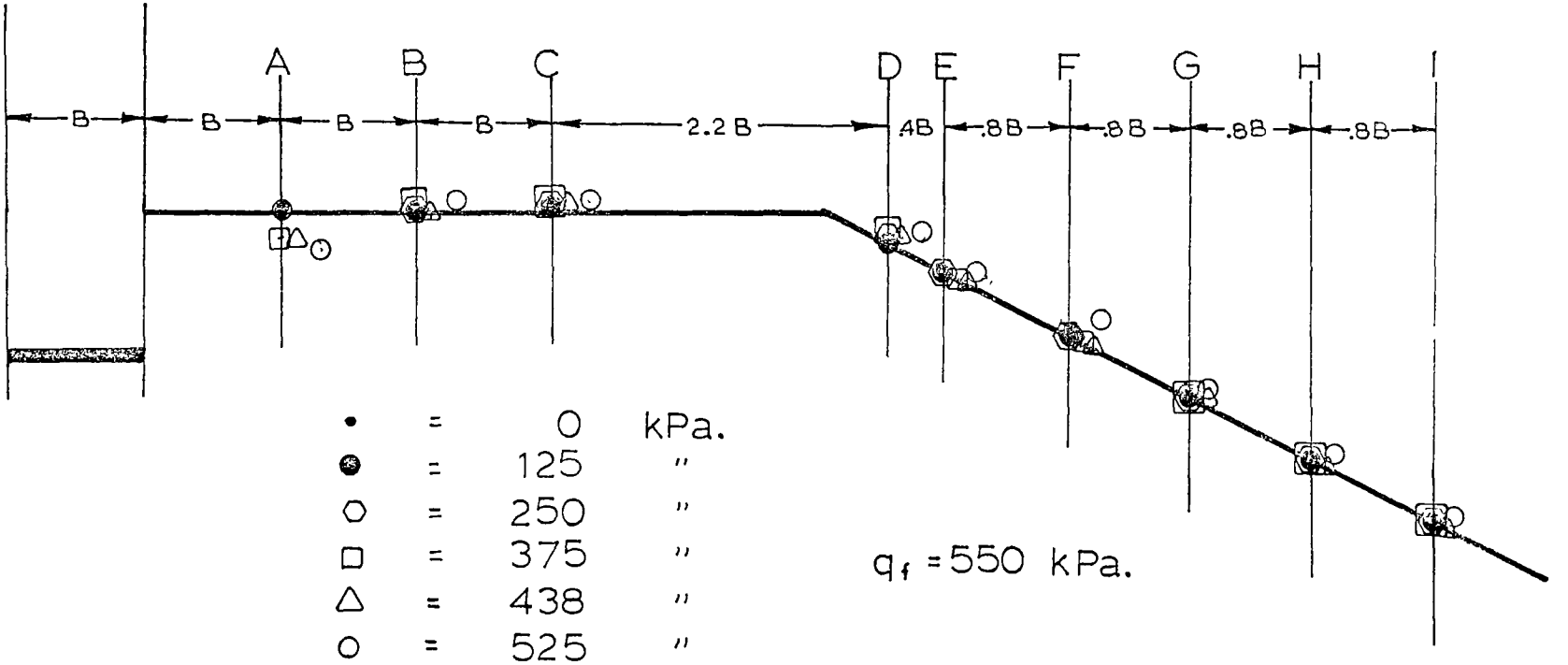

Figure 6.119

SURFACE MOVEMENTS (cm)

TEST: 5 - 1 - D

Positions		A	B	C	D	E	F	G	H	I
Horizontal distance from footing (B = footing width)		B	2B	3B	5.2B	5.6B	6.4B	7.2B	8B	8.8B
Pressure (kPa)										
0	H	0	0	0	0	0	0	0	0	0
	V	0	0	0	0	0	0	0	0	0
125	H	0	0	0	0	0	0	0	0	0
	V	0	0.1	0	0	0	0	0	0	0
250	H	0	0	0	0	0	0	0	0	0
	V	0	0.1	0.1	0.1	0	0	0	0	0
313	H	0	0	0	0	0.2	0.2	0	0	0
	V	-0.3	0.1	0.2	0.1	0	0	0	0	0
375	H	0	0	0	0	0.2	0.2	0	0	0
	V	-0.3	0.1	0.1	0.1	0	0	0	0	0
438	H	0.2	0.2	0.2	0.2	0.3	0.3	0.2	0.2	0.2
	V	-0.4	0	0.1	0.1	0	0	0.1	0	0
525	H	0.6	0.6	0.6	0.6	0.6	0.6	0.3	0.3	0.3
	V	-0.5	0.1	0.1	0.4	0.2	0.5	0.1	0.2	0.2

Figure 6.120

Test: 5 - 2 - D

PRESSURE - SETTLEMENT

TEST: 5 - 2 - D

γ = 1610 kg/m^3

B = .3 m.

Pressure q kPa	Settlement cm.	$\frac{2q}{\gamma B}$	Relative settlement $(\frac{W}{B} \times 100)$
0	0	0	0
63	0.2	26	0.7
125	0.5	50	1.7
188	0.7	75	2.3
250	1.1	101	3.7
313	1.4	125	4.7
375	1.6	150	5.3
438	2.0	176	6.7
500	2.2	200	7.3
563	2.5	226	8.3
625	2.8	251	9.3
688	3.1	276	10.3
750	3.4	301	11.3
775	3.5	311	11.7
800	3.6	321	12.0
825	3.8 - 6.2	328	12.7 - 20.7
850	6.6	341	22.0
875	6.7	351	22.3
900	6.8	361	22.7
925	6.9	371	23.0
950	7.0	381	23.3
975	7.1	391	23.7
1000	7.2	401	24.0

Figure 6.121

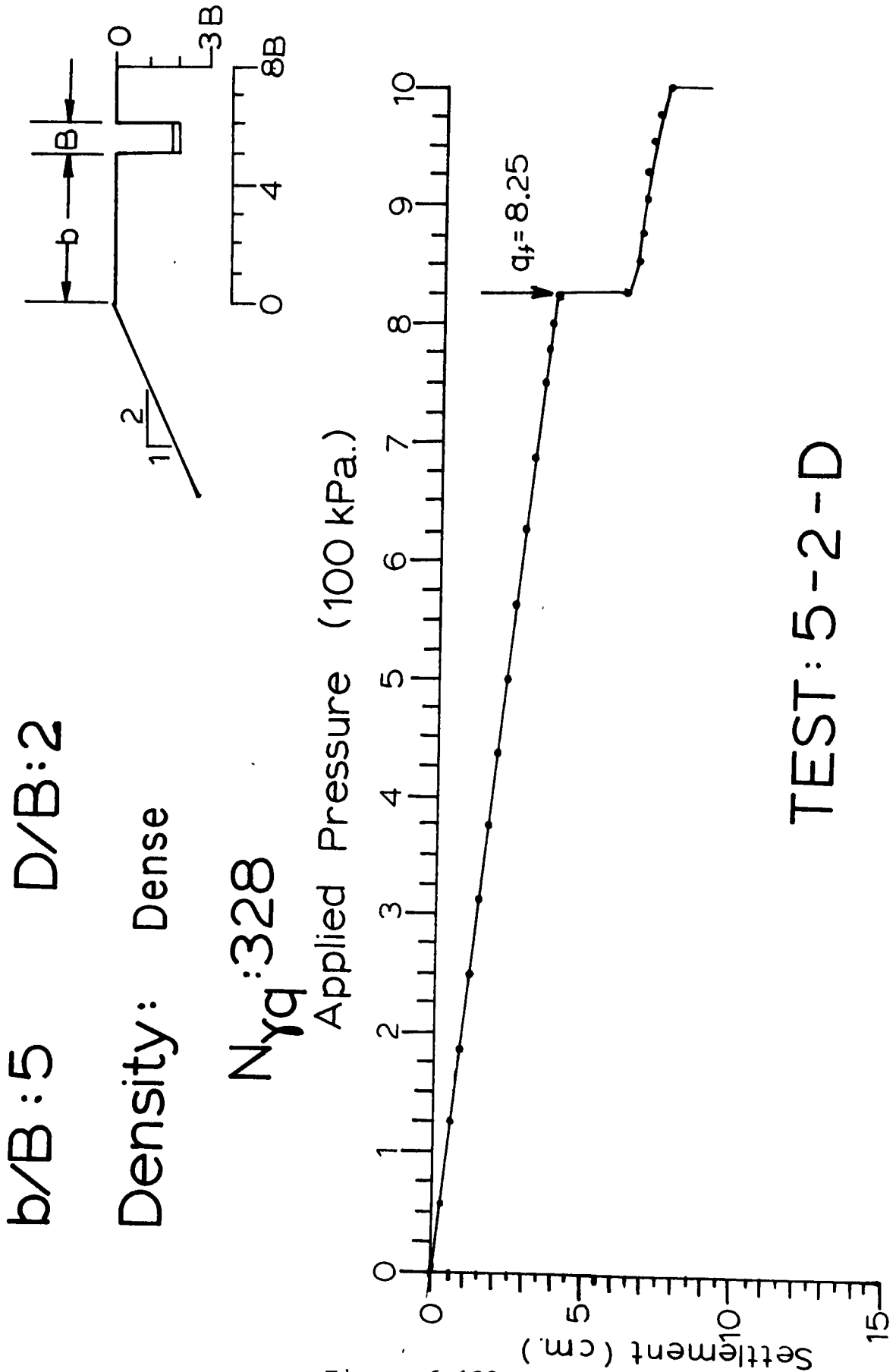
b/B:5
D/B:2
Density: Dense
$N_{\gamma q}$:328
TEST: 5-2-D
Applied Pressure (100 kPa.)
Settlement (cm.)
q_f=8.25
b
B
0
3B
8B
0
4
1
2

Figure 6.122

DENSITY MEASUREMENTS (kg/m^3)

TEST: 5 - 2 - D

Location of measurement under footing	Measurements	Average	Standard deviation
0B*	1610		
	1590		
	1610		
	1610		
1B*	1610		
	1610		
	1620		
	1630		
2B*	1610		
	1590		
	1610		
	1610		
3B*	1620		
	1620		
	1620		
	1630		
		1610	10

* B = footing width

Figure 6.123

Surface Movements

Test: 5-2-D

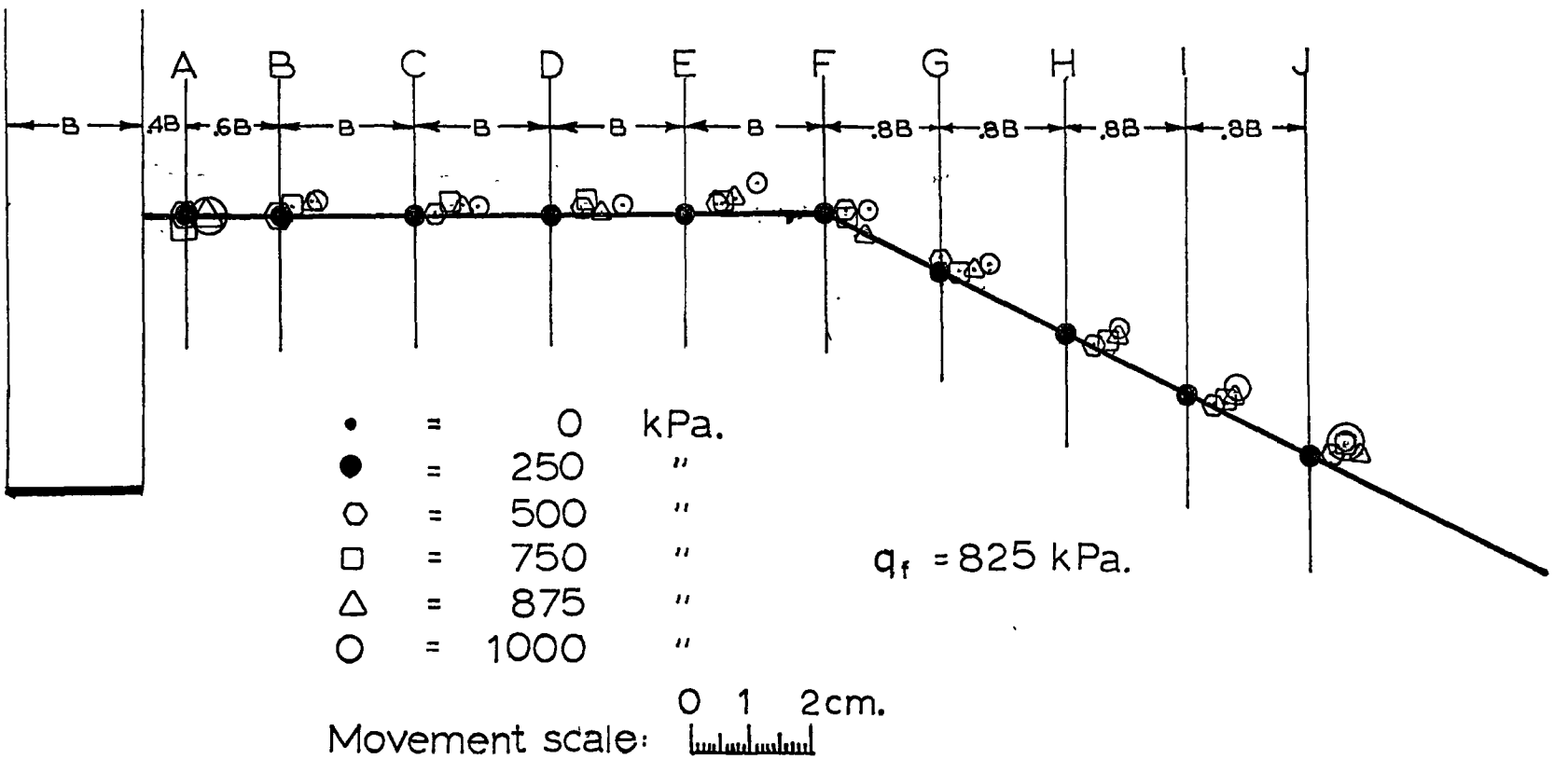

Figure 6.124

SURFACE MOVEMENTS (cm)

TEST: 5 - 2 - D

Positions		A	B	C	D	E	F	G	H	I	J
Horizontal distance from footing (B = footing width)		.4B	B	2B	3B	4B	5B	5.8B	6.6B	7.4B	8.2B
Pressure (kPa)											
0	H	0	0	0	0	0	0	0	0	0	0
	V	0	0	0	0	0	0	0	0	0	0
125	H	0	0	0	0	0	0	0	0	0	0
	V	0	0	0	0	0	0	0	0	0	0
250	H	0	0	0	0	0	0	0	0	0	0
	V	0	0	0	0	0	0	0	0	0	0
313	H	0	0	0	0	0	0	0	0	0	0
	V	0	0	0	0	0	0	0	0	0	0
375	H	0	0	0.2	0.3	0.2	0.2	0	0.3	0.3	0
	V	0	0	0.2	0.1	0.1	0.2	0.1	0	0	0
438	H	0	0	0.3	0.3	0.3	0.2	0	0.3	0.5	0.2
	V	0	0	0.2	0.2	0	0.2	0.1	0	0	0.2
500	H	0	0	0.3	0.5	0.5	0.3	0	0.5	0.5	0.3
	V	0	0	0	0.1	0.1	0.2	0.1	0	0	0.2
563	H	0	0	0.5	0.5	0.5	0.3	0.2	0.3	0.5	0.3
	V	0	0	0.1	0	0.1	0.2	0	0	0	0.2
625	H	0	0	0.5	0.6	0.6	0.3	0.3	0.5	0.6	0.6
	V	0	0.1	0	0.1	0.1	0.1	0.2	0.2	0	0.3
688	H	0	0	0.6	0.6	0.6	0.3	0.2	0.6	0.6	0.6
	V	0	0.1	0.1	0	0.2	0.1	0.1	0.1	0.2	0.3
750	H	0	0.2	0.6	0.6	0.6	0.3	0.3	0.6	0.6	0.6
	V	-0.1	0.2	0.1	0.1	0.1	0.1	0.1	0.1	0.1	0.3
775	H	0	0.2	0.6	0.6	0.6	0.3	0.3	0.6	0.6	0.6
	V	-0.1	0.2	0.1	0.1	0.1	0.1	0.2	0.2	0.1	0.3
800	H	0	0.2	0.6	0.6	0.6	0.3	0.3	0.5	0.6	0.5
	V	-0.2	0.1	0	0.1	0.1	0.1	0.2	0.2	0.1	0.3
825	H	0.2	0.6	0.8	0.8	0.8	0.6	0.6	0.8	0.8	0.8
	V	0	0.2	0	0	0.2	0	0.2	0.3	0.3	0.3
850	H	0.2	0.6	0.8	0.8	0.8	0.6	0.5	0.8	0.8	0.8
	V	0	0.1	0.1	0	0.2	0	0.3	0.3	0.3	0.3
875	H	0.3	0.5	0.8	0.8	0.8	0.6	0.6	0.8	0.8	0.8
	V	0	0.2	0.1	0	0.2	0	0.3	0.3	0.3	0.4
900	H	0.3	0.6	0.8	1.0	1.0	0.6	0.6	0.8	1.0	0.6
	V	0	0.2	0	0	0.2	0.1	0.3	0.3	0.3	0.4

Figure 6.125

SURFACE MOVEMENTS (cm)

TEST: 5 - 2 - D(cont'd)

Positions		A	B	C	D	E	F	G	H	I	J
Horizontal distance from footing (B = footing width)		.4B	B	2B	3B	4B	5B	5.8B	6.6B	7.4B	8.2B
Pressure (kPa)											
925	H	0.3	0.6	0.8	1.0	1.0	0.6	0.6	0.8	1.0	0.6
	V	0	0.2	0.1	0	0.2	0.1	0.3	0.3	0.3	0.4
950	H	0.3	0.6	1.0	1.0	1.0	0.6	0.6	0.8	0.8	0.6
	V	0	0.2	0.1	0	0.2	0.1	0.3	0.3	0.3	0.4
975	H	0.3	0.6	1.0	1.0	1.0	0.6	0.6	0.8	0.8	0.6
	V	0	0.2	0.1	0	0.2	0.1	0.3	0.3	0.3	0.4
1000	H	0.3	0.6	1.0	1.2	1.2	0.6	0.8	0.8	0.8	0.6
	V	0	0.2	0.1	0.2	0.5	0.4	0.4	0.3	0.3	0.4

Test: ∞ - 1 - D - S

PRESSURE - SETTLEMENT

TEST: ∞ - 0 - D - S

γ = 1610 kg/m^3

B = .3 m.

Pressure q kPa	Settlement cm.	$\frac{2q}{\gamma B}$	Relative settlement $(\frac{W}{B} \times 100)$
0	0	0	0
25	0.1	10	0.3
75	0.3	30	1.0
150	0.6	61	2.0
213	0.9	86	3.0
275	1.2	111	4.0
313	1.4	126	4.7
350	1.6	141	5.3
400	1.8	162	6.0
425	2.0	171	6.7
450	2.1	180	7.0

Figure 6.126

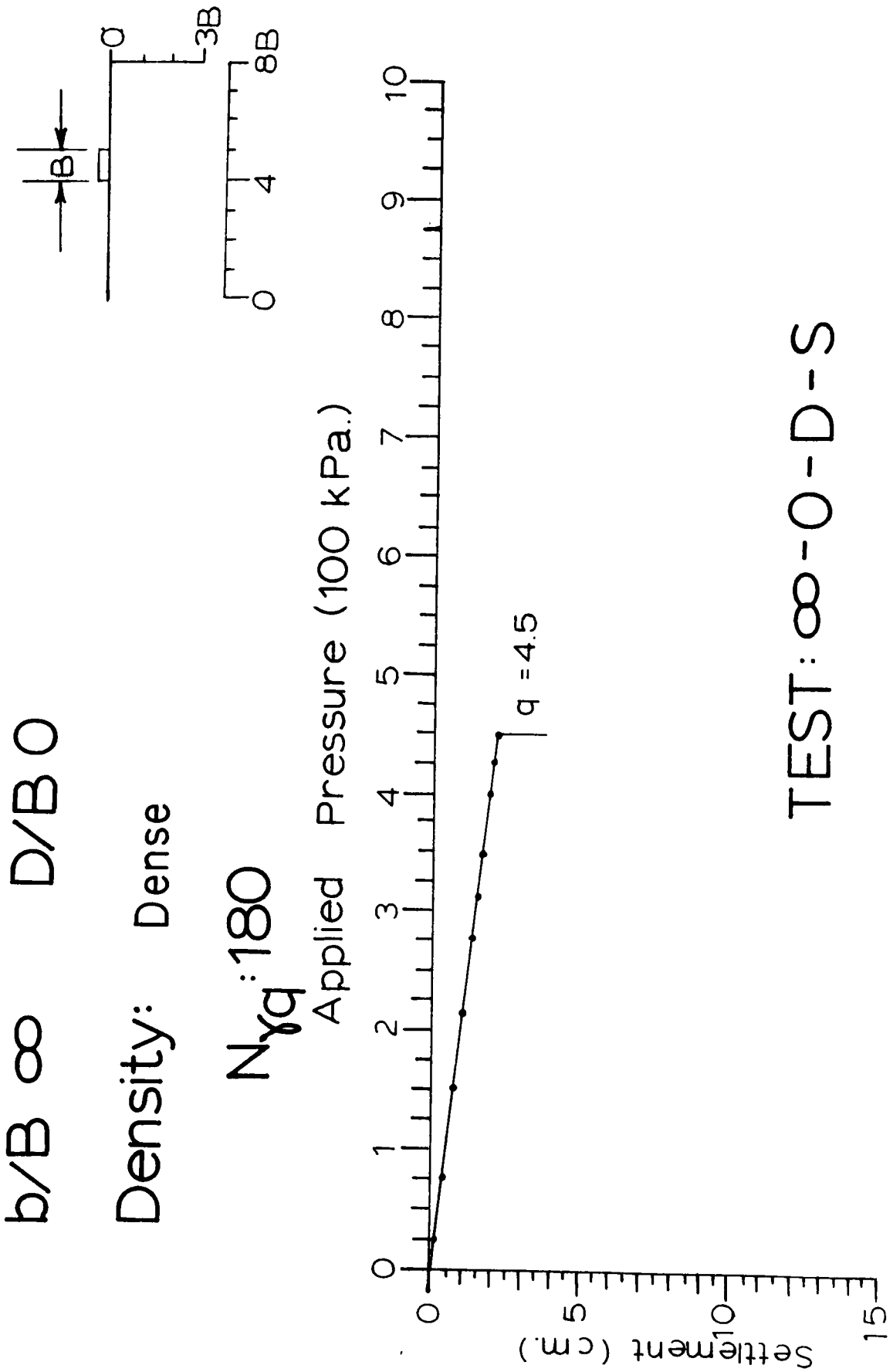
b/B ∞
D/B 0
Density: Dense
$N_{\gamma q}$: 180
B
0
3B
8B
0
4
Applied Pressure (100 kPa.)
0
1
2
3
4
5
6
7
8
9
10
q = 4.5
TEST: ∞-0-D-S
Settlement (cm.)
0
5
10
15

Figure 6.127

CHAPTER VII

DISCUSSION

7.1 Introduction

This chapter, dealing with the test results, is divided into four parts: first, the source of experimental error; second, the results of the testing program; third, the comparison of the present test results with existing theories and experimental studies; and finally, establishing a mathematical expression for the test results.

7.2 Sources of Experimental Error

7.2.1 General

The test results given in Chapter VI are the result of careful testing procedures. The equipment was operated according to the guidelines set down in Chapters IV and V in order to ensure that the results would not be influenced by external factors. The measurements show that all steps have been carried out correctly.

The only source of possible experimental error seems to be related to the process of building up the sand beds. The aim of the sand raining process is to give as homogeneous a sand bed of uniform density as possible. Because of the air currents that are set up as the sand falls, the spreader can-

not yield densities that are exactly equal throughout the length and breadth of the box. This is inherent to the raining process. This section discusses the variation in density which was measured both within the confines of the box during any one test and from test to test.

7.2.2 Density

For any particular test, a statistical analysis of the variation in density is possible because of the large number of density measurements which were made for each test. From the tables of Chapter VI, it can be seen that the density control for each test was excellent; the standard deviation for any test is lower that 17 kg/m^3 for the compact sand and 11 kg/m^3 for the dense sand.

For each test, the mean of the density measurements is considered to be representative of the state of the particular soil. Two states of density are recognized: compact and dense. The compact state is represented by tests on sands of an average density of between 1490 and 1550 kg/m^3. The average density of sands in the dense state is between 1590 and 1620 kg/m^3. The variation of 60 kg/m^3 in the compact state is larger than the variation of 30 kg/m^3 in the dense state. This can be explained by the performance of the raining device. To obtain high densities, the spreader drum is set at its lowest rotating speed, thereby yielding a low intensity of sand fall. It is easy to obtain a fairly uniform density

in dense sand because the sand is deposited in very thin uniform layers and the density is relatively independent of the height of fall of the sand.

As shown in Figure 4.29, lower densities are greatly influenced by the rotating speed of the drum and the height of fall; proper control of these variables is more critical for compact sand than for dense sand. When spreading compact sand, the height of fall and the rotating speed of the drum has to be adjusted throughout the building up of the sand beds. This is not necessary in the dense state where the height of fall has less influence and only one drum rotation speed is necessary.

Figure 7.1a) shows the average density for each footing location in the compact state; Figure 7.1b) represents the dense state. The overall average density is computed in Figures 7.2 and 7.3.

7.2.3 Reproducibility of Test Results

Four tests have been repeated: in compact sand two tests were repeated once, while in dense sand one test has been repeated twice and another was repeated once. The results are given in Figure 7.4 along with the percentage difference between the respective values. From this table, it can be seen that the results are reproducible to well within 10% and from this analysis it can be concluded that the experimental process that was designed for the present testing program is adequate.

Average Density at Each Test Location

Density in kg/m^3

A)Compact State

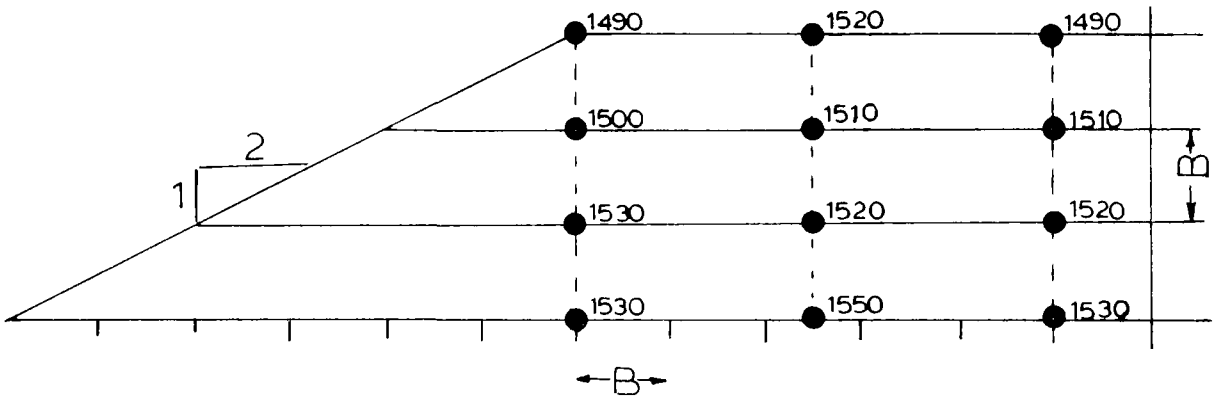

B) Dense State

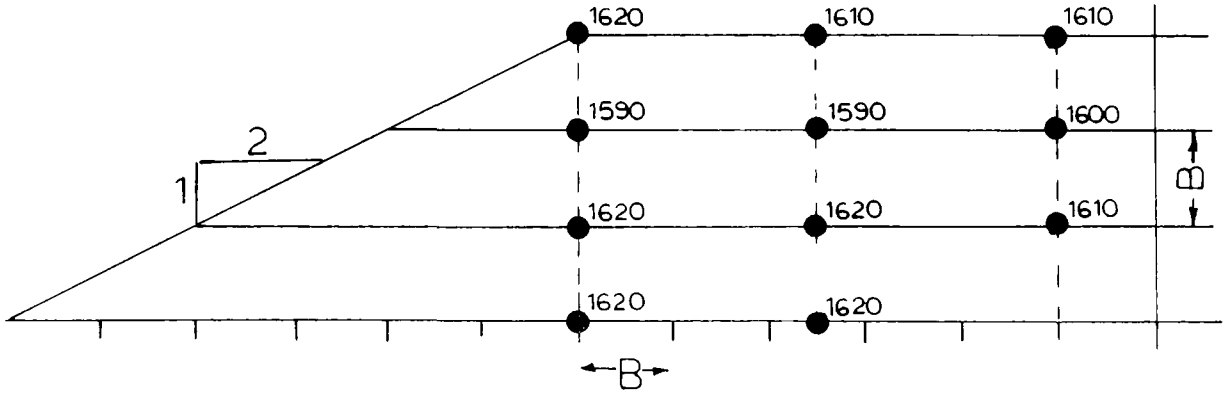

Figure 7.1

Representative Density

in Compact Sand

Test	Density kg/m^3
0 - 0 - C	1490
0 - 1 - C	1500
0 - 2 - C	1530
0 - 3 - C	1530
2.5 - 0 --C	1520
2.5 - 1 - C	1510
2.5 - 2 - C	1520
2.5 - 3 - C	1550
5 - 0 - C	1490
5 - 1 - C	1510
5 - 2 - C	1520
5 - 3 - C	1530
Overall average	1520
Standard deviation	17
Highest value	1550
Lowest value	1490

Figure 7.2

Representative Density

in Dense Sand

Test	Density kg/m^3
0 - 0 - D	1620
0 - 1 - D	1590
0 - 2 - D	1620
0 - 3 - D	1620
2.5 - 0 - D	1610
2.5 - 1 - D	1590
2.5 - 2 - D	1620
2.5 - 3 - D	1620
5 - 0 - D	1610
5 - 1 - D	1600
5 - 2 - D	1610
Overall average	1610
Standard deviation	11
Highest value	1620
Lowest value	1590

Figure 7.3

7.3 Test Results

7.3.1 General

As reported in Chapter VI, twenty-nine tests have been completed; twelve tests have been done in compact sand while eleven tests were carried out in dense sand. Furthermore, five tests were repeated, and one was performed on flat ground. In the dense sand, the test which was to be located at a horizontal distance of 5B (B = footing width) from the crest of the slope and at a vertical depth of 3B from the surface was not carried out because the two neighboring tests reached the capacity of the loading system, making it obvious that this particular test could not be taken to failure.

A general inspection of the results leads to the conclusion that the values are logical and realistic. The bearing capacities, the settlement and the surface movement all seem to agree with the expected footing behavior for their respective sand density and location. For example, the failure load was larger in dense sand than in compact sand; settlement was less in dense sand; and surface movements were larger in dense sand.

7.3.2 Trends

The bearing capacity values obtained from the tests are reported in Tables 7.5 and 7.6. This information is presented as contours of ultimate bearing pressure in Figures 7.7 and 7.8 for the compact and dense sand, respectively. It is in-

Results of Repeated Tests

Test Group #	Test #	$N_{\gamma q}$ value	Percentage difference
1	2.5-0-C	37	10%
	2.5-0-C-R	33	
2	2.5-1-C	80	5%
	2.5-1-C-R	76	
3	2.5-0-D	159	6%
	2.5-0-D-R.1	150	
	2.5-0-D-R.2	159	
4	5-0-D	180	0%
	5-0-D-R.1	180	

Figure 7.4

teresting to note that the contours are nearly horizontal in the compact sand, indicating that the proximity of the slope is not that significant. Depth of embedment plays an important role, however, since the capacity increases nearly ten fold as the footing located at the crest of the slope is placed deeper into the soil. In dense sand the contours are more steeply inclined, indicating that as the slope is approached there is a rapid decrease in capacity. Here, however, the depth of embedment is not nearly as important as in compact sand; the ultimate bearing capacity increases only threefold, from 250 kPa to 700 kPa at the crest of the slope as the depth increases from zero (surface footing) to 3B.

Multiplying the ultimate bearing capacity by two, and dividing by the unit weight and the footing width, the bearing capacity factors $N_{\gamma q}$ are determined for each test. The factors are given in Tables 7.5, and 7.6 and are plotted as contours in Figures 7.9 and 7.10. Because the footing size and the unit weight of the soil remain constant, the contours of Figures 7.9 and 7.10 have exactly the same shape as those of Figures 7.7 and 7.8.

7.3.3 Surface Movements

From the surface movement diagrams that are presented with the test results in Chapter VI, two general trends can be seen. In compact sand, no significant upward vertical movement of the sand occurs. A certain amount of downward

Ultimate Bearing Pressures in Compact Sand

Footing location	Density kg/m^3	Ultimate Bearing pressure kPa	$N_{\gamma q}$
0-0-C	1490	56	24
0-1-C	1500	163	70
0-2-C	1530	363	152
0-3-C	1530	550	230
2.5-0-C	1520	88	37
2.5-1-C	1510	188	80
2.5-2-C	1520	450	190
2.5-3-C	1550	600	250
5-0-C	1490	125	54
5-1-C	1510	225	95
5-2-C	1520	500	212
5-3-C	1530	700	250

Figure 7.5

Ultimate Bearing Pressures in Dense Sand

Footing location	Density kg/m^3	Ultimate Bearing pressures kPa	$N_{\gamma q}$
0-0-D	1620	250	99
0-1-D	1590	363	146
0-2-D	1620	525	208
0-3-D	1620	725	288
2.5-0-D	1610	400	159
2.5-1-D	1590	513	206
2.5-2-D	1620	825	328
2.5-3-D	1620	1000	397
5-0-D	1610	450	180
5-1-D	1600	550	221
5-2-D	1610	825	328

Figure 7.6

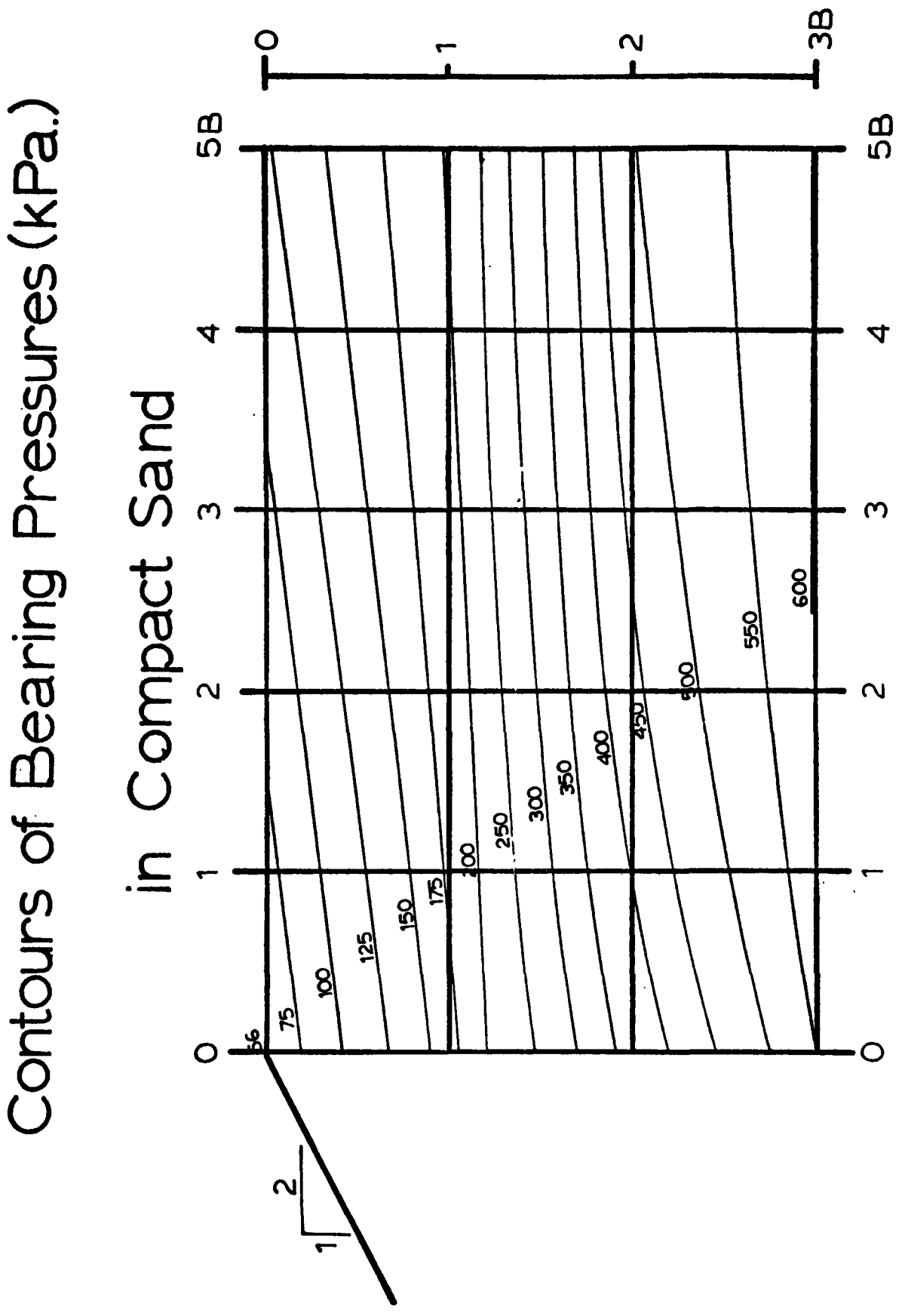
Contours of Bearing Pressures (kPa.)
in Compact Sand
0
1
2
3B
5B
4
3
2
1
0
56
75
100
125
150
175
200
250
300
350
400
450
500
550
600
2
1

Figure 7.7

Contours of Bearing Pressures (kPa.)

in Dense Sand

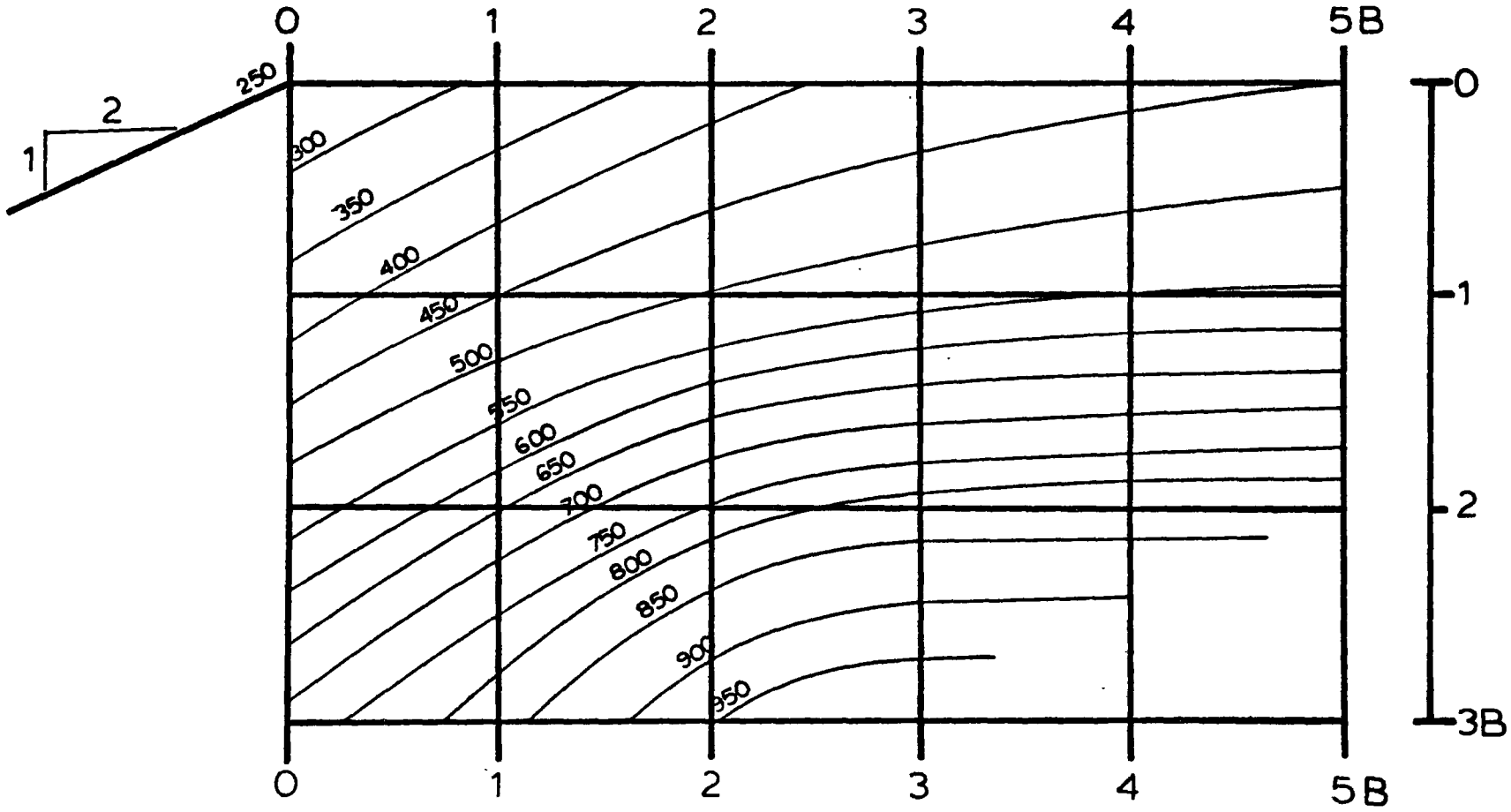

Figure 7.8

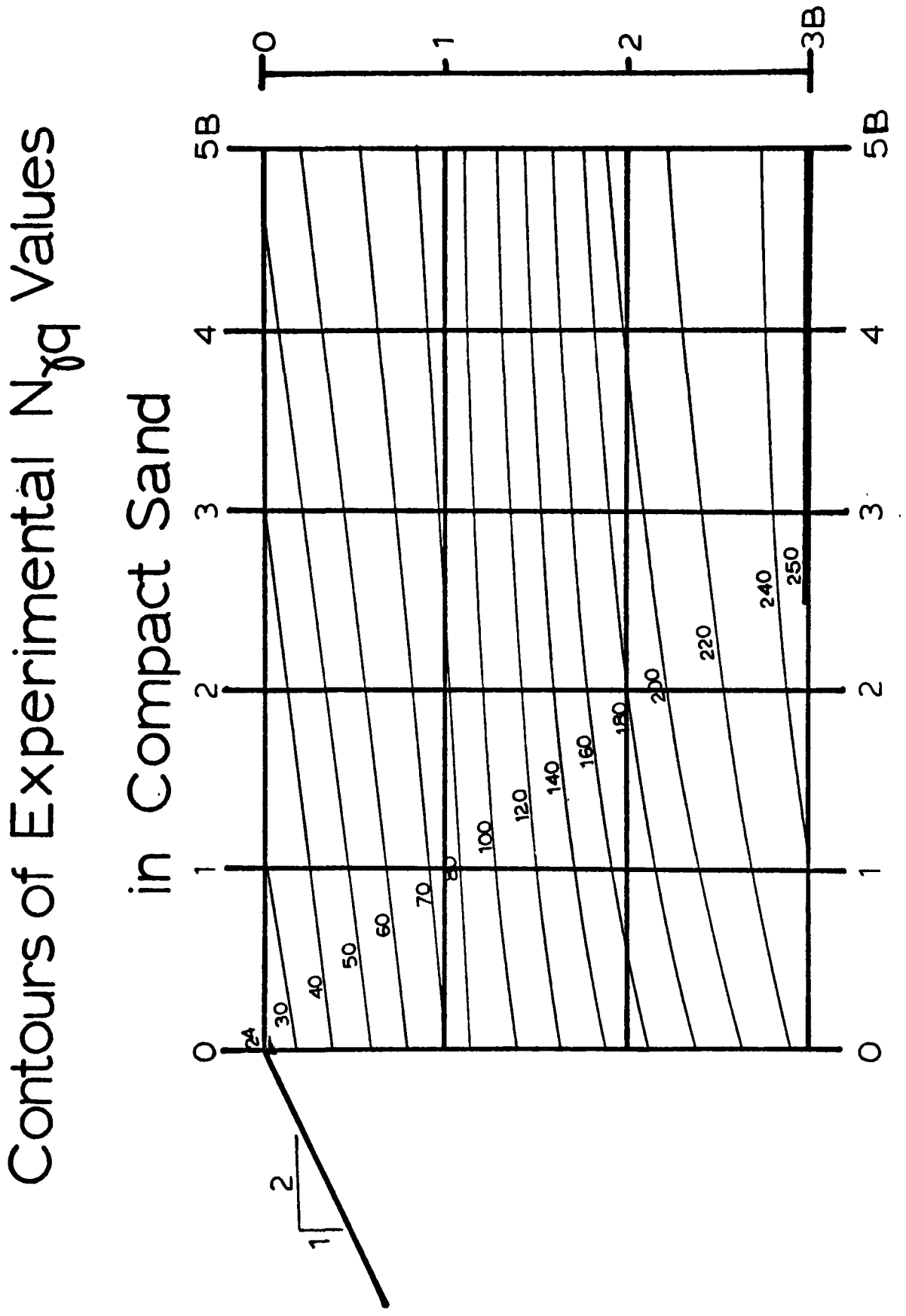
Contours of Experimental $N_{\gamma q}$ Values
in Compact Sand
0
1
2
3B
5B
4
3
2
1
0
24
30
40
50
60
70
80
100
120
140
160
180
200
220
240
250
2
1

Figure 7.9

Contours of Experimental $N_{\gamma q}$ Values in Dense Sand

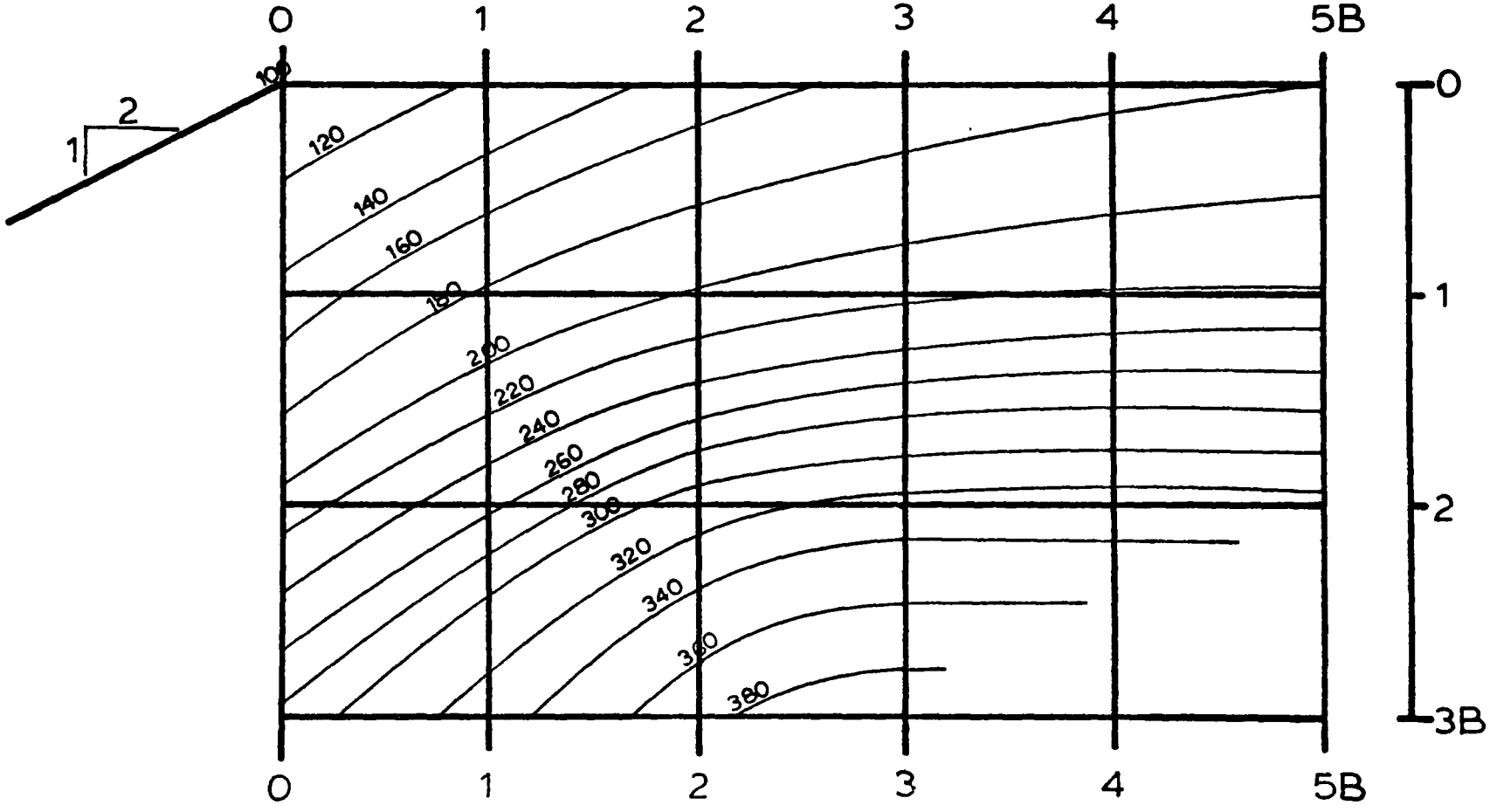

Figure 7.10

movement was obviously taking place in the vicinity of the footing. The tangential movement along the surface was small and not very important.

In dense sand, two situations occur. For footings embedded deeper than 1B, surface movements are similar to those found in compact sand: no significant vertical movement and very small tangential movement along the surface. For footings close to the surface, the results are different: upward vertical movement of the sand occurs progressively with load increase until failure. The tangential movement along the surface is also more significant in shallow dense sand tests than in compact sand or at depth in dense sand.

The formation of a definite shear surface as seen by the emergence of a shear plane was apparent only in dense sand and then only for footings located at the slope crest (Figure 7.11). This surface appeared long after failure was reached, after in fact, the footing had settled in excess of twice the settlement required to reach failure. The shear plane appeared on the sloped surface at a horizontal distance of approximately four footing widths from the crest.

7.3.4 Settlement

The table of Figure 7.12 summarizes the settlement which was measured at failure during each test. The settlement values are taken from the load settlement curves presented in Chapter VI.

Formation of the shear surface

Figure 7.11

A preliminary inspection of these settlement values shows them to be excessive. One explanation for the large values lies in the behavior of the sand under shear. All laboratory shear tests on the sand (Chapter VI) show that the material exhibits very high strains to failure. The strains at failure of the triaxial tests are shown on Figure 7.13.

The sand used in the experiments is a uniform angular silica sand. Holubec and D'Appolonia (1973) have shown that the strains at failure in a uniform angular sand are much higher than the strains at failure in either a uniform sand with round particles or a well graded granular material.

In spite of the large values of settlement the results are still useful. For one thing, it is possible to get an idea of the variation in settlement of the surface footings with distance from the slope. In compact sand, for footings loaded to 50 kPa, the settlements are:

Footing location b/B	Settlement (cm)
0	1.8
2.5	1.5
5	0.6

From these results it can be seen that a footing located at the slope crest will settle three times as much as a footing located at five footing widths from the crest of the slope (at the same bearing stress).

Analysis of Footing Settlements

Footing Location $\frac{b}{B}$	Footing Location $\frac{D}{B}$	At Ultimate Bearing Capacity	Average Normal Stress (kPa)	Triaxial Strain ε_f (%)
Compact				
0	0	1.9	6	5.1
0	1	2.7	16	5.2
0	2	1.5	36	5.4
0	3	3.1	55	5.7
2.5	0	1.4	9	5.1
2.5	0R	5.7	8	5.1
2.5	1	3.1	19	5.2
2.5	1R	3.1	18	5.2
2.5	2	2.1	45	5.5
2.5	3	3.0	60	5.7
5	0	2.2	12	5.2
5	1	5.3	22	5.3
5	2	4.4	50	5.6
5	3	5.6	60	5.7
Dense				
0	0	2.2	25	7.5
0	1	2.2	36	7.6
0	2	2.8	52	7.8
0	3	1.8	72	8.0
2.5	0	1.8	40	7.6
2.5	0R1	2.1	38	7.6
2.5	0R2	2.2	40	7.6
2.5	1	3.0	51	7.8
2.5	2	4.2	82	8.1
2.5	3	1.9	100	8.3
5	0	2.3	45	7.7
5	1	2.9	55	7.8
5	2	3.8	82	8.1

Figure 7.12

A similar comparison can be made for dense sand. The results show that a footing at the slope crest settles twice as much as a footing at five footing widths from the crest. This is illustrated in the following table for a bearing pressure of 250 kPa:

Footing location b/B	Settlement (cm)
0	2.8
2.5	1.5
5	1.4

The following table gives two examples of the variation in settlement with depth of embedment for footings at the crest of the slope.

In compact sand for 50 kPa		In dense sand for 250 kPa	
Footing Location $\frac{D}{B}$	Settlements (cm)	Footing Location $\frac{D}{B}$	Settlements (cm)
0	1.3	0	2.8
1	0.6	1	1.5
2	0.2	2	1.0
3	0.1	3	0.5

Typical Triaxial Test Results on Sand

Unit Weight kg/m^3	σ_3 kPa	σ_1/σ_3'	ε_f %	Φ°	$(\frac{\Delta V}{V})_f$	Remarks
1610	34.5	4.9	5.50	41.5°	0.042	
1620	172.5	4.8	7.00	41.0°	0.035	Dense
1620	345.0	4.6	9.00	40.0°	0.021	Sand
1630	552.0	4.4	9.60	39.0°	0.014	
1510	34.5	4.1	7.60	37.3°	0.032	
1510	172.5	4.1	7.61	37.2°	0.011	Compact
1520	345.0	4.0	10.80	36.8°	0.007	Sand
1530	552.0	3.9	14.70	36.2°	0.006	
1490	34.5	3.8	11.10	35.4°	0.028	
1450	172.5	3.7	13.20	35.2°	0.004	Loose
1470	345.0	3.7	16.30	35.0°	0.011	Sand
1480	552.0	3.6	19.20	34.5°	0.022	

Figure 7.13

7.4 Comparisons

7.4.1 Comparison with Theories

7.4.1.1 Choosing an Angle of Friction

The shearing resistance of a particular sand is usually defined by the angle of internal friction of the sand. This value is found from the Mohr-Coulomb envelope of triaxial and plane strain test results and by direct calculation of the shear box results.

During laboratory testing, the angle of internal friction is found to vary, depending on the following three factors: the type of test, the state of density of the sand and the magnitude of the normal stress. As reported in Chapter IV, the sand used in the present study was subjected to shear box, plane strain, and triaxial tests at different density states. A difficulty arises when attempting to relate the angle of shearing resistance in the laboratory to a particular footing test; even if the density is correct, there is a considerable variation in normal stress in the zone of soil which is mobilized by the footing and it is difficult to know what stress level to choose for the lab test.

Meyerhof suggested (DeBeer 1967) that the average normal stress along the failure plane should be used when choosing ϕ; this average stress would be approximately equal to 10% of the failure load. DeBeer found this approach to the problem to be satisfactory, but proposed an alternate expression to find the mean average normal stress:

$$\sigma_m = \frac{1}{1 + \tan^2\Phi} \circ \frac{1}{1 + \sin\Phi} \circ \frac{q + 3\mathbf{P}}{4} \qquad (7.2.2.1)$$

where q = failure load and $\mathbf{P}$ = the surcharge

Equation (7.2.2.1) can be converted to

$$\sigma_m = (1 - \sin\Phi)\ \frac{q + 3p}{4} \qquad (7.2.2.2)$$

or $$\sigma_m = [K_o]\ \frac{q + 3p}{4} \qquad (7.2.2.3)$$

If a realistic value of K_o is assessed to be of the order of 0.4 or 0.5 in Equation (7.2.2.3), it is obvious that the average normal stress along the failure plane will be approximately 10% of the failure load as postulated by Meyerhof.

Using the 10% rule and assuming that a slip surface forms in the sand, the average normal stress along the slip surface can be determined for each test (Figure 7.14). From the tables of Figure 7.14 it can be seen that the mean average normal stress values are all lower than 100 kPa.

Figures 4.18 through 4.24 (Mohr-Coulomb envelopes for the different types of laboratory test) show that for a normal stress of less than 100 kPa, the variation in Φ angle for a particular density is so small as to be negligeable. The relevent part of the Mohr-Coulomb envelope is almost a straight line in all cases.

Considering these observations, the proper Φ angles for both states of density for the tests are:

1- compact sand: $\Phi_t = 37°$

$\Phi_{t + 10\%} = 41°$

$\Phi_{SB} = 45°$

$\Phi_{PS} = 45°$

2- dense sand: $\Phi_t = 41°$

$\Phi_{t + 10\%} = 45°$

$\Phi_{SB} = 50°$

$\Phi_{PS} = 48°$

where: Φ_t is obtained from triaxial laboratory tests.

Φ_{SB} is obtained from shear box laboratory tests.

Φ_{PS} is obtained from plane strain laboratory tests.

$\Phi_{t + 10\%}$ is the value of the Φ angle found by triaxial test, but increased 10% for the "plane strain" condition as suggested by Meyerhof (1963).

It should be noted that the triaxial, shear box and plane strain friction angles are quite different from one another. Ideally it would be an advantage to represent each density state for the sand by a unique value of Φ, but this appears to be impossible. The next step is to see what variation there is in the theoretical $N_{\gamma q}$ values for a particular state of density given the variation in Φ.

The table of Figure 7.15 clearly illustrates the effect of the variation in Φ; the theoretical $N_{\gamma q}$ values of Giroud are compared for the four different friction angles which were measured by various means in the dense sand. It can be seen that $N_{\gamma q}$ varies as much as 710, that is from 390 to 1100 by

Approximate Mean Normal Stress Along

the Failure Surface

Test	Failure Pressure kPa	Mean Normal Stress kPa
0 - 0 - C	56	5.6
0 - 1 - C	163	16.3
0 - 2 - C	363	36.3
0 - 3 - C	550	55
2.5 - 0 - C	88	8.8
2.5 - 1 - C	188	18.8
2.5 - 2 - C	450	45
2.5 - 3 - C	600	60
5 - 0 - C	125	12.5
5 - 1 - C	225	22.5
5 - 2 - C	500	50
5 - 3 - C	600	60
0 - 0 - D	250	25
0 - 1 - D	363	36.3
0 - 2 - D	525	52.5
0 - 3 - D	725	72.5

Figure 7.14

Approximate Mean Normal Stress Along

the Failure Surface

Test	Failure Pressure kPa	Mean Normal stress kPa
2.5 - 0 - D	400	40
2.5 - 1 - D	513	51.3
2.5 - 2 - D	825	82.5
2.5 - 3 - D	1000	100
5 - 0 - D	450	45
5 - 1 - D	550	55
5 - 2 - D	825	82.5

Figure 7.14 (cont'd)

Giroud's $N_{\gamma q}$ values in Dense Sand

H	V	Experimental $N_{\gamma q}$	$\Phi = 41°$ triaxial	$\Phi = 45°$ triaxial + 10%	$\Phi = 48°$ plane strain	$\Phi = 50°$ shear box
0	0	99	25	50	90	130
0	1	146	90	160	270	340
0	2	208	215	350	520	650
0	3	288	375	600	850	1200
2.5	0	159	60	80	130	180
2.5	1	206	160	240	360	480
2.5	2	328	310	500	690	900
2.5	3	397	530	850	1090	1400
5	0	180	70	120	200	250
5	1	221	220	320	500	610
5	2	328	390	510	910	1100

H = horizontal

V = Vertical

Figure 7.15

a factor of 3 . $N_{\gamma q}$ is also strongly Φ dependent for the compact sand.

This problem can be looked at in another way. In the tables of Figure 7.16 and 7.17, Giroud's theoretical $N_{\gamma q}$ values are compared with the experimental $N_{\gamma q}$ results. In some footing locations, one particular Φ angle gives a better agreement than does any other Φ angle; in other locations a second Φ angle is better. For example, at the crest of a slope of compact sand, Φ triaxial + 10% gives a $N_{\gamma q}$ value within 4% of the actual measured value; at maximum depth, Φ triaxial (without adjustment) comes closest to the test results, but, nevertheless, overpredicts $N_{\gamma q}$ based on experiment by 30%. The same sort of comparison in dense sand indicates plane strain to be best at the crest of the slope (9% off).

In order to compare the test results with theory, it is necessary, then, to consider all possible values of Φ to represent the sand.

7.4.1.2 Comparison at the Crest of the Slope

This Section compares the experimental results at the slope crest with the $N_{\gamma q}$ values from the theories presented in Chapter II. The experimental $N_{\gamma q}$ values are 24 for the compact sand and 99 for the dense sand. Figure 7.18 gives all the theoretical values for the different Φ angles which are supposed to represent the two states of density. (These

Location of Footings		Experimental $N_{\gamma q}$	$\frac{N_{\gamma q}\text{ (Giroud's Theoretical)}}{N_{\gamma q}\text{ (Experimental)}}$ for compact sand			
H	V		$\Phi = 37°$ triaxial	$\Phi = 41°$ triaxial + 10%	$\Phi = 45°$ plane strain	$\Phi = 45°$ shear box
0	0	24	.63	1.04	2.08	2.08
0	1	70	.86	1.29	1.57	1.57
0	2	152	1.02	1.41	2.30	2.30
0	3	230	1.28	1.63	2.61	2.61
2.5	0	37	.73	1.61	2.16	2.16
2.5	1	80	1.25	1.61	2.50	2.50
2.5	2	190	1.26	1.63	2.63	2.63
2.5	3	250	1.31	2.12	3.40	3.40
5	0	54	.93	1.30	2.31	2.31
5	1	95	1.14	1.84	3.00	3.00
5	2	212	1.13	1.84	2.41	2.41
5	3	250	1.32	2.12	4.08	4.08

Ratio of $N_{\gamma q}$ (Giroud's theoretical) to $N_{\gamma q}$ (experimental) for compact sand

Figure 7.16

Location of Footings		Experimental $N_{\gamma q}$	$\frac{N_{\gamma q}\text{ (Giroud's Theoretical)}}{N_{\gamma q}\text{ (Experimental)}}$ for dense sand			
H	V		$\Phi = 41°$ triaxial	$\Phi = 45°$ triaxial + 10%	$\Phi = 48°$ plane strain	$\Phi = 50°$ shear box
0	0	99	.25	.51	.91	1.31
0	1	146	.62	1.10	1.85	2.33
0	2	208	1.03	1.68	2.50	3.13
0	3	288	1.30	2.08	2.95	4.17
2.5	0	159	.38	.50	.79	1.13
2.5	1	206	.78	1.17	1.77	2.33
2.5	2	328	.95	1.52	2.09	2.74
2.5	3	397	1.33	2.14	2.75	3.53
5	0	180	.39	.69	1.11	1.39
5	1	221	1.00	1.47	2.24	2.76
5	2	328	1.19	1.55	2.77	3.35

Ratio of $N_{\gamma q}$ (Giroud's theoretical) to $N_{\gamma q}$ (experimental) for dense sand

Figure 7.17

values were found using linear interpolation and, in some cases, extrapolation).

As seen in this figure, favorable comparison between theory and experiment can be found fairly readily in the compact sand. Meyerhof's value for Φ = 45; Mizuno's for Φ = 41° and Giroud's for Φ = 41° are close (within 4%) to the actual experimental result of 24. The other theoretical values range anywhere from 6 for Bowles (1975) and Φ = 37° (which is four times smaller than the actual result) to 200 for Bowles (1977) and Φ = 45° (which is 8 times larger than the actual result).

In the case of dense sand, only one theoretical result is equal to the experimental result of 99; this agreement is for Chen's theory assuming Φ = 50°. Other theories have values which are within 10% of the actual experimental result, for example Kovalev for Φ = 50°, Giroud for Φ = 48°, Chen for Φ = 48° and Bowles (1977) for Φ = 41°. The theoretical values representing dense sand vary from 9 for Bowles (1975) and Φ = 41° to 320 for Bowles (1977) and Φ = 50°.

A better test of the theories is the ability with which they predict $N_{\gamma q}$ in both the compact and dense sand, in other words which theory best takes into account the change in Φ. The logical way to make this test of the theories is to fix the way in which Φ is measured (to the triaxial test, for example). The important conclusion to be drawn (given the constraint of only one laboratory procedure) is the fact

$N_{\gamma q}$ Values at the Crest of a 2:1 Slope

Theories	Compact Sand							
	$\Phi_t = 37°$	%	$\Phi_t + 10\% = 41°$	%	$\Phi_{PS} = 45°$	%	$\Phi_{SB} = 45°$	%
Meyerhof (1957)	13	-46	18	-25	24	0	24	0
Mizuno (1960)	17	-29	24	0	31	+29	31	+29
Kovalev (1964)	38	+50	54	+125	70	+192	70	+192
Brinch Hansen (1970)	15	-37	21	-12	28	+17	28	+17
Giroud (1972)	15	-37	25	+4	50	+108	50	+108
Absi (1972)	8	-66	11	-54	14	-42	14	-42
Chen (1974)	27	+12	50	+108	72	+200	72	+200
Bowles (1975)	6	-75	9	-62	13	-46	13	-46
Bowles (1977)	52	+117	90	+275	200	+733	200	+733
Experimental Results	24							

Figure 7.18

$N_{\gamma q}$ Values at the Crest of a 2:1 Slope

Theories	Dense Sand							
	$\Phi_t = 41^0$	%	$\Phi_t + 10\% = 45^0$	%	$\Phi_{PS} = 48^0$	%	$\Phi_{SB} = 50^0$	%
Meyerhof (1957)	18	-82	24	-76	28	-72	30	-70
Mizuno (1960)	24	-76	31	-69	36	-64	39	-61
Kovalev (1964)	54	-46	70	-30	81	-19	89	-11
Brinch Hansen (1970)	21	-79	28	-72	33	-67	36	-64
Giroud (1972)	25	-75	50	-50	90	-10	130	+30
Absi (1972)	11	-89	14	-86	17	-83	18	-96
Chen (1974)	50	-50	72	-28	90	-10	100	0
Bowles (1975)	9	-91	13	-87	15	-85	18	-82
Bowles (1977)	90	-10	200	+100	270	+170	320	+220
Experimental Results	100							

Figure 7.18 (cont'd)

that no single theory can predict $N_{\gamma q}$ for both the dense and compact sand to within a reasonable margin of error, say $\pm$ 20%.

In fact, only three possible combinations are within $\pm$ 50% for both density states; these are Kovalev and Chen using Φ_t and Giroud with $\Phi_{t + 10\%}$. The errors for each of these cases are as follows:

Laboratory Procedure	Theory	% Error in Compact Sand	% Error in Dense Sand
Φ_t	Chen	+10%	-50%
Φ_t	Kovalev	+50%	-46%
$\Phi_{t + 10\%}$	Giroud	4%	-50%

Another way to make the test of the teories is to accept the most appropriate laboratory procedure to measure Φ. This brings the margin of error to almost $\pm$ 10% in two cases. These are:

Theory	% Error in Compact Sand	% Error in Dense Sand
Giroud	-10%	+4%
Chen	0%	+12%

However, it is necessary to use the plane strain Φ for the dense sand and $\Phi_{t + 10\%}$ for the compact sand in Giroud's

case; in Chen's case the shear box and triaxial Φ values must be used in the dense and compact sand respectively.

How the engineer is expected to know when to use which laboratory test with which theory for a particular density is not clear. However, it is important to note that the same laboratory procedure cannot be used in both compact and dense sand with either Chen's or Giroud's theories. It can, therefore, be concluded that in the case of bearing capacity factor $N_{\gamma q}$ for a footing located at the slope crest, the comparison between theories and reality is not satisfactory. A large scatter of theoretical $N_{\gamma q}$ values is found to exist, and no single theory seems to offer a reliable answer to the bearing capacity of footings located at the slope crest.

7.4.1.3 Comparison in the Mass

Comparison between theory and experiment for the bearing capacity of a footing located at the slope crest is presented in the preceeding Section. Here the experimental values at other footing locations are compared with the four theories that provide $N_{\gamma q}$ values for footings at any location in the sand mass. The four theories are those of Meyerhof, Giroud, Bowles (1975) and Bowles (1977).

One way of making the comparisons is to superimpose the contours of experimental $N_{\gamma q}$ values on the theoretical contours. In the case of compact sand this is done for Φ values of 35° and 40°. Only two Φ values are used in order to limit

the presentation to a manageable size; even then, eight figures are required, Figures 7.19 to 7.26. From these Figures 7.19 and 7.20, it can be seen that the Meyerhof values are close to the experimental results to a depth of 1B for Φ = 35°. Beyond a depth of 1B the theoretical and the experimental contours do not have the same trend. The experimental contours are almost horizontal, whereas Meyerhof's results for both Φ = 35° and Φ = 40° show that the presence of the slope has a major influence in that the theoretical contours are steeply inclined. At certain positions the experimental results are quite close to the theoretical predictions, for instance: the value of $N_{\gamma q}$ = 37 at footing location 2.5 - 0 and of $N_{\gamma q}$ = 210 at footing location 5 - 2 are equal to the theoretical predictions for their respective location for Φ = 35°. The value of $N_{\gamma q}$ = 152 at footing location 0 -2 is approximately equal (within 5%) to the theoretical value for that particular position, for Φ = 40°.

Figures 7.21 and 7.22 give the experimental contour lines in compact sand superimposed on Giroud's theoretical contour lines for Φ = 35° and 40°. The shape of the experimental and the theoretical curves for Φ = 35° match rather well. The theoretical curves are as smooth as the experimental curves. The magnitude of Giroud's $N_{\gamma q}$ values are smaller than the experimental values for Φ = 35° to a depth of 1B. Beyond this depth the values seem to agree more closely. In the case of the Φ = 40° graph, the theoretical

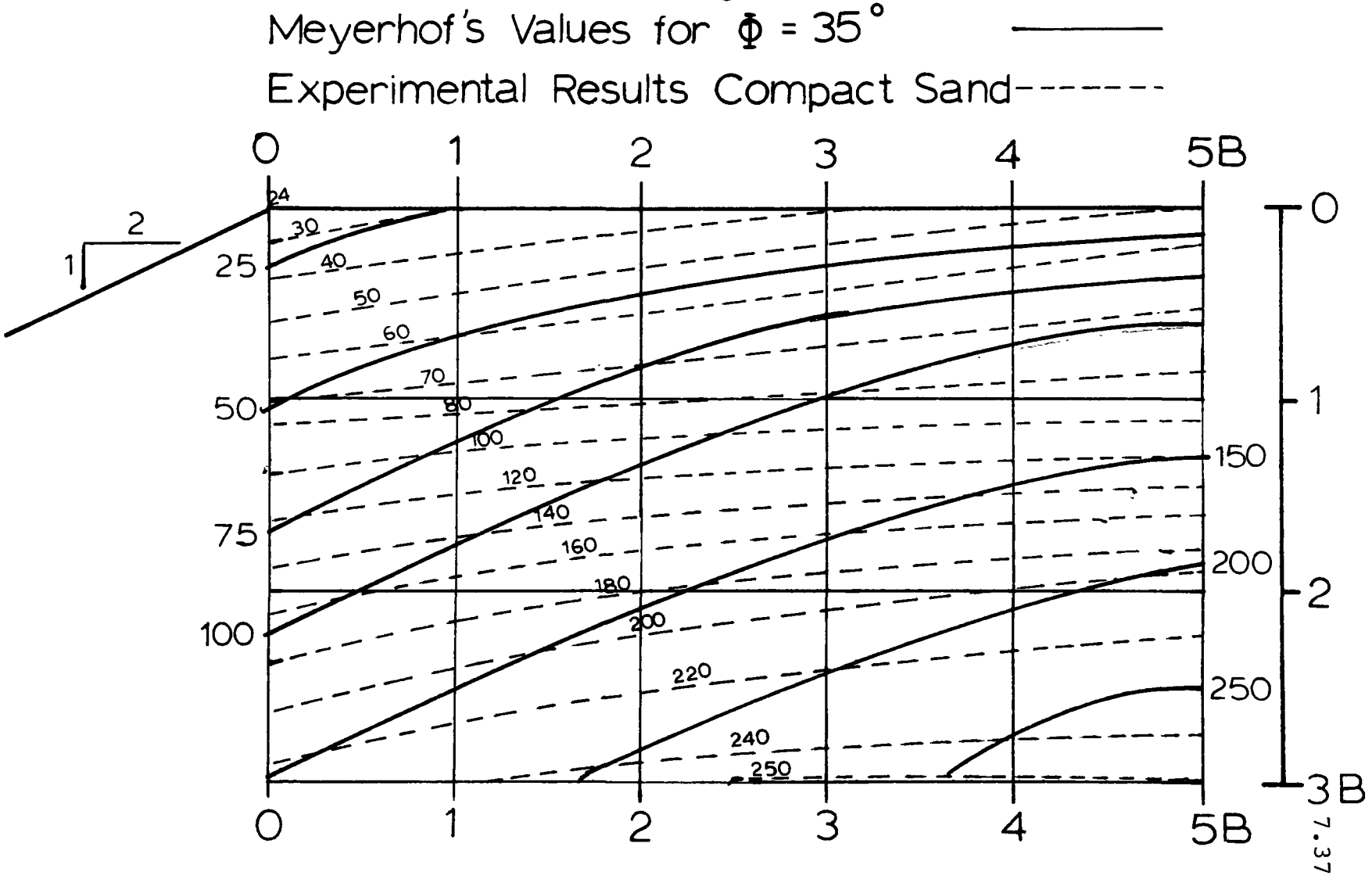
Comparison with Meyerhof's Theory
Meyerhof's Values for Φ = 35°
Experimental Results Compact Sand
0
1
2
3
4
5B
2
1
24
30
40
50
60
70
80
100
120
140
160
180
200
220
240
250
25
50
75
100
150
200
250
0
1
2
3B

Figure 7.19

Comparison with Meyerhof's Theory

Meyerhof's Values for $\Phi = 40°$ ——————

Experimental Results Compact Sand - - - - -

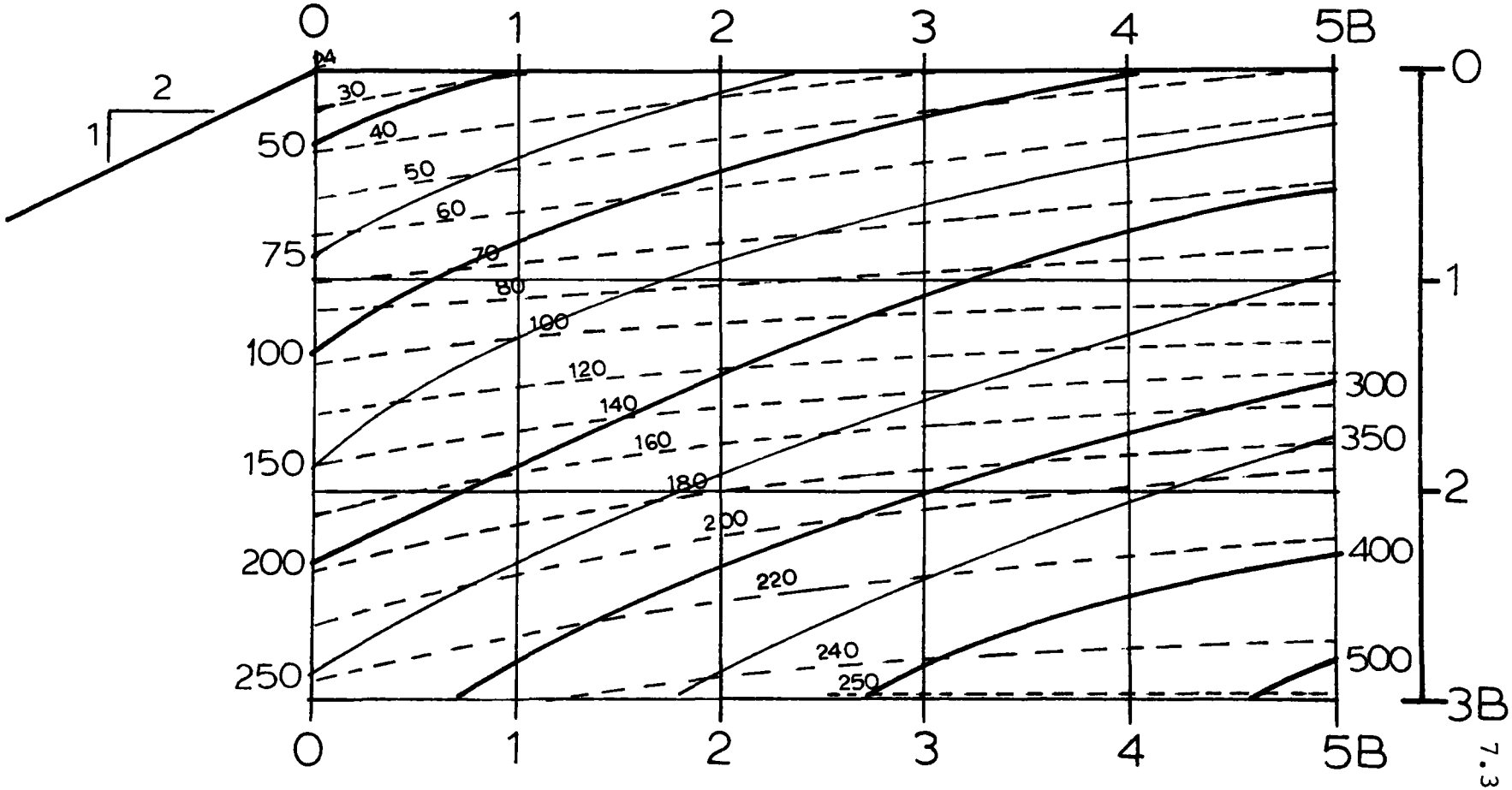

Figure 7.20

Comparison with Giroud's Theory

Giroud's Values for $\Phi = 35°$ ——————

Experimental Results Compact Sand - - - - - -

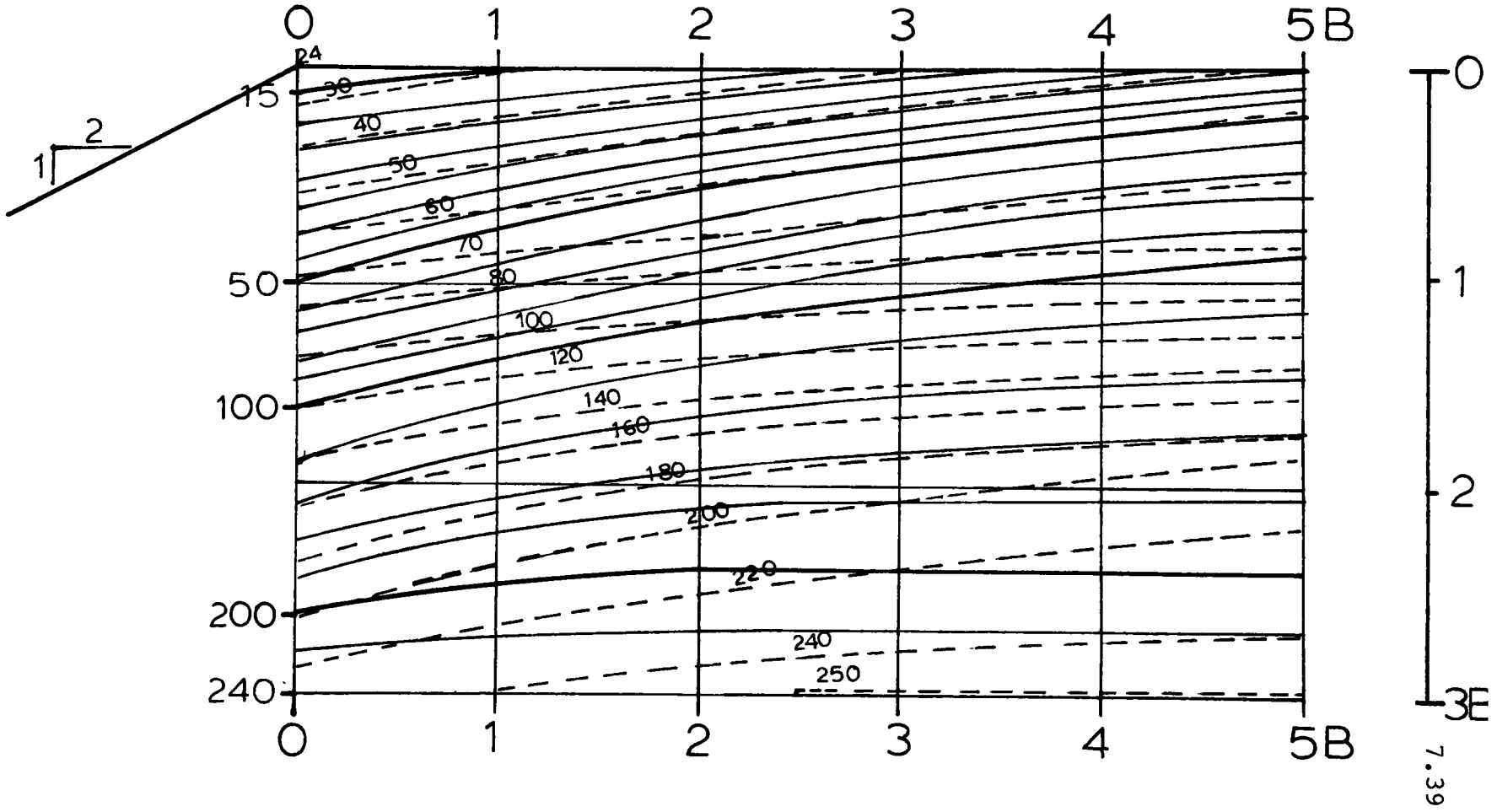

Figure 7.21

Comparison with Giroud's Theory

Giroud's Values for $\Phi = 40°$ ——————

Experimental Results Compact Sand - - - - - - - -

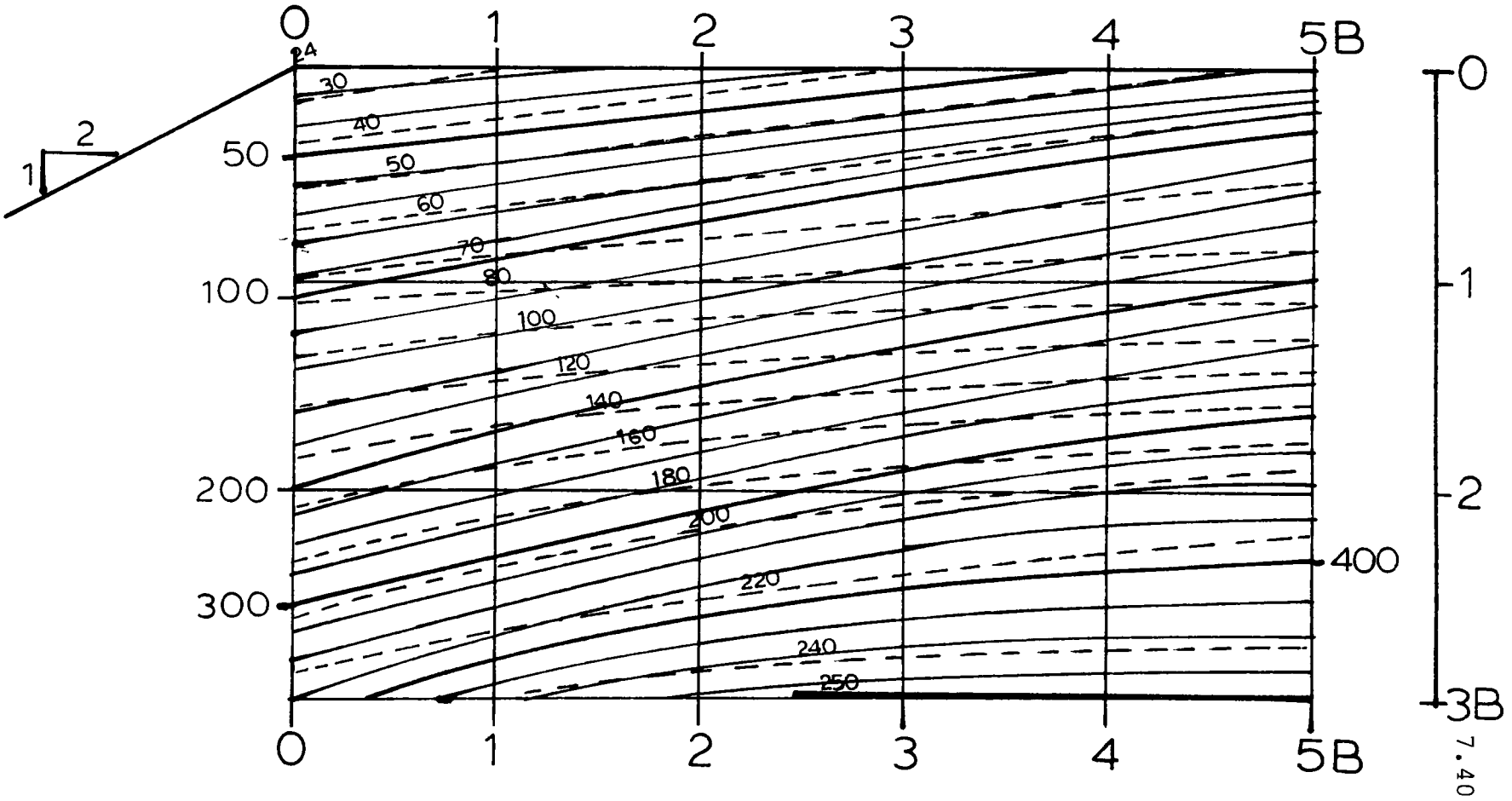

Figure 7.22

Comparison with Bowles'(1975) Theory

Bowles'(1975) Values for $\Phi = 35°$ ——————

Experimental Results Compact Sand - - - - - - -

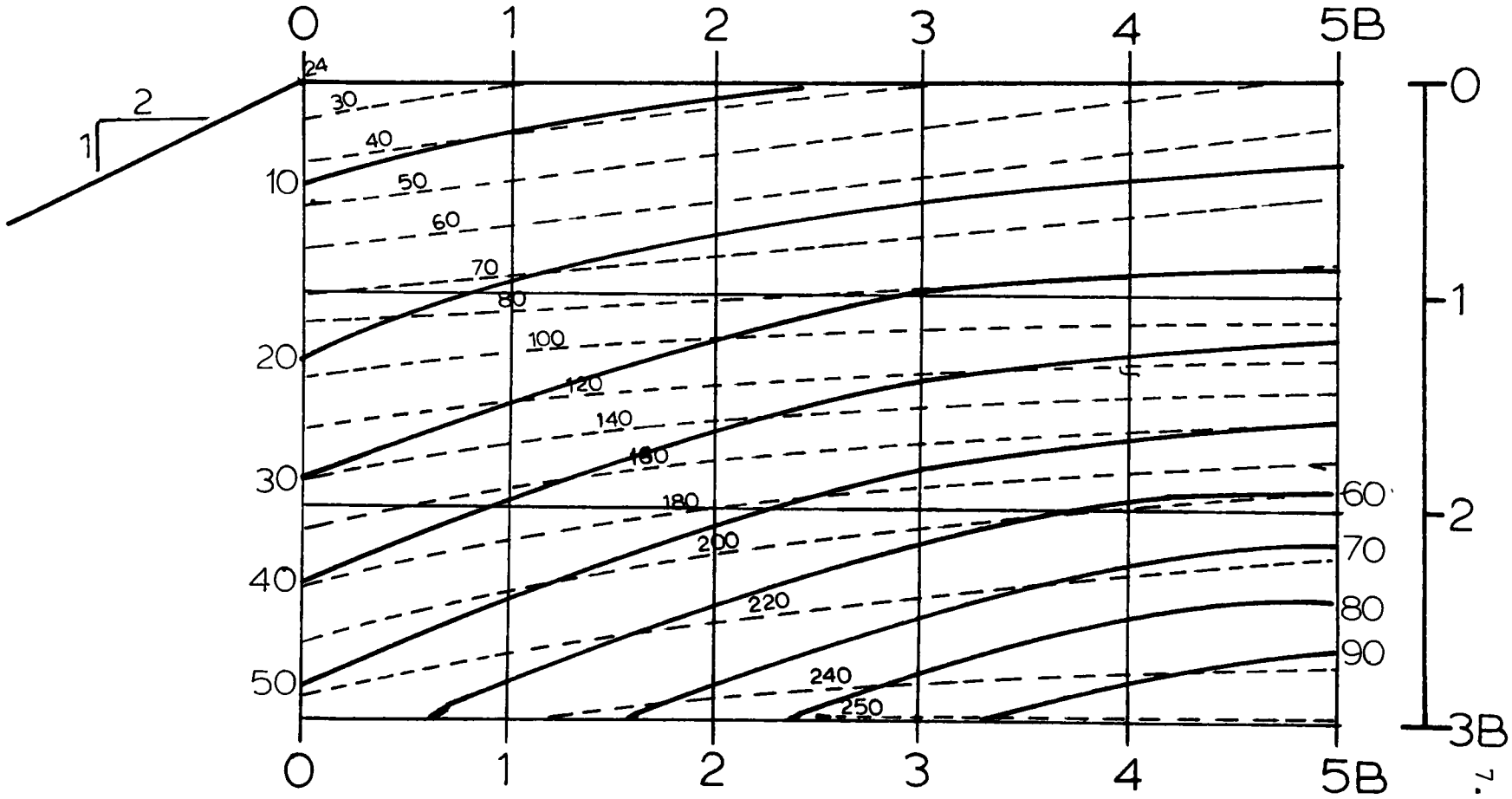

Figure 7.23

Comparison with Bowles'(1975) Theory

Bowles'(1975) Values for $\Phi = 40°$ ————

Experimental Results Compact Sand - - - - - - -

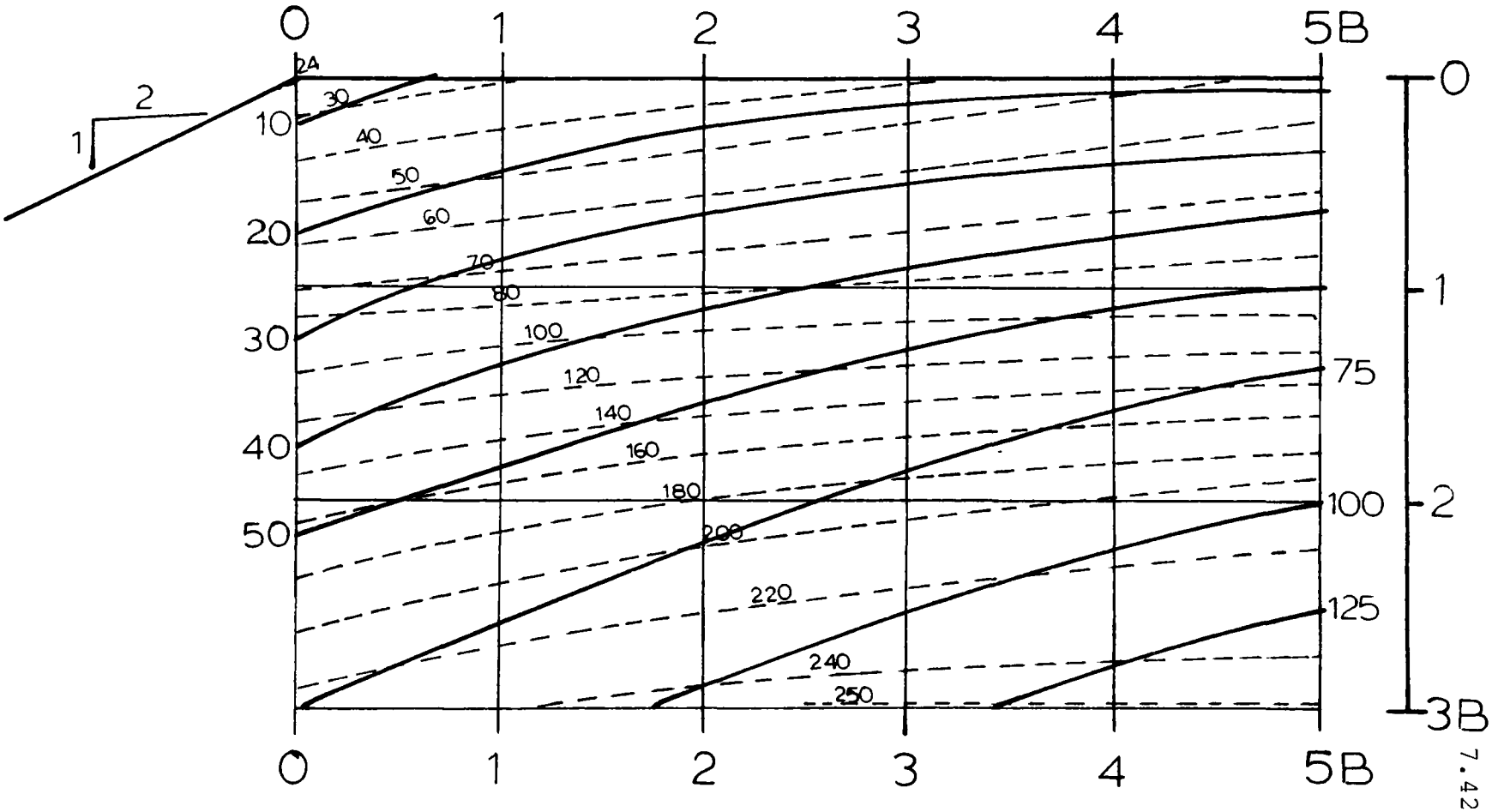

Figure 7.24

Comparison with Bowles' (1977) Theory

Bowles' (1977) Values for $\Phi = 35°$ ——————

Experimental Results Compact Sand - - - - - - -

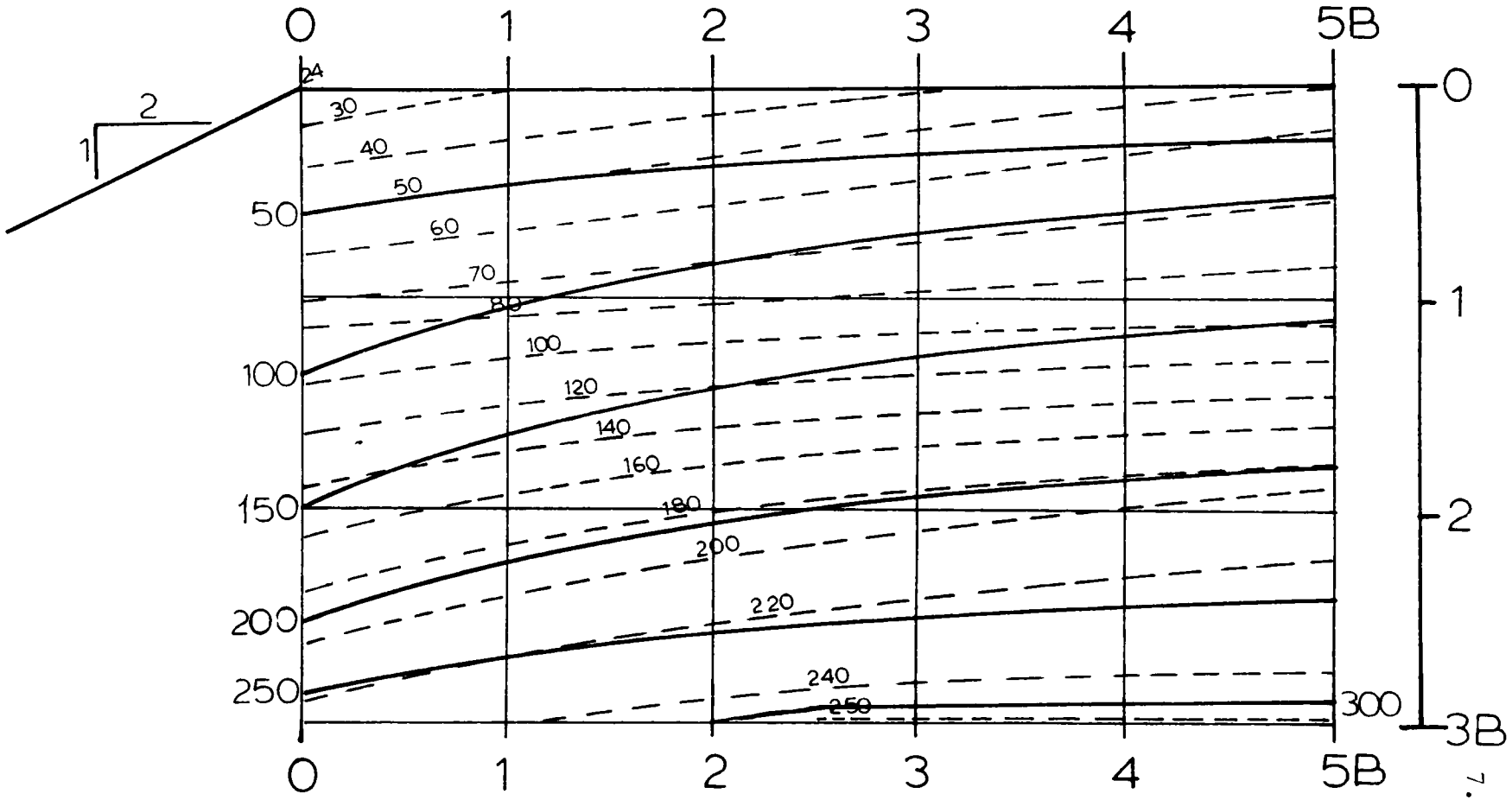

Figure 7.25

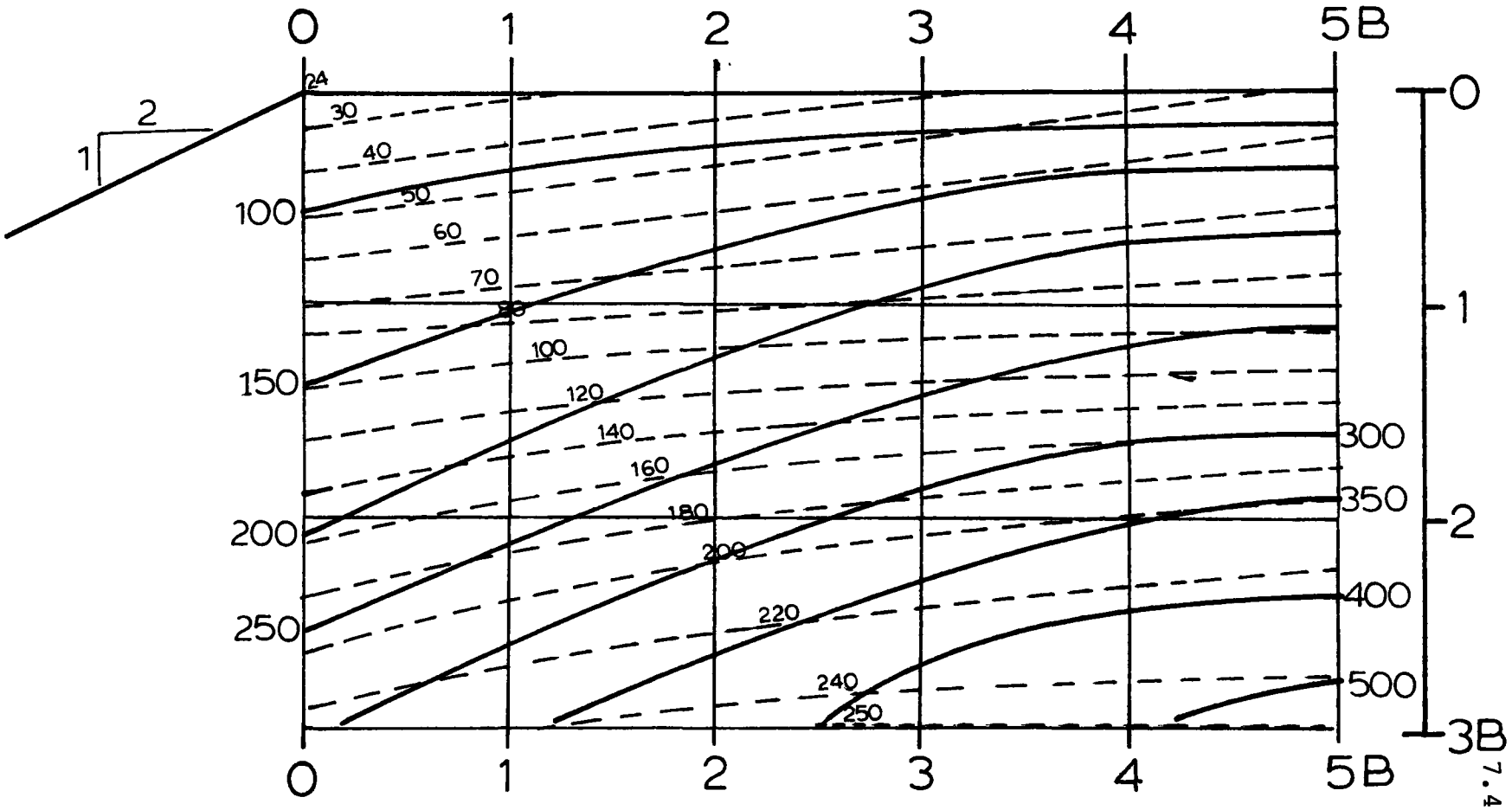
Comparison with Bowles' (1977) Theory
Bowles'(1977) Values for Φ = 40°
Experimental Results Compact Sand
0
1
2
3
4
5B
2
1
24
30
40
50
60
70
80
100
120
140
160
180
200
220
240
250
100
150
200
250
300
350
400
500
0
1
2
3B

Figure 7.26

values are close to the experimental values to a depth of 1B. Beyond this depth, the theoretical values increase rapidly and are a long way from the experimental results.

This type of analysis was also carried out for the theories proposed by Bowles (1975) and Bowles (1977) (Figures 7.23, 7.24, 7.25 and 7.26). In the case of Bowles (1975), the theoretical values for $\Phi = 35^\circ$ and $\Phi = 40^\circ$ are much smaller than the experimental results. The pattern of the theoretical curves does not match the experimental curves except for the portions beyond 2.5B from the slope crest and within a depth of 1B for $\Phi = 40^\circ$.

For Bowles (1977), the theoretical values for $\Phi = 35^\circ$ are quite close to the experimental results; for instance, the $N_{\gamma q} = 50$ contours are almost coincident. Between depths of 1B and 2B, the shape of the theoretical and the experimental curves and $N_{\gamma q}$ values do not agree. Beyond a depth of 2B, theory and experiment are in closer agreement. For Bowles (1977), no similarity exists between the experimental curves and theoretical contours for $\Phi = 40^\circ$.

An identical procedure is used to compare the experimental results in dense sand in Figures 7.27 to 7.31. The dense sand experimental contours have been superimposed on the theoretical curves of Meyerhof for $\Phi = 45^\circ$, of Giroud for $\Phi = 45^\circ$ and $\Phi = 50^\circ$ and of Bowles (1975) and Bowles (1977) for $\Phi = 45^\circ$. The Meyerhof curves match the experimental contours to a depth of 1B. The magnitude of the $N_{\gamma q}$ values

is also of the same order. Beyond this depth, however, no close relationship exists between theory and experiment, the experimental results being much smaller than the theoretical values.

For the Giroud case of $\Phi = 45^{\circ}$, the experimental and theoretical results do not agree. The theoretical curves are more nearly horizontal than the experimental contours. The experimental contours show that the slope has much greater influence than that which is predicted by theory. Total disagreement exists between the experimental contours and the theoretical contours for $\Phi = 50^{\circ}$. The contours do not follow the same trend. Furthermore, the experimental results are considerably smaller than the theoretical values.

The theoretical contours of Bowles (1975) for $\Phi = 45^{\circ}$ follow a trend similar to the experimental results, but the experimental results are much higher than the theoretical values. For the case of Bowles (1977) for $\Phi = 45^{\circ}$, the experimental results are smaller than the theoretical values. The shape of the contours is also in poor agreement.

As shown from this comparison, there is very little overall agreement between theory and experiment. Some of the experimental results do compare with theoretical values at particular locations in the soil mass, but no theory seems to offer results which are even approximately the same as the experimental results throughout the soil mass.

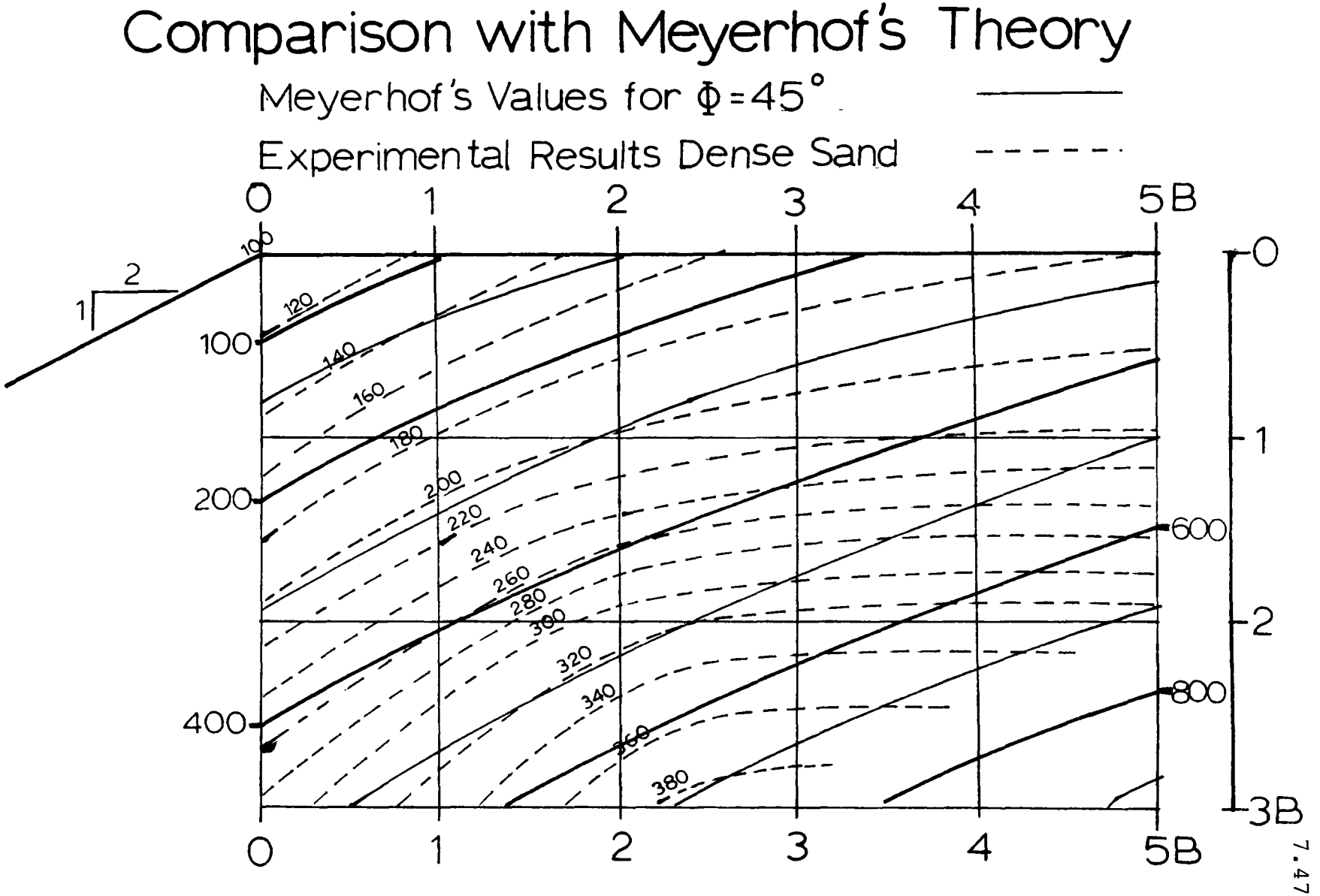
Comparison with Meyerhof's Theory
Meyerhof's Values for Φ=45°
Experimental Results Dense Sand
0
1
2
3
4
5B
2
1
100
200
400
120
140
160
180
200
220
240
260
280
300
320
340
360
380
600
800
0
1
2
3B

Figure 7.27

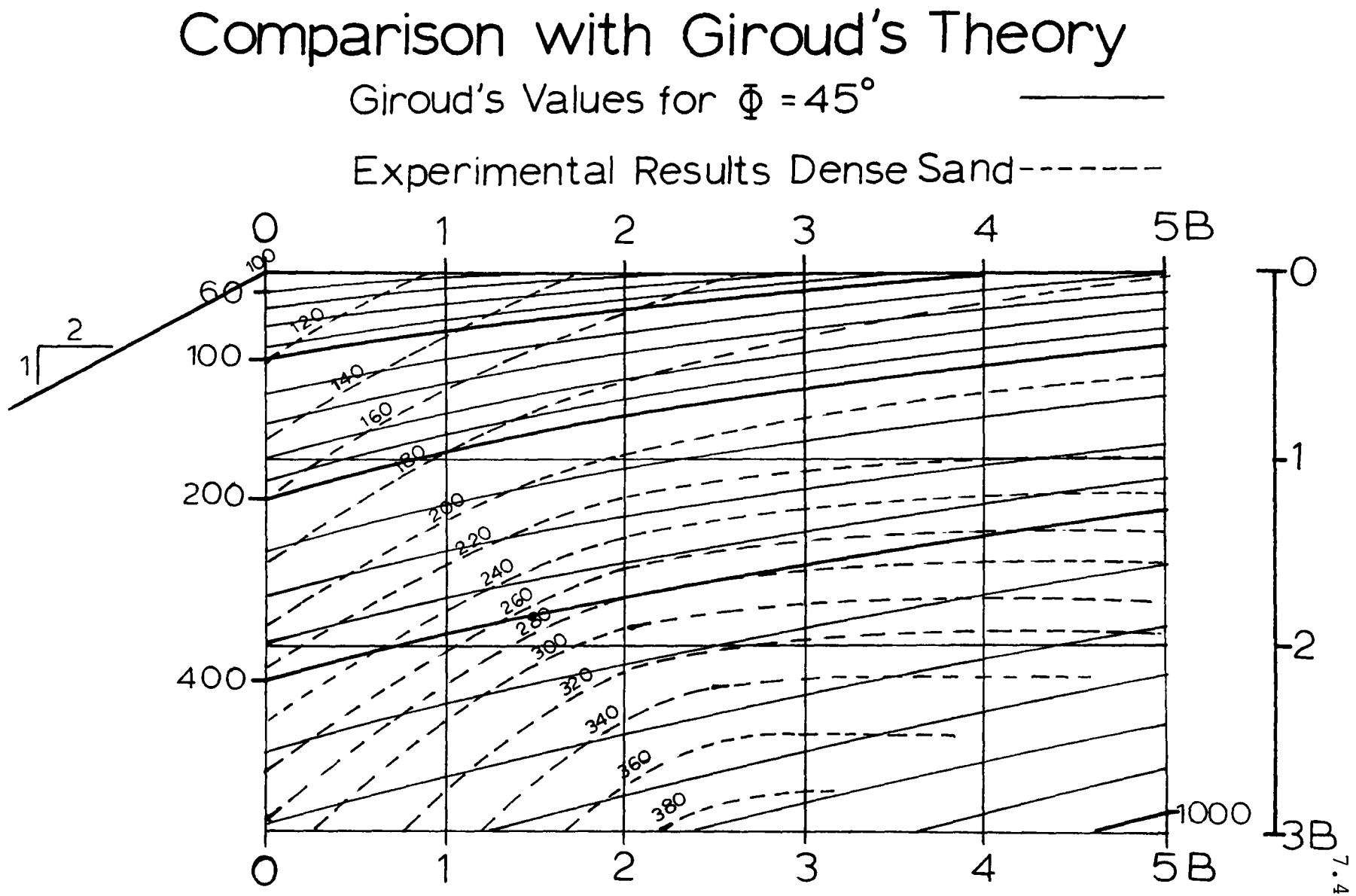
Comparison with Giroud's Theory
Giroud's Values for Φ = 45°
Experimental Results Dense Sand
0
1
2
3
4
5B
60
100
200
400
1000
2
1
0
1
2
3B
100
120
140
160
180
200
220
240
260
280
300
320
340
360
380

Figure 7.28

Comparison with Giroud's Theory

Giroud's Values for $\Phi = 50°$ ——————

Experimental Results Dense Sand - - - - - - -

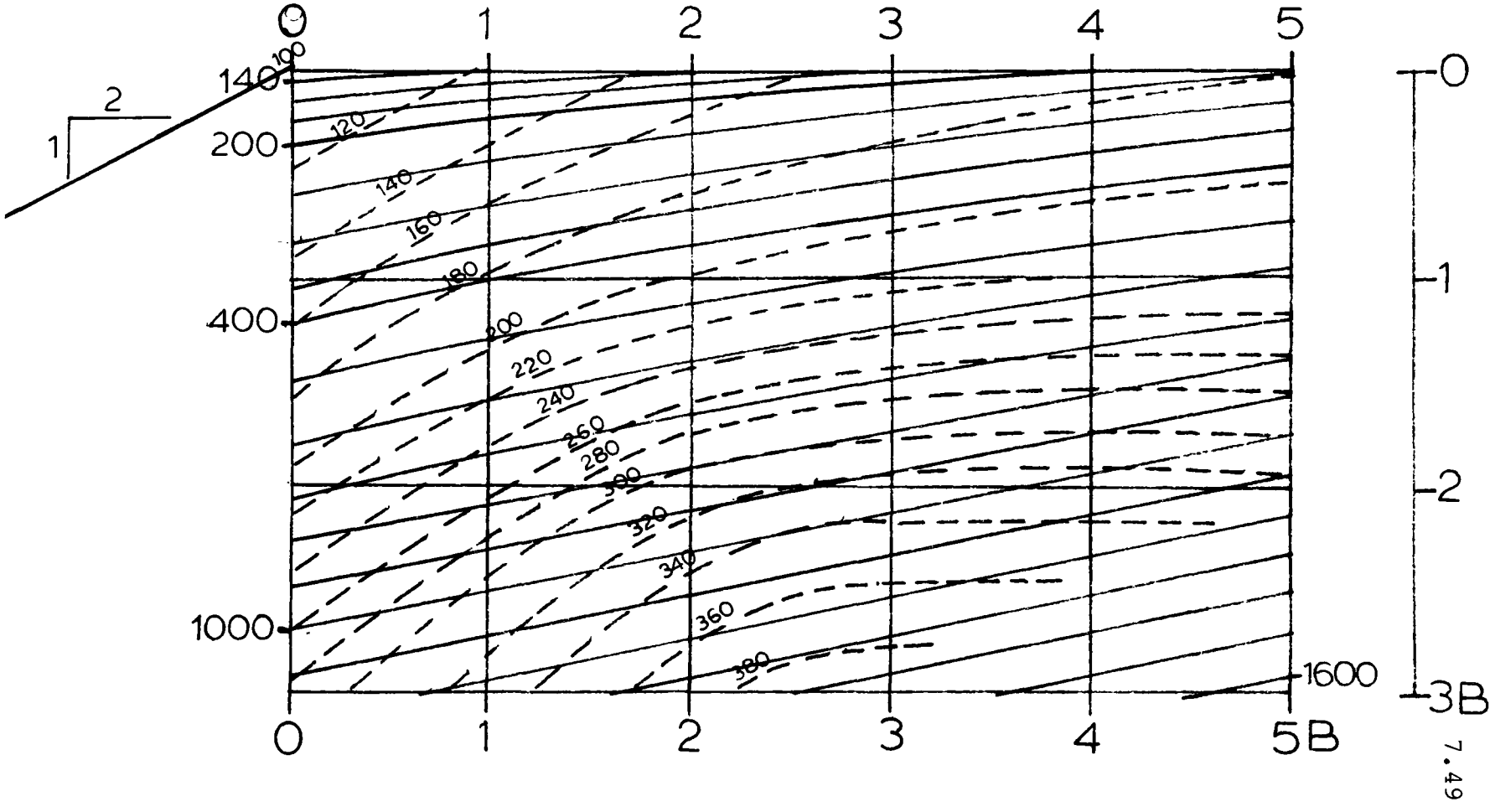

Figure 7.29

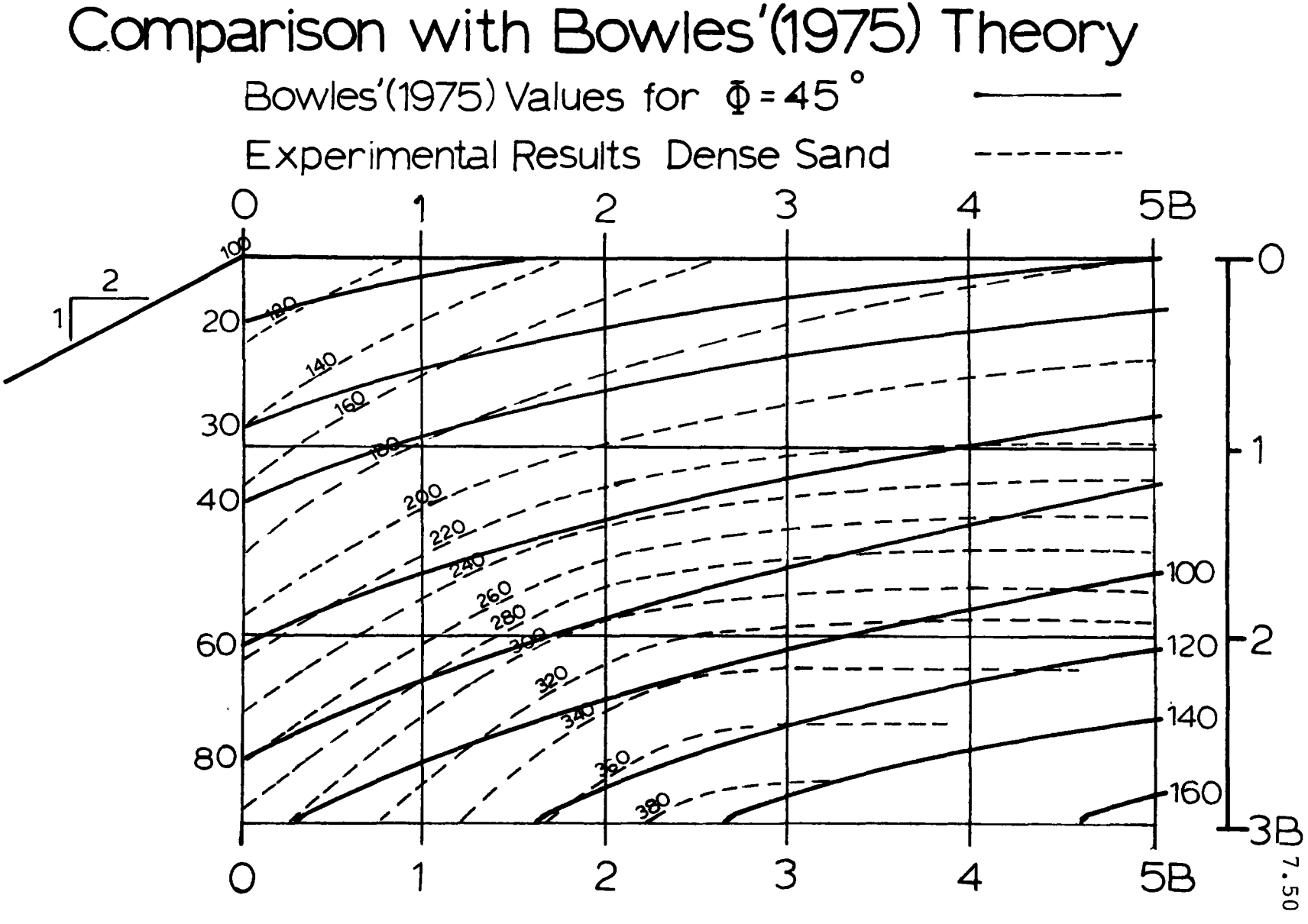
Comparison with Bowles'(1975) Theory
Bowles'(1975) Values for Φ = 45°
Experimental Results Dense Sand
0
1
2
3
4
5B
2
1
20
30
40
60
80
100
120
140
160
180
200
220
240
260
280
300
320
340
360
380
0
1
2
3B

Figure 7.30

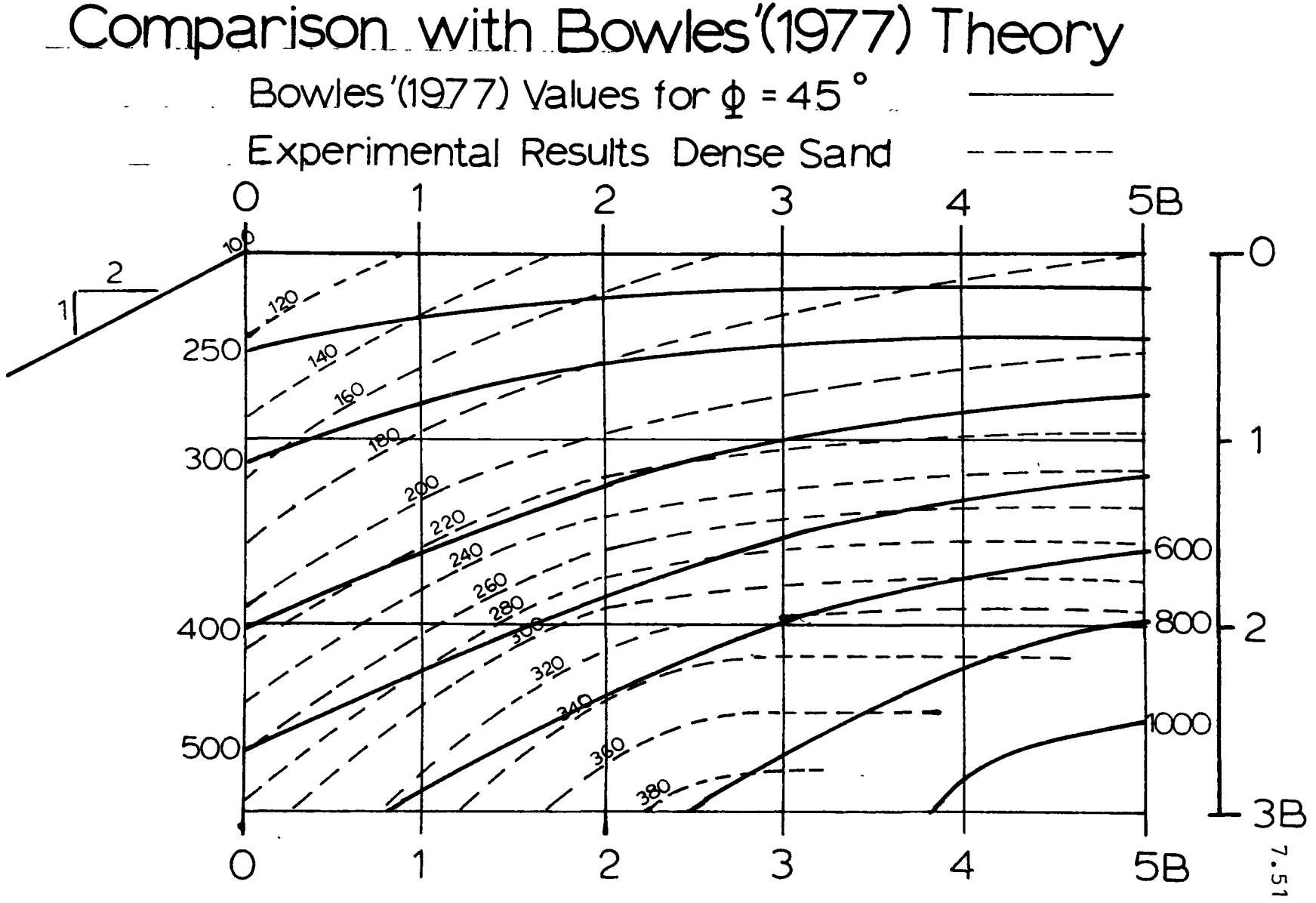
Comparison with Bowles'(1977) Theory
Bowles'(1977) Values for ϕ = 45°
Experimental Results Dense Sand
0
1
2
3
4
5B
2
1
100
120
140
160
180
200
220
240
260
280
300
320
340
360
380
250
300
400
500
600
800
1000
0
1
2
3B

Figure 7.31

7.4.1.4 The Φ to Make Theory Predict the Results

Poor agreement between theory and experiment is shown to exist in the preceeding section. Another way to make the comparison between theory and experiment is to find the Φ value that gives a theoretical $N_{\gamma q}$ value equal to the experimental $N_{\gamma q}$ result for a particular footing location. The results of this analysis are presented in tabular form in Figures 7.32 and 7.33 and in graphical form (for Meyerhof and Giroud) in Figures 7.34 to 7.37.

It can be observed that the angle Φ changes with density as might be expected, but Φ also changes with footing location for a constant density. Meyerhof's theory requires a variation in the angle of internal friction from 33° to 39° in the case of compact sand, and from 38° to 51° in the case of dense sand. The Giroud theory has a similar variation -- from 34° to 41° for compact sand, and from 37° to 49° for dense sand. The Bowles' (1975) theory yields an angle of internal friction which is in excess of 55° for the majority of test footing locations. The Bowles' (1977) theory offers a variation similar to the Meyerhof and Giroud theories, that is 33° to 38° in the case of compact sand, and 36° to 45° in the case of dense sand.

This analysis shows once again that no theory correctly predicts the distribution of $N_{\gamma q}$ in the soil; no one angle of internal friction is found at all footing locations in either state of density.

Corresponding Theoretical Φ for Experimental $N_{\gamma q}$ Results In Compact Sand

Footing Test Location	$N_{\gamma q}$ Results	Corresponding Theoretical Φ			
		Meyerhof	Giroud	Bowles(1975)	Bowles(1977)
Compact Sand					
0 - 0	24	39°	41°	48°	33°
0 - 1	70	38.5°	37.5°	52°	34°
0 - 2	152	39°	36.5°	>55°	35°
0 - 3	230	38.5°	34.5°	>55°	33.5°
2.5 - 0	37	34.5°	40°	47°	35.5°
2.5 - 1	80	33°	34.5°	>55°	31.5°
2.5 - 2	190	36.5°	35.5°	>55°	34°
2.5 - 3	250	36°	35°	>55°	33°
5 - 0	54	36°	38°	49.5°	37.5°
5 - 1	95	33°	33.5°	>55°	33°
5 - 2	212	35°	36°	>55°	35°
5 - 3	250	34°	35°	>55°	33°

Figure 7.32

Corresponding Theoretical Φ for Experimental $N_{\gamma q}$ Results

In Dense Sand

Footing Test Location	$N_{\gamma q}$ Results	Corresponding Theoretical Φ			
		Meyerhof	Giroud	Bowles (1975)	Bowles (1977)
Dense Sand					
0 - 0	100	51°	48.5°	>55°	41°
0 - 1	145	44°	44°	>55°	40°
0 - 2	208	41.5°	40.5°	>55°	37.5°
0 - 3	288	41.5°	37°	>55°	36°
2.5 - 0	160	45°	49°	>55°	43.5°
2.5 - 1	205	41°	43.5°	>55°	38.5°
2.5 - 2	330	41°	40.5°	>55°	38.5°
2.5 - 3	400	40°	38.5°	>55°	37.5°
5 - 0	180	42°	47.5°	>55°	45°
5 - 1	229	39°	41°	>55°	39.5°
5 - 2	330	38.5°	39.5°	>55°	38.5°

Figure 7.33

Contours of Φ in Compact Sand
Meyerhof's Values

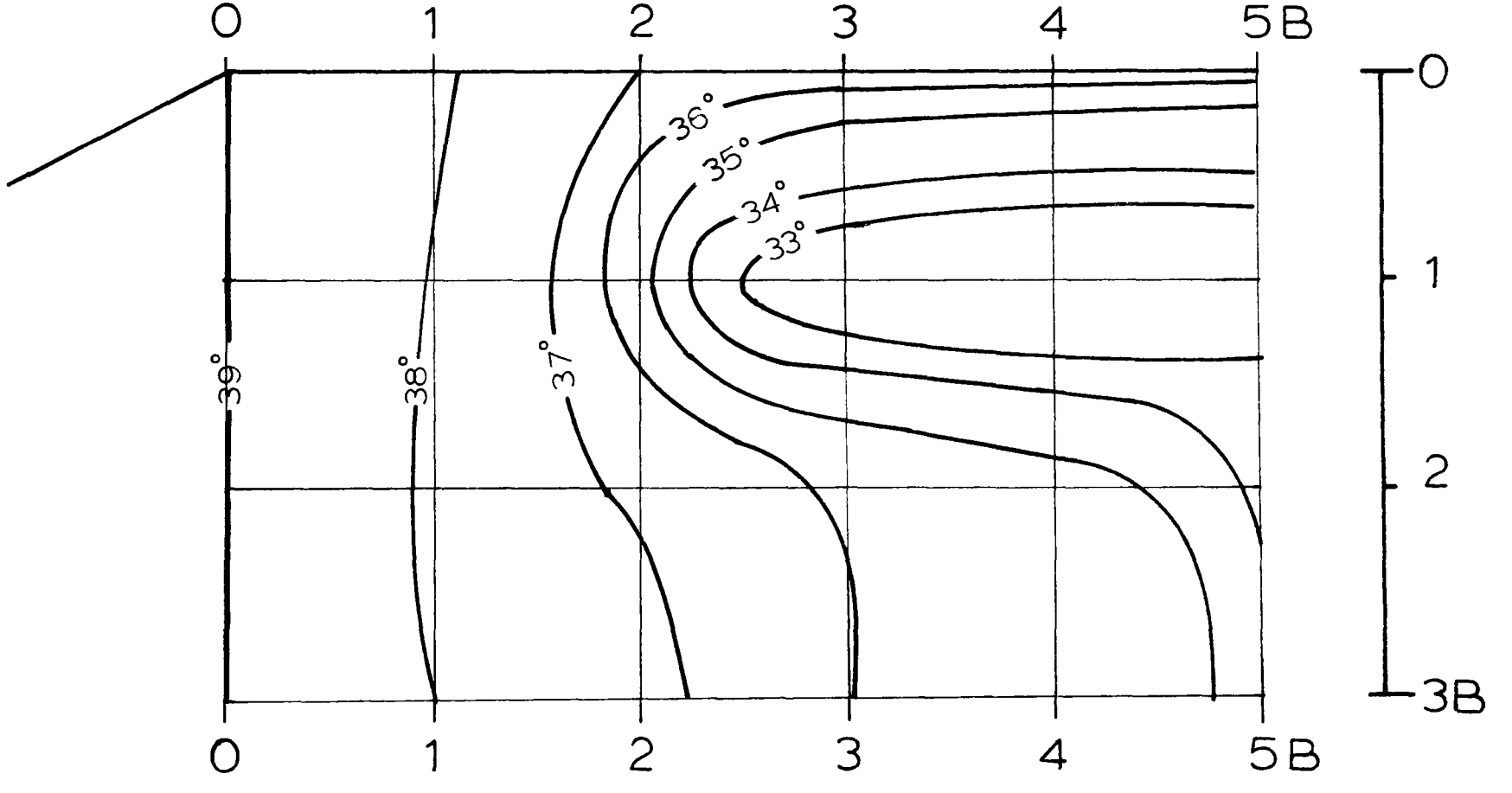

Figure 7.34

Contours of Φ in Compact Sand
Giroud's Values

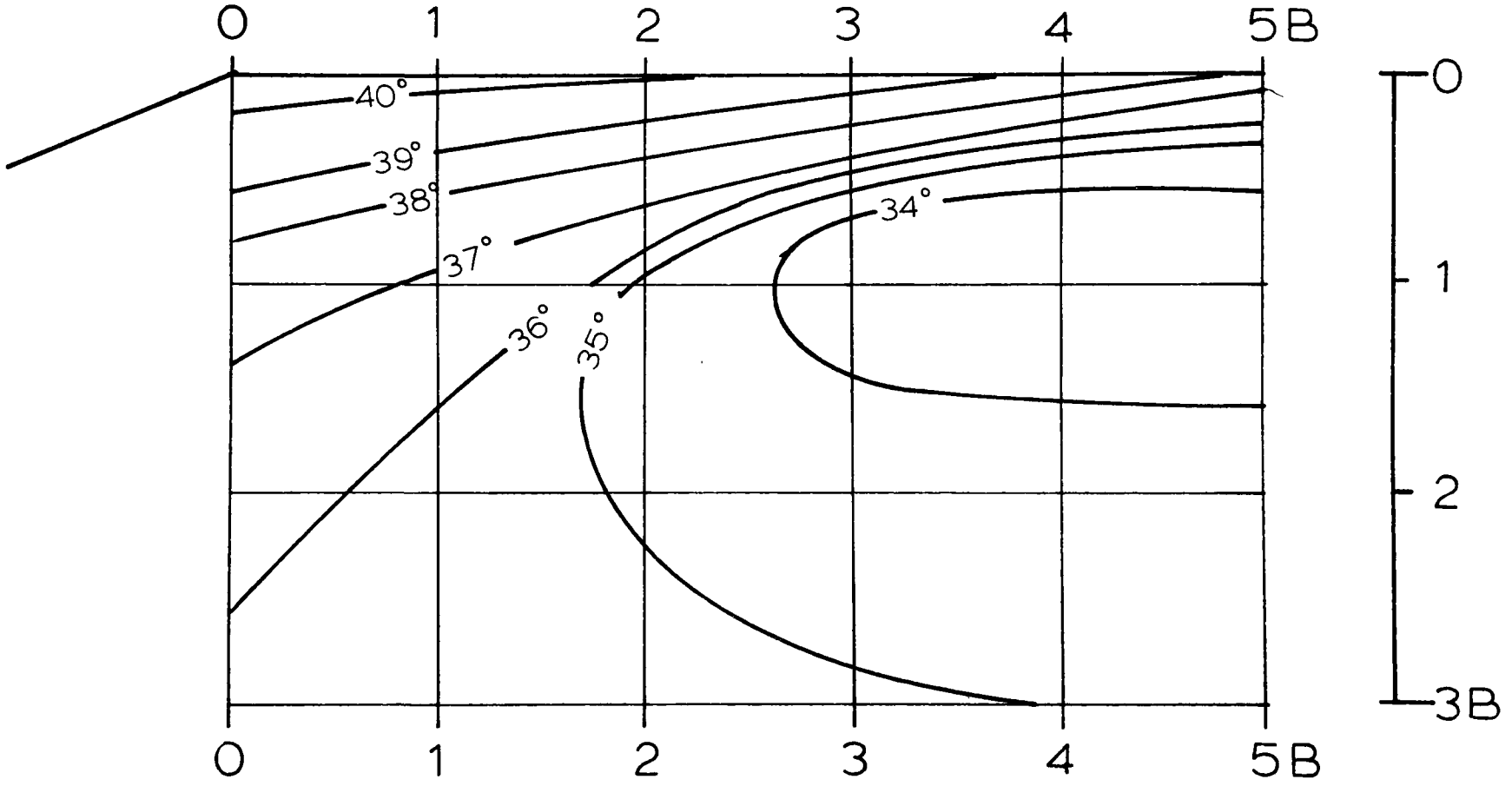

Figure 7.35

Contours of Φ in Dense Sand
Meyerhof's Values

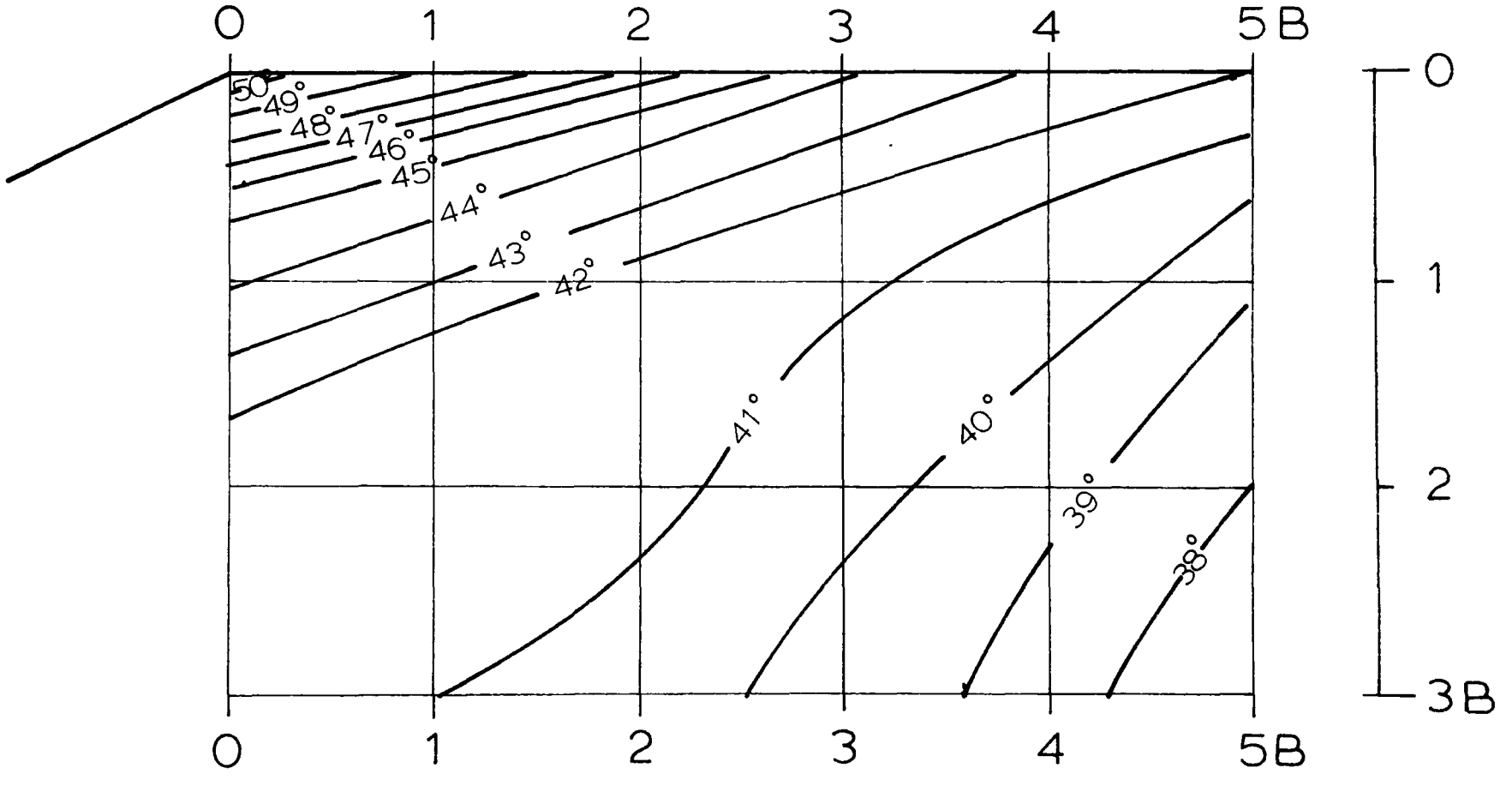

Figure 7.36

Contours of Φ in Dense Sand
Giroud's Values

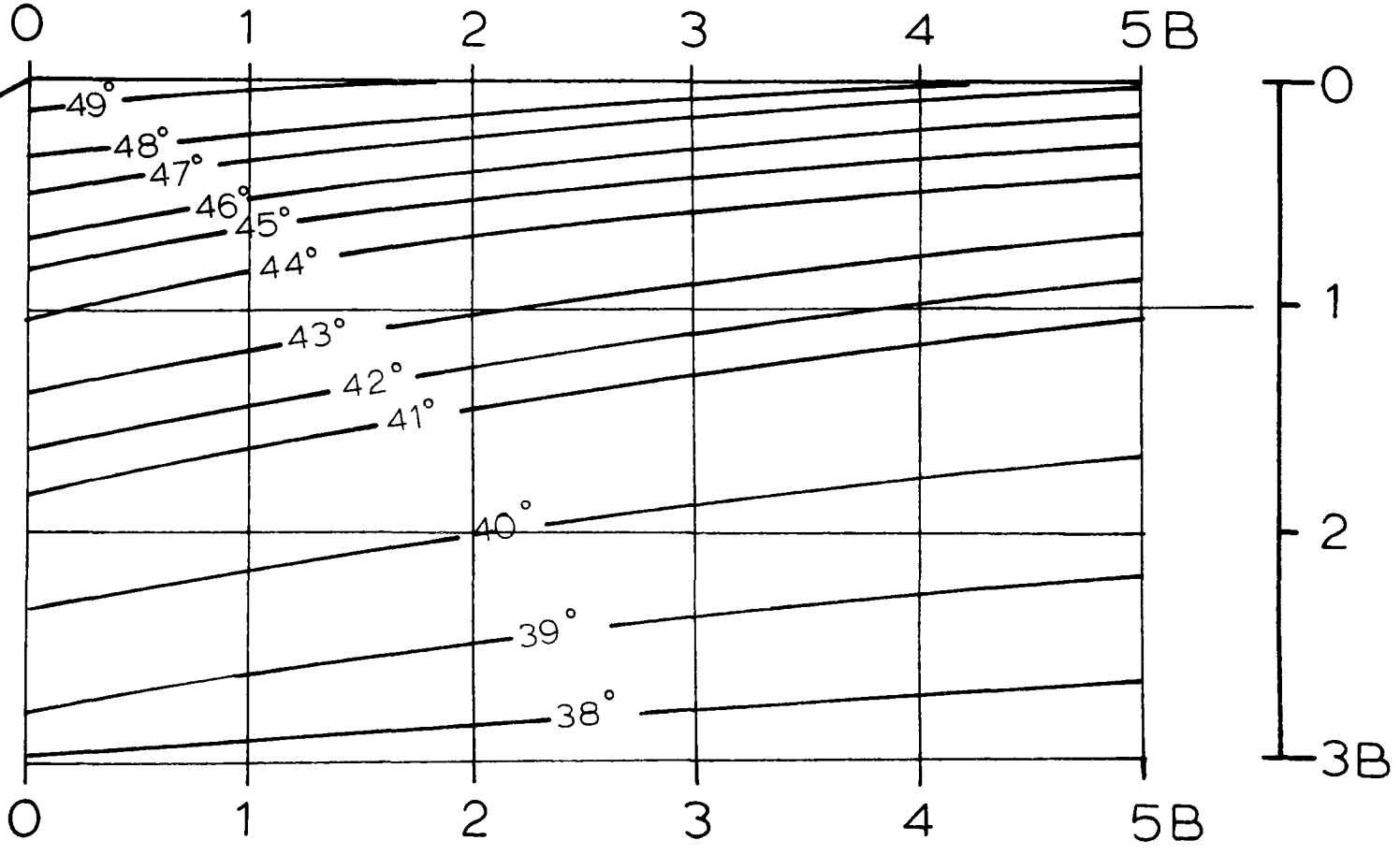

Figure 7.37

Nevertheless, one general rule evolves from Figures 7.32 and 7.33: tests where the surcharge is a minimum, correspond to angles of internal friction which are always higher than for deep buried footings. A similar rule applies to Φ versus the horizontal distances from the crest; the angle Φ is always higher close to the slope than away from it. DeBeer (1967) offered an explanation for this behavior. The choice of the proper Φ angle is dependent on the mean normal stress acting along the length of the failure surface. According to the curved Mohr-Coulomb failure envelope, low normal stresses always yield high angles of internal friction. Surface tests, especially the test at the slope crest, have low mean normal stresses acting along their respective failure surface. Therefore their Φ angle is larger than for the deep tests where a higher mean normal stress is mobilized along the failure planes.

Another possible explanation exists for the fact that Φ varies throughout the mass. This is the role that the intermediate principal stress plays in determining Φ. From Figures 7.38 and 7.41 it is possible to see that for footings located at the slope crest in dense sand, Φ obtained by the shear box matches the required Φ. The plane strain results cover locations in the dense mass that are just below the shear box results. The triaxial Φ represent a zone of footing locations that are in the middle of the mass. In compact sand only the triaxial test can be located, but the postulation probably

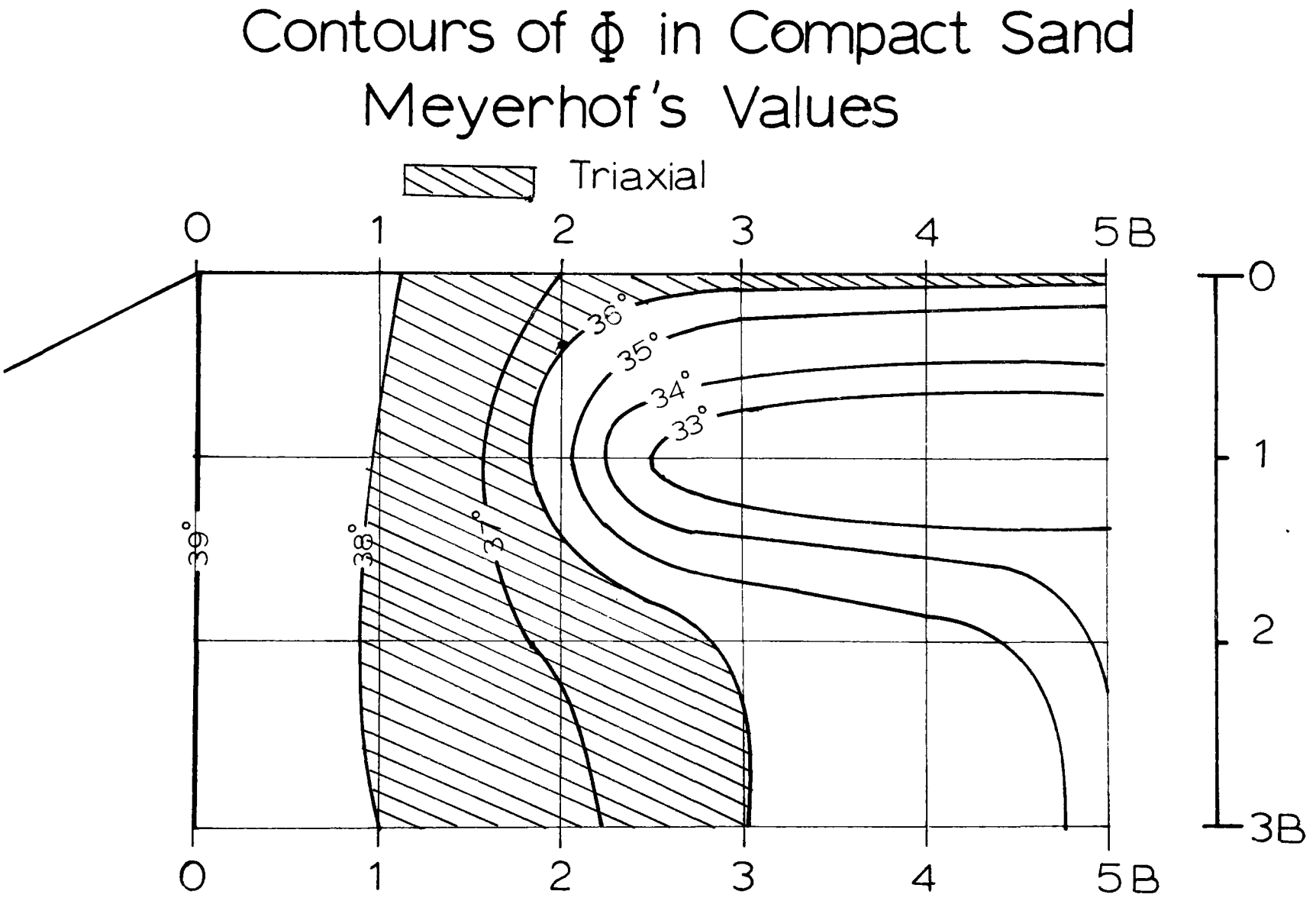
Contours of Φ in Compact Sand
Meyerhof's Values
Triaxial
0
1
2
3
4
5B
36°
35°
34°
33°
39°
38°
37°
0
1
2
3B

Figure 7.38

Contours of Φ in Compact Sand
Giroud's Values

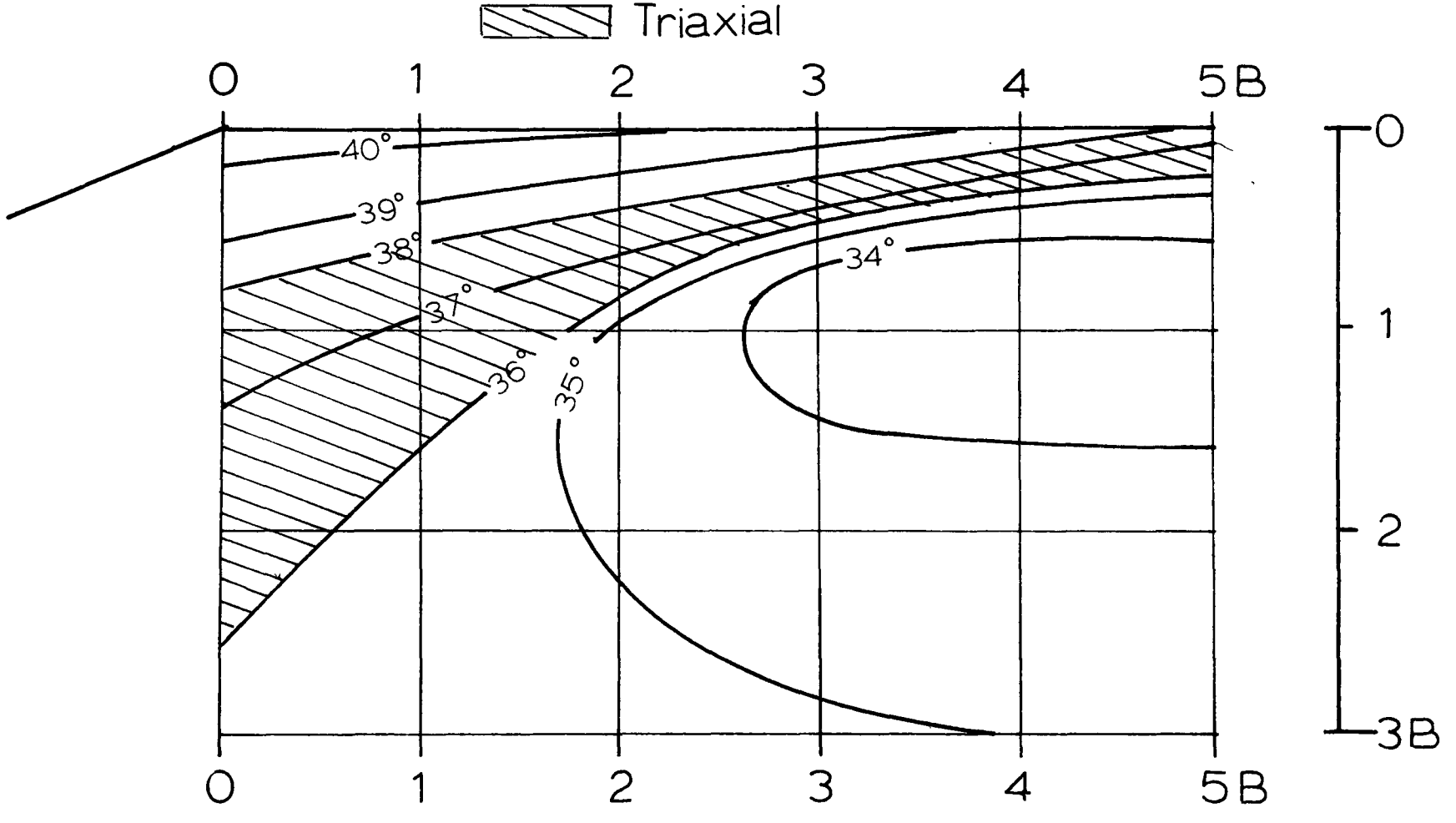

Figure 7.39

Contours of Φ in Dense Sand
Meyerhof's Values

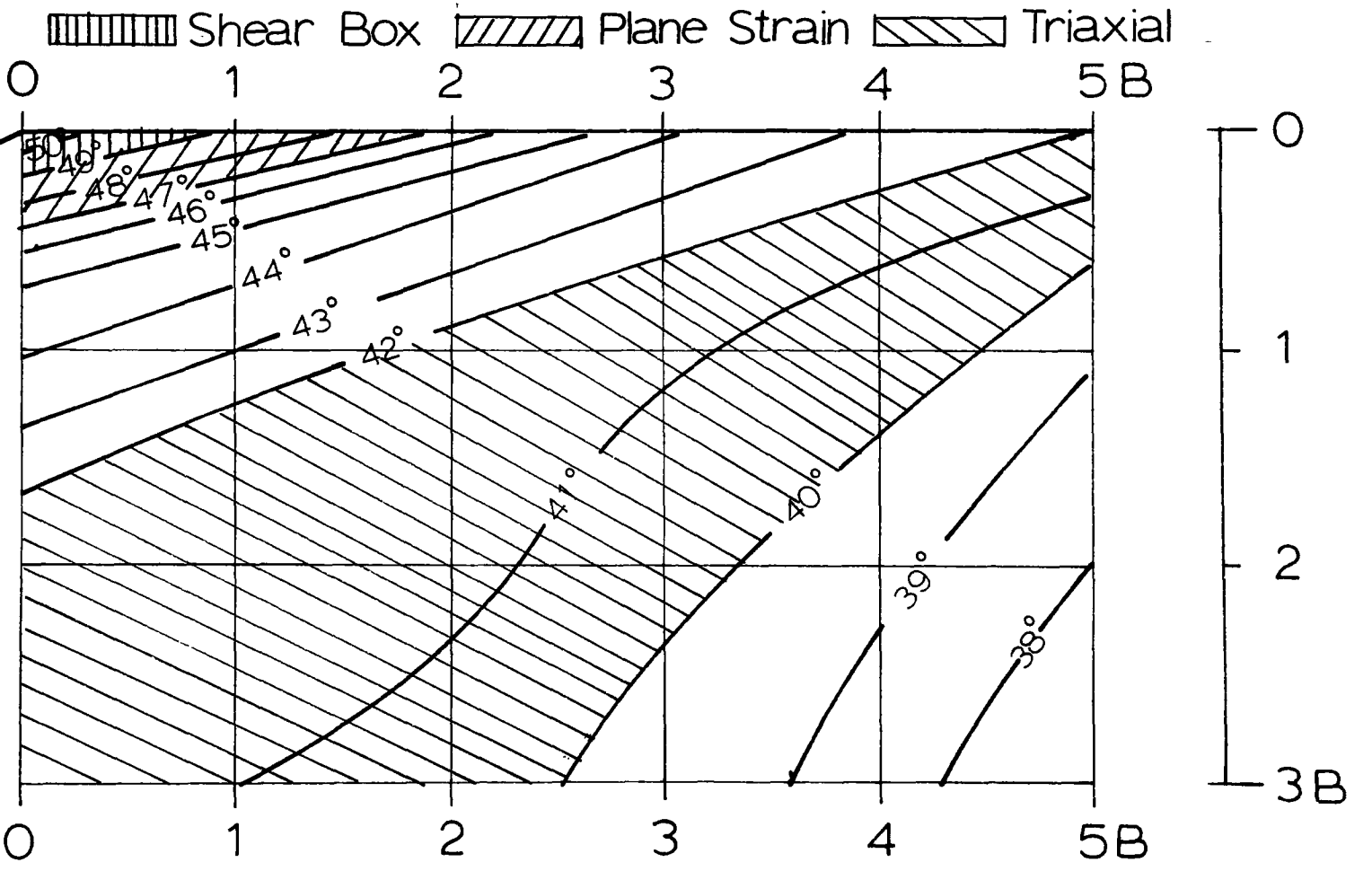

Figure 7.40

Contours of Φ in Dense Sand
Giroud's Values

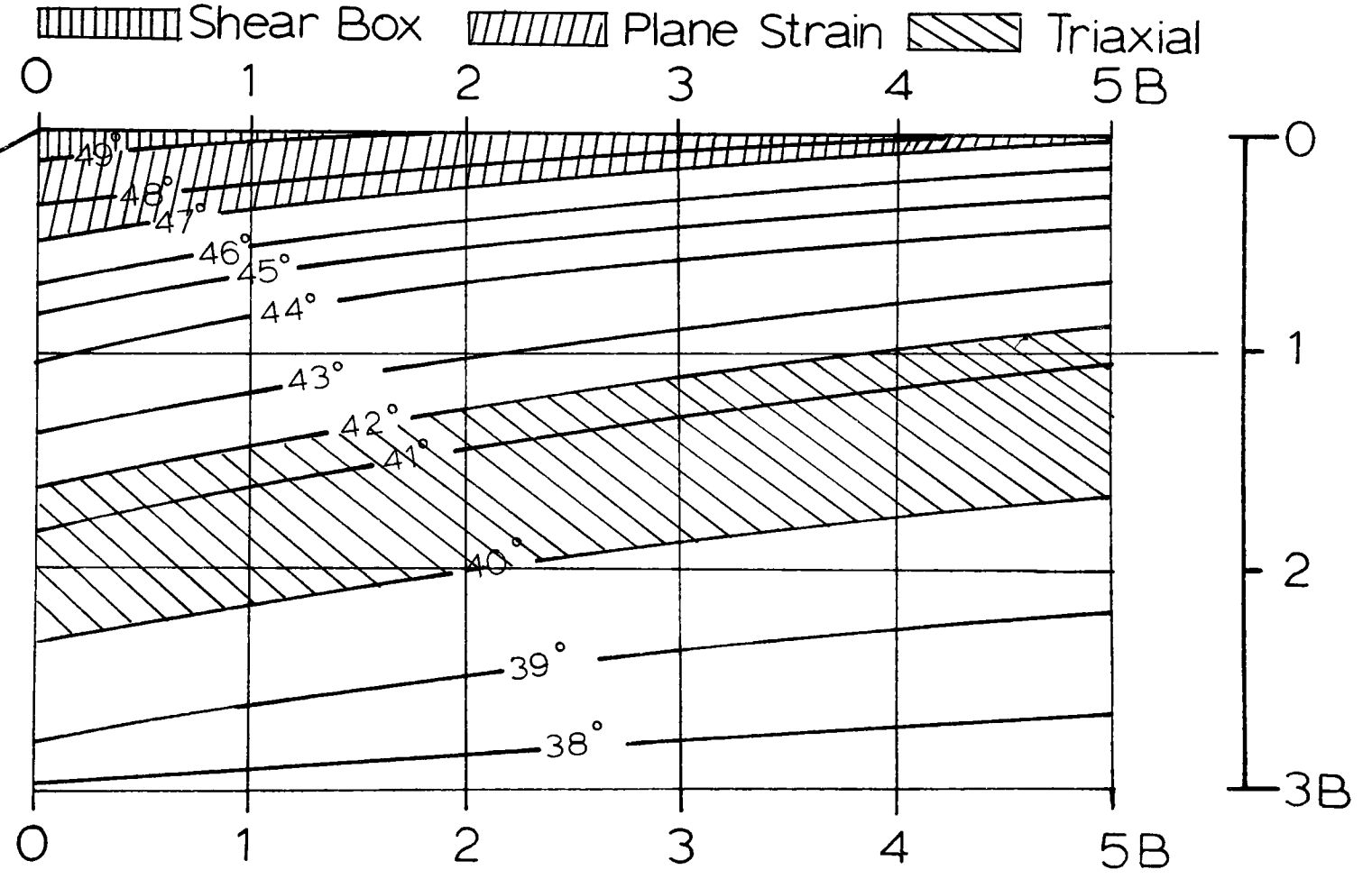

Figure 7.41

holds. The conclusion that can be drawn is that in dense sand and deeper in the mass, the minor and intermediate principal stresses are close to one another at failure, which is the condition in the triaxial test.

7.4.1.5 Comparison of Trends: Theories Vs Experiments

Even though the theoretical values do not agree very well with the experimental results, it is interesting to compare the trend in bearing capacities given by the theoretical and experimental results. From the graph of the equal $N_{\gamma q}$ contours for the theories, a comparison may be made with the contours of the experimental $N_{\gamma q}$ results. Both theory and experiment show the same trend: both sets of contours indicate a definite decrease in $N_{\gamma q}$ value in the vicinity of the slope. This decrease is more important in dense sand than in compact sand.

Another fact worth investigating is the degree to which the theories are able to predict the true increase in $N_{\gamma q}$ with depth. The theories predict a continuous increase in $N_{\gamma q}$ with depth, whereas the experimental data show that the increase is not as rapid as the predictions, and the values also seem to reach a maximum. In both compact and dense sand, the net increase in experimental $N_{\gamma q}$ values seems to occur between a depth of B and 2B.

Figures 7.42 and 7.43 show the decrease in $N_{\gamma q}$ as the footing approaches the slope crest. This analysis is made

by taking the value of $N_{\gamma q}$ for a particular footing location and dividing it by $N_{\gamma q}$ at 5B at the same depth.

In each figure the theoretical values are superimposed on the experimental results. In most cases the theoretical lines fall close to the experimental line. In compact sand the experimental line and the theoretical lines are almost identical except for the depth of 1B. In dense sand the predicted rate of $N_{\gamma q}/N_{\gamma q(5B)}$ is lower than its experimental counterpart.

The same type of comparison can be made for the change in $N_{\gamma q}$ values with depth at various horizontal positions. This comparison is shown on Figures 7.44 and 7.45. It can be seen that in compact sand, theory predicts almost the same rate of increase in $N_{\gamma q}$ as do the experiments. Though the same trend is followed in dense sand, the comparison is not as good, expecially at the slope crest where the change in $N_{\gamma q}$ with depth is less important than it is in theory.

7.4.2 Comparison with Other Experimental Results

7.4.2.1 Footings Near a Slope

This section of Chapter VII compares the experimental values of the present research program to the other experimental investigations described in Chapter III. The results of the wooden stick models will be ignored for the reasons mentioned in Chapter III. The only worthwhile testing program to date was the one carried out by Lebègue (1973).

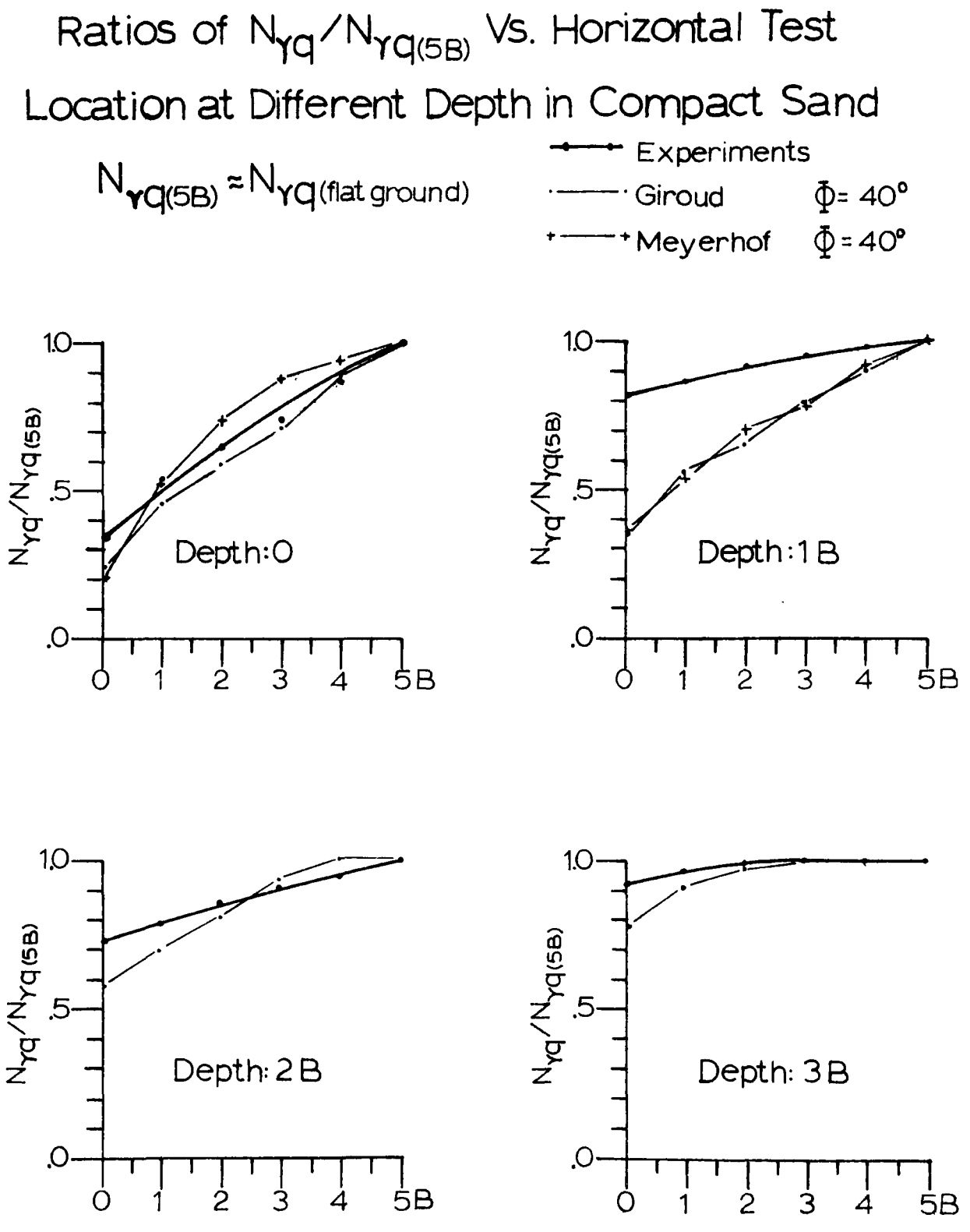
Ratios of $N_{\gamma q}/N_{\gamma q(5B)}$ Vs. Horizontal Test Location at Different Depth in Compact Sand
$N_{\gamma q(5B)} \approx N_{\gamma q\,(\text{flat ground})}$
Experiments
Giroud $\Phi = 40°$
Meyerhof $\Phi = 40°$
$N_{\gamma q}/N_{\gamma q(5B)}$
1.0
.5
.0
0 1 2 3 4 5B
Depth: 0
Depth: 1 B
Depth: 2 B
Depth: 3 B

Figure 7.42

Ratios of $N_{\gamma q}/N_{\gamma q\,(5B)}$ Vs. Horizontal Test Location at Different Depth in Dense Sand

$N_{\gamma q\,(5B)} \simeq N_{\gamma q\,(\text{flat ground})}$

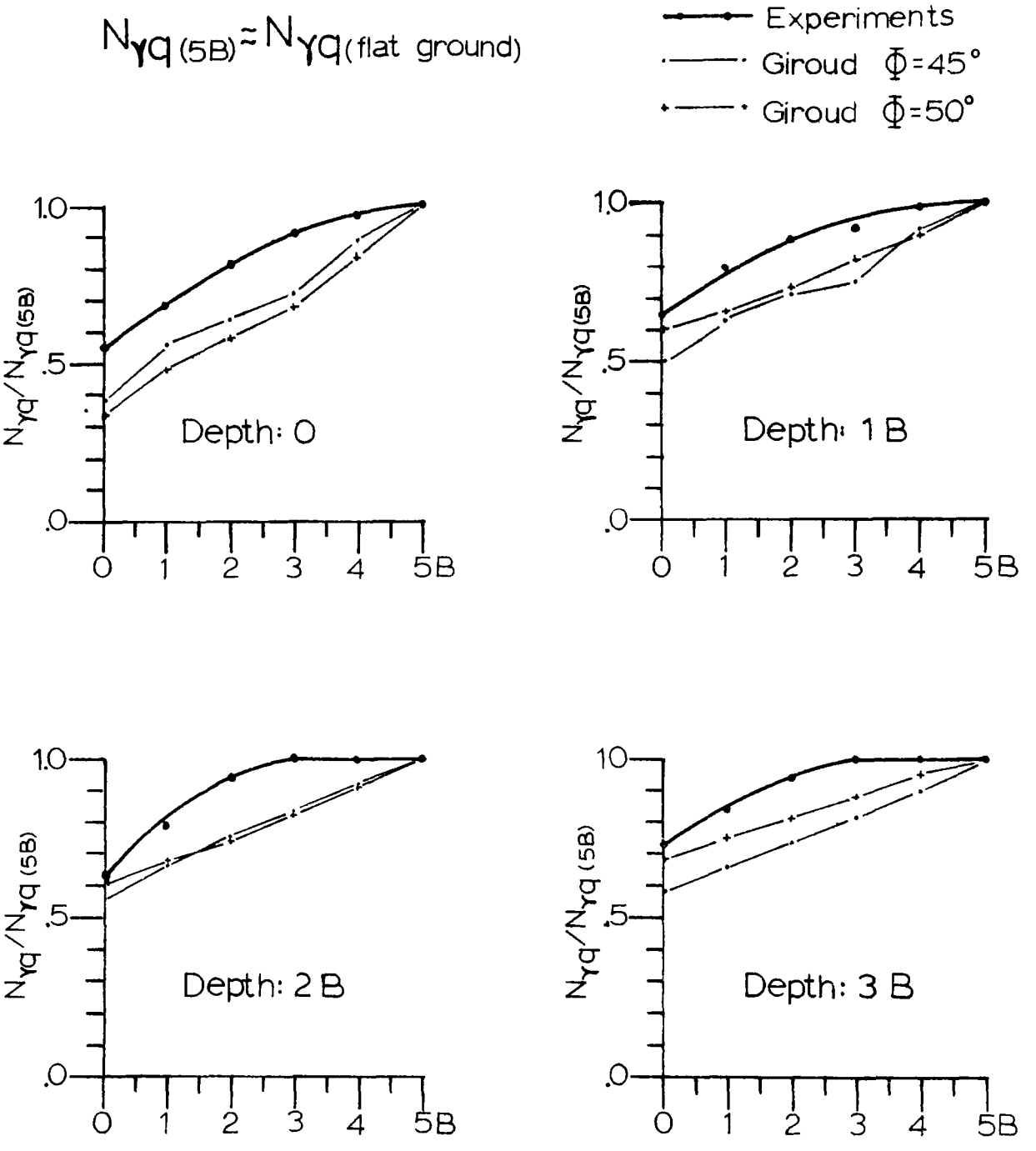

Figure 7.43

Ratios of $N_{\gamma q}/N_{\gamma q\,(Depth:3\,B)}$ Vs. Vertical Test Location at Different Distances from Slope Crest in Compact Sand

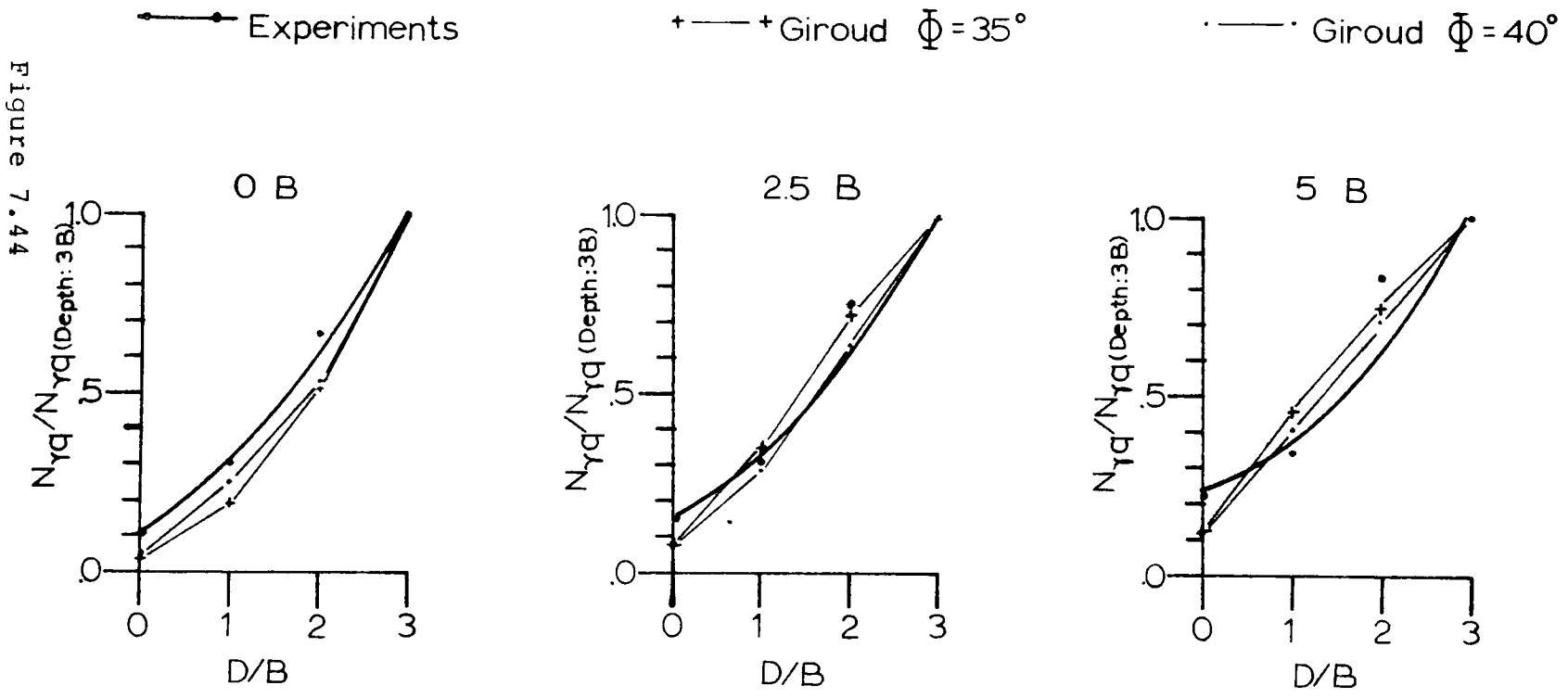

Figure 7.44

Ratios of $N_{\gamma q}/N_{\gamma q\,(Depth:3B)}$ Vs. Vertical Test Location at Different Distances from Slope Crest in Dense Sand

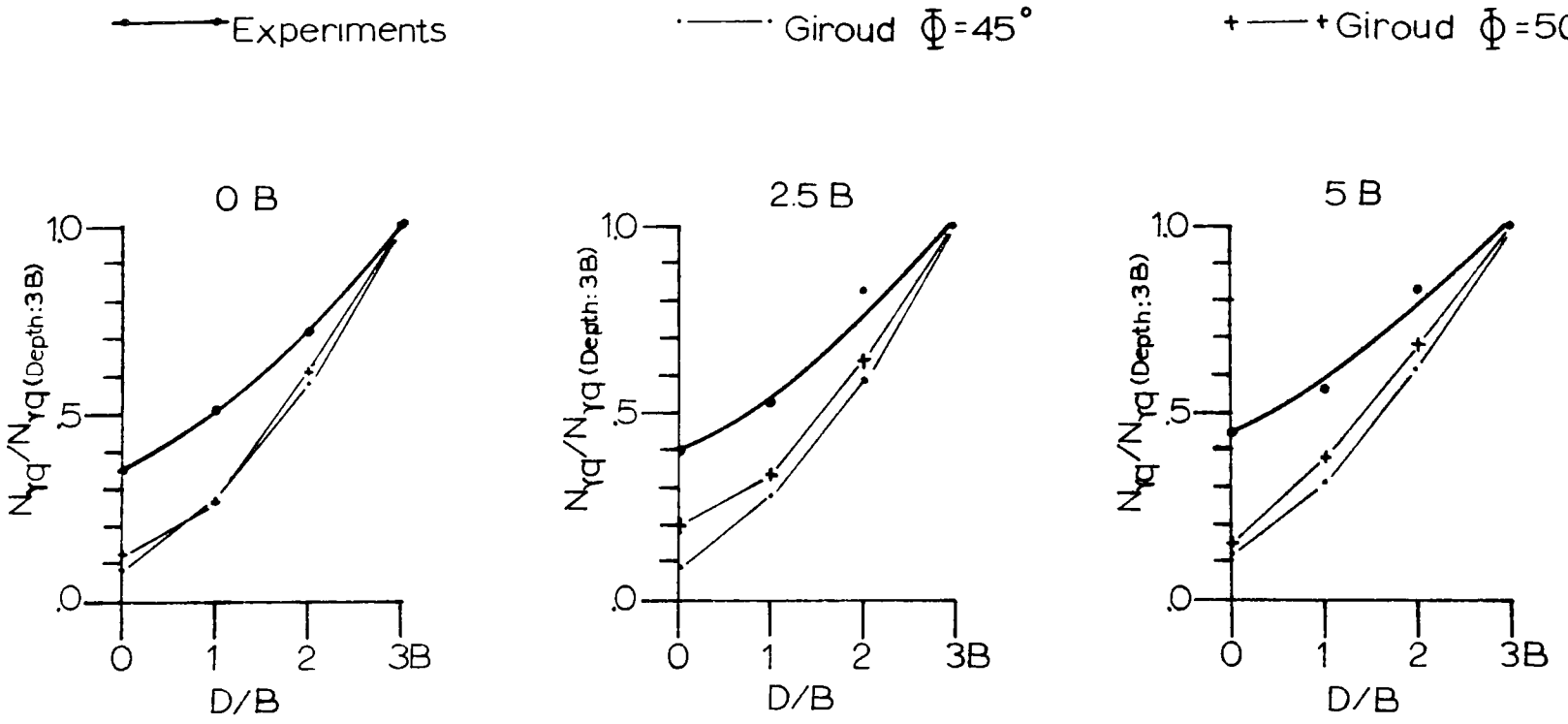

Figure 7.45

Lebègue gives only values of Φ from triaxial tests on his sand. If his values are compared to the present experimental results, Lebègue's Φ_t equal to 35° corresponds to the compact sand, while a Φ_t equal to 40° corresponds to the dense state.

The Lebègue values for a 2:1 slope are interpolated from the results he gave for slopes of 20° and 30°; these values are compared to the present experimental results, as shown in Figure 7.46. This table provides a comparison for only one footing location, that is at the slope crest which was the only location that Lebègue tested.

From Figure 7.46, it can be seen that the $N_{\gamma q}$ values of the present testing program are always lower than the values deduced from Lebègue's results. The main reason for the discrepancy is thought to be the effect of scale. Lebègue's tests were carried out on a footing 6 and 20cm wide, while the present series was on footings 30cm wide.

7.4.2.2 Footings on Flat Ground

One test was carried out on flat ground in dense sand during the present program. This test, titled ∞ - 0 - D, yielded a $N_{\gamma q}$ of 180 which is identical to the result of the test performed on the surface of the dense sand at a horizontal distance of 5B from the slope crest. This finding agrees with most theories in which the influence of the slope is shown to have no effect on the bearing capacity beyond a horizontal distance of 5B from the slope crest.

Comparison of Lebègue's Experimental N_q Values to the N_q Values of the Present Experimental Program for a 2:1 Slope

	Lebègue's $N_{\gamma q}$ values		Present program $N_{\gamma q}$	
ϕ_t	B= 6cm.	B= 20cm.	Density state	B= 30cm.
35^o	70	30	Compact	24
40^o	260	105	Dense	99

Figure 7.46

Therefore, the tests performed at 5B can be considered to be tests located on flat ground.

Figures 7.47, 7.48 and 7.49 represent the graphs of the effect of scale studied by DeBeer (1967), Tcheng and Iseux (1966) and Graham (1972). The experimental $N_{\gamma q}$ values of 54 in compact sand and 180 in dense sand obtained on the surface at a horizontal distance of 5B from the slope crest have been superimposed on the figures. It is interesting to note that the experimental results conform to the pattern of results presented by the aforementioned investigators.

7.5 Mathematical Expression of the Experimental Results

It is possible that a mathematical expression exists to express the test results. If a curve fitting procedure is used, a mathematical expression can, in fact, be found to represent the experimental values of $N_{\gamma q}$. This expression is a combination of an exponential and a power function; it incorporates the effects of slope proximity and footing depth. This expression is:

$$N_{\gamma q} = 47\left(\frac{D}{B}\right)^{1.38} + A \times 25(1.14)^{b/B} \qquad (7.5.1)$$

where A = 1 for compact sand

A = 4 for dense sand

Equation (7.5.1) has been worked out for every test location, and the $N_{\gamma q}$ value compared to the actual experimental

Scale Effect

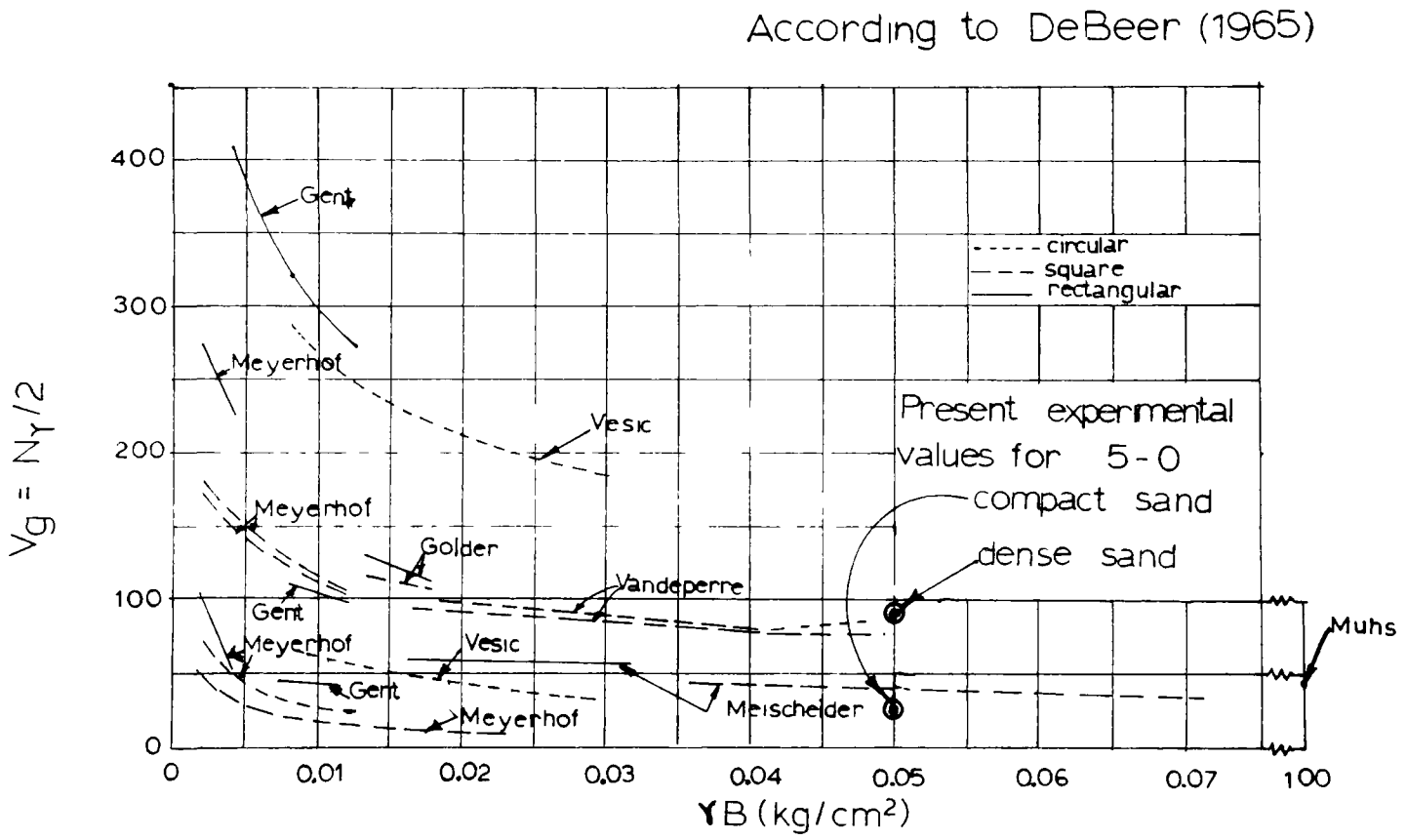

Figure 7.47

Scale Effect

According to Tcheng & Iseux (1965)

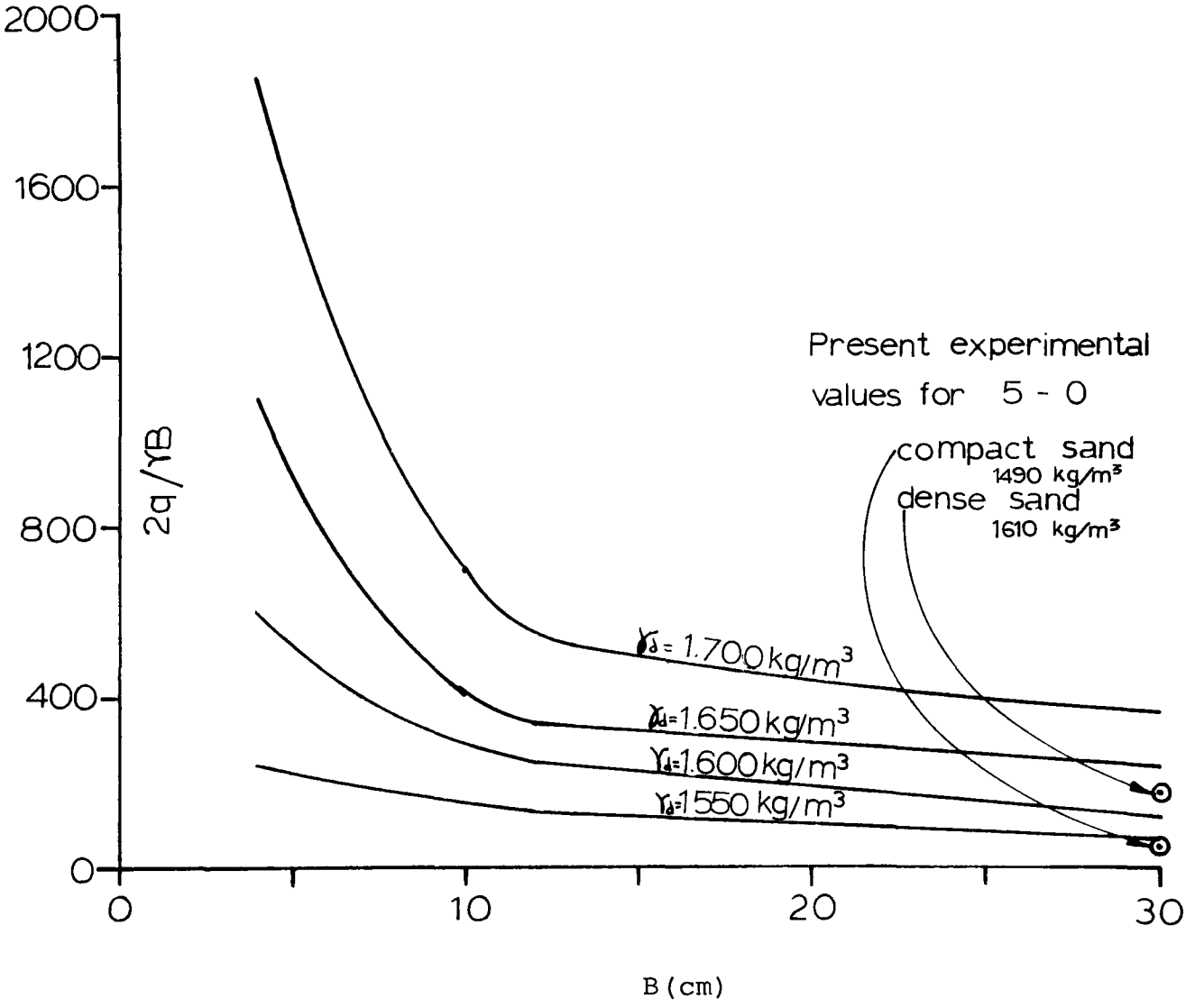

Figure 7.48

Scale Effect

According to Graham (1974)

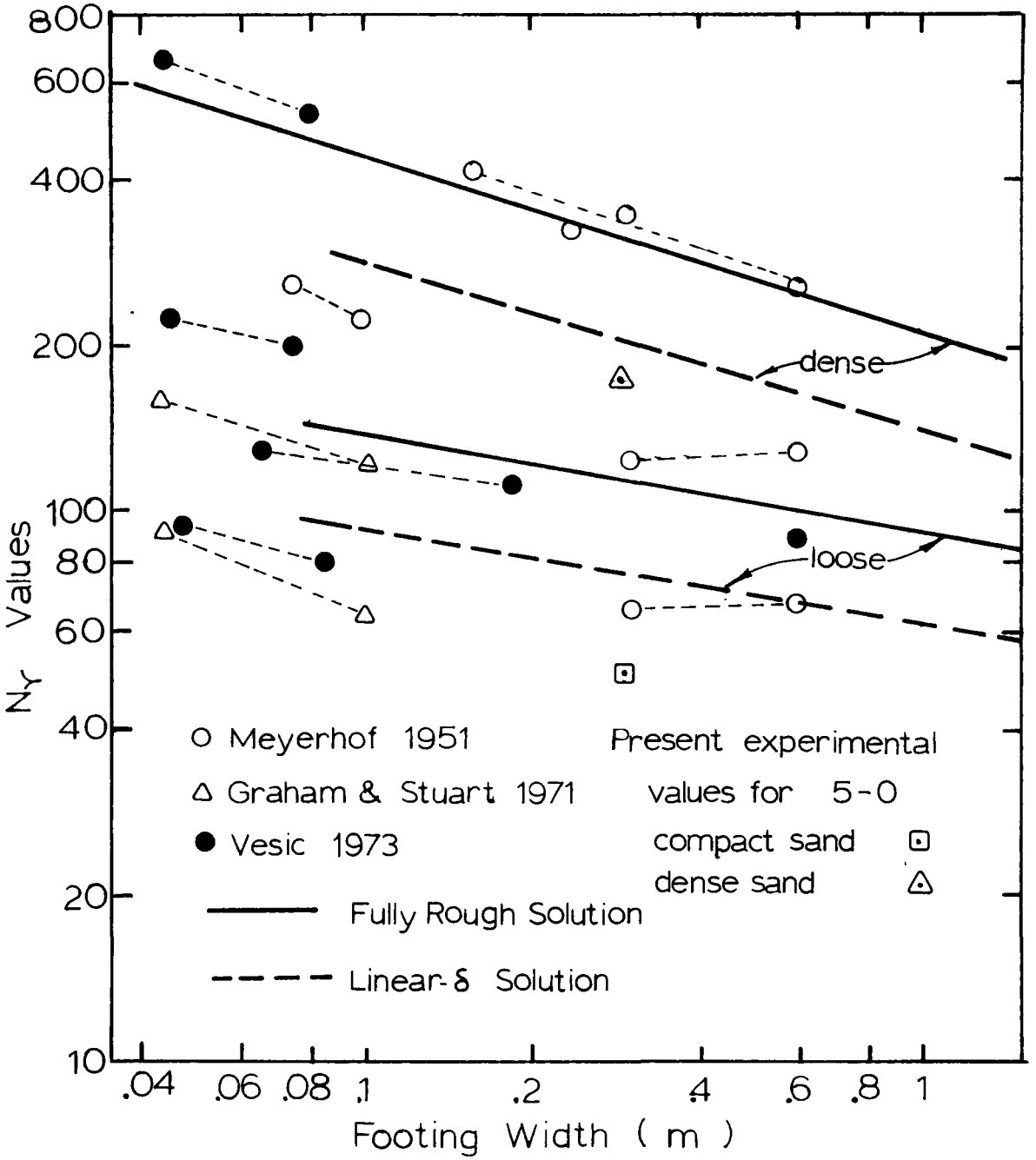

Figure 7.49

results. This comparison is presented for compact sand in Figure 7.50 and for dense sand in Figure 7.51. Interestingly, only three values disagree by more than ten percent. These values are for footings located at 2.5 - 2, 5 - 0 and 5 - 2, and Equation (7.5.1) always gives values that are on the safe side.

For the case of dense sand, the fit between the experimental results and the values given by Equation (7.5.1) is just as good as for compact sand. Again, the equation yields only three values which are more than ten percent from the experimental results, and all are on the safe side. The footing locations are at 2.5 - 0, 2.5 - 2 and 2.5 - 3. All other comparisons are well within ten percent.

Another point worth mentioning is the fact that Equation (7.5.1) is made up of two terms. The first term, $47(\frac{D}{B})^{1.38}$, takes into account the effect of depth and can be equated to the bearing capacity factor N_q. The other term can be equated to N_γ and is A x $25(1.14)^{b/B}$. The first term shows that the contribution of depth or increasing surcharge is the same for both compact sand and for dense sand and is independent of Φ. This is in contradiction to most of the theories which are presented in Chapter II, where N_q is a function of the angle of internal friction.

Therefore Equation (7.5.1) can be used to predict the values of $N_{\gamma q}$ of footings located within a horizontal distance of 5B from the slope crest. The maximum depth to which this Equation is shown to be valid is 3B.

Comparison between Experimental Results and the $N_{\gamma q}$ predicted by Equation (7.5.1) in Compact Sand

$\frac{D}{B}$	$\frac{b}{B}$	Experimental $N_{\gamma q}$ Values	$N_{\gamma q}$ from Equation (7.5.1)	Difference	%	Remarks
0	0	24	25	1	4	
0	1	70	72	2	3	
0	2	152	147	-5	-3	
0	3	230	239	9	4	
2.5	0	37	35	-2	-5	
2.5	1	80	82	2	3	
2.5	2	190	157	-33	-17	safe side
2.5	3	250	249	-1	-	
5	0	54	48	-6	-10	safe side
5	1	95	95	0	0	
5	2	212	170	-42	-20	safe side
5	3	250	262	12	5	

Figure 7.50

Comparison between Experimental Results and the $N_{\gamma q}$ predicted by Equation (7.5.1) in Dense Sand

$\frac{D}{B}$	$\frac{b}{B}$	Experimental $N_{\gamma q}$ Values	$N_{\gamma q}$ from Equation (7.5.1)	Difference	%	Remarks
0	0	99	100	1	0	
0	1	146	147	1	0	
0	2	208	222	14	7	
0	3	288	314	26	9	
2.5	0	159	140	-19	-12	safe side
2.5	1	206	187	-19	-9	
2.5	2	328	262	-66	-20	safe side
2.5	3	397	354	-43	-10	safe side
5	0	180	192	12	7	
5	1	221	239	18	8	
5	2	328	314	-14	-4	

Figure 7.51

CHAPTER VIII

THEORETICAL APPROACH

8.1 Introduction

The results of the present experimental investigation are tabulated in Chapter VI.

The fact that the results do not compare favorably with the theories of Chapter II is discussed in Chapter VII. In some instances, by coincidence, the test results compare with one theory or another but no one theory is able to predict $N_{\gamma q}$ at all footing locations nor take changes in Φ into account.

In view of the fact that no existing theory seems satisfactory, it is interesting to attempt to use a limit analysis approach to predict the test results. This approach, as discussed in Chapter II, implies that a true solution is bounded by an upper and a lower limit. An upper bound solution was worked out by Chen (1974) using velocity fields for footings located at the slope crest. These values are shown to be quite close to the Meyerhof values. Eventhough the Meyerhof values do not meet all the requirements of the upper bound theorem, they are used as an upper limit to the solution.

No lower bound solutions are available for comparison

purposes. Some existing theoretical solutions are shown to yield values that are lower than the test results, but all violate the requirements of the lower bound theorem. Most of these theoretical values were obtained using the limit equilibrium concept. To overcome this dilemma, a finite element analysis of the problem is considered since the finite element method meets all requirements of the lower bound theorem. In the following paragraphs the method is described, and various parameters are chosen.

8.2 Finite Element Analysis

8.2.1 General

Compared to other numerical methods, the finite element method has many advantages. It can treat problems with complex geometry and isotropic or anisotropic material having linear or non-linear elastic properties. Many papers have been published recently on the application of the method to geotechnical problems.

Since the principles of finite elements analysis have been described in detail by authors such as Abel and Desai (1972) and Bowes (1975), only a very brief description will be given here.

The basic concept of the finite element method is to replace the continuum by a medium that is made up of a finite number of elements. These elements are joined together at nodal points which in the simplest form are located at the

corner of each element.

The forces and the displacements at each node are interrelated by the following equation:

$$f = Ku \tag{8.2.1}$$

where f = the force

u = the displacement

K = a constant relating f and u.

For each element, Equation (8.2.1) becomes, under matrix representation:

$$\{F_e\} = [K_e]\ [u_e] \tag{8.2.2}$$

where $\{F_e\}$ = force vector matrix at the nodes of the element

$[u_e]$ = displacement vector matrix at the nodes of the element

$[K_e]$ = stiffness matrix of the element.

The nodal displacement can be represented as a polynomial with a varying degree of freedom such as:

$$u = \alpha_1 + \alpha_2 x + \alpha \tag{8.2.3}$$

$$v = \alpha_3 + \alpha_4 x \tag{8.2.4}$$

Equations (8.2.3) and (8.2.4) can be given in matrix form:

$$\begin{bmatrix} u \\ v \end{bmatrix} = \begin{bmatrix} \alpha_1 \\ \alpha_2 \\ \alpha_3 \\ \alpha_4 \end{bmatrix} \tag{8.2.5}$$

If u and v are replaced by the displacement matrix $[\delta]$

$$[\delta] = [A] \{\alpha\} \tag{8.2.6}$$

where $[\delta]$ = transformed displacement matrix

$[A]$ = position displacement matrix

$\{\alpha\}$ = coefficient matrix

From Equation (8.2.6)

$$\{\alpha\} = [A^{-1}] \{\alpha\} \tag{8.2.7}$$

Now to convert displacement into strain

$$\epsilon_{xx} = \frac{\delta u}{\delta x} \tag{8.2.8}$$

Under matrix form, this could be given as:

$$[\epsilon] = \begin{bmatrix} \text{differentiation} \\ \text{matrix} \end{bmatrix} [\delta] \tag{8.2.9}$$

$$[\epsilon] = \begin{bmatrix} \text{differentiation} \\ \text{matrix} \end{bmatrix} [A] [\alpha] \tag{8.2.10}$$

$$[\epsilon] = [B] [\alpha] \tag{8.2.11}$$

$$[B] = \begin{bmatrix} \text{differentiation} \\ \text{matrix} \end{bmatrix} [A] \tag{8.2.12}$$

Now substituting (8.2.7) into (8.2.11),

$$[\varepsilon] = [B]\ [A^{-1}]\ [\delta] \tag{8.2.13}$$

The relationship that exists between stress and strain is given as:

$$\sigma = [C]\ [\varepsilon] \tag{8.2.14}$$

[C] = the material property matrix.

From the virtual work principle, the external work is equal to internal energy:

$$[F]\ [\delta]^T = \int_{vol} [\varepsilon]^T \{\sigma\}\ d_u \tag{8.2.15}$$

$$[F]\ [\delta]^T = \int_{vol} [B]\ [A]^{-1}\ [\delta]^T\ [C][B][A][\delta]dv \tag{8.2.16}$$

$$[F] = [A^{-1}]^T\ [B]^T\ [C][B][A^{-1}]\ [\delta]vol \tag{8.2.17}$$

$$F = vol[A^{-1}]^T\ [B]^T[C][B][A^{-1}]\ [\delta] \tag{8.2.18}$$

Then

$$K = vol\ [A^{-1}]^T[B]^T[C][B][A^{-1}] \tag{8.2.19}$$

The purpose of the finite element method is to find the stresses in each element. Once the mesh has been drawn, the forces are known at nodal points where displacements are unknown, and vice versa. From the geometry and the material properties, a stiffness matrix for each element is formed.

Then the overall stiffness matrix K_A is worked out from the individual element stiffness matrices. This matrix K_A has values only along the diagonal; many entries are zero. This is why, in a computer analysis, only the diagonal is considered to reduce the size of the K_A matrix and the demand on the computer. Now the overall problem becomes,

Force equation

$$[F_A] = [K_A][U_A] \tag{8.2.20}$$

Displacement equation

$$[U_A] = [K_A^{-1}][F_A] \tag{8.2.21}$$

From Equation (8.2.10) and Equation (8.2.21) forces are found and displacements are known at each nodal point. To find the stresses in each element, Equation (8.2.14) is used. For example:

$$[\sigma(x,y)] = [C]\ [B(x,y)]\ [A^{-1}]\ [\delta(x,y)] \tag{8.2.23}$$

$[\delta(x,y)]$ = nodal displacements that are included in an element and that are found by Equation (8.2.21).

8.2.2 Analysis

8.2.2.1 Scope of the Study

The finite element program used in the present study is called ISBILD. This program calculates the stresses and displacements in embankments, simulating the actual sequence of construction involved in building the embankment. ISBILD is fully described in a publication by Ozawa and Duncan (1973).

This program is available at the University of California at Berkeley, California. The computer facilities of the University of California were used to perform the present finite element analysis.

Because of time and cost factors, only four footing locations were analysed. These were for footings located:

1- at the slope crest (0 - 0)

2- at a distance of 2.5 footing widths from the slope crest, on the surface (2.5 - 0)

3- at the slope crest, but at a depth of 0.6 footing widths from the surface (0 - 0.6)

4- at a distance of 2.5 footing widths from the slope crest, but at a depth of 0.6 footing widths from the surface (2.5 - 0.6).

The starting point of the analysis consisted of generating the finite element mesh for the four footings.

Two finite element meshes were used for the analysis. The finite element mesh shown on Figure 8.1 is used for footings 0 - 0 and 0 - 0.6, while the mesh shown on Figure 8.2 is used for footings 2.5 - 0 and 2.5 - 0.6.

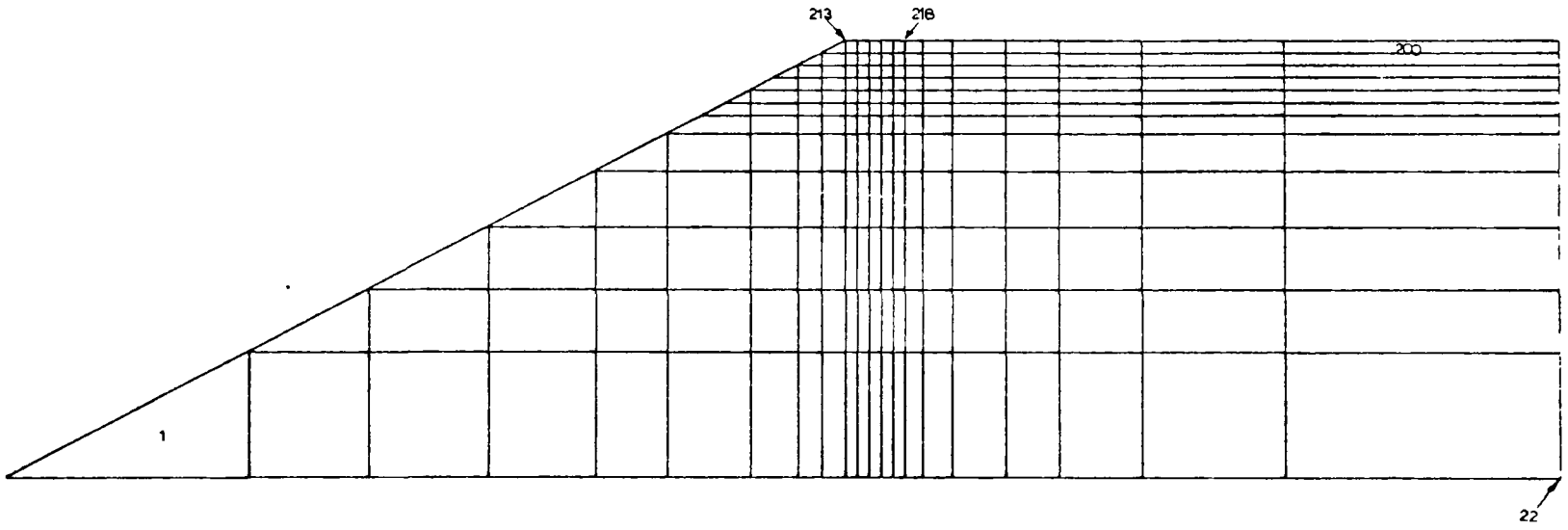

Figure 8.1

Finite Element Mesh for Locations 0-0 and 0-0.6

Finite Element Mesh for Locations 2.5-0 and 2.5-0.6

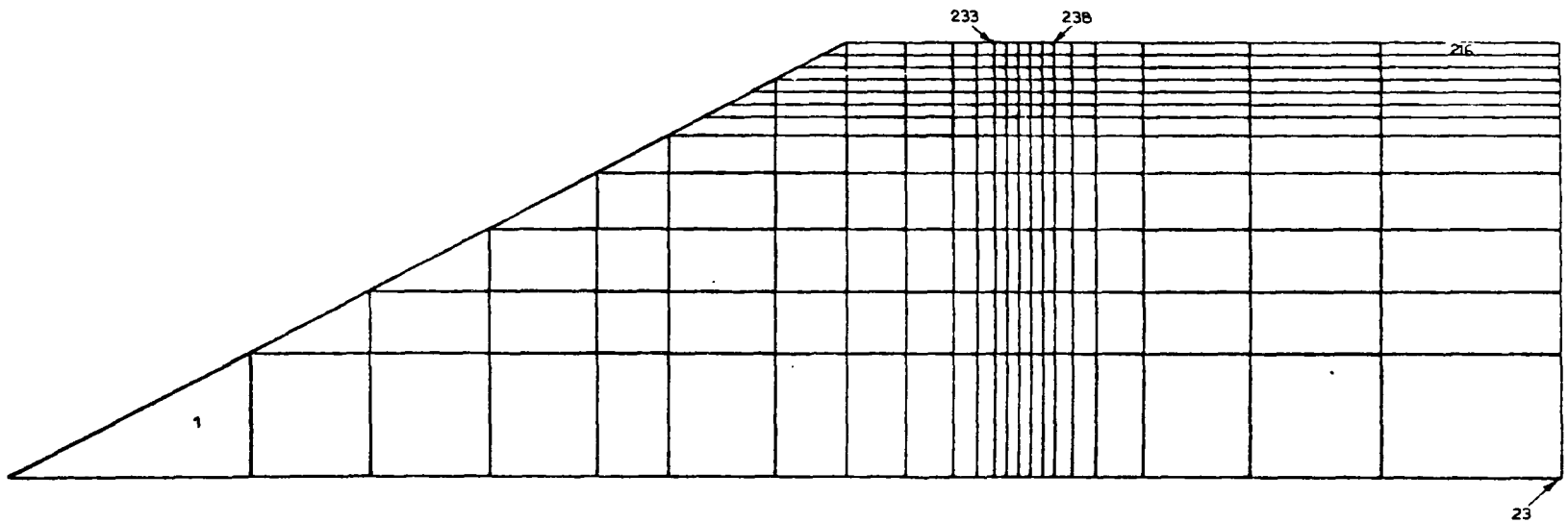

Figure 8.2

8.2.2.2 Soil Parameters

In order to be able to relate the finite element work to the theories discussed in Chapter II, the same simplifying assumptions are made regarding the soil properties. This also has the practical advantage of reducing the amount of computer time and cost. The soil is considered to be an ideal isotropic, homogeneous elastic cohesionless mass.

A linear elastic stress-strain relationship is used throughout the analysis. This simplifying assumption affects the magnitude of the displacements more than the loads. In fact, it can be shown that load or pressure results are independent of the modulus of elasticity if the soil is isotropic. This can be explained as follows:

$$[F_A] = [K_A][U_A] \tag{8.2.20}$$

$$[U_A] = [K_A^{-1}][F_A] \tag{8.2.21}$$

$[K_A^{-1}]$ is the inverse of the stiffness matrix that depends on the geometry of the elements and their material properties. It has E, which is scalar, as the denominator.

Also for each element the stresses are

$$[\sigma(x,y)] = [C]\ [B(x,y)][A^{-1}][\delta] \tag{8.2.23}$$

where $[\delta]$ = displacement matrix for a particular element.

This value is found to be a function of $[K_A]^{-1}$, and thus

is an invert function of the scalar E.

[C] = property matrix having E as numerator.

Therefore the value of $[\sigma(x,y)]$ is not a function of E beacuse the E in [C] cancels out with the E in $[\delta]$. In linear elasticity however, the displacements are linearly dependent on the magnitude of E.

In this analysis, only the stress distribution is important; therefore the value of E is not significant. Any value of E could be assigned without altering the stress results, provided the external forces remain the same.

A Poisson's ratio of 0.5 is used in the analysis. Basically, a Poisson's ratio of 0.5 means there is no volume change during shear. This is a simplification of the actual problem, because it is known that during shear, the soil will compress if it is in a loose state, and will dilate if it is in a dense state. The assumption of no volume change is consistent with Meyerhof's solution which is taken to be the upper bound.

For comparison purposes, the angle of internal friction was set at 50 degrees. As will be seen, the choice of this value is arbitrary, and any angle Φ could be used to make the comparison. The following section (8.2.2.4) discusses the choice of the failure criterion. A value of K_o equal to 0.6 is used to deduce the state of initial stress in the ground. Even though $K_o = 0.6$ is not compatible with the choice of ν (in theory $K_o = \frac{\nu}{1 - \nu}$) it is a better value to use to estimate

the initial horizontal stresses.

The program ISBILD calculates the stresses and displacements in embankments while simulating the actual sequence of construction of the embankment. The analysis is performed by placing the fill in layers. The stresses in each layer, immediately after placement and due to its own weight, are assigned rather than calculated. These assigned values are

σ_z (vertical stress) = γh

σ_x (horizontal stress) = $K_o \gamma h$

τ_{xy} (shearing stress) = $0.5\ \gamma h \sin\alpha$

Subsequent changes in stress due to the weight of additional layers are calculated by the finite element method.

The unit weight of the soil is taken to be 1600 kg/m^3.

8.2.3 Procedure

The analysis gives the elemental stresses for three loading conditions. First, the initial state of stress in a particular element is computed after the particular layer containing the element is placed on the embankment. Then, the stresses in the same element are calculated after the remaining soil layers are placed. Finally, the stresses in the element are worked out for two footing stresses, namely 250 kPa and 375 kPa of applied pressure. The stresses due to any other loading conditions can be found easily by extra-

polation because of the linear relationship between elemental stresses and external loading. A provision was made in the computer program to ensure that the loading conditions would yield uniform settlement of the footing.

All stresses in a particular soil element are calculated by the finite element method for each surface load. Once the stresses are calculated, namely σ_x, σ_z and τ_{xz}, the principal stresses acting on that element are found. This process yields a σ_1 and σ_3 for each element after each loading condition and the ratio $\frac{\sigma_1}{\sigma_3}$ is calculated for each element. This ratio is then compared to the failure $\frac{\sigma_1}{\sigma_3}$ ratio given by the Mohr-Coulomb failure criterion for the angle of internal friction chosen for the comparison.

From the Mohr-Coulomb failure criterion the failure ratio is given as:

$$\frac{\sigma_1}{\sigma_3} = \frac{1 + \sin\Phi}{1 - \sin\Phi} \qquad (8.2.24)$$

Because linear elasticity has been assumed, the values of $\frac{\sigma_1}{\sigma_3}$ in each element are not Φ dependent. This means that it is a simple procedure to check whether any element has failed for any angle of Φ.

8.3 Results

To show tha propagation of failure in the soil mass, contours of the principal stress ratio $\frac{\sigma_1}{\sigma_3}$ are plotted for

each of the footing locations. The numbers indicated on the contour lines refer to the magnitude of $\frac{\sigma_1}{\sigma_3}$ after a particular surface loading. The cases studied in this analysis use linear elasticity; the trend shown on Figures 8.3 to 8.6 is consistently the same for each footing location, irrespective of the magnitude of the load on the footing.

In these figures it is interesting to note that there is a high stress concentration in the soil on either side of the footing. From these two points of high stress concentration, failure propagates out into the soil.

The influence of the slope on the way in which failure propagates is obvious in the cases of 0 - 0 and 0 - 0.6. There is a third point of high stress concentration near the slope in the case of footing 0 - 0, and in both cases the contours are highly asymmetric. In the case of 2.5 - 0 and 2.5 - 0.6, the asymmetry of the contours is not as pronounced, and the slope certainly has less influence.

In Figures 8.7 to 8.10, the distribution of the ratio of the major principal stress to the footing load is shown in contour form. For all cases, the distribution is similar to the Boussinesg prediction. A few differences from Boussinesg are noted because the initial stresses in the soil mass are taken into account, but the slope is shown to have very little influence. In the case where the footing is located at the slope crest, (0 - 0), the contour for $\frac{\sigma_1}{q} = 0.2$ is not symmetrical with respect to the footing axis; this could possibly

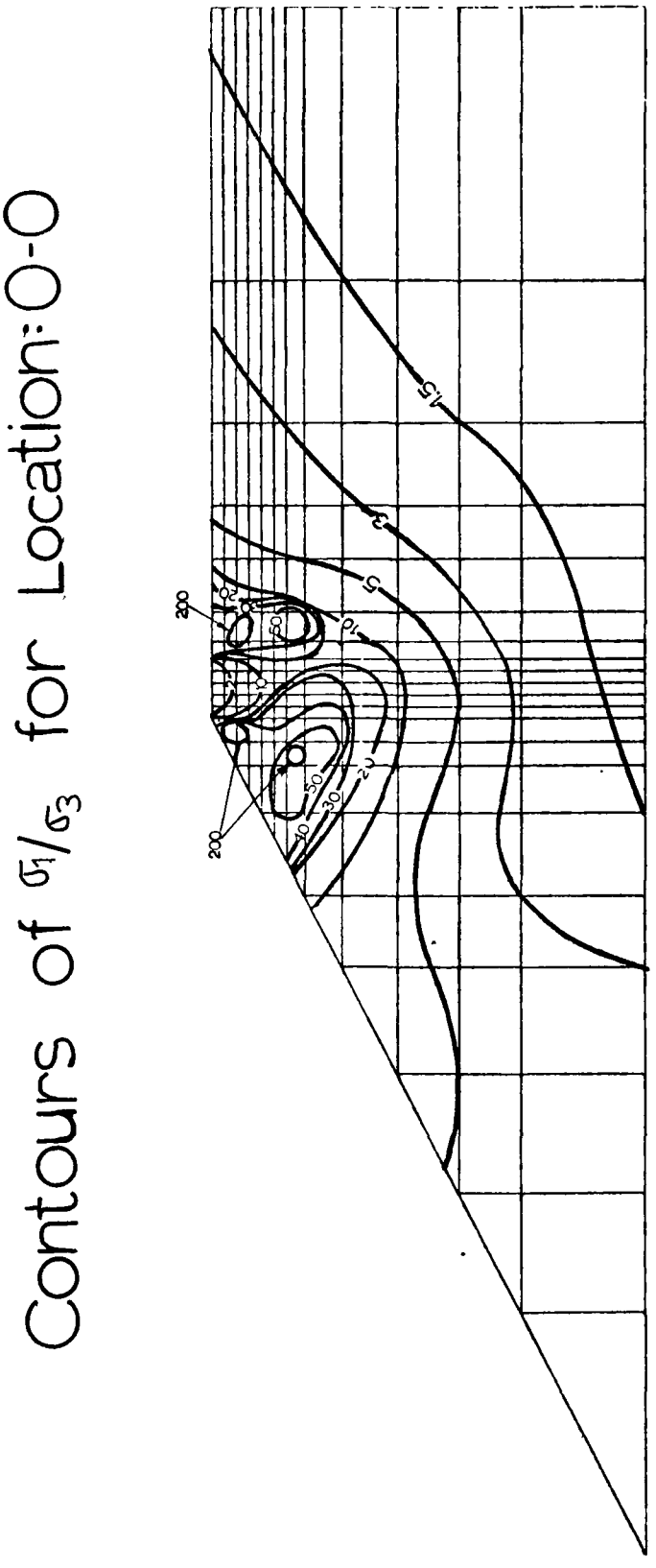
Contours of σ_1/σ_3 for Location: O-O
200
200
50
30
20
15
10
5
3
2

Figure 8.3

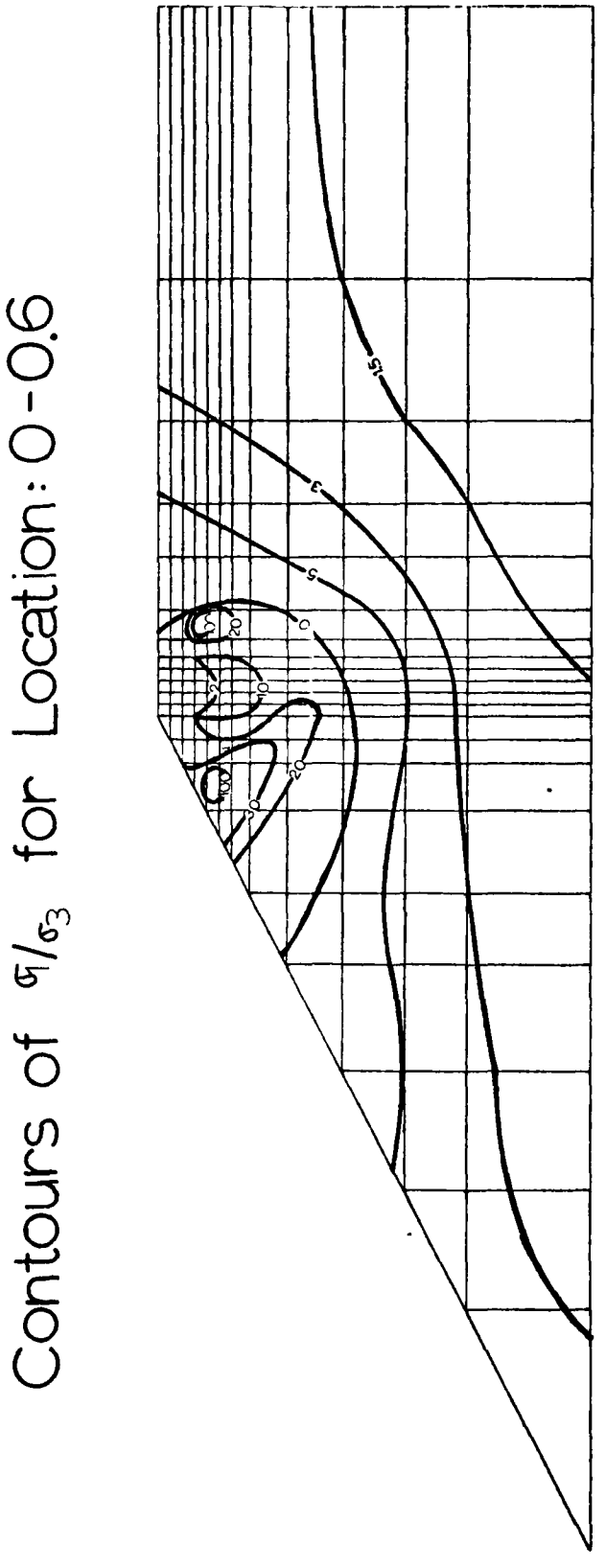

Figure 8.4

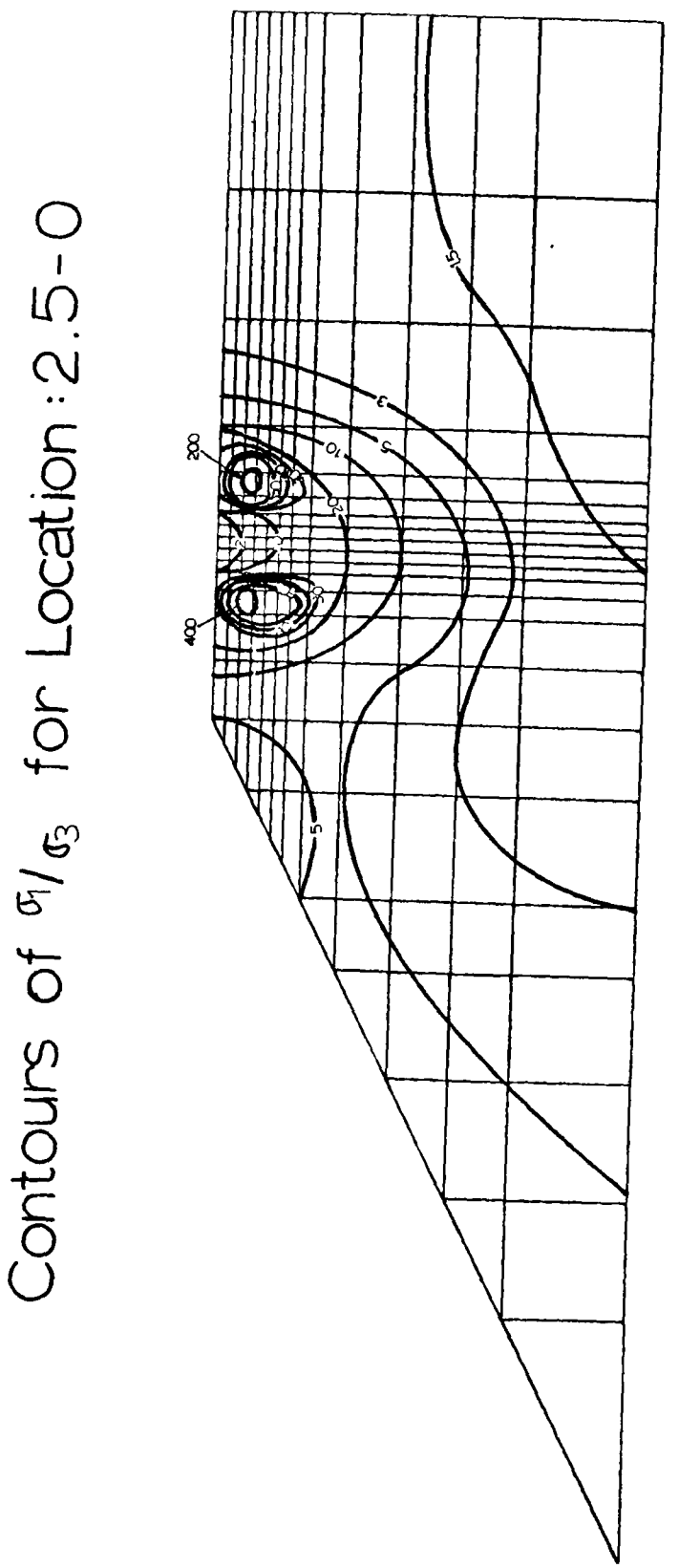
Contours of σ_1/σ_3 for Location: 2.5-0
200
400
15
3
10
5
2.5
2
5

Figure 8.5

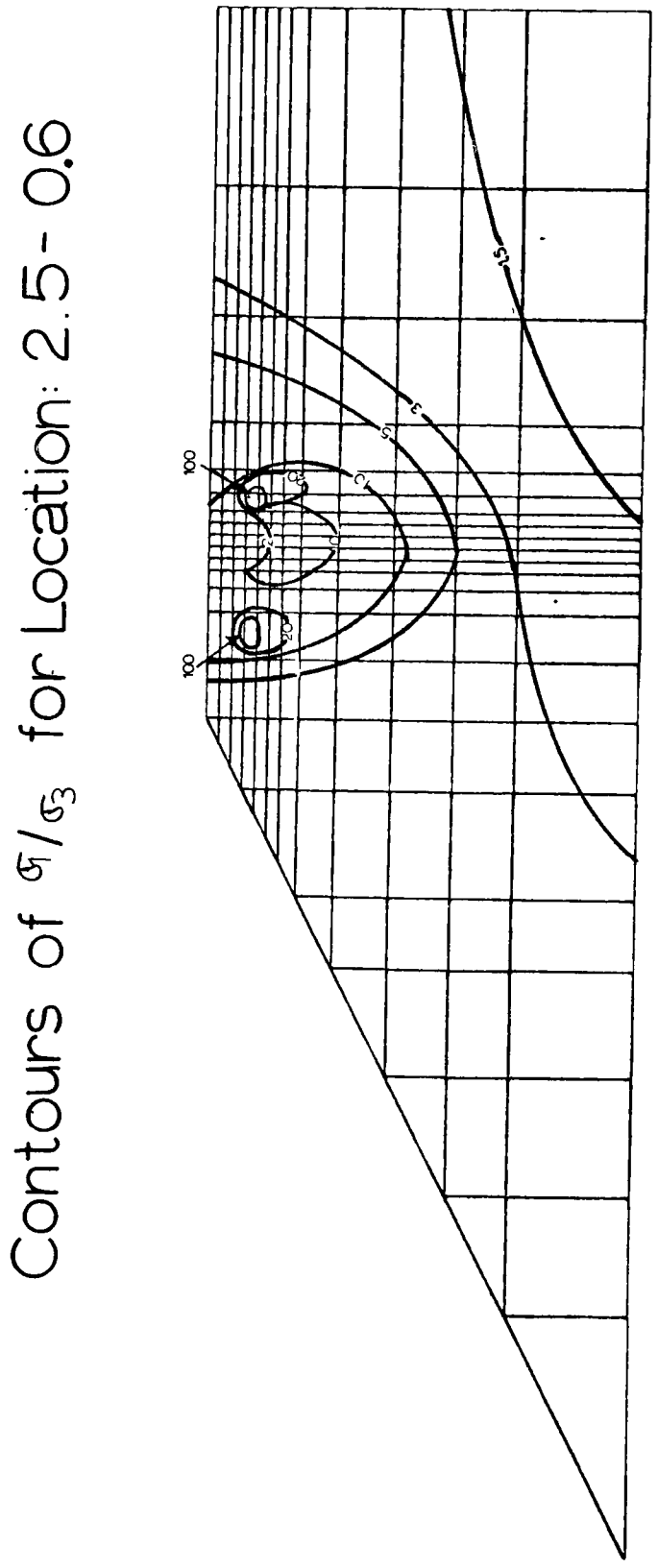

Figure 8.6

be attributed to the presence of the slope.

The concentration of the major principal stresses at the edges of the footing is due mainly to the fact that this investigation uses the simulation of a rigid footing. The principal stress under the middle of the footing is only fifty percent of the average applied bearing pressure.

In Figures 8.11 to 8.14, the distribution of the ratios of minor principal stresses to the applied load is plotted. This distribution is quite similar to the prediction given in standard references such as Lambe (1969). The distribution is the same for all cases, and the slope seems to have little or no influence.

In Figures 8.15 to 8.18, the elements that have failed under the applied load of 250 and 375 kPa for a principal stress ratio of $\frac{\sigma_1}{\sigma_3}$ equal to 7.55 or a Φ of 50° are shown. As previously mentioned, the choice of $\Phi = 50°$ is quite arbitrary. If another angle is chosen, the pattern of failed elements could be different. Nevertheless, it can be seen that a block of elements underneath the footing do not fail. This tends to confirm the assumption that a rigid wedge forms under the footing which acts as part of the footing. The geometry of the elastic wedge could be defined with more precision if a finer finite element mesh is used.

The results obtained from this computer analysis indicate that many elements fail soon after the initial application of a load. Failure propagates in the soil mass from high stress

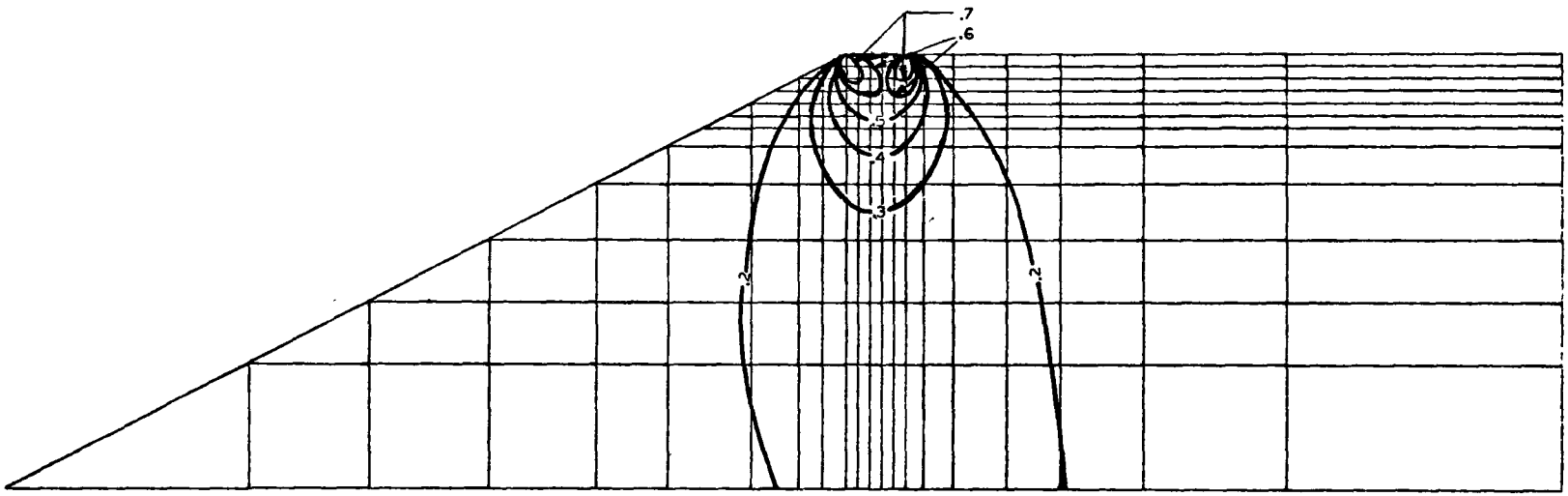

Figure 8.7

Contours of σ_1/q for Location: 0 - 0.6

q: Applied Pressure

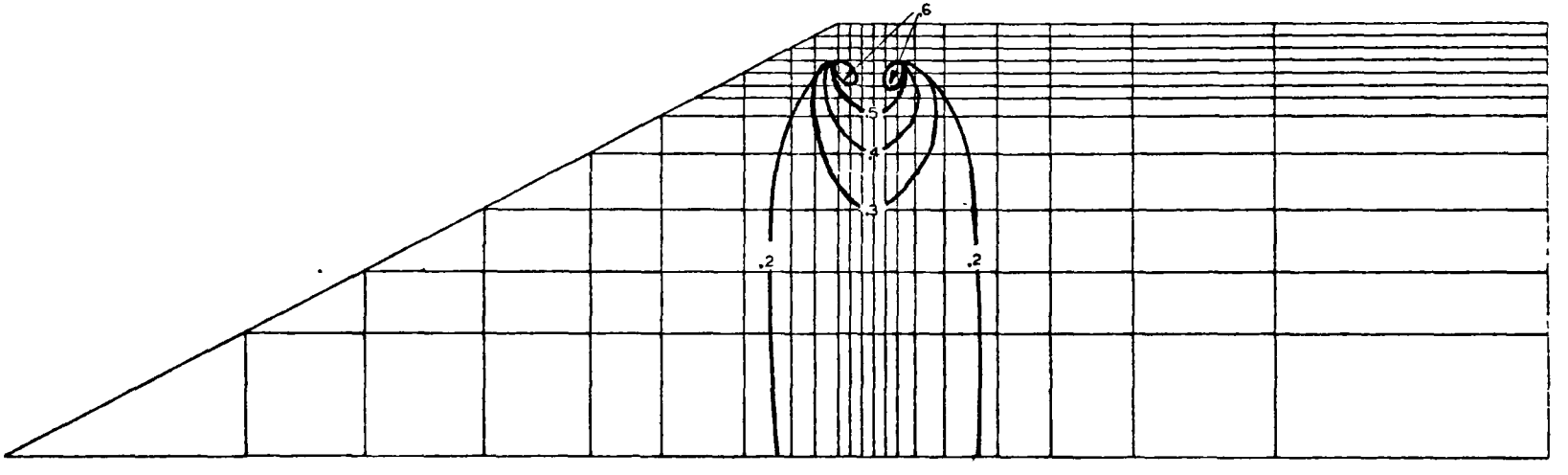

Figure 8.8

Contours of σ_1/q for Location: 2.5 - 0

q : Applied Pressure

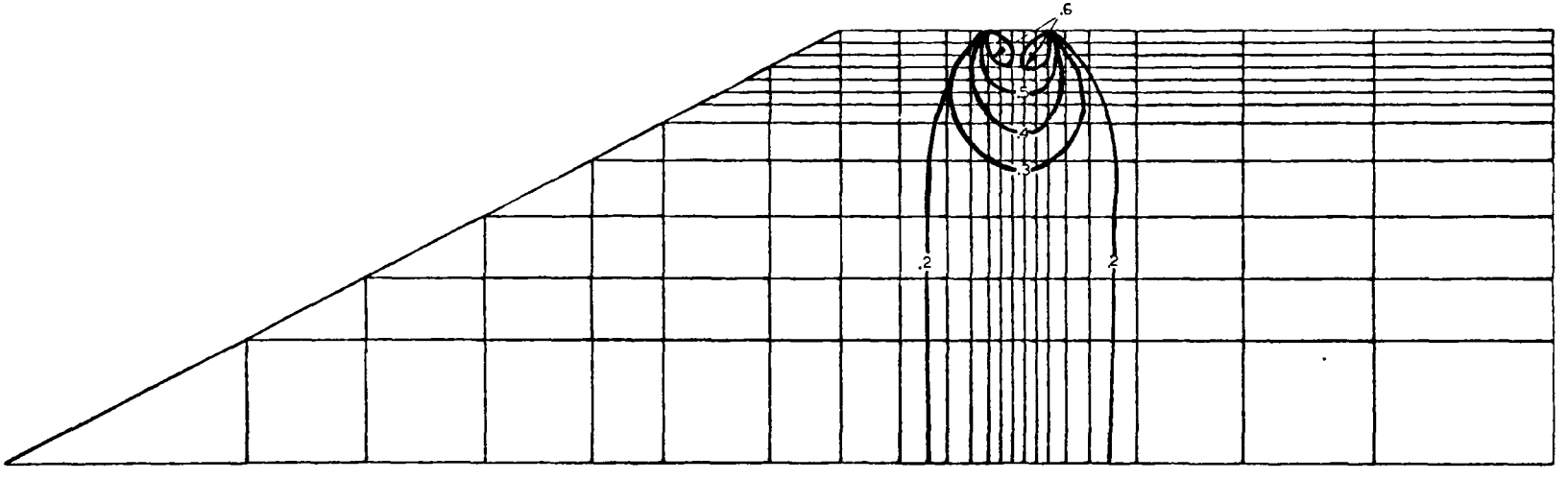

Figure 8.9

Contours of σ_1/q for Location: 2.5 - 0.6

q: Applied Pressure

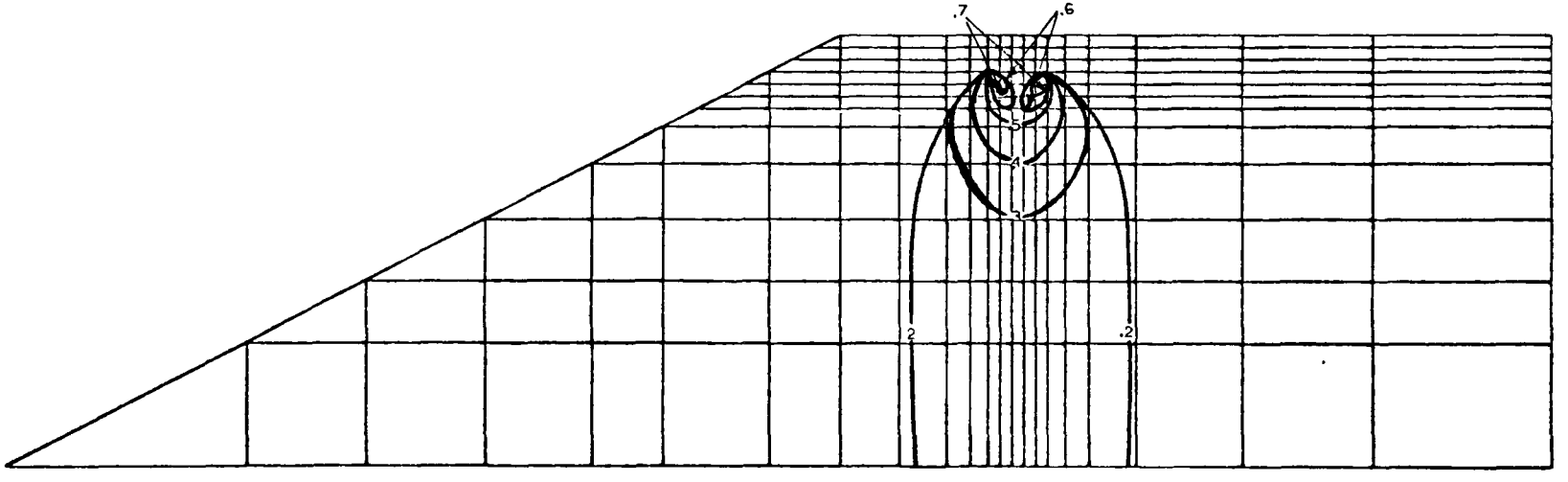

Figure 8.10

Contours of σ_3/q for Location: O-O

q : Applied Pressure

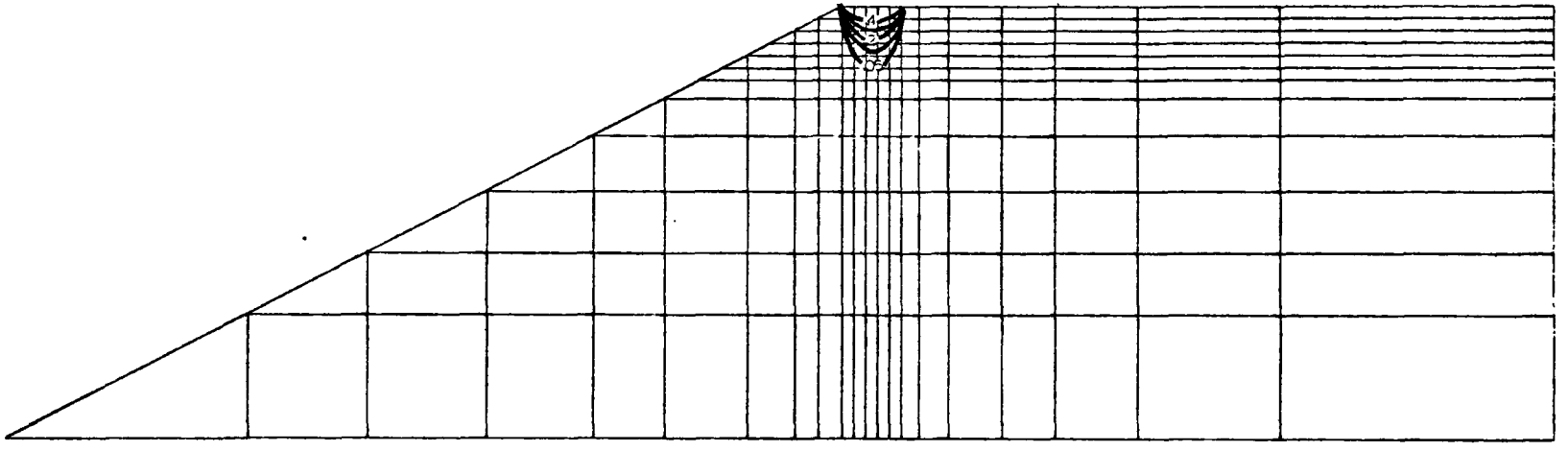

Figure 8.11

Contours of σ_3/q for Location: 0 - 0.6

q : Applied Pressure

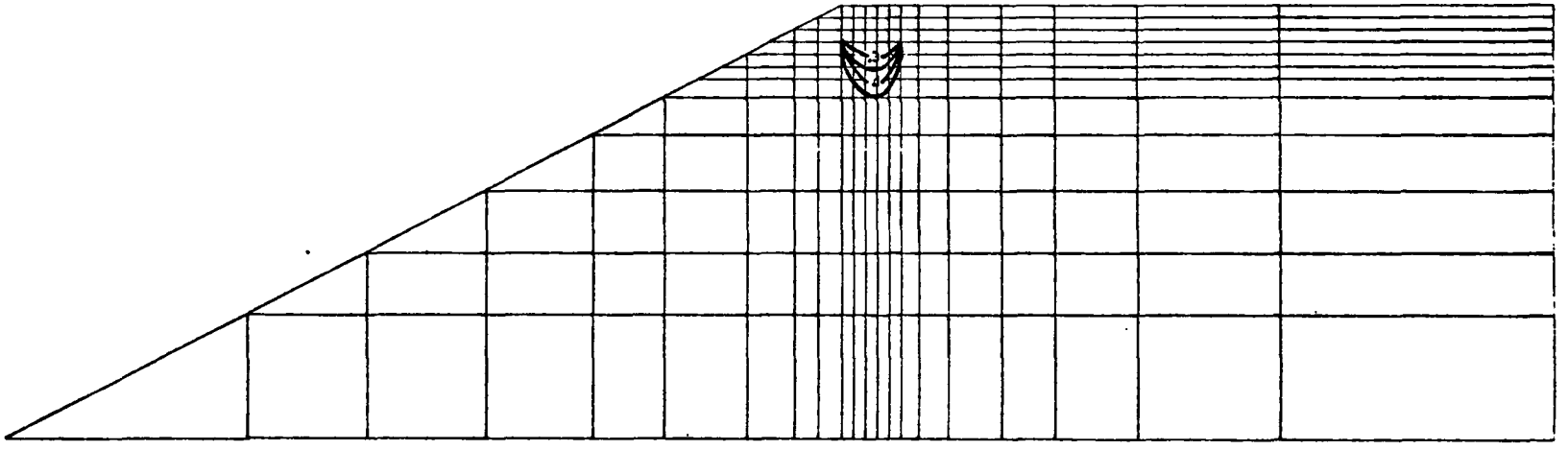

Figure 8.12

Contours of σ_3/q for Location: 2.5 - 0

q : Applied Pressure

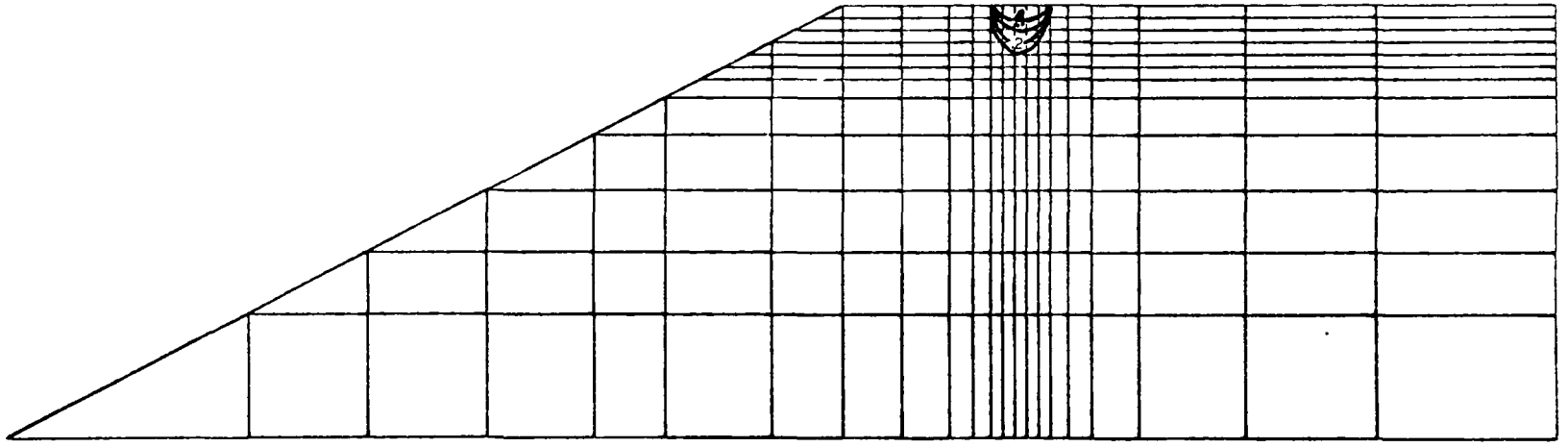

Figure 8.13

Contours of σ_3/q for Location: 2.5 - 0.6

q : Applied Pressure

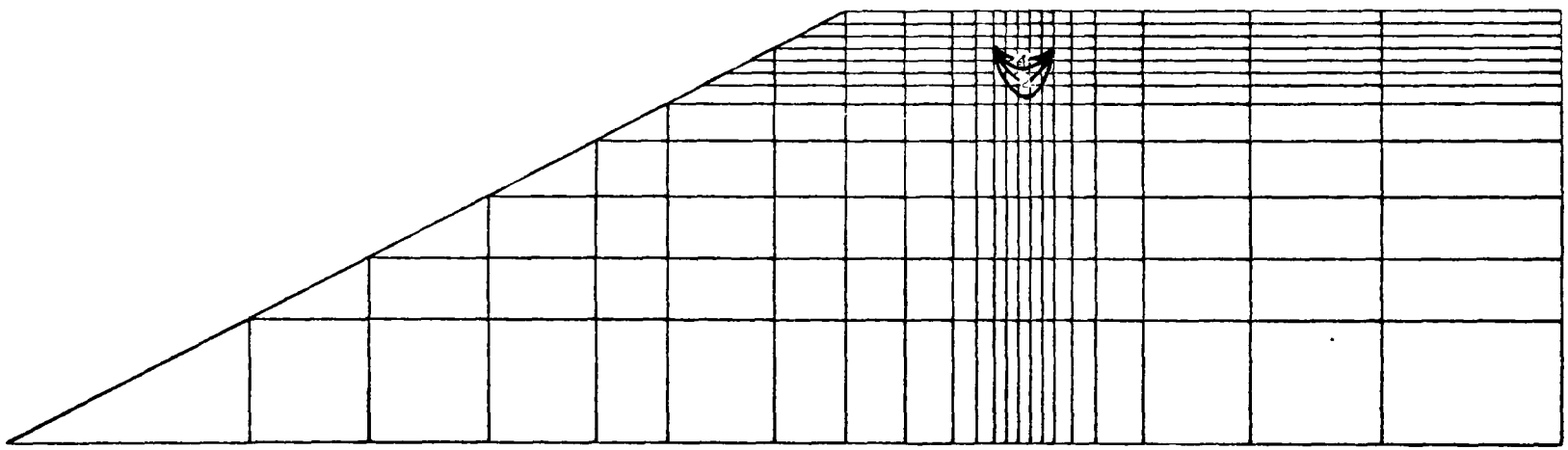

Figure 8.14

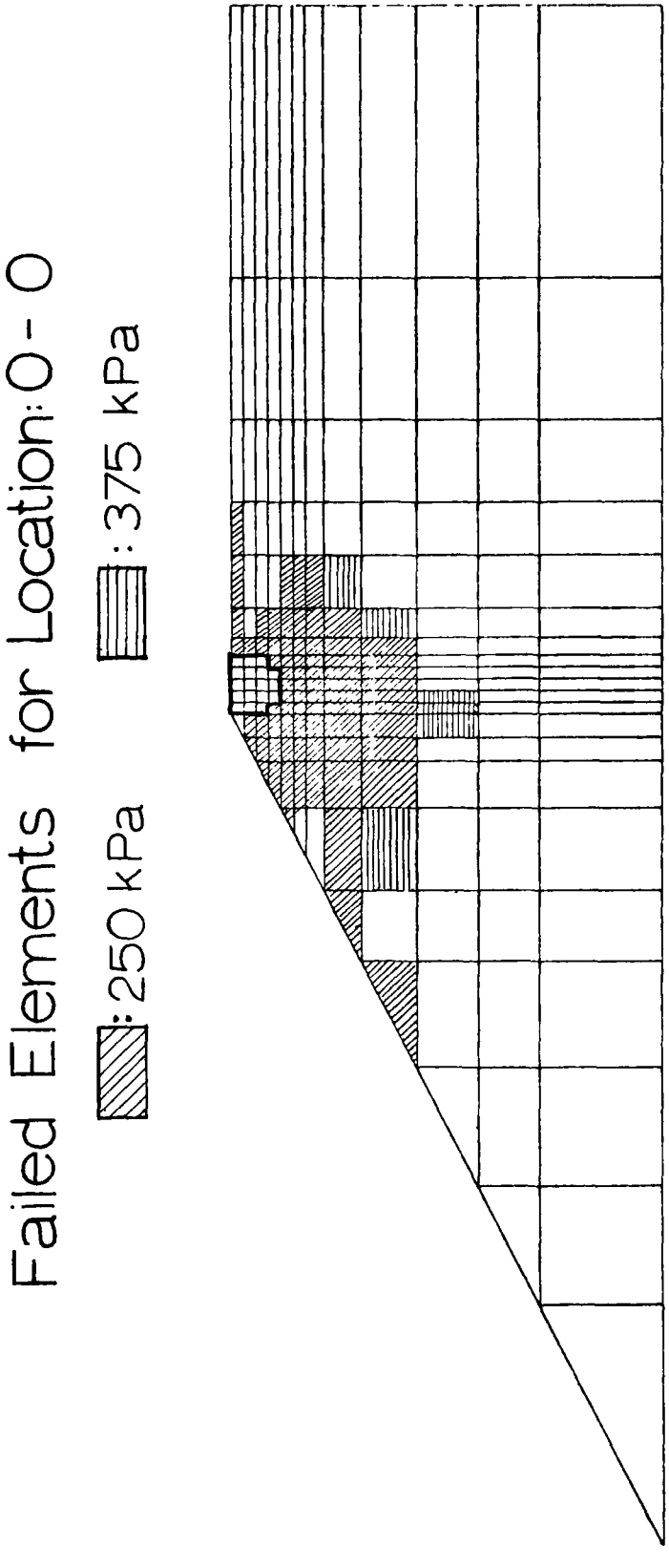

Figure 8.15

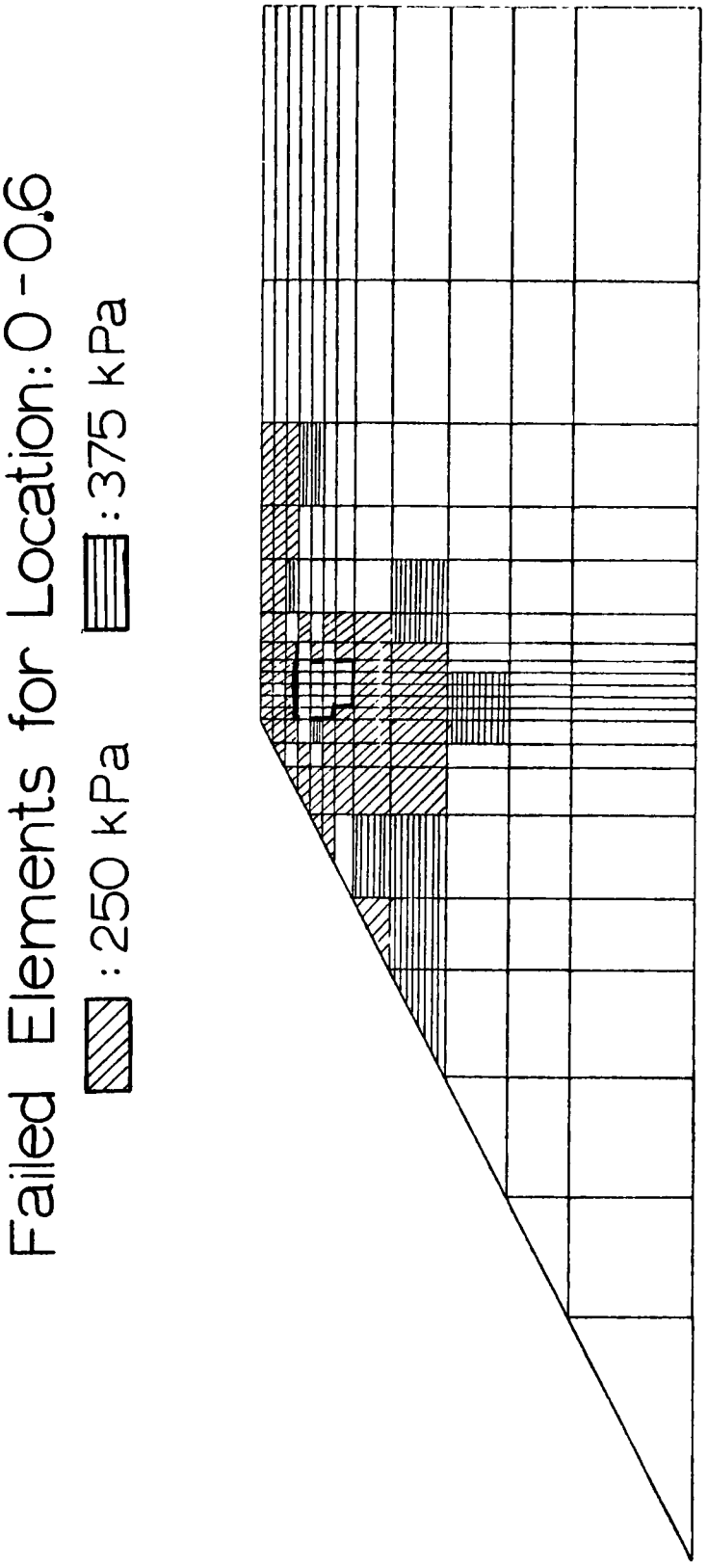

Figure 8.16

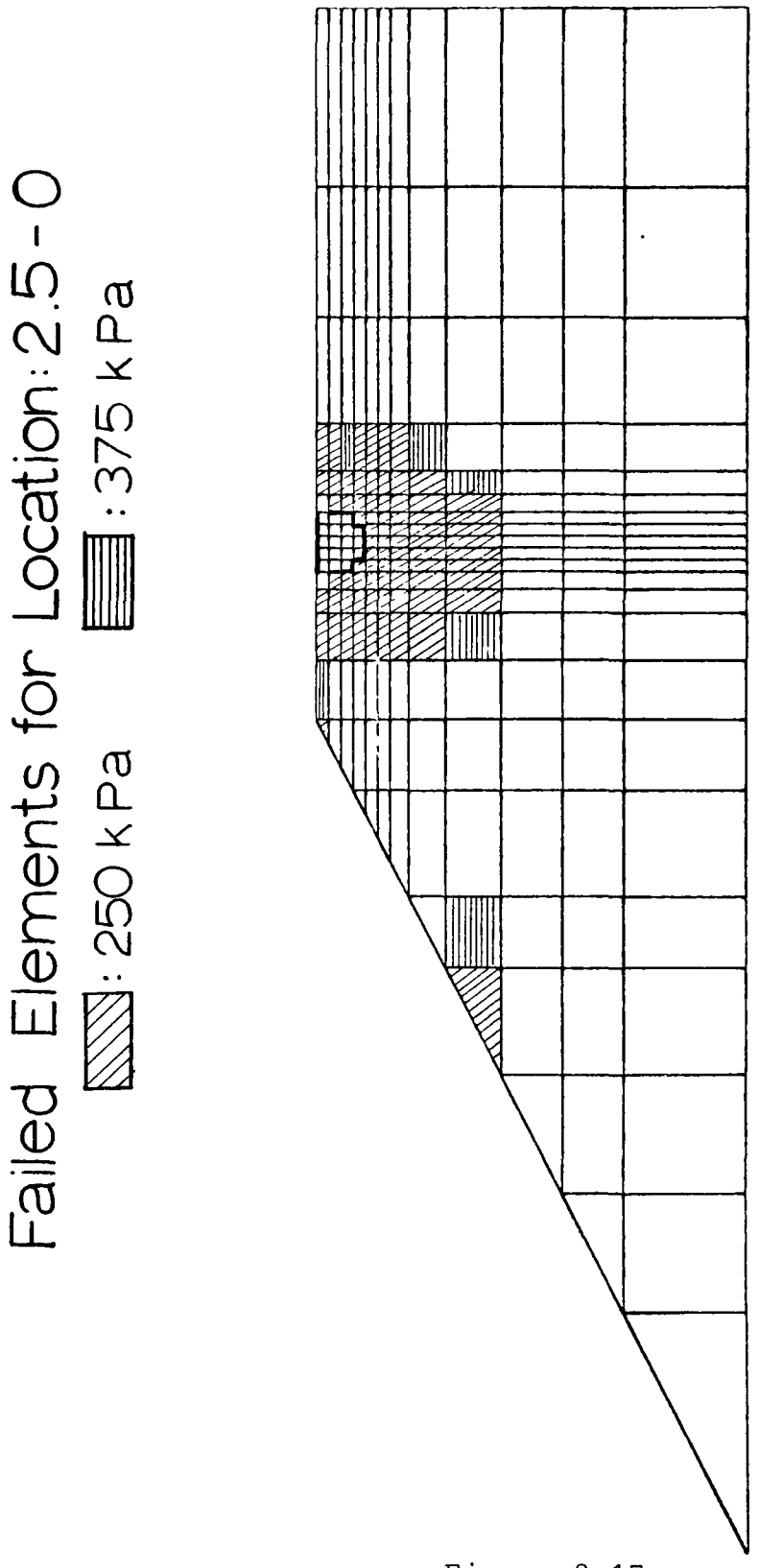

Figure 8.17

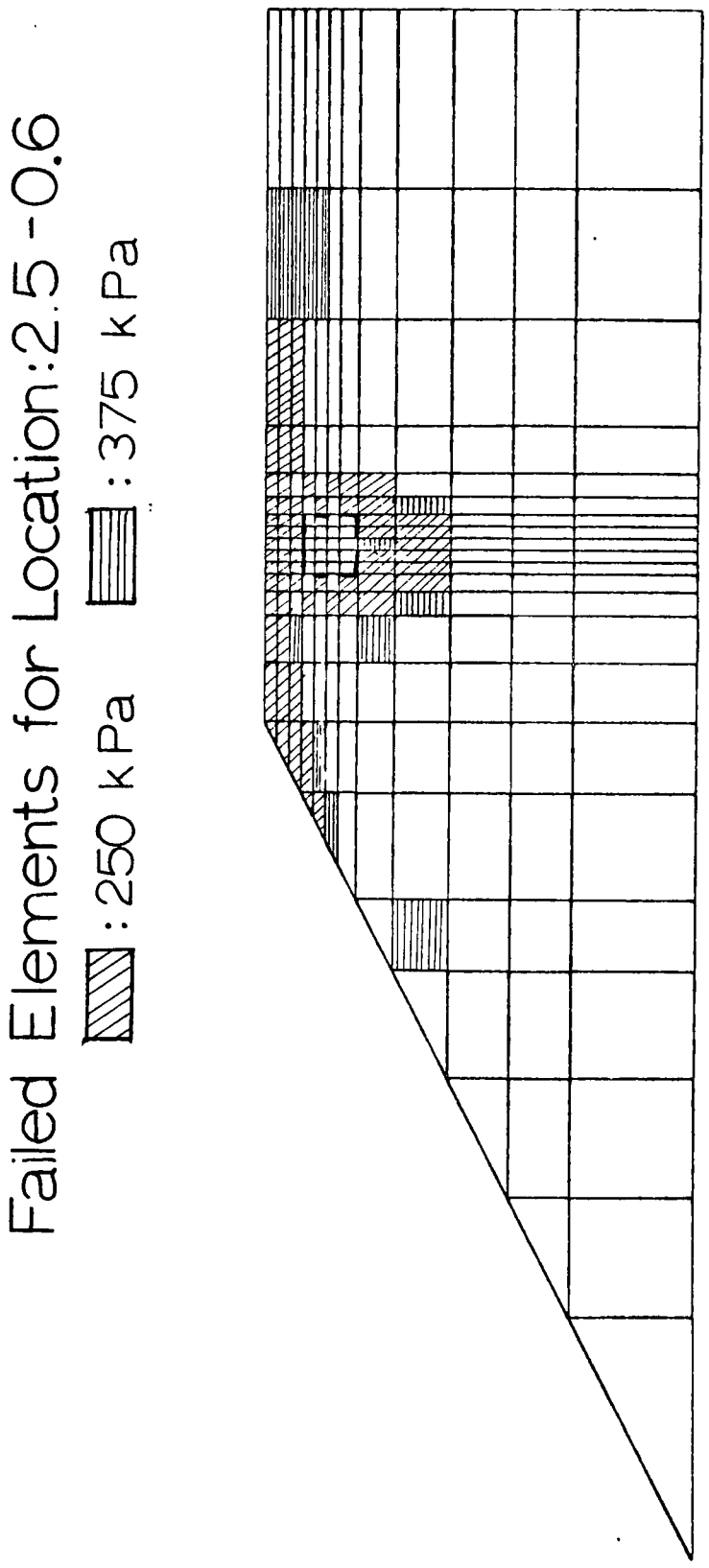

Figure 8.18

concentration points. The last elements to fail are those located beyond a radius of 3B from the middle of the footing and those located immediately under the footing.

The first element to fail is always located on the mid axis of the footing at the apex of the rigid wedge which forms under the footing. This element is located at a depth of 1B and is the element which is used to define the lower limiting value of bearing capacity. This critical element has a different number depending on the location of the footing with respect to the slope crest:

Footing Location	Element Number
0 - 0	134
0 - 0.6	86
2.5 - 0	143
2.5 - 0.6	92

The principal stresses (in kPa) acting on the critical elements for the 250 and 375 kPa loads are given in the following table:

Footing Location	Element Number	For a load of 250kPa on the footing, the principal stresses in the element are:		For a load of 250kPa on the footing, the principal stresses in the element are:	
		σ_1	σ_3	σ_1	σ_3
0 - 0	134	134	13	200	19
0 - 0.6	86	108	12	157	16
2.5 - 0	143	137	16	203	22
2.5 - 0.6	92	107	15	156	19

Advantage can be taken of the fact that since linear elasticity is being used, a linear relationship exists between the applied load and the principal stresses in each element. Equations can be established giving the principal stresses acting on an element as a function of the applied footing pressure. These equations are given here for each footing location.

1 - For footing location 0 - 0 where the critical element is number 134:

$$\sigma_1 = .53q_p + 1.6 \qquad (8.3.1)$$

$$\sigma_3 = .05\ q_p + 0.98 \qquad (8.3.2)$$

where q_p = applied pressure on footing.

Incorporating Equations (8.3.1) and (8.3.2) into the failure criterion (Equation 8.2.24), an expression for the prediction of the failure load as a function of

the angle of internal friction would be as follows:

Substituting (8.3.1) and (8.3.2) into (8.2.24)

$$\sin\Phi = \frac{\sigma_1 - \sigma_3}{\sigma_1 + \sigma_3} = \frac{(.53q_p + 1.6) - (.05q_p + .98)}{(.53q_p + 1.6) + (.05q_p + .98)} \quad (8.3.3)$$

$$\sin\Phi = \frac{.48q_p + .62}{.58q_p + 2.58} \quad (8.3.4)$$

Rearranging (8.3.4) becomes:

$$q_p = \frac{.62 - 2.58 \sin\Phi}{.48 - .58 \sin\Phi} \quad (8.3.5)$$

The load required to fail element number 134, according to the Mohr-Coulomb criterion, versus the angle of internal friction is given below.

Φ	q_p (kPa)
30°	10
35°	15
40°	23
45°	38
50°	75

These results are also shown on Figure 8.19.

2 - Following the same procedure as in 1), the pertinent equations for footing location 0 - 0.6 are:

$$\sigma_1 = .39q_p + 9.96 \quad (8.3.6)$$

$$\sigma_3 = .32q_p + 4 \qquad (8.3.7)$$

then

$$q_p = \frac{5.96 - 13.96 \sin\Phi}{0.422 \sin\Phi - 0.358} \qquad (8.3.8)$$

The failure loads for element number 86 for various angles of internal friction are:

Φ	q_p(kPa)
30°	10
35°	18
40°	35
45°	65
50°	135

These results are also shown on Figure 8.20.

3 - For footing location 2.5 - 0 the pertinent equations are:

$$\sigma_1 = .53q_p + 4.66 \qquad (8.3.9)$$

$$\sigma_3 = .05q_p + 3.98 \qquad (8.3.10)$$

then

$$q_p = \frac{.68 - 8.64 \sin\Phi}{.58 \sin\Phi - 0.48} \qquad (8.3.11)$$

The failure loads for element number 143 for various

angles of internal friction are:

Φ	q_p(kPa)
30°	19
35°	29
40°	44
45°	78
50°	149

These results are also shown on Figure 8.21.

4 - For footing location 2.5 - 0.6 the pertinent equations are:

$$\sigma_1 = .39q_p + 8.94 \qquad (8.3.12)$$

$$\sigma_3 = .03q_p + 7 \qquad (8.3.13)$$

then

$$q_p = \frac{1.94 - 15.94 \sin\Phi}{0.42 \sin\Phi - 0.36} \qquad (8.3.14)$$

The failure loads for element number 92 for various angles of internal friction are:

Φ	q_p (kPa)
30°	40
35°	60
40°	92
45°	156
50°	257

These results are also shown on Figure 8.22.

The corresponding $N_{\gamma q}$ values for all these failure loads are presented in the table of Figure 8.23. These values are obtained by multiplying the results of Equation (8.3.5), (8.3.8), (8.3.11) and (8.3.13) for different Φ angles by 2 and dividing this result by the footing width of .3m and the unit weight.

8.4 Comparison with Experimental Results

As explained in the preceeding section, a reasonable lower bound to the problem of bearing capacity of footings on top of a slope is now available. The lower limiting values of $N_{\gamma q}$ are shown in Figure 8.23. Taking the Meyerhof values to be the upper bound values and the Figure 8.23 values to be the lower bound values, Figures 8.24 to 8.27 can be drawn for the various footing locations.

The experimental $N_{\gamma q}$ values plotted on these figures are:

Compact sand		Dense sand	
Location	$N_{\gamma q}$	Location	$N_{\gamma q}$
0 - 0	24	0 - 0	99
0 - 0.6	50	0 - 0.6	130
2.5 - 0	37	2.5 - 0	159
2.5 - 0.6	65	2.5 - 0.6	190

Each experimental value appears four times in each figure

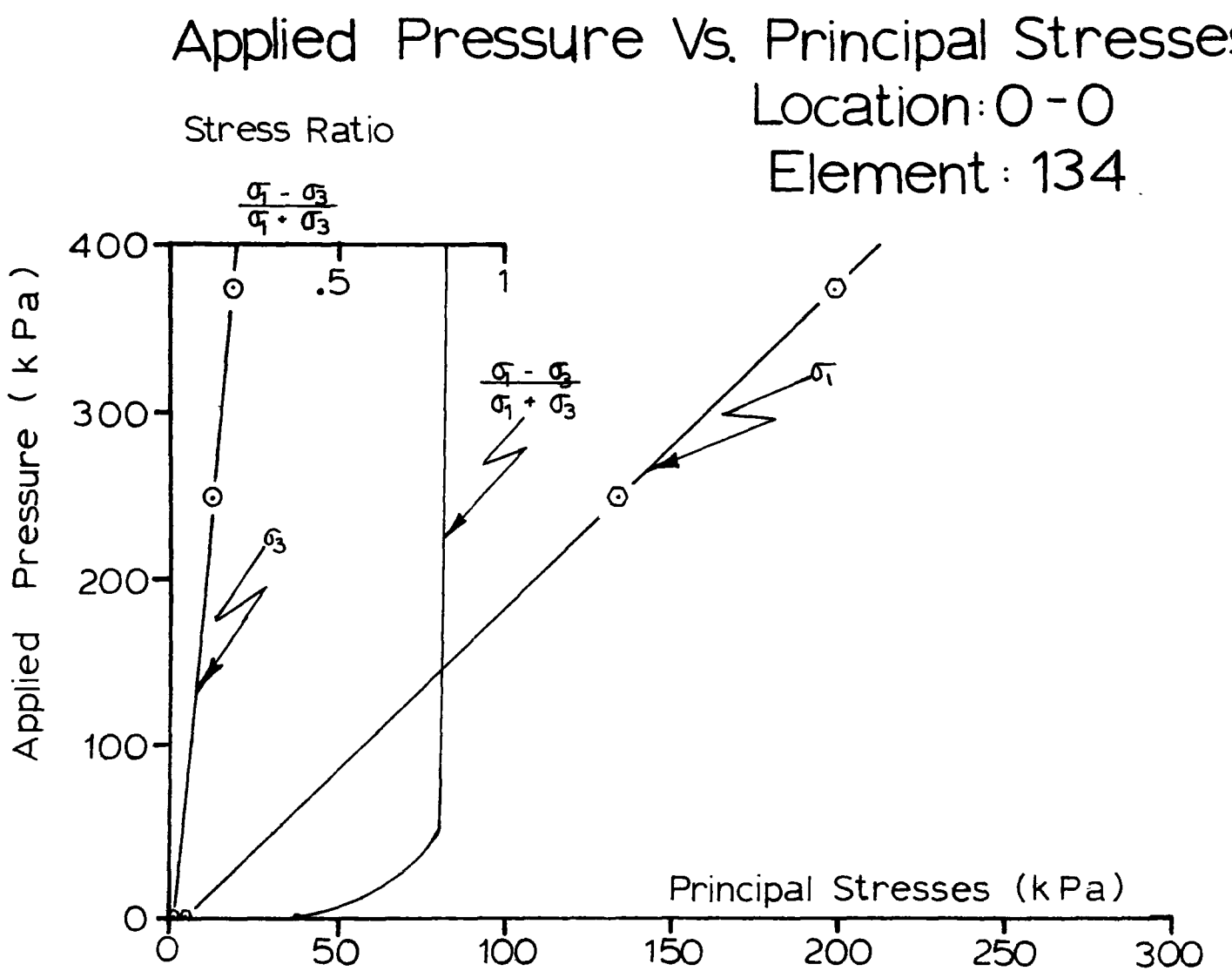
Applied Pressure Vs. Principal Stresses
Location: O - O
Element : 134
Stress Ratio
$\frac{\sigma_1 - \sigma_3}{\sigma_1 + \sigma_3}$
400
300
200
100
0
.5
1
$\frac{\sigma_1 - \sigma_3}{\sigma_1 + \sigma_3}$
σ_3
σ_1
Applied Pressure (kPa)
Principal Stresses (kPa)
0
50
100
150
200
250
300

Figure 8.19

Applied Pressure Vs. Principal Stresses

Location: 0 - 0.6

Element: 86

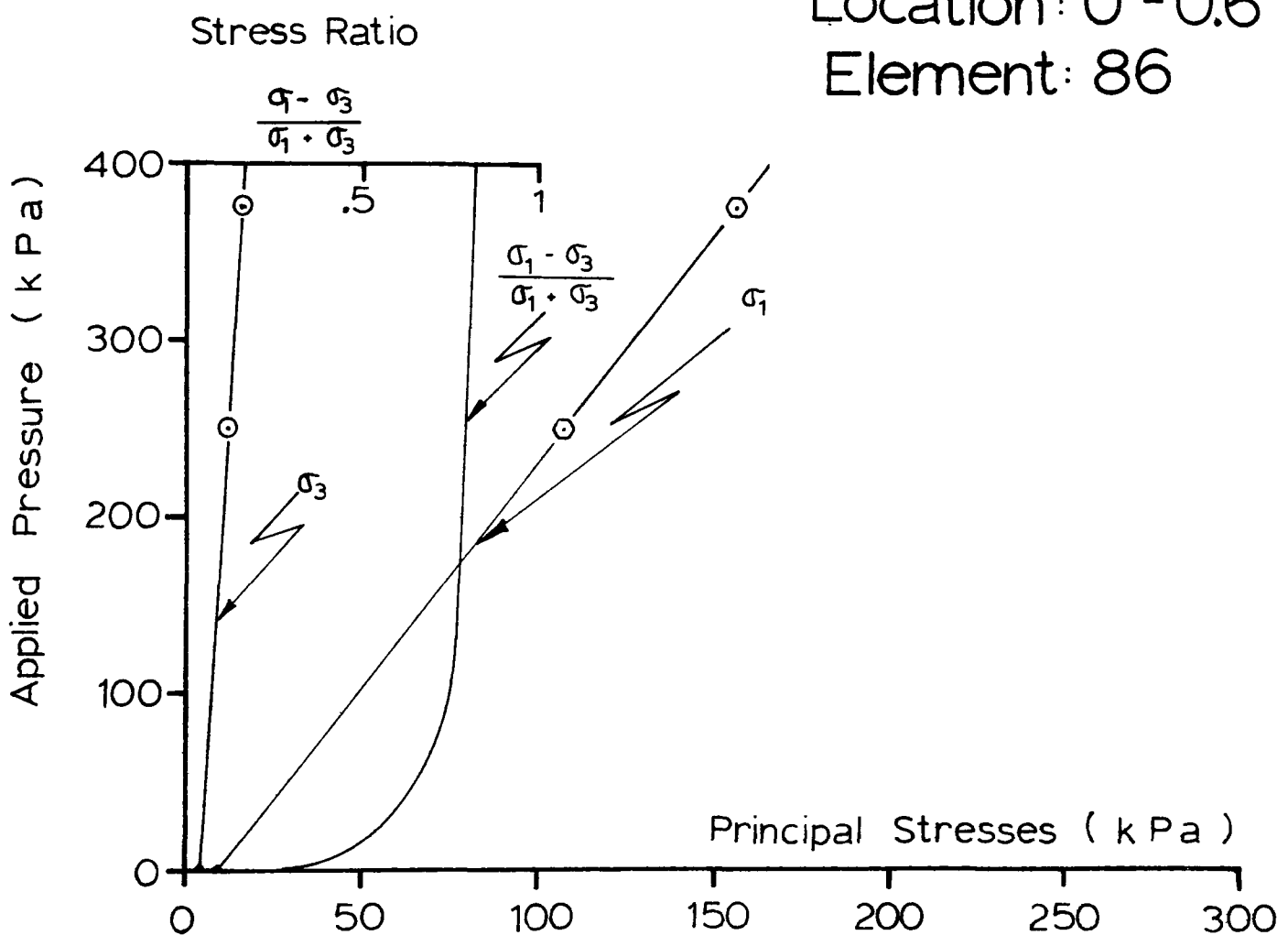

Figure 8.20

Applied Pressure Vs. Principal Stresses

Location : 2.5 - 0

Element : 143

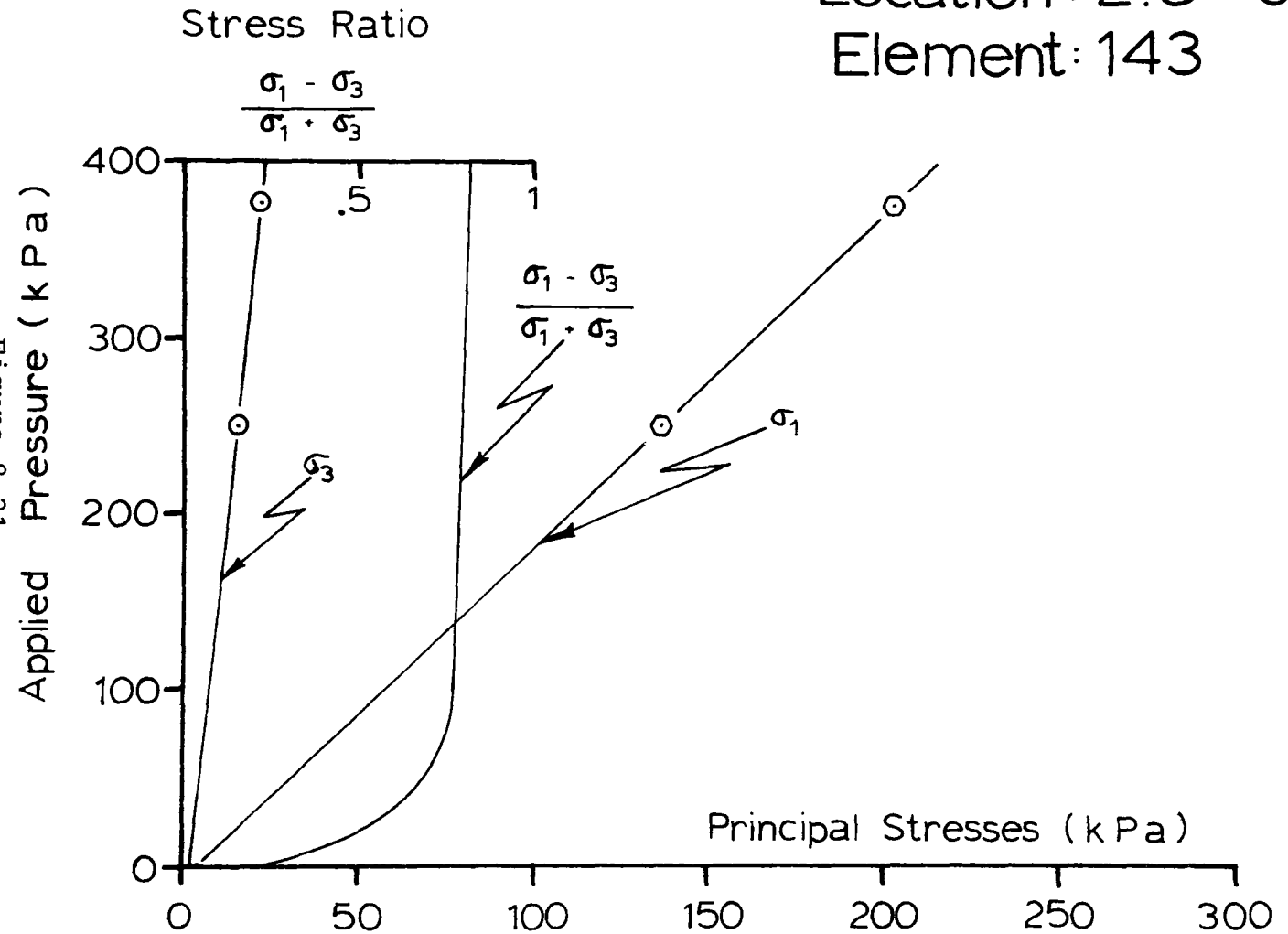

Figure 8.21

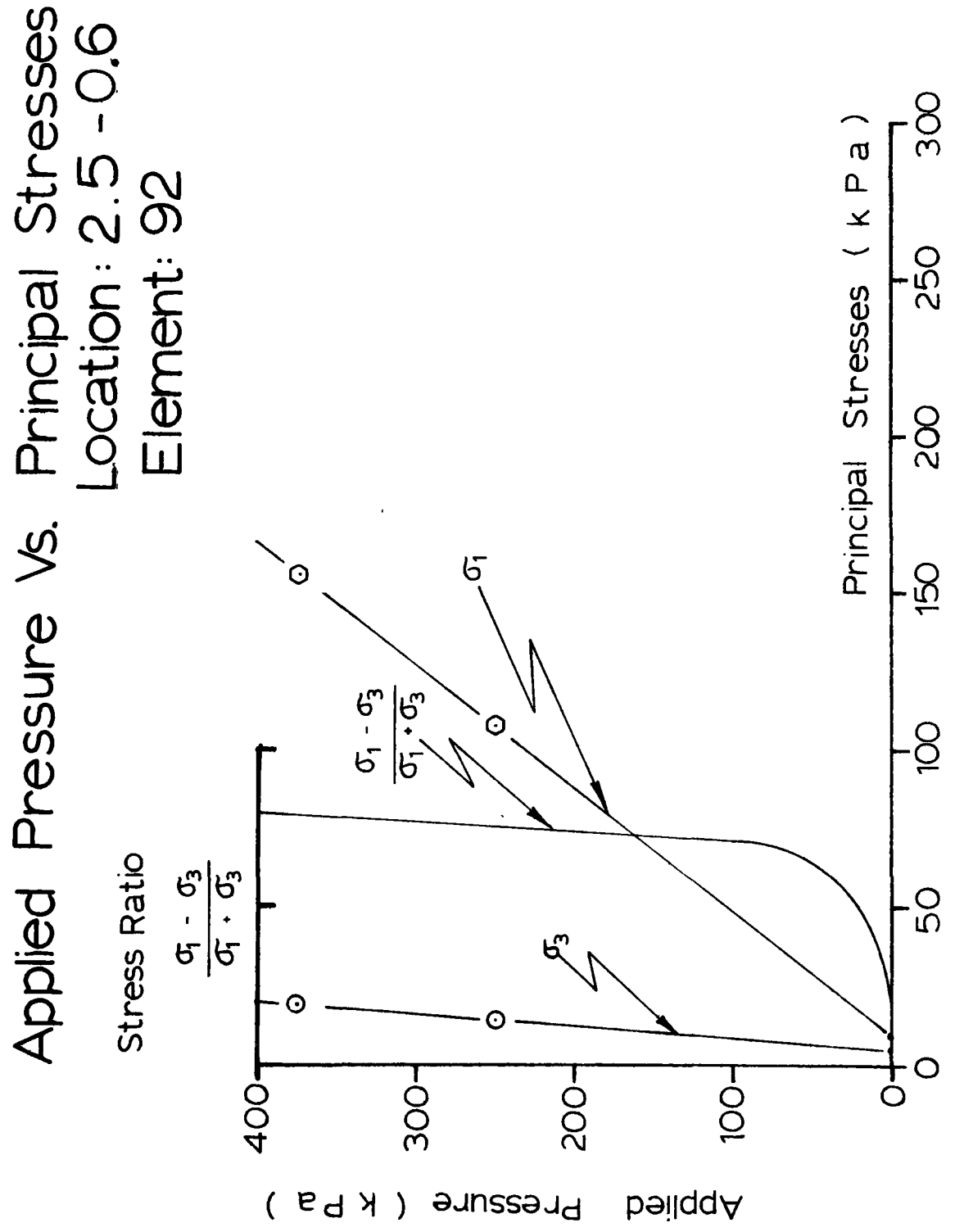
Applied Pressure Vs. Principal Stresses
Location: 2.5 -0.6
Element: 92
Stress Ratio
$\frac{\sigma_1 - \sigma_3}{\sigma_1 + \sigma_3}$
σ_1
σ_3
Applied Pressure (k P a)
Principal Stresses (k P a)
0
100
200
300
400
0
50
100
150
200
250
300

Figure 8.22

Corresponding $N_{\gamma q}$ Value of the Footing Pressure to Cause Failure in the Elements for Different Angles of Shearing Resistance.
(Lower Limiting Values of $N_{\gamma q}$)

Footing location	Element #	ϕ	q_p (kPa)	$N_{\gamma q}$
0 - 0	134	30^o	10	3
		35^o	15	7
		40^o	23	10
		45^o	38	16
		50^o	75	31
0 - .6	86	30^o	10	4
		35^o	18	8
		40^o	35	15
		45^o	65	28
		50^o	135	56
2.5 - 0	143	30^o	19	9
		35^o	29	13
		40^o	44	19
		45^o	78	33
		50^o	149	62
2.5 - .6	92	30^o	40	18
		35^o	60	26
		40^o	92	40
		45^o	156	55
		50^o	257	107

Figure 8.23

since the same $N_{\gamma q}$ is plotted for each of the Φ angles which were determined from a triaxial test, the triaxial test plus ten percent, a plane strain test, and a shear box test. These values of the angle of shearing resistance are given in Chapter VII and are:

- in compact sand

Φ_t = triaxial = 37°

$\Phi_{t + 10\%}$ = triaxial plus 10% = 41°

Φ_{PS} = plane strain = 45°

Φ_{SB} = shear box = 45°

- in dense sand

Φ_t = triaxial = 41°

$\Phi_{t + 10\%}$ = triaxial plus 10% = 45°

Φ_{PS} = plane strain = 48°

Φ_{SB} = shear box = 50°

As shown in Figures 8.24 through 8.27, the results represented by the triaxial laboratory test lie outside the upper limit in six cases (all four dense sand locations and at 0 - 0 and 0 - 0.6 in compact sand). In the case of footing location 0 - 0 in dense sand, the triaxial plus 10% and the plane strain results are outside the upper limit. All other results lie within the limits.

8.5 Conclusions

This chapter presents a finite element approach to the defining of a lower bound solution to the problem of bearing

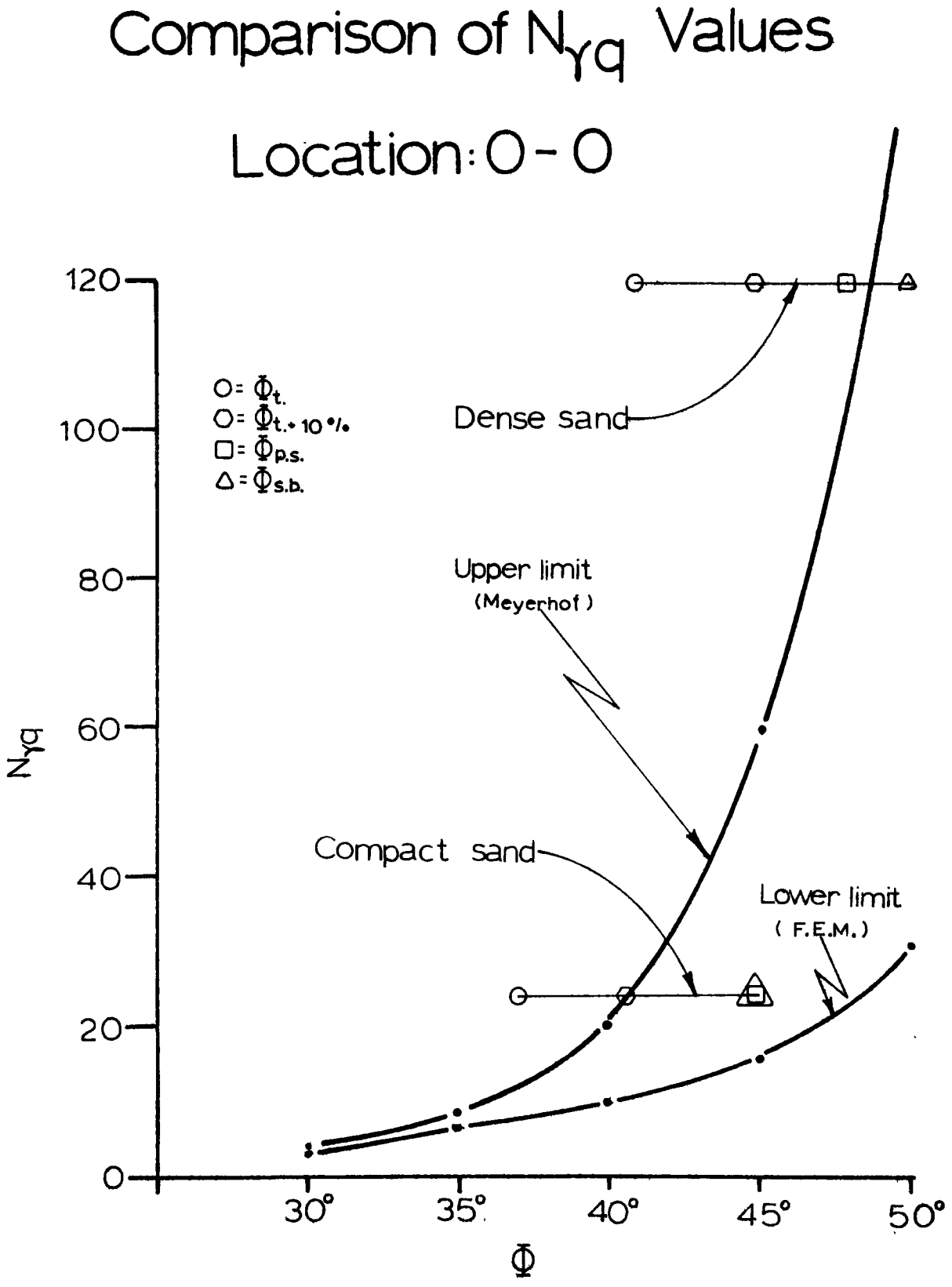
Comparison of $N_{\gamma q}$ Values
Location: O - O
O = $\Phi_{t.}$
O = $\Phi_{t.+10\%}$
□ = $\Phi_{p.s.}$
△ = $\Phi_{s.b.}$
Dense sand
Upper limit
(Meyerhof)
Compact sand
Lower limit
(F.E.M.)
$N_{\gamma q}$
120
100
80
60
40
20
0
30°
35°
40°
45°
50°
Φ

Figure 8.24

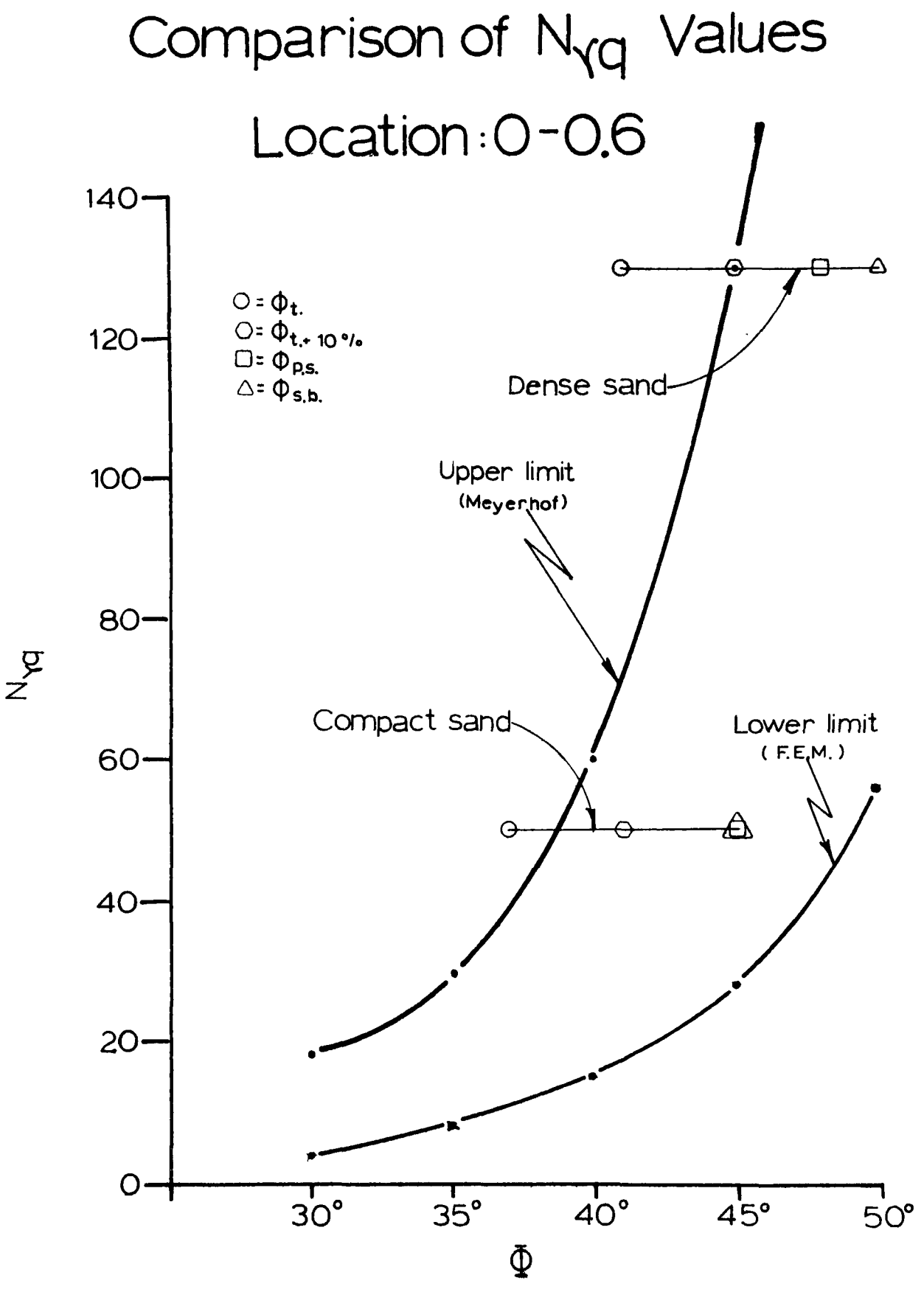
Comparison of $N_{\gamma q}$ Values
Location : 0-0.6
○ = $\Phi_{t.}$
○ = $\Phi_{t.+10\%}$
□ = $\Phi_{p.s.}$
△ = $\Phi_{s.b.}$
Dense sand
Upper limit
(Meyerhof)
Compact sand
Lower limit
(F.E.M.)
$N_{\gamma q}$
140
120
100
80
60
40
20
0
30°
35°
40°
45°
50°
Φ

Figure 8.25

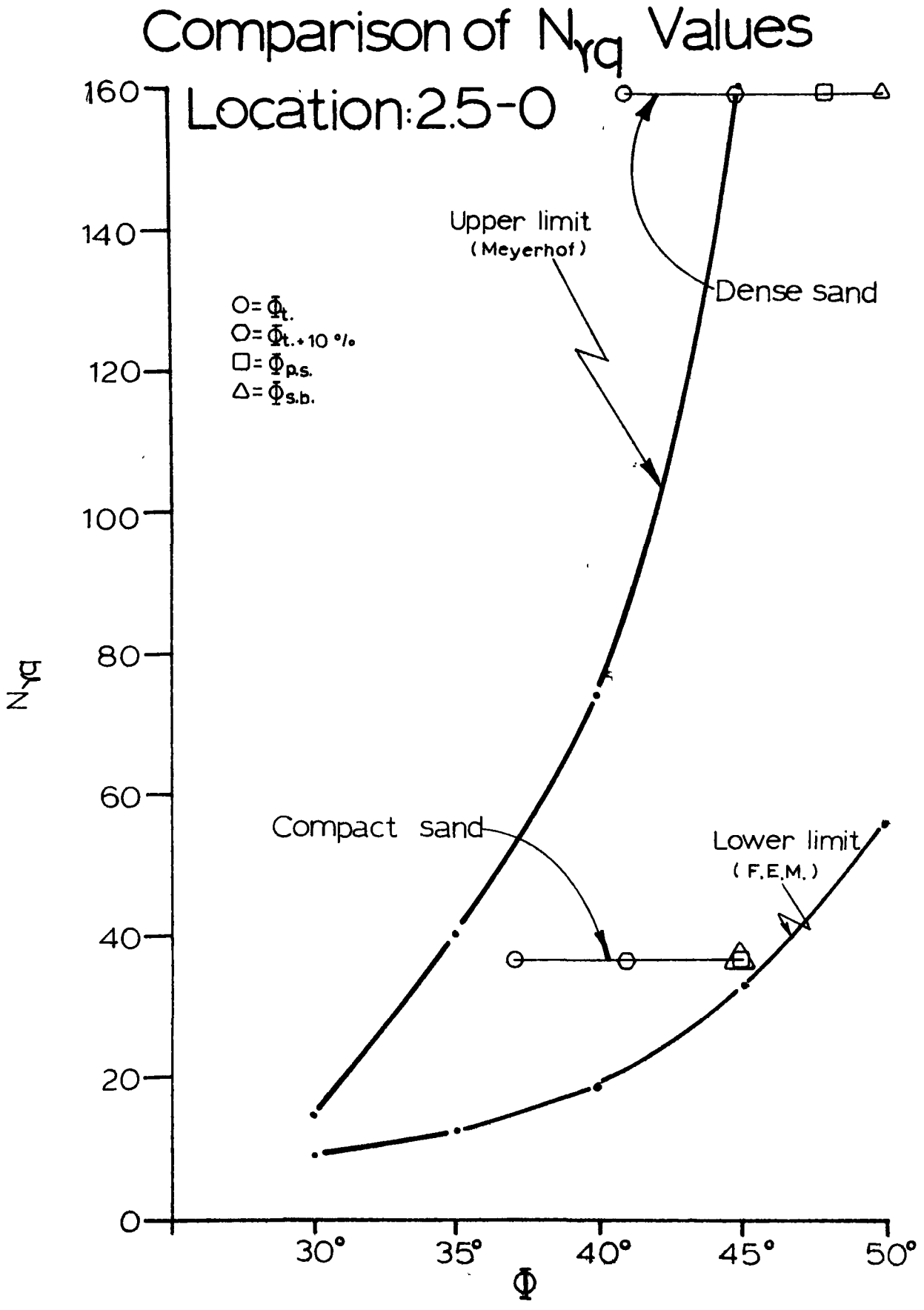
Comparison of $N_{\gamma q}$ Values
Location: 2.5-0
160
140
120
100
80
60
40
20
0
$N_{\gamma q}$
Upper limit
(Meyerhof)
Dense sand
O = $\Phi_{t.}$
O = $\Phi_{t.}$ + 10 %
□ = $\Phi_{p.s.}$
△ = $\Phi_{s.b.}$
Compact sand
Lower limit
(F.E.M.)
30°
35°
40°
45°
50°
Φ

Figure 8.26

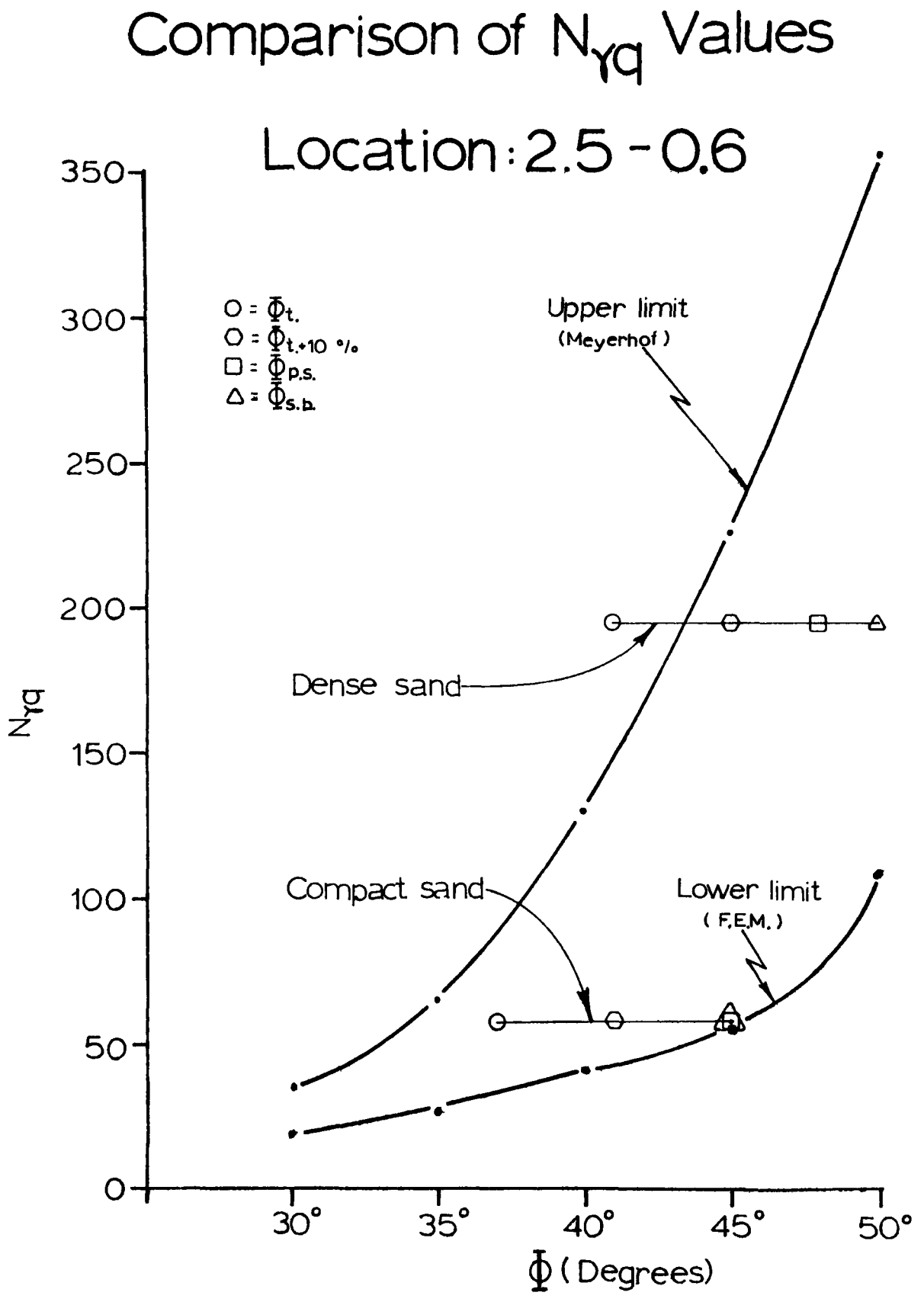
Comparison of $N_{\gamma q}$ Values
Location: 2.5 - 0.6
O = $\Phi_{t.}$
O = $\Phi_{t.+10\ \%}$
□ = $\Phi_{p.s.}$
△ = $\Phi_{s.b.}$
Upper limit
(Meyerhof)
Dense sand
Compact sand
Lower limit
(F.E.M.)
$N_{\gamma q}$
350
300
250
200
150
100
50
0
30°
35°
40°
45°
50°
Φ (Degrees)

Figure 8.27

capacity of footings on top of a slope. To achieve this analysis, certain simplifying assumptions are made:

a) Plane strain
b) The cohesionless material is represented by a linear elastic stress-strain relationship
c) The material does not exhibit volume change
d) The size of mesh immediately under the footing is equal to one fifth of the footing width.
e) The critical element that defines the lower bound is located at the bottom of the rigid soil wedge which forms under the footing. This corresponds to the element located at a depth approximately equal to the footing width.

If any of the preceeding assumptions were changed, the results might be different. Nevertheless the results obtained in this chapter are thought to be realistic. Similar stress concentration distributions and failed element distributions are reported by Loumas and Schad (1976), and Bimdi, Mastinetti, Ribacchi and Riccini (1976).

Given the above qualifications and the limited scope of the analysis, it is difficult to arrive at firm conclusions. One tentative conclusion appears to be that the true solution to the problem of the bearing capacity of footings at the top of a slope is not given by limit equilibrium analysis of the kind outlined in Chapter II. Instead, the true solution probably lies well within the band of results defined by the

upper and lower bounds. Since the problem is two dimensional it seems logical to conclude that the true solution will make use of ϕ angles given by plane strain and shear box tests on the sand. This means that the true solutions will be even closer to the lower bound.

CHAPTER IX

CONCLUSION

9.1 Summary

A large scale experimental investigation has been conducted on the bearing capacity of footings close to slopes of cohesionless material. The tests have been carried out at twelve different footing locations with respect to the slope crest.

A total of twenty-nine tests were performed; 12 were done in compact sand, and 11 were done in dense sand. Five tests were repeated, while one other test was carried out on flat ground in dense sand. Plots have been drawn relating the applied load to the settlement, and the surface movement to the loads.

An extensive literature review summarizes the existing theoretical approaches to the problem, as well as the previous experimental investigations. The test results are compared with these theoretical and experimental findings.

A special section of this thesis deals exclusively with a finite element approach to the problem. This analysis shows the way in which failure propagates in the soil mass, and gives $N_{\gamma q}$ values which are compared to the experimental results.

9.2 Conclusion

The following conclusions are based on the experimental test results, the preceeding discussions, and the interpretation of the data presented.

1) For the first time, experimental test results are available from a large scale test model.
2) All existing theories are based on similar assumptions but the results differ widely. Differences in analytical techniques account for the broad range of results.
3) The work shows that the theories presented in Chapter II, which are for the most part based on the theory of plasticity, do not predict adequately the failure loads.
4) The test results show that the existence of the slope is felt much farther back from the crest of the slope in dense sands than in compact sands. This is probably due to the failure zone being larger in dense sand than in compact sand; in compact sand the footing can be quite close to the slope and the failure zone does not encompass the slope itself. This speculation seems reasonable when the surface movements which were measured are compared.
5) The increase in bearing capacity with depth (from the the surface to a depth of 3B) is by a factor of about 10 in compact sand and only 4 in dense sand. Numerically, however, the increase in $N_{\gamma q}$ at the crest is about 200 in

both the dense and compact sand. The conclusion is that N_q increases by an amount which is independent of the state of density whereas N_γ is density dependent.

6) While numerically the predicted theoretical values of $N_{\gamma q}$ are in error when compared with the experimental results, it is shown that the theories do predict the influence of the slope with sufficient accuracy. This is evident when the predicted $N_{\gamma q}$ values are normalized by dividing them either by the predicted bearing capacity factor at a distance of 5B from the slope or by the factor at 3B depth. It is concluded that the representation of the material is in error rather than the kinematics of the problem.

7) Footings located a minimum distance of 5 footing widths back from the crest of the slope have a capacity which is the same as the capacity of a footing on flat ground.

8) The relationship between experimental $N_{\gamma q}$ values and the angle of internal friction Φ is not as clear as that which theory would predict. Compounding this problem is the fact that, for the same density condition, no unique Φ value exists; the value of Φ is dependent on the laboratory test procedure. For the same sand density, triaxial tests, plane strain tests and shear box tests all yield different Φ angles.

9) The experimental $N_{\gamma q}$ results can be predicted fairly accurately by the following mathematical expression:

$$N_{\gamma q} = 47\left(\frac{D}{B}\right)^{1.38} + A \times 25(1.14)^{b/B}$$

where A = 1 in compact sand and

A = 4 in dense sand.

It is not intended that this equation be used for design.

10) A safe design approach might be to use a lower bound solution in conjunction with a shear box Φ angle for the particular sand.

9.3 Suggestions for Further Research

Because of the large discrepency between theory and experiment discussed in this work, a major effort should be made to verify all theories pertaining to the bearing capacity of cohesionless soil.

Possible experimental research might include:

1) The bearing capacity of flat ground.
2) A testing program similar to the present one, but with all footings located in the slope. (To this end, two tests are contributed. These tests were carried out in the slope at a depth of 1B below the horizontal surface in both compact and dense sand. The test results form part of this chapter.)
3) A study of the effect of slope angle.
4) A study of the effect of inclined loading.
5) A study of the effect of eccentric loading.

6) A study of the influence of scale by using footings of different size.
7) A study of the influence of the slope on the bearing capacity of a reinforced soil mass (reinforced earth).
8) A study of the influence of the slope on the bearing capacity of a square footing.

Possible theoretical research might include:

1) Investigation of the limit loads at different footing locations other than the slope crest by limit analysis in order to formulate true upper and lower bounds.
2) Finite element analyses using hyperbolic stress-strain relationships for the soil.
3) Finite element analyses using elasto-plastic stress-strain relationships for the soil. Such analyses might consider the influence of the intermediate principal stresses and volume change.

Test: -l - l - C - S

PRESSURE - SETTLEMENT

TEST: -1 - 1 - C - S

γ = 1490 kg/m^3

B = .3 m.

Pressure q kPa	Settlement cm.	$\frac{2q}{\gamma B}$	Relative settlement $\frac{W}{B} \times 100$
0	0	0	0
25	0.5	10	1.7
31	0.7	13	2.3
38	1.0	16	3.3
44	1.2	19	4.0
50	1.4	22	4.7
56	1.6	25	5.3
63	1.9	28	6.3
69	2.4	30	8.0
75	3.4	32	11.3
81	5.0	35	16.7
88	6.1	38	20.3
100	8.8	44	29.3
113	11.8	48	39.3
125	14.6	54	48.7

Figure 9.1

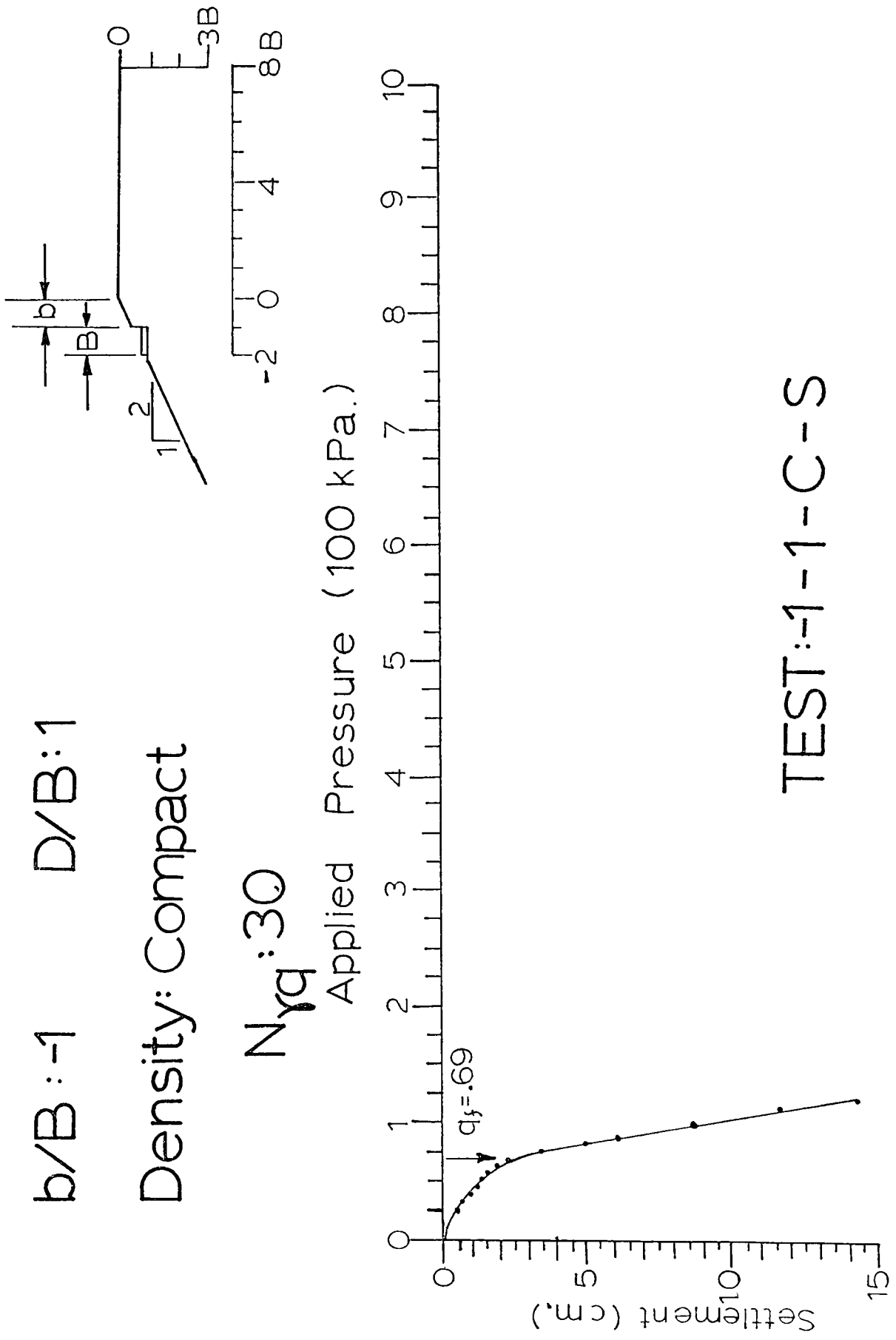
b/B : 1
D/B : 1
Density: Compact
$N_{\gamma q}$:30
TEST :-1-1-C-S
Applied Pressure (100 kPa.)
Settlement (cm.)
q_f=.69
b
B
1
2
0
3B
8B
-2
0
4
0
1
2
3
4
5
6
7
8
9
10
0
5
10
15

Figure 9.2

DENSITY MEASUREMENTS (Kg/m^3)

TEST: 1 - 1 - C - S

Location of measurement under footing	Measurements	Average	Standard deviation
1B*	1490		
	1490		
	1490		
	1500		
2B*	1490		
	1490		
	1500		
	1510		
		1490	8

* B = footing width

Figure 9.3

Surface Movements
Test:-1-1-C-S

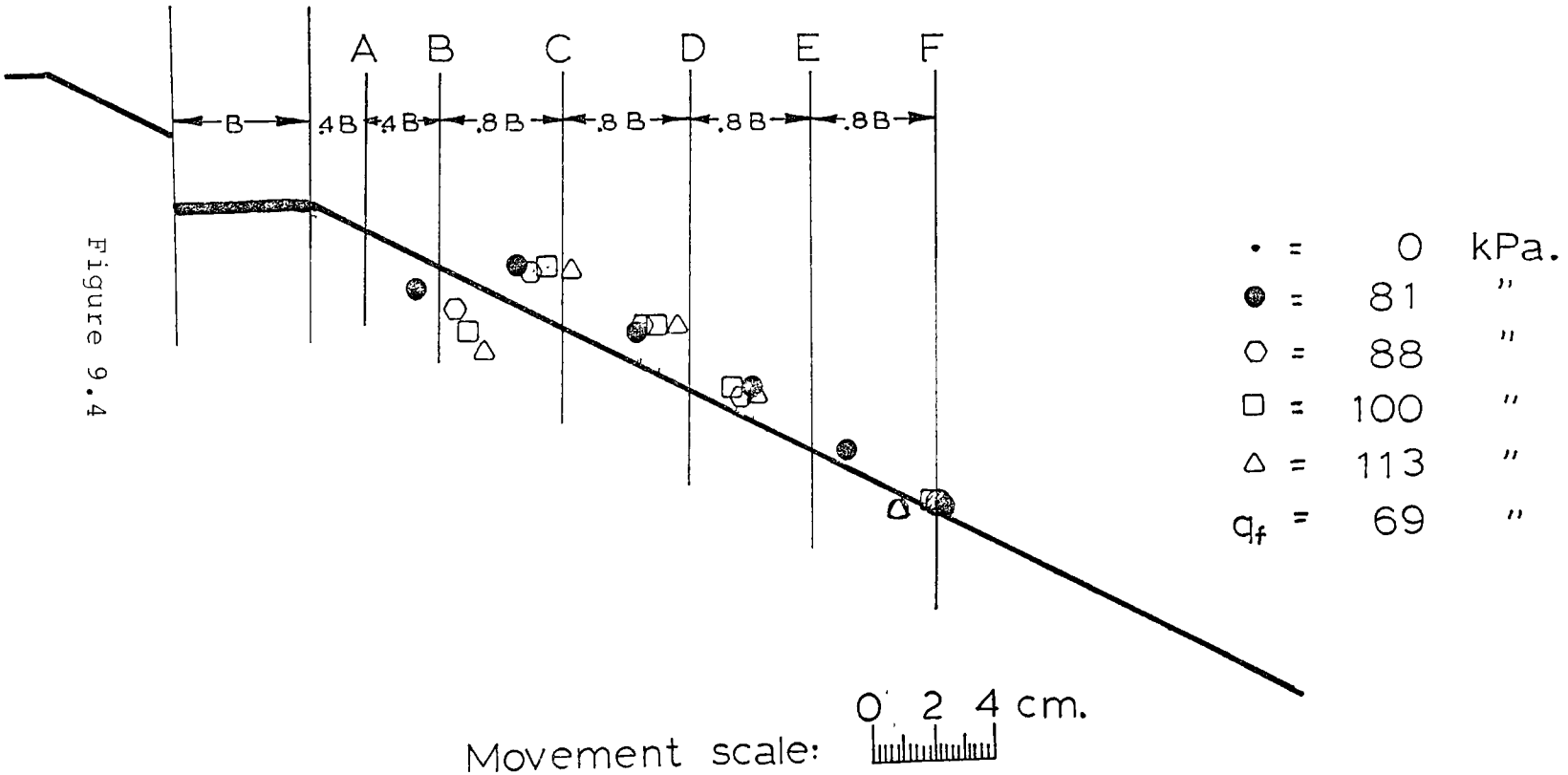

• = 0 kPa.
● = 81 "
○ = 88 "
□ = 100 "
△ = 113 "
q_f = 69 "

Movement scale: 0 2 4 cm.

Figure 9.4

SURFACE MOVEMENTS (cm)

TEST: 1 - 1 - C - S

Positions		A	B	C	D	E	F
Horizontal distance from footing (B = footing width)		.4B	.8B	1.6B	2.4B	3.2B	4B
Pressure (kPa)							
0	H	0	0	0	0	0	0
	V	0	0	0	0	0	0
25	H	0.2	0.2	0.2	0.2	0	0
	V	0	0.2	0	0.2	0	0
32	H	0.3	0.3	0.3	0.2	0	0
	V	0	0.2	0.2	0.2	0.1	0
38	H	0.5	0.5	0.5	0.5	0.3	0.2
	V	-0.1	0.3	0.2	0.3	0.2	0.1
44	H	0.6	0.6	0.5	0.3	0.2	0.2
	V	-0.2	0.3	0.2	0.3	0.2	0
50	H	0.8	0.8	0.8	0.6	0.6	0.3
	V	-0.3	0.4	0.3	0.3	0.2	0.1
56	H	0.9	1.0	1.0	0.6	0.3	0.2
	V	-0.3	0.4	0.4	0.4	0.3	0.1
63	H	1.2	1.2	1.1	1.0	0.5	0.3
	V	-0.4	0.5	0.4	0.5	0.3	0.2
69	H	1.4	1.6	1.4	1.1	0.6	0.3
	V	-0.4	0.6	0.5	0.5	0.4	0.2
75	H	2.0	2.2	2.2	1.8	0.9	0.3
	V	-0.5	0.7	0.8	0.7	0.5	0.3
81	H	2.9	2.8	2.7	2.3	1.3	0.3
	V	-0.9	1.1	0.9	1.0	0.5	0.3
88	H	3.2	3.3	2.8	2.3	1.8	0.2
	V	-1.0	1.3	1.2	1.2	0.5	0.1
100	H	3.8	3.8	3.5	2.8	1.6	-0.2
	V	-1.5	1.6	1.5	1.3	0.5	-0.1
113	H	4.5	4.8	4.1	3.5	2.2	-0.8
	V	-1.8	1.9	1.8	1.5	0.9	-0.5

Figure 9.5

Test: -l - l - D - S

PRESSURE - SETTLEMENT

TEST: -1 - 1 - D - S

γ = 1610 kg/m^3

B = .3 m.

Pressure q kPa	Settlement cm.	$\frac{2q}{\gamma B}$	Relative settlement $(\frac{W}{B} \times 100)$
0	0	0	0
25	0.2	10	0.7
50	0.3	20	1.0
75	0.6	30	2.0
100	1.0	40	3.3
125	1.2	50	4.0
150	1.4	60	4.7
175	1.8	70	6.0
188	2.1	75	7.0

Figure 9.6

b/B : -1 D/B : 1

Density : Dense

$N_{\gamma q}$: 75

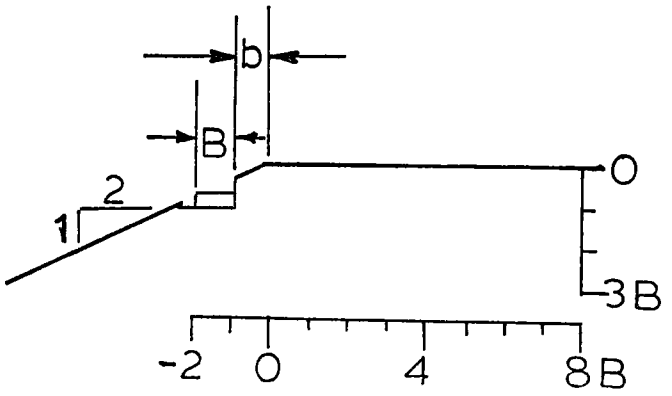

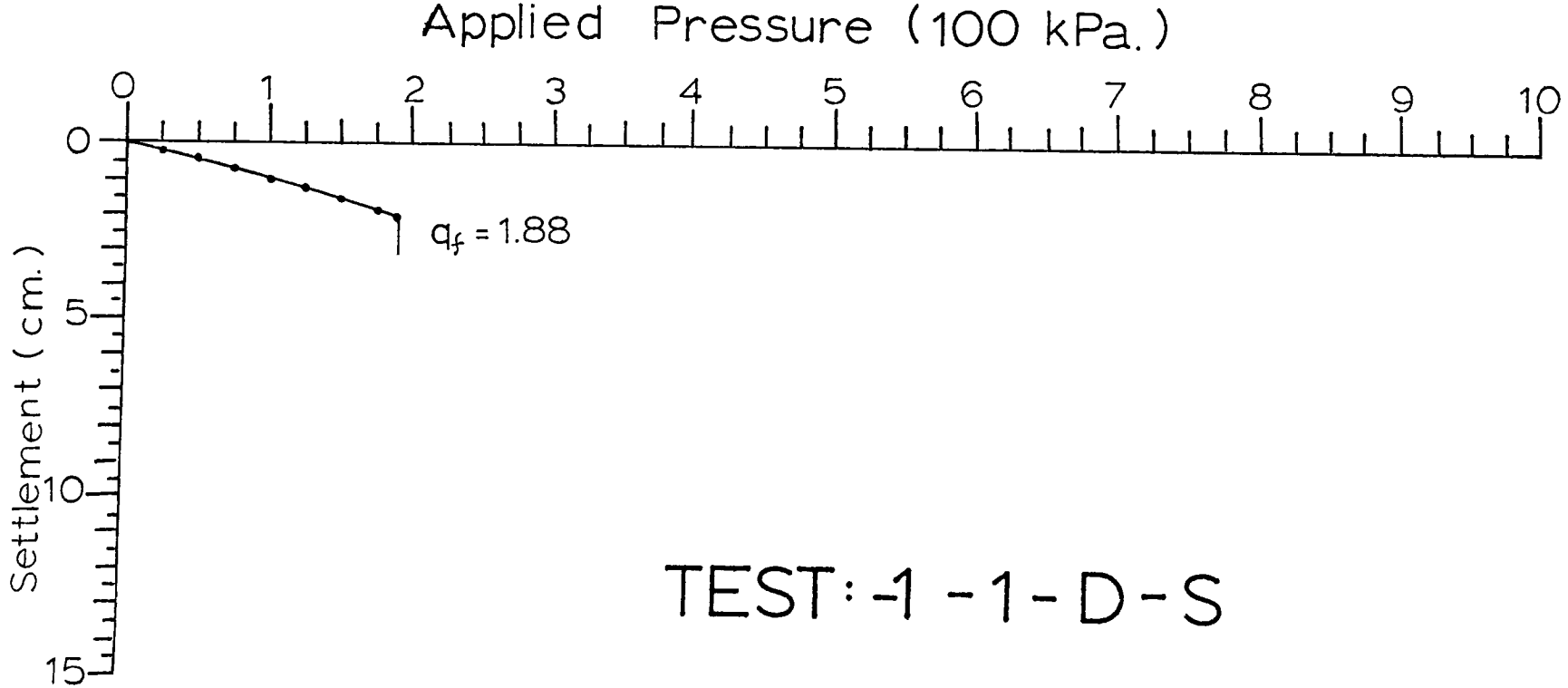

TEST : -1 - 1 - D - S

Figure 9.7

DENSITY MEASUREMENTS (kg/m^3)

TEST: 1 - 1 - D - S

Location of measurement under footing	Measurements	Average	Standard deviation
1B*	1600		
	1630		
	1610		
	1610		
	1610		
	1630		
2B*	1610		
	1620		
	1610		
	1610		
	1610		
	1610		
		1610	8

* B = footing width

Figure 9.8

Surface Movements
Test:-1-1-D-S

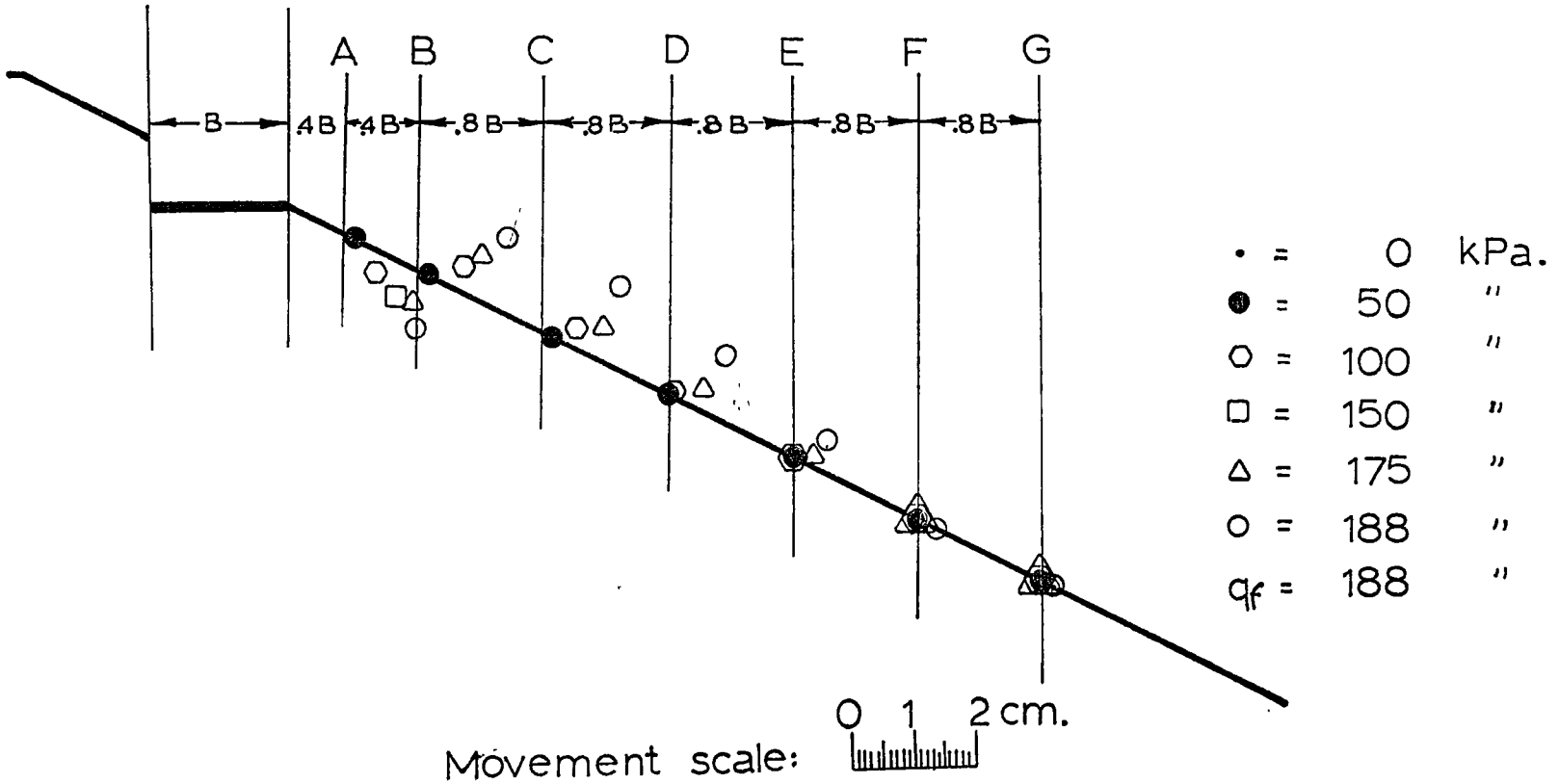

Figure 9.9

SURFACE MOVEMENTS (cm)

TEST: 1 - 1 - D - S

Positions		A	B	C	D	E	F	G
Horizontal distance from footing (B = footing width)		.4B	.8B	1.6B	2.4B	3.2B	4B	4.8B
Pressure (kPa)								
0	H	0	0	0	0	0	0	0
	V	0	0	0	0	0	0	0
50	H	0.2	0.2	0.2	0	0	0	0
	V	0	0	0	0	0	0	0
90	H	0.5	0.8	0.6	0.2	0	0	0
	V	-0.3	0.4	0.3	0.1	0	0	0
100	H	0.6	0.8	0.6	0.2	0	0	0
	V	-0.3	0.4	0.3	0.1	0	0	0
125	H	0.8	0.8	0.8	0.3	0.2	0	0
	V	-0.5	0.4	0.4	0.1	0	0	0
150	H	1.0	1.1	1.1	0.6	0.3	0	0
	V	-0.5	0.7	0.5	0.3	0.1	0	0
175	H	1.4	1.4	1.3	0.8	0.5	0.2	0
	V	-0.6	0.8	0.8	0.5	0.2	0	0
188	H	1.5	1.5	1.4	1.0	0.6	0.3	0.2
	V	-0.8	1.2	1.3	1.0	0.5	0	0

Figure 9.10

APPENDIX A

REFERENCES

A.1 References used in this thesis

Abel, J.F. and Desai, C.S. (1972). Introduction to the Finite Element Method a Numerical Method for Engineering Analysis, Van Nostrand Reinhold Company, New York, U.S.A.

Absi, E. (1972) Fondations au voisinage d'un talus, A.I.T.B.T.P. No. 289, janvier, Série théorie et méthode de calcul, No. 146, Paris, France.

Biondi, P., Manfredini, G., Martinetti, S., Ribacchi, R., and Riccioni, R. (1976). Limit Load of a Foundation in a Strain-Softening Soil, Proceedings of the Second International Conference on Numerical Methods in Geomechanics, Blackburg, Virginia, Published by A.S.C.E.

Bowes, W., and Russell, L.T. (1975). Stress Analysis by the Finite Element Method, Lexington Books, Heath Publisher, Toronto.

Bowles, J. (1975). Spread Footings, Chapter 15 of Foundation Engineering Handbook, Edited by Winterkorn and Fang, Van Nostrand Reinhold Company, New York, U.S.A.

Bowles, J. (1977). Foundation Analysis and Design, McGraw Hill, New York.

Brinch Hansen, J., (1961). A General Formula for Bearing Capacity, Bulletin No. 11, Danish Geotechnical Institute, Copenhagen, Denmark.

Caquot, A. (1934). Equilibre des massifs à frottement interne, Gauthier-Villars, Paris, France.

Caquot, A. et Kérisel, J. (1966). Traité de mécanique des sols, Gauthier-Villars, 4^{e} édition, Paris, France.

Chen, W.F. (1974). Limit Analysis and Soil Plasticity, Elsevier Scientific Publishing Company, Amsterdam.

Chen, W.F. and Davidson, H.L. (1973). Bearing Capacity Determination by Limit Analysis, J.S.M.F.D., June 1973, A.S.C.E.

DeBeer, E.E. (1965). The Scale Effect on the Phenomenon of Progressive Rupture in Cohesionless Soil, Proceeding of the Sixth International Conference S.M.F.E., Montreal, Canada, Volume 2, 1965, pp. 13-17.

DeBeer, E.E. (1965). Bearing Capacity and Settlement of Shallow Foundations on Sand, Bearing Capacity and Settlement of Foundations, Proceedings of a Symposium held at Duke University, 1965, --. 41-51.

Giroud, J.P. et Tran-Vô-Nhiem (1971). Force portante d'une fondation sur une pente, A.I.T.B.T.P., No. 283 - 284, juillet - août, Série: théorie et méthode de calcul, No. 142, Paris, France.

Graham, J. (1966). Plastic Failure in Granular Material: Plane Strain Problems in Soil Mechanics, Doctoral thesis the Queen's University of Belfast.

Graham, J. and Pollock, D.J. (1972). Scale-Dependent Plasticity Analysis for Sand, Civil Engineering and Public Works Review, March 1972.

Graham, J. (1973). Discussion on Analysis of Ultimate Loads of Shallow Foundations, by A.S. Vésic (1973), J.S.M.F.D., ASCE Volume 99, No. SM10, October, pp. 897-899.

Harr, M.E. (1966). Foundations of Theoretical Soil Mechanics, McGraw-Hill, Inc., New York.

Hasnain, M. (1974). Shear Strength Characteristics of a Crushed Quartz Sand, A Master Thesis, University of Ottawa, Department of Civil Engineering.

Holubec, I. and D'Appolonia, E. (1973). Effect of Particle Shape on the Engineering Properties of Granular Soils, Evaluation of Relative Density and Its Role in Geotechnical Projects Involving Cohesionless Soils, ASTM STP 523, American Society for Testing Materials.

Ko, H.Y. and Davidson, L.W. (1973). Bearing Capacity of Footings in Plane Strain, J.S.M.F.D., January 1973, A.S.C.E.

Kolbuszeuski, J.J. (1948). An Experimental Study of the Maximum and Minimum Porosities of Sands, Proceedings, 2nd International Conference S.M.F.E. Volume 1, 1948, pp. 158-165.

Kovalev, I.V. (1964). De la résistance ultime de fondations limitées par un talus, traduction du russe, extrait du recueil des travaux de LIIzht, fascicule 225, "Nerotovye Voprosy tonnele-i mostostroeniya", Leningrad, URSS, traduction française effectuée par L.C.P.C., Paris, 1973.

Kovalev, I.V. (1965). Calcul de stabilité des fondations limitées par une pente, traduction du russe, extrait du recueil des travaux de LIIzht, fascicule 241, Leningrad, URSS, traduction française effectuée par L.C.P.C., Paris, 1973.

Lambe, T.W. and Whitman, R.V. (1969). Soil Mechanics, Series in Soil Engineering, John Wiley and Sons, Inc., New York.

Laumans, Q. and Schad, H. (1976). Calculation of Raft Foundations on Clayery Silts, Proceedings of the Second International Conference on Numerical Methods in Geomechanics, Blackburg, Virginia, Published by A.S.C.E.

Lebègue, Y. (1972). Pouvoir portant du sol sous une charge inclinée, A.I.T.B.T.P. No. 292, avril 1972, Série Sols et fondations, No. 88, Paris.

Lebègue, Y. (1973). Essais de fondations superficielles sur talus, Proceedings 8th International Conference S.M.F.E., Col. 4.3, p. 313.

Lee, I.K., (1968). Soil Mechanics Selected Topics, Butterworths, London.

Lysmer, J. (1970). Limit Analysis of Plane Problems in Soil Mechanics, J.S.M.F.D., A.S.C.E., 96(SM4), Proc. Paper 7416.

Mandel, J. et Salençon, J. (1972). Force portante d'un sol sur une assise rigide (étude théorique), Géotechnique 22, London.

Ménard, L. (1964). Discussion sur "Essais pressiométriques destinés à déterminer la capacité portante d'une fondation près d'un talus, Sols-Soils, Paris.

Meyerhof, G.G. (1951). The Ultimate Bearing Capacity of Foundations, Géotechnique, Volume 2, pp. 301-332.

Meyerhof, G.G. (1955). Influence of Roughness of Base and Ground-Water Conditions on the Ultimate Bearing Capacity of Foundations, Geotechnique, Volume 6, pp. 227-242.

Meyerhof, G.G. (1956). Penetration Tests and Bearing Capacity of Cohesionless Soils, J.S.M.F.D., A.S.C.E. Volume 82, SM1, January 1956.

Meyerhof, G.G. (1957). The Ultimate Bearing Capacity of Foundations on Slopes, Proceeding of the 4th International Conference, S.M.F.E., Volume 1, pp. 384-386.

Meyerhof, G.G. (1961). Discussion of 'Shallow Foundations: Influence of the Dimensions and the Shape of the Foundations,' Proceeding, 5th International Conference on Soil Mechanics and Foundation Engineering, Volume 3.

Mizuno, T., (1948). On the Bearing Power of Soil in a Two-Dimensional Problem, Proceeding, 2nd International Conference on Soil Mechanics and Foundation Engineering, Volume 3, Rotterdam.

Mizuno, T., Takumitsu, Y., and Kavakami, H. (1960). On the Bearing Capacity of a Slope of Cohesionless Soil, Soil and Foundations, Volume 1, No. 2 Tokyo, Japan, November, pp. 30 - 37.

Ozawa, Y. and Duncan, J.M. (1973). ISBILD: A Computer Program for Analysis of Static Stresses and Movements in Embankments, Report #TE-73-4, Department of Civil Engineering, University of California at Berkeley.

Peynirciogly, H. (1948). Test on Bearing Capacity of Shallow Foundations on Horizontal Top Surface of Sand Fill, Proceeding, 2nd International Conference on Soil Mechanics and Foundation Engineering, Volume 3, Rotterdam.

Rowe, P.W. (1962). The Stress-Dilatancy Relation for Static Equilibrium of an Assembly of Particles in Contact, Proc. Roy. Soc. (London) A269.

Sangrelat, A. (1972). The Penetrometer and Soil Exploration, Elsevier Publishing Company, Amsterdam.

Scott, R.F. (1963). Principles of Soil Mechanics, Addison-Wesly Publishing Company Inc., Reading Massachusetts.

Sokolovski, V.V. (1965). Statics of Granular Media, Butterworth, London, England.

Tcheng, Y. et Iseux, J. (1966). Nouvelle recherche sur le pouvoir portant des milieux pulvérulents, fondations superficielles et semi-profondes, A.I.T.B.T.P., No. 227, novembre 1966, Série Essais et mesures, No. 97.

Terzaghi, K. (1943). Theoretical Soil Mechanics, John Wiley & Sons, Inc., New York.

Tournier, J.P. (1972). Comportement d'une couche compressible limitée par un substratum rigide et soumise à une charge verticale appliquée par une semelle filante, Thèse de doctorat, Département de Génie Civil, Université de Sherbrooke.

University of Ottawa (1975). Investigation of G.G. Meyerhof's Theory on Foundations in Slopes of Cohesionless Soil Using Model Footings.

Vésic, A.S. (1973). Analysis of Ultimate Loads of Shallow Foundations, J.S.M.F.D., A.S.C.E., Volume 99, No. SM1, January, pp. 45 - 73.

Vésic, A.S. (1973). Shallow Foundations, in Foundations Engineering Handbook, Edited by Winterkorn and Fang, Van Nostrand Reinhold Company, New York.

Vogel, C. and Baracos, A. (1973). Discussion on "Analysis of Ultimate Loads of Shallow Foundations", J.S.M.F.D., A.S.C.E., November 1973.

Walter, B.P., and Whitaker, T. (1962). An Apparatus for Forming Uniform Beds of Sand for Model Foundation Tests, Geotechnique, Volume 17, pp. 161 - 167.

Wu, T.H. (1968). Soil Mechanics, Allyn and Bacon, Inc., Boston, Massachusetts.

A.2 Other References

Balla, A. (1962). Bearing Capacity of Foundations, Proceedings of A.S.C.E., 88, SM5.

Biarez, J. (1967). Contributions à l'étude des propriétés mécaniques des sols et des matériaux pulvérulents, Thèse de doctorat, Université de Grenoble, France.

Bishop, A.W. (1955). Use of Slip Circle for Stability Analysis, Geotechnique, 5, London.

Gibbs, H.J. and Holtz, W.G. (1953). Research on Determining the Density of Sands by Spoon Penetration Test, Proceedings 3rd International Conference, S.M.F.E., 1.

Goodman, L.E. and Brown, C.B. (1963). Dead Load Stresses and the Instability of Slopes J.S.M.F.D., A.S.C.E., SM3, May.

Meyerhof, G.G. (1963). Some Recent Research on Bearing Capacity of Foundations, Canadian Geotechnical Journal, Volume 1.

Meyerhof, G.G. (1967). Bearing Capacity and Settlement of Pile Foundations, J.G.E.D., A.S.C.E., G.T.3.

Mitchell, R.J. (1973). An Apparatus for Plane Strain and True Triaxial Testing of Undisturbed Soil Samples, Canadian Geotechnical Journal, Volume 10, No. 3, August.

Terzaghi, K. and Peck, R.B. (1967). Soil Mechanics in Engineering Practice, John Wiley & Sons, Inc., 2nd Edition, New York.

APPENDIX B

EXTENSION OF MEYERHOF'S THEORY

B.1 Introduction

In 1957, Meyerhof proposed theoretical factors to determine the bearing capacity of spread footings on top of slopes of cohesionless soil. These factors are given for only two Φ angles and two depths. It would be interesting to expand the scope of Meyerhof's 1957 work using his bearing capacity theories of 1951 and 1955.

This appendix reviews the methods of bearing capacity determination that Meyerhof presented in 1951 and 1955. These methods are then incorporated into a computer program, to yield bearing capacity factors with respect to a wider range of Φ, depth, footing location and so on.

B.2 Theory

Of the theories proposed by Meyerhof in 1951 and 1955, the 1951 method is general and can be applied to any foundation such as a spread footing on top of a slope or deep foundation.

In 1943 Terzaghi proposed the following bearing capacity equation

$$q = CN_c + \gamma DN_q + \gamma \frac{B}{2} N_\gamma \qquad \text{(B.2.1)}$$

where N_c, N_q and N_γ are bearing capacity factors and

N_c is the cohesion term

N_q is the surcharge term

N_γ is the weight term.

Meyerhof realized that Equation (B.2.1) does not take into account the effect of the shearing resistance of the overburden of surcharge. Based on experimental evidence, Meyerhof (1948) proposed a new failure pattern which is illustrated in Figure B.2.1 and is compared to the Terzaghi assumption.

As can be seen from the illustration, in the Meyerhof theory the slip surface shears through the overburden D and reaches the surface at E, while the Terzaghi theory assumes the failure zone AE to be horizontal with an overburden pressure of D acting upon it.

In his failure pattern, Meyerhof introduces an equivalent surface BE on which the overburden normal stress, P_o, and the shear stress, S_o, act. BE is always inclined at an angle β and the angle is varied to suit the geometry of the problem. Any possible bearing capacity problem can be solved by this method.

According to Figure B.2.1, three definite zones constitute the failure.

ABC: An elastic zone that behaves as part of the footing.

BCD: The zone of radial shear, where the slip line is an arc of a log spiral with its center at B when computing

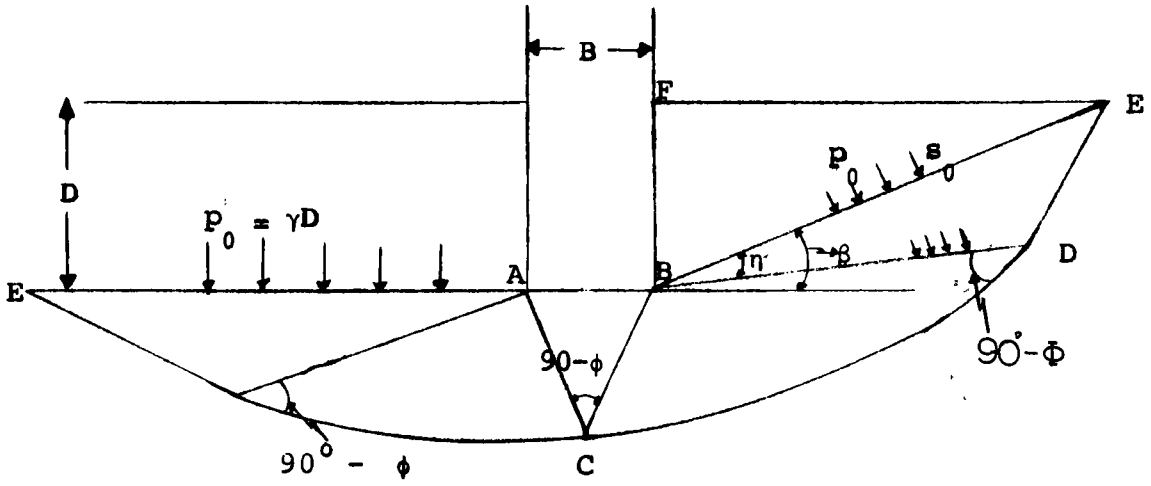

Terzaghi's theory / Meyerhof's theory

Figure B.2.1

the surcharge and cohesion terms. The location of the center of this log spiral arc is not as definite in the case of the weight term as will be seen later.

BDEF: The zone of plane shear. This zone is defined by segments of BD and DE on which the full shear strength of the soil is mobilized. The position of BD is determined by the angle η.

Investigating further zone BDEF, Meyerhof considers the normal stress (P_o) and shear tresss (S_o) acting on BE, which he calls the equivalent free surface, to be caused by the surcharge BEF. To determine the position of the slip line BD, the relationship given in the Mohr circle of Figure B.2.2 is used.

Point G denotes the stresses on BE (equivalent free surface) which are p_o and s_o. Since p_o and s_o cannot be determined until β is fixed, it is necessary to introduce the following relationship.

$$\text{Let } p_o = (c + \sigma_{\underset{0}{0}} \tan\Phi)m \qquad (0 < m < 1) \qquad (B.2.2)$$

In other words the shear strength of the soil is not fully developed along BE, and m is the fraction of the shear strength which is mobilized. The calculations can be carried out for various assumed values of "m". Since BD is a failure plane, its stresses are represented by point P on the Mohr circle. Hence, the angle GCP equals twice the angle η between

planes BD and BE. DE, the other slip line, can be located because the two sets of slip lines always intersect an angle of $90^0 + \Phi$.

Once the angle β is determined, p_o and s_o can be evaluated by considering the mass of soil BEF acting on BE. Then the angle η can be determined by the Mohr circle shown in Figure (B.2.2)

Now that the slip surface has been defined, values of N_c, N_q and N_γ can be determined. Firstly, the effect of surcharge and cohesion are computed based on the assumption that the material is weightless.

1- Effect of surcharge and cohesion on weightless material:

The stresses on BD are found directly by geometry from the Mohr circle (Figure B.2.2). The stresses on BE are indicated by point G and the stresses on BD by point P.

$$\overline{CG} = \frac{s_o}{\cos(2\eta + \Phi)} = \frac{s_1}{\cos\Phi} \qquad \text{(B.2.4)}$$

$$p_1 = p_o + \overline{HC} - \overline{IC} \qquad \text{(B.2.5)}$$

$$p_1 = p_o + \frac{s_1}{\cos\Phi}\cos(90 - \Phi - 2\eta) - \frac{s_1}{\cos\Phi}\sin\Phi$$

$$p_1 = p_o + \frac{s_1}{\cos\Phi}[\cos[90 - (2\eta + \Phi)] - \sin\Phi]$$

$$p_1 = p_o + \frac{s_1}{\cos\Phi}[\sin(2\eta + \Phi) - \sin\Phi]$$

We know that $s_1 = c + p_1\tan\Phi$

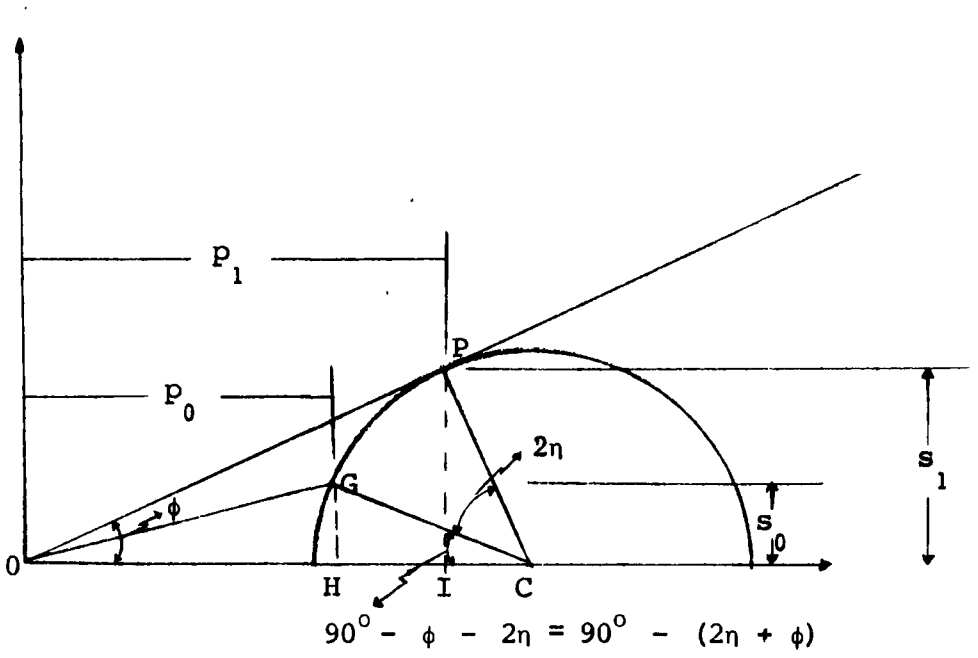

Figure B.2.2

therefore

$$p_1 = p_o + \frac{(c + p_1 \tan\Phi)}{\cos\Phi} [\sin (2\eta + \Phi) - \sin\Phi]$$

which leads to:

$$p_1 = \frac{c \cos\Phi [\sin(2\eta + \Phi) - \sin\Phi]}{1 - \sin\Phi \sin(2\eta + \Phi)} - \frac{p_o \cos\Phi}{1 - \sin\Phi \sin(2\eta+\Phi)} \qquad (B.2.6)$$

Along the arc of the log spiral the shearing strength of the soil is fully mobilized. In particular along BC and AC the normal and tangential components of the passive earth pressure are respectively (form Figure B.2.3)

$$S_p = c + P_p \tan\Phi \qquad (B.2.7)$$

$$P_p = (S_p + c) \cot\Phi \qquad (B.2.8)$$

The value of S_p is obtained as follows with the help of Figure B.2.4:

To find P_p and S_p, take moments about B

a) for the effect of surcharge

$$MB = \frac{p_1 r_1^2}{2} - \frac{P_p r_o^2}{2} = 0 \qquad (B.2.9)$$

where $r_1 = BD = r_o e^{\theta \tan\Phi}$ (B.2.10)

$$r_o = BC = \frac{B}{2\cos(45^\circ + \frac{\Phi}{2})} = \frac{B}{2\sin(45^\circ - \frac{\Phi}{2})} \qquad (B.2.11)$$

b) for the effect of cohesion (from Figure B.2.5)

$$dM_B = c\,ds\cos\Phi \times r \qquad (B.2.12)$$

$$ds = \frac{dr}{\sin\Phi} \qquad (B.2.13)$$

$$dM_B = c\frac{dr\cos\Phi}{\sin\Phi} r = \frac{c}{\tan\Phi} rdr \qquad (B.2.14)$$

$$M_B = \frac{c}{\tan} \frac{r_1^2}{2} - \frac{r_o^2}{2} \qquad (B.2.15)$$

Therefore, the full equation for the passive earth pressure acting on $\overline{BC}$ is

$$M_B = p_1 \frac{r_1^2}{2} - P_p \frac{r_1^2}{2} + \frac{c}{2\tan\Phi}(r_1^2 - r_o) = 0 \qquad (B.2.16)$$

Transforming

$$P_p r_o^2 = p_1 r_1^2 + c(r_1^2 - r_o^2)$$

$$P_p = \frac{p_1 r_1^2}{r_o^2} + \frac{c}{r_o^2} \frac{r_1^2 - r_o^2}{\tan\Phi}$$

$$P_p = p_1 \frac{r_o^2 e^{2\theta\tan\Phi}}{r_o^2} + c\frac{r_o^2(e^{2\theta\tan\Phi} - 1)}{r_o^2\tan\Phi}$$

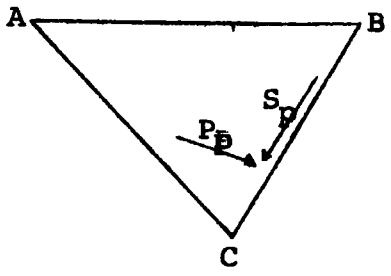

For weightless soil only

Figure B.2.3

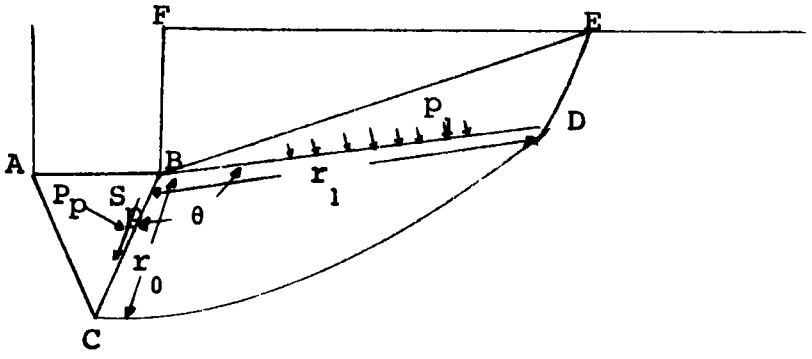

Figure B.2.4

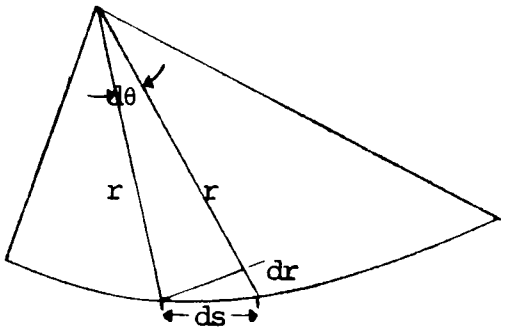

Figure B.2.5

$$P_p = p_1 e^{2\theta \tan\Phi} + \frac{c(e^{2\theta \tan\Phi} - 1)}{\tan\Phi} \qquad (B.2.18)$$

Now considering the vertical forces acting on the wedge ABC:

$$\Sigma F_{vert} = \frac{B}{2} q - P_p \frac{B}{2 \cos(45^\circ + \frac{\Phi}{2})} \cos 45^\circ + \frac{\Phi}{2}$$

$$- S_p \frac{B}{2 \cos(45^\circ + \frac{\Phi}{2})} \sin(45^\circ + \frac{\Phi}{2}) = 0 \qquad (B.2.19)$$

$$q = P_p + S_p \tan(45^\circ + \frac{\Phi}{2})$$

or $$q = P_p + S_p \cot(45^\circ - \frac{\Phi}{2}) \qquad (B.2.20)$$

Substituting (B.2.7) into (B.2.20)

$$q = P_p + (c + P_p \tan\Phi) \cot(45^\circ - \frac{\Phi}{2})$$

$$q = c \cot(45^\circ - \frac{\Phi}{2}) + P_p (1 + \tan\Phi \cot(45^\circ - \frac{\Phi}{2}) \qquad (B.2.21)$$

Now substituting (B.2.18) into (B.2.21)

$$q = c \cot(45^\circ - \frac{\Phi}{2}) + [p_1 e^{2\theta \tan\Phi} + \frac{c}{\tan\Phi} (e^{2\theta \tan\Phi} - 1)]$$

$$[1 + \tan\Phi \cot(45^\circ - \frac{\Phi}{2})]$$

After multiplying and rearranging the term:

$$q = c\,[\cot(45^\circ - \tfrac{\Phi}{2}) + e^{2\theta\tan\Phi} - 1 + e^{2\theta\tan\Phi}\tan\Phi$$

$$\cot(45^\circ - \tfrac{\Phi}{2}) + \tan\Phi\ \cot(45^\circ - \tfrac{\Phi}{2})] + p_1 e^{2\theta\tan\Phi}$$

$$[1 + \tan\Phi\ \cot(45^\circ - \tfrac{\Phi}{2})] \qquad \text{(B.2.22)}$$

Then substituting (B.2.6) into (B.2.22)

$$q = c\,[\cot(45^\circ - \tfrac{\Phi}{2}) + \frac{e^{2\theta\tan\Phi}}{\tan\Phi} - \frac{1}{\tan\Phi} + e^{2\theta\tan\Phi}\cot(45^\circ - \tfrac{\Phi}{2})$$

$$+ \cot(45^\circ - \tfrac{\Phi}{2})] - c[\frac{\sin(2\eta + \Phi) - \sin\Phi\ \cos\ e^{2\theta\tan\Phi}}{1 - \sin\Phi\ \sin(2\eta + \Phi)}$$

$$+ e^{2\theta\tan\Phi}\tan\Phi\cot(45^\circ - \tfrac{\Phi}{2})\ \ [\frac{\sin(2\eta - \Phi) - \sin\Phi]\cos\Phi}{1 - \sin\Phi\ \sin(2\eta - \Phi)}]$$

$$+ \frac{p_o e^{2\theta\tan\Phi}\cos^2\Phi}{1 - \sin\Phi\ \sin(2\eta + \Phi)}\ [1 + \tan\Phi\ \cot(45^\circ - \tfrac{\Phi}{2})]$$

Now consider the last term only of Equation (B.2.23)

$$p_o\ \frac{e^{2\theta\tan\Phi}\cos^2\Phi}{1 - \sin\Phi\ \sin(2\eta + \Phi)}\ [1 + \tan\Phi\ \cos(45^\circ - \tfrac{\Phi}{2})]$$

It is known that $\cot(45^\circ - \frac{\Phi}{2}) = \frac{1 - \sin\Phi}{\cos\Phi}$, therefore this term becomes

$$p_o\ [\frac{e^{2\theta\tan\Phi}}{1 - \sin\Phi\ \sin(2\eta - \Phi)}\ (1 - \sin\Phi)] \qquad \text{(B.2.24)}$$

Now, consider the c term of Equation (B.2.23)

By regrouping

$$c\{\cot(45^\circ - \tfrac{\Phi}{2}) + \frac{e^{2\theta\tan\Phi} - 1}{\tan\Phi}\,[1 + \tan\Phi\,\cot(45^\circ - \tfrac{\Phi}{2})]$$

$$+ \frac{e^{2\theta\tan\Phi}\sin(2\eta + \Phi) - \sin\Phi}{1 - \sin\Phi\,\sin(2\eta + \Phi)}\,[1 + \tan\Phi\,\cot(45^\circ - \tfrac{\Phi}{2})]\}$$

or

$$c\{\cot(45^\circ - \tfrac{\Phi}{2}) + [1 + \tan\Phi\,\cot(45^\circ - \tfrac{\Phi}{2})]$$

$$[-\frac{1}{\tan\Phi} + e^{2\theta\tan\Phi}(\frac{1}{\tan\Phi} + \frac{\sin(2\eta + \Phi) - \sin\Phi}{1 - \sin\Phi\,\sin(2\eta + \Phi)})]\} \qquad \text{(B.2.25)}$$

Rearranging the last factor of Equation (B.2.25)

$$-\frac{1}{\tan\Phi} + e^{2\theta\tan\Phi}$$

$$[\frac{1 - \sin\Phi\sin(2\eta + \Phi) + \tan\Phi\cos\Phi\sin(2\eta + \Phi) - \tan\Phi\sin\Phi\cos\Phi}{\tan\Phi[1 - \sin\Phi\,\sin(2\eta + \Phi)]}]$$

Transforming

$$-\frac{1}{\tan\Phi} + e^{2\theta\tan\Phi}[\frac{1 - \sin^2\Phi}{\tan\Phi[1 - \sin\Phi\,\sin(2\eta + \Phi)]}] =$$

$$e^{2\theta\tan\Phi}[\frac{\cos^2\Phi}{\tan\Phi[1 - \sin\Phi\,\sin(2\eta + \Phi)]} - \frac{1}{\tan\Phi}] \qquad \text{(B.2.26)}$$

Putting Equation (B.2.26) into Equation (B.2.25)

$$c\{\cot(45^\circ - \tfrac{\Phi}{2}) + [1 + \tan\Phi \cot(45^\circ - \tfrac{\Phi}{2})] \frac{1}{\tan\Phi}$$

$$[\frac{e^{2\theta\tan\Phi} \cos^2\Phi}{1 - \sin\Phi \sin(2\eta + \Phi)} - 1]\}$$

which leads to:

$$c\{[\cot(45^\circ - \tfrac{\Phi}{2}) + \frac{1}{\tan\Phi}] [\frac{e^{2\theta\tan\Phi} \cos^2\Phi}{1 - \sin\Phi \sin(2\eta + \Phi)}] - \frac{1}{\tan\Phi}\}$$

Knowing that $\cot(45^\circ - \frac{\Phi}{2}) = \frac{1 + \sin\Phi}{\cos\Phi}$

$$c\{(\frac{1 + \sin\Phi}{\cos\Phi} + \frac{1}{\tan\Phi}) (\frac{e^{2\theta\tan\Phi} \cos^2\Phi}{1 - \sin\Phi \sin(2\eta + \Phi)}) - \frac{1}{\tan\Phi}\}$$

or $$c\{\cot\Phi [\frac{e^{2\theta\tan\Phi}(\sin\Phi + 1)}{1 - \sin\Phi \sin(2\eta + \Phi)} - 1]\} \qquad (B.2.27)$$

Therefore, since (B.2.23) = (B.2.24) + (B.2.27)

$$q = p_o[\frac{e^{2\theta\tan\Phi}(1 + \sin\Phi)}{1 - \sin\Phi\sin(2\eta + \Phi)}] +$$

$$c\{\cot\Phi [\frac{e^{2\theta\tan\Phi}(1 + \sin\Phi)}{1 - \sin\Phi \sin(2\eta + \Phi)} - 1]\} \qquad (B.2.28)$$

which can also be written

$$q = p_o N_q + cN_c$$

where $N_q = \frac{e^{2\theta\tan\Phi}(1 + \sin\Phi)}{1 + \sin\Phi \sin(2\eta + \Phi)}$ (B.2.29)

$$N_c = \cot[\frac{e^{2\theta\tan\Phi}(1+ \sin\Phi)}{1-\sin\Phi\sin(2\eta+\Phi)} - 1] = \cot [N_q - 1] \qquad (B.2.30)$$

N_q and N_c are referred to as the bearing capacity factors to consider the effect of surcharge and cohesion respectively in a weightless soil.

Meyerhof found the values of N_c and N_q not to be very sensitive to a change in "m". It has been found that

$\eta = 0$ if $m = 1$ (full mobilization of shear on BE)

$\nu = 45 - \frac{\Phi}{2}$ if $m = 0$ (no mobilization of shear on BE)

This can be shown by the Mohr circle on Figure B.2.2.

It can be seen that if $m = 1$ and $\eta = 0$, the slip surface is a complete logarithmic spiral without the zone BDE from point C.

As a sample calculation of N_q for $\beta = 0$ and $\Phi = 30$

for $m = 1$ then $\eta = 0$ and $\Phi = 120°$

$$N_q = \frac{1 + \sin 30°}{1 - \sin 30°} \; e^{2(120)^{\pi}/180 \tan 30°} =$$

$$\frac{1 + 0.5}{1 - 0.25} \; 11.23 = 22.46$$

for $m = 0$ then $\eta = 45 - \frac{\Phi}{2}$ and $\Phi = 90°$

$$N_q = \frac{1 + \sin 30°}{1 - \sin 30°} \; e^{2(90)^{\pi}/180 \tan 30°} =$$

$$\frac{1.5}{0.5} \; e^{\pi \tan 30°} = 18.4$$

and the difference between the two N_q values is

$$22.46 - 18.4 = 4.06$$

or $\frac{4.06}{22.46} \times 100 = 20\%$

This demonstration introduces the possibility that the calculations can be simplified by assuming a full logarithmic spiral as a slip surface then reducing the resulting values of N_q and N_c by 20% to obtain a more realistic $N_{\gamma q}$ value. The soundness of the reasoning was demonstrated by Meyerhof.

2 - Considering the weight of the material

To obtain the slip surface due to the weight of the material, the configuration is the same as the one given in Figure B.2.1 except that the location of the center of the critical log spiral arc between C and D is found by trial and error.

The theory is as follows (Figure B.2.6):
Taking moments about the center of the log spiral, P_p becomes

$$P_p = \frac{P_1 l_1 + W l_2}{l_3}$$

l_1, l_2 and l_3 are dependent upon the location of the log spiral center.

Now considering the forces acting on BC

$$qB = 2P_p \cos(\psi - \Phi) - \frac{B^2}{4} \tan\psi \qquad \text{(B.2.31)}$$

$$q = 2\frac{P_p}{B} \cos(\psi - \Phi) - \frac{B}{4} \gamma \tan\psi$$

$$q = \frac{\gamma B}{2} \left[\frac{4 P_p \cos(\psi - \Phi)}{\gamma B^2} - \tfrac{1}{2} \tan\psi\right]$$

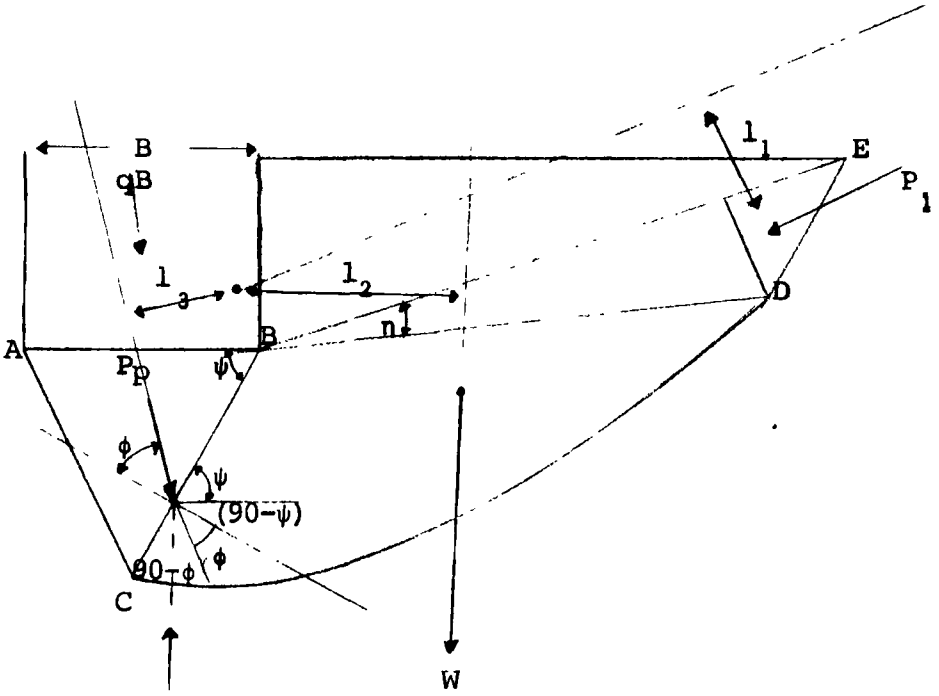

Figure B.2.6

Then $q = \frac{\gamma B}{2} N_\gamma$

where $N_\gamma = [\frac{4P_p \cos(\psi - \Phi)}{\gamma B^2} - \frac{1}{2} \tan\psi]$

Here, also, Meyerhof found that by assuming $\eta = 0$, the bearing capacity factor N_γ is approximately 20% higher than if $\eta = 45 - \frac{\Phi}{2}$ or $m = 0$. If $\eta = 0$, $P_1 = 0$, $l_1 = 0$ and $P_p = \frac{Wl_2}{l_3}$

The resulting value of N_γ should be reduced by approximately 20%.

In 1951, Meyerhof recommended that ψ should be equal to $45 + \frac{\Phi}{2}$ and that the location of the center of the log spiral be where P_p would be a minimum.

In 1955, Meyerhof again considered the factor N_γ and recommended that for a horizontal ground surface and D/B < 1

$$N_\gamma = \frac{4P_p \cos(\psi - \Phi)}{\gamma B^2} - \frac{\tan\psi}{2} \qquad \text{(B.2.32)}$$

where the minimum value of P_p is calculated by varying ψ until the critical P_p is found. Meyerhof found ψ to be approximately 1.2Φ. The 1955 method ignores the shearing strength of the overburden. The difference between ignoring the shearing strength of the overburden and taking it into account does not exceed 20% for a shallow footing (D/B < 1).

This discussion can be terminated with Meyerhof's personnal, 1955 conclusion:

".....the bearing capacity of shallow foundations in cohesionless soil can, in practice, be determined on the previous assumption of no shearing strength of the overburden (using the worst ψ for N_γ and $\psi = 45 + \frac{\Phi}{2}$ for N_q), which considerably simplifies the estimates. For foundation depth $D/B < 1$, however, the error associated with this procedure increases rapidly with D/B, and it is suggested that the more elaborate method published previously (Meyerhof, 1951), be used. That method was based on $\psi = 45 + \frac{\Phi}{2}$ (for both N_γ and N_q) which, as already shown, is reasonable for the greater foundation depth."

B.3 Computations

In his 1957 paper, Meyerhof used a combination of his 1951 and 1955 theories which are described in the preceeding section. Meyerhof gives values of the bearing capacity factors of a spread footing near or at the crest of a slope. These values are presented only for two Φ angles (namely $\Phi = 30°$ and $\Phi = 40°$) and only two depths ($D/B = 0$ and $D/B = 1$). The intention here is to devise a computer program which will yield $N_{\gamma q}$ values for $\Phi = 30°, 35°, 40°, 45°, 50°$ and $D/B = 0$, 1,2 and 3.

1- The method used to find bearing capacity factors for footings on top of a cohesionless slope.

As a first step, Meyerhof changed the original Terzaghi bearing capacity equation in cohesionless material

($N_c = 0$) from

$$q = \tfrac{1}{2} N_\gamma B\gamma + N_q \gamma D \qquad \text{(B.3.1) Terzaghi (1943)}$$

to $$q = \tfrac{1}{2} N_{\gamma q} B\gamma \qquad \text{(B.3.2) Meyerhof (1951)}$$

where $\tfrac{1}{2}N_{\gamma q} B\gamma = \tfrac{1}{2}N_\gamma B\gamma + N_q \gamma D$

and $$N_{\gamma q} = N + 2\frac{D}{B} N_q \qquad \text{(B.3.3)}$$

If γD is replaced by P_o (the stress acting on BE)

$$N_{\gamma q} = N_\gamma + 2 \frac{P_o}{B\gamma} N_q \qquad \text{(B.3.4)}$$

The aim is to find values of $N_{\gamma q}$ using Equation (B.3.4). The different steps to achieve this are:

1- Look at the geometry of the problem in two-dimensional space (Figure B.3.1).

2- From L (center of the log spiral), determine the point of intersection of BE with the slope of angle α at E (Figure B.3.2).
Assume complete log spiral with η equal to 0 (N_γ and N_q will subsequently be reduced by 20%).

3- Segment $\overline{BE}$ is drawn which determines the equivalent free surface and also angle β.

4- P_o is equal to the weight of soil in the triangle BEO multiplied by the cosine of β and divided by the length BE.

5- N_q can be found from Equation (B.2.29).

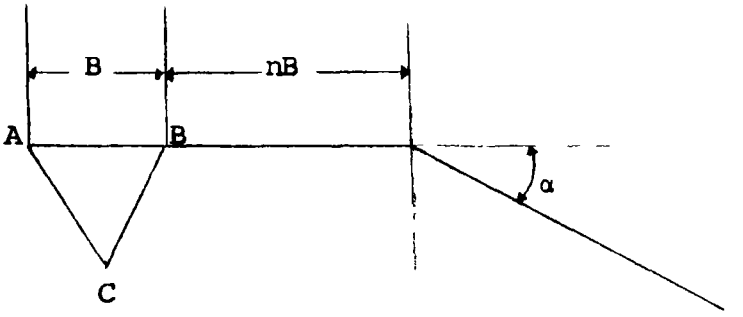

Figure B.3.1

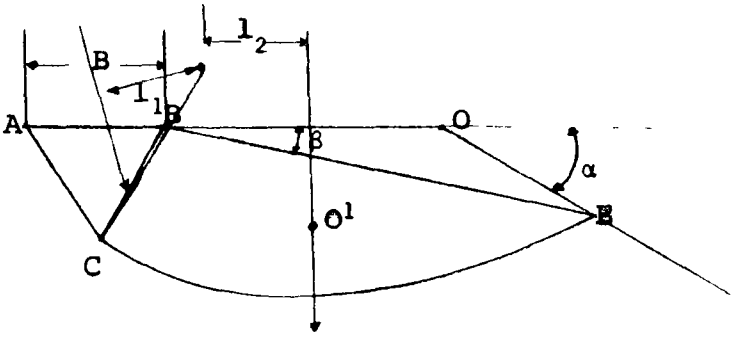

Figure B.3.2

6- The centroid of the curved area BCE is found as O' and its area must be known to find the weight of BCE.

7- Find the moment of arms l_2 and l_3.

8- N_γ is found by Equation (B.2.32)

9- Then the value of Equation (B.3.4) is calculated.

10-The process is repeated for another center of the log spiral until the minimum $N_{\gamma q}$ is found for a particular situation.

2- The computer program

First the computer chooses a set of cartesian coordinates. Figure B.3.3 shows the sign convention that has been adopted. The x axis is positive to the right of y = 0; the y coordinates will be positive below the x axis. The slope starts at the origin (0,0) and all slopes will be positive as shown in Figure B.3.3.

Then the program places the footing at the desired location as shown on Figure B.3.4 where:

(x_1, y_1): is the location of the leading edge of the footing.

(x_2, y_2): is the point below footing that defines the lowest point of the elastic wedge; this point depends on the angle ψ (which is a variable).

(x_4, y_4): is the point of the center of the log spiral.

What has been described so far is accomplished by statements 1 to 24 in the program listing which form a part of this appendix. B, the footing width, is considered to be unity throughout the calculations.

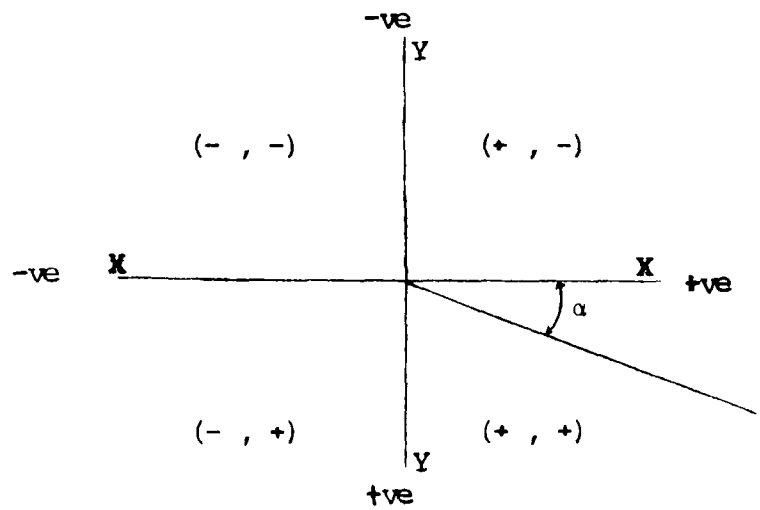

Figure B.3.3

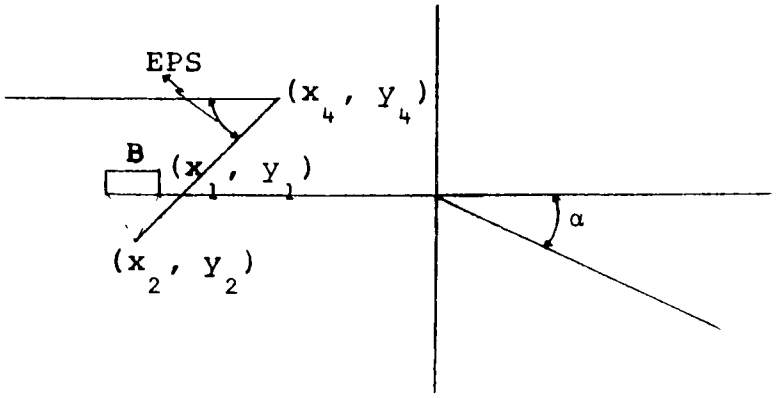

Figure B.3.4

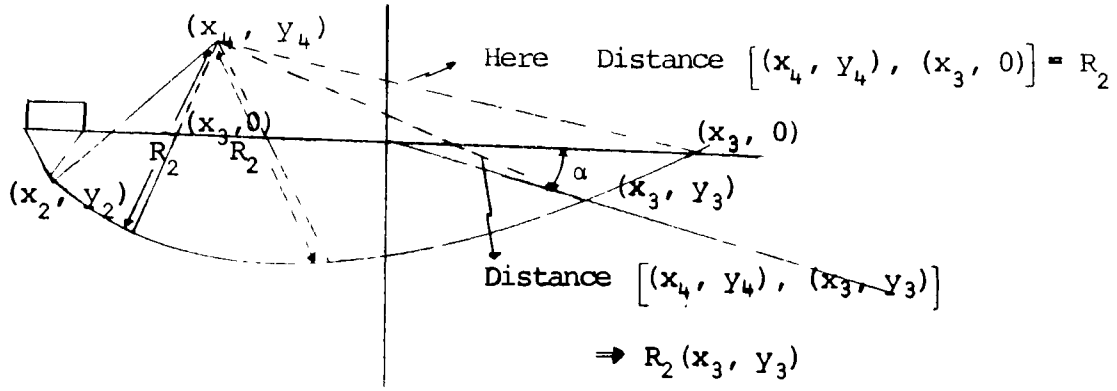

Figure B.3.5

The distance (x_4, y_4) to (x_2, y_2) is found along with the equivalent of r_o of the log spiral. Angle EPSI is worked out so that the sweep angle θ of the log spiral can be located in the two dimensional space. (Figure B.3.5)

In statements 34 to 57, the point of intersection (x_3, y_3) with the slope surface is found. This is done by an iterative process where a) y_3 is maintained equal to 0, and b) with small increments of x_3 the distance $[(x_3, 0)\ (x_4, y_4)]$ is compared to the length R_2 of the log spiral ($R_2 = R_o e^{\theta \tan\Phi}$). When the distance $[(x_3, 0)\ (x_4, y_4)]$ equals R_2, the point of intersection $(x_3, 0)$ is found as shown on Figure B.3.5. This will be very useful when the leading edge of the footing at (x_1, y_1) is very far from the slope; in this case the only intersection that is calculated is with the flat surface where x_3 is negative. Therefore, if x_3 is positive (such as is the case in Figure B.3.5) the point of intersection of the log spiral with the slope at (x_3, y_3) must be found. The procedure is the same as described previously, but the iterative process will start at the final point $(x_3, 0)$ and will go to the left until the distance $[(x_4, y_4)\ (x_3, y_3)]$ equals R_2. With convergence, (x_3, y_3) is found.

From statements 58 to 71, the program finds the area within the log spiral sector; then the centroid of this area (x_5, y_5) is located with respect to the x - y axes.

Statement 72 decides if the location of the log spiral center (x_4, y_4) is above the x axis or below.

1) When the center of the log spiral (x_4, y_4) is located above the x axis as shown in Figure B.3.6:

From (x_3, y_3) to (x_1, y_1) a segment is drawn which corresponds to the equivalent free surface described by Meyerhof and explained earlier. The angle β gives its position in space.

The point of intersection between the two segments $[(x_3, y_3), (x_1, y_1)]$ and $[(x_2, y_2), (x_4, y_4)]$ is given by (x_6, y_6). This point (x_6, y_6) is the meeting point of two triangles namely $[(x_6, y_6), (x_3, y_3), (x_4, y_4)]$ and $[(x_6,y_6), (x_2, y_2), (x_1, y_1)]$.

The area of triangle $[(x_6, y_6), (x_3, y_3), (x_4,y_4)]$ is subtracted from the area of the log spiral sector calculated previously. The centroid is adjusted to account for this as in area $[(x_6, y_6), (x_3, y_3), (x_4, y_4)]$. The centroid of triangles is found by the intersection of the medians of the triangles.

- To find the centroid of triangle $[(x_6, y_6), (x_3, y_3), (x_4, y_4)]$

  (x_7, y_7) = mid point of segment $[(x_6, y_6) , (x_3, y_3)]$

  (x_8, y_8) = mid point of segment $[(x_6, y_6), (x_4, y_4)]$

  The centroid (x_9, y_9) is then the point of intersection of segments $[(x_3, y_3), (x_8, y_8)]$ and $[(x_4, y_4), (x_7, y_7)]$.

- To find the centroid of triangle $[(x_6, y_6), (x_1, y_1), (x_2, y_2)]$

  (x_{12}, y_{12}) = mid point of segment $[(x_1, y_1), (x_6, y_6)]$

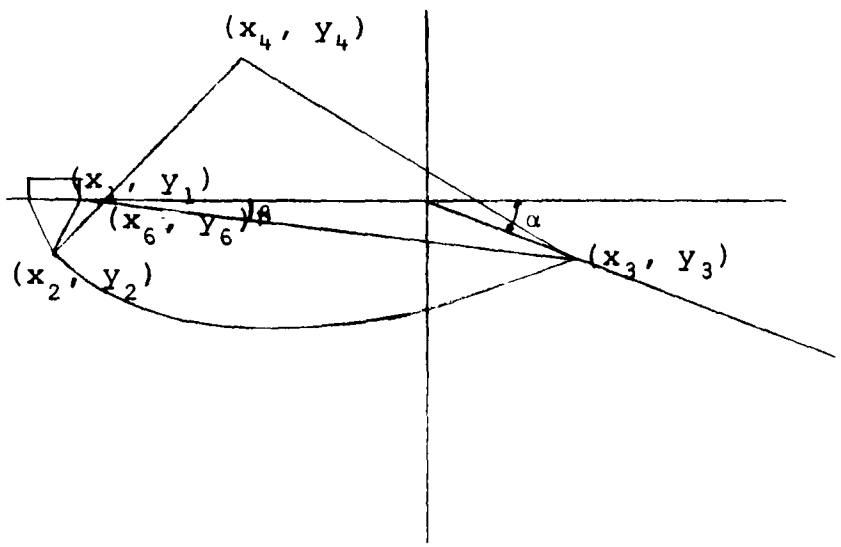

Figure B.3.6

(x_{13}, y_{13}) = mid point of segment $[(x_2, y_2), (x_6, y_6)]$

The centroid (x_{14}, y_{14}) is the point of intersection of segments $[(x_2, y_2), (x_{12}, y_{12})]$ and $[(x_1, y_1), (x_{13}, y_{13})]$.

- The new centroid (x_{15}) is given by

x_{15} = (x_5 · area of log spiral - x_9 · area of triangle $[(x_6, y_6), (x_3, y_3), (x_4, y_4)]$ - x_{14} · area of triangle $[(x_6, y_6), (x_1, y_1), (x_2, y_2)]$/ (area of log spiral - area of triangle $[(x_6, y_6), (x_3, y_3), (x_4, y_4)]$ + area of triangle $[(x_6, y_6), (x_1, y_1), (x_2, y_2)]$).

Only the position of x_{15} is necessary to define l_2

$$l_2 = x_{15} - x_4 \qquad \text{(Statement 128)}$$

2) If the center of the log spiral (x_4, y_4) is below the x axis the situation can be represented by Figure B.3.7.

This situation is treated in a similar way as when the center is above the x axis. The curved area $[(x_4, y_4), (x_2, y_2), (x_3, y_3)]$ is evaluated and its centroid is located. The triangular area $[(x_4, y_4), (x_2, y_2), (x_3, y_3)]$ is subtracted from the curved area, leaving only a second curved area $[(x_2, y_2), (x_3, y_3)]$. To this second curved area, triangle $[(x_1, y_1), (x_2, y_2), (x_3, y_3)]$ is added. The required adjustments are made to yield the proper final position of the centroid (x_{30}, y_{30})

$$l_2 = x_{30} - x_4 \qquad \text{(Statement 180)}$$

l_2 is now known for both cases and l_3 can be deduced

by analytical geometry as shown in Figure B.3.8.

P_p acts at the lower third point of segment $[(x_1, y_1), (x_2, y_2)]$ at Φ degrees to the normal; this third point is (x_{20}, y_{20}). β_{20} is easily found and, therefore, the equation for the line of action of P_p is easily determined by analytical geometry. l_3 is the directed distance from point (x_4, y_4) to the line of action of P_p.

The normal stress P_o acting on segment $[(x_1, y_1), (x_3, y_3)]$ is given by the area $[(x_1, y_1),(0,0), (x_3, y_3)]$ multiplied by $\cos\beta$ and divided by the length of the segment $[(x_1, y_1), (x_3, y_3)]$.

Then N_γ is found by Equation (B.2.32), and N_q by Equation (B.2.29). $N_{\gamma q}$ is given by the sum of $(N_\gamma + 2\ p_o N_q)$.

The process is repeated for each center of the log spiral. This repetition is concentrated in a grid 2B above and below the footing and 4B wide horizontally starting at the mid width of footing as shown in Figure B.3.9.

For every location of center (x_4, y_4) the program gives:

- Footing position (x_1, y_1)
- Intercept point (x_3, y_3)
- The center (x_4, y_4)
- N_γ
- N_q

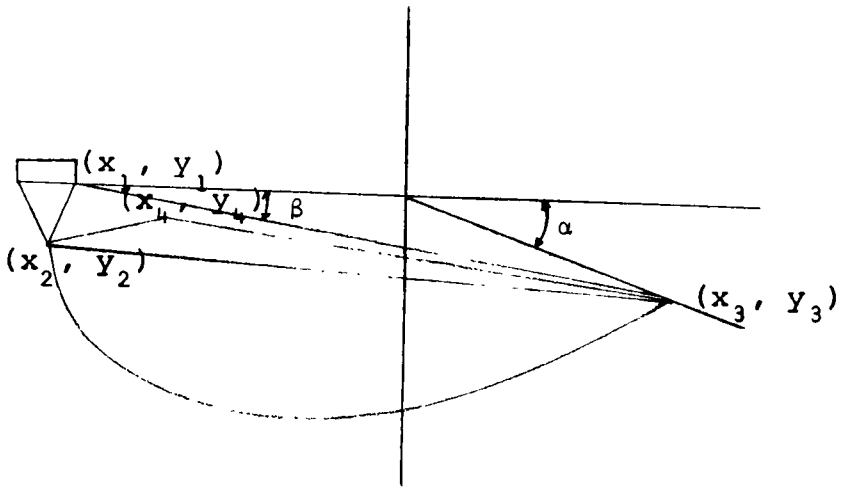

Figure B.3.7

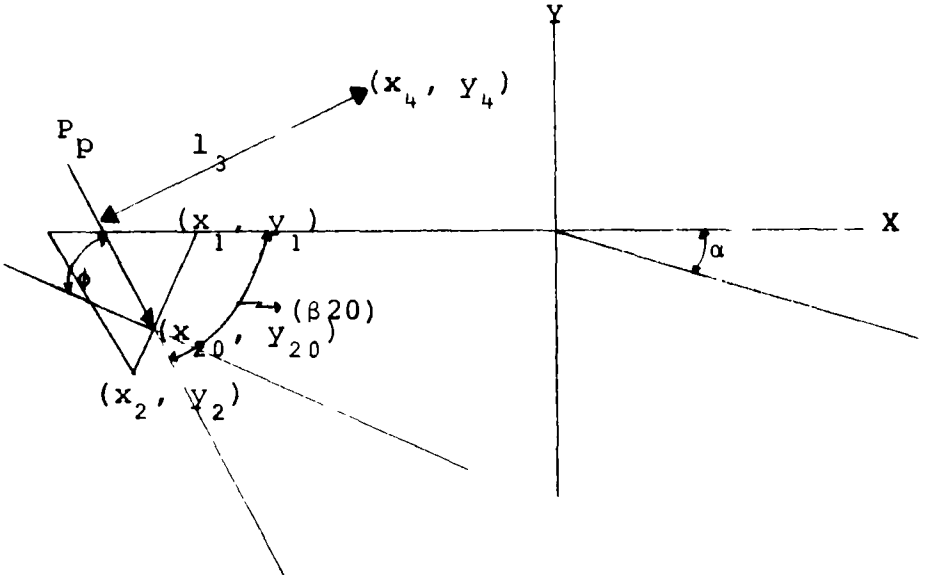

Figure B.3.8

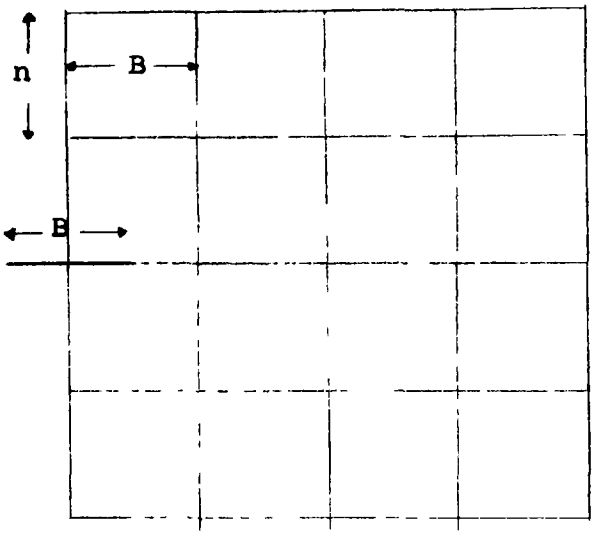

Figure B.3.9

- $N_{\gamma q}$
- R_o
- R_2
- θ (sweep angle of the log spiral)

Then the program plots the values of N_γ and $N_{\gamma q}$ on the grid and draws contours of equal N_γ and equal $N_{\gamma q}$.

B.4 Results

The computer program was run to obtain the following results:

1- The slope alpha (α) was maintained throughout the project at 2:1 (horizontal : vertical).

2- The values of Φ were 30°, 35°, 40° and 45°.

3- The footing locations horizontally with respect to the crest of the slope were b/B = 0, 1, 2, 3, 4 and 5.

4- The footing locations with respect to the ground surface were D/B = 0, 1, 2, and 3.

5- The angle of the elastic wedge under the footing was maintained throughout at

$$\psi = 45° + \frac{\Phi}{2}$$

6- The center of the log spiral was varied for every situation to yield the most critical bearing capacity factor.

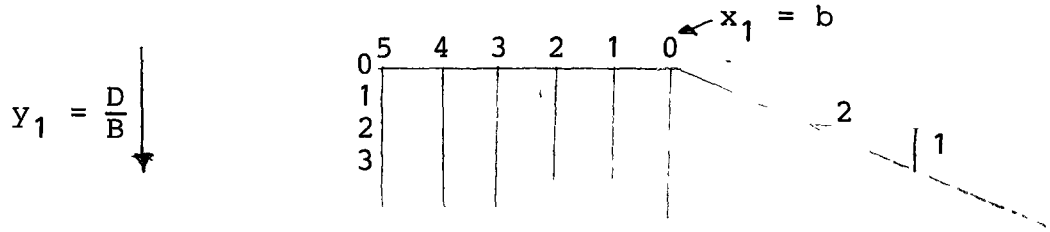

```
FC   AN IV G LEVEL  21                    MAIN                    DATE = 76336          20/46/46
      IMPLICIT REAL (M)
      DIMENSION MG(21,21),MGQ(21,21)
      PH=4[.
      PHI=PH/18[.*3.1416
      X1=-5.
      Y1=3.
      WRITE(6,51[)
  51[ FORMAT(1H1,2(1H-,/,1H ),1[X,'     PHI           X1           Y1 ')
      WRITE(6,511) PH,X1,Y1
  511 FORMAT(1H[,8X,3F10.1)
      WRITE(6,1[1)
  1[1 FORMAT(1H[,11X,'BEARING CAPACITY FACTORS MEYERHOF S METHOD ',///4X
     1'      X1           Y1           X3           Y3           X4           Y4
     2NG          NQ           NGQ          R[           R            TETA')
      Y2=.5*TAN(3.1416/4.+PHI/2.)+Y1
      X2=X1-.5
      X11=X1
      Y11=[
      X2[=X1+2.*(X2-X1)/3.
      Y2[=Y1+2.*(Y2-Y1)/3.
      BETA2[=3.1416/4.+PHI/2.
      C2[=Y2[-X2[*TAN(BETA2[)
      DO 25 JI=1,21
      X4=X2+(JI-1.)/5.
      DO 2[ JK=1.21
      Y4=Y1-2+(JK-1.)/5.
      Y21=X4*TAN(BETA2[)+C2[ -.2
      IF(Y4.GE.Y21) GO TO 25
      ALFA=ATAN(.5)
      R[=((X4-X2)**2+(Y4-Y2)**2)**.5
      IF(X2.EQ.X4) GO TO 5
      EPSI=ATAN((Y2-Y4)/(X2-X4))
      GO TO 6
    5 EPSI=3.1416/2.
    6 EPS=ABS(EPSI)
      Y3=[.
      DO 32 KL=1,R[
      X3=X2+((KL-1)/1[.)
      IF(X3.EQ.X4) GO TO 2[1
      TETA=3.1416-(EPS+ATAN(Y4/(X4-X3)))
      GO TO 2[2
  2[1 TETA=3.1416-(EPS+3.1416/2.)
  2[2 R1=R[*EXP(TETA*TAN(PHI))
      R2=((X4-X3)**2+(Y4-Y1)**2)**.5
      IF((ABS(R2-R1)).LE.(.1)) GO TO 35
   32 CONTINUE
   35 IF(X3.LE.[.[) GO TO 42
      XB=X3
      DO 45 KN=1,8[
      X3=XB-((KN-1)/1[.)
      Y3=X3*TAN(ALFA)
      IF(X3.LQ.X4) GO TO 2[3
      TETA=3.1416-(EPS+ATAN((Y4-X3*TAN(ALFA))/(X4-X3)))
      GO TO 2[4
  2[3 TETA=3.1416-(EPS+3.1416/2.)
  2[4 R1=R[*EXP(TETA*TAN(PHI))
      R2=((X4-X3)**2+(Y4-X3*TAN(ALFA))**2)**.5
      IF((ABS(R2-R1)).LE.(.1)) GO TO 42
```

```
 45 CONTINUE
 42 TET=TETA*180./3.1416
    AREA1=(R2**2-R0**2)/(4.*TAN(PHI))
    ZA=(R0**4/3)*TAN(PHI)/(9*(TAN(PHI))**2+1)
    ZAR=(R2/R0)**3
    ZAP=(R2/R0)**2-1
    AA= ZA/ZAP*(ZAR*(3*TAN(PHI)*SIN(TETA)-COS(TETA))+1)
    BB=ZA/ZAP*(ZAR-3*TAN(PHI)*SIN(TETA)-COS(TETA))
    TETAX=ATAN(AA*SIN(TETA)/(BB+AA*COS(TETA)))
    IF (TETAX.EQ.0.0) GO TO 25
    IF(TETAX.LT.0.0) TETAX=(TETAX+3.1416)
    AB=AA/SIN(TETAX)
    OMEGA=(EPS +TETAX)-3.1416/2.
    X5=X4+AB*SIN(OMEGA)
    Y5=Y4+AB*COS(OMEGA)
    IF(Y4.GE.0) GO TO 75
    IF(X3.EQ.X1) GO TO 25
    BETA=ATAN((Y3-Y1)/(X3-X1))
    CX=Y1-X1*TAN(BETA)
206 IF(EPS .EQ.(3.1416/2.)) GO TO 207
    C=Y2-X2*TAN(EPSI)
    X6=(CX-C)/(TAN(EPSI)-TAN(BETA))
    GO TO 212
207 X6=X4
212 Y6=X6*TAN(BETA)+CX
    AREA2=.5*(X3*Y6+X6*Y4+X4*Y3-X3*Y4-X6*Y3-X4*Y6)
    X7=(X6+X3)/2.
    Y7=(Y6+Y3)/2.
211 X8=(X6+X4)/2.
    Y8=(Y6+Y4)/2.
    IF(X7.EQ.X4) GO TO 213
    IF(X8.EQ.X3) GO TO 214
    PSI=ATAN((Y7-Y4)/(X7-X4))
    CPSI=Y7-X7*TAN(PSI)
    XHI=ATAN((Y3-Y8)/(X3-X8))
    CXHI=Y8-X8*TAN(XHI)
    X9=(CXHI-CPSI)/(TAN(PSI)-TAN(XHI))
    Y9=X9*TAN(PSI)+CPSI
    GO TO 224
213 X9=X4
    XHI=ATAN((Y3-Y8)/(X3-X8))
    CXHI=Y8-X8*TAN(XHI)
    Y9=X9*TAN(XHI)+CXHI
214 X9=X3
    PSI=ATAN((Y7-Y4)/(X7-X4))
    CPSI=Y7-X7*TAN(PSI)
    Y9=X9*TAN(PSI) + CPSI
224 X12=(X1+X5)/2.
    Y12=(Y1+Y5)/2.
    X13=(X2+X6)/2.
    Y13=(Y2+Y6)/2.
    IF(X2.EQ.X12) GO TO 231
    IF(X1.EQ.X13) GO TO 232
    M12=(Y2-Y12)/(X2-X12)
    C12=Y2-M12*X2
    M13=(Y13-Y1)/(X13-X1)
    C13=Y1-M13*X1
    X14=(C12-C13)/(M13-M12)
```

```
                      Y14=M12*X14+C12
                      GO TO 233
                231   X14=X12
                      M13=(Y13-Y1)/(X13-X1)
                      C13=Y1-M13*X1
                      Y14=M13*X4+C13
                232   X14=X13
                      M12=(Y2-Y12)/(X2-X12)
                      C12=Y2-M12*X2
                      Y14=M12*X14+C12
                234   AREA3=(X6*Y2+X2*Y1+X1*Y6-X6*Y1-X2*Y6-X1*Y2)/2
                      AREAN=AREA1-AREA2+AREA3
                      X15=(X5*AREA1-X9*AREA2+X14*AREA3)/AREAN
                      ML=X15-X4
                       IF(Y4.LT.Y) GO TO 76
                 75   AREA6=(X3*Y2+X2*Y4+X4*Y3-X3*Y4-X2*Y3-X4*Y2)/2
                      AREA7=(X1*Y3+X3*Y2+X2*Y1-X1*Y2-X3*Y1-X2*Y3)/2
                      AREA8=AREA1-AREA6+AREA7
                      X24=(X3+X4)/2
                      Y24=(Y3+Y4)/2
                      X25=(X4+X2)/2
                      Y25=(Y4+Y2)/2
                      IF(Y3.EQ.Y2) GO TO 25
                      IF(X24.EQ.X2) GO TO 237
                      IF(X25.EQ.X3) GO TO 238
                      M24=(Y24-Y2)/(X24-X2)
                      C24=Y24-X24*M24
                      M25=(Y3-Y25)/(X3-X25)
                      C25=Y25-X25*M25
                      X26=(C25-C24)/(M24-M25)
                      Y26=X26*M24+C24
                      GO TO 239
                237   X26=X2
                      M25=(Y3-Y25)/(X3-X25)
                      C25=Y25-X25*M25
                      Y26=X26*M25+C25
                238   X26=X3
                      M24=(Y24-Y2)/(X24-X2)
                      C24=Y24-X24*M24
                      Y26=X26*M24+C24
                239   X5=(AREA1*X5-X26*AREA6)/(AREA1-AREA6)
                      Y5=(AREA1*Y5-Y26*AREA6)/(AREA1-AREA6)
                      X27=(X1+X2)/2
                      Y27=(Y1+Y2)/2
                      X28=(X1+X3)/2
                      Y28=(Y1+Y3)/2
                      IF(X27.EQ.X3) GO TO 241
                      IF(X28.EQ.X2) GO TO 242
                      M27=(Y3-Y27)/(X3-X27)
                      C27=Y27-X27*M27
                      M28=(Y2-Y28)/(X2-X28)
                      C28=Y28-X28*M28
                      X29=(C28-C27)/(M27-M28)
                      Y29=M27*X29+C27
                      GO TO 243
                241   X29=X3
                      M28=(Y2-Y28)/(X2-X28)
                      C28=Y28-X28*M28
```

```
             Y28=X28*M28+C28
      242    X29=X3
             M27=(Y3-Y27)/(X3-X27)
             C27=Y27-X27*M27
             Y29=X29*M27+C27
      243    X30=((AREA1-AREA6)*X50+AREA7*X29)/AREA3
             Y30=((AREA1-AREA6)*Y50+AREA7*Y29)/AREA3
             ML2=X30-X4
             AREAN=AREA3
       76    ML3=(X4*TAN(BETA2 )-Y4+C2 )*COS(BETA2 )
             PP=(AREAN*ML2)/ML3
             W1=(X3*Y1+X11*Y3-X1*Y3-X11*Y1)/2.
             W2=(-X11*Y3)/2.
             DX=((X3-X1)**2+(Y3-Y1)**2)**.5
             P =(W1+W2)*COS(BETA)/DX
             THETHA=.75*3.1416-BETA-PHI/2.
             GO TO [illegible]
       [illegible] MG(JI,JK)=[illegible].
             MG=[illegible].
             MGQ(JI,JK)=0.
             RG=[illegible].
             RQ=[illegible].
             [illegible]
             [illegible]
       [illegible] MG(JI,JK)=(4.*PP*SIN([illegible].1416/4.+PHI/2.)-.5*TAN(3.1416/4.+PHI/2.))
             [illegible]=(4.*[illegible]SIN(3.1416/4.+PHI/2.)-.5*TAN(3.1416/4.+PHI/2.))
             [illegible](1.+SIN(PHI))*EXP(2.*THETHA*TAN(PHI))/(1.-(SIN(PHI))**2)
             [illegible]+2.*[illegible]*RQ
             MGQ(JI,JK)=MG(JI,JK)+2.*P[illegible]
       [illegible] WRITE([illegible])X1,Y1,X2,Y3,X4,Y4,[illegible],MGQ,RG,R2,TET
       1[illegible] FORMAT(1H,12F10.2)
       [illegible] CONTINUE
       [illegible] CONTINUE
             WRITE([illegible])
       [illegible] FORMAT(1H1,2(1H-,/,1H ),1 X,'     PHI              X1              Y1
            1                    N GAMMA VALUES')
             WRITE([illegible]1) PH,X1,Y1
       [illegible]1 FORMAT(1H ,5X,3F1 .1)
             WRITE(6,4  ) ((MG(I,J),I=1, 1),J=1,21)
       4[illegible] FORMAT(1H ,4(1H-,/,1H ),21(15X,21F5.  ,/,1H-,/,1H ))
             WRITE( [illegible] )
       [illegible] FORMAT(1H1,2(1H-,/,1H ),1 X,'     PHI              X1              Y1
            1                    N GAMMA Q VALUES')
             WRITE([illegible]1) PH,X1,Y1
       [illegible]1 FORMAT(1H ,5X,3F10.1)
             WRITE(6,[illegible]2)((MGQ(K,L),K=1,21),L=1,21)
       [illegible]2 FORMAT(1H ,4(1H-,/,1H ),21(15X,21F5.[illegible],/,1H-,/,1H ))
             RETURN
             END
```

ϕ	ψ	$b = x_1$	$D/B = Y_1$	N_γ	$N_{\gamma q}$	Meyerhof's 1957 Proposed $N_{\gamma q}$ for 2:1 slope
30°	$45 + \frac{\phi}{2} =$					
	60°	0	0	5	5	4
		1	0	9	12	13
		2	0	13	19	15
		3	0	18	19	15
		4	0	19	19	15
		5	0	19	19	15
		0	1	13	25	30
		1	1	18	37	37
		2	1	23	49	49
		3	1	30	58	57
		4	1	37	60	60
		5	1	37	60	60
		0	2	23	54	N/A
		1	2	30	68	"
		2	2	38	83	"
		3	2	45	96	"
		4	2	53	102	"
		5	2	54	102	"
		0	3	38	88	"
		1	3	45	107	"
		2	3	53	120	"
		3	3	63	121	"
		4	3	65	121	"
		5	3	65	121	"

ϕ	ψ $45 + \frac{\phi}{2}$	$b = x_1$	$D/B = Y_1$	N_γ	$N_{\gamma q}$
35°	62.5°	0	0	11	11
		1	0	17	24
		2	0	24	36
		3	0	32	43
		4	0	41	43
		5	0	43	43
		0	1	24	44
		1	1	32	64
		2	1	41	83
		3	1	51	102
		4	1	62	117
		5	1	74	120
		0	2	41	90
		1	2	51	116
		2	2	62	140
		3	2	74	164
		4	2	88	186
		5	2	103	207
		0	3	62	148
		1	3	74	178
		2	3	88	208
		3	3	103	235
		4	3	118	263
		5	3	134	287

ϕ	ψ $45 + \frac{\phi}{2}$	$b = x_1$	$D/B = Y_1$	N_γ	$N_{\gamma q}$	Meyerhof's 1957 proposed $N_{\gamma q}$ for slope of 2:1
40°	65°					
		0	0	25	25	20
		1	0	37	48	47
		2	0	48	70	68
		3	0	63	92	80
		4	0	78	104	85
		5	0	95	104	90
		0	1	48	82	82
		1	1	63	118	120
		2	1	80	153	155
		3	1	96	184	180
		4	1	112	215	210
		5	1	135	248	240
		0	2	78	162	N/A
		1	2	96	205	"
		2	2	112	247	"
		3	2	134	290	"
		4	2	155	331	"
		5	2	177	370	"
		0	3	112	259	"
		1	3	135	310	"
		2	3	155	360	"
		3	3	177	412	"
		4	3	201	459	"
		5	3	230	506	"

ϕ	ψ $45 + \frac{\phi}{2}$	$b = x_1$	$D/B = Y_1$	N_γ	$N_{\gamma q}$
45°					
	67.5°	0	0	60	60
		1	0	81	104
		2	0	105	149
		3	0	128	191
		4	0	157	235
		5	0	189	271
		0	1	106	165
		1	1	128	231
		2	1	157	294
		3	1	189	355
		4	1	222	417
		5	1	255	501
		0	2	157	309
		1	2	189	388
		2	2	220	463
		3	2	255	545
		4	2	292	623
		5	2	335	700
		0	3	220	477
		1	3	250	572
		2	3	292	671
		3	3	332	755
		4	3	375	845
		5	3	418	930

B.5 Conclusion

As can be seen the results appear to be reasonable and they compare favorably with the 1957 Meyerhof values of $N_{\gamma q}$.

The results presented herein are based on Meyerhof's 1951 theory and do not take into account the reduction in $N_{\gamma q}$ that is possible if ψ is varied. The reason why the values compare is thought to be due to the fact that when $\psi = 45^{\circ} + \frac{\Phi}{2}$ the most critical center of log spiral is not located at the footing edge but is in fact located somewhere above the footing.

As a check on the importance of varying ψ, the case of $\psi = 1.2\Phi$ for $\Phi = 40^{\circ}$ was investigated. $N_{\gamma q}$ was found to be not very different from the case of $\psi = 45^{\circ} + \frac{\Phi}{2}$ (within 5%).

PHI K1 Y1 N GAMMA VALUES

40.0 0.0 0.0

25. 26. 27. 30. 34. 39. 47. 55. 66. 78. 94. 112. 135. 161. 193. 229. 267. 315. 367. 423. 4

25. 26. 28. 30. 33. 40. 48. 56. 67. 82. 99. 121. 145. 172. 206. 248. 288. 345. 399. 459. 5

27. 25. 27. 30. 34. 39. 47. 57. 71. 87. 104. 127. 156. 188. 224. 268. 317. 370. 434. 504. 5

27. 27. 27. 29. 34. 40. 48. 61. 73. 92. 113. 137. 168. 201. 244. 290. 348. 404. 472. 554. 634

27. 26. 26. 30. 35. 42. 52. 63. 77. 97. 120. 148. 185. 221. 271. 321. 382. 448. 529. 608. 702

28. 27. 26. 30. 34. 43. 53. 67. 83. 107. 130. 165. 204. 247. 295. 354. 426. 497. 583. 676. 776

29. 27. 28. 30. 36. 45. 55. 72. 92. 117. 146. 183. 225. 277. 334. 405. 475. 560. 652. 762. 869

29. 28. 28. 31. 38. 47. 60. 78. 102. 129. 164. 209. 254. 316. 378. 454. 538. 639. 738. 856. 983

32. 26. 28. 31. 40. 52. 66. 88. 113. 147. 190. 238. 293. 361. 436. 527. 618. 727. 845. 972.1123

38. 28. 29. 34. 42. 58. 73. 99. 135. 172. 225. 278. 345. 427. 509. 609. 719. 849. 978.1116.1279

47. 31. 31. 37. 48. 64. 87. 121. 161. 207. 265. 339. 413. 504. 604. 725. 845. 983.1143.1292.1468

34. 33. 42. 60. 76. 109. 147. 197. 255. 328. 413. 502. 614. 737. 869.1014.1160.1328.154[illegible] 1719

45. 51. 69. 121. 142. 192. 256. 3[illegible]. 422. 515. 630. 756. 8[illegible].1041.1214.1391.1575.1792.20[illegible]

B.43

0. 0. 0. 0. 76. 143. 194. 264. 347. 442. 549. 667. 798. 953.1131.1299.1467.1677.1873.2115.2366

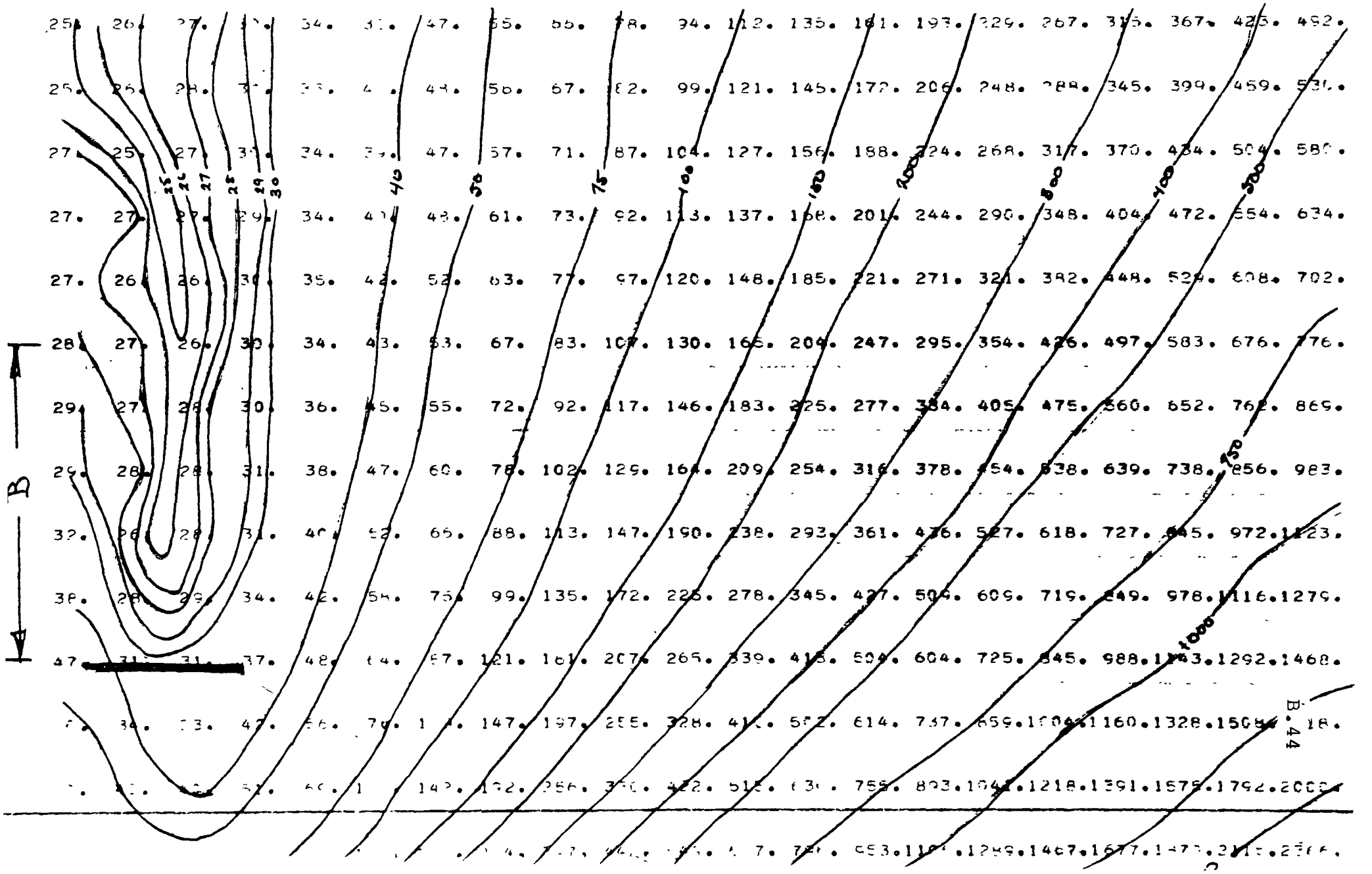
PHI
X1
Y1
N GAMMA VALUES
B
B.44

[illegible]	X1	Y1	N GAMMA VALUES															
[illegible]	[illegible]	[illegible]																
64.	7.	31.	[illegible]	[illegible]	[illegible]	59.	71.	89.	107.	134.	168.	194.	237.	283.	342.	394.	467.	553.	631.
67.	6.	[illegible]	[illegible]	[illegible]	[illegible]	58.	69.	73.	92.	114.	143.	175.	215.	260.	310.	371.	437.	516.	598.	693.
72.	4.	29.	28.	33.	39.	48.	61.	76.	96.	122.	152.	190.	233.	286.	338.	409.	480.	560.	658.	759.
83.	3.	27.	28.	33.	39.	51.	64.	83.	103.	135.	166.	212.	257.	313.	375.	451.	535.	626.	724.	841.
120.	4.	28.	28.	33.	41.	54.	67.	90.	115.	149.	187.	236.	290.	350.	424.	505.	594.	701.	805.	930.
0.	3.	26.	27.	33.	42.	57.	74.	97.	129.	164.	210.	262.	326.	398.	478.	574.	669.	783.	906.	1039.
0.	3.	24.	27.	34.	44.	60.	81.	110.	148.	192.	241.	304.	374.	460.	546.	649.	762.	898.	1030.	1172.
0.	2.	25.	27.	36.	50.	70.	97.	128.	169.	223.	283.	359.	435.	529.	632.	756.	878.	1024.	1181.	1333.
0.	3.	23.	28.	39.	57.	81.	115.	154.	205.	271.	336.	421.	524.	627.	751.	874.	1020.	1178.	1347.	1527.
0.	4.	24.	31.	46.	68.	99.	141.	190.	254.	327.	419.	512.	625.	750.	886.	1034.	1194.	1382.	1566.	1761.
0.	7.	26.	38.	57.	90.	130.	183.	254.	327.	427.	523.	639.	766.	918.	1069.	1232.	1424.	1611.	1829.	2047.
0.	6.	34.	53.	84.	127.	187.	258.	341.	435.	553.	671.	815.	958.	1129.	1295.	1493.	1704.	1908.	2146.	2384.
0.	7.	[illegible]	[illegible]	141.	[illegible]	[illegible]	[illegible]	482.	605.	742.	877.	1041.	1218.	1417.	1615.	1813.	2045.	2291.	2551.	2798.
[illegible]	[illegible]	[illegible]	[illegible]	[illegible]	[illegible]	[illegible]	[illegible]	[illegible]	[illegible]	[illegible]	[illegible]	[illegible]	[illegible]	[illegible]	[illegible]	[illegible]	[illegible]	[illegible]	[illegible]	[illegible]